Design and Experimental Evaluation of a Hybrid Wheeled-Leg Exploration Rover in the Context of Multi-Robot Systems

von
Dipl.-Ing. Florian Cordes

Kumulative Dissertation
zur Erlangung des akademischen Grades eines
Doktors der Ingenieurwissenschaften (Dr.-Ing.)

Vorgelegt im Fachbereich 3
Informatik und Mathematik
der Universität Bremen

Bremen, im August 2018

Datum des Promotionskolloquiums: 12.12.2018

Gutachter:
Prof. Dr. Dr. h.c. Frank Kirchner

Zweitgutachter:
Prof. Dr. Udo Frese

Zusammenfassung

In der vorliegenden Dissertation werden das Design, die Implementierung, die Kontrolle und eine experimentelle Evaluation eines neuartigen Rovers mit aktivem Fahrwerk beschrieben. Durch das hybride Fahrwerk wird eine Basis für vielfältige Lokomotionsformen geschaffen. Das entworfene Kontrollsystem abstrahiert die komplexe Kinematik des Fahrwerks und stellt ein Interface zur Kommandierung des Rovers über wenige Parameter bereit. Das Hauptaugenmerk dieser Arbeit liegt auf Design und Kontrolle des Fahrwerks sowie der experimentellen Evaluation des resultierenden Rovers.

Der Rover ist Teil eines heterogenen, modularen Multi-Robotersystems welches für eine Probenrückführmission am lunaren Südpol oder in mit derzeitigen Systemen schwer oder gar nicht erreichbaren Gegenden des Mars vorgesehen ist. Die Anforderungen an den Rover, die durch den Einsatz in einem Multi-Robotersystem entstehen, werden dargestellt und in das Design einbezogen. Somit wird die Entwicklung des Multi-Robotersystems als Hintergrund der Entwicklungen des Einzelsystems ebenfalls in dieser Arbeit dargestellt.

Insgesamt wird durch die Entwicklungen eine Kombination verschiedener Lokomotionsformen sowohl im einzelnen Roversystem als auch im heterogenen Multi-Robotersystem angestrebt. Die folgenden Punkte werden im Rahmen dieser Arbeit bearbeitet:

- Es wird ein aktives Fahrwerk für einen planetaren Rover entworfen, welches aus dem Bereich laufender Systeme wie auch dem Bereich rädriger Lokomotion inspiriert ist. Es werden zwei aufeinander aufbauende Versionen des Fahrwerks entwickelt und integriert. Hierzu zählt das elektromechanische Design ebenso wie die Lokomotionskontrolle des resultierenden Roboters. Die finale Version wird einer detaillierten experimentellen Evaluation unterzogen.
- Es werden modulare, heterogene Multi-Robotersysteme mit Fokus auf planetarer Exploration entworfen und untersucht. Verschiedene Kombinationen von fahrenden und laufenden/kletternden Systemen werden instanziiert: Insgesamt werden drei Multi-Robotersysteme unterschiedlicher Ausprägung und mit verschiedenen Fähigkeiten zur Durchführung unterschiedlicher Aufgaben aufgebaut.

In der Arbeit wird gezeigt, dass durch die Kombination verschiedener Lokomotionsarten erhöhte Fähigkeiten in der Bewältigung von schwierigem Gelände möglich sind. Im Fall der Multi-Robotersysteme betrifft dies zum Beispiel das Erreichen des Inneren von Kratern am Mondsüdpol. Im Rahmen der Untersuchungen des hybriden Einzelsystems wird eine erhöhte Anpassungsfähigkeit des Systems an unstrukturierte Untergründe gezeigt. Hierzu werden sowohl Experimente in einer Laborumgebung als auch ausgedehnte Versuche im Rahmen einer Feldtestkampagne durchgeführt und ausgewertet. Es werden insbesondere der Energiebedarf des aktiven Fahrwerks, die Qualität der Bodenadaption sowie die Fähigkeit der Bewältigung von Steigungen in verschiedenen Fahrwerkskonfigurationen untersucht und untereinander verglichen.

Abstract

With this dissertation, the electromechanical design, electromechanical implementation, locomotion control, and experimental evaluation of a novel type of hybrid wheeled-leg exploration rover are presented. The actively articulated suspension system of the rover is the basis for advanced locomotive capabilities of a mobile exploration robot. The developed locomotion control system abstracts the complex kinematics of the suspension system and provides platform control inputs usable by autonomous behaviors or human remote control. Design and control of the suspension system as well as experimentation with the resulting rover are in the focus of this thesis.

The rover is part of a heterogeneous modular multi-robot exploration system with an aspired sample return mission to the lunar south pole or currently hard-to-access regions on Mars. The multi-robot system pursues a modular and reconfigurable design methodology. It combines heterogeneous robots with different locomotion capabilities for enhanced overall performance. Consequently, the design of the multi-robot system is presented as the frame of the rover developments. The requirements for the rover design originating from the deployment in a modular multi-robot system are accentuated and summarized in this thesis.

With the active suspension rover on the one hand and a heterogeneous multi-robot system on the other hand, a combination of different locomotion modes is pursued in both, individual (sub-)systems and heterogeneous multi-robot systems. The two main topics of this thesis are:

- Electromechanical system design, motion control design and experimental evaluation of an active suspension system. The developed rover suspension takes inspiration from wheeled and legged locomotion. Two versions of an active suspension consecutively building on each other are implemented within this thesis.
- Design of heterogeneous modular multi-robot systems for planetary exploration missions. Different combinations of heterogeneous robots with driving, walking and climbing capabilities are instantiated. Three different multi-robot systems, subsequently building on each other, are developed in the scope of this thesis.

With this thesis it is shown that the combination of different locomotion modes results in improved capabilities for negotiating challenging terrain. In case of multi-robot systems this is for example related to soil sampling within permanently shaded crater regions at the lunar south pole. In the context of the hybrid rover system an increased adaptability to natural terrain is shown. Experiments in laboratory indoor tests as well as an extended four week field trial are conducted and evaluated in this thesis. Special attention is given to the energy consumption of the suspension system, the quality of ground adaption, and the ability of slope climbing in different configurations of the suspension system.

Danksagung

Es sind immer viele verschiedene Personen, die mit ihren speziellen Fähigkeiten die Arbeit an und mit robotischen Systemen ermöglichen. Somit ist auch diese Dissertation schlussendlich durch die Zusammenarbeit mit verschiedenen Kollegen am DFKI Robotics Innovation Center (RIC) in Bremen möglich geworden.

Allen voran möchte ich meinem Doktorvater Prof. Dr. Dr. h.c. Frank Kirchner für die exzellenten Rahmenbedingungen danken, die er mir am DFKI RIC geboten hat. Auch für das Vertrauen, welches er mir entgegengebracht hat, als er mir bereits früh in meiner beruflichen Laufbahn die Projektleitung großer Projekte mit verschiedenen Partnern aus Industrie und Wissenschaft zutraute, möchte ich ihm ausdrücklich danken. In mittlerweile über zehn Jahren wissenschaftlicher Arbeit am DFKI RIC konnte ich verschiedenste Bereiche der Robotik, vor allem die Lokomotionskontrolle mobiler Roboter und das mechatronische Design komplexer (Multi-Roboter)Systeme bearbeiten. Diese Arbeit ist jeden Tag aufs neue fordernd, spannend und voller neuer Erfahrungen und ich freue mich, ein Teil des Teams am RIC sein zu können.

Prof. Dr. Udo Frese möchte ich für seine Bereitschaft als Zweitprüfer dieser Arbeit zu fungieren danken. Seine Kommentare halfen, die Grundstruktur dieser kumulativen Dissertation sinnvoll zu gestalten.

Grundsätzlich ist die Arbeit an den in dieser Dissertation beschriebenen Systemen ohne die technischen und administrativen Kollegen nicht möglich; mein Dank gilt also allen Kollegen am DFKI. Namentlich möchte ich vor allem das Feld-Team aus dem Vorhaben FT-Utah erwähnen. Mit den Kollegen Leif Christensen, Steffen Planthaber, Thomas M. Röhr, Roland U. Sonsalla und Tobias Stark durfte ich einen vierwöchigen Feldversuch in der Wüste des US-Bundesstaates Utah durchführen. Die ausgezeichnete Zusammenarbeit unter den widrigen Bedingungen hat die Versuche mit dem Multi-Robotersystem sowie dem Einzelsystem SherpaTT möglich gemacht. Dank der hervorragenden Stimmung im Team konnte die gute Laune auch an den langen und arbeitsreichen Tagen aufrecht erhalten werden.

Besonderer Dank gilt meinem Freund und Kollegen Dr. Daniel Kühn. Über die Jahre der gemeinsamen Arbeit hat er mit kritischen Nachfragen und Hinweisen immer wieder meinen Blick für die Dinge geschärft. Die Diskussionen mit ihm im Rahmen von Projektbesprechungen sowie an längeren Abenden im Privaten möchte ich auch nach Abschluss dieser Dissertation nicht missen.

Gleiches gilt für meine Freunde und Kollegen Ajish Babu, Dr. Sebastian Bartsch und Alexander Dettmann. In den Jahren der Arbeit an dieser Dissertation haben die Diskussionen und Debatten zu verschiedenen Themen mit ihnen immer wieder neue Blickwinkel eröffnet und diese Arbeit schlussendlich mit ermöglicht.

Für die Korrektur der schriftlichen Ausarbeitung dieser Arbeit möchte ich zudem Dr. Jose de Gea und meinem Bruder Sebastian Cordes danken. Die verschiedenen Sichtweisen führten zu kleinen und größeren Verbesserungen der Qualität dieser Arbeit.

Zu guter letzt möchte ich meinen Eltern, meinem Bruder und meiner Frau für all die Unterstüzung danken, die mir jederzeit in allen Lebenslagen geboten wurde. Insbesondere meiner Frau Stefanie Cordes möchte ich für ihre Geduld und ihr Verständnis während der Feldversuche in den USA bis wenige Tage vor der Geburt unseres Sohnes, sowie ihre moralische Unterstützung während der Schreibphase dieser Dissertation danken.

Contents

Preface

Thesis

Bibliography

Appendix

List of Figures

List of Tables

Acronyms

BCS Body Coordinate System

BHC Body Height Control
(A motion controller in SherpaTT's MCS)

BLDC Brushless Directed Current

CAD Computer Aided Design

CMMB Central Module Management Board

CoG Center of Gravity

CPMB Central Power Management Board

COS Coordinate System

DGPS Differential GPS
(GPS: Global Positioning System)

DoF Degree of Freedom

EGC Ensure Ground Contact
(A motion controller in SherpaTT's MCS)

EMI Electromechanical Interface

FLC Force Leveling Control
(A motion controller in SherpaTT's MCS)

FPGA Field Programmable Gate Array

FTS Force-Torque Sensor

GAP Ground Adaption Process
(Central motion controller in SherpaTT's MCS)

GCS Ground Control Station

IMU Inertia Measurement Unit

LCS Leg Coordinate System

LEP Leg End Point

LRO Lunar Reconnaissance Orbiter
(A satellite mission to Moon)

LVDS Low Voltage Differential Signaling

MC3D Motion Command 3D

MCS Motion Control System
(Middleware for SherpaTT locomotion control)

ME Module Electronics
(as used within PLIs of described MRSs)

MER Mars Exploration Rover
("Spirit" and "Opportunity")

MRS Multi-Robot System

MSL Mars Science Laboratory
(The "Curiosity" rover)

PLI Payload-Item

PSR Permanently Shaded Region
(particularly on lunar poles)

RMS Root Mean Square

RPA Roll-Pitch Adaption
(A motion controller in SherpaTT's MCS)

SCS Shadow Coordinate System

SIMA Symmetrical Interface Manipulator
(Modular arm in TransTerrA system)

WCP Wheel Contact Point

WCS Wheel Coordinate System

WSS Wheel Steering Support
(A motion controller in SherpaTT's MCS)

1 Introduction

This chapter provides a motivation for the thesis and defines the scope of the topics covered. The contributions are outlined, and a clarification of the terminology as used throughout the thesis is provided. Additionally, the structure of the thesis with an overview of the chapters and related publications is presented in this chapter. The chapter is closed with a content summary of the author's publications contributing to this thesis.

1.1 Motivation and Scope

With the exploration of the solar system, mankind follows an ancient pursuit of widening horizons, expanding habitable areas and increasing knowledge of their sourroundings, natural phenomena and environmental processes. Questions that currently drive missions to Moon, Mars or beyond include the evolutionary history of our solar system and the search for former or present life on celestial bodies other than Earth. A key factor for answering these questions is the search for traces of water on celestial bodies which is also a prerequisite for possible inhabitation by humans in the future. Hence, NASA's general theme for the Mars exploration program is "Follow the Water" [Figueroa and Garvin, 2018].

After the manned Apollo-Missions to Moon in the late 1960ies and the early 1970ies, exploration of celestial bodies nowadays is conducted by robotic devices only. These systems can be categorized into three groups:

- (orbiting) satellites
- stationary surface landers
- mobile robots

Satellites are a method to gain general knowledge about the celestial body while passing by or orbiting it. In this case, data can only be acquired by remote sensing. Mars Odyssey is an example for such a satellite, indicating subsurface water ice on Mars using its Gamma-Ray Spectrometer instrument [Boynton et al., 2002].

Opposed to satellites, stationary landers are deployed on the surface of the celestial body. Being equipped with a manipulation arm or similar devices, instruments can be placed on the surface. This allows measurements in the direct vicinity of the landing spot. One example of such a system is the Phoenix lander on Mars [Goldstein and Shotwell, 2009]. This lander was sent to the polar regions to confirm the findings of the Mars Odyssey Orbiter. In general, the scientific return is limited to the immediate surroundings of the lander platform. Powered decent is required for precision landing on specific spots of scientific interest. However, exhaust plumes from the landing propulsion might impede the measurements conducted with the stationary lander.

The third alternative, using mobile robots, provides the possibility to take measurements independent of the landing site. Scientific investigation several kilometers away from the lander is made possible with mobile systems [Volpe, 2005]. All mobile surface robots that have been deployed in extraterrestrial exploration (Mars and Moon) so far are single systems with all instrumentation and capabilities included in one rover. All of these systems feature a passive suspension providing good performance at low complexity, e.g. NASA's Mars Exploration Rovers (MERs) [Lindemann and Voorhees, 2005] and Mars Science Laboratory (MSL) [Heverly et al., 2013] on Mars or China's Yutu rover on Moon[(a)].

However, the areas and types of terrain these robots negotiate are quite conservative in terms of locomotive challenges. Scientifically interesting sites, especially in terms of geologic history and traces of former or present water, can be found in very challenging terrain such as cliffs, crevasses, on top of inverted river beds or in permanently shaded regions of lunar polar craters. These areas are out of safe reach for the currently deployed types of robots [Schenker et al., 2001], [Huntsberger et al., 2007], [Nesnas et al., 2012].

To advance the accessibility of these remote areas and to be able to respond to unforseen terrain challenges, a new rover locomotion system is developed, integrated and experimentally evaluated in this thesis. The presented approach is an active suspension system for a rover maintaining an energy-efficient wheeled locomotion but also allowing to actively change the position of the wheels with respect to the rover's central body. Hence a wide range of motion capabilities is opened. For example, wheels can be lifted off the ground to be freed in case they are stuck in very soft soil or broken through a crust into a cavity. Generally, even walking locomotion patterns become possible which can be employed in very challenging situations. However, these might be not the preferred locomotion modes for a wheeled system and would be limited to exceptional cases.

Accessability of scientifically interesting areas might pose contradicting requirements on a robotic system: A longer distance from the landing site to the sampling site is preferably covered by energy efficient (e.g. wheeled) locomotion. Steep slopes and vertical cliffs required to be negotiated for reaching the sampling site might call for another locomotion approach e.g. with climbing capabilities. Hence, the combination of robotic systems with different locomotive capabilities into one multi-robot exploration system is proposed in this thesis to further increase the overall locomotive capabilities. The different robots' capabilities can match the requirements of different phases of a mission, one example being the exploration of the interior of a crater: During the traverse from a landing spot to the crater, a comparatively energy-efficient wheeled robot transports a highly capable climbing robot. For the second exploration phase, both systems are detached and the climbing robot descends into the crater.

The rover system with active suspension in this thesis is developed as part of such a heterogeneous modular Multi-Robot System (MRS). Being part of such a *system of systems* generates extra requirements for each individual robotic subsystem in terms of physical interaction and cooperation abilities. Additionally, specific mission scenarios generate specific requirements for functionality and capabilities of the robot. Consequently, an analysis of the different heterogeneous MRSs as background for the individual rover developments is part of this thesis.

[(a)] Unfortunately there seems to be no English conference or journal publication on the findings of the Yutu mission available. Images from the Chinese original webpage have been republished in [Lakdawalla, 2016]

1.2 Thesis Contributions

The main contribution of this thesis is the design of an active suspension rover and its locomotion control, cumulating in the design of the rover SherpaTT. The experimental evaluation of the system in laboratory environment and during a field test in Mars analogue terrain is part of this contribution. It is shown that an active adaption to unstructured terrain can be achieved without prior knowledge of the terrain. Furthermore, with the design presented, the additional power requirements for actuating the suspension can be kept low in comparison to the overall power requirement.

The path leading to the development of the active suspension for the rover SherpaTT went through the design of three multi-robot systems. From iteration to iteration, the systems are more tightly integrated and of increasing sophistication in subsystem performance as well as capabilities of the combined heterogeneous system.

Consequently, the second major contribution of this thesis is the design of heterogeneous multi-robot systems for planetary exploration scenarios. These scenarios include, but are not limited to, crater exploration with climbing robots descending into the crater as well as landing a mission into a crater and building a logistics chain for sample return. The described missions and systems can be transferred to terrestrial applications as well, as shown with a submarine version of the exploration rover.

Figure 1.1 illustrates the contributions of this thesis along the line of systems developed. The first row shows pictures of the three MRSs which are part of the contributions of this thesis.

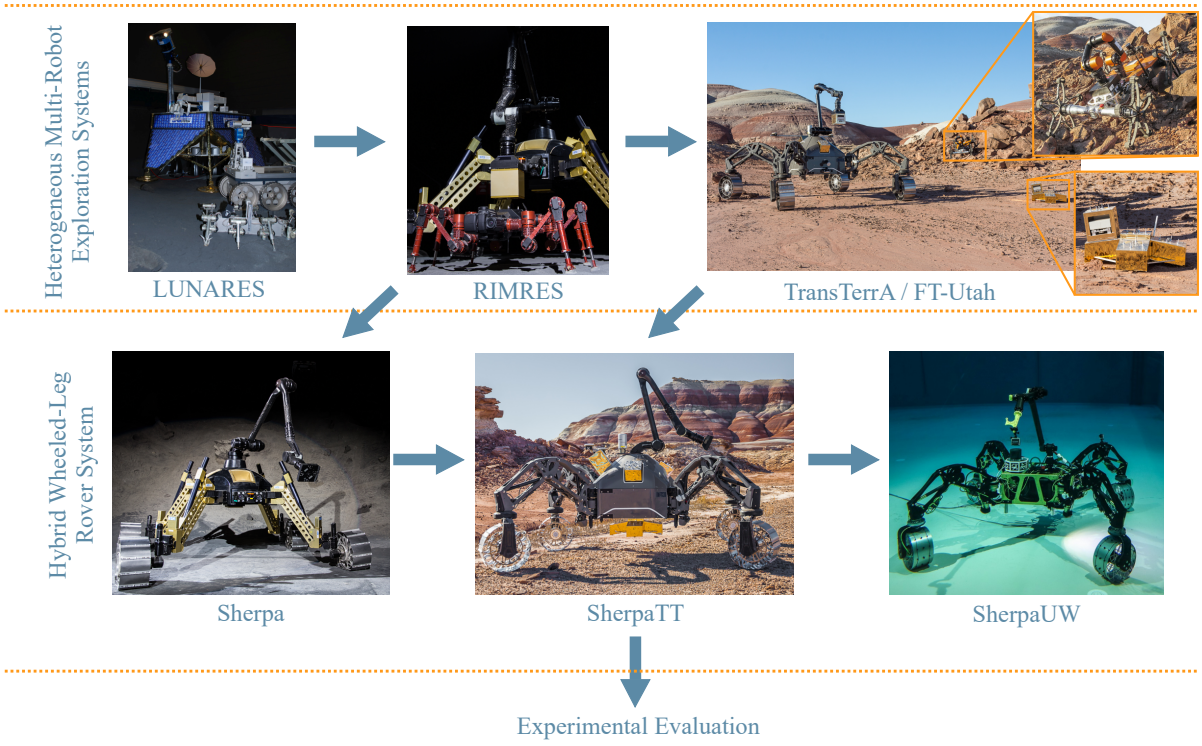

Figure 1.1: *Multi-robot systems and active suspension rovers as part of this thesis. Derivations are indicated by arrows.*

The second row illustrates the individual wheeled-leg rovers which are part of these multi-robot systems. Their electromechanical design and control system design are described in the thesis. The rover SherpaTT is taken out of the MRS for detailed experimental evaluation as an individual rover system, which is indicated in the third row of the image.

The multi-robot system LUNARES[(b)] is shown as the origin of the thesis' developments in Figure 1.1. This feasibility study consists of a lander mock-up equipped with a manipulation arm, a wheeled platform and an eight-legged scout robot. With the system RIMRES[(c)] a tighter coupling of the subsystems is achieved by introducing a common Electromechanical Interface (EMI). The TransTerrA MRS[(d)], makes use of a shuttle rover between the exploration rover and a lander unit. The EMI is updated to a second generation in this MRS. The TransTerrA systems are deployed in a four week field test in the desert of Utah[(e)]. Experiments from this field trip are used for rover evaluation in this thesis.

The *wheeled-leg* platform Sherpa of the RIMRES MRS introduces the first version of an active suspension system described in this thesis. The active suspension of the exploration rover is updated, resulting in the rover SherpaTT and its submarine pendant SherpaUW, as indicated in the second row of Figure 1.1.

Essential for tight coupling of heterogeneous robots is the common EMI, facilitating power sharing, communication and mechanical interconnection of different systems. The EMI is used for transporting immobile payload-items and mobile units, assembly of basic infrastructure elements, as well as adding new sensor modalities to mobile systems. Thus, a flexible, adaptable and extendable multi-robot system is made possible with this interface. The EMI is developed as essential part of the MRSs and presented in this thesis as an additional contribution.

1.3 Terminology

The following list defines several terms in the context of this work. It serves to clarify the usage of the terms within this thesis, since there might be similar, yet slightly different understandings of these terms.

System of Systems In this thesis the term is following the definition from [Kotov, 1997]: "System of systems are large-scale concurrent and distributed systems the components of which are complex systems themselves".

Multi-Robot System (MRS) A MRS is considered to be a system composed of two or more robot systems operating in the same environment [Farinelli et al., 2004]. Consequently, a MRS is a subcategory of the more general term system of systems. Individual robot systems of the MRS are called *subsystems* in the context of a MRS.

Wheeled-Leg The term *wheeled-leg* is used to describe a structure attached to a robot's body with one or more active DoF (the "leg") that features an active or passive wheel in contact with the ground. In literature such structures can also be found under the terms "wheel-on-leg". Alternatively, a robot is said to be "wheel-legged".

(b) Project LUNARES: Lunar Crater Exploration Scenario, BMWi Grant-No.: 50 RA 0706 and big Grant-No.: INNO 1036 A

(c) Project RIMRES: Reconfigurable Integrated Multi-Robot Exploration System, BMWi Grant-No.: 50 RA 0904

(d) Project TransTerrA, BMWi Grant-No.: 50 RA 1301

(e) Project FT-Utah: field Trials in Utah, BMWi Grant-No.: 50 RA 1621 and 50 RA 1622

Legged-Wheel As opposed to a wheeled-leg, a *legged-wheel* is defined as one or more legs that are oriented around a common hub, hence forming a rimless wheel. Alternative formulations from literature include "leg(s)-on-wheel" structure and "paddle-wheel".

Leg End Point (LEP) The term *LEP* is used to kinematically describe a wheeled-leg of a robot. The LEP is considered to be the idealized point of contact of a rigid wheel on rigid ground. The location of an LEP is considered to be described by a vector in cartesian coordinates $\boldsymbol{p} = (p_x\ p_y\ p_z)^T$ or cylindrical coordinates $\boldsymbol{p} = (p_\alpha\ p_r\ p_z)^T$.

Wheel Contact Point (WCP) The real contact point between wheel and ground might be different from the LEP and is defined as the *WCP*. A wheel can have more than one WCP or no WCP when the wheel is lifted off the ground, but there is always exactly one LEP.

1.4 Structure of Thesis

The structure of this thesis is illustrated in Figure 1.2. From the publications forming this cumulative thesis, those related to each chapter are provided in the respective box. Further publications of the author are cited at the appropriate places in each paragraph.

Following this introductory chapter are two chapters laying the foundations of the thesis: An overview on the relevant state of the art is presented in Chapter 2. The rover of the subsequent chapters is part of a multi-robot system. Therefore, requirements originating from the modularity and mission design have to be considered for the rover. Hence, Chapter 3 is dedicated to the design of heterogeneous MRSs.

The electromechanical design of the rover system is described in Chapter 4, two different suspension system implementations are addressed. The control system design is discussed in Chapter 5. These two chapters represent the design part of the thesis.

Both, electromechanical design and the control of the suspension system are experimentally evaluated as presented in Chapter 6. The thesis is wrapped up with a conclusion in Chapter 7 additionally providing an outlook on future developments.

Additional system information and additional experimental data not published yet is provided in the tables and plots of Appendix A. Appendix B provides a statement on the author's contributions to the publications forming this cumulative dissertation, and briefly lists the contents of additional publications of the author. Finally, Appendix C accumulates the full length publications forming this cumulative thesis.

1.5 Bibliography Remarks

To better distinguish between the author's own publications and citations from literature, different citation marks are applied:

- Citations from the author's own publications are plain numbered, e.g. [1], [4].
- Citations from literature are using the author-year format, e.g. [Wilcox, 2012].

Following list briefly introduces the contents of the accumulated publications. The publications are attached in Appendix C in full length.

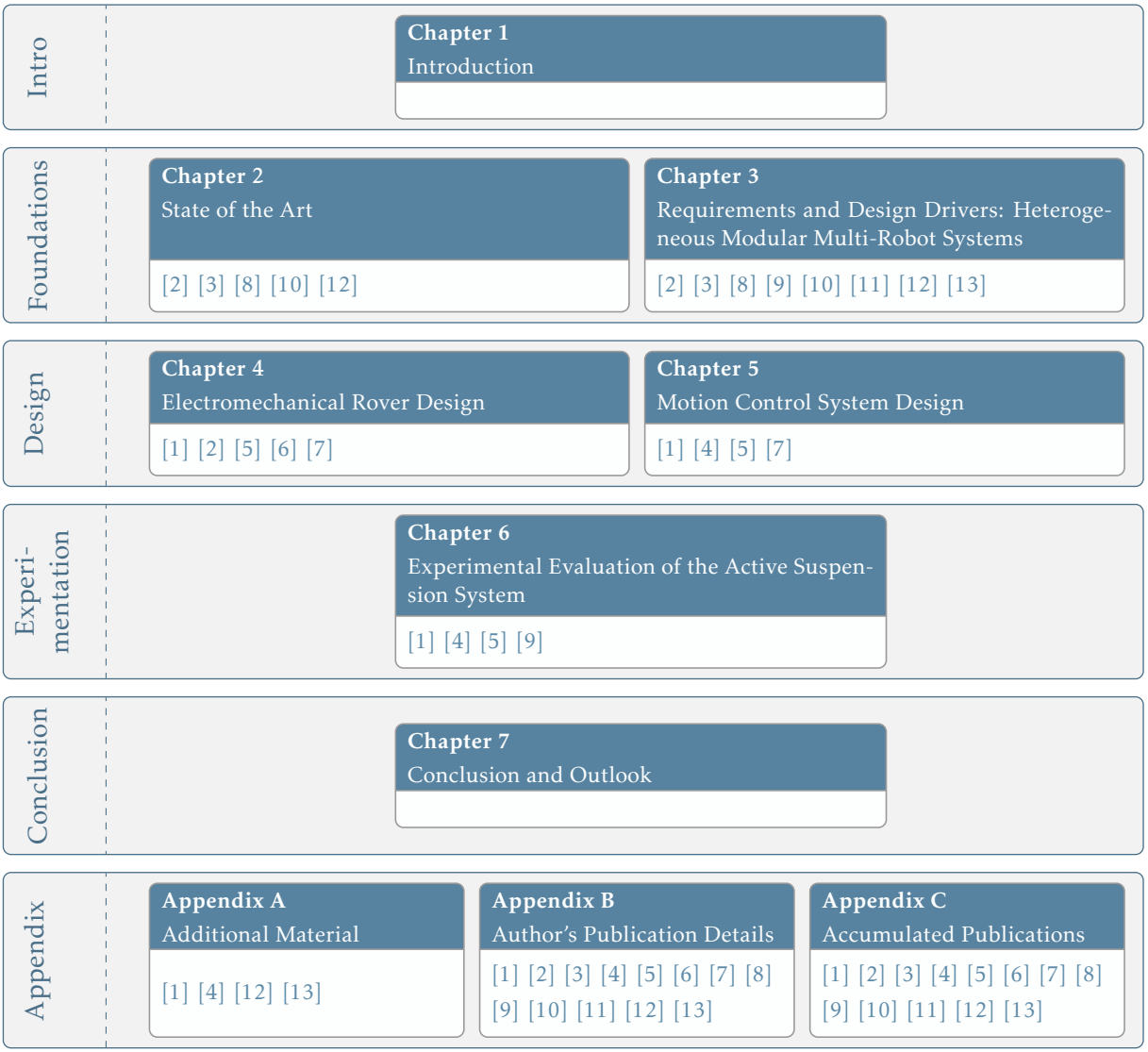

Figure 1.2: *Structure of this thesis and related accumulated publications.*

[1] **Design and Field Testing of a Rover with an Actively Articulated Suspension System in a Mars Analogue Terrain**
This journal publication provides the main experimental evaluation of the rover SherpaTT. Exhaustive data analysis of the field experimentation in Mars analogue terrain is conducted in this publication. Additionally, the electromechanical design as well as the motion control system and its individual ground adaption processes are discussed.

[2] **Reconfigurable Integrated Multirobot Exploration System (RIMRES): Heterogeneous Modular Reconfigurable Robots for Space Exploration**
This journal publication presents the final results of the RIMRES multi-robot system. System design, experimental evaluation of cooperative behaviors and lessons learned from the work with the system are presented.

[3] **Lunares: Lunar Crater Exploration with Heterogeneous Multi Robot Systems**
This journal publication summarizes all results and lessons learned with the concept study of a heterogeneous multi-robot system. The novel approach of combining a wheeled rover with a legged scout robot for lunar polar crater exploration is evaluated in an artificial lunar crater.

[4] **Static Force Distribution and Orientation Control for a Rover with an Actively Articulated Suspension System**
In this publication, experiments in a laboratory environment with the rover SherpaTT are presented. Main focus is on the evaluation of the ground adaption processes. The basic motion control system is outlined.

[5] **SherpaTT: A Versatile Hybrid Wheeled-Leg Rover**
This publication provides an early stage of the motion control system for SherpaTT and provides first experimental results in an indoor laboratory environment.

[6] **An Active Suspension System for a Planetary Rover**
This publication reviews the design of the rover Sherpa and identifies drawbacks of the initial design. The review leads to the introduction of the new suspension system for SherpaTT. Consequently, this publication links the two suspension system versions with each other.

[7] **Locomotion Modes for a Hybrid Wheeled-Leg Planetary Rover**
Locomotion modes for the wheeled-leg system Sherpa are proposed in this publication. An analytical solution for wheel orientation and wheel rotational velocity calculation to match motion commands under varying footprint configurations is presented.

[8] **Heterogeneous Robotic Teams for Exploration of Steep Crater Environments**
In this workshop publication the LUNARES multi-robot system is reviewed and the aspired RIMRES multi-robot system as follow-on system with tightly integrated subsystems is presented. The six-legged SpaceClimber robot is presented as antetype for the RIMRES scout robot CREX.

[9] **Field Testing of a Cooperative Multi-Robot Sample Return Mission in Mars Analogue Environment**
This publication presents the test site of the field deployment with the TransTerrA multi-robot system. Additionally, multi-robot system experimentation as well as individual system experiments are highlighted.

[10] **Performance Evaluation of an Heterogeneous Multi-Robot System for Lunar Crater Exploration**
This publication provides experimental results from the LUNARES multi-robot system. The scout's climbing capabilities in an artificial crater environment are experimentally evaluated. Furthermore, an autonomous sample approach with the legged scout, sample detection and sample pick-up are evaluated.

[11] **Towards a Heterogeneous Modular Robotic Team in a Logistic Chain for Extraterrestrial Exploration**
The TransTerrA multi-robot system with its aspired logistics chain is introduced in this publication. A detailed lunar mission layout is provided and the subsystems of the multi-robot system are presented.

[12] **Heterogeneous Modules with a Homogeneous Electromechanical Interface in Multi-Module Systems for Space Exploration**
This publication recapitulates the developments of the first generation electromechanical interface for the RIMRES multi-robot system. Experimental evaluation in terms of mechanical loads, mechanical docking as well as communication quality with dust contaminated interface connections is conducted and documented in this publication.

[13] **A Robust Electro-Mechanical Interface for Cooperating Heterogeneous Multi-Robot Teams**
This publication introduces a second generation electromechanical interface. Differences to the first design are highlighted and mechanical load experimentation is provided.

2 State of the Art

This chapter gives a brief overview on the state of the art of the main topics of this dissertation. An overview of MRS can be found in Section 2.1, including multi-robot systems for space exploration as well as modular reconfigurable systems. Rover systems with focus on suspension systems for mobile robots are presented in Section 2.2. The section highlights the differences between passive suspension and active suspension systems and draws the conclusions for design of the active suspension system presented in this thesis. Section 2.3 concludes this chapter with a statement on the contributions of the author's publications assigned to this chapter. This survey does not claim to be exhaustive, more details on specific parts of the state of the art can be found in each publication contributing to this cumulative thesis.

The following publications from Appendix C – Accumulated Publications contribute to the contents of this chapter:

[2] **Reconfigurable Integrated Multirobot Exploration System (RIMRES): Heterogeneous Modular Reconfigurable Robots for Space Exploration**; *T. M. Roehr, F. Cordes, Frank Kirchner*; Journal of Field Robotics, 2014.

[3] **Lunares: Lunar Crater Exploration with Heterogeneous Multi Robot Systems**; *F. Cordes, I. Ahrns, S. Bartsch, T. Birnschein, A. Dettmann, S. Estable, S. Haase, J. Hilljegerdes, D. Koebel, S. Planthaber, T. M. Roehr, M.Scheper, F. Kirchner*; Journal of Intelligent Service Robotics, 2010.

[8] **Heterogeneous Robotic Teams for Exploration of Steep Crater Environments**; *F. Cordes, F. Kirchner*; Planetary Rovers Workshop at ICRA 2010.

[10] **Performance Evaluation of an Heterogeneous Multi-Robot System for Lunar Crater Exploration**; *S. Bartsch, F. Cordes, S. Haase, S. Planthaber, T. M. Roehr, F. Kirchner*; i-SAIRAS 2010.

[12] **Heterogeneous Modules with a Homogeneous Electromechanical Interface in Multi-Module Systems for Space Exploration** ; *A. Dettmann, Z. Wang, W. Wenzel, F. Cordes, F. Kirchner*; ICRA 2011.

2.1 Multi-Robot Systems

To the best of the author's knowledge, there currently exists no heterogeneous MRS directly comparable to the systems described in this thesis in Chapter 3. These systems provide reconfiguration capabilities and modular extendability while at the same time integrating self-contained mobile systems into a system of systems. All heterogeneous MRSs developed in the scope of this thesis tackle a broad range of research topics, only a few of which shall be highlighted in this section. An exhaustive survey on this particular state of the art is provided in [Parker et al., 2016] and [Farinelli et al., 2004].

2.1.1 Types of Multi-Robot Systems

Generally, the term multi-robot system describes a system composed of more than one robot, see also the definition in Section 1.3. This might include stationary robots as for example industrial robot arms and other dual- or multi-arm manipulation systems. Multi-robot systems always exhibit a *collective behavior*, being defined as *any behavior* of subsystems in a MRS [Cao et al., 1997]. *Cooperative behavior* is a subclass of collective behavior and distinguished by cooperation, i.e. interaction of subsystems.

This thesis focusses on mobile robots, hence the term multi-robot system as used in this document is with special focus on multiple *mobile* robot systems. This system class can be subdivided into two categories: (i) *collective swarm systems* and (ii) *intentionally cooperative systems* [Parker et al., 2016]. The first category is generally covering large scale systems, i.e. more than five mobile robots. Typically the entities of a swarm system are identical in hardware and software. Only local control on each robot is used to generate an emergent and coherent overall system behavior. Opposed to that, systems of the second category have knowledge of their team mates and take into account the actions of other team mates.

The type of cooperation of subsystems in a MRS can be described as (i) *strongly cooperative* or (ii) *weakly cooperative*. Strongly cooperative systems require tight cooperation of the subsystems; particularly, the tasks cannot be serialized or otherwise accomplished with one single robot in strongly cooperative systems [Brown and Jennings, 1995]. Opposed to that, the latter category allows single robots of the team to have periods of independent operations [Parker et al., 2016] or to decompose the multi-robot task in order to be serialized.

Modular (self-)reconfigurable robots are a subclass of MRSs and typically constituted from small units with common electromechanical interfaces. Connecting the units into new compound systems allows to generate robots with different morphologies and capabilities. One of the first publications describing a modular reconfigurable robot is [Fukuda and Nakagawa, 1988]. Most of present modular self-reconfigurable systems follow this initial concept.

2.1.2 Cooperating Multi-Robot Systems for Space Exploration

Nearly two decades ago, multi-robot systems have already been considered for future space exploration missions. Applications conceived include wide-baseline observations with fused data from multiple agents, distributed mapping and navigation as well as collective locomotion tasks [Schenker et al., 2000]. However, currently no multi-robot surface systems are deployed in any space mission. At most the MERs twin rovers can be considered as a multi-robot system in the widest sense of the term, yet they are deployed on opposite sides of the planet Mars,

hence no interaction or cooperation is present [NASA-JPL, 2018a]. Several research groups are currently proposing multi-robot teams for celestial body surface exploration, the architectures and their aspired advantages over single rover systems are highlighted in this subsection.

With the TRESSA system (Teamed Robots for Exploration and Science on Steep Areas), a heterogeneous multi-robot system is developed, demonstrating the reach of areas not accessible for a single robot [Huntsberger et al., 2007]. In literature the system is also known as Cliffbot [Pirjanian et al., 2002], [Mumm et al., 2004]; it consists of two anchoring robots each connected with a tether to a mobile robot descending a cliff surface. By combining the two types of robots the overall system proved to be able to navigate in rocky slopes up to 85° [Huntsberger et al., 2007]. The rappelling robot on the cliff face is a wheeled rover, which would not be able to manage the traverse without anchors and tethers.

A similar approach is described with the Axel system: A wheeled rover with comparatively high mass such as the MSL lowers the small two-wheeled Axel rover into a steep cliff. The tether management is proposed to be on the smaller descending robot [Abad-Manterola et al., 2010], reducing the wear on the cable when compared to the anchor rolling out the tether during descent. In field experiments the system was able to demonstrate the applicability to crater exploration with steep cliffs and tethered descent.

A different approach for inner crater exploration with a heterogeneous MRS is investigated with the LUNARES system [3]. With LUNARES former separately developed systems are combined into one heterogeneous robotic team. In this concept study, an eight-legged walking and climbing robot is used to climb down an artificial crater, take a soil sample and head back to a wheeled rover waiting at the crater rim. Descent and ascent are conducted without a tether system. The wheeled rover is used to transport the legged scout between lander unit and crater rim. After ascent from the crater, the robots jointly return to a landing unit where the soil sample is taken from the mobile robots onto the lander. The performance of the overall system is evaluated in an artificial crater environment as presented in [10], [18]. In the study, the general feasibility of a heterogeneous MRS combining legged and wheeled locomotion is shown. The LUNARES system is described in Chapter 3 as part of this thesis.

The RIMRES system [8] is building on and expanding the LUNARES experiences. The system consists of a wheeled-leg rover and a six-legged scout system aspired for lunar crater exploration [2]. By introducing an EMI for the system, modular extendability and reconfigurability are achieved [12]. While connected via the EMI, both robots can share electrical power and establish a reliable wired data connection. Further details on mechanical robustness and power management of the EMI are presented in [24] and [25], respectively. Furthermore, surface-deployable sensor-stacks and basic infrastructure elements can be constructed using modular payload-items in this system [12]. The main focus of the developments in this project is on the cooperation and reconfiguration of the single systems using modular payloads. The RIMRES MRS is described in more detail in Chapter 3.

With the Mars Sample Return concept, a multi-robot mission to Mars is conceived [Nilsen et al., 2012]. In this concept subsequent missions to Mars realize a sample return to earth: A first mission lands a sample caching rover for selection and collection of geological and atmospherical samples, a second mission lands a sample fetching rover to retrieve the samples and either bring them back to the landing unit or transporting a return stage on its own. The latter option became available with the successful landing of MSL with the Sky Crane concept [Prakash et al., 2008].

2.1.3 Modular Self-Reconfigurable Robot Systems

As opposed to MRS with self-contained rover systems, modular (self-)reconfigurable robot systems are typically built up from small building blocks with limited capabilities. Since the first definition of a modular reconfigurable robotic system [Fukuda and Nakagawa, 1988], many different systems have been conceived. Systems with very good representation in literature are Polybot [Yim et al., 2000], CKBot [Park and Yim, 2009], Molecube [Zykov et al., 2007], M-TRAN [Kamimura et al., 2005], Superbot [Shen et al., 2010], and ATRON [Ostergaard et al., 2006]. Other modular systems exist in literature, an extended overview of the state of the art in the field of modular robotics is provided in [Stoy et al., 2010] and [Yim et al., 2009]. Classifications and examples for the classes of modular reconfigurable robots are also provided in [Parker et al., 2016]. Three main benefits drive the development of modular self-reconfigurable robot systems [Yim et al., 2009]:

Versatility Through rearrangement of interconnected modules, adding new modules or removing modules, a wide range of morphologies can be adopted to tackle various tasks.

Robustness A system is built up from many similar or identical parts, malfunctioning units can be replaced to maintain the function of the overall system.

Low cost A set of modules can adopt different morphologies, as opposed to several single use-case robot systems reducing cost due to re-usability. Furthermore, a potentially great number of single units forms a modular self-reconfigurable system. Hence, mass production of modules might reduce fabrication costs.

Typically, the subsystems are connected via interfaces providing at least mechanical connection; additionally, communication and power sharing might be possible with the chosen interface. Connecting the simple subsystems generates robot systems of various shapes; rolling chains, four-legged robots, snake-like systems and driving (i.e. car-like) systems have been reported in literature. The MRSs developed in this thesis and presented in Chapter 3, make use of such an interface in order to include above listed benefits into the multi-robot exploration systems. However, an atomic reconfiguration with complete morphological changes as pursued with the modular (self-) reconfigurable systems cited above is not the goal for the MRSs of this thesis.

2.1.4 Multi-Robot Systems: Summary and Conclusion

Two types of MRS are described in this section: (i) cooperating ("complex") mobile systems and (ii) atomic reconfigurable systems, composed of "simple" subsystems. Systems of the first type are advanced in the sense that viable application scenarios e.g. in the context of planetary exploration, particularly in terms of locomotion capabilities, exist. Even though [Shen et al., 2010] describe a mission scenario for planetary exploration, the systems of the second type are more in the state of basic research and lacking specific application scenarios not feasible without deployment of atomic reconfigurable systems.

However, these systems promise increased versatility and robustness due to ease of exchange of modules and flexibility in terms of overall system extension, which are important properties for robotic space exploration systems. The MRSs developed in this thesis aim at this goal by combining multiple sophisticated mobile robots into a system of systems. Aspects of the modular reconfigurable systems are used to exploit the benefits of these system types, resulting in a heterogeneous modular multi-robot system.

2.2 Rover Suspension Systems

This section presents several different (rover) locomotion systems with emphasis on wheel and leg combinations. For comparability, "classical" passive suspension systems are described, before the enhancement of such passive suspensions with active elements is tackled. Systems relying on predominantly active suspension are presented, additionally, walking robots with rolling motion capabilities are briefly discussed.

2.2.1 Passive Suspension Systems

One of the best known passive suspension systems for planetary rovers is the so-called *rocker-bogie* suspension [Bickler, 1989]. Figure 2.1a illustrates the kinematics of a rocker-bogie suspension. It features six independently driven wheels, three on either side of the vehicle. The front wheel and the center wheel of one side are connected rigidly with a bogie. The rear wheel is mounted on the rear end of a rocker arm, the front end of which is connected via a passive rotational joint to the bogie of the front and center wheel. The linkage of one side is connected via a differential gear to an identical linkage on the other side of the rover. Each of the four corner wheels is steerable, resulting in ten active DoF for driving and steering the six wheels. Straight drive, arc turns and point turn manoeuvers are possible. The height of obstacles that can be overcome with this type of suspension ranges in the size of a wheel's diameter [Lindemann and Voorhees, 2005].

The Sojourner microrover with a mass of 10.5 kg was a flight experiment aboard the Mars Pathfinder mission, featuring the rocker-bogie suspension system [Stone, 1996]. Both MERs are featuring a rocker-bogie suspension as well, [Harrington and Voorhees, 2004]. These rovers have a mass of about 170 kg. The latest deployed Mars rover MSL/Curiosity has a mass of about 900 kg and features a rocker-bogie suspension, too [Welch et al., 2013]. The wide range of mass over nearly two orders of magnitude proves a general feasibility of the rocker-bogie for a wide range of vehicle classes. Due to the kinematics, all wheels are kept in permanent ground contact and the mass of the vehicle is approximately evenly distributed onto all six wheels. All deployed rovers with this suspension showed an exceptional performance on Mars, however, with the rover "Spirit" getting stuck in soft soil, a fatal failure is reported, ending the mission in May 2011 [NASA-JPL, 2018c].

Many derivations of a rocker-bogie system exist, one being the triple-bogie suspension, also referred to as 3-bogie suspension, Figure 2.1b. ESA's ExoMars rover is equipped with this type of suspension [Michaud et al., 2008]. A system with a triple-bogie configuration has three independent bogies with two wheels each, resulting in six wheels in total. The bogies are mounted on the two sides and the rear end of the rover's body, each bogie rotating around its mounting point independent of the other bogies. For the ExoMars rover nearly all test-scenarios showed a good terrain performance, however getting entangled on certain types of obstacles is reported in [Apfelbeck et al., 2011]. Variations of passive suspension systems for the ExoMars rover are discussed in [Kucherenko et al., 2004].

With the Artemis rover, a variation of the triple-bogie system is presented, [Manz et al., 2014]. In this configuration, the bogies are supported by spring elements for improved ground traction. The springs were introduced after the observation that the thrust of a middle wheel was able to lift the front wheel off the ground in certain situations. All six wheels are drivable and steerable, hence omnidirectional manoeuvers are possible with the Artemis robot.

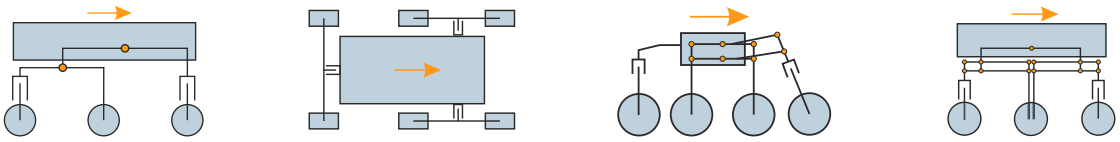

(a) *Rocker-bogie type (side view)* **(b)** *Triple-bogie type (top view)* **(c)** *Shrimp type (side view)* **(d)** *CRAB type (side view)*

Figure 2.1: *Illustrations of discussed passive suspension systems. Arrow indicates nominal forward movement of robot.*

A further variation can be found in the rovers Shrimp [Lamon and Siegwart, 2003] and SOLERO [Lamon and Siegwart, 2004]. This type of suspension makes use of six wheels providing two wheels on each side of the rover and additionally one wheel in the front and one wheel at the rear end of the rover. Figure 2.1c illustrates this suspension setup. The two bogies on the sides are constructed as parallelograms with one wheel at each end. An articulated spring-loaded fork holds the front wheel, while the rear wheel is mounted with a rigid arm to the main body of the rover. Front and rear wheel are both steerable.

The forward/backward symmetry of the CRAB type of suspension is claimed to have similar performance characteristics as the rocker-bogie type, yet its inherent symmetry enables the same terrain capability in both, forward and backward motion [Thueer et al., 2006]. Figure 2.1d illustrates the kinematic principle of this type of passive suspension: Each side of the robot has three wheels, the front and rear wheel are both connected to the center wheel via a parallelogram, in effect connecting front and rear parallelogram at the center wheel. As in the other types of suspension discussed, a differential reduces the pitch angle of the chassis.

All the examples above show that passive suspension systems are designed in a way that all wheels are kept in permanent ground contact. The gravitational load is distributed between the wheels and roll and pitch angles of the central rover's body are reduced when traversing sloping terrain. Active control of the mechanisms is not possible, the adaption to sloping terrain is a result of the chosen kinematics. Yet, failure from getting stuck in soft soil or entanglement with obstacles rendering a robot immobile are reported. Furthermore, sufficient wheel thrust is required in order to push wheels onto and over obstacles. Particularly in slopes this might not always be guaranteed, reducing the performance in such a scenario.

2.2.2 Passive Suspension Supplemented with Active Elements

This subsection presents systems mainly relying on passive ground adaption, similar to those described in the previous section. However, the systems described here feature active elements of various types. The active elements are reported to improve the capabilities of the respective system, when compared to the pure passive adaption.

In [Kucherenko et al., 2004] additional "walking drives" for the ExoMars suspension are proposed, effectively adding active suspension elements to the otherwise passive triple-bogie suspension system described in the previous subsection. The actuators initially planned for deployment only – i.e. to get the rover from its stow configuration to the surface operation configuration – are proposed to be considered for advanced locomotion as well.

The proposed solution with six driven and steerable wheels, each equipped with a walking actuator is experimentally evaluated on the ExoMars Testing Rover ("ExoTeR"). Three scenarios including getting stuck in soft soil, up-slope climbing abilities and lander egress are tested and

described in [Azkarate et al., 2015]. It is found that the rover using only its passive suspension reaches a slip ratio of 97% in soft soil. After 45 s runtime, only 3 cm are driven. Enabling the wheel-walking mode in the same test-setup frees the rover completely after 20 s runtime. With regard to slope climbing, the wheel-walking showed increased performance over the purely passive system in the same setups. The performance gap increases with increasing slope angles. In lander-egress tests, the tip-over angle is improved.

A four-wheeled rover with passive and active suspension elements is the Sample Return Rover (SRR). The rover has four drivable and steerable wheels, two mounted on a rocker on each side of the central body. The rockers are shaped like an inverted "V", the opening angle of each rocker can be individually controlled by an actuator. Experimentation on sloping terrain showed improved locomotion performance especially in terms of stability margins in steeper slopes, when the active elements of the rockers are used to adapt to the slope. With fixed suspension, the rover reached stability margins as low as 2.1°, with 0° resulting in tipover, while the minimum stability margin in the runs with active articulation was 15.0° [Iagnemma et al., 2003]. The rover is not permanently adapting to the terrain, it traverses a distance in a fixed rocker configuration, relying only on the passive suspension elements, then stops for evaluation of terrain slopes and rover stability margins and then adapts the rocker configuration accordingly. Control strategies for locomotion system reconfiguration and terrain adaption strategies including repositioning of the Center of Gravity (CoG) using SRR's manipulator arm are described in [Schenker et al., 2003] and discussed in detail in [Iagnemma and Dubowsky, 2004].

Combining passive and active suspension in a similar manner is presented with the Scarab rover for lunar polar crater exploration [Bartlett et al., 2008]. In contrast to the SRR, Scarab has no steering actuators and relies purely on skid steering. The two rockers with active actuation are used for active adaption of the body-ground clearance and active locomotion modes such as the so-called "inch-worming" motion mode [Wettergreen et al., 2009b]. The active inch-worming motion mode and the possibility of CoG control are stated to greatly increase Scarab's locomotion performance in steep slopes [Wettergreen et al., 2009a].

The examples from this subsection substantiate a locomotion performance gain when active elements are employed in the suspension system. Depending on the arrangement and usage of the active elements, the boundaries between passive and active suspension systems are often blurry: The SRR makes use of active elements to bias the otherwise purely passive suspension; Scarab does the same but also allows for active crawling modes. The ExoTeR can change its locomotion strategy between using (i) a purely passive triple-bogie passive suspension, (ii) biasing the suspension as well as (iii) active crawling motion. Significantly increased locomotion performance is reported using the active elements of these robots' suspensions. Yet, all these systems still require wheel thrust to overcome obstacles, a drawback inherited from the passive suspension design. Furthermore, wheels stuck in cavities can only be freed with driving manoeuvers, repositioning of wheels with deliberate loss of ground contact is not possible.

2.2.3 Active Suspension Systems

This subsection is focussed on systems with mainly actively articulated suspension systems. In literature these systems are also referred to as "hybrid" systems due to their combination of legs and wheels, bridging the domain of walking robots and driving robots. The mobilities of such systems allow to actively adapt to the terrain and/or to control the body posture.

The Hylos system [Grand et al., 2004a] is a rover with 16 active DoF: Its suspension system is constructed from four legs with two DoF each, ending in a 2 DoF (drivable and steerable) wheel. A decoupled control approach for posture control and trajectory following is presented in [Besseron et al., 2008]. A reactive control approach is used to keep the body at zero roll and pitch angle. The footpoints are chosen to minimize the distance between CoG and center of support polygon. With this control strategy, the wheel contact forces are balanced due to the kinematic design of the robot. In simulation and real world experiments the capability of keeping the desired posture while traversing sloping terrain is confirmed. Body angle errors are ranging around 3° with single peaks up to 15° due to actuator velocity constraints [Grand et al., 2004a].

The All-Terrain Hex-Limbed Extra-Terrestrial Explorer (ATHLETE) is a hexagonally shaped six-wheeled platform. Each of the actively driven wheels is mounted on a six active DoF leg, resulting in a total of seven active DoF per leg. Each leg can also be used as a manipulator arm and provides an interface for connecting tools such as a drill or a gripper. ATHLETE is designed for lunar missions and can be used as a cargo or crew transporting device. Multiple systems can be connected via a mechanical latching mechanism [Wilcox et al., 2007]. Active load balancing between the wheels is conducted using ground contact force estimates based on joint torques of each leg. The forces are then distributed evenly by retracting or stretching single legs. Additionally, the main body is kept in the center of the support polygon spanned by the ground contact points in order to distribute the weight equally to all wheels. An Inertia Measurement Unit (IMU) mounted on the main frame is used to measure roll and pitch angle of the central platform. The control of these angles is possible independent of the foot positions for slopes up to 15°. Apart from rolling motion in flat terrain, walking in obstacle covered areas is possible [Townsend et al., 2010].

With the Sherpa rover, an actively articulated rover system with four wheeled-legs is introduced. Each of the four legs has six active DoF, including a drivable and steerable wheel. A centrally mounted six DoF manipulation arm is used for assembling payloads and is able to support the robot weight, hence can be considered as a fifth limb for locomotion support, resulting in 30 active DoF in total [2]. Passive flexibility is achieved using springs serially mounted to the linear drives acting on the parallelogram structure of a leg and by using flexible metal wheels. A discussion on possible locomotion modes with Sherpa is presented in [7]. The successor of Sherpa is the rover SherpaTT [5], a comparison of both systems is presented in [6]. Both systems are part of this thesis and are described in more detail in the subsequent chapters with special emphasis on the system SherpaTT.

A kinematically similar system to Sherpa is presented in [Reid et al., 2014]. The Mammoth rover makes use of four legs with four active DoF each, including the two DoF for driving and steering the leg's wheel. The control approach for active ground adaption with this system relies on the availability of terrain maps in front of the rover. The wheel trajectories are then pre-planned and executed, a reactive correction to deal with uncertainties is currently not implemented. Consequently, ground contact loss during obstacle traverse is reported in [Reid et al., 2016] and assigned to improper environment models.

Altogether, the active suspension systems presented in this subsection are essentially wheeled-leg systems, hence a combination of legs from the domain of walking robots and wheels from the domain of driving systems is realized for improved locomotion performance. Using legs, single wheels can be lifted off the ground and placed in various locations relative to the cen-

tral body. Planning approaches as well as reactive approaches for suspension configuration in sloping terrain are present in literature, a slight performance advantage can be seen with reactive control. A combination of planned wheel trajectories with reactive control altering the planned trajectories has not been investigated so far with above mentioned systems. Reactive control for wheel-contact forces relies on estimated force values from IMU measurements or joint torque estimates in all of the described systems. Explicit force measurement at the wheels has not been implemented in any of these systems.

2.2.4 Walking Robots with Additional Driving Capabilities

This subsection presents primarily walking robots with additional driving capabilities. The hybrid architecture of these systems allows to exploit the benefits of legged as well as wheeled locomotion. This thesis is aimed at the deployment of a rover system in predominantly unstructured terrain where energy-efficient wheeled locomotion is aspired to be the main locomotion mode. Hence the systems in this subsection illustrate the benefits of a hybrid locomotion architecture, while not being direct antetypes for the proposed rover system.

A four legged walking robot equipped with passive wheels for skating motion is presented with the Roller-Walker in [Endo and Hirose, 1999]. The system makes use of an active ankle joint that flips the passive wheels to a foot configuration for walking in rough terrain or to rolling configuration on flat surfaces. The rolling motion is stated to have an improved energy efficiency by factor eight when compared to crawling gait. The specific resistance, defined as "energy per unit distance" is used for the evaluation [Endo and Hirose, 2011].

A highly dynamic wheeled-leg robot is the Handle robot. The system features two legs ending in actively driven wheels and is equipped with two arms for manipulation and dynamic balancing during rolling motion. Jumping onto and off obstacles, managing stairs and transporting loads of nearly half of the robot's own weight have been demonstrated [Boston Dynamics, 2018].

In the 2015 DARPA Robotics Challenge (DRC) Finals, four out of the five best ranked-teams made use of robots combining driving and walking locomotion [Krotkov et al., 2017]. Ranked first place was the robot DRC-HUBO, a humanoid robot equipped with wheels on knees and ankles for driving in flat terrain and walking locomotion for example on stairs [Lim et al., 2017]. Ranked second was the humanoid robot Atlas with no driving capabilities from the team IHMC robotics [Johnson et al., 2017]. Ranked third was Chimp, a robot with mainly hominid shape, featuring track drives for rolling motion on forearms and legs [Haynes et al., 2017]. With Momaro [Schwarz et al., 2017] on the fourth rank, a further hybrid wheeled-leg system was amongst the five best robots in the challenge. The system RoboSimian achieved the fifth rank, this system is mainly oriented towards walking and climbing motion, however, active wheels in the body allow for driving motions on flat terrain [Karumanchi et al., 2017].

2.2.5 Rover Suspension Systems: Summary and Conclusion

Overall a good performance at low maintenance can be asserted for passive ground adaption systems. However, as shown for example with the triple-bogie system of the ExoMars rover, adding active elements to the previously passive system can greatly improve locomotion performance, particularly in non-nominal i.e. stuck situations. Yet, merely adding active

elements to an otherwise passive suspension system might not generate the locomotive capabilities needed. A multitude of solutions for active suspension systems exists in literature, several of which are highlighted in this section. As indicated in above subsections, systems with active elements or fully actively articulated suspension bear the potential of superior terrain performance. As described with the skating motions of the RollerWalker [Endo and Hirose, 2011] the locomotion modes are not necessarily discrete driving vs. walking but can be a hybrid of both. Most prominently the benefits from hybrid systems are demonstrated with the results of the 2015 DARPA Robotics Challenge, where four of the five highest ranked teams made use of a combination of wheeled and legged locomotion [Krotkov et al., 2017].

An intrinsic overhead of control is needed for active suspension, since a sensing and actuation control scheme is needed for coordination of active DoF. As suggested in literature [Townsend et al., 2010] and also shown in this thesis, proprioceptive data such as force readings and roll and pitch angle measurements allow sophisticated control of an active suspension system. In many cases simple strategies already show improvements using active locomotion [Haynes et al., 2017], reducing the computational and sensory requirements.

Furthermore, employing active articulation does not automatically increase the overall system mass; Wilcox argues that a wheeled-leg system can be about 25% lighter compared to a passively articulated vehicle designed for the same range of terrain types [Wilcox, 2012]. The mass savings result from actuators being chosen for a narrower band of torque requirements due to relaxed worst case scenarios; additionally smaller wheel actuation with smaller gearboxes as well as smaller wheels are possible, since a wheel could be lifted over an obstacle or out of a cavity. With the full scope of a space mission in mind, hence including a lander system, the mass savings with active suspension for the surface rover can be further increased: Ramps for egress and payload deployment mechanisms might be neglected if the system is able to climb off the lander and retrieve payloads from the lander deck using its limbs [Heverly et al., 2010], [Haarmann et al., 2012]. Furthermore, active elements can improve the safety while driving off of the lander in rough terrain [Azkarate et al., 2015].

2.3 Contributions of the Corresponding Publications

Altogether, the publications associated to this chapter are contributing to the state of the art: A novel approach of combining individual robot systems via a electromechanical coupling is introduced. The publications include the early design stage with a feasibility study, conclusions and derivations from the study as well as the realization of a new multi-robot exploration system.

The journal publication [3] summarizes all results and lessons learned from the LUNARES MRS concept study. An artificial crater environment is developed, including realistic lighting conditions and crater slopes. Automated experiment documentation, a motion tracking system, and a gantry crane for support of gravity compensation are installed within the environment. Furthermore, a mission control system for the heterogeneous system is introduced. The novel approach of combining a wheeled rover with a legged scout robot for lunar polar crater exploration is evaluated successfully in the test laboratory and documented in this publication.

The publication [10] is concerned with the evaluation of single aspects of the LUNARES study. As such, it details aspects also presented in [3] but additionally presents the experimental validation of the scout's locomotion in the artificial crater environment. In particular, climbing is

analyzed with regard to time and power requirements, as well as slippage in the crater slope. Furthermore, docking between different subsystems using a visual approach is part of the experiments presented in this paper.

The results presented in both papers laid the foundation for the design of a tightly integrated reconfigurable MRS with electromechanically coupled subsystems: The RIMRES MRS. A review of the results of the LUNARES demonstrator and derived requirements for the co-design process in the RIMRES system are described in [8]. This publication links the two multi-robot systems with regards to development strategies and experiences with system control.

The final results of the RIMRES project are presented in the journal publication [2]. The combination of sophisticated individual robots in a team equipped with a common EMI, primarily known from the class of modular (self-)reconfigurable robots, represents a novel approach for planetary surface robot systems. The benefits listed in Subsection 2.1.3 resulting from modularity and reconfigurability are thus transferred to a complex MRS in a lunar exploration scenario. Autonomous docking between mobile and immobile systems equipped with the interface is presented and evaluated substantially in experiments with the hardware.

The publication [12] details the design of the electromechanical interface used for connecting and tight coupling of the single systems in RIMRES. Connectors from modular (self-) reconfigurable systems are reviewed and a proposal for an interface usable in the aspired RIMRES MRS is made. Furthermore, the publication provides an overview of the power management, internal and external communications and mechanical design. Experiments concerning dust resistance are conducted, a feature indispensable for a modular planetary surface system which is, however, not covered broadly in literature so far.

3 Requirements and Design Drivers: Heterogeneous Modular Multi-Robot Systems

This chapter provides the background for the design of the hybrid wheeled-leg rover described in the subsequent chapters: Requirements and drivers for the rover design originating from its deployment in a heterogeneous modular multi-robot exploration system are presented.

A general mission scenario for a heterogeneous modular multi-robot system is motivated and presented in Section 3.1. The central part for such a modular multi-robot system is a common electromechanical interface for interconnection of subsystems. Consequently, an overview on the interface developed in this thesis is provided in Section 3.2.

The three physical implementations of multi-robot systems, namely LUNARES, RIMRES and TransTerrA, are described in Section 3.3, Section 3.4 and Section 3.5, respectively. The RIMRES and TransTerrA multi-robot systems make use of the developed electromechanical interface.

Section 3.6 recapitulates the lessons learned from the multi-robot systems and derives requirements for the rover design resulting from the presented multi-robot interaction as well as from the modularity approach. A summary of this chapter is provided with Section 3.7; Section 3.8 details the contributions of the included publications for this chapter.

The following publications from Appendix C – Accumulated Publications contribute to the contents of this chapter:

[2] **Reconfigurable Integrated Multirobot Exploration System (RIMRES): Heterogeneous Modular Reconfigurable Robots for Space Exploration**; *T. M. Roehr, F. Cordes, Frank Kirchner*; Journal of Field Robotics, 2014.

[3] **Lunares: Lunar Crater Exploration with Heterogeneous Multi Robot Systems**; *F. Cordes, I. Ahrns, S. Bartsch, T. Birnschein, A. Dettmann, S. Estable, S. Haase, J. Hilljegerdes, D. Koebel, S. Planthaber, T. M. Roehr, M.Scheper, F. Kirchner*; Journal of Intelligent Service Robotics, 2010.

[8] **Heterogeneous Robotic Teams for Exploration of Steep Crater Environments**; *F. Cordes, F. Kirchner*; Planetary Rovers Workshop at ICRA 2010.

[9] **Field Testing of a Cooperative Multi-Robot Sample Return Mission in Mars Analogue Environment**; *R. U. Sonsalla, F. Cordes, L. Christensen, T. M. Roehr, T. Stark, S. Planthaber, M. Maurus, M. Mallwitz, E. A. Kirchner*; ASTRA 2017.

[10] **Performance Evaluation of an Heterogeneous Multi-Robot System for Lunar Crater Exploration**; *S. Bartsch, F. Cordes, S. Haase, S. Planthaber, T. M. Roehr, F. Kirchner*; i-SAIRAS 2010.

[11] **Towards a Heterogeneous Modular Robotic Team in a Logistics Chain for Extraterrestrial Exploration**; *R. Sonsalla, F. Cordes, L. Christensen, S. Planthaber, J. C. Albiez, I. Scholz, F. Kirchner*; i-SAIRAS 2014.

[12] **Heterogeneous Modules with a Homogeneous Electromechanical Interface in Multi-Module Systems for Space Exploration**; *A. Dettmann, Z. Wang, W. Wenzel, F. Cordes, F. Kirchner*; ICRA 2011.

[13] **A Robust Electro-Mechanical Interface for Cooperating Heterogeneous Multi-Robot Teams**; *W. Wenzel, F. Cordes, F. Kirchner*; IROS 2015.

3.1 General Mission Scenario

The overall mission goal of the envisioned exploration systems in this thesis is a prolonged science mission with geological sampling from multiple sites. Generally, multiple mobile robots allow simultaneous sampling at different sites, potentially increasing surface coverage and science return. Furthermore, distributing tasks to different robotic (sub-)systems increases overall system robustness and resilience: Fatalities of individual robots do not necessarily result in failure of the complete mission [2]. Including a modular approach in a multi-robot system allows to gradually increase functionalities and robotic capabilities in subsequent missions. Additionally, replacement of malfunctioning modular units becomes possible to further increase the overall system robustness.

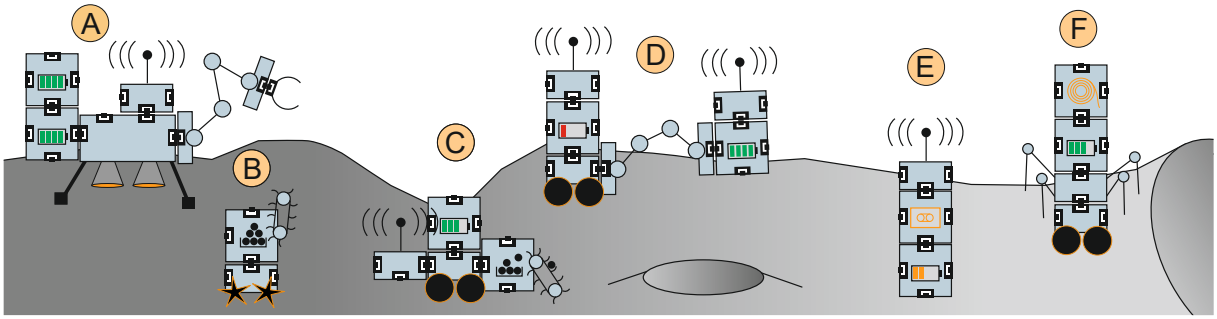

Figure 3.1: *Illustration of a possible heterogeneous modular multi-robot exploration system.*
(A) Lander with power packs and modular manipulation arm (B) shuttle rover returning sample container to lander (C) wheeled rover taking soil samples (D) wheeled rover deploying communication beacon (E) deployed scientific payload (F) wheeled rover transporting legged system to crater rim

An illustration of possible components of the aspired modular multi-robot exploration system is provided in Figure 3.1, see also [8]. In the anticipated scenario, a landing unit would serve as depot for Payload-Items (PLIs) and possibly as a science lab with sophisticated analytical tools or alternatively a return stage for sample return to earth. Various mobile systems make use of immobile PLIs to conduct scientific experiments, collect soil samples or to set up basic infrastructure elements.

Figure 3.1 is a basic illustration of aspired mission elements. Depicted battery packs for example could be exchanged by solar panels without loss of the general idea of the scenario. Further modules and functionalities are conceivable. A multitude of research and operational aspects are covered in this multi-robot scenario [2], including, but not limited to:

- Interface-design (physical connection and software)
- System design for cooperation
- (Cooperative) locomotion
- (Cooperative) navigation and mapping
- Manipulation, particularly PLI handling
- Logistics coordination
- Replanning and reconfiguration after failure

All of these topics are covered in the three MRSs described in the subsequent sections. However, from above list, the focus of this thesis lies on the enabling components facilitating the high-level objectives. These components include the electromechanical interface design for physical coupling of subsystems as well as mechatronic design aspects for the rover subsystem that is part of a MRS.

3.2 Modularity in a Multi-Robot Exploration System

A common electromechanical interface is a crucial component for a modular robotic system, as it is the device that allows for reconfiguration and modularity in the first place. Such an interface has been developed within the scope of this thesis. Mechanical as well as electrical design are specifically described in [12], [13], an overview can be found in [2] and [21]. Further details are published in [24], [25], [26], [27]. The interface is shown in the center of Figure 3.2. Oriented around the center are all mobile and immobile systems that up to date have been equipped with the modular interface. A gender principle was chosen: The passive part is completely sealed and without moving parts. This increases robustness against contamination with surface material, see [13].

Experimentation with the EMI and PLIs has been documented in several publications: Hot-swap of power sources during an automated payload assembly from two PLIs is documented in [2]. Experimentation with the first interface generation concerning docking angles, dust-resistance and mechanical loads is published in [12] and [24]. Electrical characteristics with focus on power switching and power management of the EMI are described and experimentally evaluated in [25]. Usage of the EMI as end-effector for a rover's manipulator is described and experimentally evaluated in [26]. Finally, [27] presents all implemented PLIs and highlights experiments conducted in terms of reconfiguration and PLI functionality.

The first generation latch mechanism was successfully tested with static loads of up to 400 N, while the second generation latch was tested successfully with up to 1300 N static load. These values are well above the aspired maximum loads for a scout robot like CREX in earth gravity.

Orientation experiments showed that undocking between two EMIs with orientations up to 30° rolled or pitched from the gravitational axis is possible. In regular operations such orientations would be avoided using the DoF of the manipulation arm or the rover's body pose control.

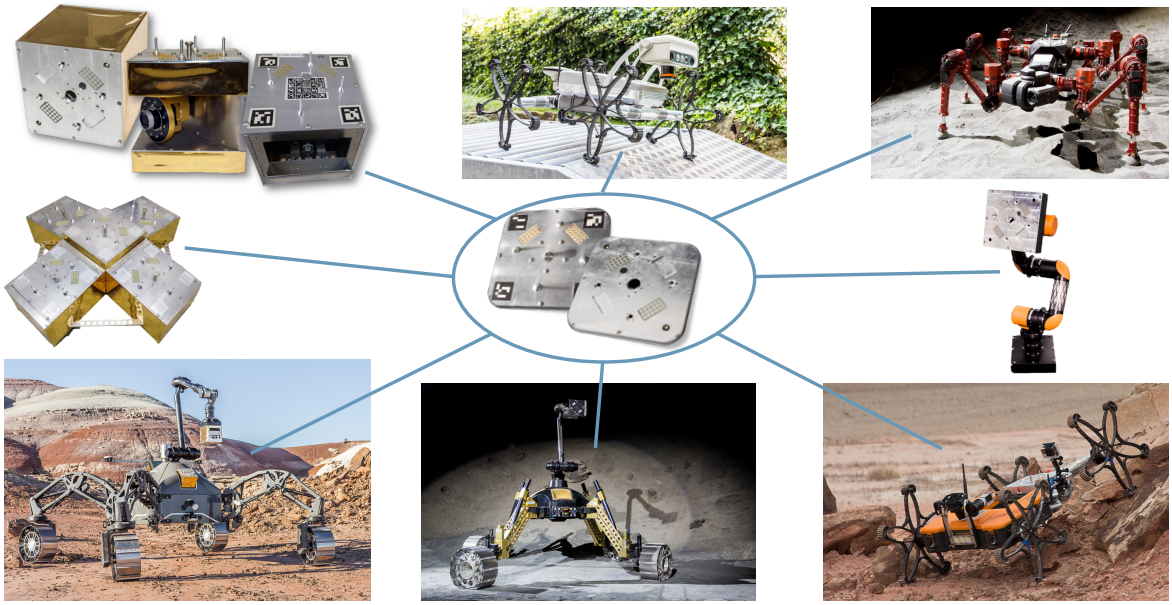

Figure 3.2: *The Electromechanical Interface (EMI) as central part of the proposed heterogeneous multi-robot systems connects all mobile and immobile subsystems.*
From top left counter clockwise: Various payload-items, a BaseCamp, rover SherpaTT, rover Sherpa, shuttle rover Coyote III, modular arm SIMA, scout robot CREX, Asguard v4

Experiments with dirt contaminations on both, the passive interface as well as the latch mechanism of the active interface were conducted successfully. Figure 3.3 shows examples from the conducted experiments. Complete coverage of the passive interface in basalt with a layer thickness of up to 2 mm is tolerated, both mechanically and electrically. Extreme contamination of the latch mechanism did not render it inoperable. Power switching tests showed a hardware reaction mean time to short circuits of 71.1 μs; constant currents of up to 10 A were tested without critical temperature increase on pins or Module Electronics (ME) board.

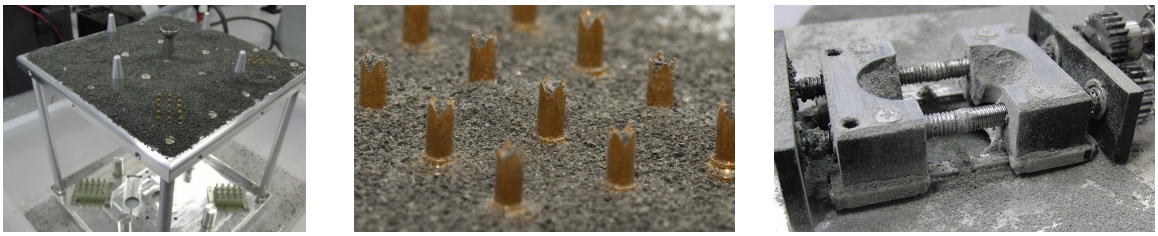

(a) *Distance pins tolerate up to 2 mm layer of granulate*

(b) *Crown headed pins allow electrical contact*

(c) *Latch mechanism still operable despite heavy contamination*

Figure 3.3: *EMI experimentation concerning contamination with geological surface material*

3.3 Sample Return from a Lunar Polar Crater: LUNARES

The system LUNARES is a MRS built up from preexisting robots, brought together for a feasibility demonstration of a lunar crater exploration with a heterogeneous robotic team. Functionless mock-ups are used to demonstrate payload transport and exchange. Establishing a software framework for an exploration mission with a heterogeneous multi-robot system and the locomotive capabilities of the legged scout are of special interest in this system.

3.3.1 Subsystems

The LUNARES MRS is composed of following robotic components [3]:

- A stationary lander mock-up with manipulation arm and sensor tower
- A rigid suspension six-wheeled rover
- An eight-legged climbing scout robot

Figure 3.4 shows the employed systems in an artificial crater test environment. The test environment along with the installed ground truth sensor suite is presented in [3]. Robot control, ground control station and mission control are presented in [3] and [17].

3.3.2 Mission Scenario

A mission with multiple sampling is assumed, hence the demonstration mission starts with an arbitrary relative pose between wheeled rover and stationary lander. The rover docks to the lander in a visual servoing approach and is equipped with a payload. Afterwards it drives to the crater rim, where the legged scout robot is deployed. The scout climbs into the crater, locates a geological sample, picks it up using a gripper mounted on a leg and climbs back to the wheeled rover. After the scout is in its transportation bay on the rover, both systems drive back to the lander, where the sample container is retrieved using the lander's manipulation arm. Detailed mission descriptions with images and experimental results are available in [3] and [8].

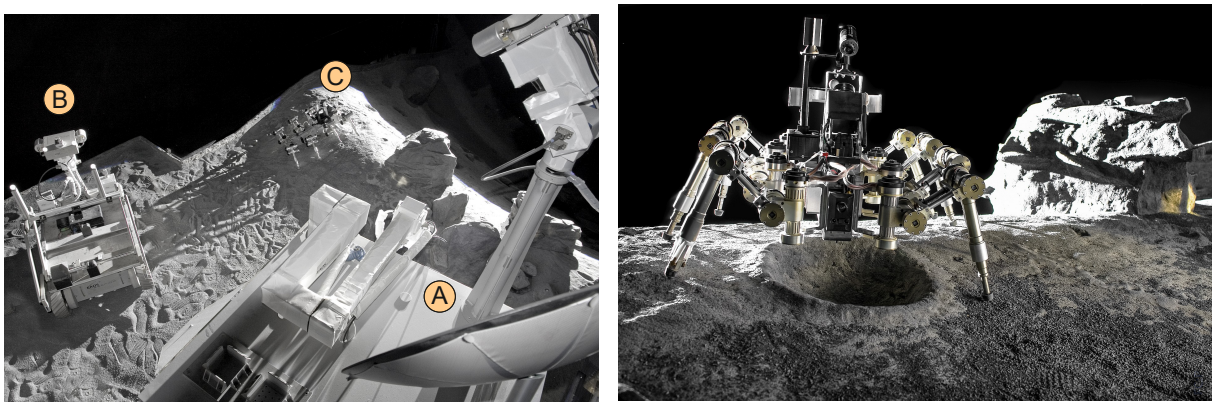

(a) *Lander-mockup with sensor mast and six DoF manipulation arm (A), six-wheeled rover (B) and eight-legged scout robot (C)*

(b) *Fully equipped scout robot Scorpion. Camera, laser scanner and sample container are mounted on top of the central body.*

Figure 3.4: *Multi-robot system LUNARES*

3.3.3 Experimental Evaluation

Experimental evaluation of the multi-robot system is documented in several publications. Autonomous docking between scout and rover as well as rover and lander is presented in [3], [10], and [18]. Autonomous sampling with the gripper of the legged scout robot is described in [3] as well as in [10]. Climbing with different locomotion parameters in the artificial crater slope is experimentally evaluated and documented in [10]. Acceleration data analysis for slip detection of the legged scout is presented in [17]. Payload exchange between lander platform and rover is highlighted in [17] and experimentally evaluated in [3].

3.3.4 Multi-Robot System LUNARES: Conclusion / Lessons Learned

From the experiences of the feasibility study several requirements for the follow-up system RIMRES are derived, as presented in [8]. Following main issues are contained in the lessons learned from LUNARES, see also [3]:

- Active payload containers are needed to be able to further improve the evaluation in a more realistic scenario.
- For transporting those payloads, an electromechanical interface is needed, in order to advance the simple "box-in-a-bucket" principle used for the LUNARES study. Such an interface would also facilitate the modularity which has been prepared within the demonstration study.
- A co-design process for the two mobile systems is needed for seamless integration. Using the aspired common interface, both systems could act as one single system when connected and independent of each other when disconnected.
- A manipulator is needed on the rover: It can pick-up/deploy samples from/onto the lander and can equip the scout with additional payloads. Furthermore a manipulator arm on the rover allows assembly and deployment of immobile payloads independent of the lander location.
- For greater distances and a more realistic demonstration of approaching the crater rim, a suspension system for the rover is needed.

3.4 Sample Return from a Lunar Polar Crater: RIMRES

The RIMRES MRS takes up the principle ideas of the LUNARES MRS and refines several aspects of the preliminary study. Three major advancements in terms of hardware are made with the introduction of (i) a standardized EMI for interconnection of all subsystems (see also Section 3.2), (ii) a newly designed rover system with an active suspension system, and (iii) a newly designed six-legged scout robot. The aspired tight integration of subsystems and the design specifically for reconfiguration, modularity, and locomotion in crater environments is facilitated with the new hardware.

3.4.1 Subsystems

The MRS consists of the following subsystems [2]:

- A wheeled-leg rover system (Sherpa), Figure 3.5a
- A six-legged scout robot (CREX), Figure 3.5b
- Several immobile payload-items, Figure 3.5c

The four-wheeled rover Sherpa is a hybrid wheeled-leg rover. Details of the design of the active suspension are provided in Chapter 4 of this dissertation. In the context of the MRS, the rover has several tasks, including transport, deployment and connection with the scout robot, traverse in sloping terrain and handling of PLIs to (i) assemble and deploy payloads and (ii) equip the scout with PLIs. A design review of the rover is presented in [6].

As in the previous scenario, the legged scout robot has the task of climbing down into a crater, retrieving a sample and climbing back out of the crater for sample return to the lander. Mechatronic design and control of CREX is based on the design of the SpaceClimber robot [28], [29], [30]. A capacious discussion on the design and locomotive capabilities of CREX's antetype SpaceClimber is presented in [Bartsch, 2013]. CREX's main variations with respect to SpaceClimber are the sensor head with two instead of one DoF and being equipped with an EMI for seamless integration into the modular MRS.

The mobile systems Sherpa and CREX are two separate mobile robots that can act independent of each other. However, using the EMI, both systems are connected electromechanically and can act as one single unit. Transport of the legged scout to the crater rim is conducted using the EMI connection. The scout is fixed below the wheeled rover and can share electrical power as well as data using the interface connection [2], see Figure 3.5a.

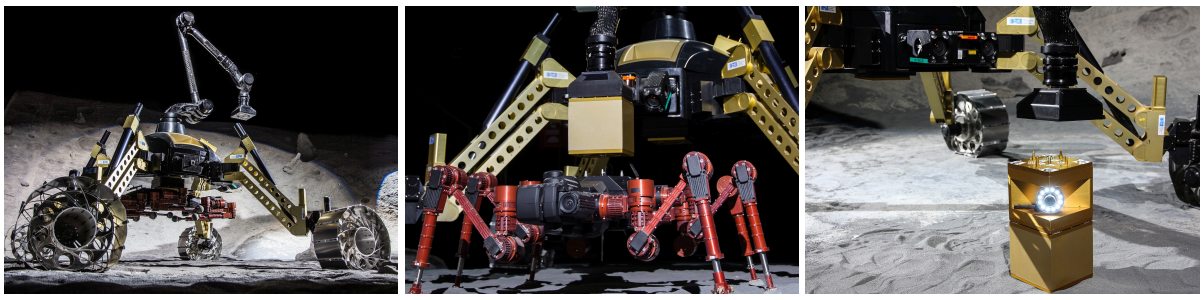

(a) *Wheeled-leg rover Sherpa with six-legged scout CREX*

(b) *CREX being equipped with an additional battery module*

(c) *A battery/camera payload is deployed by Sherpa*

Figure 3.5: *Multi-robot system RIMRES*

Each of the immobile PLIs features one active and one passive EMI in order to be connected to other PLIs or the mobile systems [12]. Various PLI have been conceived and implemented within the RIMRES scenario. The so-called Battery Module, Camera Module, as well as the REIPOS system are described in [2], [19], and [Bindel and Bruns, 2010]. Furthermore, [27] gives an overview on all implemented modular payload-items.

Mobile systems can be equipped with additional devices using the EMI. Figure 3.5b shows CREX being equipped with a battery module for extension of the system's own internal battery. In Figure 3.5c the rover is shown retracting its arm after deploying a payload on the surface. The payload is constructed from a Battery Module and a Camera Module. The latter simulates any data generating scientific device in a real lunar mission.

3.4.2 Mission Scenario

The lunar sample return mission scenario presented in Section 3.3 is used as the baseline for the RIMRES MRS: A wheeled rover and a legged scout jointly traverse from the landing site to a crater rim, where the scout is deployed in order to retrieve a sample from within the crater. After successful (re-)ascend from the crater, both systems return to the lander. The scenario is refined in terms of subsystem integration and sophistication as well as autonomy of procedures, e.g. docking or payload-assembly [2]. Main focus of the RIMRES system is the modularity and reconfigurability of the systems. These aspects are taken into account explicitly in the design phase [19]. Furthermore, the mission control and system control are addressed, the preliminary work from LUNARES in this field is extended within the RIMRES system [21].

3.4.3 Experimental Evaluation

The journal publication [2] contains the documentation of the experiments concerning assembly of payload-items using the manipulation arm and docking between legged scout and wheeled rover. Additionally, statements on the general feasibility of the chosen communication and software architecture for control of the MRS are made based on the experiences during experimentation. The manipulation arm for Sherpa is tested in a simulation environment for parameter optimization, the procedure is described in [15]. Deformation sensing for flexible metallic wheels for Sherpa is evaluated in preliminary experiments in [16]. Furthermore, most of the experiments described for the EMI in Section 3.2 are part of the experimentations with the RIMRES MRS.

3.4.4 Multi-Robot System RIMRES: Conclusion / Lessons Learned

Several experiences were made during the setup and experimentation with the RIMRES MRS. The most prominent aspects are provided in the following list, a more detailed description is provided in [2] and [21].

- Isolated tests of the EMI validated the feasibility of the design mechanically as well as electrically. However, the guidance pins showed to be to short in the initial design for the autonomous docking procedures.
- The optical markers are designed such that markers in two different heights are required for pose reconstruction. Hence a marker needed to be laser-imprinted on the central pin. This is costly and showed to be limited in automatic detection in the video stream.

- The serial point-to-point communication between two EMIs proved to be a useful backup, e.g. when a wireless connection was unreliable or not established yet, see also discussion on communication reconfiguration in Subsection 4.2.4.
- The EMI is a seemingly "simple" device, especially when compared to the mobile robots. Yet, it is the central device for modularity and reconfiguration in the MRS. As such, extended experimentation was conducted with the device to establish a transparent interface, enabling reconfiguration of robotic systems at runtime, see Section 3.2.
- The manipulation arm demonstrated being precise enough for manipulation and strong enough to support the rover during locomotion, e.g. by acting as a leg [2], [15].
- Each leg of the rover has six active DoF, yet mostly only four were required. Especially with employment of flexible wheels it can be argued that the design was overly complex. For a detailed review on the rover design, refer to [6].
- With CREX being developed on the experiences of SpaceClimber, a sophisticated climbing robot for the RIMRES MRS is developed. The co-design process with Sherpa has particular focus on the electrical specifications and connectivity using the EMI.
- The co-design process with developments from low-level hardware to high-level autonomy software within the MRS development proved to be of great benefit. All systems employ the same software framework and are, despite their diversity and heterogeneity (of the "phenotype"), quite similar in a considerable amount of hard- and software [21]. This underlying homogeneity (of the "genotype") should be advanced in further steps to facilitate developments and maintenance.
- The (semi-) autonomous control of the systems with action sequences, e.g. for payload stacking or scout-rover docking allowed integrating single actions into complex tasks. In the example of scout-rover docking, a control loop between both robots is established, where the rover effectively generates posture commands for the scout [2].
- Even though the legged scout is a highly capable climbing robot, direct landing of the MRS within a lunar crater might reduce overall mission risk by eliminating the need for descent of steep crater slopes. Landing a mission within a lunar polar crater for search of volatiles in permanently shaded regions has been proposed for example in [Bartlett et al., 2008].

3.5 Sample Return Using a Logistics Chain: TransTerrA System

With the TransTerrA system a paradigm change concerning the composition, task assignment and objectives for the MRS was done, based on the lessons learned from the RIMRES system. Firstly, the mission concept foresees landing a mission within a lunar polar crater and direct deployment of the systems at the crater bottom [11]. The selected crater of the reference mission provides areas with high illumination for solar power generation and permanently shaded regions as candidate regions for in-situ evidence of volatile materials. Secondly, the establishment of a logistics chain promises to reduce the need of multiple paths for a sample taking rover and hence the potential to reduce rover traverse distance requirements [Klein et al., 2014]. Finally, the task of sampling is shifted from the scout to the exploration rover, while the scout's role is altered to that of a shuttle. Hence, it fetches the samples from the exploration rover and transports them to the return stage at the lander. Furthermore, the shuttle has the task of transporting energy packs between exploration rover and charging locations, hence implementing a logistics chain in the exploration system. To match the new

(a) *Exploration rover SherpaTT* **(b)** *Shuttle rover Coyote III* **(c)** *Modular manipulation arm SIMA* **(d)** *BaseCamp with three PLIs attached*

Figure 3.6: *Subsystems of the TransTerrA MRS*

requirements of a shuttle robot (speed and mechanical simplicity), the walking and climbing robot CREX is exchanged with the hybrid legged-wheel robot Coyote III [Sonsalla et al., 2015].

3.5.1 Subsystems

The TransTerrA MRS consists of the following subsystems [11]:

- The wheeled-leg exploration rover SherpaTT, Figure 3.6a
- The legged-wheel shuttle robot Coyote III, Figure 3.6b
- The modular five DoF Symmetrical Interface Manipulator (SIMA), Figure 3.6c
- Several cubic PLIs with a common EMI, Figure 3.6d
- A BaseCamp as special case of a PLI with five passive EMIs, Figure 3.6d

The exploration rover SherpaTT is the successor system of the rover Sherpa from the RIMRES MRS [6]. Details of the design of SherpaTT and the heritage from Sherpa are described in Chapter 4 of this dissertation. In the context of the TransTerrA MRS the rover has several tasks, including deployment of BaseCamps, assembly of surface deployable payloads, soil sampling with a modular sampling device and transfer of filled sample containers to the shuttle system. The manipulation arm [15], [Manz et al., 2012] is basically the identical hardware as on the predecessor Sherpa, apart from the first joint being exchanged and the active EMI that serves as an end-effector being updated to the second generation [26].

Coyote III is a platform with four actively driven legged-wheels. A passive DoF allows a rotation of the rear wheel pair around the forward axis, ensuring ground contact of all four wheels in most terrains. The rover is equipped with two EMIs in order to be able to transport payload-items or to make use of the modular manipulator SIMA. The design of rover and manipulation arm are described in [Sonsalla et al., 2015].

With SIMA a symmetrical manipulation arm is introduced in the TransTerrA system. The five DoF arm features an active EMI at either end. The arm itself has no power source, it needs a mobile unit, a BaseCamp or a battery PLI to be fully operational. Within the TransTerrA MRS, the arm is mostly used on Coyote III for payload deployment. Equipped with an additional battery it could act as a snake-like robot for alternative locomotion capabilities in the MRS.

Several payload-items are implemented for the TransTerrA system. The functionalities of the RIMRES PLIs are re-used, additionally, a sampling module [26] and a Differential GPS (DGPS) module for ground truth data are implemented. The BaseCamp as a special type of PLI is integrated and used as communication beacon in the TransTerrA MRS. All available PLIs are described in more detail in [27].

3.5.2 Mission Scenario

The conceived reference mission contains elements for technology demonstration, e.g. installation of a robotic logistics chain on the lunar surface and elements to meet scientific interests, e.g. soil sampling from Permanently Shaded Regions (PSRs) in a lunar polar crater. A lunar sample return mission was chosen [23], following the heritage of LUNARES and RIMRES. However, a mission e.g. to Mars instead of Moon would impose no changes on the MRS in its current state as earth demonstrator. Environmental conditions are not in the focus of the electromechanical design of the systems. A detailed definition of a reference mission including reasoning for the chosen sites, estimates for driving distances and height profiles as well as line of sight for communication is provided in [11].

3.5.3 Experimental In-Field Evaluation

The approach of a logistics chain for sample return has been evaluated in a field deployment in a Mars analogue terrain in Utah, USA [9]. Since subsystem locomotion, cooperative navigation and mapping, payload handling and the general establishment of a logistics chain are the main research interests for the TransTerrA MRS, the choice of Mars analogue terrain does not impede the findings for the system when compared to a lunar analogue terrain. Environmental issues such as radiation, vacuum and temperatures are excluded in the current development state.

During the field test campaign, several aspects of the cooperative mission sequences for a sample return mission and a logistics chain were experimentally evaluated. Additionally, remote operations with a mission control located in Bremen, Germany were conducted successfully via satellite link under considerable communication delays of up to 20 s [22]. Apart from the MRS mission sequence tests, subsystem tests were conducted with Coyote III and SherpaTT, with focus on the locomotive capabilities [9]. SherpaTT demonstrated slope climbing in inclinations of up to 28° with loose soil covered slopes, see also Chapter 6. Coyote III climbed slopes of up to 42° covered in duricrust and up to 32° inclines covered with bed-rock. Descriptions of test area, conducted demonstration mission, communication link and results of the MRS experiments as well as an overview of single system tests are provided in [9]. The in-field experiments with SherpaTT are discussed in [1] and Chapter 6 of this dissertation.

In the evaluated multi-robot mission sequence, a part of the reference mission described in [11] was conducted: Figure 3.7a shows the testing area with superimposed trajectories and waypoints for both mobile subsystems. Both robots start at the (virtual) landing spot (C0/S0); the exploration rover SherpaTT is sent directly to a location for soil sampling (S0→S1), while the shuttle rover takes another traverse (C0→C1→C2) to meet the rover at the rendezvous point (C2/S1). All waypoints are generated by a human operator in the Ground Control Station (GCS) in Bremen. To gain an overview of the surroundings, maps are requested by the operator and displayed in the GCS. Figure 3.7b shows a multi-level surface map as generated by SherpaTT. At the rendezvous point, SherpaTT deploys a sample container onto Coyote III for sample return to the lander, Figure 3.7c. After the PLI has been received by Coyote III, it heads back to the lander (C2→C3).

The conducted mission demonstrated cooperative mapping and rendezvous, handover of sample containers as well as the interaction with a GCS connected via a low-bandwith communication link. In single system tests, mapping and waypoint-navigation of both individual mobile systems were evaluated prior to the cooperative mapping during the demonstration mission.

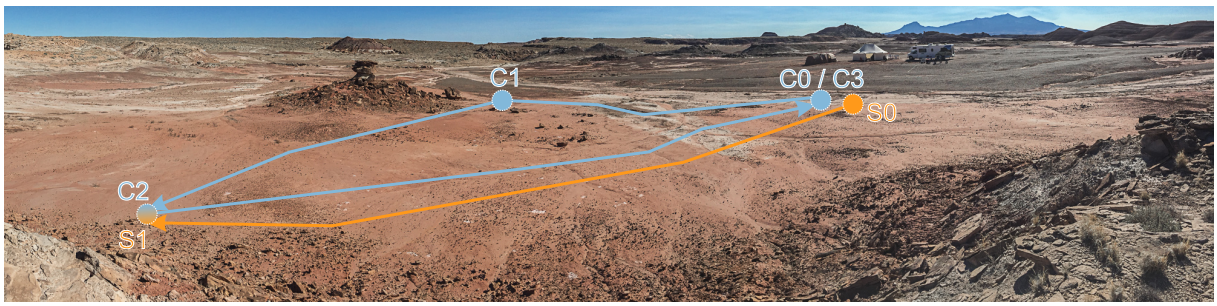

(a) *Conducted mission in field trials with waypoints for SherpaTT (orange) and Coyote III (blue)*

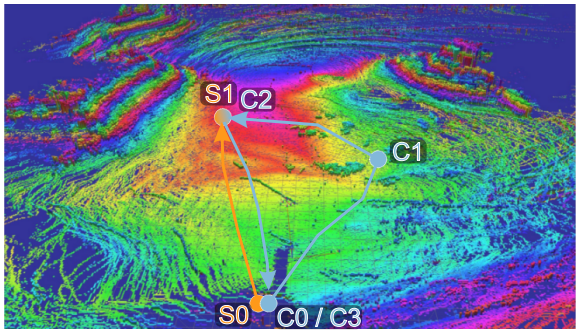

(b) *Multi-level surface map from SherpaTT laser scans. Color cycle repeats each 1 m height.*

(c) *Sample container hand-over at rendezvous S1/C2*

Figure 3.7: *Field testing of TransTerrA MRS in the desert of Utah, USA*

Furthermore, soil sampling with SherpaTT using a sampling PLI was conducted, as well as remote manipulator arm control with a human wearing an exoskeleton in the GCS in Bremen. For improved manipulator remote control, force feedback via the satellite communication link was included in the control loop [22].

3.5.4 Multi-Robot System TransTerrA: Conclusion / Lessons learned

The TransTerrA system builds on the experiences from both previously built MRSs described in the above sections. A slightly different mission approach was chosen for decreased mission risk and increased potential for science return. The system was experimentally tested in a four week field deployment with the robotic systems and local control station being day and night in the harsh environmental conditions of a desert in Utah, USA. Following experiences are made from laboratory experiments and field deployment:

- Individual tests with the EMI further evaluated the chosen design and the revisions conducted for the second generation [13]
- Two dimensional optical markers (so-called ArUco markers[(f)]) proved to be beneficial for pose estimation during the visual servoing process
- A sampling device was integrated into a standard PLI container. The rover is able to use such a modular sample device to take soil samples using its manipulation arm [26].
- BaseCamp transport and deployment are demonstrated in natural terrain [27].
- A high degree of re-usability of software on systems as different in size and morphology as SherpaTT and Coyote III showed to be beneficial for integration and debugging.

[(f)] https://docs.opencv.org/3.1.0/d5/dae/tutorial_aruco_detection.html

- Key elements of the multi-robot logistics chain were demonstrated successfully in laboratory environment and in natural terrain [9]. These include payload exchange between mobile units, payload drop-off from Coyote III using its modular manipulation arm, soil sampling, cooperative mapping and navigation of heterogeneous mobile systems, and remote manipulator control using an exo-skeleton.
- Integration of a satellite link between mission control center in Bremen, Germany and robot systems in Utah, USA was successfully conducted [22].

3.6 Requirements Derivation for Rover Design

The MRS scenarios described in this chapter allow to derive various requirements and design drivers for the exploration rover subsystem. The list below recapitulates the requirements with effect on the electromechanical design of the rover. The requirements marked with a star* are added due to the changes for the TransTerrA system commented on in Section 3.3.

Transport of PLIs For transport of PLIs, the rover needs to be equipped with at least one EMI.

Handling of PLIs For handling of PLIs, for example to construct payloads or to equip another subsystem with payload containers, a manipulation arm is required. The arm needs a compatible EMI to grasp PLIs. The workspace of the arm needs to be designed such that payloads can be deployed on the surface around the rover.

Exploit PLI functionality Connected subsystems shall be usable by the rover, for example to add new functionalities in subsequent missions or to replace broken components with new modular containers. Hence, a module management, including for instance a modular power bus and a modular communication bus is required in the system.

Transport of legged scout The rover shall be able to pickup, transport and deploy a scout robot. Appropriate ground clearance has to be kept. The legged scout possibly can support deployment and pickup using its own active DoF.

Transport of BaseCamp* The rover shall be able to pickup, transport and deploy a BaseCamp. A BaseCamp is immobile, placement needs to be done by the rover.

Taking soil samples* Handling of payloads and exploitation of PLI functionality is combined in this requirement: A sampling module needs to be attached to the arm, powered and commanded through the interface, and be brought into contact with the soil, in order to collect a sample.

Slope Climbing The scenarios LUNARES and RIMRES assume a deployment of a scout after climbing the outside of the Shakelton crater at the lunar south pole. For the TransTerrA scenario, a landing inside the Amundsen crater with ascend/descent of a central peak and ascent into the inner crater wall is assumed. The online mapping tool [LROC-Team, 2018] allows to extract lunar terrain data generated by the Lunar Reconnaissance Orbiter (LRO) mission. Figure 3.8a shows exemplary paths for a LUNARES/RIMRES type of mission and a TransTerrA type of mission, additionally the extracted data and the corresponding slope angles for the two craters are provided. From the data, slopes of 20°-25° need to be negotiated by the rover in the Shakelton scenario. In the Amundsen scenario slopes are seldom exceeding 15°, a maximum of 20° is present in the nominal scenario.

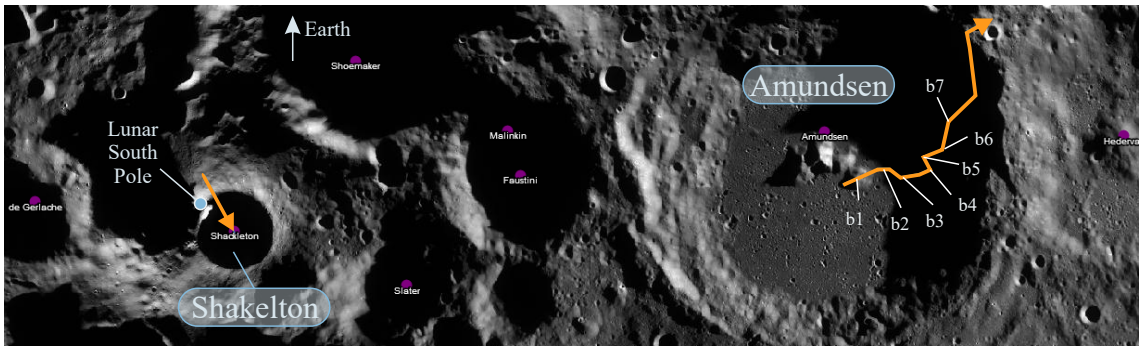

(a) *Chosen paths (orange arrows) in craters for profile height extraction of lunar polar craters Shakelton and Amundsen. Points of interest b1-b7 are described in [9].*

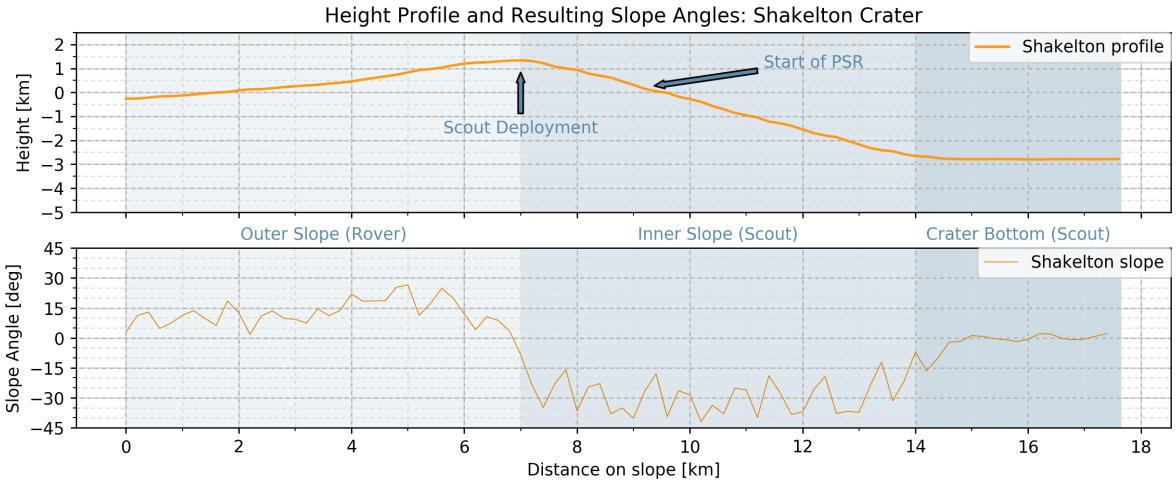

(b) *Profile and slope angles of linear path into Shakelton crater.*

(c) *Profile and slope angles of rover path out of Amundsen crater onto plateau.*

Figure 3.8: *Reference areas for MRS mission: Shakelton and Amundsen lunar polar craters.*
Data is based on [LROC-Team, 2018] from LRO-mission. Note that the scaling of the x-axes is different due to the different crater diameters. The same holds for the scaling of the crater height on the y-axes.

3.7 Summary and Conclusion

This chapter presents a general mission scenario for heterogeneous modular multi-robot systems. In order to cover the modular approach, an electromechanical interface is introduced, allowing functional extensions of existing systems, assembly of scientific instruments or infrastructure elements as well as "drop-in replacement" of building blocks. Modular payload-items are introduced as such building blocks, with battery packs, a sampling tool and sensor units being exemplarily implemented in hardware.

Three multi-robot systems are presented in this chapter. In the proposed multi-robot approach, heterogeneous robots with specialized locomotion capabilities for different terrains are constituting one heterogeneous multi-robot system. A wheeled rover and a legged scout [3], a wheeled-leg rover and a legged scout [2], or a wheeled-leg rover and a legged-wheel shuttle [11] are combined into an exploration system.

To cope with possible failures in a prolonged mission, modular system aspects are incorporated in the design. All subsystems of the proposed MRSs make use of a common electromechanical interface to connect to each other and to construct scientific devices and infrastructure elements from modular building blocks [13]. Surface deployable payloads can take long-term measurements at designated sites, allowing to allocate other tasks to the mobile systems. Examples for long-term measurements of surface deployed payloads include (geo-)thermal activity monitoring, atmospheric measurements, seismic experiments or subsurface sampling with energy-efficient but slow devices, such as the PLUTO Mole system [19]. Radio beacons deployed on the surface and on mobile systems can be used for communications as well as for relative positioning, hence constructing rudimentary infrastructure elements [19], [31].

According to the definitions provided in Subsection 2.1.1, the classification of the three MRS developed in the scope of this thesis can be defined as *intentionally cooperative systems*. Since all described MRSs in this thesis are explicitly designed for periods of independent subsystem operations, all systems are falling into the definition of *weakly cooperative systems*. Furthermore, elements of *modular (self-) reconfigurable systems* are present, particularly with the introduction of a general electromechanical interface in the RIMRES and TransTerrA MRSs.

Most components of the aspired mission scenario illustrated in Figure 3.1 have been developed and physically integrated with the presented systems. This includes a modular manipulation arm, the coupling of two mobile systems via a common electromechanical interface and usage of payload containers for adding new functionalities to mobile systems.

Table 3.1 shows the possible physical combinations of the integrated subsystems in RIMRES when using the EMI. The check mark for the rover-rover combination is set in parentheses since only one rover system has been integrated; generally, a connection using the manipulation arm of one rover and a payload-bay of a second rover is possible. A direct connection of two scout robots is not possible, since a scout features only one passive interface in this scenario.

Similarly, possible combinations of subsystems in the TransTerrA context are listed in Table 3.2. The check mark for the combination of BaseCamps is set in parentheses: Stacking of BaseCamps is accounted for in the design phase, however, since only one entity is physically integrated, an active EMI on the bottom of this module is excluded from integration.

Using a walking and climbing robot as scout for inner crater exploration generally proved to be feasible: Inclines similar to those expected in the inner crater walls have been covered with

Table 3.1: *Possible combinations of subsystems in RIMRES*

	Rover	Scout	PLI
Rover	(✓)	✓	✓
Scout	✓	×	✓
PLI	✓	✓	✓

Table 3.2: *Possible combinations of subsystems in TransTerrA*

	Rover	Shuttle	PLI	SIMA	BaseCamp
Rover	(✓)	✓	✓	✓	✓
Shuttle	✓	×	✓	✓	×
PLI	✓	✓	✓	✓	✓
SIMA	✓	✓	✓	×	✓
BaseCamp	✓	×	✓	✓	(✓)

the climbing scouts Scorpion [10] and SpaceClimber [28], [Bartsch, 2013]. In these mission scenarios the Shakelton crater at the lunar south pole is the designated destination. Figure 3.8b shows the height profile of the crater when approaching from a potential landing site. It can be seen that a traverse of ≈ 7.5 km in a terraced slope with recurring inclines of 30°-45° is required for the climbing scout robot to reach the crater bottom. For reaching the edge of Shakelton's PSR within the crater slope, still a distance of roughly 2.5 km needs to be travelled by the climbing scout robot.

During field-testing with the TransTerrA system, the legged-wheel shuttle system Coyote III demonstrated ample terrain trafficability [9]. With only four actuators Coyote III has the potential to be at least energetically favorable over a multi-DoF walking machine. The possibility of embedding the actuators in the central body instead of having extended limbs with "free" actuators would furthermore facilitate the thermal management in the PSR with temperatures being close to absolute zero. Therefore, an improvement of the RIMRES and LUNARES scenarios could be the use of a legged-wheel robot for descent into a crater, possibly using a tether for improved stability and as umbilical connecting the anchoring rover (placed in a sunlit area) electrically with the descending robot. This was shown in preliminary experiments documented in [9].

Another scenario advancement is shown with the TransTerrA reference scenario, where the complete MRS is landed directly within a crater: The PSR can be accessed by the exploration rover with potentially lower risk compared to the crater descent. Additionally, the slopes shown in the example profile of the chosen Amundsen crater are mostly around and below 15°. Partially steeper slopes still not exceeding 30° are present in the traverse beyond the nominal mission, Figure 3.8c. The system requirements introduced by the slope inclines might be relaxed in both scenarios with careful path planning e.g. by avoiding small impact craters and planning serpentine paths in steep terrain.

3.8 Contributions of the Corresponding Publications

The publications associated to this chapter describe the design path of a heterogenous modular multi-robot system. Three system iterations are designed and evaluated, each iteration building on the experiences of the prior multi-robot system. Furthermore, the design of an electromechanical interface for coupling of the individual rover systems is presented in the publications contributing to this chapter. Altogether, the results from these publications lay the foundations for the rover system design discussed in the subsequent chapters of this thesis.

The journal publication [3] describes the LUNARES demonstrator system. It lays out the mission sequence and deals with the overall lessons learned from the implementation of the het-

erogeneous multi-robot system. Major topics covered in the publication are locomotion with a legged scout in crater environments and docking procedures between subsystems of the MRS.

These experiences are further detailed in [10], where performance aspects of several subsequences are experimentally evaluated. This includes experiments with the legged scout robot Scorpion in the artificial crater environment. Main focus is on determining favorable locomotion parameter sets for power consumption and stability optimization.

In the workshop publication [8], the aspects of the LUNARES system are summarized and the experiences gained are transferred into a new system design with tightly coupled systems. This publication furthermore proposes the SpaceClimber system as antetype for the scout CREX.

For the aspired tight electromechanical coupling of heterogeneous robotic systems, a suitable physical interface is needed. The developments concerning this electromechanical interface for a heterogeneous modular multi-robot system are recapitulated in [12]. This publication provides an overview of both, mechanical as well as electrical aspects of the developed first generation EMI. Experimental evaluation in terms of mechanical loads, docking with dust contaminated interfaces as well as communication quality with contaminated interface connections is conducted and documented in this publication.

With [13] an advancement of the modular interface is presented. In this publication, the second generation EMI is described, changes and differences with respect to the first generation are highlighted. Experimentation with the new EMI design is focussed on docking under heavy loads and durability of the latch mechanism with dust contaminations.

The EMI is part of the two MRSs RIMRES and TransTerrA. RIMRES is described in detail in the journal publication [2]. This includes the mechatronic design of the mobile subsystems (Sherpa, CREX) as well as immobile subsystems (PLIs and EMI). Furthermore, durability experiments with the EMI and experimental evaluation of docking between the two mobile systems as well as stacking of payload elements are covered in the publication.

The TransTerrA system is initially described in [11]. This publication contains details about the mission aspect of establishing a robotic logistics chain within a lunar polar crater. A reference mission with technical and scientific aspects is defined in this publication, including the presentation of a landing spot selection as well as mission and communication architecture.

In [9] experimental evaluation of elements of the logistics chain in a field trial campaign is described. An overview of the field campaign and the test environment is provided along with the communication architecture from the experiment area in Utah, USA via satellite to the GCS in Bremen, Germany. Lessons learned from the field testing in general as well as the subsystem locomotion tests and the mission sequence experiments are provided in this publication.

4 Electromechanical Rover Design

This chapter details the electromechanical design of a rover with an active suspension system. Focus is on the actual suspension system design, however, the influences of the rover being part of a multi-robot system are addressed as well. Hence central electronics, manipulation arm design and integration of the modular electromechanical interface are part of this chapter. Two different rover systems, Sherpa and SherpaTT, are presented; Sherpa makes use of the first suspension design and is part of the RIMRES system. With the lessons learned from the RIMRES system, new requirements for the TransTerrA multi-robot system arise, and a new suspension system design is realized for SherpaTT to meet the new requirements.

The chapter is structured as follows: Section 4.1 provides general design decisions originating from the requirements provided in the previous chapter. The initial suspension design is presented in Section 4.2. This section includes an overview on the manipulator design process as well as lessons learned from the first design. Section 4.3 picks up the lessons learned and provides the description of the second rover design, including updates on the central electronics.

The chapter is summarized in Section 4.4. The contributions of the supporting publications are provided in Section 4.5.

The following publications from Appendix C – Accumulated Publications contribute to the contents of this chapter:

[1] **Design and Field Testing of a Rover with an Actively Articulated Suspension System in a Mars Analogue Terrain**; *F. Cordes, F. Kirchner, A. Babu*; Journal of Field Robotics 2018.

[2] **Reconfigurable Integrated Multirobot Exploration System (RIMRES): Heterogeneous Modular Reconfigurable Robots for Space Exploration**; *T. M. Roehr, F. Cordes, Frank Kirchner*; Journal of Field Robotics, 2014.

[5] **SherpaTT: A Versatile Hybrid Wheeled-Leg Rover**; *F. Cordes, A. Babu*; i-SAIRAS 2016.

[6] **An Active Suspension System for a Planetary Rover**; *F. Cordes, C. Oekermann, A. Babu, D. Kuehn, T. Stark, F. Kirchner*; i-SAIRAS 2014.

[7] **Locomotion Modes for a Hybrid Wheeled-Leg Planetary Rover** ; *F. Cordes, A. Dettmann, F. Kirchner*; RoBio 2011.

4.1 General Rover Design Considerations

The following list provides the reasoning for the fundamental design decisions. These decisions are valid for both rover versions the design of which is described in this chapter.

Manipulation arm A manipulation arm is required on the system to be able to handle the PLIs and fulfill the tasks of the rover within the modular MRS. The arm needs to be equipped with an active EMI for interaction with PLIs. Since specialized end-effectors, e.g. a multi-fingered gripper, could easily be implemented as payload-devices, no other end-effector is required for the arm design.
The arm shall be mounted centrally on the rover in order to be able to equally reach the ground around the entire rover and hence reduce manoeuvering required for surface deployment of PLIs and payload exchange with other subsystems.

Payload bays oriented around central manipulator Four payload bays shall be oriented symmetrically around the manipulation arm, such that the arm can freely rotate with two PLIs stored in either payload bay, allowing a total of at least eight PLIs transported by the rover. Implementing the payload bays on top of the central body facilitates usage of solar modules and extraction of stored payloads by the manipulation arm.

Powerbus All possible power sources shall be usable for the rover. Hence, a power bus connecting all EMIs is required. With the power bus, usage of external batteries or solar power modules connected to a payload bay becomes available.

Modular communication structure To be able to communicate with all connected payloads and subsystems, an appropriate communication bus shall be implemented.

Body height change Active influencing of the body height, and hence the body-ground clearance, is desired. Connecting mobile and immobile subsystems below the rover's main body (see next items) reduces ground clearance. Without other subsystems being connected, an unnecessary high ground clearance results in an unfavorable high CoG, leading to decreased stability margins in sloping terrain.

Active, down-facing EMI in body An active, down-facing EMI shall be mounted centrally at the ground plate of the rover's main body: It can be used for connecting to as well as transport and deployment of a multitude of subsystems, as exemplary demonstrated with a legged scout in the RIMRES scenario and BaseCamps in the TransTerrA scenario.

Changing mass The role of the rover in the scenarios described in Chapter 3 requires it to cope with significant mass changes during the mission. Prior to design following masses are estimated: $m_{PLI} \leq 5\,\text{kg}$ for one payload-item and $m_{scout} \approx 25\,\text{kg}$. Consequently mass changes of up to $\Delta m = 8 \cdot m_{PLI} + m_{scout} \approx 65\,\text{kg}$ have to be supported by the suspension system. A total rover mass of 150 kg is estimated during the design phase. Hence, the additional payloads can add up to 43% of the rover mass during mission runtime. These mass changes are not allowed to impede the locomotive capabilities of the system.

Manipulator locomotion support A manipulator being able to reach the ground around the rover might be used as additional limb for locomotion support [Schenker et al., 2003]. For example, (partial) unloading of wheels can support locomotion in soft soils. Hence, the arm developed shall be able to support locomotion.

Active suspension Above considerations call for an active suspension system: Passive elements (i.e. springs) might be problematic with the estimated mass changes during mission runtime. Furthermore, the position of the CoG changes during the mission, compli-

cating the usage of a passively suspended body. On the other hand, active body height control becomes possible with active suspension. Additionally, an active suspension system can be considered to facilitate lander egress and locomotion capabilities in difficult terrain, which is required for the aspired mission setting in lunar crater environments.

Powerless posture keeping The actuation of the suspension system shall be designed such that a posture of the system can be kept without expending power. This calls for self-locking gear-boxes or breaks in the actuators.

Four-wheeled system Four wheels are considered as baseline design: With an active suspension, more wheels do not nessecarily increase system performance. For lifting one wheel off the ground the remaining three wheels provide the possibility of static stability. Additionally, the manipulation arm can be used as fifth limb if required.

4.2 Initial Suspension System Design: Sherpa

This section describes the initial rover developments under the requirements imposed from the RIMRES MRS. An overview on the resulting rover Sherpa is provided before the suspension system design is discussed. The manipulation arm design is highlighted and modular aspects resulting from the reconfigurable modular MRS design are described. Various aspects of the rover design are published in [2], [6], [7], [14], [15], [21], and [23].

4.2.1 Rover System Overview

The fully integrated rover system Sherpa is depicted in Figure 4.1. The system has a total mass of about 160 kg, each leg as well as the manipulation arm weights about 25 kg, [21]. It is powered by a 44.4 V internal battery with 8 Ah capacity. Main sensors for autonomous locomotion are a stereo camera and a tiltable laser range finder mounted at the front face of the main body. Table A.4 provides the key values of the system, see also [2].

The developed manipulation arm is strong enough to support the rover when lifting two adjacent wheels off the ground, Figure 4.1a. The active suspension system can be used to lower the body to the ground, even a negative ground clearance is possible, resulting in all four LEPs lifted off the ground and the rover's body being on the surface. Figure 4.1b shows another benefit of negative ground clearance: The wheels can be lifted onto high obstacles [6]. The obstacle in the figure is around 600 mm high. Due to the sag in the flexible wheels this is about

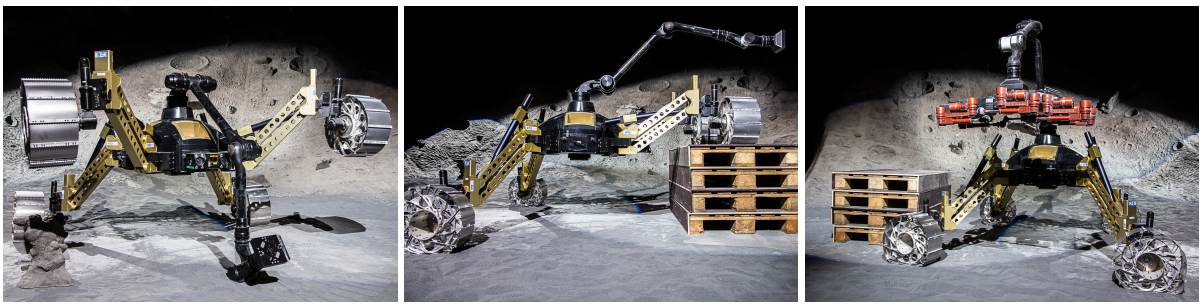

(a) *Using the manipulation arm for locomotion support*

(b) *Stepping onto obstacles*

(c) *Scout deployment from lander platform*

Figure 4.1: *Sherpa rover*

the body-ground clearance of the system. The wheels can be lifted above the ground clearance height and be placed on the obstacle.

Sherpa features six EMIs in total: four payload bays each equipped with a passive EMI are mounted around the central manipulation tower, the manipulation arm itself makes use of an active EMI, and a second active EMI is mounted below the central body.

An additional use-case of the manipulation arm is provided in Figure 4.1c, where the scout is lifted off a lander mock-up. Further usage of this scenario is conceivable: The attached scout robot could in principle serve as a six-fingered hand. Due to the mass of the scout this might not be a nominal scenario, yet it shows reconfiguration possibilities and options to respond to unforeseen events during a mission [2].

4.2.2 Suspension System Design

The baseline for designing the active suspension system for Sherpa is to avoid power consumption for maintaining a certain posture. Hence, self-locking gears or the employment of breaks are a requirement for all DoF (excluding the wheel actuators) of the suspension system. Following the requirements formulation from Section 3.6 and the design considerations from Section 4.1, a body height change needs to be possible, furthermore each wheel shall be steerable and drivable. An adaption to slopes on rigid as well as soft surfaces needs to be possible.

According to the four-wheel design decision stated above, the active suspension system of Sherpa is composed of four identical units, also referred to as legs. Each leg is ending in a drivable and steerable wheel and hence forming a wheeled-leg. Six active DoF are present in each leg, resulting in a total of 24 DoF for the full suspension system. Figure 4.2a provides a sectional view and dimensions of a leg with all joints in their defined zero position. Figure 4.2b shows the CAD design of one leg of the suspension system with the joint's naming convention [6]. The leg is shown with the wheel pushed down, hence the Lift actuator being in its maximum positive position. Each of the four legs is mounted in one corner of the central body, resulting in a quadratic footprint, when all Pan joints are set to zero and all Lift actuators are in the same position.

The Pan joint's rotational axis coincides with the z-axis of a leg's coordinate system as shown in Figure 4.2a. Using the Pan joints allows to change the general footprint from square to wide or long rectangles or an arbitrary tetragon [7]. With the Lift joint, the LEP can be lifted 450 mm up and pushed 450 mm down from the position illustrated in Figure 4.2a. The actuation of the Lift joint is realized with a linear pushing actuator in the parallelogram. For kinematics calculations, the virtual rotation axes Ba1 and Ba2 are introduced [14]. The Lift joint's rotational angle β is measured around Ba1, while Ba2 has a constraint angle $\hat{\beta} = -\beta$ to represent the parallelogram structure.

Due to the parallelogram structure of this joint, the WheelSteering axis is not rotated from the vertical by moving the Lift actuator. By changing the height of the LEP, the distance to the leg's origin is changed as well. Using geometric constraints and the values provided in Figure 4.2a and Table A.5, the movement in x-direction calculates as $\Delta x_{Lift} = \cos\beta_{max} \cdot 520\,\text{mm} = 260\,\text{mm}$ for a stroke from zero to maximum up or down position of the LEP. Such movements on the ground have to be followed by proper wheel alignment and wheel rotational speed adaption in order to avoid unfavorable stress, eventually leading to slip of the wheel. Further details on kinematics of the system Sherpa are published in [7] and [14].

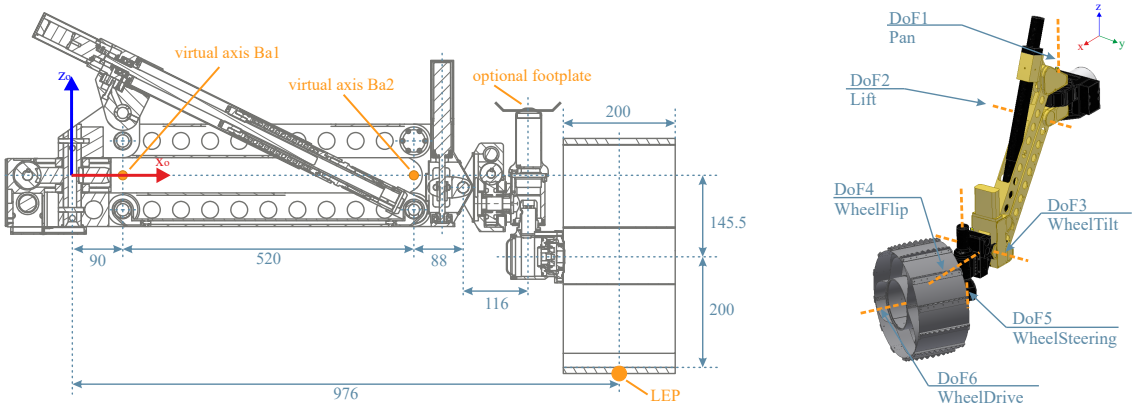

(a) *Leg with all DoF in zero position, dimensions are provided in mm* **(b)** *Leg's DoF and naming*

Figure 4.2: *Sherpa suspension unit: Dimensions and joint names*

The two joints Pan and Lift are the main articulation DoF for the suspension system, the resulting workspace is illustrated in Figure 4.3a: The Pan joint is responsible for the circular movement depicted in the plane, the Lift joint is responsible for the circular up-down movement, resulting in a workspace in the shape of the surface of a sphere [7]. The minimum volume configuration of the rover results in an envelope of $V_{min,Srp} = 2.24\,\mathrm{m}^3$ and is shown in Figure 4.3b, see also [6].

In order to be able to orient the wheel's steering axis to the normal of the slope while the rover is keeping the body's roll and pitch angle[g] at zero, the WheelTilt and WheelFlip joints are introduced. On rigid surfaces, the wheels can keep maximum ground contact using these two DoF, Figure 4.3c. On soft surfaces, e.g. sand, it might be beneficial to keep the steering axes parallel to the gravitational normal, in order to dig step-like trenches into the soil and thus maximize traction and avoid slippage on slopes. Consequently, in soft soil covered slopes the angles of WheelTilt and WheelFlip can be kept zero, when the rover's roll and pitch angles are controlled to be zero. A second usage of the WheelFlip joint is to rotate the WheelSteering/WheelDrive subassembly by 180°. When rotated, an optional footplate on top of the WheelSteering joint comes into ground contact for increased traction. Such a footplate is depicted in Figure 4.2a.

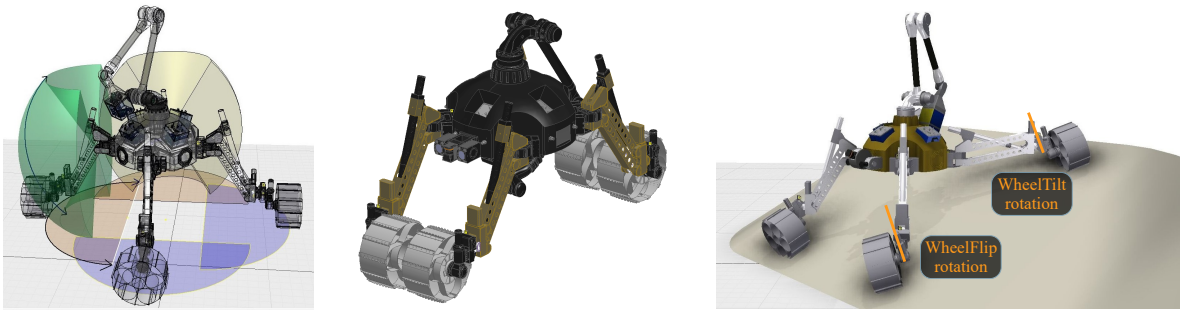

(a) *Illustration of movement range of suspension units* **(b)** *Minimum volume configuration* **(c)** *Usage of WheelTilt and WheelFlip for adaption in slopes*

Figure 4.3: *Sherpa active suspension system*

[g] Roll and pitch are measured against gravity with a body-mounted IMU

WheelSteering and WheelDrive are realized in one housing. The wheel is placed off-axis from the steering rotational axis, which has two main advantages: The configuration (i) reduces stress induced from a wheel rotating around a single point on the ground and (ii) allows the wheel actuator to support steering motions and thus to employ a smaller actuator for orienting the wheel. Both actuators are controlled using a single control board with two driver channels. When the WheelSteering actuator moves due to a new position command, the controller automatically adapts the WheelDrive's rotational speed to match the movement of the wheel around the steering axis. The actuation units are a heritage from the design of the AILA robot [Lemburg et al., 2011] and have been used for the ARTEMIS robot as well [Manz et al., 2014]. The range of motion, angular velocity and strength of the suspension's actuators in terms of torque and force is provided in Table A.5.

Flexible metallic wheels are providing a small-scale passive adaption to ground irregularities. Three development stages are foreseen for the flexible wheel [16]: (i) passive flexible adaption, (ii) integration of sensors to measure deformation, (iii) integration of actuation for active stiffness control. So far, only the passive adaption has been integrated into the wheels.

4.2.3 Manipulation Arm Design

The manipulation arm for the Sherpa rover is designed using an evolutionary optimization to find an optimal morphology for the concurrent requirements for the arm [15]. The arm is predefined to have six DoF as illustrated in Figure 4.4a; the goal of the simulation is to optimize the link lengths between the DoF to minimize the torque requirements for the defined use-cases. In a physical simulation environment a trajectory for the arm is generated to cover the following use-cases:

Locomotion support The arm is set into ground contact with lifting the two adjacent wheels off the ground, Figure 4.4b. The end-effector is folded away and the housing of DoF5 is used as ground contact point. The arm needs to reach over a PLI in one of Sherpa's payload bays.

Pickup PLI A 5 kg PLI is grasped from a payload bay to consider a kinematic solution for a single PLI in a payload bay.

Wrist torques The PLI is moved to generate maximum torques at the three wrist joints.

Two PLI in one bay The payload is stacked onto another payload to consider a kinematic solution for two PLI in one payload bay, Figure 4.4c.

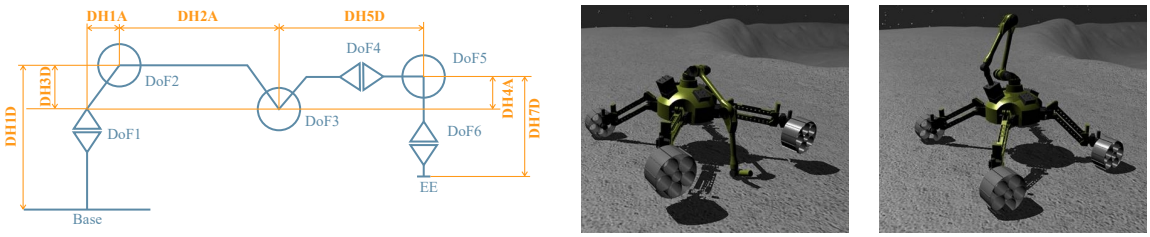

(a) *Fixed number of DoF and evolutionary variable link lengths (Denavit-Hartenberg notation)*

(b) *Way point criterion: Locomotion support*

(c) *Way point criterion: Stacking of PLIs*

Figure 4.4: *Manipulator arm: Evolutionary optimization of morphology*

To evaluate the current fitness, the sum of all average joint torques of the currently evaluated individuum is used. The single joint torques are furthermore an indication for the dimensioning of the actuators for integration of the physical arm. Contact of the arm with any rover structure is penalized to exclude such configurations. The final link lengths resulting from the evolutionary process are provided in Table A.2. Full details on the evolutionary design are covered in [15]. Details on the physical integration using light-weight materials and biologically inspired structural design methods is presented in [Manz et al., 2012], the joint specification with torques, movement range and maximum possible angular velocities of the final arm are provided in Table A.3.

4.2.4 Rover Design for a Heterogeneous Modular Multi-Robot System

Connecting several PLIs results in a linear structure with one PLI having one neighbour when it is the topmost or bottommost element. Two neighbours are present, when it is an element in the center of the structure. In the context of the heterogeneous modular MRS, Sherpa can be regarded as a special type of PLI. With its four passive and two active EMIs, Sherpa is able to build a tree structure and can have more than two neighboring modules. In order to cope with the increased structural complexity, a so-called Central Power Management Board (CPMB) is introduced in the central electronics of the rover. Apart from the control of the power bus it is also responsible for the communication between the single EMIs on Sherpa.

Figure 4.5a shows the CPMB and its connections to the power bus. The CPMB is connected to the internal battery (or alternatively an external power supply) and the modular power bus. The connection to the power bus can be an input or an outlet while the battery port is an input only. Sherpa's internal consumers (e.g. main PC, sensors, etc) can be powered either via the modular power bus or by the internal battery. The legs' actuators are always powered by the internal battery, since the first generation EMI only provides up to 5 A of constant current[(h)].

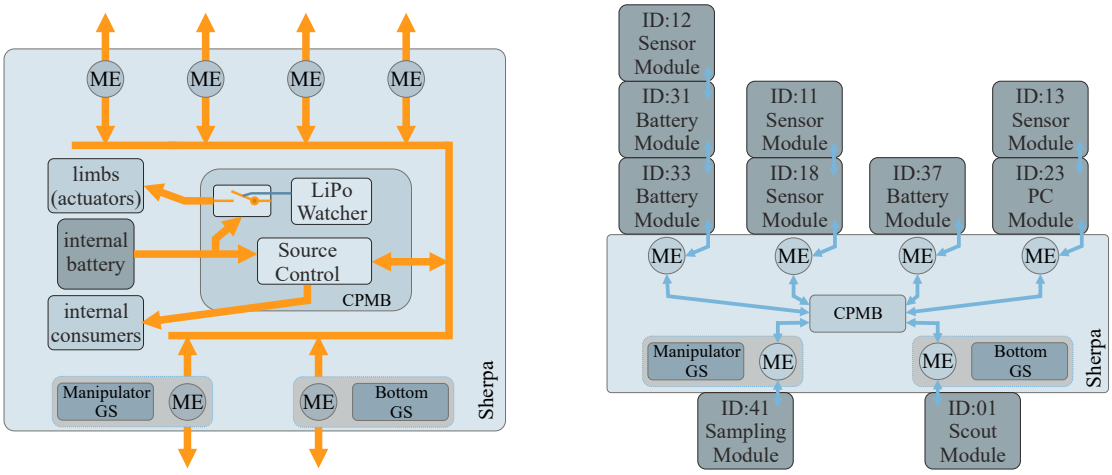

(a) *Model of power bus and source management* **(b)** *Example of modular communication bus*

Figure 4.5: *Central power management board (CPMB) in Sherpa: Management of modularity*

[(h)] The EMI's power bus has been updated to 10 A constant current in the second generation, enough current to drive the actuators of SherpaTT, see Section 3.2 and Section 4.3

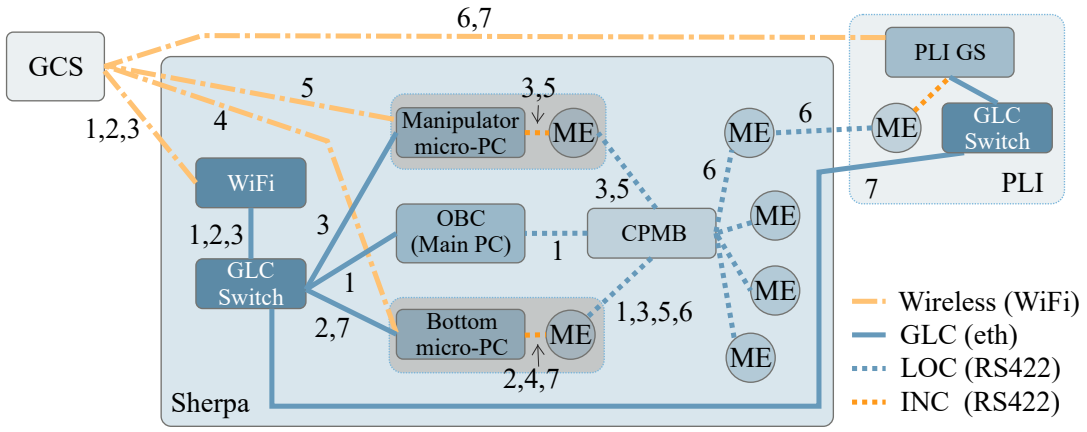

Figure 4.6: *Modular communication bus example: Seven paths for sending command* `open_latch` *from GCS to bottom EMI of Sherpa with one connected PLI to a payload bay.*

Topology reconstruction i.e. detecting connected PLIs in the order of connection is also possible using the CPMB. Generally, each payload-item in a stack retrieves its neighbouring modules via local communication. As each PLI also provides the information of the lower neighbouring module to the upper neighbour and vice versa, gradually a complete topology list is established in every item of the stack. When such a stack is present on one of Sherpa's EMIs, the corresponding module electronic of Sherpa acts similar to any other of the connected PLIs. Consequently, each of the EMIs of Sherpa has a topology of its connected modules. The information is gathered at the CPMB where the full topology for Sherpa is constructed, this is illustrated in Figure 4.5b.

An example for redundancy resulting from the modularity is illustrated in Figure 4.6: Assuming, that a certain point in the mission the bottom EMI of Sherpa needs to be opened, e.g. to release the scout robot, different communication paths are possible to achieve this goal. From the seven different paths illustrated, path (1) would be the nominal case: A high-level command is issued from the Ground Control Station (GCS) and sent to the Sherpa main PC; the connection between GCS and Sherpa is wireless, within the rover wired communication is used. The main PC forwards the low level command `open_latch` to the corresponding bottom module electronic. If for some reason the main PC is not reachable, it is still possible to open the latch of the bottom EMI. The path marked with (2) in the illustration shows the connection from GCS via the bottom EMI's micro-PC board. The low-level command is then sent via internal module communication to the module electronic. At least in case of the earth demonstration, the WiFi capability of the micro-PC board can be exploited as shown with path (4), where Sherpa's global communication bus is completely bypassed. Similarly, the manipulator's micro-PC board can be reached via (3) or (5) from the GCS, its module electronic can then connect via the CPMB to the bottom EMI to issue the `open_latch` command. With a connected PLI the communication options further increase, as shown with (6) and (7).

The example shows that, assuming an operational bottom EMI, the scout robot can be detached in a multitude of error cases of the rover. The illustrated communication reconfigurations have been demonstrated in the RIMRES scenario [2], [21]. Further pursuing these thoughts, even a complete failure of the main PC could possibly be compensated by using the micro-PC boards as replacement.

4.2.5 Sherpa Design Review / Lessons Learned

The lessons learned and resulting considerations for a suspension system redesign are presented in [6]. The main issues are summarized in the following.

A beneficial design aspect of Sherpa's suspension system is the employment of self-locking gears in the suspension unit's joints. The system keeps its current posture when being without power. Impact loads of 90 kg falling from 10 cm on the central body have been successfully tested without damage to the suspension units.

However, a drawback is inherent in this design philosophy: since no current is needed to keep a joint's position, no torque estimation from motor currents is possible. Integration of sophisticated load balancing between the wheels therefore requires employment of force and/or torque senors at joint or leg level which are not present in the Sherpa design. Only model based load balancing as presented in [Grand et al., 2004b] for the Hylos robot is possible with Sherpa.

The off-axis positioning of the wheel from the steering axis allows the wheel to support the WheelSteering actuator. However, a wheel orientation change always results in a movement of the LEP relative to the body, which might be unfavorable in certain situations. As described above, lifting a wheel of the Sherpa rover always results in a change of distance between wheel and central body, due to the circular LEP path when moving the Lift actuator. Hence, to avoid stress and unfavorable loads, the wheel needs to be oriented properly for lifting the wheel off the ground. Consequently, active unloading of the wheel in Sherpa is not possible without imposing stress onto the structure: The wheel cannot be oriented properly, which was the reason for triggering active unloading in the first place.

The joints WheelTilt and WheelSteering are intended for advanced wheel-ground adaption and maximizing the traction. However, the flexible wheels with passive ground adaption showed to be completely sufficient for the intended use-cases. Consequently, DoF3 and DoF4 were used only sparsely in the conducted experiments and could be removed in a re-design to reduce system complexity.

Generally, even though highly actuated, no useable internal mobilities are present in Sherpa. An internal mobility according to the definition in [Iagnemma et al., 2000] would be any movement, that can be conducted without the wheels moving on the terrain. Only the three rotations around the idealized LEP are allowed for the wheel. As such, only a movement of the lift-actuator counteracted by the WheelTilt actuator provides an internal mobility. This internal mobility has a very limited movement range. Platform movements, i.e. central body movements, are possible only when the wheels are moved on the ground.

4.3 SherpaTT – Less Actuators, Improved Workspace

This section deals with the electromechanical design of SherpaTT under the requirements imposed from the TransTerrA MRS and the lessons learned from the Sherpa design. The description of central electronics is constrained to highlighting the differences with respect to Sherpa, the basic functionality is similar in both systems. Special focus is given on the design of the new suspension system, which is the basis for the motion control developments and experimental evaluation in Chapter 5 and Chapter 6, respectively. A detailed design description is provided in [1]; [5] provides additional information on the workspace and actuators, while [6] relates the SherpaTT developments with the Sherpa lessons learned.

4.3.1 Rover System Overview

The fully integrated rover system SherpaTT is depicted in Figure 4.7 in different suspension system configurations. Changing the rear Pan joint angles results in the Quasi-Tripod pose shown in Figure 4.7a. The rear wheels are very close to each other, resulting in a load-distribution similar to a tripod. A compact stow pose with an envelope of $V_{min,SrpTT} = 1.67\,\mathrm{m}^3$ for interplanetary transport is possible as shown in Figure 4.7b, note that the arm is not in its stow configuration in the image. The ground clearance can be changed, Figure 4.7c shows the robot in a high body pose. Adaption to sloping terrain is shown in Figure 4.7d – Figure 4.7f.

The rover has a total mass of 170 kg; each leg as well as the manipulation arm are having a mass of about 26 kg, the mass is similar to that of Sherpa. The rover is powered from two internal 44.4 V batteries with 10 Ah capacity each. Total runtime on batteries is approximately 3.5 hours, depending on velocities and terrain roughness.

For autonomous locomotion, a rotating lidar sensor is mounted on top of the rover. The sensor position rotates with the first arm joint, hence allowing to compensate for the occlusion of the arm. Additionally, a tiltable laser range finder is mounted on the front along with a wide angle camera. Table A.6 lists the main system specifications.

As in the previous design, SherpaTT features six EMIs in total; four passive EMIs are mounted around the central manipulation tower, one active EMI is mounted at the bottom of the central body and one active EMI is used as end-effector for the manipulation arm. The functionalities of the CPMB version present in Sherpa are splitted for SherpaTT: Management of the modular system functionalities is conducted using the newly introduced Central Module Management Board (CMMB) which is the central node for the EMIs' power bus and provides a single power bus line to the CPMB. The new version of the CPMB board is responsible for power source management for the central rover electronics and the limbs, see also Figure 4.12 on Page 50.

(a) *Quasi-Tripod pose*

(b) *Compact stow pose of legs*

(c) *High body pose in CrossStance*

(d) *Body roll-pitch control in sloping natural terrain*

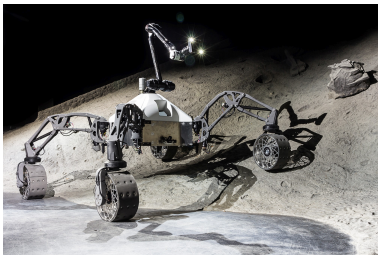

(e) *Body roll-pitch control in artificial crater*

(f) *Approaching a sampling spot in natural terrain*

Figure 4.7: *SherpaTT: Examples for configurations of the active suspension system*

4.3.2 Kinematic Suspension System Design

The new suspension system design follows the same baseline as the initial design: Self-locking gears are employed in order to be able to keep the current posture without power draw from the actuators. Additionally, internal mobilities are required for facilitating the deployment and pickup of passive payloads connected to the bottom EMI in the context of the TransTerrA MRS. In the RIMRES MRS, the legged scout robot's internal mobilities were used for the docking procedure [2]. Furthermore, the identified drawbacks discussed in Subsection 4.2.5 are tackled with the new design [6]. Figure 4.8a shows the new leg's design with all DoF in their respective zero position, Figure 4.8b provides the naming convention of the joints in one leg.

The new leg design features five instead of six DoF; the WheelFlip actuator has been removed from the design, while the WheelTilt actuator is designed to have more influence on the LEP positioning, resulting in a serial chain of two parallelograms connected by a knee link. The former Lift joint and WheelTilt joint from the initial design are now referred to as InnerLeg and OuterLeg joints [1]. The introduction of the knee link enables internal movements: The rover's body can be moved in 6 DoF with all four wheels being stationary on the ground. Both parallelograms in the leg structure have the same baseline of 400 mm reducing the 520 mm of the single parallelogram in the original design. However, when stretched in zero position the total leg length from Pan rotation axis, i.e. the origin of a leg's coordinate system, to the LEP with $L_{0,SrpTT} = 977$ mm is basically the same as $L_{0,Srp} = 976$ mm in the initial design. Three-dimensional placement of an LEP relative to the rover's body is now conducted using the three DoF Pan, InnerLeg and OuterLeg.

A further notable difference is the positioning of the WheelSteering axis over the LEP of the leg. Generally this requires a higher torque for steering the wheel, since the the WheelDrive cannot support the steering manoeuver any more. However, orientation of the wheel and position of the LEP are now decoupled, facilitating locomotion control of the system. A Force-Torque Sensor (FTS) is mounted at the flange of the wheel, Figure 4.8b, enabling precise load balancing between the wheels as well as ground contact loss detection. With active load balancing comes the opportunity of active wheel unloading for steering support and hence a relaxed torque requirement for the steering actuator [1], see Subsection 5.4.

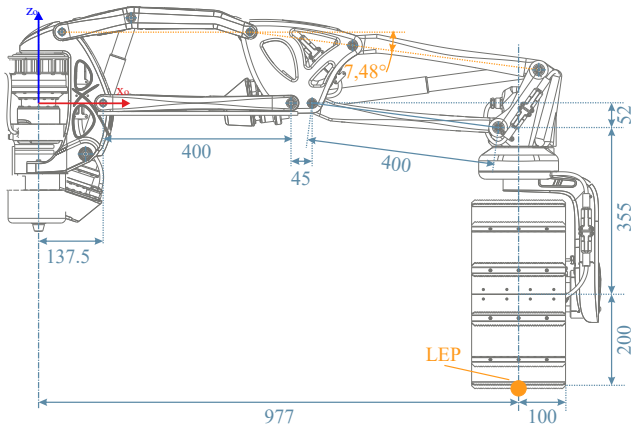

(a) *Leg with all DoF in zero position, dimensions in mm*

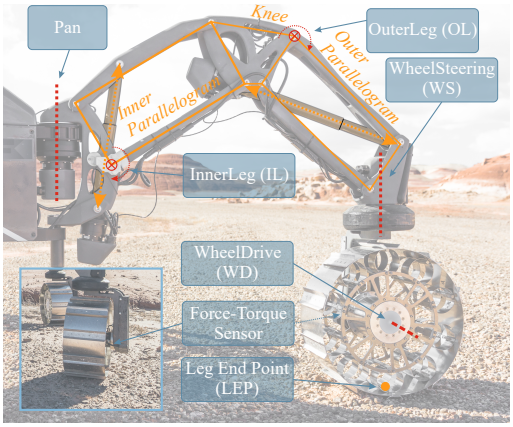

(b) *Leg's DoF and naming convention*

Figure 4.8: *SherpaTT suspension unit: Dimensions and DoF naming*

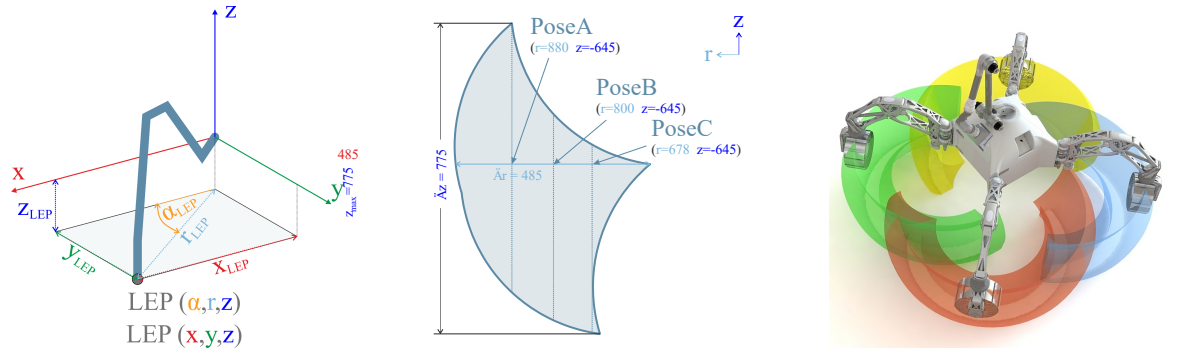

(a) *Cartesian vs cylindrical coordinates for LEP description*

(b) *Workspace of InnerLeg and OuterLeg actuators. Dimensions in mm.*

(c) *Three dimensional workspace. Rover shown in CrossStance with LEPs in PoseA.*

Figure 4.9: *SherpaTT suspension unit: Workspace description*

Figure 4.9a illustrates a suspension leg from the origin of the leg's Coordinate System (COS) to the LEP. Depicted are the LEP's coordinates as measured in cartesian and cylindrical coordinates. Describing the LEP in cylindrical coordinates allows to decouple the Pan joint from the InnerLeg and OuterLeg joints: The former is responsible for the angle α, while the latter two are used for controlling r and z in cylindrical (α, r, z) coordinates. Note that the z-coordinate is identical in both representations.

Figure 4.9b illustrates the two dimensional leg subworkspace spanned by the InnerLeg and OuterLeg actuators. The LEP position denoted as Pose A in combination with a Pan joint with zero angle is defined as the standard pose for SherpaTT [1]. In this pose, a maximum stroke in z-direction (up/down) is possible for the LEP without changing the wheel's distance to the body. Pose B is close to the center of the possible radius movement (cylindrical coordinates) and provides a compromise in possible z-movements. Pose C is limited in the upward movement of the LEP but provides the highest body posture with a linear z-stroke of all LEP [5]. The full three dimensional workspace is spanned by the movement of the Pan joint, resulting in the toroidal volumes illustrated for each leg in Figure 4.9c.

To achieve a constant cartesian velocity for an LEP, varying rotational speeds for the InnerLeg and OuterLeg joints are required; the angular velocity is dependent on the current joint angle. The maximum angular velocity for both actuators is 5 deg/s, as specified in Table A.7. The required angular velocities $\dot{\beta}$ of InnerLeg and $\dot{\gamma}$ of OuterLeg actuator when the LEP is moved with constant vertical velocity are shown in Figure 4.10. Three vertical velocities $\dot{z} = 0.01 m/s$, $\dot{z} = 0.02 m/s$, and $\dot{z} = 0.03 m/s$ are illustrated. A vertical velocity of $\dot{z} = 0.03 m/s$ violates the maximum angular velocity of the InnerLeg actuator at the lower points of the workspace. The maximum constant cartesian velocity for the whole motion range is 0.024 m/s. When the movement range of the LEP is restricted, higher constant cartesian velocities are possible, examples are given in Figure A.1 of the appendix.

Table A.7 provides the movement range, velocities and torque or force specifications of the individual joints of a leg in SherpaTT's suspension system. Dimensioning of the actuators according to expected load-cases is presented in [1]. Generally, the WheelSteering joint is not mechanically limited in its movement range, however, the cabling of the WheelDrive actuator is routed through the structure and limits the movement range. Currently, the software limits are set to ±175° in order to avoid cable damage.

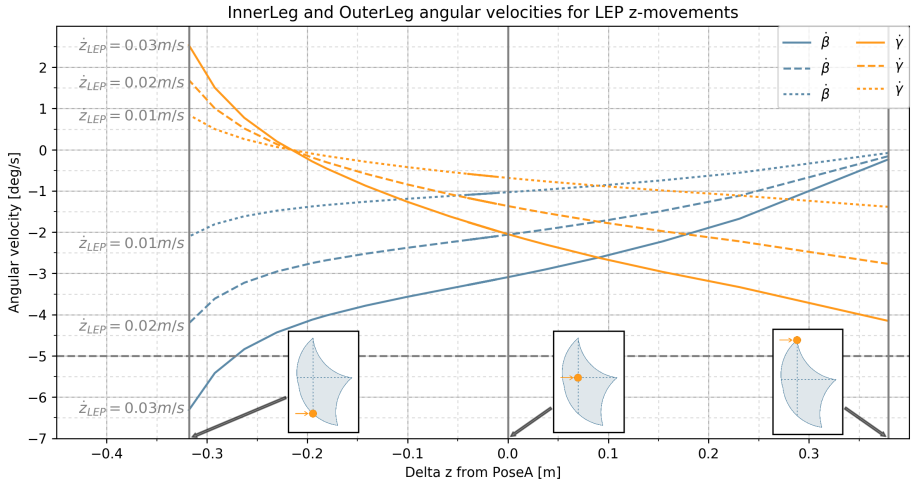

Figure 4.10: *Angular velocities for InnerLeg and OuterLeg with different LEP cartesian velocities. Movement vertically up through Pose A, inset pictures illustrate LEP position.*

In contrast to the various types of actuators employed for the initial active suspension design in Sherpa, a set of modular actuators is used for driving the DoF of the SherpaTT suspension. The actuators employed are based on the developments described in [Bartsch et al., 2016], see also [6].

Different sizes of motor modules using Brushless Directed Current (BLDC) motors are used in combination with a modular gear box in order to implement a wide range of actuator types. For SherpaTT, two different motor modules are combined with four different gear boxes to realize the actuators for a leg. A linear spindle drive is additionally placed on the two actuators for the InnerLeg and OuterLeg joints. All actuator types are controlled by the same custom electronic stack, featuring an FPGA-based controller unit, power electronics and custom communication using the NDLCom protocol [Zenzes et al., 2016].

Figure 4.11 illustrates several footprint configurations possible with the suspension system [1]. All of the displayed footprints allow up/down movements of an LEP without changing the footprint shape. Hence, active ground adaption is possible in a multitude of footprint configurations / support polygon shapes.

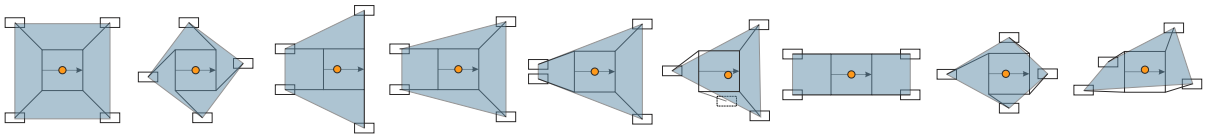

Figure 4.11: *Illustration of footprint possibilities for SherpaTT as seen from top [1]. Orange dot represents approximate position of CoG.*
Left to right: Cross-Stance, P90, Turtle-Front, Y-Shape, Quasi-Tripod, Tripod (one wheel disabled), Long-Stance, Kite-Shape, and an arbitrary/asymmetric footprint.

4.3.3 Manipulator Arm Design

For SherpaTT the manipulation arm of Sherpa described in Subsection 4.2.3 is used. The arm's first joint is updated with an actuation unit as used for SherpaTT's Pan joints. Additionally, the end-effector EMI is updated with the new version [26]. Furthermore, the FPGA-based control software is updated to match the communication definitions for the new motor drivers. Other than that the exact same hardware is used.

4.3.4 Components for Deployment in a Modular Multi-Robot System

The central electronics of SherpaTT are similar in function to those of Sherpa as described in Subsection 4.2.4. The main components of SherpaTT's central electronics are illustrated in Figure 4.12, see also [1]. The same amount of EMIs is present, however, the interfaces are updated to the second generation EMI. Unlike in Sherpa, the passive EMIs do not feature an own electronics board, a centralized management is introduced with the CMMB, which takes over all features connected with the modular system approach from the first CPMB version described above for Sherpa. The newly designed CPMB in SherpaTT is responsible for managing all power sources in the rover. It provides more power inputs to select from: Two internal batteries and one external power supply can be connected in parallel. Batteries can be charged in the system, which is a step further into real applications, where solar panels might be present. Additionally, an input/output interface is provided for the modular power bus which is now provided by the CMMB.

Currently locomotion control as well as autonomy are executed on the on board computer (denoted OBC in the image), which is connected to a custom FPGA/ARM processor board (the so-called *Zynq-Brain*) [1]. The Zynq-Brain is responsible for communication with the limbs of the system via a the custom NDLCom protocol also used for internal and local communication in the modular system part.

All limb power lines are connected in one central node on the CPMB, for clarity this node is illustrated outside the CPMB box in Figure 4.12. The wheels of SherpaTT are backdrivable; the central node allows to use power generated from the wheels in other joints of the suspension or in the manipulation arm, hence reducing power draw from batteries [1]. This is also discussed in the experiment chapter in Section 6.3.

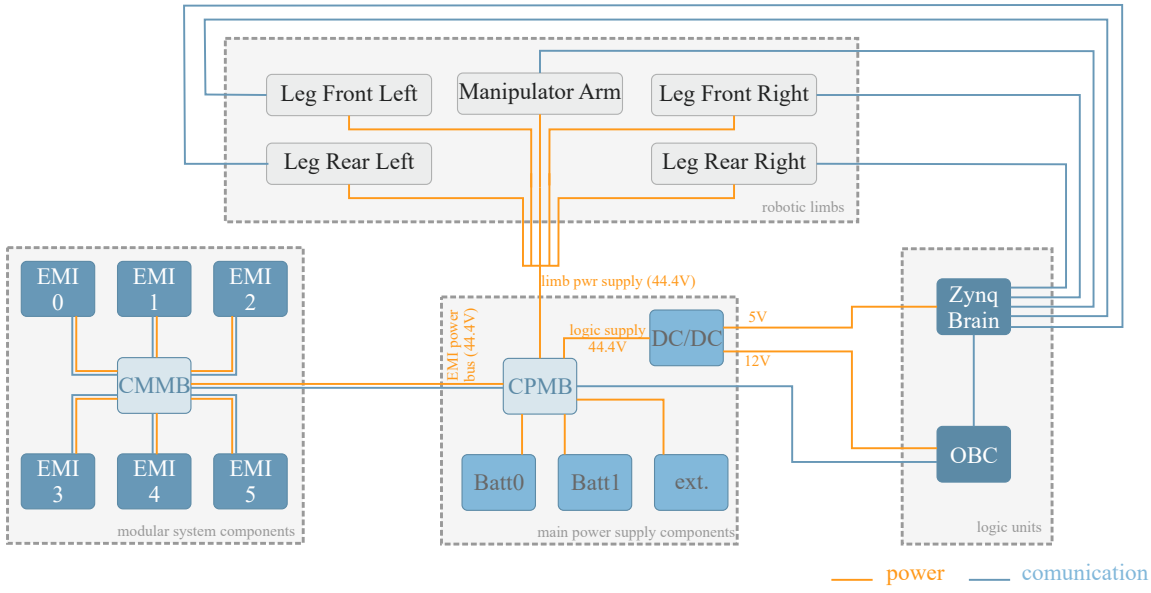

Figure 4.12: *Simplified overview of SherpaTT's updated central electronics components. Sensors and auxiliary electronics are left out for readability.*

4.4 Summary and Conclusion

This chapter presents the electromechanical system design of the two rover versions Sherpa and SherpaTT. General design decisions valid for both systems are presented with the main influences resulting from the respective MRS. Apart from the kinematic design of the suspension systems, the central power management is discussed as this is a central part for the rovers to be a fully functional subsystem of a modular MRS.

A manipulation arm for both rovers is developed using an evolutionary algorithm for morphology optimization. Several use-cases are defined and a trajectory for the arm is built to test the use-cases in a physical simulation for fitness evaluation of the respective individuum. The arm is then manufactured following a biologically inspired manufacturing methodology.

Comparing the main features of both implemented rover systems shows basically the same leg length of the first and second suspension generation, Table 4.1. The mass per leg as well as the total system mass are nearly identical as well. With five DoF per leg, the second generation suspension has one DoF less per leg. Horizontal and vertical LEP movements in Sherpa are coupled, while they are independent in SherpaTT. Note that the vertical and horizontal stroke listed for SherpaTT in the table are those resulting from the currently set software-joint limits as also shown in Figure 4.9b. Exploiting the full mechanical range as provided in Table A.7 results in 860 mm vertical and 629 mm horizontal stroke.

Table 4.1: *Comparison of main features of suspension system generations and rovers.*

System	Leg length zero pose	Mass (leg)	Mass total	DoF (leg)	vert. stroke	horz. stroke	min stow volume	compactness footprint	compactness volume
Sherpa	976 mm	25 kg	160 kg	6	900 mm	260 mm	2.24 m^3	0.40	0.64
SherpaTT	977 mm	26 kg	170 kg	5	775 mm	485 mm	1.67 m^3	0.79	0.72

Due to improved arrangement of the DoF, the minimum stow volume is reduced from 2.24 m^3 to 1.67 m^3. This is also reflected in the values of compactness provided in the table; these values are based on the isoperimetric quotient: The ratio of the area of the footprint to the area of a circle with the same perimeter is built. A circle is the most compact shape in two-dimensional space, therefore, the ratio ranges between 0 and 1 with high compactness being close to 1. Similarly the compactness of the three-dimensional envelope volume is calculated using a sphere as most compact volume. In both cases, the new design achieves higher compactness values.

Apart from the compactness, the new arrangement of the DoF allows to place the LEP in a three-dimensional workspace compared to a two-dimensional spherical surface. This design generates internal mobilities, that can be used to facilitate deployment and pickup of immobile elements in the MRS. Furthermore, the position and orientation of the central body in the support polygon can be changed without moving the wheels over the ground, which is beneficial for CoG relocations in intricate slopes with low traction surface material.

A six DoF FTS is present in each leg of the new suspension system design. Direct ground contact force measurement becomes available with this sensor, which in turn allows improved load balancing between the rover's ground contact points.

To conclude, with basically the same dimensioning (size, weight), superior properties are presented with the second suspension system design. The subsequent chapters focus on the control and evaluation of this new suspension system and the rover SherpaTT.

4.5 Contributions of the Corresponding Publications

Overall, the publications contributing to this chapter provide the design steps from initial to final suspension system design. Electromechanical development with design rationales and redesign are provided over the course of these publications.

The journal publication [2] provides an overview of the finally integrated version of the first suspension design. The role of the rover in the multi robot scenario is described and experimentation concerning manipulation is conducted. The publication summarizes the design of the first suspension system and provides a conclusion for example on the number of DoF present in this design.

The suspension system design of the Sherpa rover is further described in [7]. Joint's naming and workspace are presented along with the joint's limits and performance specifications. A subset of possible postures is presented. Furthermore, the kinematics are analyzed for implementation of a posture-independent motion controller.

The publication [6] picks up on the lessons learned from the initial suspension system design in the Sherpa rover. The implications for the new design are discussed. An early design study of the second generation suspension system is presented in this publication. The expected workspace of the rover's legs and an initial estimate of the stow envelope volume is given with this publication. Furthermore, the publication details the modular actuator design for SherpaTT's suspension system.

With [5] the final suspension system design of SherpaTT is presented for the first time. The first integration stage of SherpaTT with only the central body and the four legs of the suspension system is presented. Dimensions of a leg's workspace are given and coordinate frames for locomotion control are defined in this publication.

In the journal publication [1] a detailed design review of SherpaTT is provided. Dimensioning of actuators is discussed and the central electronics, particularly the power management, are highlighted. Details on coordinate systems, LEP pose description and workspace of a leg are published in this article. Preferred poses in the OuterLeg/InnerLeg subworkspace are discussed and a subset of available footprints is presented.

5 Motion Control System Design

This chapter reviews the motion control system for a hybrid wheeled-leg rover. A reactive adaption control scheme is chosen for the motion control. Consequently, wheel-ground contact models, mapping and modelling of the environment or any planning for future system states is not required for locomotion control. The control system is implemented as a layer between deliberate high-level processes and the low-level hardware layer. With the control system, the complex kinematic suspension is articulated in a "black box"-manner: In effect a passive suspension with controllable properties is mimicked from the point of view of the deliberate software layer.

The general software stack of the rover and particularly the structure of the motion control system is described in Section 5.1 of this chapter. Coordinate systems used to describe the kinematics and control the articulated suspension are highlighted in Section 5.2.

With the DriveMode module described in Section 5.3, an important component of the motion control system is presented. Different DriveModes define how the motion command for the rover platform is transferred into actual propulsion, using all or a subset of available suspension actuators.

The main part of this chapter is the discussion of the active ground adaption process, which is the central part of the motion control system. The general structure and the submodules responsible for coherent locomotion in rough terrain are presented in Section 5.4.

A short detour to the system's low-level control is provided with Section 5.5 to give a comprehensive image of the motion control systems' interface with the hardware. The chapter is summarized in Section 5.6, the contributions of the corresponding publications to the contents of this chapter are stated in Section 5.7.

The following publications from Appendix C – Accumulated Publications contribute to the contents of this chapter:

[1] **Design and Field Testing of a Rover with an Actively Articulated Suspension System in a Mars Analogue Terrain**; *F. Cordes, F. Kirchner, A. Babu*; Journal of Field Robotics 2018.

[4] **Static Force Distribution and Orientation Control for a Rover with an Actively Articulated Suspension System**; *F. Cordes, A. Babu, F. Kirchner*; IROS 2017.

[5] **SherpaTT: A Versatile Hybrid Wheeled-Leg Rover**; *F. Cordes, A. Babu*; i-SAIRAS 2016.

[7] **Locomotion Modes for a Hybrid Wheeled-Leg Planetary Rover** ; *F. Cordes, A. Dettmann, F. Kirchner*; RoBio 2011.

5.1 General Structure of the Motion Control System

This section provides the general layout of the rover's Motion Control System (MCS). The single modules are briefly introduced, more details are provided in the publications [1], [4], and [5] as well as in the subsequent sections. The overall rover control scheme including the autonomy is a hybrid architecture with deliberative and reactive elements. A separation into three software layers as listed in the following is assumed.

High-Level This is the autonomy level of the robot's control system. It includes for example navigation and mapping, path following and other deliberate behaviors. These behaviors are independent of the physical robot and can generally be identical on different robots with different morphology.

Middle-Layer The middle-layer is an abstraction of the physical robot. It provides command inputs for interfacing the high-level processes and calculates according joint movements for coordinated motions. The middle-layer reacts to sensor inputs such as for example deformation sensing (springs, flexible soles, etc), IMU data or FTS values in order to conform to terrain. Furthermore, system stability is maintained at this level, e.g. by monitoring the position of the CoG with respect to the support polygon and using the locomotive system for adaption to avoid tip-over.

Low-Level The low-level is considered to be close to the physical hardware. This includes sensors and local pre-processing of sensor data, for example large scale contact sensor fields calculating the center of pressure. If present, local joint controllers are part of the low-level as well, using for example PID controllers for position or velocity control of an individual joint.

The MCS developed in this thesis is a reactive system. No ground interaction models or terrain maps are required for the active ground adaption. The current state of the robot is sufficient for control, no future actions are planned within the MCS. Reactive controllers have the advantage to be able to run on relatively limited hardware and thus are better suited for deployment on space qualified hardware [Mumm et al., 2004]. Consequently, deliberative behaviors are not part of this thesis. However, experiments concerning mapping and path planning with SherpaTT in natural terrain are highlighted in [9].

Figure 5.1 illustrates the general structure of the MCS. The MCS provides three basic command input classes for controlling the motions of a wheeled-leg rover. Sensor inputs are IMU readings in the central body as well as force measurements at the wheel mounting points. Outputs are the joint commands for the suspension system. The MCS runs at an update frequency of 100 Hz [4].

The modules illustrated as orange boxes in Figure 5.1 are described in more detail in the subsequent sections. The three command inputs classes shown at the top of the image can be used by autonomous behaviors, e.g. a motion command generated by a path follower module. Alternatively the commands can be set directly from a human operator. The input command classes are defined as listed below, see also [1].

Motion Command 3D (MC3D) The MC3D is represented by the vector $\dot{\xi}$. It contains the velocity commands for forward $\dot{x}$, lateral $\dot{y}$ and turn velocity $\dot{\Theta}$. The three components are independent of each other in the implementations presented in this thesis.

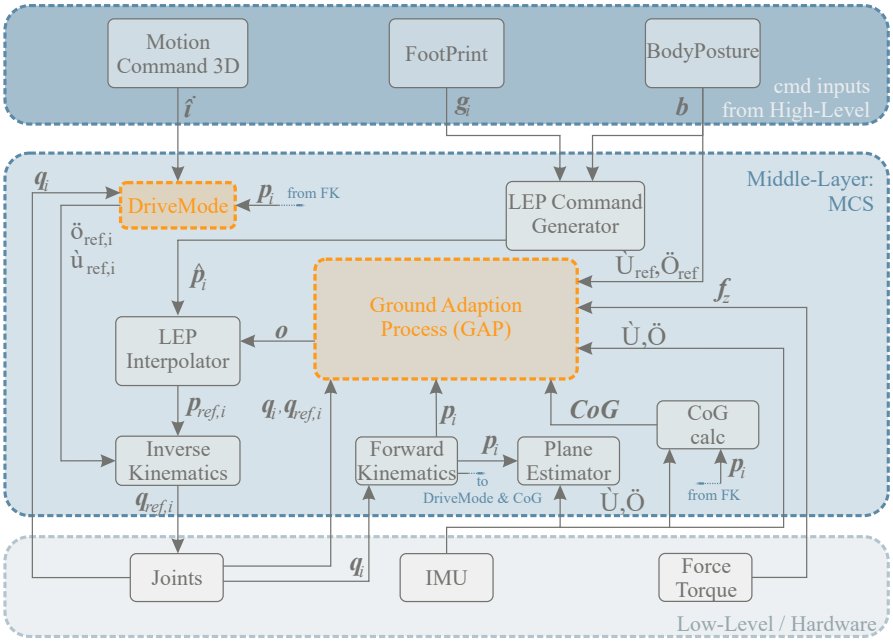

Figure 5.1: *Simplified illustration of the MCS structure*

FootPrint The footprint of the robot is commanded with a three dimensional vector for each leg i: $\boldsymbol{g_i} = (r_i, \alpha_i, z_i)^T$. Varying r_i and α_i results in footprint variations, examples of which are illustrated in Figure 4.11 of the previous chapter. Additionally, the height z can be manipulated, for example to deliberately take a wheel off the ground.

BodyPosture The central body's posture can be commanded using the six-dimensional vector $\boldsymbol{b} = (x_b\ y_b\ z_b\ \Omega\ \Phi\ \Psi)^T$. This command allows to shift the position of the central body within the support polygon by setting the lean values x_b and y_b as well as the body height / ground clearance z_b. Furthermore, roll (Ω), pitch (Φ) and yaw (Ψ) of the body can be set independently of the FootPrint. With $\boldsymbol{b} \equiv \boldsymbol{0}$, the robot is defined to be in its standard pose which is called *Cross-Stance*. All Pan joints are at zero and the LEPs are in Pose A in this pose.

Internally, several modules are used to merge the commands into consistent joint motions and to make use of the sensor feedback for active ground adaption, Figure 5.1. The MC3D command is processed by the *DriveMode* module. It takes the current LEP positions $\boldsymbol{p}_i$ as well as the current joint velocities from $\boldsymbol{q}_i$ as additional inputs. The correct wheel orientations φ_i and velocities ω_i are calculated within this module, see Section 5.3 for more details.

FootPrint and BodyPosture command are merged within the *LEP Command Generator* module to generate unambiguous LEP commands. When a new LEP command is generated, the *LEP Interpolator* module generates a smooth trajectory between current and new LEP position.

The *Inverse Kinematics* module uses the interpolator output to calculate the corresponding joint commands for Pan, InnerLeg and OuterLeg. The complete joint command vector $\boldsymbol{q}_{ref,i}$ for each leg is constructed by combining the inverse kinematics output with the DriveMode output.

A *Plane Estimator* module is implemented in the MCS. This module estimates a ground plane from all wheels with ground contact. In case of three wheels with ground contact, this is a plane fitting through all three wheels. In the nominal case with four wheels on the ground, a

least square approximation of a plane through all four wheels is constructed. The fitted plane is corrected by the body's roll and pitch measurements to generate a representation in a fixed world coordinate frame. The plane estimator can be used to assess the terrain with proprioceptive data and possibly support map generation. The module is part of the experiments presented in Chapter 6. Further details are available in [1].

5.2 Coordinate Systems for Locomotion Control

Several coordinate systems are used to facilitate the calculations and descriptions required for controlling the active suspension system of SherpaTT. Details on the used coordinate frames are published in [1], [5], and in [14] for the initial suspension system. All coordinate systems are right-handed.

The Body Coordinate System (BCS) is used to describe all internal movements of the robot. The Shadow Coordinate System (SCS) is a virtual coordinate system, that remains at the nominal body pose for SherpaTT [5]: When $\boldsymbol{b} \equiv \mathbf{0}$, SCS and BCS are identical. The Leg Coordinate System (LCS) is introduced in Subsection 4.3.2. A Wheel Coordinate System (WCS) is present at each wheel of the rover [1].

Following indices, naming and contact axes (one contact axis is containing two wheels) are defined for the wheels and/or legs and used in the subsequent sections:

- *font left*, FL, index $i = 0$ $\rightarrow$ part of contact axis a_0
- *front right*, FR, index $i = 1$ $\rightarrow$ part of contact axis a_1
- *rear left*, RL, index $i = 2$ $\rightarrow$ part of contact axis a_0
- *rear right*, RR, index $i = 3$ $\rightarrow$ part of contact axis a_1

5.3 The DriveMode Module

The *DriveMode* module is responsible for the actual propulsion of the rover. In [7] different locomotion strategies for a wheeled-leg rover are presented. Each of these strategies can be seen as an individual DriveMode module; simply exchanging this module in the MCS structure results in a different locomotion strategy for the rover. With an appropriate DriveMode selector, this can be done during runtime. More generally, a DriveMode module takes in the MC3D and generates appropriate commands for the suspension system joints to match the commanded platform speed. All joints or a subset of joints might be used to propel the robot.

For the evaluation of the suspension system in this thesis the rover relies on a so-called *OmniDrive* mode. In this mode, WheelSteering and WheelDrive actuators are used for propulsion, while Pan, InnerLeg and OuterLeg joints are used exclusively for active ground adaption. In [7], an analytical kinematics calculation for controlling the wheeled-leg rover Sherpa in an OmniDrive mode is presented. The approach is an extension of the one proposed by [Campion et al., 1996]: variable footprints are considered and the off-axis steering of wheels in Sherpa is accounted for. However, the approach presented in [7] assumes a quasi static state of the suspension for each calculation step. Velocities resulting from leg movements are not taken into account, hence the full potential of the suspension is not exploited.

For SherpaTT the approach was further extended to include the suspension system motions in the calculations for φ_i and ω_i [1]. The MC3D vector is transformed to the wheel coordinate frame to generate $\dot{\boldsymbol{\xi}}_i^{WCS}$. In this frame the velocity $\dot{\boldsymbol{\lambda}}_i$ resulting from the movements of

the Pan, InnerLeg and OuterLeg DoF is added to form the velocity vector $\dot{\boldsymbol{p}}_i^{WCS}$ at the wheel coordinate frame which is the basis for calculation of orientation and rotational speed of each wheel i according to Equation (5.1) and Equation (5.2). This is basically the same calculation approach as presented in [7] for Sherpa but including the current leg motion. Full detail on this methodology is provided in [1].

$$\varphi_i = \arctan2\left(\dot{p}_{i,x}^{WCS}, \dot{p}_{i,y}^{WCS}\right) \qquad \varphi_i\text{: steering angle wheel } i \tag{5.1}$$

$$\omega_i = \frac{\left|\dot{\boldsymbol{p}}_i^{WCS}\right|}{r_w} \qquad \begin{array}{l}\omega_i\text{: rotational velocity wheel } i \\ r_w\text{: wheel radius}\end{array} \tag{5.2}$$

5.4 The Ground Adaption Process: Central Motion Control Modules

The Ground Adaption Process (GAP) is the main part of the middle-layer in SherpaTT's software stack. In the most general sense, the GAP is responsible to mimic a passive suspension using the active DoF of the rover's legs. Hence, the coordination of the legs is encapsulated within the GAP and a high-level process or a human operator can rely on simple motion commands for robot control. The advantage using active DoF and the GAP as controller is that different ground adaption strategies can be modeled and a reconfiguration of the suspension during runtime is possible, whereas the properties of a passive suspension cannot be changed without re-assembly of its mechanical components. In order to model different adaption strategies, several modules with different objectives are implemented within the GAP. All submodules run in parallel and can be individually activated or deactivated to match the current adaption strategy.

Figure 5.2 shows the general structure of the GAP with the currently available submodules for ground adaption. Each module can be described as a behavior in the sense of a perception-action unit as for example described in [Mumm et al., 2004]. The general approach is to have each module M generating its own offset vector $\boldsymbol{o}_i^M$ for each LEP i. With four LEPs, each having three DoF, the dimension of this vector is $\dim(\boldsymbol{o}_i^M) = 12$. However, in the current setting only the z-coordinate of an LEP is manipulated by the adaption modules described below.

The two main sensor inputs for the GAP are

- the forces $\boldsymbol{f}_z$ ($\dim(\boldsymbol{f}_z) = 4$) in z-direction at each LEP and
- the IMU readings of roll Ω and pitch Φ.

Additionally, "internal" values originating from other MCS modules are used, including (i) the actual LEP positions $\boldsymbol{p}_i$, which are including the last GAP offset, (ii) the joint status $\boldsymbol{q}_i$ and reference values $\boldsymbol{q}_{ref,i}$, and (iii) the CoG as calculated from the respective module.

5.4.1 Force Leveling Control Module

The main task of the Force Leveling Control (FLC) is to maintain the expected forces at all wheels of the system in the actual suspension configuration and hence keep all wheels in ground contact. Consequently, the FLC module is the main ground adaption module. Two different implementations are developed during this thesis. The initial version is used for the indoor experiments [4], [5], while the revised version is descibed and experimentally evaluated in [1].

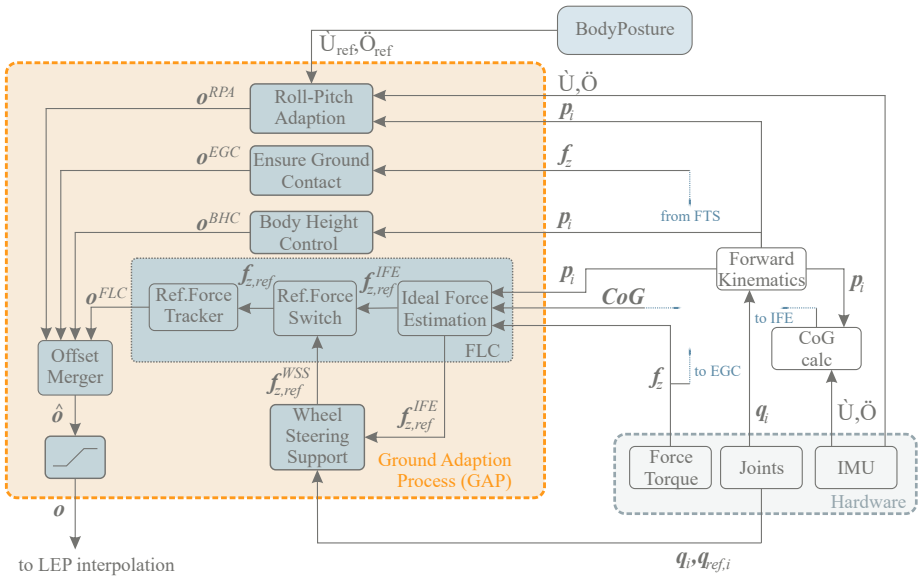

Figure 5.2: *Illustration of GAP structure*

The FLC consists from several submodules. As illustrated in Figure 5.2 these are (i) *Ideal Force Estimation*, (ii) *Reference Force Switch*, and (iii) *Reference Force Tracker*. The actual forces f_z at the wheels, the current LEP positions and the robot's CoG are the main inputs for the FLC [4].

The Ideal Force Estimation submodule is used to calculate the expected contact forces; a naive formulation of the submodule's calculation result is "the closer a wheel is to the CoG the higher its load share". For calculation of reference forces, a static equilibrium with only the gravitational force F_g at the robot's CoG and the reaction forces at the wheels is assumed [4]. Oscillations for example resulting from slip might violate this assumption.

An underdetermined equation system with three equations and four unknowns – the reaction forces – can be established and solved using a Moore-Penrose pseudoinverse [1], [4]. The three equations are built from the zero moment constraint around x and y axis of the robot, and the gravitational force which is the sum of all reaction forces. With $(x_c\ y_c)^T$ being the location of the CoG in a two dimensional plane perpendicular to the gravity vector and $(x_i\ y_i)^T$ the coordinates of LEP i in that plane, the three constraint equations are then given by:

$$0 = \sum_i (x_i - x_c) \cdot f_{z,ref,i}^{IFE} \qquad \text{zero moment around y-axis,} \tag{5.3}$$

$$0 = \sum_i (y_i - y_c) \cdot f_{z,ref,i}^{IFE} \qquad \text{zero moment around x-axis,} \tag{5.4}$$

$$F_g = \sum_i f_{z,ref,i}^{IFE} \qquad \text{sum of all forces.} \tag{5.5}$$

Where $f_{z,ref,i}^{IFE}$ is the estimated reaction force at LEP i that shall be maintained through FLC. Writing Equation (5.3) through Equation (5.5) in matrix form yields:

$$\boldsymbol{t} = \boldsymbol{A} \cdot \boldsymbol{f}_{z,ref}^{IFE} \quad \text{with } \boldsymbol{A} = \begin{pmatrix} x_0 - x_c & x_1 - x_c & x_2 - x_c & x_3 - x_c \\ y_0 - y_c & y_1 - y_c & y_2 - y_c & y_3 - y_c \\ 1 & 1 & 1 & 1 \end{pmatrix} \text{ and } \boldsymbol{t} = (0\ 0\ mg)^T. \tag{5.6}$$

Equation (5.6) can be solved using the pseudoinverse $\boldsymbol{A}^{+} = \boldsymbol{A}^{T} \cdot \left(\boldsymbol{A} \cdot \boldsymbol{A}^{T}\right)^{-1}$. The result is provided in Equation (5.7) allowing to calculate a reference force per wheel for the force tracking module's four individual force-controllers.

$$\boldsymbol{f}_{z,ref}^{IFE} = \boldsymbol{A}^{+} \cdot \boldsymbol{t} \tag{5.7}$$

The Reference Force Switch of the FLC module can change the reference force forwarded to the Reference Force Tracker depending on the system state. When a WheelSteering actuator gets stuck, the Wheel Steering Support (WSS) module generates alternative reference forces to free the wheel, as described in Subsection 5.4.3.

The third FLC submodule, the Reference Force Tracker, takes in the set of reference forces and generates an offset for each LEP to reduce the force error. This implementation was tested in the indoor experiments described in Chapter 6. With all wheels writing an independent offset, slight inaccuracies in modelling of system masses and consequently an error in the position of the CoG can lead to drift of the offsets and undesired oscillations. Unloading of one wheel adds load to the remaining wheels and vice versa: Each wheel's adaption has an effect on the controllers of all other wheels. To reduce the effect of individual wheels pushing into the ground, the offset changes are defined to be small (slow up/down movements of wheels). To react to sudden changes in the ground resulting in wheel ground contact loss (e.g. when leaving a step-like obstacle), the Ensure Ground Contact (EGC) module is used along with the FLC module, Subsection 5.4.2.

Following the indoor experiments, the force tracking was revised as described in [1]. Assuming a rigid suspension system and the rover in its standard pose with Cross-Stance, slight ground irregularities cause individual wheels to loose ground contact. The two adjacent wheels of the one with ground contact loss then take the main load and the robot tends to rock over this axis, which is defined as *strong contact axis* [5]. Since the wheels have a track width of 200 mm, a small support polygon is spanned between the wheels' contact areas (as opposed to idealized contact points). Two wheels can support nearly the complete rover's weight when the CoG is within this sub-support polygon. The axis with the wheel that lost ground contact is defined as *weak contact axis*. Due to symmetry, the wheels $i = 0$ and $i = 3$ and as well as $i = 1$ and $i = 2$ constitute one axis each, the former being on contact axis a_0, the latter on a_1, see Section 5.2.

Both wheels of the strong contact axis need to be moved up, both wheels of the weak contact axis need to be moved towards the ground. Hence, for reduction of number of single controllers, as well as for stability and speed of execution, the Reference Force Tracking module adds the forces on each axis and makes use of one instead of four independent controllers to generate wheel offsets: Offsets for both LEPs on the strong axis are positive (move up), while both LEP on the weak axis are getting negative offsets (move down) of the same absolute value. The offsets are thus $o_0^{FLC} = o_3^{FLC}$, $o_1^{FLC} = o_2^{FLC}$ and $\sum_i o_i^{FLC} = 0$. This strategy keeps all LEP modifications resulting from the FLC around the desired posture and does not change the body ground clearance over time [1]. This approach is called *cross leveling* in the following.

With the introduction of cross leveling, only one controller is present for all wheels. The reaction to ground irregularities is sped up by writing bigger offsets, because the influence of one wheel to all other wheels is removed. This in turn removes the need for the EGC module described in Subsection 5.4.2, when cross leveling is employed.

5.4.2 Ensure Ground Contact Module

Ground contact loss of individual wheels can result in undesired rover tilt and traction loss. The task of the EGC module is to keep all wheels in ground contact when fast changes of terrain, e.g. driving over a hole in the ground, occur and the intentionally slow offset adaptions of the first implementation of the FLC component are not enough to keep all wheels in ground contact. The EGC is a module that pushes the wheel down with a predefined speed as long as no ground contact is detected. When a wheel is in ground contact, the offset $\boldsymbol{o}^{EGC}$ is reduced until it is zero. With reducing $\boldsymbol{o}^{EGC}$ while ground contact is detected, the offset is shifted to that of the force leveling module.

This module is only used in the indoor experiments described in Chapter 6. For the outdoor experiments, the cross leveling method is employed.

5.4.3 Active Wheel Steering Support Module

The WSS module is a module calculating alternative reference forces for unloading single wheels in case a wheel support event is triggered. Different triggers are possible, including

- the current of a WheelSteering joint is greater than the predefined maximum $I_{WS,max}$,
- the difference between actual steering angle φ_i and reference $\varphi_{ref,i}$ is greater than the predefined maximum $\Delta\varphi_{max}$ while the joint is not moving ($\dot{\varphi}_i \leq \dot{\varphi}_{min}$), and
- time in system state `reorienting hold` is longer than predefined maximum $t_{ro,max}$.

A current limiter implemented on the low-level joint control prohibits exceeding $I_{WS,max}$. In effect this current limitation acts as a torque limitation for each joint. Hence, the second trigger becomes active, once a WheelSteering joint cannot act against the resistance of the ground. The timed trigger is a backup in case of errors in sensor readings of the other triggers.

Unloading of wheels is conducted by manipulating the reference forces for the Reference Force Tracker module as indicated in Figure 5.2. The reference force for the wheel j to be unloaded is reduced by a predefined value f_s which is shifted to the remaining three wheels. In case of cross leveling, this has the effect of generating a weak contact axis. The wheel in need of WSS is then placed on the weak contact axis to be able to align the wheel correctly.

5.4.4 Roll and Pitch Adaption Module

The platform's roll angle of a rover with passive suspension such as the rocker-bogie is dependent on the terrain angle and cannot be actively influenced. The internal mobilities of SherpaTT's suspension system allow tracking of ground contact forces and platform roll-pitch control independently of each other. Active roll and pitch control (i) allows to manipulate the position of the CoG within the support polygon, (ii) can support specific sensors mounted on the rover platform, (iii) facilitates payload deployment with SherpaTT, and (iv) can increase the usable workspace for improved ground adaption, see Subsection 5.4.5.

The Roll-Pitch Adaption (RPA) module in SherpaTT's ground adaption process takes the IMU readings and compares it against the commanded values Ω and Φ. Roll and pitch errors are combined into angle-axis form $\{\boldsymbol{e}, \Theta_e\}$ with the axis of rotation $\boldsymbol{e}$ ($\|\boldsymbol{e}\| = 1$) and the error angle Θ_e, [4]. The required offset for each wheel is calculated using the distance $d_i = \|\boldsymbol{d}_i\|$ of LEP i to the rotation axis (in the xy-plane). Depending on the sign of Θ_e and the position of the LEP with respect to $\boldsymbol{e}$, the offset is positive or negative, details are presented in [1].

5.4.5 Body Height Control Module

Various modules with individual offsets in the GAP can lead to the case where all finally written offsets to the four wheels have the same sign. This effectively results in a change of ground clearance of the robot: When all offsets are negative, the body is pushed up, possibly resulting in an unfavorable high CoG with the consequence of a reduced stability margin in slopes. In case all written offsets are positive, the body is effectively lowered to the ground, hence increasing the danger of getting entangled with objects such as rocks and boulders.

Furthermore, the usable workspace for ground adaption is reduced when all offsets have the same sign. Figure 5.3a illustrates the case, where all LEPs are close to the lower workspace limit, with one LEP being at the limit. No further stretching of this leg is possible, resulting in ground contact loss or improper roll-pitch adaption.

The Body Height Control (BHC) module is used to keep a desired body height and to maximize the usable workspace for the other ground adaption modules. The base offset $o_{fix}^{BHC} = -b_z$ defines the center of all LEPs in order to keep control of the desired body height. For maximizing the usable workspace, all LEPs are shifted to be around this value. Figure 5.3b shows the effect of shifting the LEPs with $o_{fix}^{BHC} = 0$, i.e. moving the LEPs around Pose A.

A further extension of the approach is illustrated in Figure 5.3c: Rolling/pitching the body can result in further increased workspace for the LEPs. This can only be conducted, when the roll and pitch of the body are not required at certain values for current rover operations. An automatic roll-pitch command manipulation is currently not implemented in the BHC module, however manual pitch control showed to increase the workspace for driving in steep slopes and indicates an improvement of force distribution between the wheels, [1].

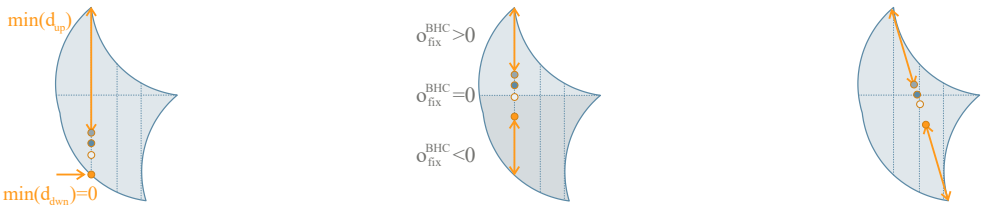

(a) *No BHC: An LEP reaches the lower workspace limit*

(b) *BHC shifts all LEPs to the center of the workspace.*

(c) *Further extension with roll-pitch control.*

Figure 5.3: *Body height control: increasing usable workspace for ground adaption.*

5.5 Low Level Control

Low-level control is conducted on joint-level of the limbs (legs and arm) of the rover. Each actuator has its own FPGA-based controller, all controllers of one limb are communicating on the same bus. The Zynq-Brain (Subsection 4.3.4) is the central node of low-level communications.

The joint command vectors $\boldsymbol{q}_{ref,i}$ are forwarded from the on board computer to the Zynq-Brain and from there to the respective joints. Each joint of each limb is locally running a cascaded position-velocity-current PID controller. An exception are the wheels featuring a velocity-current cascade. Each joint k is periodically sending its telemetry vector $\boldsymbol{t}_{k,i}$ containing the joint status information, such as position, velocity, current measurements (three phases and overall), supply voltage, and temperatures. A joint hardware driver module then constructs the joint status vector $\boldsymbol{q}_i$ containing position, velocity and current of each limb.

5.6 Summary and Conclusion

This chapter reviews the design of the motion control system for a rover with an actively articulated suspension. The general software stack with its three layers is outlined. The motion control system is the main focus of this chapter. Particularly the software modules for realizing an active ground adaption are discussed in this chapter.

Ground adaption is based on reactive behaviors, deliberative control is not employed; the controllers rely on the current robot state and do not preplan future actions. These controllers have the advantage to be able to run on hardware with processing limitations and thus are better suited for deployment on space qualified hardware.

Currently, five submodules constitute the GAP: Force Leveling Control, Ensure Ground Contact, Wheel Steering Support, Roll-Pitch Adaption, and Body Height Control. The submodules are independently generating offsets for the four LEPs of the rover SherpaTT. One exception is the Wheel Steering Support which generates alternative reference forces for unloading of single wheels. An add-merge is used to merge the individual module's offsets, facilitating future development of adaption modules: a new module can simply add to the overall offset. Furthermore, the general modular approach allows to exchange individual modules with updated versions. Single GAP modules can be switched on and off at runtime of the system, alternatively the influence of individual modules can be adapted during runtime using the module's gain values without affecting the other modules.

5.7 Contributions of the Corresponding Publications

Overall, the publications contributing to this chapter document the development steps of a control system for a hybrid wheeled-leg rover. Over the course of the publications, the structure is refined and several motion modules are implemented and improved.

In [7] an analytical solution for the wheel orientation and velocity resulting from a three dimensional velocity command for a rover with varying footprint is presented. Non-fix positions of the wheel-steering axes are considered in the calculations. Several locomotion modes are conceived for the rover system Sherpa, including an inch-worming mode, tripod mobility and manipulation arm support in locomotion.

An initial version of the MCS and the GAP for SherpaTT is presented in [5]. FLC and EGC are two separate, mutually exclusive modules in the development state presented in this publication. When a wheel is not in ground contact, the contact module controls the wheel's offset, when ground contact is made, the FLC component takes over control.

In [4] an updated motion control is presented. The FLC module is used for keeping all wheels in ground contact. Switching between different modules is not required for the implementation presented in this publication. EGC and FLC run in parallel, the EGC module writes offsets only when FLC cannot react fast enough. Each wheel has an own FLC controller in the MCS version presented in this publication.

The journal publication [1] reviews the final motion control strategy. Usage of the different coordinate systems for locomotion control is discussed. The cross leveling approach as described in Subsection 5.4.1 is introduced and evaluated in this publication, the EGC module is obsolete in this implementation. A detailed discussion of the implemented GAP submodules is provided.

6 Experimental Evaluation of the Active Suspension System

This chapter of the thesis summarizes the experiments and results conducted for evaluation of the active suspension system and its control with the motion control system. The results of the corresponding publications are reviewed and set into relation with each other. Details on setup, conduction and results of all experiments are provided in the publications.

A set of indoor experiments on artificial wooden obstacles is used to evaluate the general feasibility of the chosen approach as well as the system behavior close to the limits of its physical abilities. The outdoor experimentation substantiates the findings and evaluates the system in a natural Mars analogue terrain.

In Section 6.1 the general setup of the experiments conducted for the rover evaluation is provided. The performance of the ground adaption processes is discussed in Section 6.2. Particularly the ground force tracking and the body angle control are addressed. An analysis of the system's power consumption is conducted in Section 6.3, while the slope climbing abilities of the system in natural terrain are presented in Section 6.4.

A summary and conclusion of the experimental results is provided in Section 6.5. The chapter is completed by the statement of the contributions of the corresponding publications in Section 6.6.

The following publications from Appendix C – Accumulated Publications contribute to the contents of this chapter:

[1] **Design and Field Testing of a Rover with an Actively Articulated Suspension System in a Mars Analogue Terrain**; *F. Cordes, F. Kirchner, A. Babu*; Journal of Field Robotics 2018.

[4] **Static Force Distribution and Orientation Control for a Rover with an Actively Articulated Suspension System**; *F. Cordes, A. Babu, F. Kirchner*; IROS 2017.

[5] **SherpaTT: A Versatile Hybrid Wheeled-Leg Rover**; *F. Cordes, A. Babu*; i-SAIRAS 2016.

[9] **Field Testing of a Cooperative Multi-Robot Sample Return Mission in Mars Analogue Environment**; *R. U. Sonsalla, F. Cordes, L. Christensen, T. M. Roehr, T. Stark, S. Planthaber, M. Maurus, M. Mallwitz, E. A. Kirchner*; ASTRA 2017.

6.1 General Experimental Setup and Evaluation Methods

This section provides the general experimental setups. The data of all runs is used for analysis of the rover suspension system performance. In total, 99 runs are used for the evaluation of the system. Thereof 29 runs are conducted in the indoor environment ([4] and [5]), while 70 runs are conducted in the field tests which are highlighted in [9] and described in detail in [1].

6.1.1 Indoor Setting

Modular elements are used to built up the obstacles in this setting. One modular unit is a 1.2 m × 1.2 m wooden plate with an up-down ramp with a height of 0.2 m at the peak. Two units are connected to establish the obstacle shown in Figure 6.1. The modules are part of a standardized set of obstacles which are oriented in design at the standard published in [American Society for Testing and Materials, 2011].

The obstacle is designed such that a frequent change in wheel height is forced when driving over the obstacle. The height represents approximately 30% of the available vertical stroke with the LEP in its standard configuration. The wheels of the rover are stiff without passive adaption, thus all adaption to the obstacle needs to be realized by the active suspension.

Two velocity commands for the rover are used: 0.05 m/s and 0.10 m/s. With the obstacle height changing by 0.2 m per 0.6 m driving distance, LEP velocities of $\dot{z}_{LEP} \approx 0.017$ m/s and $\dot{z}_{LEP} \approx 0.033$ m/s are required, respectively. These correspond to 52% and 92% of the maximum velocity achievable in the motion range of ±0.2 m around Pose A, see also Section A.5.

As a baseline, the rover drives without active ground adaption over the obstacle (referred to as *noAdap* runs), the suspension system is rigid. Afterwards, runs with EGC active (referred to as *EGConly* runs), RPA active (*RPAonly*), EGC and RPA active (*EGC+RPA*), as well as FLC, EGC and RPA active (*FLC+EGC+RPA*) are conducted. When RPA is active, roll and pitch reference angles are 0°.

Preliminary tests showed that a *FLConly* setting is not feasible: The rover showed a tendency to shift its body pitch over time most likely due to improper mass modelling of the rover and consequently a wrong CoG calculation see also [4]. The modifications resulting in cross leveling as described in Subsection 5.4.1 were made following the indoor experiment results.

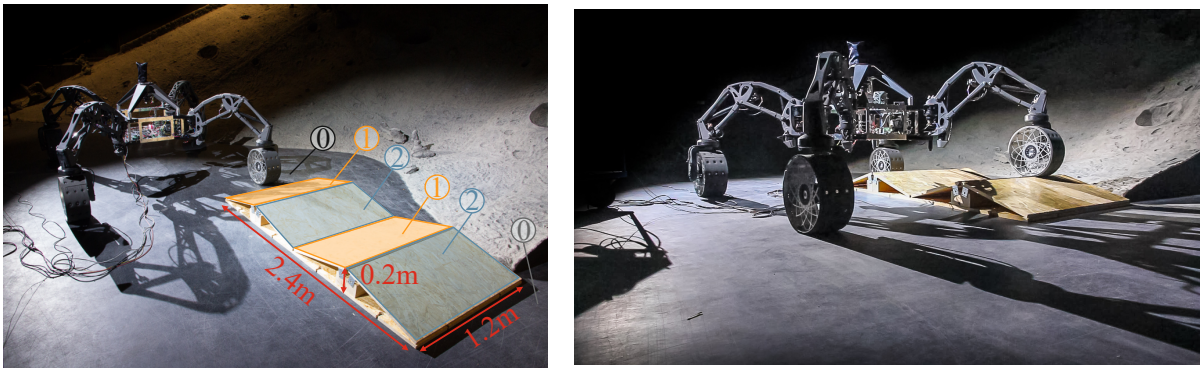

(a) *Single sided obstacle. Color overlays for up - and down ramps.*

(b) *Screenshot from experiment video: SherpaTT on obstacle with active adaption*

Figure 6.1: *Indoor setup with wooden obstacle track*

Experiment markers with value 0, 1, or 2 are set manually in the log-file, when the front left and rear left wheel enter the corresponding slope, respectively: When a wheel is on laboratory floor its marker is (0), while being on rising slopes (when driving forward) the corresponding marker is (1), falling slopes are marked with (2), see Figure 6.1a. Both right side wheels are driving on the laboratory floor for the whole experiment run. The indoor experiments are described in detail in the publications [4] and [5].

6.1.2 Outdoor Setting

The test site in the desert of Utah, USA was chosen due to its reported similarity to areas on Mars, [Clarke and Stoker, 2011], [Dupuis et al., 2016]. Bed rock, loose soil, varying slopes and inverted river beds are some of the features in this area. The test site is described in [9], it is considered to be a representative of areas the TransTerrA MRS would be deployed in.

Three different setups varying in the type of terrain are used in the outdoor experiments. In each setup different footprints are used, as described in the following list. The GAP modes *noAdap*, *FLConly* and *FLC+RPA* are used in the outdoor experiments. As a result from the indoor experiments, *RPAonly* runs are not conducted in the outdoor evaluation due to the tendency of ground contact loss with single wheels. The FLC implementation employed during the field-trials is using cross leveling. The settings of the outdoor experimentations as well as the rationales for the chosen footprints and GAP modes are described in detail in [1]. Illustrations of the footprints are given in Figure 4.11 of Chapter 4.

The commanded velocity is $\dot{x} = 0.1\,\mathrm{m/s}$, which is the desired velocity for nominal operations. A slow velocity setting as in the indoor experiments is neglected due to the mostly smooth surfaces with low frequency height changes. For the steep slope terrain, however, a low speed setting with $\dot{x} = 0.04\,\mathrm{m/s}$ is chosen additionally to the $\dot{x} = 0.1\,\mathrm{m/s}$ setting: After five successful preliminary runs with $\dot{x} = 0.1\,\mathrm{m/s}$ in the slope, the duri-crust was brocken and fine powdered sand was present on the track. The rover ended in 100% slip in mid-slope. Further tests showed a reduced velocity of $0.04\,\mathrm{m/s}$ to be the maximum possible for successful slope climbing, see also explanation in [1]. With active roll-pitch control, the commanded angles are $\Omega_{ref} = \Phi_{ref} = 0°$. In the steep slope setting, however, manual adaption of the pitch angle is necessary in the steepest part of the slope to keep the LEPs from their workspace limits and allow further ground adaption.

Setup A: Flat Terrain This track is illustrated in Figure 6.2. A mostly flat track is used to generate baseline values for comparison with the other two setups. The rover is commanded to drive a 20 m straight line in GAP modes *noAdap* and *FLConly*. *FLC+RPA* is skipped due to the flat terrain without inclinations. Three different footprints are used for each GAP mode: Cross-Stance as the standard footprint, P90 with a compact footprint, see Figure 6.2c, and Turtle-Front as footprint presumed to be favorable in steep slopes due to the shifted CoG. A total of 22 runs is conducted in this setup [1].

Setup B: Moderate Slope This test track is shown in Figure 6.3, it has a length of 12 m, segmented in three parts. The first and last 4 m segments each feature mostly flat ground, while the middle segment of 4 m has a 8° slope. All three above listed GAP modes are used with the footprints Cross-Stance and Quasi-Tripod. Using basically three contact points as in Quasi-Tripod eliminates the undefined contact distribution and is expected

to provide more stable ground contact only from the flexible wheels (hence in *noAdap* mode). A total of 30 runs is conducted in this setup [1].

Setup C: Steep Slope The steep slope setting is illustrated in Figure 6.4. The slope angle varies with around 10° at the start of the test track, a peak of 28° in the center of the slope and a flat top of the hill. The inclinations separated in 1 m segments of the slope are provided in [9]. A distance of 17 m is driven on the slope. Due to the risk of damage in the steep slope, *noAdap* runs are not conducted, hence only *FLConly* and *FLC+RPA* runs are conducted on this track. Five runs in Cross-Stance with $\dot{x} = 0.1\,\mathrm{m/s}$ are conducted, while 13 runs with $\dot{x} = 0.04\,\mathrm{m/s}$ are conducted using the footprints Cross-Stance and Y-Shape. Runs in Y-Shape are conducted as a substitute for Turtle-Front to avoid the risk of system damage due to unfavorable loads, see explanations in [1].

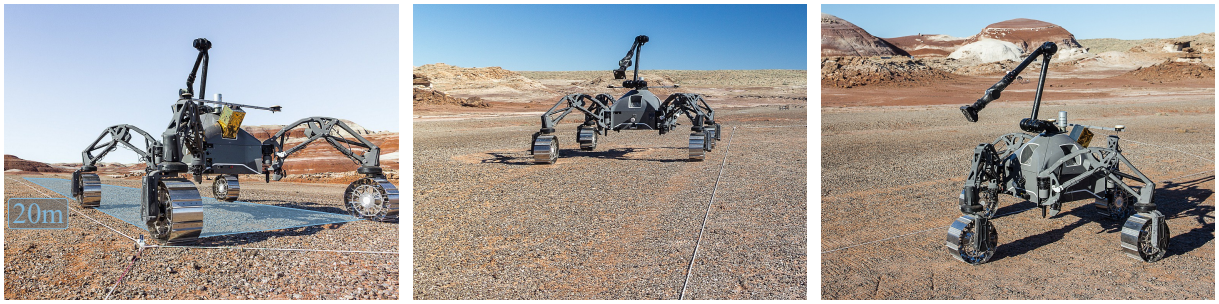

(a) *Start of track. SherpaTT is equipped with DGPS module.*

(b) *SherpaTT in Cross-Stance during a run*

(c) *SherpaTT in P90 footprint configuration during a run*

Figure 6.2: *Outdoor setup A: Flat ground as reference. Track length 20 m.*

(a) *Start of run. SherpaTT in Cross-Stance, segmentation of track provided in overlay.*

(b) *SherpaTT in Quasi-Tripod during a run*

Figure 6.3: *Outdoor setup B: Moderate slope. Track length 12 m, height difference ≈0.55 m.*

6.1.3 Evaluation Methods

Comparison of two individual indoor runs shows the progression of the values to be very similar: Figure A.2 in the Appendix shows the force error plots at all wheels for two runs. Despite the difference in the commanded velocity, the force error plots are nearly identical. Hence, the indoor evaluation relies on single run data, see also [4] and [5].

In case of the force tracking experiments, a Root Mean Square (RMS) error value $\hat{e}_{f,i}$ of the force error for each wheel i is calculated. The mean of all four RMS values over all runs is used as value for comparison of the GAP settings. Similarly, the mean of roll and pitch RMS error

(a) *SherpaTT on top of the slope. Colored overlay indicates approximate track.*

(b) *SherpaTT just passed the steepest part of the slope in a* FLConly *setting*

Figure 6.4: *Outdoor setup C: Steep Slope. Track length 17 m, height difference ≈5 m.*

values is calculated. For power evaluation of the indoor runs, the mean power draw per run is calculated. The mean of all runs per GAP setting is calculated to compare the settings.

The evaluation methods for the outdoor runs are explained in detail in [1]. All runs of the same setting are used to build a mean of the error values, which are used for the plots in the subsequent sections. The RMS error value of the means over all runs per GAP setting and footprint is used to generate a measure of quality for comparison of different settings.

The data of indoor and outdoor runs from the publications contributing to this chapter is recompiled into the same format for better comparability. This previously unpublished format is provided in the tables of Appendix A.6. These tables also contain the number of runs used per footprint and GAP mode.

6.2 Ground Adaption Performance: Force Leveling and Body Angle Control

This section recapitulates the results concerning the force-leveling and body angle control. Indoor as well as outdoor experiments are conducted to evaluate the performance of the GAP modules. Without proper force leveling, system stability is decreased. Unbalanced loads between the wheels lead to high torques required for wheels with high load and low torques for wheels without load. Roll and pitch control can further increase system stability. Furthermore, precise roll-pitch adaption facilitates payload handling in the multi-robot scenario.

6.2.1 Presumption

Significant ground contact loss of single wheels is expected for the *noAdap* baseline runs since the suspension is rigid and no contour following is conducted. Switching of a_0 and a_1 being the strong contact axis is expected with individual wheels loosing ground contact.

Quality of ground contact in *EGConly* runs is expected to be improved, however without the FLC module oscillations around the ground contact loss might occur. Runs with active FLC module should show the best ground adaption performance, independent of other activated modules. Body angle tracking with RPA active is expected to keep the commanded body an-

gles, independent of other activated modules. Generally, no significant performance drop is expected for any module, when another ground adaption process is activated.

Cross leveling was introduced assuming the standard footprint Cross-Stance. The outdoor experiment series are used to evaluate the performance with other footprint configurations. Generally, all stable footprints result in the contact axes a_0 with wheel FL and wheel RR and a_1 with wheel FR and wheel RL as defined in Section 5.2. Consequently, the cross leveling approach is expected to be working independently of the chosen footprint.

6.2.2 Results and Discussion

The discussion of the results is kept short with exemplary plots as supplement. More detailed information can be found in the respective publications [1], [4], and [5]. Additionally, the experiment data is compiled into values for quantitative comparison of all experiments as presented in the tables of Subsection A.6.2 of the Appendix.

Plots of force tracking errors e_{fi} at all four wheels as well as the roll and pitch errors e_r and e_p are shown in Figure 6.5 for exemplary indoor runs. The background of the force error plot is colored to highlight the wheels on strong and weak contact axes. Ideally, both, the force error plots as well as the body angle error plots would show a flat line at zero. The experiment markers introduced above are plotted along with the body angles for improved understanding.

The *noAdap* plots from Figure 6.5a illustrate the ground contact loss when not using any ground adaption strategy. A clear separation between strong (upper half of force error plot) and weak contact axis (lower half) is visible. At the beginning of a run, a_0 is the strong contact axis, the front right wheel is lifted into the air during the run. At the middle of the run, the axes change: a_1 becomes the strong contact axis, when the rear left wheel enters the obstacle and the rear right wheel is lifted off the ground. This can also be seen in the body orientation plot: The pitch error (yellow line) basically follows the obstacle contour. The roll error has peaks, when the rover rocks about the strong contact axis.

In Figure 6.5b, a *FLC+EGC+RPA* run is shown. Throughout the whole run, no ground contact loss occurs, consequently, the EGC component is not writing any offset and the result is effectively the same as a *FLC+RPA* run would have.

The indoor experiments are conducted without batteries in the rover and without the manipulation arm mounted on the rover, see Figure 6.1; the gravitational force of the rover is $F_{g,lab} = 1459\,N$. All forces are mostly within a ±100 N band around the setpoint, the error per wheel is thus below 7% of the rover gravitational force. Spikes occur, when the two wheels are rolling over slope changes as well as obstacle start and end. The force error exceeds the ±100 N band twice (approximately 45 s and 55 s) when both wheels are changing the slope shortly after each other. This is due to the comparatively slow adaption of the FLC module. Between these events, the force errors are narrowed towards ±50 N (< 3.5% of rover gravitational force). The roll and pitch errors are kept in a ±0.5° band with spikes corresponding to those seen in the force error plot. An elaborated discussion of these values is presented in [4], similar results are presented with the experiments in [5].

Force error plots representative for the results from the outdoor experiments are shown in Figure 6.6. The means over all runs with the GAP modes *noAdap*, *FLConly* and *FLC+RPA* in Setting B (moderate slope) are plotted exemplarily for the front left wheel, the remaining wheels show corresponding values. Extended discussion of the data is available in [1].

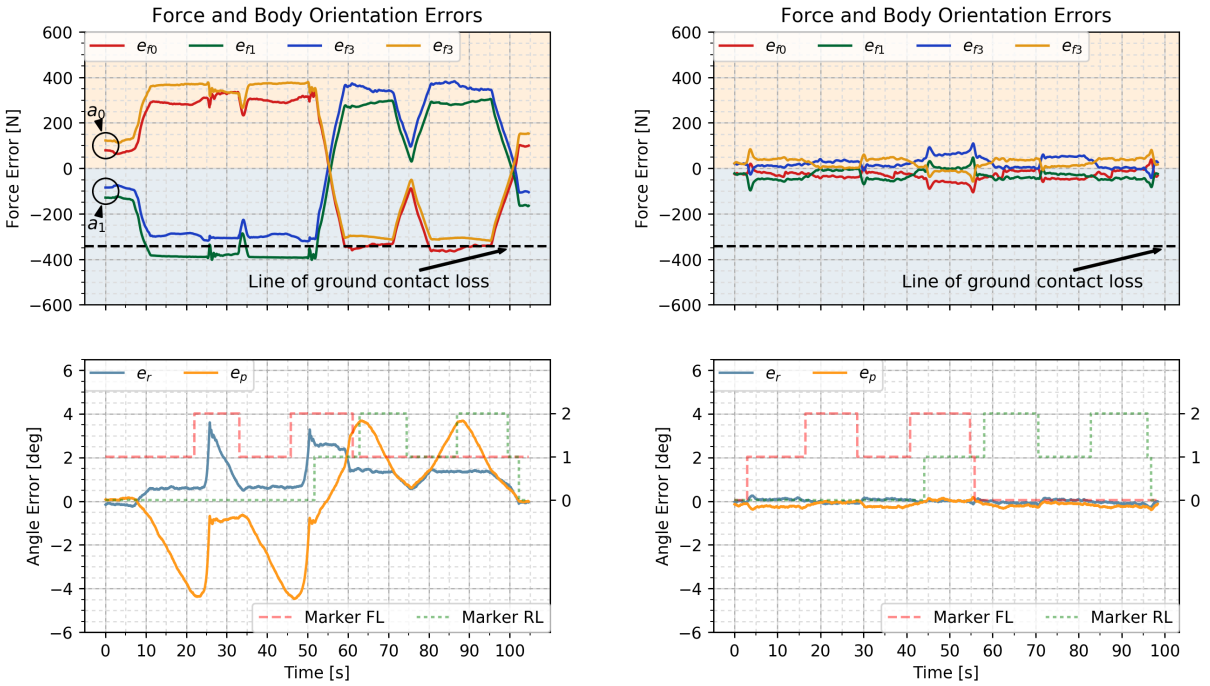

(a) noAdap*: Force contact axes clearly separated. Long periods of ground contact loss. Obstacle shape reflected in pitch angle.*

(b) FLC+EGC+RPA*: Small force deviations around setpoint. Body angle errors kept at minimum.*

Figure 6.5: *Force and body orientation error plots from selected indoor runs. Details in [4] and [5]*

The plot in Figure 6.6a shows that the Cross-Stance footprint experiences ground contact loss of the front left wheel in *noAdap* mode. Compared to that, Figure 6.6b shows the tripod configuration to have only moderate force errors even without active adaption, which matches the presumption.

Other than that, both GAP modes with active force leveling have similar results in both footprints illustrated, showing the ability of the force leveling control to cope with different footprints. Furthermore, the force errors are similar with and without additional roll-pitch adaption module. A quantitative comparison is possible from the data listed in Table A.10: It shows

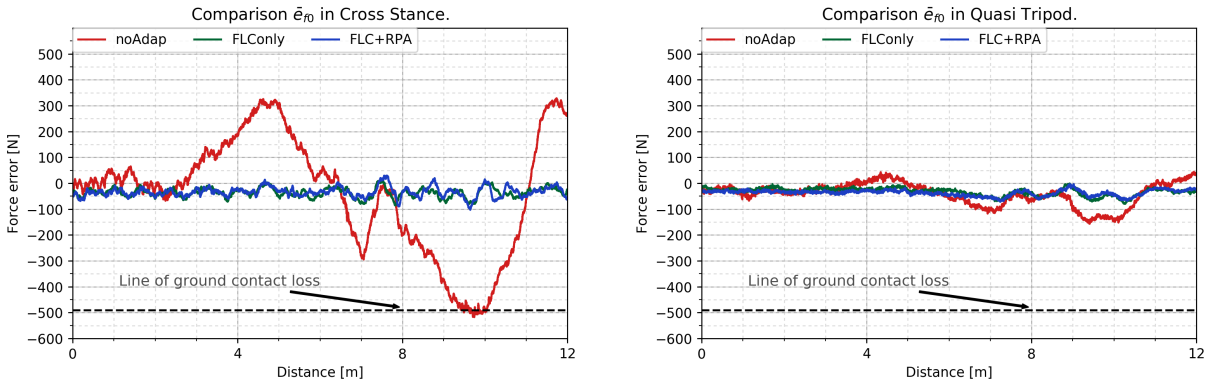

(a) *Cross-Stance: Ground contact loss of wheel FL*

(b) *Quasi-Tripod: Small force error in* noAdap.

Figure 6.6: *Force error wheel FL in outdoor Setting B (moderate slope) over three GAP modes: Quasi-Tripod with significantly lower force error in* noAdap *setting.*

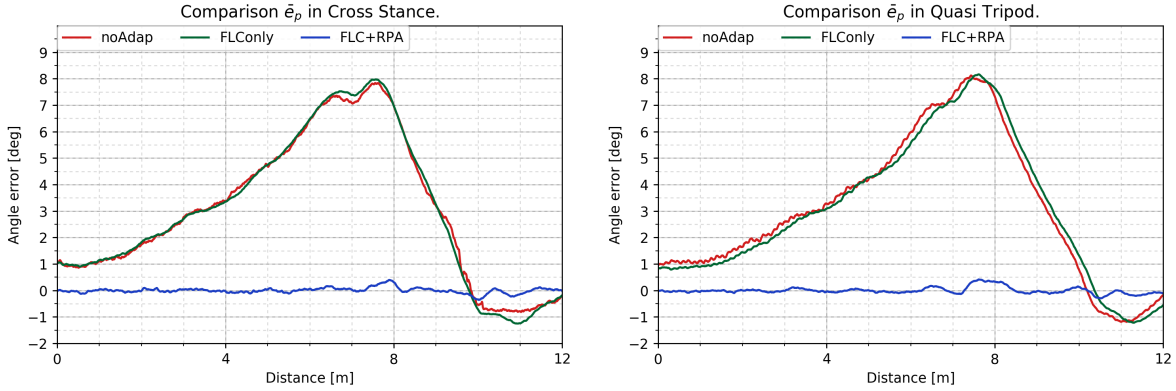

(a) *Cross-Stance* **(b)** *Quasi-Tripod*

Figure 6.7: *Pitch error in outdoor Setting B (moderate slope) over three GAP modes: no significant difference between footprints. Without roll-pitch adaption, body angle follows slope.*

similar values of the force errors in *FLConly* and *FLC+RPA* modes in both footprints. Actually, a slightly better performance is achieved in *FLC+RPA* mode for both footprints, resulting from improved load distribution between the wheels, see also Section 6.4.

In the outdoor runs, the rover is fully equipped with manipulation arm, batteries and GPS module, its gravitational force is $F_{g,out} = 1901\,N$. The mean force error plotted for the front left wheel is not exceeding the ±100 N band, which is around 5% of the gravitational force of the rover. The RMS error values for these runs are ranging between 31 N and 38 N (see Table A.10), which is below 2% of $F_{g,out}$.

Figure 6.7 shows the progression of the pitch error on the moderate slope track for the three applied GAP modes and separated in Cross-Stance and Quasi-Tripod suspension configurations. The rover shows basically the same pitch error for *noAdap* and *FLConly* modes over the two footprints. These values show that the rover's body angle is not influenced from the offsets written by the FLC module. Comparing the *FLC+RPA* mode in both footprints shows a very similar progression of the pitch error, which indicates the RPA's independence of the chosen footprint. The mean RMS error of roll and pitch is 0.11° in Cross-Stance and 0.16° in Quasi-Tripod, see Table A.10.

6.2.3 Conclusion

The developed suspension system in conjunction with the reactive control approach is able to cope with high frequency changes of ground height as well as with natural terrain. The remaining steady state force error is due to the intentionally simplistic implementation of a proportional gain controller and has a similar absolute value in the indoor and the outdoor experiments. Adding an integrative part bears the potential to further decrease the error. However, the mass deviation between individual wheels is kept around 50 N, satisfying stable locomotion and equal load distribution between the wheels.

The relative force error is kept below 2% of the rover's total mass with the cross leveling implementation in the outdoor runs. Due to the lower mass in the indoor runs, the force errors at the wheels are kept below 7% of the rover's gravitational force in this setting. Absolute force errors are similar in both cases. System stability is maintained, all wheels are kept in permanent ground contact.

Body angle errors can be kept below 1° with active RPA module. This is the case for the high frequency obstacle indoors as well as for the outdoor runs in natural terrain. The EMI tolerates up to 7° angle error between interfaces [13]. Consequently, a high precision body control independent of the terrain shape is shown, the remaining angle error is small enough e.g. for picking up a BaseCamp with the rover's body interface.

Despite the individual offsets of force and body angle controllers, both do not influence each other significantly in moderate terrain: Different ground adaption objectives can be matched independently with the proposed suspension and its control system. However, a minor improvement of force tracking errors is suggested from the data in Table A.8 and Table A.10 when activating roll-pitch control. For the steep slope experiments, this cannot be confirmed: Table A.11 shows the force leveling quality to be decreased by activating the RPA module in steep slopes. However, all runs in steep slope with *FLC+RPA* mode showed increased slippage, see also Section 6.4. Slip leads to oscillations, which in turn leads to an increased RMS force error due to high frequency loading and unloading of individual wheels. The dynamic loads introduced by the oscillations violate the static equilibrium assumption used for calculating the reference forces, see Subsection 5.4.1.

6.3 Power Consumption Analysis of the Active Suspension System

This section recapitulates the experimental results concerning the power consumption of the active suspension system. Indoor and outdoor experiments are used to evaluate the power requirements in different terrain conditions. The data from the experiments published in [1] and [4] is compiled into a comparable format in the tables provided in Subsection A.6.3.

It is straightforward that an active suspension requires more power than a passive suspension without actuators. For determination of the power overhead induced by the active articulation, the power for locomotion P_l is split into P_s for the suspension system (all Pan, InnerLeg and OuterLeg joints) and P_d for the drive system (WheelSteering and WheelDrive actuators). P_s is assumed to be the power overhead compared to a passive suspension. Due to non-backdrivable joints, $P_s = 0\,W$ when no movements of the suspension are present (i.e. *noAdap* mode).

Additionally, a base power draw P_b is present. This is the power required for sensors, computing units, DC/DC converters, attached payload-items and other electronics in the central body of SherpaTT. Due to the early integration stage during the indoor experiments, less electronics are active in the robot. The presented indoor experiments have a base power draw of $P_{b,lab} \approx 130\,W$, while the base power draw during the outdoor tests is $P_{b,out} \approx 160\,W$ with DGPS-module and $P_{b,out} \approx 150\,W$ without DGPS module.

6.3.1 Presumption

Power requirements are expected to increase with the number of control objectives for the rover. Consequently, the GAP mode *FLConly* is expected to require less power than the *FLC+RPA* mode, which also controls the body orientation.

Generally, terrain roughness plays an important role in power consumption. More frequent changes in the suspension system require more power. Hence, the indoor experiments with a high frequency adaption close to the velocity limits of the suspension should show the worst case power draw.

6.3.2 Results and Discussion

Figure 6.8 illustrates the results from the power analysis. Plotted is the mean suspension power $\bar{P}_s$ as well as the mean total locomotion power $\bar{P}_l$ of all runs of the same settings. The area between the two lines represents the mean power $\bar{P}_d$ for driving the rover. The full data sets are provided in the tables of Subsection A.6.3 in the appendix.

Figure 6.8a shows the power requirements for locomotion in different GAP modes on the high frequency obstacle of the indoor experiments. Plotted are the mean values of the 0.05 m/s velocity setting. It can be seen, that the power for driving the rover is nearly constant, while the suspension power increases depending on the chosen control mode. *noAdap* does not move the legs, hence no power is consumed, *EGConly* controls individual legs if ground contact is lost. The roll-pitch adaption controls all four legs to match the body angle commands, consequently the power draw increases significantly in *RPAonly* compared to the former two modes. Adding ground contact control in the *EGC+RPA* setting further increases the power requirement. When ground contact is not lost during the *FLC+EGC+RPA* runs, the power requirement decreases: No fast movements are required and a more constant leg motion is conducted.

In the worst case of the high frequency obstacle with *EGC+RPA* mode, the suspension draws around 60% of the total locomotion power or 19% of the total rover power when considering $P_{b,lab}$ as well. This is a considerable share of the overall power for the rover. However, as stated above, the obstacle is designed such that the rover is driven close to the physical limits of the system. If power draw is crucial, as can be expected for a planetary mission, reduction of rover velocity can be a simple method to reduce power requirements in terrains with high frequency changes. Additionally, a path planner could penalize terrain roughness in the optimization process in order to avoid terrain considered unfavorable from the point of view of power draw.

The data from the outdoor runs in Table A.14 and Table A.16 confirms the observation of increasing power draw with additional control modes. Each mean value of $\bar{P}_s$ with *FLConly* setting is significantly lower than the corresponding value in *FLC+RPA* mode.

Figure 6.8b illustrates the power requirements in the different outdoor tracks. Plotted are the mean values of runs in Cross-Stance with *FLConly* setting. For the non flat terrain, only upslope runs are plotted. It can be seen that the main driver for power requirement increase is the drive system of the rover, i.e. those actuators also present in a passive suspension system. Compared to the increase in drive power, only a slight increase of the suspension power is present from flat terrain over the moderate slope to the steep slope setting. Reducing the velocity in the steep slope setting decreases the power requirements in both, suspension system and drive system.

The suspension system's share of the total power for locomotion ranges from 18% in the moderate slope setting down to 12% in the steep slope setting, see Tables in Subsection A.6.3. Taking $P_{b,out}$ into account, the suspension system's share of the total rover power is between 3% and 6% in the *FLConly* runs of all terrains.

Driving downslope with the rover allows the wheels to generate power when the slope is steep enough. In Setting C, runs down the slope with high velocity show a netto power generation of the wheels, Table A.15. In cases of power generation from the wheels, the indication value $P_s/P_l > 1$ and the suspension system consumes more power than the total power required for locomotion. The generated power can be used in the suspension joints for ground adaption, releasing the load on the batteries, see also [1]. Consequently, the power share value P_s/P_l is not useful for comparison in these cases.

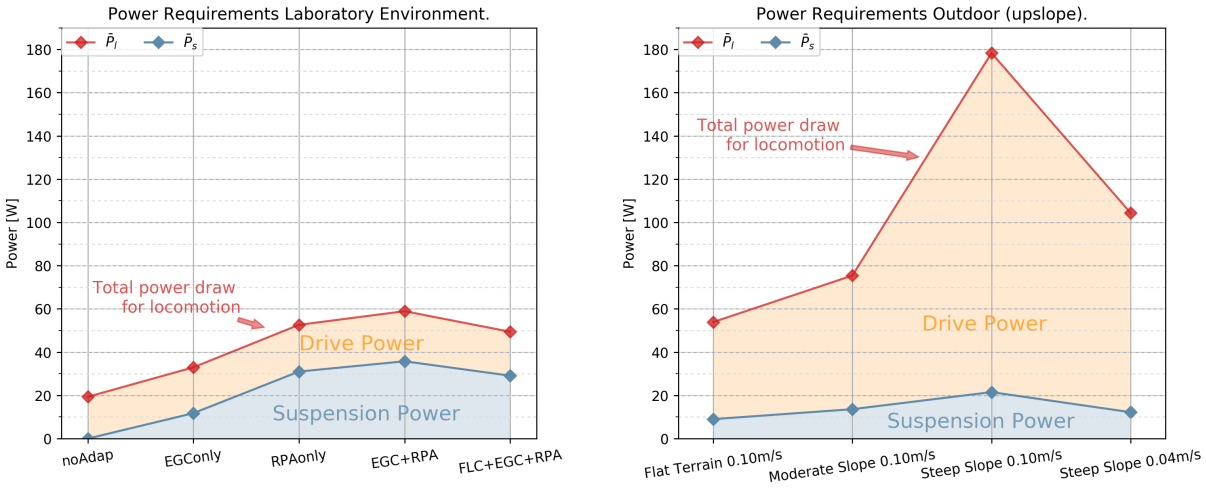

(a) *Mean power for locomotion on high frequency obstacle with different GAP modes.*

(b) *Mean power for locomotion in different terrains (upslope drives in* FLConly *and Cross-Stance)*

Figure 6.8: *Power analysis with different GAP modes and different terrains*

6.3.3 Conclusion

Power consumption of the suspension is mostly independent of the slope angle the rover is driving as well as of the chosen footprint of the system. All outdoor settings show comparable suspension power draw, despite the wide range of slope inclinations and the different footprint settings. However, power draw of the suspension system is dependent on the terrain surface type: The similar power draw of the outdoor runs is due to the mostly smooth surface on the slopes. High frequency changes of the surface require the suspension to permanently change the LEPs' positions and consequently would require comparable high amounts of power as shown on the artificial obstacle in the indoor runs.

Furthermore, the individual control modes require different amounts of power for adapting the suspension system. Permanent ground contact of all wheels showed to be favorable, since only small adaptions of the wheels are required in this case. Body angle control needs to adapt all four wheels independently of each other, hence a comparably high amount of movements in the legs is needed for this control mode. If a body angle control is not required in the current mission profile, it should be omitted to reduce the power requirements of the rover.

The outdoor tests were conducted in a terrain considered a Mars analogue terrain, [9]. Hence the power results from the outdoor evaluation give a more realistic result of the power requirements in a real mission. The mean power overhead for active ground adaption of around 10 W found in the outdoor experiments is considered justifiable given the flexibility and reconfigurability of the active suspension system, which bears the potential for advanced fault recovery in various terrain types.

6.4 Steep Slope Climbing

This section summarizes the results from the slope climbing evaluation in the steep slope of the outdoor experiments. A detailed analysis is provided in [1]. The amount of slippage is used as indicator for ground adaption quality and hence to compare different GAP modes and foot-

prints. The slip s of the rover is calculated according to Equation (6.1) using the proprioceptive distance from odometry d_{odo} (distance the rover "believes" to be driven) and the ground truth distance d_{gps} as measured with the DGPS module on SherpaTT.

$$s = 1 - \frac{d_{gps}}{d_{odo}} \qquad \text{with} \quad \begin{array}{ll} s > 0\text{: slip} & \text{(typically driving upslope)} \\ s < 0\text{: skid} & \text{(typically driving downslope)} \end{array} \tag{6.1}$$

6.4.1 Presumption

It is expected that shifting the CoG to the upslope wheels has a positive effect on the slope climbing ability. A forward shift can be achieved by moving front and/or rear wheels to the back, which has the effect of the body being oriented to the front edge of the (new) support polygon. Another way to shift the CoG to the front is by pitching the rover against the slope, e.g. by commanding a zero pitch with respect to the gravity vector. Thus less slippage and improved slope climbing ability is expected for the Y-Shape configuration compared to the Cross-Stance as well as for *FLC+RPA* mode when compared to the *FLConly* mode.

6.4.2 Results and Discussion

Figure 6.9 illustrates the effect of CoG shift through rover pitch control. The reference forces for all four wheels are plotted in the upper half of each subfigure. Below the reference force plot is a plot of the slope angle and the body pitch command. The slope angle is the output of the plane estimator module; for details on the evaluation of the module see [1].

The reference forces are calculated according to the current configuration of the rover. Hence, the reference forces reflect the load distribution due to the location of the CoG within the support polygon. The CoG's position is dependent of slope incline, body shift and body angle.

When driving in *FLConly* mode, a decrease of the front wheel loads can be seen with increasing slope angle. This is indicated by the $f_{0,ref}$ and $f_{1,ref}$ plots in Figure 6.9a. The loads to the rear wheels increase with the slope angle, correspondingly. The maximum slope angle is reached at $d_{odo} = 5\,m$. Each right sided wheel shows a higher load than the corresponding left sided wheel, this is due to the roll angle of the system which can also be seen in Figure 6.4b.

The reference forces of a run in steep slope with active roll-pitch adaption are shown in Figure 6.9b. The rover starts with commanded zero angles for roll and pitch, the reference forces are close to an evenly distributed load on all four wheels, the front wheel pair has a slightly higher load share than the rear wheel pair. Two results can be seen in this plot: (i) the load distribution is kept constant in varying inclines when the pitch angle is kept constant with respect to gravity and (ii) it is possible to influence the load distribution by manipulating the rover's body pitch angle. This result confirms the presumption presented above.

As a consequence of the improved force distribution, an increased slope climbing capability is assumed. A comparison of slip and skid values for all conducted runs (with velocity setting 0.04 m/s) in the steep slope setting is shown in Figure 6.10. Note that the small values of d_{odo} and d_{gps} in conjunction with sensor noise cause fluctuations in the values of s in the beginning of the plot. The plot illustrates that the two tested footprints have similar slip and skid values, when the same GAP setting is used. This result indicates that the choice of GAP mode is more important than the choice of footprint. With less slip in *FLConly* upslope the result contradicts the presumption.

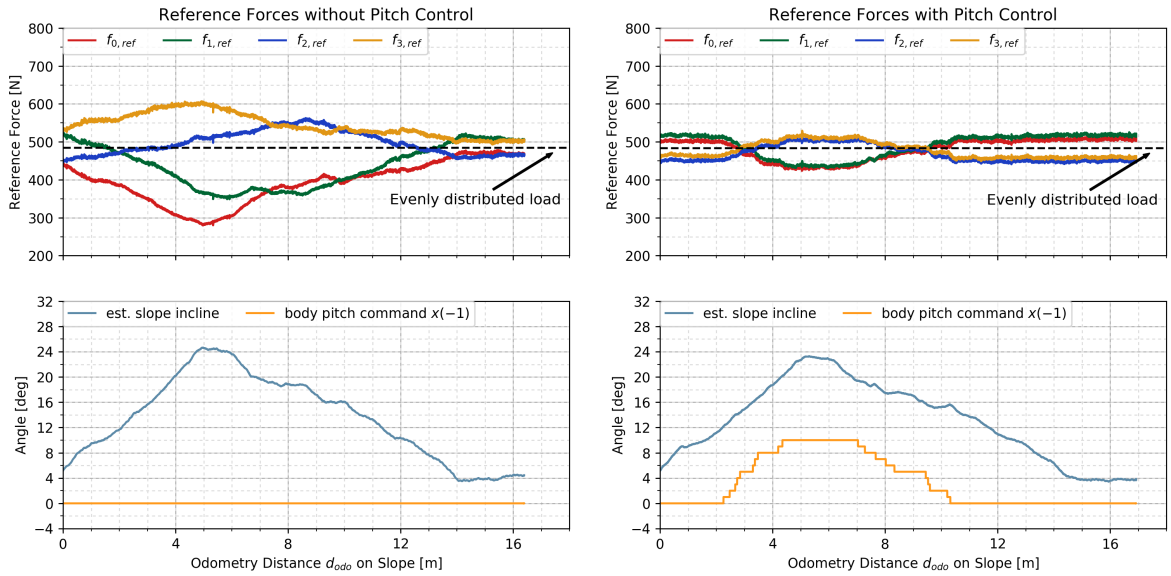

(a) *Run in* FLConly *mode. No pitch adaption to slope is conducted.*

(b) *Run in* FLC+RPA *mode. Body pitch adaption to slope leads to improved reference forces*

Figure 6.9: *Reference force comparison in two steep slope settings*

6.4.3 Conclusion

The steep slope experiments demonstrate the general ability of the rover system to climb slopes of at least 28° incline in different footprints and GAP modes. Several runs were successful with a high velocity setting (0.1 m/s), before the duri-crust was broken and fine powdered sand led to 100% slip in the subsequent runs. Reducing the rover velocity to 0.04 m/s allowed further slope climbing in the soft soil[(i)]. The rover was able to repeatedly climb the slope in the reduced velocity setting, no run had to be aborted due to slippage.

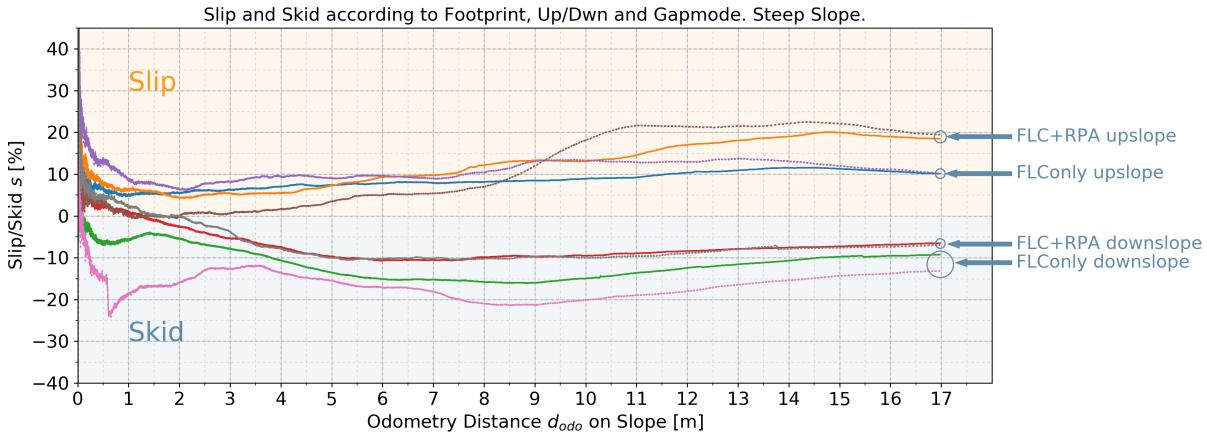

Figure 6.10: *Slip/Skid values separated by footprint, movement direction and GAP-mode. Solid lines: Cross-Stance, dashed lines: Y-Shape*

[(i)] For comparison: The MER top speed on hard flat ground is 0.05 m/s, its average velocity is 0.01 m/s [NASA-JPL, 2018b]

Influencing of reference forces by manipulating the rover's pitch angle is shown in the steep slope experiment. The load distribution onto the wheels can be positively influenced when controlling the pitch angle during slope ascend or descend. In the experiment, the pitch angle was manually adapted, an autonomous pitch control module can be implemented based on the data from the experiments.

Despite the improved load balancing between the wheels, the runs with active roll-pitch control show higher slip than the runs in *FLConly* mode. The reason is most likely to be found in the manual pitch changes: These are made stepwise when the LEPs approach the workspace limits. With step inputs, fast movements of the suspension legs can lead to temporary high force errors and consequently to increased slip. An automated gradual control needs to be implemented to exploit the benefits of improved load distribution. To conclude, positive influence of improved load balancing resulting from body pitching could not be found in this experiment setup. However, the improvement is aspired to be found with an appropriate GAP module.

The current result further substantiates to prefer the *FLConly* over *FLC+RPA* mode if not otherwise required, see also the results of the power analysis in Section 6.3. Concerning the choice of footprint, no significant performance difference was found between the chosen footprints.

6.5 Summary and Conclusion

This chapter of the thesis connects the results from the indoor and outdoor experiments. The experiments and results from the corresponding publications are presented in condensed form. Indoor experiments [4] [5] for general validation of active ground adaption strategies and system analysis close to physical limits are presented as well as an extensive field test campaign [1] [9] in Mars analogue terrain.

Force tracking errors are kept below 2% of the rover's gravitational force in the field experiments. On the indoor high frequency obstacle similar absolute errors are achieved, due to the reduced rover mass, the relative force tracking error is below 7% of the total rover mass. With active roll-pitch control, the absolute body angle errors on the high frequency obstacle is not exceeding ±0.5° neither for roll nor for pitch error values. The mean combined roll-pitch error (angle-axis representation) is reduced to 0.2° in the indoor experiments and the steep slope outdoor experiment. In the moderate slope setting it is reduced to 0.1°. These values demonstrate the ability of precise body angle control and general suspension system control while driving through rough terrain. This sophisticated control is achieved with simplistic offset generation, which facilitates future implementation on limited performance space qualified hardware.

Around 3%-6% of the total rover power requirement are due to the active ground adaption in natural terrain using the *FLConly* adaption mode. Power requirement increases when the roll-pitch control is added in the *FLC+RPA* mode but still does not exceed 10% of the rover total power. With the high frequency obstacle in the indoor experiments, the rover is tested close to the velocity limits of its suspension joints. Consequently, a higher power share for the suspension is found in this setting. In the high speed *FLC+EGC+RPA* setting, 21% of the total rover power are required for adaption to the artificial obstacle.

Particularly the power overhead found in the natural terrain experiments is considered to be tolerable given the reconfiguration possibilities, flexibility and redundancy introduced by the

active suspension system. The higher power overhead of the indoor experiments can be decreased with velocity adaption of the rover: The velocities tested by far exceed those executed by deployed rovers in planetary missions. The high speed setting uses a velocity one order of magnitude higher than current velocities of deployed systems [NASA-JPL, 2018b].

Steep slope climbing is successfully conducted in natural terrain slopes with inclines of up to 28°. Runs with 0.1 m/s are conducted, yet after the first runs the harsh crust of the surface is broken and the exposed soft soil on the slope results in 100% slip of the rover. With reduced velocity of 0.04 m/s all subsequent runs are conducted successfully. Rover slip is used as quality indication for slope climbing, less slip is considered to be a result of better ground adaption. Generally, the experiments indicated the slippage to be more dependant on the choice of GAP mode (*FLConly* vs. *FLC+RPA*) than on the footprint. However, a more detailed investigation with a broader range of footprints is required for a final conclusion in this matter.

6.6 Contributions of the Corresponding Publications

The publications contributing to this chapter present various experiments with the rover SherpaTT. Refinements of the motion control as presented in Chapter 5 are due to the experiments from these publications.

Both publications, [4] and [5], are presenting an experimental evaluation of the GAP module in a laboratory test environment. The evaluation focusses on the errors in force leveling and body angle control. Power requirements for the suspension system are not analyzed in these publications. For comparison with the outdoor settings, power analysis of the indoor experiments from [4] is conducted in the scope of this document.

In [5] the first set of experiments is presented. The approach is already shown to be viable, however, tuning of the controller parameters is suggested for improvements. With the experiments published in [4] improved results are reported on the same obstacle. However, an influence of each wheel on all remaining wheels in force leveling is revealed in this experiment set, leading to the revision of the implementation as described in Section 5.4 of this thesis.

The publication [9] provides a first overview on the conducted experiments with SherpaTT in the field test campaign. The test site for conduction of the experiments is described in this publication. Not only the experiments with SherpaTT but also the experimentation with the whole multi-robot system is highlighted in this publication.

A very broad discussion on the locomotive capabilities of SherpaTT is provided in the journal publication [1]. Detailed experiment setup descriptions with illustration of the ground characteristics are provided. Elaborate description of results and discussion of the findings is provided for the topics (i) power requirements, (ii) quality of load balancing between wheels, (iii) quality of body angle control, (iv) ground plane estimation, and (v) slope climbing capabilities in the three terrain settings.

7 Conclusion and Outlook

In this thesis the electromechanical design, implementation, locomotion control and experimental evaluation of a novel type of hybrid wheeled-leg exploration rover are presented. The electromechanical design of the active suspension provides the basis for advanced locomotive capabilities of the rover. Its control approach is reactive: no external data or a priory information as for example a terrain model is required to adapt the rover to irregular terrain. Only force readings at the wheels as well as body orientation from IMU data are required for the active ground adaption described in this thesis. The developed locomotion control system abstracts the complex kinematics of the suspension system and provides control inputs usable by autonomous behaviors or for human remote control. A central module of the motion control system is the ground adaption process with several controllers running in parallel. Each controller writes an own offset to the wheel position to match its ground adaption objective. This "simplistic" approach is an important benefit and crucial for future implementation on space relevant hardware with limited processing capabilities.

The rover is developed as part of a multi-robot system. A general mission scenario for heterogeneous modular multi-robot teams is developed and presented in this thesis. Possible tasks of the multi-robot system include, but are not limited to, cooperative mapping and exploration, sample retrieval, geological and biological research and infrastructure setup. The scenario is used as a guideline for the development of three multi-robot systems consecutively building on each other. With each incrementation a refinement of the system is conducted, bringing the developments towards increased feasibility and sophistication. A central part for modularity and reconfiguration within the multi-robot system is a common electromechanical interface. The design and implementation of this crucial part is presented. Experimental evaluation of the interface is highlighted, demonstrating its robustness and feasibility. Experiments concerning the cooperation of subsystems within the multi-robot systems are summarized in this thesis. The experiments include autonomous docking of two mobile systems, assembly of payload-devices from simple payload-items as well as legged scout climbing in an artificial crater environment and cooperative mapping in a multi-robot scenario.

Main focus of this thesis is on the locomotive capabilities of the rover with an actively articulated suspension system. The robot is evaluated independently of the multi-robot system as an individual robotic system. Experiments in laboratory environment and during an outdoor field deployment demonstrate the capabilities of the rover system. In the indoor environment, an obstacle simulating high surface roughness is used, while the field tests are conducted in a natural, Mars analogue terrain.

The active ground adaption is able to limit the ground contact force errors below 2% of the rover's gravitational force. Keeping all wheels in ground contact and reducing the load difference between the wheels reduces the torque differences between wheels and consequently

keeps the actuators close to their designated working point. With active body angle control the absolute error of roll and pitch can be kept well below 1° in all tested scenarios. The RMS error is reduced to 0.2° or below in all tested terrains and footprints. These values demonstrate the precision of body orientation control in rough terrain. Precise body angle control enables the robot to interact with mobile and immobile modular elements of the multi-robot deployment scenarios: The developed interface tolerates angle displacements of up to 7°.

Clearly, an active suspension needs to be powered in order to move its actuators. The experiments presented in this thesis show that the developed suspension system requires around 3%-6% of the total rover power to keep all wheels in ground contact in natural terrain. The mean absolute power for the suspension actuation can be as low as 7 W and is around 12 W in most cases for these experiment sets. Given the system's potential for fault recovery, e.g. getting out of sand pits, its locomotion reconfiguration possibilities and the general flexibility offered by the system, this power overhead is considered tolerable.

All experiments are conducted with velocities exceeding by far those employed by currently deployed space rovers. Despite these high velocities, steep slopes with up to 28° incline in natural terrain are negotiated with the system. Reducing the velocities bears the potential for reducing the power draw and increasing the difficulty of manageable terrain.

Due to the demonstrated capabilities of the rover, it will will be deployed in several projects and mission demonstration scenarios in the near future. Currently it is being prepared for a 1 km autonomous traverse in the Moroccan desert end of 2018. Additionally it will be used for deployment in a search and rescue scenario in the context of decontamination and deconstruction. Even though the rover already demonstrated its locomotion capabilities, further developments of the control system can be conducted to exploit the capabilities of the locomotive system.

The force leveling control presented is currently adapting the rover to the expected forces at each wheel resulting from terrain inclination and footprint configuration. A further module indirectly manipulating the reference forces can bear the potential for increased locomotive performance. Load distribution and thus the share of overall torque for each wheel is already shown to be improved with pitch control of the body. In moderate slopes active roll-pitch adaption indicates improved force tracking. With the manual control and step inputs for the commanded pitch angle in the steep slope setting this observation was not confirmed. Reactive body angle control dependent on the terrain inclines with a gradual adaption due to the current slope incline can thus be a part of a future active ground adaption behavior. Improved locomotion performance in slopes using an inclination-dependent lean behavior has already been shown for legged robots, e.g. the scout robot in the LUNARES scenario [10].

So-called reorientation holds of the system can be avoided by moving the wheel on a trajectory that ensures a smooth position and velocity trajectory for the WheelSteering joint. This is a behavior currently in development for SherpaTT.

An adaption module implementing a virtual spring is currently planned. The module shall make use of all three dimensions of the LEP offsets. When a force acts on the wheel, for example resulting from a rock the wheel is driving onto, a force-proportional displacement of the wheel is conducted using the offsets, which models the behavior of a mechanical spring. Improved obstacle negotiation is aspired using this module.

Alternative drive modes to the OmniDrive employed for the experiments presented in this thesis will be employed in future work. The comparison of different drive modes in terms of terrain performance allows to establish a metric for locomotion mode selection depending on terrain types.

Generally, all behaviors presented in this thesis are hand-crafted. With the rapidly growing field of artificial neural networks and (deep) learning strategies, further locomotive capabilities of the system can be explored and implemented.

In terms of the multi-robot systems, steep cliff exploration is aspired as the next research direction. It is planned to use the shuttle rover Coyote III as a rappelling robot, while the heavier SherpaTT is used as an anchor. The tether would be included in a modular payload-item, allowing settings with tether payout from the anchor or the rappelling robot. Locomotion control of the rappelling rover and tether management are of special interest in this scenario. Preliminary experiments into this direction were conducted in the field deployment and are highlighted in [9].

In general, the rover SherpaTT is designed for hostile environments as found on Mars and Moon. The rover is a self-contained system that can be used as an individual robot or in a multi-robot scenario. This bears the potential to be employed not only in heterogeneous multi-robot systems in extraterrestrial exploration but also for terrestrial application scenarios. Particularly in maritime environments more and more applications arise where robots are considered to be deployed, due to high risks for human life or high costs associated with human personell. This includes inspection of maritime infrastructure, e.g. offshore power plants as well as prospection and exploitation of maritime resources.

At the point of writing this thesis, an underwater version of SherpaTT is integrated and initially tested. The rover makes use of the same kinematics as presented for SherpaTT. The motion control system presented in this thesis can thus be used without functional adaptions for this rover as well. Figure 7.1 depicts SherpaUW, the underwater version of SherpaTT. Special attention is given to the sealing and waterproofness of the actuators. The deployment scenario is that of submarine resource utilization: The rover can harvest manganese nodules with reduced impact on the flora and fauna of the sea floor. In upcoming work, the rover will be subject to quantitative experimentation and evaluation in the context of a multi-robot submarine exploration system.

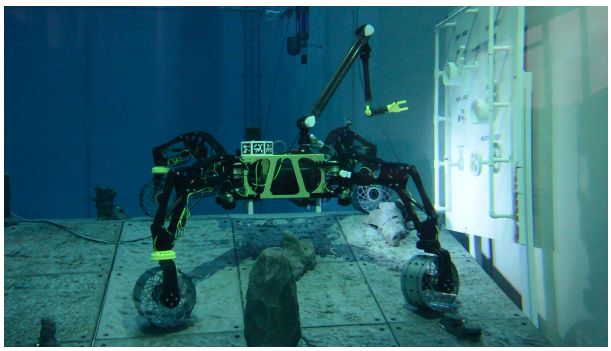

(a) *SherpaUW in an underwater manipulation scenario*

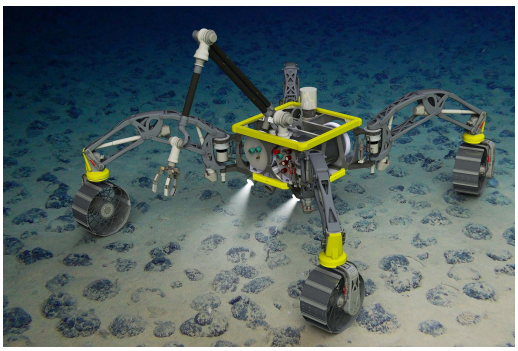

(b) *Artist rendering of submarine resource utilization*

Figure 7.1: *Terrestrial application example: SherpaUW*

Literature References

[Abad-Manterola et al., 2010] Abad-Manterola, P., Burdick, J. W., Nesnas, I. A. D., Chinchali, S., Fuller, C., and Zhou, X. (2010). Axel rover paddle wheel design, efficiency, and sinkage on deformable terrain. In *2010 IEEE International Conference on Robotics and Automation (ICRA'10)*, Anchorage, Alaska, USA.

[American Society for Testing and Materials, 2011] American Society for Testing and Materials (2011). Standard test method for evaluating emergency response robot capabilities: Mobility: Confined area terrains: Crossing pitch/roll ramps. Technical report, ASTM International, 100 Barr Harbor Drive, PO Box C700, West Conshohocken, PA.

[Apfelbeck et al., 2011] Apfelbeck, M., Kuss, S., Rebele, B., Michaud, S., Boesch, C., Krpoun, R., and Schaefer, B. (2011). Exomars phase b2 breadboard locomotion sub-system testcampaign. In *11th Symposium on Advanced Space Technologies for Robotics and Automation, (ASTRA'11)*.

[Azkarate et al., 2015] Azkarate, M., Zwick, M., Carrio, J. H., Nelen, R., Wiese, T., Joudrier, P. P. A., and Visentin, G. (2015). First experimental investigations on wheel-walking for improving triple-bogie rover locomotion performances. In *13th Symposium on Advanced Space Technologies for Robotics and Automation, (ASTRA'15)*.

[Bartlett et al., 2008] Bartlett, P., Wettergreen, D., and Whittaker, W. R. L. (2008). Design of the scarab rover for mobility and drilling in the lunar cold traps. In *9th International Symposium on Artificial Intelligence, Robotics and Automation in Space (i-SAIRAS'08)*.

[Bartsch, 2013] Bartsch, S. (2013). *Development, Control, and Empirical Evaluation of the Six-Legged Robot SpaceClimber Designed for Extraterrestrial Crater Exploration*. PhD thesis, University of Bremen, FB3, Bremen.

[Bartsch et al., 2016] Bartsch, S., Manz, M., Kampmann, P., Dettmann, A., Hanff, H., Langosz, M., v. Szadkowski, K., Hilljegerdes, J., Simnofske, M., Kloss, P., Meder, M., and Kirchner, F. (2016). Development and control of the multi-legged robot mantis. In *47st International Symposium on Robotics (ISR'16)*, pages 1–8.

[Besseron et al., 2008] Besseron, G., Grand, C., Amar, F. B., and Bidaud, P. (2008). Decoupled control of the high mobility robot hylos based on a dynamic stability margin. In *2008 IEEE/RSJ International Conference on Intelligent Robots and Systems (IROS'08)*, pages 2435–2440.

[Bickler, 1989] Bickler, D. B. (1989). Articulated suspension system. US-Patent US4840394 (A) – 1989-06-20 https://ntrs.nasa.gov/search.jsp?R=19900007837. Last access: 2018-02-06.

[Bindel and Bruns, 2010] Bindel, D. and Bruns, R. (2010). Reipos - relative interferometric position sensor. In *61st International Astronautical Congress, IAC 2010*.

[Boston Dynamics, 2018] Boston Dynamics (2018). Handle. Legs & wheels: The best of both worlds. Boston Dynamics homepage https://www.bostondynamics.com/handle. Last access 2018-02-08.

[Boynton et al., 2002] Boynton, W. V., Feldman, W. C., Squyres, S. W., Prettyman, T. H., Brückner, J., Evans, L. G., Reedy, R. C., Starr, R., Arnold, J. R., Drake, D. M., Englert, P. A. J., Metzger, A. E., Mitrofanov, I., Trombka, J. I., d'Uston, C., Wänke, H., Gasnault, O., Hamara, D. K., Janes, D. M., Marcialis, R. L., Maurice, S., Mikheeva, I., Taylor, G. J., Tokar, R., and Shinohara, C. (2002). Distribution of hydrogen in the near surface of mars: Evidence for subsurface ice deposits. *Science*, 297(5578):81–85.

[Brown and Jennings, 1995] Brown, R. G. and Jennings, J. S. (1995). A pusher/steerer model for strongly cooperative mobile robot manipulation. In *1995 IEEE/RSJ International Conference on Intelligent Robots and Systems (IROS'95)*, volume 3, pages 562–568 vol.3.

[Campion et al., 1996] Campion, G., Bastin, G., and Dandrea-Novel, B. (1996). Structural properties and classification of kinematic and dynamic models of wheeled mobile robots. *IEEE Transactions on Robotics and Automation*, 12(1):47 –62.

[Cao et al., 1997] Cao, Y. U., Fukunaga, A. S., and Kahng, A. (1997). Cooperative mobile robotics: Antecedents and directions. *Autonomous Robots*, 4(1):7–27.

[Clarke and Stoker, 2011] Clarke, J. D. and Stoker, C. R. (2011). Concretions in Exhumed and Inverted Channels near Hanksville Utah: Implications for Mars. *International Journal of Astrobiology*, 10(3):161–175.

[Dupuis et al., 2016] Dupuis, E., Picard, M., Haltigin, T., Lamarche, T., Rocheleau, S., and Gingras, D. (2016). Results from the csa's 2015 mars analogue mission in the desert of utah. In *13th International Symposium on Artificial Intelligence, Robotics and Automation in Space (i-SAIRAS'16)*, Bejing, China.

[Endo and Hirose, 1999] Endo, G. and Hirose, S. (1999). Study on roller-walker (system integration and basic experiments). In *1999 IEEE International Conference on Robotics and Automation (ICRA'99)*, volume 3.

[Endo and Hirose, 2011] Endo, G. and Hirose, S. (2011). Study on roller-walker – energy efficiency of roller-walk. In *2011 IEEE International Conference on Robotics and Automation (ICRA'11)*, Shanghai, China. IEEE.

[Farinelli et al., 2004] Farinelli, A., Iocchi, L., and Nardi, D. (2004). Multirobot systems: a classification focused on coordination. *IEEE Transactions on Systems, Man, and Cybernetics, Part B (Cybernetics)*, 34(5):2015–2028.

[Figueroa and Garvin, 2018] Figueroa, O. and Garvin, J. (2018). Following the water: The mars exploration program. Online Presentation https://www.hq.nasa.gov/mars/presentations/FTW/index.html. Last access: 2018-02-09.

[Fukuda and Nakagawa, 1988] Fukuda, T. and Nakagawa, S. (1988). Dynamically reconfigurable robotic system. In *1988 IEEE International Conference on Robotics and Automation (ICRA'88)*, pages 1581–1586 vol.3.

[Goldstein and Shotwell, 2009] Goldstein, B. and Shotwell, R. (2009). Phoenix: The first mars scout mission. In *2009 IEEE Aerospace Conference (IAC'09)*, pages 1 –20, New York, USA.

[Grand et al., 2004a] Grand, C., BenAmar, F., Plumet, F., and Bidaud, P. (2004a). Decoupled control of posture and trajectory of the hybrid wheel-legged robot hylos. In *2004 IEEE International Conference on Robotics and Automation (ICRA 2004)*, volume 5, pages 5111–5116.

[Grand et al., 2004b] Grand, C., Benamar, F., Plumet, F., and Bidaud, P. (2004b). Stability and traction optimization of a reconfigurable wheel-legged robot. *The International Journal of Robotics Research*, 23(10-11):1041–1058.

[Haarmann et al., 2012] Haarmann, R., Jaumann, R., Claasen, F., Apfelbeck, M., Klinkner, S., Richter, L., Schwendner, J., Wolf, M., and Hofmann, P. (2012). Mobile payload element (mpe): Concept study for a sample fetching rover for the ESA lunar lander mission. *Planetary and Space Science*, 74(1):283 – 295. Scientific Preparations For Lunar Exploration.

[Harrington and Voorhees, 2004] Harrington, B. D. and Voorhees, C. (2004). The challenges of designing the rocker-bogie suspension for the mars exploration rover. In *37th Aerospace Mechanisms Symposium*.

[Haynes et al., 2017] Haynes, G. C., Stager, D., Stentz, A., Vande Weghe, J. M., Zajac, B., Herman, H., Kelly, A., Meyhofer, E., Anderson, D., Bennington, D., Brindza, J., Butterworth, D., Dellin, C., George, M., Gonzalez-Mora, J., Jones, M., Kini, P., Laverne, M., Letwin, N., Perko, E., Pinkston, C., Rice, D., Scheifflee, J., Strabala, K., Waldbaum, M., and Warner, R. (2017). Developing a robust disaster response robot: Chimp and the robotics challenge. *Journal of Field Robotics*, 34(2):281–304.

[Heverly et al., 2010] Heverly, M., Matthews, J., Frost, M., and McQuin, C. (2010). Development of the tri-athlete lunar vehicle prototype. In *40th Aerospace Mechanisms Symposium*, NASA Kennedy Space Center.

[Heverly et al., 2013] Heverly, M., Matthews, J., Lin, J., Fuller, D., Maimone, M., Biesiadecki, J., and Leichty, J. (2013). Traverse performance characterization for the mars science laboratory rover. *Journal of Field Robotics*, 30(6):835–846.

[Huntsberger et al., 2007] Huntsberger, T., Stroupe, A., Aghazarian, H., Garrett, M., Younse, P., and Powell, M. (2007). Tressa: Teamed robots for exploration and science on steep areas. *Journal of Field Robotics*, 24(11-12):1015–1031.

[Iagnemma and Dubowsky, 2004] Iagnemma, K. and Dubowsky, S. (2004). *Mobile Robots in Rough Terrain – Estimation, Motion Planning, and Control with Application to Planetary Rovers*, volume 12 of *Springer Tracts in Advanced Robotics*. Springer-Verlag Berlin Heidelberg.

[Iagnemma et al., 2003] Iagnemma, K., Rzepniewski, A., Dubowsky, S., and Schenker, P. (2003). Control of robotic vehicles with actively articulated suspensions in rough terrain. *Autonomous Robots*, 14(1):5–16.

[Iagnemma et al., 2000] Iagnemma, K. D., Rzepniewski, A., Dubowsky, S., Pirjanian, P., Huntsberger, T. L., and Schenker, P. S. (2000). Mobile robot kinematic reconfigurability for rough-terrain. In *2000 Sensor Fusion and Decentralized Control in Robotic Systems Conference*, pages 413–420.

[Johnson et al., 2017] Johnson, M., Shrewsbury, B., Bertrand, S., Calvert, D., Wu, T., Duran, D., Stephen, D., Mertins, N., Carff, J., Rifenburgh, W., Smith, J., Schmidt-Wetekam, C., Faconti, D., Graber-Tilton, A., Eyssette, N., Meier, T., Kalkov, I., Craig, T., Payton, N., McCrory, S., Wiedebach, G., Layton, B., Neuhaus, P., and Pratt, J. (2017). Team ihmc's lessons learned from the darpa robotics challenge: Finding data in the rubble. *Journal of Field Robotics*, 34(2):241–261.

[Kamimura et al., 2005] Kamimura, A., Kurokawa, H., Yoshida, E., Murata, S., Tomita, K., and Kokaji, S. (2005). Automatic locomotion design and experiments for a modular robotic system. *IEEE/ASME Transactions on Mechatronics*, 10(3):314–325.

[Karumanchi et al., 2017] Karumanchi, S., Edelberg, K., Baldwin, I., Nash, J., Reid, J., Bergh, C., Leichty, J., Carpenter, K., Shekels, M., Gildner, M., Newill-Smith, D., Carlton, J., Koehler, J., Dobreva, T., Frost, M., Hebert, P., Borders, J., Ma, J., Douillard, B., Backes, P., Kennedy, B., Satzinger, B., Lau, C., Byl, K., Shankar, K., and Burdick, J. (2017). Team robosimian: Semi-autonomous mobile manipulation at the 2015 darpa robotics challenge finals. *Journal of Field Robotics*, 34(2):305–332.

[Klein et al., 2014] Klein, E., Nilsen, E., Nicholas, A., Whetsel, C., Parrish, J., Mattingly, R., and May, L. (2014). The mobile mav concept for mars sample return. In *2014 IEEE Aerospace Conference (IAC'14)*, pages 1–9.

[Kotov, 1997] Kotov, V. (1997). Systems of systems as communicating structures. Technical Report HPL-97-124, Hewlett Packard (Computer Systems Laboratory), http://www.hpl.hp.com/techreports/97/HPL-97-124.pdf. Last access: 2018-02-14.

[Krotkov et al., 2017] Krotkov, E., Hackett, D., Jackel, L., Perschbacher, M., Pippine, J., Strauss, J., Pratt, G., and Orlowski, C. (2017). The darpa robotics challenge finals: Results and perspectives. *Journal of Field Robotics*, 34(2):229–240.

[Kucherenko et al., 2004] Kucherenko, V., Bogatchev, A., and van Winnendael, M. (2004). Chassis concepts for the exomars rover. In *8th ESA Workshop on Advanced Space Technologies for Robotics and Automation (ASTRA'04)*.

[Lakdawalla, 2016] Lakdawalla, E. (2016). Fun with a new data set: Chang'e 3 lander and yutu rover camera data. The Planetary Society http://www.planetary.org/blogs/emily-lakdawalla/2016/01281656-fun-with-a-new-data-set-change.html. Last Access: 2018-02-21.

[Lamon and Siegwart, 2003] Lamon, P. and Siegwart, R. (2003). 3d-odometry for rough terrain – towards real 3d navigation. In *2003 IEEE International Conference on Robotics and Automation (ICRA'03)*, volume 1, pages 440–445.

[Lamon and Siegwart, 2004] Lamon, P. and Siegwart, R. (2004). Inertial and 3d-odometry fusion in rough terrain – towards real 3d navigation. In *2004 IEEE/RSJ International Conference on Intelligent Robots and Systems (IROS'04)*, volume 2, pages 1716–1721 vol.2.

[Lemburg et al., 2011] Lemburg, J., de Gea Fernandez, J., Eich, M., Mronga, D., Kampmann, P., Vogt, A., Aggarwal, A., Shi, Y., and Kirchner, F. (2011). Aila - design of an autonomous mobile dual-arm robot. In *2011 IEEE International Conference on Robotics and Automation (ICRA'11)*, pages 5147–5153.

[Lim et al., 2017] Lim, J., Lee, I., Shim, I., Jung, H., Joe, H. M., Bae, H., Sim, O., Oh, J., Jung, T., Shin, S., Joo, K., Kim, M., Lee, K., Bok, Y., Choi, D.-G., Cho, B., Kim, S., Heo, J., Kim, I., Lee, J., Kwon, I. S., and Oh, J.-H. (2017). Robot system of drc-hubo+ and control strategy of team kaist in darpa robotics challenge finals. *Journal of Field Robotics*, 34(4):802–829.

[Lindemann and Voorhees, 2005] Lindemann, R. and Voorhees, C. (2005). Mars exploration rover mobility assembly design, test and performance. In *2005 IEEE International Conference on Systems, Man and Cybernetics (SMC'05)*, volume 1, pages 450–455 Vol. 1.

[LROC-Team, 2018] LROC-Team (2018). LROC (lunar reconnaissance orbiter camera) quickmap tool. Lunar mapping tool (online): http://target.lroc.asu.edu/q3/. Last access: 2018-02-20.

[Manz et al., 2012] Manz, M., Dettmann, A., Hilljegerdes, J., and Kirchner, F. (2012). Development of a lightweight manipulator arm using heterogeneous materials and manufacturing technologies. In *11th International Symposium on Artificial Intelligence, Robotics and Automation in Space (i-SAIRAS'12)*. o.A.

[Manz et al., 2014] Manz, M., Sonsalla, R. U., Hilljegerdes, J., Oekermann, C., Schwendner, J., Bartsch, S., and Ptacek, S. (2014). Design of a rover for mobile manipulation in uneven terrain in the context of the spacebot cup. In *12th International Symposium on Artificial Intelligence, Robotics and Automation in Space (i-SAIRAS'14)*.

[Michaud et al., 2008] Michaud, S., Gibbesch, A., Thueer, T., Krebs, A., Lee, C., Despont, B., Schaefer, B., and Slade, R. (2008). Development of the exomars chassis and locomotion subsystem. In *9th International Symposium on Artificial Intelligence, Robotics and Automation in Space (i-SAIRAS'08)*.

[Mumm et al., 2004] Mumm, E., Farritor, S., Pirjanian, P., Leger, C., and Schenker, P. (2004). Planetary cliff descent using cooperative robots. *Autonomous Robots*, 16(3):259–272.

[NASA-JPL, 2018a] NASA-JPL (2018a). Mars exploration rover mission. http://marsrovers.jpl.nasa.gov/overview/. Last access 2018-02-06.

[NASA-JPL, 2018b] NASA-JPL (2018b). Spacecraft: Surface Operations: Rover. https://mars.nasa.gov/mer/mission/spacecraft_rover_wheels.html. Last Access: 2018-04-11.

[NASA-JPL, 2018c] NASA-JPL (2018c). Spirit (MER-A) Mission. https://www.jpl.nasa.gov/missions/mars-exploration-rover-spirit-mer/. Last Access: 2018-02-06.

[Nesnas et al., 2012] Nesnas, I. A., Matthews, J. B., Abad-Manterola, P., Burdick, J. W., Edlund, J. A., Morrison, J. C., Peters, R. D., Tanner, M. M., Miyake, R. N., Solish, B. S., and Anderson, R. C. (2012). Axel and duaxel rovers for the sustainable exploration of extreme terrains. *Journal of Field Robotics*.

[Nilsen et al., 2012] Nilsen, E., Whetsel, C., and Mattingly, R. (2012). Mars sample return campaign status. In *2012 IEEE Aerospace Conference*, Big Sky, MT, USA.

[Ostergaard et al., 2006] Ostergaard, E., Kassow, K., Beck, R., and Lund, H. (2006). Design of the atron lattice-based self-reconfigurable robot. *Autonomous Robots*, 21(2):165–183.

[Park and Yim, 2009] Park, M. and Yim, M. (2009). Distributed control and communication fault tolerance for the ckbot. In *2009 ASME/IFToMM International Conference on Reconfigurable Mechanisms and Robots (ReMAR'09)*, pages 682–688.

[Parker et al., 2016] Parker, L. E., Rus, D., and Sukhatme, G. (2016). *Multiple Mobile Robot Systems*, chapter 53, pages 1335–1379. Springer Handbook of Robotics.

[Pirjanian et al., 2002] Pirjanian, P., Leger, C., Mumm, E., Kennedy, B., Garrett, M., Aghazarian, H., Farritor, S., and Schenker, P. (2002). Distributed control for a modular, reconfigurable cliff robot. In *2002 IEEE International Conference on Robotics and Automation (ICRA'02)*, volume 4, pages 4083–4088 vol.4.

[Prakash et al., 2008] Prakash, R., Burkhart, P. D., Chen, A., Comeaux, K. A., Guernsey, C. S., Kipp, D. M., Lorenzoni, L. V., Mendeck, G. F., Powell, R. W., Rivellini, T. P., Martin, A. M. S., Sell, S. W., Steltzner, A. D., and Way, D. W. (2008). Mars science laboratory entry, descent, and landing system overview. In *2008 IEEE Aerospace Conference (IAC'08)*, pages 1–18.

[Reid et al., 2014] Reid, W., Göktogan, A. H., and Sukkarieh, S. (2014). Moving mammoth: Stable motion for a reconfigurable wheel-on-leg rover. In *2014 Australasian Conference on Robotics and Automation*.

[Reid et al., 2016] Reid, W., Perez-Grau, F. J., Goetogan, A. H., and Sukkarieh, S. (2016). Actively articulated suspension for a wheel-on-leg rover operating on a martian analog surface. In *2016 IEEE International Conference on Robotics and Automation (ICRA)*, pages 5596–5602, Stockholm, Sweden.

[Schenker et al., 2001] Schenker, P. S., Huntsberger, T. L., Pirjanian, P., Baumgartner, E., Aghazarian, H., Trebi-ollennu, A., Leger, P. C., Cheng, Y., Backes, P. G., Tunstel, E. W., Propulsion, J., and Dubowsky, L. S. (2001). Robotic automation for space: Planetary surface exploration, terrain-adaptive mobility, and multi-robot cooperative tasks. In Hall, D. P. C. E. L., editor, *2001 Intelligent Robots and Computer Vision XX: Algorithms, Techniques, and Active Vision conference*, volume 4572, pages 12–28, Boston, MA, USA.

[Schenker et al., 2003] Schenker, P. S., Huntsberger, T. L., Pirjanian, P., Baumgartner, E. T., and Tunstel, E. (2003). Planetary rover developments supporting mars exploration, sample return and future human-robotic colonization. *Autonomous Robots*, 14(2-3):103–126.

[Schenker et al., 2000] Schenker, P. S., Pirjanian, P., Balaram, B., Ali, K. S., Trebi-ollennu, A., Huntsberger, T. L., Kennedy, H. A. B. A., Baumgartner, E. T., Rzepniewski, A., and Dubowsky, S. (2000). Reconfigurable robots for all terrain exploration. In *Sensor Fusion and Decentralized Control in Robotic Systems III*, volume 4196 of *SPIE*, pages 419–6.

[Schwarz et al., 2017] Schwarz, M., Rodehutskors, T., Droeschel, D., Beul, M., Schreiber, M., Araslanov, N., Ivanov, I., Lenz, C., Razlaw, J., Schueller, S., Schwarz, D., Topalidou-Kyniazopoulou, A., and Behnke, S. (2017). Nimbro rescue: Solving disaster-response tasks with the mobile manipulation robot momaro. *Journal of Field Robotics*, 34(2):400–425.

[Shen et al., 2010] Shen, W.-M., Hou, F., Rubenstein, M., Chiu, H., and Kamimura, A. (2010). Recent progress of superbot. In *ICRA 2010 Workshop "Modular Robots: State of the Art"*.

[Sonsalla et al., 2015] Sonsalla, R., Akpo, J. B., and Kirchner, F. (2015). Coyote III: Development of a modular and highly mobile micro rover. In *13th Symposium on Advanced Space Technologies in Robotics and Automation (ASTRA'15)*.

[Stone, 1996] Stone, H. (1996). Mars pathfinder microrover a small, low-cost, low-power spacecraft. In *1996 AIAA Forum on Advanced Developments in Space Robotics*.

[Stoy et al., 2010] Stoy, K., Nagpal, R., and Shen, W.-M., editors (2010). *2010 IEEE International Conference on Robotics and Automation (ICRA'10). Workshop Modular Robots: The State of the Art*, Anchorage, AK, USA. IEEE.

[Thueer et al., 2006] Thueer, T., Krebs, A., and Siegwart, R. (2006). Comprehensive locomotion performance evaluation of all-terrain robots. In *2006 IEEE/RSJ International Conference on Intelligent Robots and Systems (IROS'06)*, pages 4260–4265.

[Townsend et al., 2010] Townsend, J., Biesiadecki, J., and Collins, C. (2010). Athlete mobility performance with active terrain compliance. In *2010 IEEE Aerospace Conference (IAC'10)*, pages 1–7.

[Volpe, 2005] Volpe, R. (2005). Rover technology development and mission infusion beyond mer. In *2005 IEEE Aerospace Conference (IAC'05)*, pages 971–981.

[Welch et al., 2013] Welch, R., Limonadi, D., and Manning, R. (2013). Systems engineering the curiosity rover: A retrospective. In *2013 IEEE International Conference on System of Systems Engineering (SoSE'13)*, pages 70–75.

[Wettergreen et al., 2009a] Wettergreen, D., Jonak, D., Kohanbash, D., Moreland, S., Spiker, S., and Teza, J. (2009a). Field experiments in mobility and navigation with a lunar rover prototype. In *7th International Conference on Field and Service Robotics*, Cambridge, Massachusetts.

[Wettergreen et al., 2009b] Wettergreen, D., Jonak, D., Kohanbash, D., Moreland, S. J., Spiker, S., Teza, J., and Whittaker, W. R. L. (2009b). Design and experimentation of a rover concept for lunar crater resource survey. In *47th AIAA Aerospace Sciences Meeting Including The New Horizons Forum and Aerospace Exposition*.

[Wilcox et al., 2007] Wilcox, B., Litwin, T., Biesiadecki, J., Matthews, J., Heverly, M., Morrison, J., Townsend, J., Ahmad, N., Sirota, A., and Cooper, B. (2007). Athlete: A cargo handling and manipulation robot for the moon. *Journal of Field Robotics*, 24(5):421.

[Wilcox, 2012] Wilcox, B. H. (2012). Athlete: A limbed vehicle for solar system exploration. In *2012 IEEE Aerospace Conference (IAC'12)*, pages 1–9.

[Yim et al., 2000] Yim, M., Duff, D. G., and Roufas, K. D. (2000). Polybot: A modular reconfigurable robot. In *2000 IEEE International Conference on Robotics and Automation (ICRA'00)*, San Francisco, CA. IEEE.

[Yim et al., 2009] Yim, M., White, P., Park, M., and Sastra, J. (2009). *Modular Self-Reconfigurable Robots*, pages 5618–5631. Springer New York, New York, NY.

[Zenzes et al., 2016] Zenzes, M., Kampmann, P., Stark, T., and Schilling, M. (2016). Ndlcom: Simple protocol for heterogeneous embedded communication networks. In *Embedded World Exhibition & Conference*, Nürnberg, Germany.

[Zykov et al., 2007] Zykov, V., Mytilinaios, E., Desnoyer, M., and Lipson, H. (2007). Evolved and designed self-reproducing modular robotics. *IEEE Transactions on Robotics*, 23(2):308 –319.

Own Publications

[1] F. Cordes, F. Kirchner, and A. Babu, "Field testing of a rover with active suspension system in a mars analogue terrain.," *Journal of Field Robotics*, 2018.

[2] T. M. Roehr, F. Cordes, and F. Kirchner, "Reconfigurable integrated multirobot exploration system (RIMRES): Heterogeneous modular reconfigurable robots for space exploration," *Journal of Field Robotics*, vol. Special Issue on Space Robotics, Part 2, pp. 3–34, 2014.

[3] F. Cordes, I. Ahrns, S. Bartsch, T. Birnschein, A. Dettmann, S. Estable, S. Haase, J. Hilljegerdes, D. Koebel, S. Planthaber, T. Roehr, M. Scheper, and F. Kirchner, "Lunares: lunar crater exploration with heterogeneous multi robot systems," *Intelligent Service Robotics*, pp. 1–29, 2010. 10.1007/s11370-010-0081-4.

[4] F. Cordes, A. Babu, and F. Kirchner, "Static force distribution and orientation control for a rover with an actively articulated suspension system," in *2017 IEEE/RSJ International Conference on Intelligent Robots and Systems (IROS'17)*, (Vancouver, Canada), ©2017 IEEE. Reprinted with permission, Sept. 2017.

[5] F. Cordes and A. Babu, "SherpaTT: A versatile hybrid wheeled-leg rover," in *13th International Symposium on Artificial Intelligence, Robotics and Automation in Space (i-SAIRAS'16)*, (Bejing, P.R. China), June 2016.

[6] F. Cordes, C. Oekermann, A. Babu, D. Kuehn, T. Stark, and F. Kirchner, "An active suspension system for a planetary rover," in *12th International Symposium on Artificial Intelligence, Robotics and Automation in Space (i-SAIRAS'14)*, (Montreal, Canada), June 2014.

[7] F. Cordes, A. Dettmann, and F. Kirchner, "Locomotion modes for a hybrid wheeled-leg planetary rover," in *2011 IEEE International Conference on Robotics and Biomemetics (RoBio'11)*, (Phuket, Thailand), ©2011 IEEE. Reprinted with permission, Dec. 2011.

[8] F. Cordes and F. Kirchner, "Heterogeneous robotic teams for exploration of steep crater environments," in *2010 IEEE Conference on Robotics and Automation (ICRA'10), Planetary Rovers Workshop*, (Anchorage, AK, USA), May 2010.

[9] R. U. Sonsalla, F. Cordes, L. Christensen, T. M. Roehr, T. Stark, S. Planthaber, M. Maurus, M. Mallwitz, and E. A. Kirchner, "Field testing of a cooperative multi-robot sample return mission in mars analogue environment," in *14th Symposium on Advanced Space Technologies in Robotics and Automation (ASTRA'17)*, (Leiden, The Netherlands), June 2017.

[10] S. Bartsch, F. Cordes, S. Haase, S. Planthaber, T. M. Roehr, and F. Kirchner, "Performance evaluation of an heterogeneous multi-robot system for lunar crater exploration," in *10th International Symposium on Artificial Intelligence, Robotics and Automation in Space (iSAIRAS'10)*, (Sapporo, Japan), Sept. 2010.

[11] R. Sonsalla, F. Cordes, L. Christensen, S. Planthaber, J. Albiez, I. Scholz, and F. Kirchner, "Towards a heterogeneous modular robotic team in a logistic chain for extraterrestrial exploration," in *12th International Symposium on Artificial Intelligence, Robotics and Automation in Space (i-SAIRAS'14)*, (Montreal, Canada), June 2014.

[12] A. Dettmann, Z. Wang, W. Wenzel, F. Cordes, and F. Kirchner, "Heterogeneous modules with a homogeneous electromechanical interface in multi-module systems for space exploration," in *2011 IEEE International Conference on Robotics and Automation (ICRA'11)*, (Shanghai, P.R. China), ©2011 IEEE. Reprinted with permission, May 2011.

[13] W. Wenzel, F. Cordes, and F. Kirchner, "A robust electro-mechanical interface for cooperating heterogeneous multi-robot teams," in *2015 IEEE International Conference on Intelligent Robots and Systems (IROS'15)*, (Hamburg, Germany), pp. 1732–1737, ©2015 IEEE. Reprinted with permission, Sept. 2015.

[14] J. H. Carrio and F. Cordes, "Kinematics modeling of a hybrid wheeled-leg planetary rover," in *11th International Symposium on Artificial Intelligence, Robotics and Automation in Space (i-SAIRAS'12)*, (Turin, Italy), June 2012.

[15] A. Dettmann, M. Roemmermann, and F. Cordes, "Evolutionary development of an optimized manipulator arm morphology for manipulation and rover locomotion," in *2011 IEEE International Conference on Robotics and Biomemetics (RoBio'11)*, (Phuket, Thailand), ©2011 IEEE. Reprinted with permission, Dec. 2011.

[16] O. Kroemer, D. Beermann, F. Cordes, C. Lange, B. Littau, R. Rosta, M. Scharringhausen, T. van Zoest, and C. Grimm, "Adaptive flexible wheels for planetary exploration," in *62nd International Astronautical Congress (IAC'11)*, (Cape Town, South Africa), Oct. 2011.

[17] F. Cordes, S. Planthaber, I. Ahrns, S. Bartsch, T. Birnschein, and F. Kirchner, "Cooperating reconfigurable robots for autonomous planetary sample return missions," in *ASME/IFToMM International Conference on Reconfigurable Mechanisms and Robots (ReMAR'09)*, (London, United Kingdom), pp. 665–673, June 2009.

[18] T. M. Roehr, F. Cordes, I. Ahrns, and F. Kirchner, "Cooperative docking procedures for a lunar mission," in *41st International Symposium on Robotics and 6th German Conference on Robotics (ISR/Robotik'10)*, (Munich, Germany), June 2010.

[19] F. Cordes, D. Bindel, C. Lange, and F. Kirchner, "Towards a modular reconfigurable heterogenous multi-robot exploration system," in *10th International Symposium on Artificial Intelligence, Robotics and Automation in Space (i-SAIRAS'10)*, (Hokkaido, Japan), pp. 38–45, Sept. 2010.

[20] F. Cordes, T. M. Roehr, and F. Kirchner, "RIMRES: A modular reconfigurable heterogeneous multi-robot exploration system," in *11th International Symposium on Artificial Intelligence, Robotics and Automation in Space (i-SAIRAS'12)*, (Turin, Italy), June 2012.

[21] T. M. Roehr, F. Cordes, and F. Kirchner, "RIMRES: A project summary," in *2013 IEEE Conference on Robotics and Automation (ICRA'13), Workshop proceedings*, (Karlsruhe, Germany), May 2013.

[22] S. Planthaber, M. Maurus, B. Bongardt, M. Mallwitz, L. M. V. Benitez, L. Christensen, F. Cordes, R. U. Sonsalla, T. Stark, and T. M. Roehr, "Controlling a semi-autonomous robot team from a virtual environment," in *Human Robot Interaction Conference (HRI'2017)*, (Vienna, Austria), Mar. 2017.

[23] W. Brinkmann, S. Bartsch, R. U. Sonsalla, F. Cordes, D. Kuehn, and F. Kirchner, "Advanced robotic systems in the context of future space exploration," in *69th International Astronautical Congress (IAC'18)*, 2018.

[24] W. Wenzel, F. Cordes, A. Dettmann, and Z. Wang, "Evaluation of a dust-resistant docking mechanism for surface exploration robots," in *15th International Conference On Advanced Robotics (ICAR'11)*, (Talinn, Estonia), pp. 495–500, June 2011.

[25] Z. Wang, F. Cordes, A. Dettmann, and R. Szczuka, "Evaluation of a power management system for heterogeneous modules in self-reconfigurable multi-module systems," in *2011 IEEE/RSJ International Conference on Intelligent Robots and Systems (IROS'11)*, (San Francisco, CA, USA), ©2011 IEEE. Reprinted with permission, Sept. 2011.

[26] W. Brinkmann, T. M. Roehr, S. Natarajan, F. Cordes, R. U. Sonsalla, R. Szczuka, S. Bartsch, and F. Kirchner, "Design and evaluation of an end-effector for a reconfigurable multi-robot system for future planetary missions," in *2018 IEEE Aerospace Conference (AeroConf'18)*, (Big Sky, MT, USA), ©2018 IEEE. Reprinted with permission, Mar. 2018.

[27] W. Brinkmann, F. Cordes, T. M. Roehr, L. Christensen, T. Stark, R. U. Sonsalla, R. Szczuka, N. A. Mulsow, and D. Kuehn, "Modular payload-items for payload-assembly and system enhancement for future planetary missions," in *2018 IEEE Aerospace Conference (AeroConf'18)*, (Big Sky, MT, USA), ©2018 IEEE. Reprinted with permission, Mar. 2018.

[28] S. Bartsch, T. Birnschein, F. Cordes, D. Kuehn, P. Kampmann, J. Hilljegerdes, S. Planthaber, M. Roemmermann, and F. Kirchner, "SpaceClimber: Development of a six-legged climbing robot for space exploration," in *41st International Symposium on Robotics and 6th German Conference on Robotics (ISR/Robotik'10)*, (Munich, Germany), June 2010.

[29] F. Cordes, S. Bartsch, T. Birnschein, D. Kuehn, and F. Kirchner, "Towards an intelligent foot for walking and climbing robots," in *Proceedings of the 41st International Symposium on Robotics and 6th German Conference on Robotics, (ISR Robotik-2010)*, 2010.

[30] T. Birnschein, G. Natarajan, S. Bartsch, F. Cordes, D. Kuehn, and F. Kirchner, "Terrain recognition and environment modeling in legged robots," in *11th European Regional Conference of the International Society for Terrain-Vehicle Systems (ISTVS'09)*, (Bremen, Germany), Oct. 2009.

[31] Y. Dobrev, C. Reustle, T. Pavlenko, F. Cordes, and M. Vossiek, "Mobile robot 6d pose estimation using a wireless localization network," in *2016 IEEE MTT-S International Conference on Microwaves for Intelligent Mobility (ICMIM'16)*, (San Diego, CA, USA), pp. 1–4, May 2016.

[32] M. Roemmermann, D. Kuehn, F. Cordes, Y.-H. Yoo, and F. Kirchner, "Concept evaluation of modeling terrain mechanics by a neural network," in *11th European Regional Conference of the International Society for Terrain-Vehicle Systems (ISTVS'09)*, (Bremen, Germany), Oct. 2009.

[33] T. Lutz, C. Gu, S. Gardecki, F. Cordes, T. Homingo, A. Boeljes, and P. de Maagt, "Startiger dropter project: Development and flight experiment of a skycrane-like terrestrial lander demonstrator," in *ESA GNC 2014: 9th International ESA Conference on Guidance, Navigation and Control Systems, (GNC'14)*, (Oporto, Portugal), June 2014.

[34] T. Hormigo, C. Gu, T. Lutz, S. Gardecki, F. Cordes, A. Boeljes, J. Bolz, and P. D. Maagt, "Startiger dropter project: Integrated, closed-loop vision-aided navigation with hazard detection and avoidance," in *ESA GNC 2014: 9th International ESA Conference on Guidance, Navigation and Control Systems, (GNC'14)*, (Oporto, Portugal), June 2014.

A Additional Material

This chapter contains additional material such as system specifications and experiment data previously not published in this form. All data presented here is based on the publications [1] [4] [12] [13].

A.1 System Specification Tables: EMI

The key specifications of the EMI are listed in Table A.1.

Table A.1: *EMI system specifications. Valid for both genreations if not otherwise stated.*

Description	Value	Comments
	Main Features	
Orientations for connection	4	
Powerbus	✓	44.4 V nom (36 V-52 V)
Local Communication	✓	RS422
Global Communication	✓	100Mbit ethernet
Maintain connection powerless	✓	
In-system charging	(✓)	Second generation only
	Mechanical Interface	
Max tested static load	400 N	First generation
Max tested static load	1300 N	Second generation
Max angle for undocking	30°	Roll or pitch. Max for passive EMI to slide out of latch of active EMI
Max dust layer	2 mm	Closed layer of dust. Not interfering mechanical nor electrical connection.
	Electrical Interface	
Number of connection pins	15	First generation: 4× RS-422, 4× eth, 2× PWR, 4× EMI-ctrl, 1× N.C.
	18	Second generation: Additionally 2× power and 1× orientation detection
Max permanent current on power bus	5 A	First generation
	10 A	Second generation
	Sensors	
Camera	e-cam32	For visual servoing in docking process. 640px × 480px, 7fps.
Position of latch	Potentiometer	
IMU	MPU6050	Acceleration and gyroscope. Second generation only.
Voltage and current sensing	✓	Multiple sensors per EMI

A.2 System Specification Tables: Manipulation Arm

This section contains the specification data tables for the manipulation arm. The arm is employed on both rover versions.

Table A.2: *Resulting link lengths of evolutionary arm optimization*

Link	Length
DH1D	500 mm
DH1A	225 mm
DH2A	735 mm
DH3D	30 mm
DH4A	30 mm
DH5D	695 mm
DH7D	300 mm

Table A.3: *Specification of the manipulator arm joints*

Joint	Range	Angular Velocity	Repeatable Peak Torque
DoF1 (vert)	720°	31°/*s*	520 Nm
DoF2 (horiz)	200°	7.0°/*s*	866 Nm
DoF3 (horiz)	280°	7.0°/*s*	433 Nm
DoF4 (wrist)	720°	130°/*s*	92 Nm
DoF5 (wrist)	270°	130°/*s*	92 Nm
DoF6 (wrist)	720°	130°/*s*	92 Nm

A.3 System Specification Tables: Sherpa

This section provides some key values of Sherpa. Table A.4 provides key features of Sherpa, while Table A.5 lists the actuator specifications.

Table A.4: *Sherpa system specifications [2]*

Description	Value	Comments
Performance Characterization		
Step & Obstacle Height	900 mm	Active stepping nessecary
Max. ground clearance	711 mm	
Min. ground clearance	-189 mm	LEPs above body; body touching ground
Locomotion Speed	0.1 m/s (0.9 m/s)	nominal (maximum)
Dimensions		
Square-shaped footprint	2100 mm	Minimum, presupposing max ground clearance
in cross stance	2500 mm	Maximum: Body close to ground
Number of active DoF	30	six per leg, six in arm
Minimum stow envelope volume	2.24 m^3	
Masses		
Total Mass	≈ 160 kg	w/o scout or payload-items
– thereof: manipulator	25 kg	
– thereof: each leg	25 kg	four legs present in suspension
Power-Supply		
Internal DC-Power	1x 44.4 V / 8 Ah	
External DC-Power	50 V / 20 A	Tethered power supply
Manipulator Arm		
Length of fully stretched arm	1955 mm	
Max. static load on stretched arm	183 N	(stretched wrist)
	537 N	(hanging wrist)
Force Torque Sensor	FT-mini 45	
Sensors		
Laser Range Finder	Hokuyo UTM-30LX	Tiltable
Stereo Camera Pair	2×GC1380	Tiltable
Attitude and Heading	Xsens MTi	
Joint Level Sensors	various	Current, Temperature, Voltage Speed, Position
Communication		
External Wireless	2.4 GHz (802.11n)	WiFi
External Cable Connection	GbE	Ethernet switch with Main PC, Suzaku Board and WiFi
Internal Joint Communication	Custom	Low Voltage Differential Signaling (LVDS)-based
Remote Emergency Switch	868 MHz	
Modularity / Interfaces		
Passive EMIs	4×	Mounted as "payload-bays" around arm mount
Active EMIs	2×	Mounted below central body and as arm end-effector
Power Bus via any EMI	44.4 V / 5 A	Bi-directional power transfer possible
Ethernet via any EMI	100Mbit/s	4Pin Fast Ethernet
Local Communication	RS422	Between Modules, i.e. for organization of topology

Table A.5: *Actuator specification for Sherpa's suspension system*

DoF	Joint Name	Angle Identifier	Movement Range	Angular Velocity	Torque / Force (nom)
1	Pan	α	± 90°	12°/s	241 Nm
2	Lift	β	± 60°	5.5°/s	2 328 N
3	WheelTilt	γ	± 30°	15°/s	414 Nm
4	WheelFlip	ζ	± 180°	60°/s	75 Nm
5	WheelSteering	φ	± 90°	75°/s	34 Nm
6	WheelDrive	ω^*	inf	165°/s	59 Nm

* ω denotes an angular velocity.

A.4 System Specification Tables: SherpaTT

The key specifications of SherpaTT are listed in Table A.6, see also [1]. The actuator specifications are provided in Table A.7.

Table A.6: *SherpaTT System Specifications, as presented in [1]*

Parameter Name	Value	Comments
	Performance Characterization	
Step & Obstacle Height	0.772 m	Active stepping necessary for step-like obstacles
Ground Clearance	0.10 m – 0.80 m	Variable, can be commanded
Locomotion Speed	0.1 m/s (nom)	
	0.7 m/s (max)	Currently limited by software to 0.2 m/s
Turning Arc	1 m (min)	Wheel track radius with point turn
(circular wheel path)	2.1 m (nom)	Point turn in nominal suspension configuration
	Dimensions	
Footprint Size	variable from 0.79 m^2 to ≈6.76 m^2	Smallest footprint: a square with 0.89 m edge length. Biggest: 2.6 m edge length. Abritrary non-symmetric footprints possible [5][7]
Leg Length (to LEP)	1.082 m	Fully stretched leg (i.e. not "Zero-Pose")
	0.880 m	Nominal configuration: PoseA (see Figure 4.9b)
Number of active DoF	26	4×5 suspension system, 1×6 arm
Minimum stow envelope	1.67 m^3	
	Masses	
System Mass m_g	170 kg	Total mass, w/o payloads, w/o batteries
– thereof: Legs	25.75 kg	(×4)
– thereof: Arm	25 kg	
– thereof: Central Body	≈ 42 kg	Includes structure, electronics, hull, arm mount, EMI mounts
Payload Capacity	≈ 80 kg	Based on 4×2 PLI with 5 kg/ in payload bays, one BaseCamp with 15 kg and a 25 kg payload at the manipulator.
	Power-Supply	
Internal DC-Power	2× 44.4 V/10 Ah	Autonomous switching from empty to full battery
External DC-Power	50 V / 20 A	External AC/DC-converter with power tether
	Sensors	
Lidar	Velodyne HDL-32E	Main navigation sensor. Sensor mount rotates with first manipulator arm joint.
Laser Range Finder	Hokuyo UST-20LX	Tiltable. Mounted on front face. Used mainly for manipulation.
Camera	Allied Vision GC1380	1360×1024px, 20.2fps, 12bit, CCD camera for human operator.
Attitude and Heading	Xsens MTi-300	
Force Torque Sensors (Legs)	FT-DELTA 160	Mounted at each wheel for autonomous ground adaption
Force Torque Sensor (Arm)	FT-mini 45	Part of manipulation interface
Joint Level Senors		Current (total and phase), voltage, speed, position, temperature
	Communication	
External Wireless	2.4 GHz (802.11n)	WiFi
External Cable Connection	GbE	Ethernet switch connected to WiFi, control PC and modular interfaces
Internal Joint Com.	NDLCom via LVDS	Custom protocol / inter-hardware communication
Remote Emergency Switch	868 MHz Xbee-Pro	Custom hardware
	Modularity / Interfaces	
Passive EMIs	4×	Mounted as "payload-bays" around arm mount
Active EMIs	2×	Mounted below central body and used as manipulation interface
Power Bus via any EMI	44.4 V / 10 A	Bi-directional power transfer possible
Ethernet via any EMI	100Mbit/s	4Pin Fast Ethernet
Local Communication	RS422	Between Modules, i.e. for topology reconstruction

Table A.7: *Actuator specification for SherpaTT's suspension system.*
Movement range as provided by hardware. Software safety limits are set smaller. Particularly the WS joint's rotation is limited by cabling only.

DoF	Joint Name	Angle Identifier	Movement Range Min	Movement Range Max	Angular Velocity	Torque / Force (nom)
1	Pan	α	-90°	+135°	7.0 deg/s	433 Nm*
2	InnerLeg (IL)	β	-55°	+20°	5.0 deg/s **	3 500 N
3	OuterLeg (OL)	γ	-5°	+80°	5.0 deg/s **	3 500 N
4	WheelSteering (WS)	φ	<-180°	>+180°	175.0 deg/s	60 Nm
5	WheelDrive (WD)	ω***	inf	inf	210.0 deg/s	74 Nm

* Theoretically the motor gear combination provides more than 2200 Nm; 433Nm is the repeated torque rating of the gear box. A momentary peak torque of 841Nm is rated for the gear box.
** Note that the angular velocity is dependent on the position for the linear joints. Provided is the limit that is possible in all angular positions. Max linear velocity is 12 mm/s
*** ω denotes an angular velocity

A.5 Cartesian Velocity Limits for an LEP

Figure A.1 shows the angular velocities $\dot{\beta}$ of the InnerLeg actuator for three different cartesian velocities of the LEP. Limiting factor is the 5 deg/s rotational velocity limit for the joint.

I Maximum linear velocity for the full vertical range through Pose A is $\dot{z} = 0.024\,\text{m/s}$.
II Maximum linear velocity with constraining the movement range to max 0.2 m below Pose A is $\dot{z} = 0.036\,\text{m/s}$.
III Maximum linear velocity with constraining the movement range to max 0.1 m below Pose A is $\dot{z} = 0.042\,\text{m/s}$.

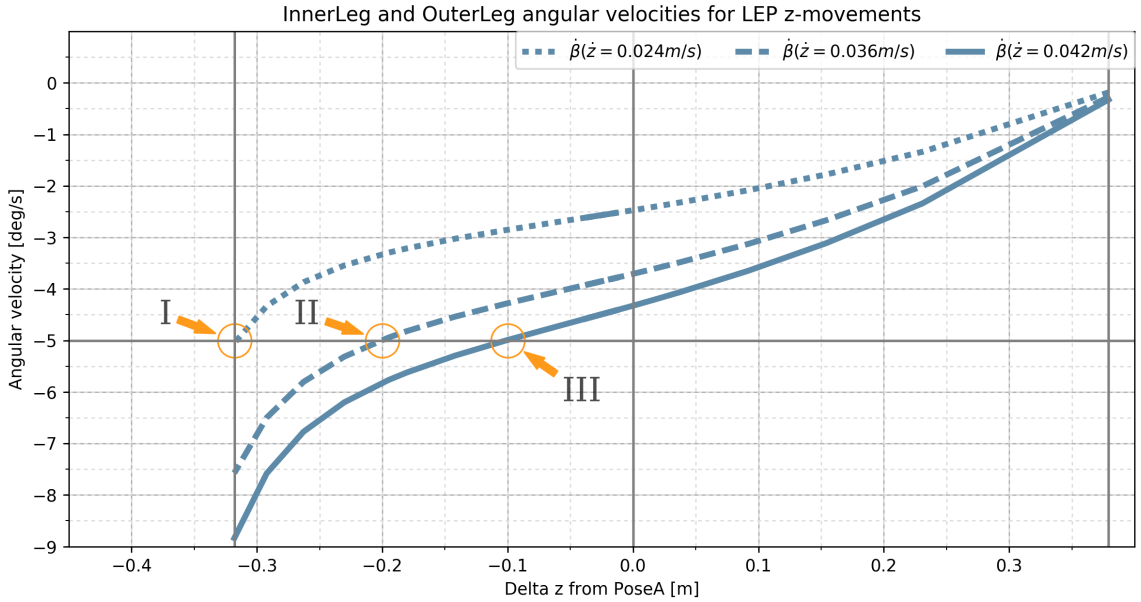

Figure A.1: *Limitation examples for maximum vertical velocity of an LEP with Pose A. Full movement range (I), limitation to 0.2 m (II) and limitation to 0.1 m (III) below Pose A.*

A.6 Additional Experiment Data

This section provides additional experiment data. References to this section are made in the full text from Chapter 6.

A.6.1 Comparison of Single Runs Indoor

The plot in Figure A.2 shows the force errors of all four wheels in two different experiment runs on a wooden obstacle as described in Chapter 6. The upper plot is from a run with a commanded velocity of 0.05 m/s, while the lower plot is from a run with velocity 0.10 m/s. Even though different velocity settings are present (note the different time on the x-axes), the general force error progression is nearly identical when the rover is at the same spot on the obstacle. The plots are taken from *RPAonly* runs.

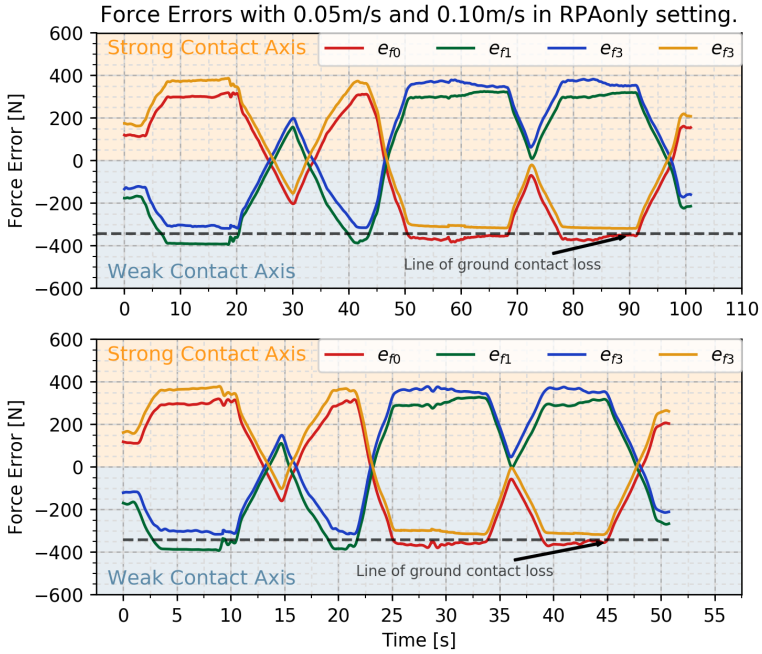

Figure A.2: *Comparison of wheel contact forces of two runs with different velocity settings*

A.6.2 Force Leveling and Body Orientation Control

A plot of an *EGConly* run on the wooden obstacle from Chapter 6 is shown in Figure A.3a. Between 5 s and 15 s oscillations on all four contact forces can be seen. These are resulting from the offset written to wheel FR: Pushing that wheel towards ground releases the load on wheel FL and wheel RR (hence reducing the plotted error value) from a_0, while the load on wheel RL is increased. With wheel FR in ground contact, wheel FL is experiencing a lower load when being on a downslope of the obstacle, consequently the contact axis with strong contact switches several times. Despite the oscillations, the time of ground contact loss during the run is reduced significantly when compared to rigid suspension. Both body angle errors are uncontrolled and increase in comparison to a *noAdap* run.

The plot in Figure A.3b shows the force errors and body angle errors, when EGC and RPA are working in parallel on the wooden obstacle. The force plot is quite similar to that of *EGConly*

with oscillations and switching of the strong contact axis. Interesting is the fact, that the EGC module influences the RPA quality. At the beginning of the run (0 s - 20 s), wheel FR is pushed down to stay in ground contact. Since relative big offsets are written by the EGC module for fast adaption, this results in a slight lifting of the body, which can be seen in the oscillations in the pitch. Similarly, wheel RR is pushed down to stay in ground contact when wheel RL enters the obstacle at around 50 s. When wheel RL changes over to a falling slope around 60 s, the wheel is pushed faster to the ground than the RPA module can counter act. This results in the pitch and roll error from 50 s-70 s and also shifts the strong axis to a_0.

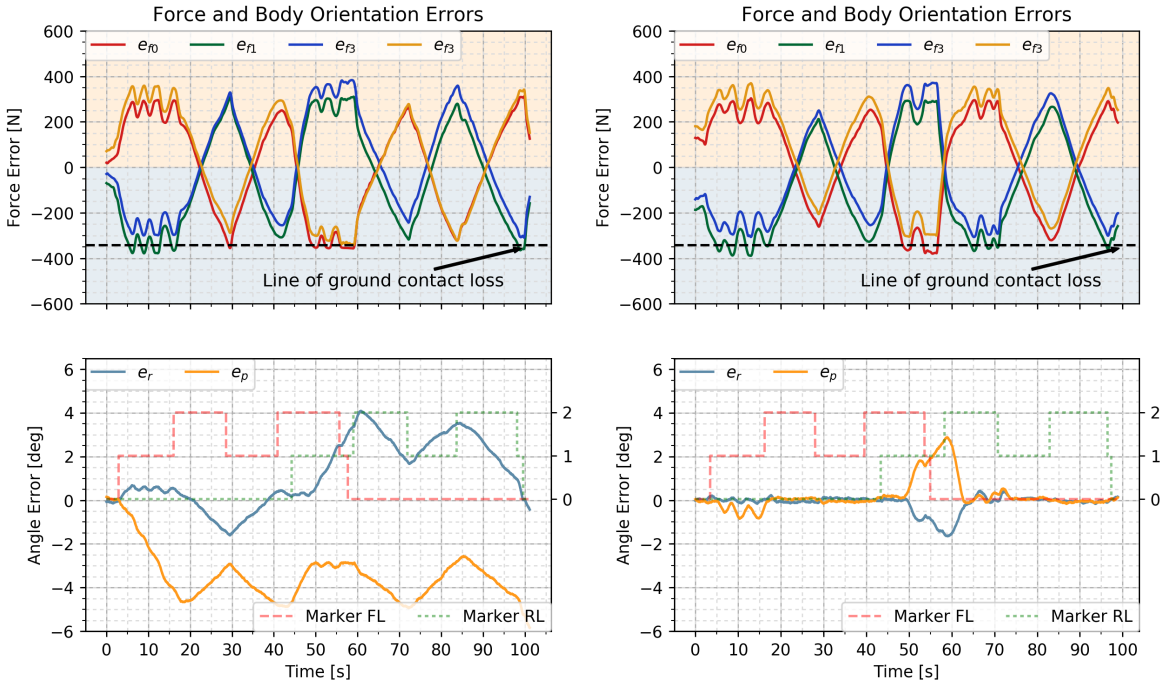

(a) EGConly*: Adaption of single wheels reflected in oscillations of all forces.*

(b) EGC+RPA*: Ground contact recovered in case of loss. Body angle tracking negatively influenced.*

Figure A.3: *Previously unpublished plots of force and body orientation errors of indoor runs, data from [4]*

All experiment data of the indoor experiments from [4] and the outdoor experiments from [1] is compiled into the same format for better inter-comparability. Consequently, the tables provided in in the following have not been published in this form before.

Table A.8 summarizes the results from the indoor experiments: The means of the RMS values $\hat{e}_{fi}$ for all forces as well as for the RMS error values for roll and pitch, $\hat{e}_r$ and $\hat{e_p}$ are used as quality indication of ground contact and body orientation, respectively. The number of runs used to build the mean is provided in the table. It can be seen, that the force error is the biggest for the *noAdap* case, followed by the *RPAonly* setting, which does not influence the wheels for ground contact. Using the EGC module alone shows a clear improvement in the contact force error. The quality of ground contact is slightly attenuated by adding the RPA module with the *EGC+RPA* setting. An improvement of one order of magnitude for the ground adaption can be seen in the *FLC+EGC+RPA* setting.

Concerning the body orientation, the *EGConly* setting shows a worse result than the baseline

noAdap setting. However, the EGC alone does not actively influence the body angle, hence arbitrary relative heights of all LEP are possible as long as the wheels are kept in ground contact which in turn generates arbitrary body orientations. In *RPAonly* setting an improvement of one order of magnitude is achieved for the body angle tracking. This result is negatively influenced, when the EGC module is activated which is due to oscillations from the EGC module, see also additional explanations above. The quality of body angle tracking is further improved, when the FLC component is included in the *FLC+EGC+RPA* setting.

Table A.8: *Means of RMS values for force tracking and body angle indoor and improvement compared to baseline values: $g > 1$ indicates impairment, $g < 1$ indicates improvement. Data from [4].*

Setting	Runs	mean $\hat{e}_{fi}$	g_f	mean $\hat{e}_{rp}$	g_{rp}
noAdap	2	287.03 N	baseline	1.82°	baseline
RPAonly	4	265.19 N	0.92	0.31°	0.17
EGConly	2	211.07 N	0.74	3.10°	1.70
EGC+RPA	4	225.98 N	0.79	0.66°	0.36
FLC+EGC+RPA	4	46.92 N	0.16	0.20°	0.11

Table A.9 provides the force leveling and body angle data of the flat terrain outdoor runs. Without adaption a high variance of the observed force errors can be seen. With active force leveling, all error values are within the same range around and below 50 N, indicating the independence of the force leveling module from the footprint. Since the *noAdap* mode in P90 has already a small force error, the improvement g_f is not so significant as for the Turtle-Front case. The body angles are not manipulated in the *FLConly* setting. Consequently the angles are similar for both modes. An exception is Turtle-Front, here a stronger tilt was observed during the *noAdap* run due to ground contact loss of single wheels. Hence, in specific cases, *FLConly* can already reduce roll-pitch changes.

Table A.9: *Means of RMS values for force tracking and body angle in outdoor Setting A: flat terrain and improvement compared to baseline values: $g > 1$ indicates impairment, $g < 1$ indicates improvement. Data from [1].*

Footprint	GAP mode	Runs	mean $\hat{e}_{fi}$	g_f	mean $\hat{e}_{rp}$	g_{rp}
	*noAdap*	6	96.58 N	baseline	0.45°	baseline
	FLConly	2	46.94 N	0.49	0.47°	1.05
	*noAdap*	4	56.12 N	baseline	0.51°	baseline
	FLConly	4	52.33 N	0.93	0.53°	1.03
	*noAdap*	4	207.32 N	baseline	1.04°	baseline
	FLConly	2	43.85 N	0.21	0.63°	0.61

Table A.10 provides the force leveling and body angle data of the moderate slope outdoor runs. A clear improvement in force leveling can be seen from *noAdap* case to *FLConly* mode. Both footprints show similar mean RMS force error values, further substantiating the presumption of independence of the force leveling quality from the footprint. The Quasi-Tripod suspension configuration shows a smaller force error in *noAdap* than the Cross-Stance. With active body

control, the body angle error is reduced to a fraction of a degree, the error has only 4% to 6% of the baseline value.

Table A.10: *Means of RMS values for force tracking and body angle in outdoor Setting B: moderate slope and improvement compared to baseline values: $g > 1$ indicates impairment, $g < 1$ indicates improvement. Data from [1].*

Footprint	GAP mode	Runs	mean $\hat{e}_{fi}$	g_f	mean $\hat{e}_{rp}$	g_{rp}
	*noAdap*	2	230.69 N	baseline	2.68°	baseline
	FLConly	8	37.88 N	0.16	2.64°	0.98
	FLC+RPA	6	32.62 N	0.14	0.11°	0.04
	*noAdap*	2	93.88 N	baseline	2.77°	baseline
	FLConly	6	32.00 N	0.34	2.74°	0.99
	FLC+RPA	6	31.06 N	0.33	0.16°	0.06

Table A.10 provides the force leveling and body angle data of the steep slope outdoor runs. Both velocity settings are presented in the table. The force errors are significantly lower in *FLConly* mode than in the corresponding *FLC+RPA* mode. Body angle tracking errors are well below 1°, with 0.20° in case of Cross-Stance and 0.16° in case of Y-Shape stance.

Table A.11: *Means of RMS values for force tracking and body angle in outdoor Setting C: steep slope. Data from [1].*

Footprint	GAP mode	Vel	Runs	mean $\hat{e}_{fi}$	mean $\hat{e}_{rp}$
	*FLConly*	0.1 m/s	5	63.87 N	7.87°
	FLConly	0.04 m/s	5	27.84 N	9.39°
	FLC+RPA	0.04 m/s	4	52.36 N	0.20°
	*FLConly*	0.04 m/s	2	21.49 N	10.51°
	FLC+RPA	0.04 m/s	2	41.75 N	0.16°

A.6.3 Power Requirement Analysis

This section provides the data of power requirement analysis from indoor and outdoor runs. Discussion of the values is provided in Section 6.3. All tables provide the footprint, GAP mode, number of runs for building the mean values and the commanded velocity. The power values are the mean power $\bar{P}_s$ for the suspension actuators, $\bar{P}_d$ for driving the rover and $\bar{P}_l = \bar{P}_s + \bar{P}_d$ as total locomotion power. The share of the suspension power to the locomotion power and to total rover power ($\bar{P}_l + P_b$) are provided.

Table A.12 shows the power requirements on the high frequency obstacle from the indoor experiments. In the high velocity setting the power can reach up to 60 W for adaption to the obstacle. The up-down slopes with short period in combination with the tested velocities are close to the limits of the suspension actuation. Force leveling errors proved to be small (see previous section), however, the power required to adapt the rover to this obstacle is comparatively high.

Table A.13 provides the power requirement from flat terrain in the outdoor experiments. The power requirement is low, in all tested footprints, less than 10 W are required for the force

Table A.12: *Means and deviations of power values in indoor experiment. Data from [4].*

Footprint	Mode	Runs	Velocity	$\bar{P}_s$	$\bar{P}_d$	$\bar{P}_l$	$\bar{P}_s/\bar{P}_l$	$\bar{P}_s/(\bar{P}_l+P_b)$
	*noAdap*	2	0.05 m/s	0.0 W	19.3 W	19.3 W	0.00	0.00
	EGConly	2	0.05 m/s	11.8 W	21.2 W	33.0 W	0.36	0.07
	RPAonly	2	0.05 m/s	31.0 W	21.6 W	52.6 W	0.59	0.17
	RPAonly	2	0.10 m/s	48.7 W	37.9 W	86.6 W	0.56	0.22
	EGC+RPA	2	0.05 m/s	35.8 W	23.2 W	58.9 W	0.61	0.19
	EGC+RPA	2	0.10 m/s	58.7 W	41.4 W	100.1 W	0.59	0.25
	FLC+EGC+RPA	2	0.05 m/s	29.1 W	20.3 W	49.4 W	0.59	0.16
	FLC+EGC+RPA	2	0.10 m/s	43.2 W	35.6 W	78.9 W	0.55	0.21

leveling of the robot.

Table A.13: *Power data from outdoor Setting A: flat terrain, data from [1]*

Footprint	GAP mode	Runs	Velocity	$\bar{P}_s$	$\bar{P}_d$	$\bar{P}_l$	$\bar{P}_s/\bar{P}_l$	$\bar{P}_s/(\bar{P}_l+P_b)$
	*noAdap*	6	0.10 m/s	0.0 W	44.8 W	44.8 W	0.00	0.00
	FLConly	2	0.10 m/s	9.0 W	44.9 W	53.9 W	0.17	0.04
	*noAdap*	4	0.10 m/s	0.0 W	45.1 W	45.1 W	0.00	0.00
	FLConly	4	0.10 m/s	6.8 W	47.2 W	54.0 W	0.13	0.03
	*noAdap*	4	0.10 m/s	0.0 W	48.8 W	48.8 W	0.00	0.00
	FLConly	2	0.10 m/s	7.3 W	47.3 W	54.6 W	0.13	0.03

Table A.14 provides the power requirement in moderate slope. Suspension power for *FLConly* mode in the tested footprints is around 12 W. The power required to adapt the suspension in Y-Shape is lower than that in Cross-Stance, most likely due to the inherently better force distribution (see also previous section). With active body angle control, the required mean power increases to values around 22 W.

Table A.14: *Power data from upslope drives in outdoor Setting B: moderate slope, data from [1].*

Footprint	GAP mode	Slope	Runs	Velocity	$\bar{P}_s$	$\bar{P}_d$	$\bar{P}_l$	$\bar{P}_s/\bar{P}_l$	$\bar{P}_s/(\bar{P}_l+P_b)$
	*noAdap*	up	1	0.10 m/s	0.0 W	64.8 W	64.8 W	0.00	0.00
	FLConly	up	4	0.10 m/s	13.6 W	61.7 W	75.4 W	0.18	0.06
	FLC+RPA	up	3	0.10 m/s	21.4 W	60.9 W	82.3 W	0.26	0.09
	noAdap	down	1	0.10 m/s	0.0 W	49.9 W	49.9 W	0.00	0.00
	FLConly	down	4	0.10 m/s	13.4 W	45.4 W	58.8 W	0.23	0.06
	FLC+RPA	down	3	0.10 m/s	21.5 W	45.0 W	66.4 W	0.32	0.10
	*noAdap*	up	1	0.10 m/s	0.0 W	65.8 W	65.8 W	0.00	0.00
	FLConly	up	3	0.10 m/s	11.1 W	60.9 W	72.0 W	0.15	0.05
	FLC+RPA	up	3	0.10 m/s	23.7 W	61.9 W	85.6 W	0.28	0.10
	noAdap	down	1	0.10 m/s	0.0 W	49.0 W	49.0 W	0.00	0.00
	FLConly	down	3	0.10 m/s	11.1 W	45.5 W	56.6 W	0.20	0.05
	FLC+RPA	down	3	0.10 m/s	23.4 W	45.1 W	68.5 W	0.34	0.11

Table A.15 provides the power requirement data for the steep slope runs with high velocity setting. Suspension power is around 20 W. In case of driving down the slope, the wheels are generating power, consequently, the share of power for locomotion is above 100% for the suspension system. The relative value is not meaningful for comparison in case of power generation at the wheels.

Table A.15: *Power data from outdoor Setting C: steep slope, data from [1].*

Footprint	GAP mode	Slope	Runs	Velocity	$\bar{P}_s$	$\bar{P}_d$	$\bar{P}_l$	$\bar{P}_s/\bar{P}_l$	$\bar{P}_s/(\bar{P}_l + P_b)$
	*FLConly*	up	2	0.10 m/s	21.5 W	156.8 W	178.3 W	0.12	0.06
	FLConly	down	3	0.10 m/s	18.4 W	-7.0 W	11.4 W	1.61	0.11

Table A.16 provides the power requirement data for steep slope runs with reduced velocity setting. In *FLConly* mode, the power for suspension is around 12 W, in *FLC+RPA* mode the value is around 20 W. These values are obtained in both footprints for driving upslope and downslope.

Table A.16: *Power data from outdoor Setting C: steep slope (reduced velocity), data from [1].*

Footprint	GAP mode	Slope	Runs	Velocity	$\bar{P}_s$	$\bar{P}_d$	$\bar{P}_l$	$\bar{P}_s/\bar{P}_l$	$\bar{P}_s/(\bar{P}_l + P_b)$
	*FLConly*	up	2	0.04 m/s	12.2 W	92.1 W	104.3 W	0.12	0.05
	FLC+RPA	up	2	0.04 m/s	22.2 W	95.9 W	118.1 W	0.19	0.08
	FLConly	down	3	0.04 m/s	12.2 W	2.3 W	14.5 W	0.84	0.07
	FLC+RPA	down	2	0.04 m/s	20.0 W	0.5 W	20.5 W	0.98	0.11
	*FLConly*	up	1	0.04 m/s	11.6 W	89.2 W	100.8 W	0.12	0.04
	FLC+RPA	up	1	0.04 m/s	19.2 W	99.5 W	118.7 W	0.16	0.07
	FLConly	down	1	0.04 m/s	12.4 W	2.7 W	15.1 W	0.82	0.07
	FLC+RPA	down	1	0.04 m/s	21.2 W	0.9 W	22.0 W	0.96	0.12

B Author's Publication Details

B.1 Statement of Contribution to Accumulated Publications

The publications listed in Table B.1 are part of this cumulative dissertation. In the table the declaration of this thesis author's contributions to each publication is provided. An abstract of each paper's content is given in Section 1.5.

Table B.1: *Publications and Thesis' Author's contributions.*
(Type J: Journal, C: Conference, W: Workshop at Conference.)

Ref	Type	Individual Contribution	Share
[1]	J	All experiments were conceived by me and conducted by me, with the help of the field team. The paper was written entirely by me. The conceptual design of SherpaTT was developed by me, execution of electro-mechanical construction and implementation of parts of the MCS were done by colleagues at DFKI RIC.	95%
[2]	J	I wrote a major part of the introduction, the system-design related parts of the state-of-the-art chapter, and the multi-robot system overview chapter. I am responsible for the evaluation of stacking payload-items in the experimental section. Additionally, I contributed to the conclusion of the article. Technically I was responsible for the electro-mechanical design of Sherpa and CREX as well as the implementation of both system's locomotion control.	45%
[3]	J	I was responsible for the main frame and finalization of the publication. The sections introduction, mission description, conclusion and outlook were written by me.	30%
[4]	C	The experiments described in this publication were conceived and conducted entirely on my own. The paper was completely written by me. Parts of the implementations of the MCS are the work of the co-authors.	90%
[5]	C	The experiments described in this publication were conceived and conducted entirely on my own. The paper was completely written by me. The co-author contributed in conceptual design and implementation of the control system.	95%
[6]	C	The main part of the paper is written by me, particularly, the comparison of both systems was done by me. Co-Authors supported physical realization of the robot and contributed in the control system conceptual design.	90%
[7]	C	I wrote the complete paper. Kinematics modelling and locomotion mode conceptual design was done by me. Co-Authors with contribution concerning physical simulation and manipulator arm.	95%
[8]	W	The entire paper was written by me. The co-author added conceptual design of the two multi-robot systems and the presented climbing robot. The design of the climbing robot is done by colleagues not appearing as authors on this publication.	95%
[9]	C	I wrote parts of the general test campaign and infrastructure descriptions, and the SherpaTT parts of the paper. Furthermore I contributed to the lessons learned and conclusions section.	15%
[10]	C	I am the main author of this publication (authors appear in alphabetical order). I am responsible for the main structure of the article. I conducted the climbing experiments with the legged scout robot and wrote the introduction, description of the climbing experiments and the conclusion of the paper.	40%
[11]	C	I wrote the robotic systems overview section. I contributed in the mission design for the multi-robot system and revised the paper before final submission.	15%
[12]	C	The three first mentioned authors conducted the experiments. I was involved in the conceptual design phase and wrote the introduction, state of the art, general concept of RIMRES as well as the conclusion of the paper.	25%
[13]	C	The experiments were conceived, conducted and evaluated by the first author. I wrote most of the paper, particularly Introduction, System Overview and Conclusion and contributed in the experimental evaluation.	45%

B.2 Additional Publications

Following publications are contributing to a deeper understanding of the topics covered in this thesis and as such are cited at the appropriate places, but are not included in the accumulated publications:

[14] A kinematic model for Sherpa is developed in this publication. The model is used for pose estimation in robot localization.

[15] The evolutionary optimization of a manipulator arm for both rovers described in this thesis is presented in this publication.

[16] This publication presents flexible metal wheels for an actively articulated rover. Three design steps are illustrated: Passive wheels, wheels with deformation sensing, wheels with active stiffness control.

[17] The multi-robot system of LUNARES is introduced. Experiments concerning docking and scout locomotion are highlighted in this publication.

[18] Experimental evaluation of the LUNARES system is presented. Focus in this publication is on the autonomous docking between subsystems.

[19] The RIMRES MRS is introduced in this publication. Plans for the system and first designs of individual subsystems are presented.

[20] This publication illustrates the developments within the RIMRES multi-robot system. The journal publication [2] is an invited publication based on this conference paper.

[21] A final review with lessons learned within the RIMRES MRS is presented in this publication.

[22] This video publication presents the mission control and conduction of the field experiments with the TransTerrA MRS in the desert of Utah in November 2016.

[23] An overview of robotic systems developed at the DFKI RIC is provided in this publication.

[24] The development of the first generation EMI is presented in this paper. Emphasis is put on the experimental evaluation of the mechanical components.

[25] The power management for the EMI is presented and evaluated in this publication.

[26] The EMI as end-effector for a manipulation arm is presented in this publication.

[27] All exemplarily implemented payload-devices using the EMI are presented in this paper.

[28] The SpaceClimber robot is presented in this publication. The robot is the antetype for the CREX scout robot of the RIMRES multi-robot system.

[29] An intelligent foot for a walking robot is presented. The sensors in the foot facilitate an underground assessment of the terrain the robot is currently walking on. These feet have been integrated into the six-legged robots SpaceClimber and CREX.

[30] The lower leg and foot for a climbing legged robot are described and experimentally evaluated for ground property estimation.

[31] A relative positioning device for a multi-robot exploration system is experimentally evaluated. Experiments include localization of the rover SherpaTT with the developed device.

The following publications of the author are not directly related to the topics of this thesis:

[32] A concept for a neural network to model contact dynamics of a legged robot in rough terrain is presented. The neural network is used to build a model of the ground contact dynamics.

[33] A concept for a new landing device is presented in this publication. A SkyCrane-like powered descend on Mars is experimentally evaluated in an earth demonstration scenario using an octocopter, equipped with a winch and bridle mechanism and a rover-mockup.

[34] This publication focusses on the in-flight hazard detection for a SkyCrane like drop-ship for rover deployment on Mars.

C Accumulated Publications

In the following, all publications contributing to the cumulative dissertation are included in full length. Due to copyright restrictions, several included publications are in the layout as submitted instead of the layout eventually published. The finally published version of each paper is available online:

[1] **Design and Field Testing of a Rover with an Actively Articulated Suspension System in a Mars Analogue Terrain**
https://onlinelibrary.wiley.com/doi/abs/10.1002/rob.21808

[2] **Reconfigurable Integrated Multirobot Exploration System (RIMRES): Heterogeneous Modular Reconfigurable Robots for Space Exploration**
https://onlinelibrary.wiley.com/doi/abs/10.1002/rob.21477

[3] **Lunares: Lunar Crater Exploration with Heterogeneous Multi Robot Systems**
http://dx.doi.org/10.1007/s11370-010-0081-4

[4] **Static Force Distribution and Orientation Control for a Rover with an Actively Articulated Suspension System**
https://ieeexplore.ieee.org/document/8206412/

[5] **SherpaTT: A Versatile Hybrid Wheeled-Leg Rover**
https://tinyurl.com/cordes2016-SherpaTT

[6] **An Active Suspension System for a Planetary Rover**
https://tinyurl.com/cordes2014-ActiveSuspension

[7] **Locomotion Modes for a Hybrid Wheeled-Leg Planetary Rover**
https://ieeexplore.ieee.org/document/6181694/

[8] **Heterogeneous Robotic Teams for Exploration of Steep Crater Environments**
https://pdfs.semanticscholar.org/6993/dc4a4ab5023671535912c721d4f13cb90658.pdf

[9] **Field Testing of a Cooperative Multi-Robot Sample Return Mission in Mars Analogue Environment**
https://tinyurl.com/sonsalla2017-FieldTestingMRS

[10] **Performance Evaluation of an Heterogeneous Multi-Robot System for Lunar Crater Exploration**
https://tinyurl.com/bartsch2010-PerformanceEval

[11] **Towards a Heterogeneous Modular Robotic Team in a Logistic Chain for Extraterrestrial Exploration**
https://tinyurl.com/sonsalla2014-TransTerrA

[12] **Heterogeneous Modules with a Homogeneous Electromechanical Interface in Multi-Module Systems for Space Exploration**
https://ieeexplore.ieee.org/document/5980051/

[13] **A Robust Electro-Mechanical Interface for Cooperating Heterogeneous Multi-Robot Teams**
https://ieeexplore.ieee.org/document/7353601/

Design and Field Testing of a Rover with an Actively Articulated Suspension System in a Mars Analogue Terrain

Florian Cordes*, Frank Kirchner*†, and Ajish Babu*

Reformatted version. Original version in: Journal of Field Robotics ©John Wiley & Sons, Inc. 2018
https://onlinelibrary.wiley.com/doi/abs/10.1002/rob.21808

This article presents the electro-mechanical design, the control approach and the results of a field test campaign with the hybrid wheeled-leg rover SherpaTT. The rover ranges in the 150 kg class and features an actively articulated suspension system comprising four legs with actively driven and steered wheels at each leg's end. Five active degrees of freedom are present in each of the legs, resulting in 20 active degrees of freedom for the complete locomotion system. The control approach is based on force measurements at each wheel mounting point and roll-pitch measurements of the rover's main body, allowing active adaption to sloping terrain, active shifting of the center of gravity within the rover's support polygon, active roll-pitch influencing and body-ground clearance control. Exteroceptive sensors such as camera or laser range finder are not required for ground adaption. A purely reactive approach is employed, rendering a planning algorithm for stability control or force distribution unnecessary and thus simplifying the control efforts. The control approach was tested within a four week field deployment in the desert of Utah, USA. The results presented in this paper substantiate the feasibility of the chosen approach: The main power requirement for locomotion is from the drive system, active adaption only plays a minor role in power draw. Active force distribution between the wheels is successful in different footprints and terrain types, and is not influenced by controlling the body's roll-pitch angle in parallel to the force control. Slope climbing capabilities of the system were successfully tested in slopes of up to 28° inclination, covered with loose soil and duricrust. The main contribution of this article is the experimental validation of the actively articulated suspension of SherpaTT in conjunction with a reactive control approach. Consequently, hardware and software design as well as experimentation are part of this article.

1 Introduction

Nature provides a vast amount of examples that legged, walking or climbing locomotion is an excellent means to cover even the steepest cliffs and to reach literally any place on a planetary surface. Goats climbing steep rocky surfaces, Geckos with adhesive feet managing smooth surfaces or many types of insects are only a few examples of impressive locomotive capabilities to be found in the animal domain.

In the robotic domain, walking robots are of increasing interest as for example shown at the Darpa Robotics Challenge (DRC) (Krotkov et al., 2017). The majority of robots taking part in the DRC finals were walking robots, most of them in some kind of humanoid form. Despite the high number of walking robots in the contest, and recent advances in developing walking and climbing robots, most of the highest ranked systems in the challenge where those combining walking and driving locomotion in one way or the other. This contest's result illustrates the advantages of combining different modes of locomotion in a robotic system and adapting the locomotive system according to the current task and environment.

Looking into the application area of space robotics, all mobile robots deployed for exploration of celestial bodies are up to now purely wheeled systems, equipped with a performant passive suspension system, yet without the possibility to adapt the locomotive system to a wider range of terrain types or non-nominal situations (sinkage in soft soil, getting entangled between rocks or alike). The employed systems provide the possibility to carry scientific instruments to locations several kilometers away from the landing spot (Lindemann and Voorhees, 2005) (Volpe, 2005). However, new mission scenarios with additional requirements concerning sample return, sites to take samples from and their reachability with robotic systems as well as improved fault-recovery abilities demand for new solutions.

The approach presented in this paper is to combine benefits of the domain of legged locomotion with those of the domain of wheeled locomotion to form an active suspension system (Cordes and Babu, 2016), (Cordes et al., 2017). As a result the hybrid wheeled-leg rover *SherpaTT* was designed, integrated and tested. In this paper the rover system is presented in terms of electro-mechanical design, control approach and testing within a field test campaign during October and November 2016 in the desert of Utah, USA. The extensive experimental validation in a field deployment is the main contribution of this paper. Several aspects of the chosen test site are good representatives of terrain on Mars, including segmented and inverted river beds that can be found on Mars, providing a potential source of astrobiological data, (Clarke and Stoker, 2011). Due to the geological similarity other Mars analogue tests were con-

*DFKI Robotics Innovation Center Bremen, Bremen, Germany `firstname.lastname@dfki.de`
†University of Bremen, Faculty 03: Mathematics/Computer Science, Bremen, Germany

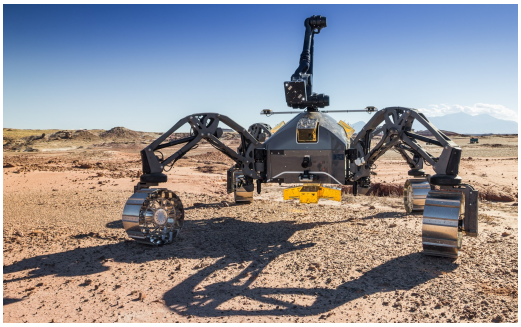

Figure 1: The hybrid wheeled-leg rover SherpaTT during the field test campaign. In the photograph, the system is equipped with modular units used in a multi-robot scenario. The two antennae of the DGPS-system used for ground truth-data can be seen behind the central manipulator.

ducted in the area as well, (Dupuis et al., 2016), (Caudill et al., 2016), (Gingras et al., 2017).

Figure 1 shows the final design of SherpaTT as deployed in the field test campaign with connected modular payload-containers. During the field tests, locomotion experiments, navigation and autonomous control tests and a multi-robot sample-return mission were conducted. This article focusses on the suspension design and the locomotion experiments conducted with SherpaTT during the field tests. An overview on the experiments conducted and general field experiences are presented in (Sonsalla et al., 2017).

We define the following terms as used throughout the paper:

Definition 1.1: Wheeled-Leg.
In this paper, a *wheeled-leg* is considered as a limb of a robot that, instead of a foot for ground contact, makes use of a wheel at the ground contact point. Alternatively the term wheel-on-leg can be found in literature.

Definition 1.2: Leg End Point (LEP).
The term *LEP* in this article is used to kinematically describe a wheeled-leg of a robot. A LEP is considered to be the idealized point of contact of a rigid wheel on rigid ground. The location of a LEP is considered to be described by a vector in cartesian coordinates $p = (p_x\ p_y\ p_z)^T$ or cylindrical coordinates $p = (p_\alpha\ p_r\ p_z)^T$. Currently, the LEP is used as reference for controlling the active ground adaption, see Section 5.

Definition 1.3: Wheel Contact Point (WCP).
The real contact point between wheel and ground might be different from the LEP and is defined as the *WCP*. A wheel can have more than one WCP or no WCP when the wheel is lifted off the ground, but there is always exactly one LEP. In a further advanced control, the ground adaption would react to the WCP(s) and not the LEP.

The remainder of this article is structured as follows. The following chapter gives an overview of the related work. This encompasses passive and active suspension system rovers and a comparison of benefits and drawbacks of both approaches. Chapter 3 gives an overview on the full rover system, while he mechanical design and kinematics analysis of the system is detailed in Chapter 4.. The control approach of the suspension system and how to take advantage of the kinematic structure for locomotion is described in Chapter 5. With Chapter 4.4 a brief discussion on the effect of individual joint failures and other operative risks is provided. Chapter 6 focusses on the experiments conducted with SherpaTT and the results and conclusions from these experiments. The article closes with lessons learned and a summarizing conclusion in Chapter 7.

2 Rover Suspension Systems: Passive vs. Active

One means of exploration of celestial bodies is remote sensing, for example with satellites passing or orbiting a planet or moon. A more direct approach is a lander equipped with a robotic arm, like the Phoenix lander (Smith, 2004). Such stationary units can provide data in the direct vicinity of the landing spot, for example by soil sampling and analysis with appropriate instruments on the landing unit. Depending on the type of lander, propulsion plumes might contaminate the direct vicinity of the landing spot and thus if not rendering impossible at least complicate the interpretation of data from soil samples. To gather data from "in-situ" measurements at multiple locations on a celestial body's surface with more distance to the landing spot, mobile robotic devices are required.

2.1 Passive Suspension Systems

Recently deployed mobile robots on Mars (Mishkin et al., 1998), (Lindemann and Voorhees, 2005), (Welch et al., 2013) or China's Yutu-rover from Chang'e 3 mission to Moon feature wheeled locomotion with passive adaptive suspension systems. All these rovers are equipped with a suspension system known as *rocker-bogie* suspension (Bickler, 1989), (Harrington and Voorhees, 2004). Two identical linkage mechanisms are fixed on either side of the rover, connected via a differential. Each linkage consists of a rocker which has one wheel mounted on the front end of the vehicle and a bogie with two wheels pivoting at the rear end of the rocker. The effect of the connecting differential between the two rockers is that the pitch angle of the rovers's body maintains the average angle of the two rocker angles. The size of negotiable obstacles is related to the wheel size. A rover with a rocker-bogie suspension can typically overcome obstacles of a height in the range of a wheel's diameter: The MER systems have a wheel diameter of 25 cm and are stated to safely traverse obstacles of 25 cm height (Lindemann and Voorhees, 2005).

Similar to a rocker-bogie suspension is a mechanism known as triple bogie or 3-bogie configuration as found in the ExoMars rover (Michaud et al., 2008). One bogie

with two wheels is mounted on the left, right and rear of the robot in this type of suspension configuration. No differential or other connection is present between the single bogies, the rear bogie acts as a leveling mechanism for roll angles. Apfelbeck et al. (Apfelbeck et al., 2011) report on obstacles that might get the rover stuck, yet most test-cases showed a good terrain performance of this passive suspension system. A triple bogie configuration with supporting spring elements is presented in (Manz et al., 2014).

Another bogie configuration can be found in the CRAB rover (Thueer et al., 2006). As opposed to the rocker-bogie or triple bogie configuration, a symmetrical design with two parallelograms attached to one rocker is chosen for this system. A further passive suspension is shown for example in the rovers Shrimp (Lamon and Siegwart, 2003) and SOLERO (Michaud et al., 2002) which are six-wheeled rovers with two wheels on each side central body and one wheel in the front and one wheel at the rear end of the rover.

All the above mentioned passive suspension systems are designed to keep all wheels in ground contact and to equally distribute loads between the wheels. Furthermore, the roll and pitch angles of the rover bodies are reduced by the design of the suspension when compared to fixed suspension in equally sloping terrain. A clear benefit of these systems is that no active control of linkages is needed, the kinematics of the passive suspension ensure optimal ground contact in most situations.

However, certain stuck situations are reported from which the rover cannot free itself. This is a clear drawback of a passive suspension system. Furthermore, the body angle with respect to gravity can not be influenced arbitrarily. For climbing obstacles, enough traction is required to be able to push a wheel up an obstacle. In cases with low ground traction, the rover might fail to overcome the obstacle.

2.2 Active Suspension Systems

Wilcox et al. (Wilcox et al., 2007) argue that using wheeled-legs for propulsion creates the possibility to walk out of stuck situations. Additionally, a wheel can be actively lifted to climb an obstacle, reducing the risk of entangling robot structures with the obstacle. Unlike in passive suspension, the wheels remaining on the ground do not need to provide thrust to push a wheel up an obstacle. This bears the potential for better obstacle negotiation in slopes: slippage of wheels compromises the thrust needed in passive suspension to push the wheel onto the obstacle.

When a rover can walk out of a stuck situation, the wheel torque requirements can be relaxed: For dimensioning a wheel's actuator, a worst-case scenario where one wheel is stuck in a hole and the rover is tilted onto that wheel can be assumed. This load case implies that the wheel needs to generate a torque that allows to push half of the rover's mass vertically up (Wilcox, 2012). If the suspension system can actively pull the wheel out of the stuck situation the peak thrust requirement for each wheel can be reduced. Reducing the peak thrust allows to reduce the gear-box size and hence reduce the weight of the actuator. Additionally, the motors can operate closer to their specific working point, since the ratio between thrust in nominal operation and in worst-case operation is significantly smaller. Combined with the reduction of the wheel size due to reduced requirements for ground pressure limits, a wheeled-leg system can be about 25% lighter compared to an alternative all-terrain mobility system (Wilcox, 2012). Hence, combining legs and wheels to wheeled-legs has the potential to combine the benefits of both, walking and driving locomotion.

Active suspension systems, depending on their design can further reduce the overall system mass which includes the lander system: Using such a suspension can render ramps or other rover deployment systems unnecessary (Haarmann et al., 2012) (Townsend et al., 2010). At least an increase in safety for lander egress when using ramps can be achieved using active elements in a suspension as shown in (Azkarate et al., 2015).

A combination of walking and rolling motion using the deployment actuators of ExoTeR (ExoMars Testing Rover) showed increased performance when compared to only rolling motion in three different experimental scenarios, namely freeing from a stuck situation in soft soil, up-slope capabilities and lander egress (Azkarate et al., 2015). The ExoTeR makes use of a triple bogie suspension as the ExoMars platform does. Furthermore, each wheel has a deployment actuator, that is responsible for the transition of the folded stow configuration to the unfolded driving configuration after the landing manoeuver.

Another system combining active and passive suspension is the Scarab rover (Bartlett et al., 2008). Passive terrain adaptability is achieved by a differential rocker mechanism connecting the two rockers on each side. The opening angle of each of the two rockers can be set with an actuator, providing two active Degrees of Freedom (DoFs) in the suspension system. In (Wettergreen et al., 2009) the outcome of field testing the Scarab rover is presented.

Similar in suspension design to Scarab is the Sample Return Rover (SRR), which has four wheels that are mounted on a similar two-rocker system with controllable shoulder joints. As opposed to Scarab the wheels can be independently steered, allowing explicit steering maneuvers. In (Iagnemma et al., 2003) the SRR rover demonstrates improved terrain stability when roving in undulating terrain with active adaption of the suspension system.

A rover with an actively actuated suspension designed for lunar mission is the ATHLETE rover (Wilcox et al., 2007) (Heverly et al., 2010). The ATHLETE family of rovers employs an actively articulated suspension composed of six limbs with six Degree of Freedom (DoF) each. Each limb can be used as a general purpose manipulator with a tool adapter. The size of of a ATHLETE

SDM rover is 2.75 m in diameter with a total mass of 850 kg.

In (Reid et al., 2016) a rover with an actively articulated suspension system is presented. The rover has four wheeled-legs with four active DoF each. The ground adaption strategy is based on a planned trajectory for the rovers body. With the terrain information gathered from a RGB-D sensor, joint movements in the limbs are planned that lead to the desired body trajectory in unstructured terrain.

The rover SherpaTT presented in this paper is a system that fits into the category of active suspension systems described in this section. In contrast to the systems described above, SherpaTT has a six-axis force-torque sensor mounted at each wheel, allowing a direct measurement of the interaction with the ground. A force estimation using joint displacements or joint currents is not required, which in turn allows the employment of self-locking gears that do not need to be powered to keep the current position. Apart from flexible metal wheels (Kroemer et al., 2011), no passive suspension is implemented in SherpaTT The reactive control approach implemented in SherpaTT (Cordes et al., 2017) together with the chosen workspace of the legs of the suspension system allow for active ground adaption during a continuous drive in sloping terrain. A sequential "drive-stop-adapt" motion strategy is not necessary.

2.3 Conclusion

Above examples show that passive suspension systems as employed or envisioned for current space exploration robots provide good terrain traversability in many cases. However, limits of theses systems occur in steeper slopes covered with obstacles and in non-nominal situations, especially in cases where a robot gets stuck in soft soil. Actively articulated suspension systems bear the potential to increase the rover's locomotive capabilities and hence increase the margin before reaching non-nominal states or increase possibilities to recover from non-nominal system states.

The additional actuators required for active suspension do not necessarily increase the system mass as savings in actuator size and – having the full space system in mind – lander system are possible due to the increased capabilities of the mobile robot (Wilcox, 2012) (Townsend et al., 2010) (Haarmann et al., 2012).

However, it is clear that any active element in a suspension system needs an input (i.e. sensors) and a control strategy, hence processing power, to be able to actively adapt to the terrain at hand. In many cases simple strategies already show improvements in active locomotion (Haynes et al., 2017), reducing the computational and sensory requirements. The strategy pursued for SherpaTT and presented in this article relies basically on four force measurements at the wheels as well as roll and pitch measurements of the body as the only exteroceptive data for ground adaption. No terrain models are employed, a purely reactive control approach is pursued.

Figure 2: Multi-Robot Scenario: SherpaTT is handing over a sample container to Coyote III for return to the lander. Coyote III has the modular manipulation arm SIMA attached which is currently in a pose to facilitate the container hand-over.

3 SherpaTT: System Overview

The rover SherpaTT is a four-wheeled mobile robot with an actively articulated suspension system and a manipulation arm. The five limbs of the system add up to 26 active DoF in total, five in each of the four legs and six DoF in the manipulator arm. Apart from the active suspension system, a modular system approach with exchangeable Payload-Items (PLIs) is another key feature of the rover. Figure 2 shows SherpaTT during a multi-robot system test. Details on the modularity and the multi-robot scenario can be found in (Roehr et al., 2014), (Sonsalla et al., 2014), (Wenzel et al., 2015), (Sonsalla et al., 2017).

SherpaTT is the successor of the system Sherpa (Cordes et al., 2011) improving the workspace of the legs while having a reduced number of active DoF (Cordes et al., 2014). Both Sherpa-versions are designed to work together with other robots in unstructured terrain; while Sherpa has to transport a highly mobile six-legged walking robot (Roehr et al., 2014), SherpaTT has to transport immobile payloads requiring a higher flexibility in the rover's body pose control for deployment and pick-up. Compared with the design of the predecessor Sherpa, SherpaTT's suspension provides a three- instead of two-dimensional positioning of the LEP by introducing a second parallelogram in the leg and thus creating a "knee".

Overall, SherpaTT has a mass of 166 kg and a payload capacity of at least 80 kg. Each of the four suspension system units (legs) has a weight of 25.75 kg, the manipulator arm has a mass of 25 kg and the central body including the manipulator mount and the mounts for the Electro-Mechanical Interfaces (EMIs) has a mass of approximately 38 kg excluding batteries. The payload capacity results from a fully equipped system with two PLIs in each of the four available payload-bays, a BaseCamp mounted beneath the robot (15 kg) and a 25 kg mobile robot lifted with the manipulator arm. The rover can vary its support polygon spanned by the four Leg End Points (LEPs) between one square meter in stow pose with a 1 m×1 m footprint and around six square

meters with fully stretched legs spanning a 2.4 m×2.4 m polygon.

The main power supply consists of two 44.4 V Lithium Polymer batteries with 10 Ah each. A power management system switches autonomously between the two batteries, an external power supply or power from the modular bus when a battery module is present. The priority is (1) external power supply (2) internal LiPo-batteries (3) attached battery module. Table 1 lists the key system specifications of the rover system, including dimensions, mass and performance characteristics.

Currently, a standard i7 PC running Linux is used for locomotion and high level control implementation. Motion control and high level processes for navigation and planning are implemented using the Rock[1] framework.

4 System Design

This chapter describes the mechanical design of the rover SherpaTT with a focus on the suspension system. The methodology for actuator selection is highlighted. For completeness, the manipulation arm is briefly introduced as well.

4.1 Kinematics of the Suspension System

Figure 3 shows the final design of a leg with annotations for DoFs and the placement of a six-axis force-torque sensor. The suspension system of SherpaTT consists of four identical legs ending in a drivable and steerable wheel. Each of the legs has five active DoF in total. Three out of the five DoF are used for placing the LEP in three dimensions relative to the body. The two outermost DoF are used to orient the wheel for steering and to drive the wheel, respectively. Figure 4(a) provides the definition of the leg index (starting with $i = 0$ at front left leg), and shows a schematic of the Pan joints angle $\alpha = 0$. The zero positions of InnerLeg β, OuterLeg γ and WheelSteering φ are provided in Figure 4(b).

The linear drives responsible for the movement of the parallelograms are mounted such that the weight of the robot pulls on the actuator, hence undesired bending forces from pushing the linear drive are avoided. The WheelSteering joint is placed over the center of the wheel, avoiding a movement of the wheel on a circular path around the joint's axis during a steering manoeuver. Furthermore, the WheelSteering actuators are not experiencing loads from WheelDrive torques.

Figure 5 illustrates the workspace of the rover's suspension system. Rotating the Pan joint creates a circular path of the leg's LEP around the joint's rotational axis which is also defined as the z-axis of the Leg Coordinate System (LCS). Movements with InnerLeg and OuterLeg joints allow to control the distance of the wheel to the LCS origin as well as the height of the wheel w.r.t. the body. Combining all three joints creates the toroid

[1] Robot Construction Kit http://rock-robotics.org

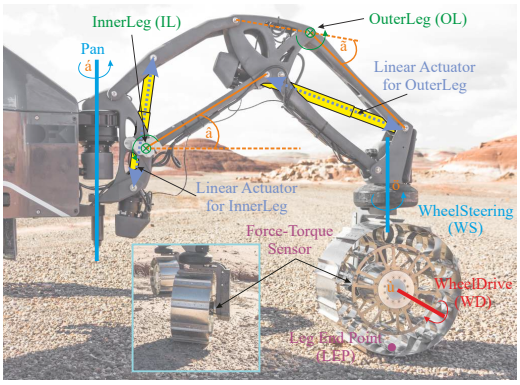

Figure 3: Description of DoF present in SherpaTT's suspension system and placement of force-torque sensor.

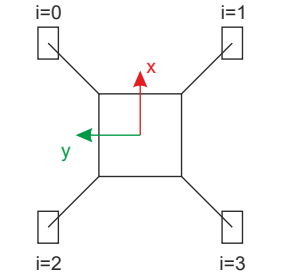

(a) Leg index and zero position of Pan joint α. Top view.

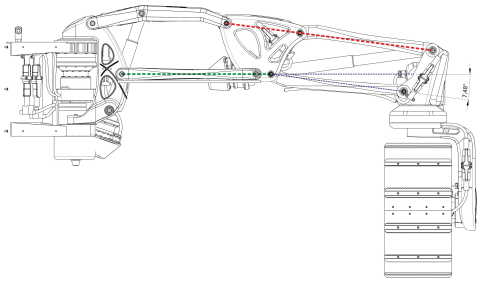

(b) Definition of zero positions. Note that OuterLeg zero position is not defined as horizontal.

Figure 4: Kinematics: Joint positions and leg indexing.

Table 1: SherpaTT System Specifications

Parameter Name	Value	Comments
Performance Characterization		
Step & Obstacle Height	0.772 m	Active stepping necessary for step-like obstacles
Ground Clearance	0.10 m – 0.80 m	Variable, can be commanded
Locomotion Speed	0.1 m/s (nom)	
	0.7 m/s (max)	Currently limited by software to 0.2 m/s
Turning Arc	1 m (min)	Wheel track radius with point turn
(circular wheel path)	2.1 m (nom)	Point turn in nominal suspension configuration
Dimensions		
Foot Print Size	variable from 1 m^2 to ≈6.76 m^2	Smallest footprint: a square with 1 m edge length. Biggest: 2.6 m edge length. Abritrary non-symmetric foot prints possible (Cordes et al., 2011) (Cordes and Babu, 2016)
Leg Length as distance between	1.082 m	Fully stretched leg
Leg Pivot (Pan) and LEP	0.880 m	Nominal configuration: PoseA in Figure 5(c)
Number of active DoF	26	4×5 suspension system, 1×6 arm
Masses		
System Mass m_g	166 kg	Total mass, w/o payloads, w/o batteries
Thereof: Legs	25.75 kg	(×4)
Thereof: Arm	25 kg	
Thereof: Central Body	38 kg	Includes structure, electronics, hull, arm mount, EMI mounts
Payload Capacity	≈ 80 kg	Based on 4×2 PLI with 5 kg/ in payload bays, one BaseCamp with 15 kg and a 25 kg payload at the manipulator.
Power-Supply		
Internal DC-Power	2× 44.4 V/10 Ah	Autonomous switching from empty to full battery
External DC-Power	50 V / 20 A	External AC/DC-converter with power tether
Nominal Power	≈150 W	Base load P_b of processors, DC/DC converters, sensors etc
	≈200 W/225 W/250 W	Total mean power when driving in flat/moderate/steep terrain. Peak loads up to 350 W possible.
Sensors		
Lidar	Velodyne HDL-32E	Main navigation sensor. Sensor mount rotates with first manipulator arm joint.
Laser Range Finder	Hokuyo UST-20LX	Tiltable. Mounted on front face. Used mainly for manipulation purposes.
Camera	Allied Vision GC1380	1360×1024px, 20.2fps, 12bit, CCD camera for human operator. With Fisheye lens Fujinon FE185C086HA-1
Attitude and Heading Sensor	Xsens MTi-300	
Force Torque Sensors (Legs)	FT-DELTA 160	Mounted at each wheel for autonomous ground adaption
Force Torque Sensor (Arm)	FT-mini 45	Part of manipulation interface
Joint Level Senors		Current (total and phase), voltage, speed, position, temperature
Communication		
External Wireless	2.4 GHz (802.11n)	WiFi
External Cable Connection	GbE	Ethernet switch connected to WiFi, control PC and modular interfaces
Internal Joint Communication	NDLCom via LVDS	Custom protocol / inter-hardware communication
Remote Emergency Switch	868 MHz Xbee-Pro	Custom hardware
Modularity / Interfaces		
Passive EMIs	4×	Mounted as “payload-bays” around arm mount
Active EMIs	2×	Mounted below central body and used as manipulation interface
Power Bus via any EMI	44.4 V / 10 A	Bi-directional power transfer possible
Ethernet via any EMI	100Mbit/s	4Pin Fast Ethernet
Local Communication	RS422	Between Modules, i.e. for organization of topology

shown in Figures 5(a) and 5(b). The toroid is the leg's workspace in which the LEP can be positioned relative to the body.

Figure 5(c) displays a cross-section of the workspace with indications for preferred poses of the leg. The nominal robot configuration is named Cross-Stance and has the LEPs at PoseA together with $\alpha = 0$. In this nominal configuration, the vertical stroke of the LEP is 671 mm, without changing the distance to the body. Pose B is a compromise between maximizing the possible body height and still having a feasible vertical stroke, while Pose C is the distance of the LEP to the leg coordinate origin that allows the highes body configuration. The total vertical stroke is 775 mm when moving the LEP from PoseA-up to PoseC-down. Note that the defined preferred poses are valid for all Pan joint positions, as they are only dependent on the InnerLeg and OuterLeg joints.

Combining the motion range of the three DoF Pan, InnerLeg, and OuterLeg results in various footprints that can be adopted. Figure 6 illustrates different defined stances and resulting footprint shapes for SherpaTT. The nominal height of a LEP in all stances is defined as shown in Figure 5(c) for the preferred poses. All illustrated stance examples are possible with different distances of the LEP from the origin of the respective leg's coordinate system. If not otherwise stated, a footprint shape is generally used in the preferred PoseA.

The chosen kinematic design has the following key-features:

- Linear actuators are placed in a way that the loads and moving-distances are almost equal for both actuators, so the same parts can be used for fabrication.
- All linear actuators experience a pull-force with the robot on ground, which leads to less slackness and simplified design of the actuator's bearings.
- High maneuvrability: the rover can shift its body parallel to the ground plane (x and y direction) which allows center of gravity shifts in sloping terrain and facilitates easier pick-up and more precise deployment of a payload as for example a BaseCamp compared to moving the body in small increments by driving motions.
- The rover's body can be rolled and pitched w.r.t. the ground and execute yaw movements, further facilitating the pick-up of payloads with the body's EMI
- Providing a knee like structure significantly reduces the stow volume of the robot, due to the possibility of compact folding.
- Pure vertical movement of a wheel is possible, hence no change of the footprint, when the rover's body is lifted or the wheels are adapted to sloping terrain.

Surely this kinematic setup also has drawbacks, one being a complex design process. Furthermore the torque that can be introduced to the Pan joints when the rover is moving in slopes can cause high structural loads in the whole leg. The knee and the additional actuator introduce moving parts and bearings that are subject to those structural loads.

4.2 Actuators for the Suspension System

All actuators employed for the suspension system are based on the design presented in (Bartsch et al., 2016). Each actuator consists of three main parts: A gear stage on the drive side, a motor, and a stack of three printed circuit boards for local joint control. Depending on the location of the actuator in the leg, different combinations of motors and gears are used, while the control electronics are identical for all actuator types.

The Pan actuator has to provide the highest torque of all suspension actuators. To estimate the required torque, a worst case scenario was used. From the initial dimensions in the design process, a radius of $\tilde{r}_{Pan} = 1\,m$ was taken as maximum lever to generate a torque from the forces acting on the wheel[2]. Furthermore, a slope of $\psi_s = 40°$ with the rover's body being parallel to the slope was assumed, and a rover mass of $m_g = 150\,kg$ was estimated during the design phase[3]. This results in a force $F_{s,wc}$ for the worst case along the slope:

$$F_{s,wc} \;=\; m_g \cdot g \cdot \sin(\psi_s) \;\approx\; 946\,N \qquad (1)$$

As a safety margin, only two legs were considered to be bearing the full load. Using the radius $\tilde{r}_{Pan}$, the worst case torque a pan joint actuator has to bear was estimated as $T_{Pan,wc}$:

$$T_{Pan,wc} \;=\; \frac{1}{2} \cdot F_{s,wc} \cdot \tilde{r}_{Pan} \;=\; 473\,Nm \qquad (2)$$

As shown in Table 2, the employed gear combination is limited to a repeatable peak torque of 433 Nm, and an allowable momentary peak torque of 841 Nm according to the manufacturer's specification. Theoretically, the chosen motor-gear combination can provide more than 2200 Nm. Since a worst case scenario with only two wheels was assumed, and the calculation done with a slope beyond the systems's specification, the chosen combination was considered to be suitable for the system. This assumption was confirmed in all use-cases so far for the physical system. The actuators did not stall in any scenario as for example moving the legs for footprint changes in natural terrain or slope climbing with impulses and oscillations resulting from slip in steep slopes.

Similar scenarios were considered for the dimensioning of all actuators in the suspension system. A spindle drive mechanism driven by a rotational actuator is used for the linear drives for InnerLeg and OuterLeg joints. For ease of fabrication, integration and control, both

[2] In the final design, the preferred PoseA has a lever of $r_{Pan} = 0.88\,m$, a fully stretched leg in kinematic singularity has a length of $r_{Pan,max} = 1.08\,m$

[3] Final mass $m_g = 166\,kg$, c.f. Table 1

(a) Overlapping workspaces of the legs mounted on the central body. Rover model shown in standard Cross-Stance configuration.

(b) Overlapping workspaces as seen from side. Rover model shown in standard Cross-Stance configuration.

(c) Cross-section of a workspace with indication of preferred poses as measured from leg's origin (dimensions in mm).

Figure 5: Workspace of the suspension system

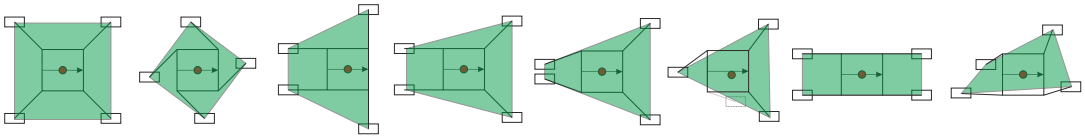

Figure 6: An extract of possible foot print configurations and resulting support polygons. From left to right: Cross-Stance, P90 (Pan joints at $\alpha_i = 90°$), Turtle-Front, Y-Shape, Quasi-Tripod, Tripod (one wheel disabled), Long-Stance, and arbitrary or asymmetric foot print.

linear drives of a leg are using the same hardware. For dimensioning the WheelSteering and WheelDrive actuator the aspired wheel dimensions are used together with worst case loads to estimate the required torques. The final actuator dimensioning is listed in Table 2.

4.3 Manipulator Arm and Body Concept

For completeness, this section briefly gives a description of the central body and the manipulation arm. The arm is not used for the experiments described in this article, details on the manipulator arm design are described in (Dettmann et al., 2011) and (Manz et al., 2012).

The manipulator arm is the hardware taken from the predecessor Sherpa. For SherpaTT the EMI is updated to the new design as presented in (Wenzel et al., 2015) and the first joint is exchanged for the same type of double stage gear actuator as used for the leg's Pan joints.

The arm is mounted centrally on the body of the rover, to be able to reach the ground all around the system. Mounted around the central manipulation tower are four EMIs that are used in the multi-robot scenario. For navigation, a HDL-32E rotating lidar is mounted on the arm such that the sensor rotates with the first DoF of the manipulation arm.

4.4 Robustness and Failure Response of an Actively Articulated Suspension System

Assuming the rover to get stuck in soft soil, several options to free the system exist. If a wheel breaks through a crust and gets stuck in soft soil, the wheel can be lifted and placed in a different location. If required, the manipulation arm can add stability during the repositioning of the wheel, (Roehr et al., 2014). Alternatively, the footprint can be changed for stable tripod-stance if the arm support is not feasible. Generally, a maneuver to free a wheel from soft soil can be conducted in arbitrary footprint configurations. Detection of soft soil or other ground parameters might be possible using the force and torque information available at each wheel, this is, however, not implemented nor experimentally validated up to now.

When all wheels are subject to heavy slip and a wider area of soft soil is present, subsequent repositioning of all wheels is possible. This would lead to a kind of walking behavior to free the rover from very soft soil. The rover is not primarily designed for walking, yet the kinematics of the suspension system allow for implementation of motion patterns similar to walking locomotion.

The performance of a complex system as presented with the active suspension of SherpaTT can be impeded by failure of single joints. This is surely a factor of risk in a space mission, where currently no maintenance and repair is possible. However, the advanced locomotive capabilities allow to reach scientifically interesting and hard-to-access areas in the first place: Cliffs, crevasses and the top of inverted river beds promise to be spots with increased science return, for example in terms of geologic history and traces of former or actual presence of water. These areas cannot be safely reached with the currently deployed robots (Schenker et al., 2001), (Huntsberger et al., 2007), (Nesnas et al., 2012).

Table 2: DoF naming and actuator specifications for SherpaTT. Note that the range of motion of each DoF is generally not symmetric around the respective zero position. Pan joints use a double-stage gear.

Joint name	Index j	Angle identifier	Gear	Speed	Torque/ Force (nominal)	DoF Range of Motion
Pan	0	α	1:30 + 1:100	7 °/s	433 Nm*)	223°
InnerLeg	1	β	1:30 + linear TR14x4	12 mm/s	3500 N	70°
OuterLeg	2	γ	1:30 + linear TR14x4	12 mm/s	3500 N	81°
WheelSteering	3	φ	1:120	175 °/s	60 Nm	340°
WheelDrive	4	ω	1:100	210 °/s	74 Nm	inf.

*) theoretically the motor gear combination provides more than 2200 Nm; 433 Nm is the repeated torque rating of the gear box. A momentary peak torque of 841 Nm is rated for the gear box.

Analysing the individual joints in each of SherpaTT's legs, the Pan joint is the least critical joint for failure: A Pan joint not able to move anymore results in less flexibility in the choice of footprints and can impede the roll-pitch adaption capabilities. General driving capabilities and ground adaption control are not affected: Force leveling control, which is the main ground adaption process (see next section), would not be affected from a failure of the Pan joints.

When InnerLeg or OuterLeg actuators fail, a rudimentary ground adaption would still be possible with all legs: Loading and unloading of the wheel is possible, however, for adaption, the wheel moves relative to the body, possibly resulting in undesirable slip or shear of the wheel on the ground. Generally, this would be counteracted by correct wheel orientation, as presented in Section 5.3; the approach is working independently from failure of individual joints and can be used without changes.

Failure of WheelSteering and WheelDrive joints results in the same problems that a passive suspension system would experience. However, the active suspension can be used to permanently remove a wheel from ground contact and drive on in a three wheel configuration as described above. If a failed WheelDrive does not block the wheel, the three remaining wheels provide enough thrust for the robot to move, the locomotion capabilities are only affected marginally. The maximum manageable slope inclines would be reduced in this case. Locomotion of SherpaTT on four wheels with only three of them powered has already been tested successfully in a qualitative experiment setting in flat outdoor terrain .

With the four wheeled-legs the loss of one leg can be generally compensated, assuming that it can at least be moved up high enough to not be in ground contact any more. This requires at least the InnerLeg or OuterLeg joint to be still functional. The remaining three wheeled-legs are then oriented in a tripod stance that distributes the wheels on a circumference around the robot's center. The distribution is chosen such that the disabled leg's weight is shared from the two adjacent legs. Calculation of reference forces is actually simplified with only three contact points, however, arbitrary changes in footprints are not possible anymore and roll-pitch control might also be impeded.

5 Control System Design

The rover's autonomy and locomotion control are running in the Rock framework. Three basic software layers can be identified in the robot control stack:

1. *High Level, running on On-Board Computer (OBC)*: Autonomous navigation and control
2. *Middle Ware, running on OBC*: Motion control, responsible for suspension articulation
3. *Low Level, running on FPGA and microcontrollers*: Joint control and sensor pre-processing

Both, high level and middle ware are implemented using the Rock framework. The system can be used with autonomous components for navigation, mapping and exploration of unknown terrain by using the highest software level. However, by only running the levels 2 and 3, direct remote operation of the system is possible by a human operator. Direct (tele-)operation and autonomous behaviors both use the same software interfaces on level 2.

This paper focusses on the experimental validation of the rover's level 2, the *Motion Control System (MCS)*, hence the following sections focus on describing the middle ware layer. Special focus is given on the active *Ground Adaption Process (GAP)* and its submodules enabling the locomotion of the system on a natural terrain. The GAP is the software module responsible for generating LEP offsets from force measurements and body roll-pitch data in order to adapt the suspension system to the current terrain conditions.

5.1 Motion Control System Overview

Figure 7 provides an overview on the general structure of the MCS for SherpaTT. The three main command input types are used for human operator control or autonomous control. The commands are defined as follows:

Definition 5.1: Motion Command 3D (MC3D).
The three dimensional command vector $\dot{\xi} = (\dot{x}\ \dot{y}\ \dot{\Theta})^T$ is used to command forward ($\dot{x}$), lateral ($\dot{y}$) and rotational ($\dot{\Theta}$) velocity of the rover. All three components are independent of each other.

Definition 5.2: BodyPosture.
A six dimensional vector $\mathbf{b} = (x_b\ y_b\ z_b\ \Omega\ \Phi\ \Psi)^T$ containing lean values of the body within the support polygon (x_b, y_b), the body height (z_b) and roll (Ω), pitch (Φ) and yaw (Ψ) commands of the body.

Definition 5.3: FootPrint.
Four three dimensional vectors $\mathbf{g_i} = (r_i, \alpha_i, z_i)^T$ ($i = \{0 \dots 3\}$) define the foot print of the robot in cylindrical coordinates (origin is the leg coordinate system, see below). This command is mainly used to alter the support polygon of the robot in the projected plane beneath the robot by changing the r- and α-coordinates of each LEP. In addition to the body-height command, the z-coordinate of each LEP might be commanded individually. Figure 6 illustrates several possible foot prints resulting in different support polygons for the robot.

Internally all commands are processed such that a consistent locomotion of the system is possible. The *DriveMode* module handles the MC3D to orient the wheels according to the current velocity command for the rover. Additionally, the module integrates possible motions of the suspension's legs, i.e. resulting from foot print changes, to avoid internal stress that would result in slippage of the wheels. Hence, foot print changes and body posture changes can be conducted while driving, a system stop for reorganizing the suspension system is in general not required, see also Section 5.3.

BodyPosture and FootPrint commands are merged within the *LEP Command Generator* module to a single LEP-Command $\mathbf{p}_{ref,i}$ for each leg i. The resulting command is forwarded to the *LEP Interpolator* module. The interpolator generates smooth trajectories between actual and commanded LEP, the final LEP commands $\mathbf{p}_{ref,i}$ are written to an inverse kinematics module. The inverse kinematics module calculates the joint commands $\mathbf{q}_{ref,i} = (\alpha_{ref,i}\ \beta_{ref,i}\ \gamma_{ref,i}\ \varphi_{ref,i}\ \omega_{ref,i})^T$ for each leg i of the suspension system.

The central GAP takes the merged LEP commands from the command generator as reference input and uses sensor data as to generate LEP output commands modifications (i.e. offsets) $\mathbf{o}_i$. The offsets are depending on the control modules and current ground adaption strategy. These offset values are written to the interpolated LEP commands.

In the rover's motion control system a *Ground Plane Estimator* is implemented. The ground plane is estimated by fitting a plane in a least square approach through all LEPs of wheels with ground contact. If there are only two wheels with ground contact – which can happen for short periods of time due to the width of the wheels – the plane calculation is considered not valid and the last valid plane is assumed. The fitted plane is corrected by the measured roll and pitch of the body in order to achieve a representation in a fixed coordinate frame. This module is currently not used for autonomous ground adaption, however, an experimental validation was conducted during the field tests as presented in Section 6.

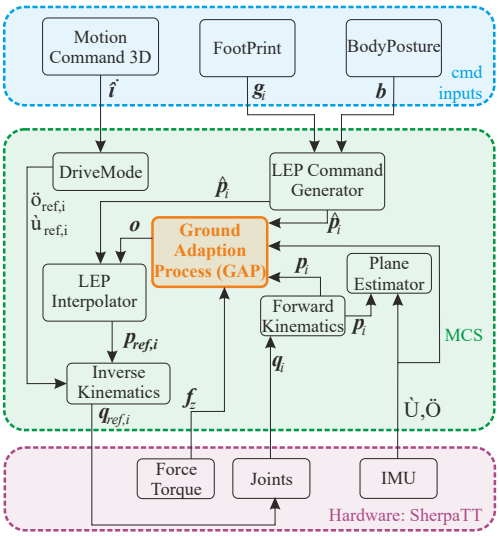

Figure 7: Simplified control structure of SherpaTT's Motion Control System (MCS) with inputs from high-level or human operator, sensor inputs and outputs to the hardware. The central Ground Adaption Process (GAP) is responsible for active terrain adaption.

5.2 Coordinate Systems for Locomotion Control

For locomotion control, different coordinate systems are used for ease of description and implementation of locomotion behaviors. All employed coordinate systems are right-handed.

Figure 8 illustrates the locomotion coordinate systems. The depicted coordinate systems are:

Definition 5.4: Body Coordinate System (BCS).
All commands for the leg end points are internally represented in this coordinate frame. Its origin is located in the center of the robot's body, x pointing forward, z pointing up, Figure 8(a).

Definition 5.5: Shadow Coordinate System (SCS).
At startup of the MCS, shadow coordinate system and body coordinate system BCS are identical. Body posture commands $\mathbf{b}$ are describing the movement of the body from this initial position. Motion commands $\dot{\xi}$ are interpreted in this frame.

Definition 5.6: Leg Coordinate System (LCS).
Used for intuitive description of a foot print. Cylindrical coordinates are used in this frame for describing each LEP: $\mathbf{g}_i = (r_i, \alpha, z_i)^T$.

Definition 5.7: Wheel Coordinate System (WCS).
Used internally for accumulating all movements due to motion command and footprint changes. Wheel orientation and velocity are calculated in this frame.

Figure 8(b) illustrates the advantage of using a shadow coordinate system: With unchanged body posture ($\mathbf{b} = \mathbf{0}$), LEP commands are the same in body coordinates

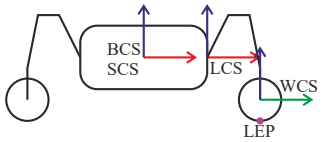

(a) Body in standard posture (side view). Commands in BCS and SCS are identical.

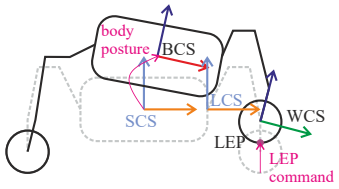

(b) Body posture changed, LEP command input is in SCS, i.e. moving a LEP "up" is independent of the body's pose.

Figure 8: Important coordinate systems: Body Coordinate System BCS, Shadow Coordinate System SCS, Leg Coordinate System LCS, and Wheel Coordinate System WCS.

and in shadow coordinates. In the example illustration, a body height change together with a positive body pitch is commanded. If the odometry be described in body coordinates, movement would no longer be only in x-direction but also in z-direction. Using shadow coordinates, a forward-velocity command does not need to incorporate the body's actual orientation. Considering the LEP control, a change in the LEP's z-component is always perpendicular to the ground, since the leg coordinate system is also a shadow coordinate system.

5.3 Commanding a Rover with a Variable Footprint

Moving a rover with adaptive suspension that allows changing footprints and thus changing the location of the wheels w.r.t. the body requires some consideration of the orientation control of the wheels for locomotion. Incorrect orientation of wheels results in structural stress, undesired forces, possible slip and might lead to failure following trajectories which in turn can cause hazards for system stability and integrity.

With fixed wheel positions and assuming motion on a flat plane, all wheels need to be oriented such that all wheel axes intersect at a common point, which is the Instantaneous Center of Rotation (ICR). An ICR in infinity of the y-axis of the SCS corresponds to a pure forward movement, while positioning the ICR at the origin of the SCS results in a pure point turn of the robot[4]. In (Cordes et al., 2011) an explicit calculation of the wheel orientation and wheel velocity for a rover with variable footprint is presented for the system Sherpa. The calculation assumes quasi static states and neglects the current movement of the suspension system. For SherpaTT the rover's current velocity resulting from the commanded vector $\dot{\xi}^{SCS}$ is transformed to the frame of each wheel i to form the vector $\dot{\xi}_i^{WCS}$ of velocities at each wheel resulting from the MC3D according to Eqn. (3), where $\mathbf{T}_{WCS,i}^{SCS}$ is the instantaneous homogeneous transformation matrix between SCS and WCS_i, which is dependent on the current pose of leg i.

$$\dot{\xi}_i^{WCS} = \mathbf{T}_{WCS,i}^{SCS} \; \dot{\xi}^{SCS} \qquad i \in \{0,1,2,3\} \tag{3}$$

The velocity of an LEP resulting from the movement of the respective suspension leg i is described as $\dot{\lambda}_i$ and calculated using the measured angular velocities of each DoF. The combined velocity $\dot{\mathbf{p}}$ at each LEP resulting from both, leg movement and robot movement is then calculated as

$$\dot{\mathbf{p}}_i = \dot{\xi}_i^{WCS} + \dot{\lambda}_i. \tag{4}$$

The condition for slip free motion with intersection of the wheel axes in the ICR holds only for fixed LEP positions. Introducing the component $\dot{\lambda}_i$ in $\dot{\mathbf{p}}$ resulting from a leg's motion renders the condition invalid. Figure 9(a) shows the velocity vector $\dot{\xi}^{WCS}$ at a wheel due to the rover's motion as well as a velocity vector $\dot{\lambda}$ of the respective leg's motion and the combination $\dot{\mathbf{p}}$ of both velocities for wheel alignment.

The orientation φ_i and velocity ω_i of wheel i are based on $\dot{\mathbf{p}}$ and can be calculated by

$$\varphi_i = \arctan2\left(\dot{p}_{i,x}, \dot{p}_{i,y}\right) \tag{5}$$

$$\omega_i = \frac{|\dot{\mathbf{p}}_i|}{r_w} \qquad r_w\text{: wheel radius} \tag{6}$$

In general, two orientations of φ are possible for correct movement. For locomotion control in SherpaTT the solution with smaller difference to the current orientation is preferred, minimizing the movement needed in the joint to reach the desired configuration. Depending on the chosen orientation φ_i, the calculated wheel velocity ω_i might need to be inverted.

With smooth trajectories, only small changes in the commanded velocity for the rover occur, resulting in incremental changes of the wheels' steering angles. However, jumps in the reference angles $\varphi_{ref,i}$ might occur, for example, when a FootPrint change is commanded during drive and a sudden non-zero value for $\dot{\lambda}$ is measured.

Figure 9(b) illustrates the change of direction when a leg movement is introduced between time step $t-1$ and t. The difference between current and last reference steering angle is $\Delta\varphi_{ref}$. Since the physical WheelSteering actuator cannot change its position instantaneously to the new slip-free orientation, the whole robot has to switch into a so called re-alignment state where the

[4]The parallel wheel axes then are defined to intersect in infinity.

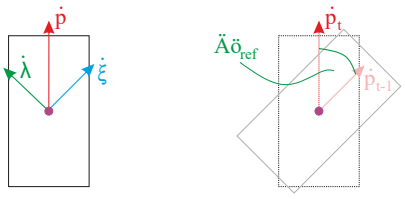

(a) Velocity combination in wheel frame. $\dot{\mathbf{p}}$ is pointing in y-direction of WCS.

(b) Velocity direction changes result in changes of the steering angle φ. A sudden change results in a large $\Delta\varphi$ which cannot be followed instantaneously by the actuator.

Figure 9: Velocity components at a leg's LEP and sudden velocity direction change.

current reference values of all joints are stored and all movements are stopped until the desired wheel orientation is reached. Since in stopped state both, $\dot{\lambda} = \mathbf{0}$ and $\dot{\xi}^{WCS} = \mathbf{0}$, a fading between the stored non-zero reference velocities and the actual velocities is done until the robot regains its speed, to avoid excessive WheelSteering reference angle switching.

5.4 Ground Adaption Process

This section describes the Ground Adaption Process (GAP) by detailing the single subcomponents and how the components interact with each other to achieve a consistent active ground adaption of the system. Generally, each of the subcomponents described in the following sections generates an LEP offset value that is added to the LEP command before passing the modified LEP command to the inverse kinematics module.

Figure 10 illustrates the structure of the GAP. The modules described in the following paragraphs are highlighted in the blue boxes. *Force Leveling Control (FLC)* and *Roll and Pitch Adaption (RPA)* are running in parallel and are writing offsets to the LEP commands. The *Active Wheel Steering Support* module is acting as an input to the Force Leveling Control by generating new reference forces in case of a stuck WheelSteering joint. After adding the LEP command and all submodules' offsets the new command is passed to the *Body Height Control* module to shift all LEPs such that the available workspace is maximized by keeping the FLC and RPA objectives, the latter prohibiting the control case shown in Figure 12(c).

5.4.1 Force Leveling Control Module

An important role for SherpaTT's active ground adaption is taken by the FLC component. For each wheel a contact force can be expected that is related to the position of the wheel w.r.t. the body. Using the FLC module, the expected force for each wheel is maintained, deviations due to sloping terrain are corrected and the ground contact of all wheels is ensured.

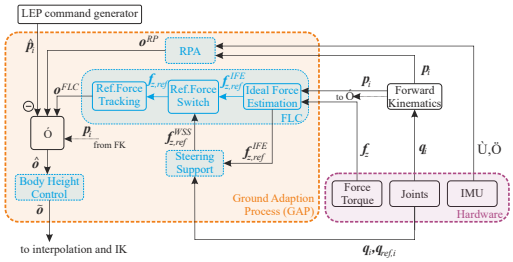

Figure 10: Structure of GAP and connection of components.

Inputs for the FLC component are the measured forces at each wheel, the location of the Center of Gravity (CoG) as well as the current coordinates of each wheel's LEP. Note that the task of FLC is to maintain the *expected* forces derived from the current foot print configuration of the robot. Improving the force distribution for locomotion, i.e. by shifting the robot's body forward when driving upslope is not the task of the FLC. The reference force switch displayed in Figure 10 is used to forward the modified reference forces as final input $\mathbf{f}_{z,ref}$ to the force tracking in case a wheel steering support is active (see Section 5.4.2).

For each wheel i the ideal contact force $f_{z,ref,i}$ is estimated in terms of the current footprint under the assumption of static equilibrium with only the gravitational forces and their reaction forces from the ground acting on the robot. Three constraint equations with four unknowns can be established, the resulting underdetermined system is solved using a Moore-Penrose pseudoinverse. The output of the FLC are offsets for the z-coordinates of the LEPs in order to increase or decrease the force acting on a wheel.

To generate the reference forces, the LEPs and the CoG of the robot are projected onto a gravity perpendicular 2D plane using the Inertial Measurement Unit (IMU) measurements, resulting in the 2D position of the LEPs $\begin{pmatrix} x_i & y_i \end{pmatrix}^T$ and the 2D position of the CoG $\begin{pmatrix} x_c & y_c \end{pmatrix}^T$. A vector $\mathbf{t} = \begin{pmatrix} 0 & 0 & mg \end{pmatrix}^T$ is constructed containing zero-moments around x and y axis and gravitational force with m the mass of the robot and g the acceleration due to gravity. The vector of expected reaction forces at each LEP is the vector of reference forces $\mathbf{f}_{z,ref} = \begin{pmatrix} f_{z,ref,0} & f_{z,ref,1} & f_{z,ref,2} & f_{z,ref,3} \end{pmatrix}^T$. Equation (7) shows the underdetermined equation system.

$$\mathbf{A} \cdot \mathbf{f}_{z,ref} = \mathbf{t} \tag{7}$$

The matrix $\mathbf{A}$ is defined as provided in Equation (8).

$$\mathbf{A} = \begin{pmatrix} x_0 - x_c & x_1 - x_c & x_2 - x_c & x_3 - x_c \\ y_0 - y_c & y_1 - y_c & y_2 - y_c & y_3 - y_c \\ 1 & 1 & 1 & 1 \end{pmatrix} \tag{8}$$

Constructing the Moore-Pensrose pseudoinverse $\mathbf{A}^+ = \mathbf{A}^T \cdot (\mathbf{A} \cdot \mathbf{A}^T)^{-1}$ allows to calculate $\mathbf{f}_{z,ref}$ according to

Equation (9).

$$\mathbf{f}_{z,ref} = \mathbf{A}^{+} \cdot \mathbf{t} \tag{9}$$

In each time step of MCS execution, $\mathbf{f}_{z,ref}$ is recalculated, updating the reference values according to the current footprint and CoG location within the support polygon.

Without active leg end point control ground contact loss of one wheel can occur even in slightly irregular terrain, as there are more than three wheels on the rover that generally make ground contact. In its preferred posture the rover has a square shaped support polygon. When one of the wheels looses ground contact, the two neighbouring wheels share the main load of the system and form what is defined as *strong contact pair*. As with a rocking table the other two wheels of the *weak contact pair* tend to change their ground contact state. The two diagonals a_0 (between front left and rear right) and a_1 (between front right and rear left) of the support polygon are defined as *strong axis* and *weak* axis depending on the ground contact state of the wheels, (Cordes et al., 2017).

Since the strong axis has always a higher contact force than required and the weak axis always has a lower force than required, a simplified control can be used to (i) increase the speed of adaption since one pair is moving up and the other pair is moving down the same amount, (ii) reduce the number of independent controllers from four to one, and (iii) reduce interferences in force controllers of one wheel to all other wheels, since unloading one wheel results in increased load of three other wheels.

Note that the whole approach is reactive; no models of terrain-ground interaction, digital elevation maps or planning algorithms are required. This approach is chosen deliberately to keep the processing efforts as low as possible and to be able to deploy the control system on lower performance hardware in the future. Generally, reactive controllers have a better chance of being deployed successfully on space hardware with limited performance (Mumm et al., 2004). The experiments described in Section 6.4 are conducted to characterize the validity of this approach for other than the nominal Cross-Stance foot print.

5.4.2 Active Wheel Steering Support

Generally, the bigger the contact area of a wheel with the ground the better the traction of the wheel. However, with the steering axis above the wheel center, a bigger contact area requires a higher steering torque and also causes higher stresses in the wheel structure when steering against the ground resistance. With the possibility to lift single wheels off the ground comes the opportunity to actively unload wheels for steering support. This can be used in situations where the wheels get stuck between rocks or are subject to heavy sinkage in soft soil. Furthermore, the strength of the actuators for steering the wheel can be smaller as the actuator does not have to be designed for worst case scenarios.

SherpaTT's MCS has a trigger for active wheel steering support which is based on the difference of actual steering angle φ_i and the commanded reference value $\bar{\varphi}_i$. The steering joints are limited conservatively in the drawable current (hence a torque limit is established) to limit mechanical loads introduced through the wheel during a steering manoeuver. Thus when the required torque is bigger than the threshold, actual angle and reference angle for the steering DoF diverge as the wheel cannot be turned against the resistance.

Unlike most of the GAP subcomponents which are generating LEP offsets, the wheel steering support module manipulates the reference forces $\mathbf{f}_{z,ref}$ of each wheel for unloading the wheel being stuck. In case the steering support is triggered for wheel j, the reference ground contact force $f_{z,ref,j}$ is reduced (see also Section 5.4.1) by shifting a part k of the ground contact force to the remaining three wheels. During a wheel steering support event, the modified reference forces are used in the FLC component, once the wheel orientation reached the reference angle, the regular ground contact reference forces $\mathbf{f}_{z,ref}^{IFE}$ from the *Ideal Force Estimation* module are used for each wheel. The value k is chosen such that the stuck wheel becomes part of the *weak contact pair*.

5.4.3 Roll-Pitch Adaption Module

The Roll and Pitch Adaption (RPA)-module is responsible for controlling the body's roll and pitch angles. Both, roll and pitch angle are measured with respect to gravity. To calculate an offset o_i^{RP} for each LEP, measured and commanded roll and pitch angles are compared in angle-axis form $\{\mathbf{e}, \theta_e\}$, where $\mathbf{e}$ is the normalized rotation axis and θ_e is the rotation error. As the yaw angle is not included in the RPA calculations, $e_z = 0$, hence $\mathbf{e}$ is lying in the xy-plane. The distance d_i of an LEP from the rotation axis is a scaling factor for the offset, simply put, the further away a leg from the rotation axis, the greater the offset for the same rotational effect, which follows from the intercept theorem of geometry. The sign of o_i^{RP} (adapting up or down) is determined by the sign of θ_e and the LEP location in the xy-plane $\mathbf{p_i} = \begin{pmatrix} x_i & y_i & 0 \end{pmatrix}^T$ w.r.t. $\mathbf{e}$. Figure 11 illustrates the angle-axis representation.

$$o_i^{RP} = \pm\, d_i \tan\theta_e \tag{10}$$

$$d_i = \|\mathbf{e} \times \mathbf{p}_i\| \quad \text{because } \|\mathbf{e}\| = 1 \tag{11}$$

$$o_i^{RP} = \operatorname{sgn}(\mathbf{p} \cdot \mathbf{n})\, \|\mathbf{e} \times \mathbf{p}\|\, \tan\theta_e \tag{12}$$

Where $\mathbf{n}$ is the normal of the plane spanned by the rotation axis $\mathbf{e}$ and the basis vector along the robot's z-axis $\hat{k} = \begin{pmatrix} 0 & 0 & 1 \end{pmatrix}^T$. Each leg's index is represented by $i = \{0, 1, 2, 3\}$.

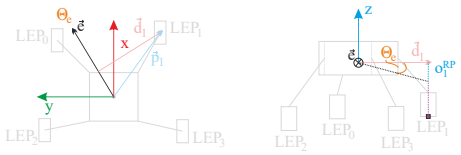

Figure 11: Illustration of angle-axis calculations for RPA-module. Left: top-view onto SCS; right: view in direction of **e**.

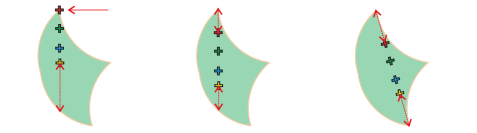

(a) One LEP reaches the upper limit of its workspace while all others are well away from workspace limits

(b) Shifting the body up increases the workspace by shifting all LEPs down

(c) Further increase of available workspace by rolling or pitching the body

Figure 12: Body Height Control module: Shifting body to increase overall workspace of active ground adaption. This module might be not usable when specific body commands are required.

5.4.4 Body Height Control Module

The Body Height Control (BHC) module is used to tailor all written offsets such that the rover's body height is altered in a way that maximizes the workspace of the legs. Figure 12(a) shows the situation, when an LEP (illustrated as red cross) reaches its upper workspace limit, rendering it impossible to further unload the wheel. In the example, all other LEPs, are still some distance from their respective limits. Hence, shifting all LEP-offsets by the same amount allows further adaption of the overall system, as shown in Figure 12(b). This effectively results in a change in body-ground clearance and hence is only possible in situations where the system is not required to keep a certain body height. A further increase of the workspace is possible by allowing the BHC module to manipulate the roll and pitch angle of the body as well, as illustrated in Figure 12(c). Again, a decision has to be made whether body roll and pitch or the quality of ground contact are of more importance in the current situation.

6 Experiments

This chapter describes the experiments conducted during the field trials with the rover system SherpaTT. The site for the experiments was chosen due to its reported similarity to areas on Mars (Clarke and Stoker, 2011), (Dupuis et al., 2016), (Caudill et al., 2016), (Balme et al., 2017). Preliminary indoor-experiments with SherpaTT for validation of the GAP behavior prior to the field tests are described in (Cordes et al., 2017) and (Cordes and Babu, 2016).

Experiments in three different test tracks in natural terrain were conducted during the field trip to evaluate different aspects of the rover in natural terrain. Each test track was driven in forward and backward motion, with different GAP-modes and different rover footprints. The following sections provide a description of the three terrain setups and the results from data analysis from the runs in these setups.

From the log-data of the experiments, following aspects are analysed and described in this article:

- power requirements in natural terrain, Section 6.3,
- force reference tracking and body angle control, Section 6.4,
- terrain slope estimation from proprioceptive data, Section 6.5, and
- slope climbing capabilities of SherpaTT in Section 6.6.

Summarizing the results of the following sections, it can be stated that in terms of power requirement the expectation of a general higher power draw using active suspension is confirmed. However, the extra amount of power is low compared to the overall system power requirements, at least in the presented terrain types and footprint configurations. Concerning the force reference tracking, all tested footprints showed to be usable with the force leveling methodology described in this article. The body angle control is able to keep the Root Mean Square (RMS) error below 0.5° in all tested terrains and footprints. In moderate slopes, the error is reduced to 0.2° or below. Terrain slope estimation can be confirmed to be invariant of the chosen footprint. A slight problem can be identified in the estimation when wheels loose ground contact. In terms of slope climbing experimentation, it is found that the slip in steep slopes seems to be more influenced by the chosen ground adaption mode than by the chosen footprint.

Further experimentation was conducted but is not explicitly covered in this article. This includes qualitative experiments such as successfully driving over individual high obstacles, as shown in Figure 13(a) or traversing terrain covered in small rocks of up to 100 mm height with occurrence of individual lager rocks as shown in Figure 13(b). Both of these mentioned scenarios did not pose a problem for the locomotion system, however, a quantitative experimental setup was not conducted in these areas.

6.1 Experimental Setups

This section describes the different setups for conducting the evaluation experiments with SherpaTT. In total three test tracks, namely Flat-Terrain, Moderate-Slope, Steep-Slope are used. In each test track, single runs of the robot are conducted, while varying the driving direction (forward and backward), the footprint (two to three footprints per test track) and the GAP-mode.

The following GAP-modes are used in the experiments:

(a) Crossing a ≈450 mm high obstacle on one side of the rover

(b) Negotiating undulating terrain abundantly covered with rocks

Figure 13: SherpaTT during additional experimentation not covered in this article (Screenshots from video material)

- *noAdap* – a stiff suspension system, only the flexible metal wheels are providing adaption. This setting is chosen as a baseline to be compared with the following two other settings.
- *FLConly* – the LEP of each leg is adapted such, that the calculated reference force at the leg's wheel is maintained
- *FLC+RPA* – force leveling control and body angle control (roll-pitch) are both active and working in parallel

Since preliminary experiments showed that using pure roll-pitch adaption without force leveling control can lead to undesired wheel-ground contact loss (Cordes et al., 2017), the GAP-mode *RPAonly* was not tested in any of the setups. The contact loss occurs for example, when a one-sided obstacle causes a pitch error of the body. To counteract the error, both front wheels are lifted up, effectively taking the wheel without obstacle off of the ground.

In each test track the footprint Cross-Stance is used. This is the nominal configuration of the rover and allows a direct comparison between the different test tracks. Additional footprints are chosen according to the rationales described in the following subsections.

6.1.1 Setup Flat-Terrain

Figure 14 illustrates the setup for Flat-Terrain. Main driver for this setup is baseline-data without slopes for the rover. In this setup, a straight drive for a distance of 20 m with a velocity setting of $\dot{x} = 0.1\,\mathrm{m/s}$ is commanded. The rover drives alternating forward and backward on the test track. The footprints Cross-Stance, P90, and Turtle-Front as illustrated in Table 3 are used, all with LEP in the preferred PoseA. A total of 22 runs is conducted in this setup. In this setting the ground adaption options *noAdap* and *FLConly* are used. Since there are basically no slopes in this setting, the option *FLC+RPA* was not used. Table 3 lists the conducted runs.

Table 3: Conducted runs in Flat-Terrain. Idx: Run index.

	 Cross-Stance		 P90		 Turtle-Front	
	Amount	Idx	Amount	Idx	Amount	Idx
noAdap	6	1-6	4	9-12	4	17-20
FLConly	2	7-8	4	13-16	2	21-22
Total	8		8		6	

6.1.2 Setup Moderate-Slope

Figure 15 shows the general test setup of the Moderate-Slope runs. The main driver for this setup is the evaluation of the force leveling component and the combination of force leveling and roll-pitch adaption in moderate slopes.

In each run, the rover drives a 12 m traverse over the depicted natural terrain with a constant commanded velocity of $\dot{x} = 0.1\,\mathrm{m/s}$. The track is separated into three segments of about 4 m where the first and last segment have nearly no slope, while the middle segment has a slope of approximately 8°. The rover drives alternatively forward and backward on the test-track, hence runs with an odd index have a negative slope, while runs with an even index are those driving upslope (rear wheels first). The front wheel pair is used to determine the traveled distance, Figure 15 shows the situation before a forward run. When stopping the rover in a forward run the rear wheels are at about the center of the third segment, this is the starting condition of the backward runs which stop in the setting as depicted in the figure.

Table 4 lists the conducted runs for this test track. A total of 30 runs is conducted in this setup, separated into the two different footprints Cross-Stance and Quasi-Tripod as illustrated in Figure 6, both with LEP in the preferred PoseA. In each footprint, runs without any active ground adaption (labeled *noAdap*), with active FLC and inactive RPA (labeled *FLConly*) and with both controllers active (labeled *FLC+RPA*) are conducted.

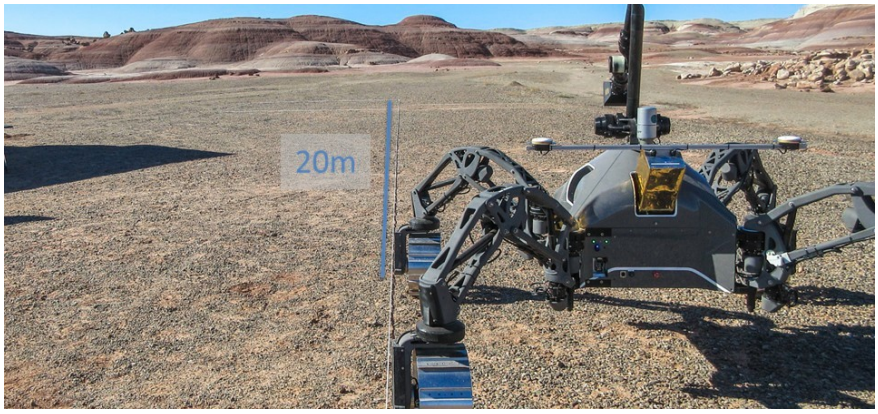

Figure 14: Experiment setup in Flat-Terrain. The DGPS module is connected to SherpaTT's rear EMI.

Table 4: Conducted runs in Moderate-Slope.

	Cross-Stance		Quasi-Tripod	
	Amount	Idx	Amount	Idx
noAdap	2	1-2	2	17-18
FLConly	8	3-10	6	19-24
FLC+RPA	6	11-16	6	25-30
Total	16		14	

The footprint Turtle-Front from Flat-Terrain is altered to Quasi-Tripod, as the tripod configuration is especially interesting for force leveling: Using basically three contact points eliminates the undefined contact distribution and is expected to provide more stable ground contact with only the passive adaptive wheels and without active ground adaption.

6.1.3 Setup Steep-Slope

In this experiment series, the rover is commanded to drive on a hill with varying slope inclination of up to 28°. A photograph of the test slope is shown in Figure 16. For reference, 1 m long segments of the slope angle are recorded with an angle-meter. Table 5 shows the 1 m segmented slope angles on the test track.

A Differential Global Positioning System (DGPS) system is mounted on the rover for ground truth, as the main objective of this setting is the evaluation of slippage in slopes under different footprint and GAP settings. The slippage is recorded as a difference between Global Positioning System (GPS) distance and odometry distance.

The rover is commanded to drive a 17 m long distance on the slope. The runs are alternating as upslope runs and downslope runs. After each run the robot was set manually to the starting position for the next run in order to compensate for slip and deviations from the track. Downhill runs start on top of the hill, uphill runs start at the lower end of the track, with the front wheel pair as reference, hence in downslope runs (rear wheels first) the rear wheel pair is already ≈2 m into the track.

The first four (pre-test) runs were conducted with a velocity of $0.1m/s$, after those runs, the duricrust was broken and the system ended in 100% slippage in mid-slope for the next trials. A velocity setting of $0.04m/s$ was then used for all remaining runs, allowing the rover to climb the slope without getting stuck in the soft soil of the broken duricrust. Nine of the runs are conducted in Cross-Stance, four runs in Y-Shape are recorded, resulting in a total of 13 valid runs on the slope.

The runs with 0.1m/s are excluded from the detailed analysis in this paper. However, two successful upslope and two successful downslope runs from the pre-tests are used for comparison in the power requirement analysis in Section 6.3.

Originally, Turtle-Front was thought to be a good shape for the steep slope since the CoG of the robot is shifted to the front of the support polygon, which proved beneficial with a walking/climbing robot (Bartsch et al., 2010). However, runs in this footprint had to be aborted due to the structural loads, that were introduced to the front legs, being perpendicular to the downhill-slope force. Rotating the front leg pair into the slope results in the tested Y-Shape, which showed a higher structural stability of the rover and still has a forward shifted CoG when compared to Cross-Stance.

Further preliminary runs showed that a completely stiff suspension system (in *noAdap*-setting) poses a risk on the system stability as ground contact loss is imposing high loads to the remaining legs with ground contact and ground contact loss leads to high slip values on the remaining wheels. Even though the loads were accounted for in the mechanical design phase, the rover was not put to this risk in the field trials, hence all runs are conducted with active force leveling module in order to have all four wheels in permanent ground contact during slope drive (*FLConly* or *FLC+RPA* settings). Out of the 13 runs, six are conducted with active roll-pitch

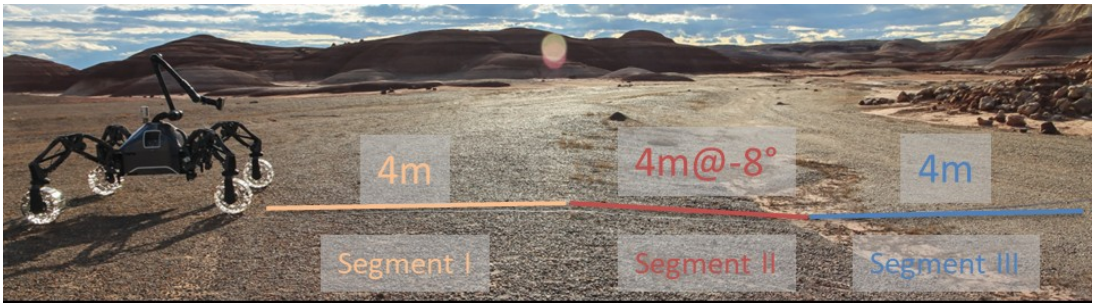

Figure 15: Experiment setup in Moderate-Slope with indicated approximate slope profile.

adaption (*FLC+RPA*). Table 6 lists the number of conducted runs and ground adaption settings.

In the steepest part of the slope, the rover reaches the workspace limit of one or more legs, even with body height correction module. In these cases, the pitch command for the rover's body is manually altered in order to keep all LEP in the workspace for the FLC module to be able to level the forces acting on the wheels, effectively realizing a control mode as illustrated in Figure 12(c). Hence, the body angle tracking is subject to changing reference values that the rover shall maintain w.r.t. gravity.

6.2 Data Evaluation Methods

All evaluated data resulting from the MCS is logged at 100 Hz as this is the execution frequency of the motion control. From the data logged in the runs, most important for the following analysis are joint telemetry (current, speed, position) of all 20 DoF, force measurements at each wheel, body orientation readings from the IMU and the supply voltage of the system.

The DGPS module for ground truth in the experiments makes use of the miniature GPS aided inertial measuring system *Spacial Dual* manufactured by Advanced Communication (Advanced Navigation, 2017). With satellite based augmentation system, the horizontal position accuracy achieved is at 0.5 m, while the vertical position accuracy is at 0.8 m. The logging frequency is 20 Hz, which is the update frequency of the DGPS software module. All distances in the evaluation are calculated from latitude and longitude using python's geographiclib, and filtered with a low pass filter for noise cancellation. For synchronization with MCS-data, absolute timestamps in the log-data streams are used to match MCS and GPS data samples.

For comparison of single runs, construction of mean values, RMS error values and alike, the log data is tailored such that all data is synchronised with the beginning of the movement of the robot[5]. Consequently, the plots providing a distance on the x-axis are all starting with a distance of zero meters. This travelled distance on the x-axis is an estimated value from the robot's proprioceptive data, thus a slight error in synchronicity due to slip and sensor inaccuracy might be present in the data.

All experiments are conducted with the robot running on battery power. Once the primary battery is low, the system automatically switches to the (identical) secondary battery. For power calculations presented in Section 6.3, always the actual supply voltage is used. Pulse Width Modulation (PWM) duty cycle and joint currents are taken from the respective joint's telemetry data stream.

When comparing the data of different runs, a mean value is calculated with a standard deviation around that mean value. In the plots presented in the following, a light band around each mean-plot illustrates the standard deviation of the runs. For power analysis, first a mean power draw for each single run is calculated. All runs with same settings (same footprint, GAP-mode, test track) are then used to build a mean power value for this setting.

The RMS error values of force tracking provided in the tables are generated from the means over all respective runs, resulting in a single value for comparison of the effects of footprints and active adaption modes. Based on the RMS error values, a percentual change between the runs with and without active ground adaption is calculated. Absolute errors are denoted as e with appropriate index, RMS values of errors are denoted $\hat{e}$, while the mean of errors over several runs is denoted as $\bar{e}$. General definitions of the most commonly used symbols in the following sections are provided in Table 7.

6.3 Power Requirements for Active Ground Adaption

One of the main questions when analysing a rover with an active suspension is the power requirement for the active adaption to the terrain. The experiments in this section shall determine the "power overhead" for the active suspension system.

[5]The start of movement is not equidistant (time-wise) from the start of logging in all runs.

Table 5: Slope angles for Steep-Slope tests.

Segment [m]	0-1	1-2	2-3	3-4	4-5	5-6	6-7	7-8	8-9
Slope	9.5°	10°	10°	11°	15°	16°	28°	22°	25°
Segment [m]	9-10	10-11	11-12	12-13	13-14	14-15	15-16	16-17	17-18
Slope	28°	28°	20°	20°	15°	10°	10°	0°	0°

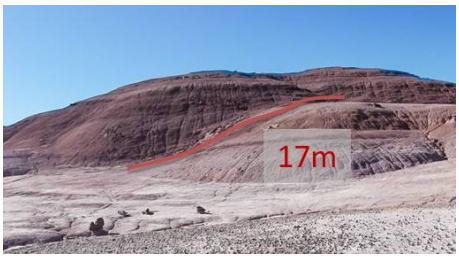

(a) Photograph of the slope with indication of test track. Length of track is 17 m.

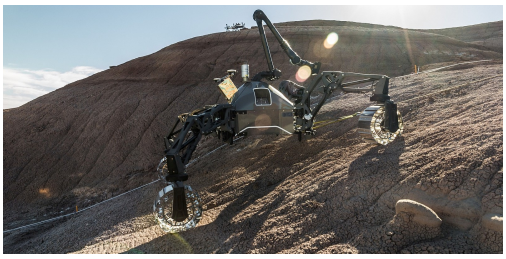

(b) SherpaTT in the steepest section of the slope with active roll-pitch adaption.

Figure 16: Experimental setup for Steep-Slope tests.

Table 6: Conducted runs in Steep-Slope.

	Cross-Stance		Y-Shape	
	Amount	Idx	Amount	Idx
FLConly	5	1-5	2	10-11
FLC+RPA	4	6-9	2	12-13
Total	9		4	

6.3.1 Presumption

A system with passive suspension has basically no power requirement for ground adaption, only actuators for steering and driving the wheels need to be powered. For active suspension, all actuators that are responsible for terrain adaption add to the power requirements of the system. Consequently, the analysis in this section splits SherpaTT's power for locomotion P_l into the power for the drive system P_d (all WheelSteering and WheelDrive joints) and for the suspension system P_s (all Pan, InnerLeg and OuterLeg joints).

It is expected that more power is required for the suspension with increasing terrain difficulty. Furthermore, a simple force leveling requires less movements of the suspension's actuators, when compared to force leveling and body roll-pitch control. Hence, the cases with active roll-pitch adaption are expected to consume more power.

All three settings described in Section 6.1 are used to characterize the power overhead for active adaption in SherpaTT, additionally two pre-test runs with 0.1 m/s velocity setting are analysed for better comparability with the runs in Flat-Terrain and Moderate-Slope. All power values presented are based on current measurements on joint level as well as central supply voltage measurement for the legs.

6.3.2 Results

In the current integration state, the base power consumption from the logic units, sensors, wireless communication, and DC/DC converters is for all runs in all settings $P_b \approx 160\,W$ when a DGPS module is connected and $P_b \approx 150\,W$ without connected DGPS module. This power is required regardless of the locomotion state of the robot. P_b is a constant power requirement and not taken into account in the following analysis, which focusses on the locomotion power requirements.

Table 8 lists the mean power values from Flat-Terrain runs. As can be expected, inactive adaption results in no power consumption from the suspension system. The total power in the runs with *noAdap* is thus equal to the power consumption from the WheelSteering and WheelDrive joints and is around 45 W to 48 W for all footprints. With active force leveling control, the rover mean power increases by 7 W - 9 W for controlling the 12 active DoF of the suspension system. The deviation for the suspension system power consumption means is below 1 W, indicating a very constant power consumption over the different runs.

For Moderate-Slope a similar behavior can be found, as provided in Table 9. In the case with *FLConly* adaption mode, 13.6 W and 11.1 W of power are required for adaption to the ground in Cross-Stance and Quasi-Tripod, respectively. When adding the roll-pitch control in *FLC+RPA* mode, the power requirement increases in both footprints. The reason for the increased power requirement is that the InnerLeg and OuterLeg actuators have to adapt more to the terrain in order to keep the body in constant orientation w.r.t. gravity. Again the standard deviation for the suspension system's power consumption is below 1 W in all shown cases.

Comparing Cross-Stance in Flat-Terrain with Moderate-Slope, an increase in power requirement P_l can be seen from flat terrain (around 54 W) to mod-

Symbol	Explanation	Symbol	Explanation
P_b	Basic power consumption	$P_l = P_d + P_s$	Power for locomotion
P_d	Power for drives	P_s	Power for suspension
e_{a0}	Force error on Axis 0 (FL/RR)	e_{a1}	Force error on Axis 1 (FR/RL)
e_{fi}	Force error at wheel i		
e_r	Roll error	e_p	Pitch error
σ_X	Standard deviation for $\bar{X}$		

Table 7: Main symbols for evaluation

Table 8: Mean values and standard deviation for power consumption for locomotion in Flat-Terrain. Locomotion velocity $v = 0.1\,\mathrm{m/s}$

	Cross-Stance		P90		Turtle-Front	
	noAdap	*FLConly*	*noAdap*	*FLConly*	*noAdap*	*FLConly*
$\bar{P}_l$ / σ_{Pl}	44.8 W / 3.5 W	53.9 W / 4.7 W	45.1 W / 4.8 W	54.0 W / 3.3 W	48.8 W / 4.6 W	54.6 W / 5.2 W
$\bar{P}_d$ / σ_{Pd}	44.8 W / 3.5 W	44.9 W / 4.0 W	45.1 W / 4.8 W	47.2 W / 3.5 W	48.8 W / 4.6 W	47.3 W / 5.4 W
$\bar{P}_s$ / σ_{Ps}	0.0 W / 0.0 W	9.0 W / 0.7 W	0.0 W / 0.0 W	6.8 W / 0.4 W	0.0 W / 0.0 W	7.3 W / 0.2 W

erate slope (around 75 W "up"). The increase is mostly from the wheel drives: when comparing Cross-Stance in *FLConly* the suspension system requires a mean of 9.0 W for force control in flat terrain and 13.6 W in the moderate slope of Moderate-Slope.

In the Steep-Slope setting, the suspension system power requirement for controlling the wheel-ground contact forces is not significantly higher when compared to the other two settings.

Table 10 shows the data from Steep-Slope with velocity setting of 0.04 m/s. The upslope and downslope runs in *FLConly* mode show a mean power requirement of around 12 W for both footprints. Due to the steeper inclination the power requirement P_s for *FLC+RPA* mode is noticeably higher, as the steeper slope requires more adaption from the suspension joints, around 20 W are required in this locomotion mode. The standard deviation over the suspension power consumption means of all runs is below 1 W for all shown cases of the table.

For better comparison the power requirements from the two pre-test upslope runs (Cross-Stance, *FLConly*, $\dot{x} = 0.1\,m/s$) are provided as follows: Mean total locomotion power $\bar{P}_l = 178.3\,W$, separated into $\bar{P}_d = 156.8\,W$ and $\bar{P}_s = 21.5\,W$. Looking at the pre-test downslope runs shows that the wheels have a netto power generation of $\bar{P}_d = -6.98\,W$, which is due to less power required for braking the rover. Table 11 lists all mean power values for upslope runs in Cross-Stance and *FLConly* as measured in the three terrain profiles and with two velocity settings in Steep-Slope.

In the table, the mean values from Moderate-Slope are taken as baseline values, the other settings are compared against these values. absolute change and relative change w.r.t. Moderate-Slope are provided in the table. Due to the very low power consumption of the suspension system in flat terrain, the relative change of P_s in Moderate-Slope is with 51.1% higher than that of P_d (37.4%). However, in Steep-Slope with reduced velocity setting, the P_s is only 35.6% higher than in Moderate-Slope, while P_d increases by 105.1%.

The last row of Table 11 indicates the fraction of the suspension system power of the overall locomotion power. In flat terrain and moderate slopes, the share of the suspension system is at 17% and 18% of the overall locomotion power. For the Steep-Slope setting, regardless of the commanded speed, the suspension power share drops to 12%, because of the main increase in power for the drive system. The mean power values are also illustrated in Figure 17

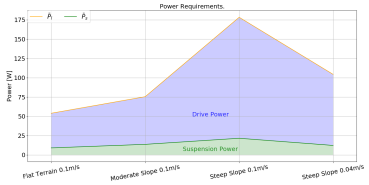

Figure 17: Power for locomotion in different terrains

The most noticeable difference in power consumption in Steep-Slope is neither the footprint nor the GAP-mode, the main difference in power consumption is between up- and downslope runs. Figure 18 shows the power mean values for each single run in Steep-Slope setup ($\dot{x} = 0.040\,\mathrm{m/s}$). A clear difference in the mean power consumption $\bar{P}_{l,n}$ from the battery can be seen when comparing the downslope runs (odd index) with the upslope runs (even index). The mean downslope power requirement regardless of the GAP-mode is around 17 W in Cross-Stance and at ≈19 W for Y-Shape. Upslope power over all runs of one GAP-mode is 104 W and 118 W for Cross-Stance and 101 W and 119 W for Y-Shape.

A high standard deviation of the single-run mean values can be observed, as indicated by the black bars in the

Table 9: Mean values and standard deviation for power consumption for locomotion in Moderate-Slope. Locomotion velocity $v = 0.1\,\mathrm{m/s}$

Footprint	mean/dev	Up *noAdap*	Up *FLConly*	Up *FLC+RPA*	Dwn *noAdap*	Dwn *FLConly*	Dwn *FLC+RPA*
	$\bar{P}_l$ / σ_{Pl}	64.8 W / n.a.*)	75.4 W / 1.0 W	82.3 W / 2.3 W	49.9 W / n.a.*)	58.8 W / 1.1 W	66.4 W / 2.4 W
	$\bar{P}_d$ / σ_{Pd}	64.8 W / n.a.*)	61.7 W / 0.8 W	60.9 W / 2.1 W	49.9 W / n.a.*)	45.4 W / 0.9 W	45.0 W / 2.2 W
	$\bar{P}_s$ / σ_{Ps}	0.0 W / n.a.*)	13.6 W / 0.7 W	21.4 W / 0.3 W	0.0 W / n.a.*)	13.4 W / 0.8 W	21.5 W / 0.2 W
	$\bar{P}_l$ / σ_{Pl}	65.8 W / n.a.*)	72.0 W / 1.2 W	85.6 W / 2.0 W	49.0 W / n.a.*)	56.6 W / 1.3 W	68.5 W / 1.5 W
	$\bar{P}_d$ / σ_{Pd}	65.8 W / n.a.*)	60.9 W / 1.3 W	61.9 W / 2.0 W	49.0 W / n.a.*)	45.5 W / 1.4 W	45.1 W / 1.6 W
	$\bar{P}_s$ / σ_{Ps}	0.0 W / n.a.*)	11.1 W / 0.2 W	23.7 W / 0.0 W	0.0 W / n.a.*)	11.1 W / 0.2 W	23.4 W / 0.4 W

*) single runs: no std-deviation values

Table 10: Mean values and standard deviation for power consumption for locomotion in runs in Steep-Slope. Values are separated for up- and downslope drives and GAP-mode. Locomotion velocity $v = 0.040\,\mathrm{m/s}$

Footprint	Pwr mean/dev	Up *FLConly*	Up *FLC+RPA*	Dwn *FLConly*	Dwn *FLC+RPA*
	$\bar{P}_l$ / σ_{Pl}	104.3 W / 1.5 W	118.1 W / 6.0 W	14.5 W / 0.3 W	20.5 W / 0.5 W
	$\bar{P}_d$ / σ_{Pd}	92.1 W / 1.4 W	95.9 W / 6.4 W	2.3 W / 0.2 W	0.5 W / 0.2 W
	$\bar{P}_s$ / σ_{Ps}	12.2 W / 0.0 W	22.2 W / 0.3 W	12.2 W / 0.1 W	20.0 W / 0.3 W
	$\bar{P}_l$ / σ_{Pl}	100.8 W / n.a.*)	118.7 W / n.a.*)	15.1 W / n.a.*)	22.0 W / n.a.*)
	$\bar{P}_d$ / σ_{Pd}	89.2 W / n.a.*)	99.5 W / n.a.*)	2.7 W / n.a.*)	0.9 W / n.a.*)
	$\bar{P}_s$ / σ_{Ps}	11.6 W / n.a.*)	19.2 W / n.a.*)	12.4 W / n.a.*)	21.2 W / n.a.*)

*) single runs: no std-deviation values

Table 11: Example Cross-Stance, *FLConly*: Change of mean power consumption over terrain settings

	Flat-Terrain 0.1 m/s	Moderate-Slope 0.1 m/s			Steep-Slope 0.1 m/s			Steep-Slope 0.04 m/s		
	abs	abs	change		abs	change		abs	change	
$\bar{P}_l$	53.9 W	75.4 W	+21.5 W	+39.9 %	178.3 W	+124.4 W	+230.9 %	104.3 W	+50.4 W	+93.5 %
$\bar{P}_d$	44.9 W	61.7 W	+16.8 W	+37.4 %	156.8 W	+111.9 W	+249.3 %	92.1 W	+47.2 W	+105.1 %
$\bar{P}_s$	9.0 W	13.6 W	+4.6 W	+51.1 %	21.5 W	+12.5 W	+138.9 %	12.2 W	+3.2 W	+35.6 %
	ratio $\bar{P}_s/\bar{P}_l$									
$\frac{\bar{P}_s}{\bar{P}_l}$	0.17	0.18			0.12			0.12		

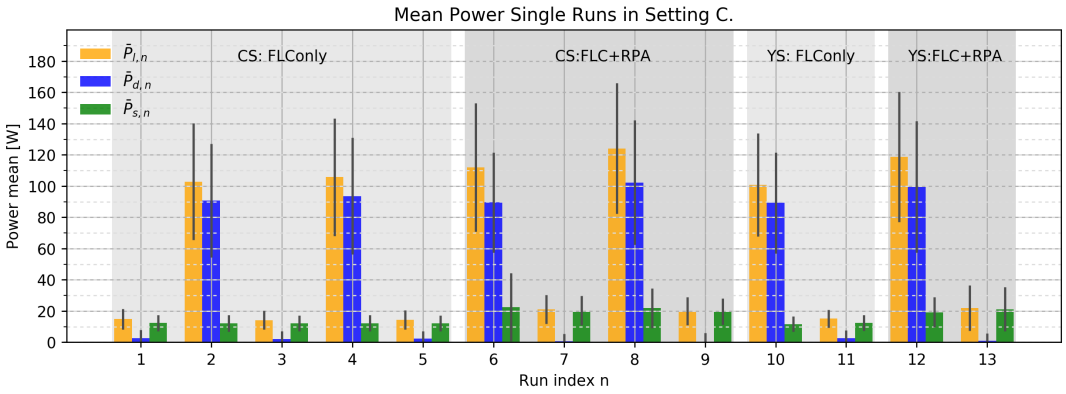

Figure 18: Individual run power consumption in Steep-Slope (mean values per run). Black error bars indicate the standard deviation for each run's mean value. CS: Cross-Stance; YS: Y-Shape.

figure. This is due to the changing power consumption during the run which starts in moderate slopes, has a peak slope in the middle of the run and a zero degree slope on top of the test hill. Figure 19 shows the mean power consumption over all runs in Steep-Slope with Cross-Stance to illustrate the power consumption over the locomotion distance in the slope.

In moderate inclinations at the begin and end of a run, only a small amount of power is required when compared to the steepest parts of the slope. Upslope it can be seen that a moderate 40 W are from the wheel's joints in the first two meters of the slope. The maximum mean value is around 11-12 m into the slope, where 160 W are required. Downslope the wheels require around 10 W in the moderate slopes at start and stop of the runs but temporarily generate power in the steeper parts.

The power for the suspension units is comparatively constant, yet there is a peak around 7.5 m visible in Figure 19(a), which results from one single run event: In Run 6 there was a heavy slip event with 100% slip in mid-run, causing the robot to shake due to the wheels' grousers until slip-value dropped below 100%. During that event, the suspension system tried to compensate the loading and unloading of the wheels, resulting in a higher power consumption from the suspension system to compensate the contact loss, Figure 20.

6.3.3 Conclusion: Power Analysis

With the presented experiments it is shown that the active adaption to the surface is not the main power consumer in the system SherpaTT. In fact in moderate terrain (Settings A and B), the power consumption is around 10 W for *FLConly* mode, while the overall power consumption in these cases is 54 W in flat terrain and around 75 W in moderate slopes. The change in power requirement is mostly due to the higher power requirements of the rover drive system, the suspension has the same power requirements in both settings. In steep slopes with *FLConly* the overall power requirement rises to above 100 W in upslope runs with reduced velocity, while the suspension system requires less than 12.5 W (*FLConly*). The fraction of power requirement of the active suspension drops from moderate terrain with about 20% to 12% in steep slopes. Thus, while enabling the rover to drive in steep terrain, the fraction of power for the suspension system in these terrains plays a smaller role in the overall power consumption of the rover.

Figure 17 shows the development of power requirement for locomotion over the three terrain settings. For Steep-Slope there are also the pre-test runs with velocity setting 0.1 m/s included in the plot. It is clearly visible that the main increase in power consumption with increasing terrain inclines is due to the drive system, hence the WheelSteering and WheelDrive actuators also present in a comparable rover with passive suspension system are the main power sinks.

The final conclusion concerning the power requirements for active ground adaption is that there is indeed a higher power requirement than in passive suspension would be. However, the extra amount of power is low compared to the variance of power at the wheels required for different terrains. Furthermore the active suspension provides more abilities than passive suspension with active body angle control or flexible footprint configurations not being possible with a passive suspension. It can be expected, that the power requirement for the suspension increases in undulating terrain, as the legs need to move the wheels longer distances and more frequently. This needs further consideration in upcoming experiments.

6.4 Force Reference Tracking and Body Angle Control

The FLC module is used for permanent ground contact of each wheel. For roll and pitch adaption for the body the RPA module is used. Both modules of GAP are evaluated in this chapter.

6.4.1 Presumption

In the presented experiments the ability of the force leveling control module to cope with different footprints shall be evaluated. Since a simplified controller based on the strong and weak contact axis and combined control for two wheels is used, it is expected, that other footprints than Cross-Stance impede the capability of FLC to track the reference forces. Furthermore, the effect of different terrain inclinations on the quality of ground adaption is analysed.

The body angle control is expected to have no significant differences between the footprints as it is implemented independent of the footprint, each LEP's distance to the rotation axis is regarded separately.

6.4.2 Results

All three experiment settings are used to validate the reference force tracking of the FLC component while Moderate-Slope and Steep-Slope are used to evaluate the body angle tracking of the RPA component as well. The results for the FLC component presented in this section are mainly based on the force tracking errors e_{a0} on the contact axis 0 (front left and rear right wheel). An evaluation based on one contact axis is valid, since all tested footprints have a left-right symmetry, resulting in symmetrical force errors on the two contact axes, hence $e_{a0} = -e_{a1}$ for all runs.

Figure 21 shows the mean error plots with standard deviations for the runs from Flat-Terrain, while Table 12 lists all RMS results from this setting and indicates the changes resulting from the active adaption process with negative values indicating an improvement (reduction of the error). The errors $\hat{e}_r$ and $\hat{e}_p$ for body attitude control are small (mostly below 1°), due to the flat terrain. Since no runs with active roll-pitch adaption are conducted in Flat-Terrain, these values are not discussed in

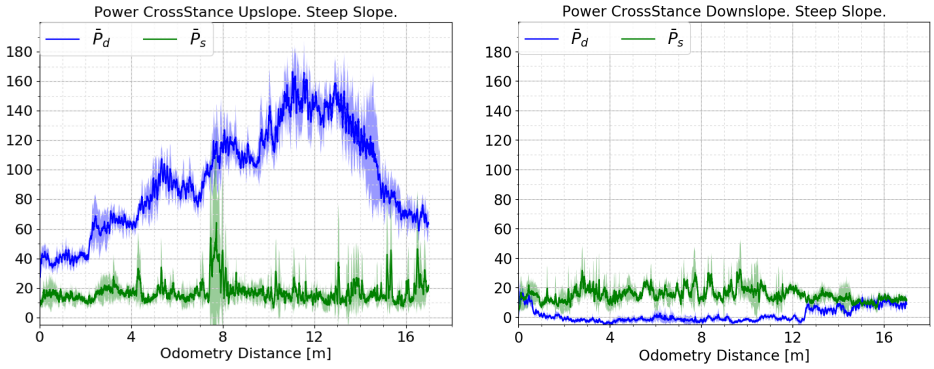

(a) Power over all upslope runs: Power $\bar{P}_d$ increases with slope.

(b) Power over all downslope runs: Temporary power generation from wheel drives.

Figure 19: Power over up- and downslope runs in Steep-Slope. Means over all runs in Cross-Stance.

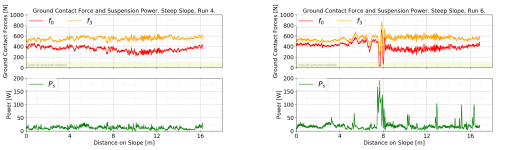

(a) Run 4 in Steep-Slope. Regular slip in slope, all wheels with permanent ground contact. Power consumption for suspension system without significant peaks.

(b) Run 6 in Steep-Slope. Heavy Slip (100%) in the middle of the slope leads to loading and unloading of the wheels. Loss of ground contact for front left wheel around 7.5 m into the slope leads to high energy consumption for the suspension system in order to get all wheels into ground contact as quick as possible.

Figure 20: Comparison of regular run and run with heavy slip: Forces FL and RR and power for suspension system.

detail.

Without active adaption, the forces deviate from the reference forces due to temporary ground contact loss and non ideal force distribution. As obvious from the plot and visible in the data in Table 12, the P90 setting has smaller force errors without active adaption in this flat ground traverse than Cross-Stance. The reason for this might be found in the smaller footprint, which reduces the tendency to tip over one of the two contact axes, this can also be seen in the smaller amount of power needed for adaption in this footprint, see Table 8.

Using the force leveling control module reduces the errors in all footprint settings. As the absolute error is already small for P90 without active adaption, the relative improvement is not that high, yet the absolute values with force leveling are comparable to those of Moderate-Slope with different footprints (see below).

All runs with active ground adaption in Cross-Stance for Flat-Terrain had a re-orientation phase of the wheels in the beginning of the run, leading to higher force errors due to changing reference values. Consequently a higher RMS error value (≈56 N compared to ≈38 N in Moderate-Slope) is observed. This is also visible in the data plot in Figure 21(b), where a peak of $\bar{e}_{a0}$ in Cross-Stance is visible at the beginning and the end of the runs. Excluding the peaks results in $\hat{e}_{a0}(1\,m \ldots 19\,m) \approx 43\,N$ for Cross-Stance.

A separate analysis has to be done for the Turtle-Front runs. The plot for the runs without adaption in Figure 21(a) shows a nearly constant mean error $\bar{e}_{a0}$. In fact, in this footprint the rear right wheel was without ground contact most of the time in all four runs, effectively leading to a tripod configuration. This is also the reason for the seemingly great improvements in the body angle error values $\Delta\hat{e}_r = -60\%$ and $\Delta\hat{e}_p = -30\%$ for this footprint even without active RPA-module: All wheels had ground-contact with *FLConly* setting, reducing the roll and pitch error even without active RPA-module. Note that the absolute values of improvement are only around 0.4°.

As listed in Table 3, only two runs were conducted for the active adaption case in Turtle-Front. In one of the two runs a reorientation of the wheels occurred in the first few meters of the run, explaining the higher RMS error value $\hat{e}_{a0}$ of about 81 N. After the reorientation event the FLC module was able to reduce the force error to comparable values as in the other two footprint configurations, Figure 21(b). Using only the error values between 3 m and 19 m for RMS calculation results in a value $\hat{e}_{a0}(3\,m \ldots 19\,m) \approx 34\,N$ for Turtle-Front which is well in the range of the other footprints and the runs in Moderate-Slope. However, due to the small number of runs, the values for Turtle-Front in Table 12 cannot be taken into account of the analysis. Qualitatively the adaption seems to be able to cope with this footprint, yet a more thorough analysis is needed for a quantitative statement.

A similar result as in Flat-Terrain can be observed for Moderate-Slope. Figure 22 shows the force errors on the FL-RR contact axis for Cross-Stance and Quasi-Tripod

Table 12: RMS error values of forces, roll and pitch in Flat-Terrain. Percentual change when compared to *noAdap*. Gravitational force of rover is $F_g \approx 1628\,\text{N}$.

Footprint	GAP mode	$\hat{e}_{f0}$	$\hat{e}_{f1}$	$\hat{e}_{f2}$	$\hat{e}_{f3}$	$\hat{e}_{a0}$	$\hat{e}_{a1}$	$\hat{e}_r$	$\hat{e}_p$
	*noAdap*	123.64 N	74.36 N	117.54 N	70.77 N	183.43 N	183.43 N	0.34°	0.57°
	FLConly	47.77 N -61 %	45.94 N -38 %	44.32 N -62 %	49.72 N -30 %	55.96 N -69 %	55.96 N -69 %	0.36° +7 %	0.59° +3 %
	*noAdap*	35.21 N	70.70 N	79.10 N	39.47 N	61.75 N	61.75 N	0.59°	0.44°
	FLConly	29.74 N -16 %	76.04 N +8 %	74.65 N -6 %	28.90 N -27 %	39.64 N -36 %	39.64 N -36 %	0.64° +9 %	0.41° -6 %
	*noAdap*	126.97 N	92.32 N	322.34 N	287.64 N	414.51 N	414.51 N	0.64°	1.44°
	FLConly	32.28 N -75 %	21.05 N -77 %	63.54 N -80 %	58.52 N -80 %	81.43 N -80 %	81.43 N -80 %	0.25° -60 %	1.02° -30 %

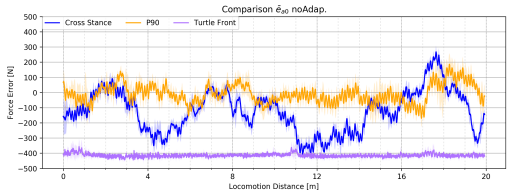

(a) Comparison with no active ground adaption

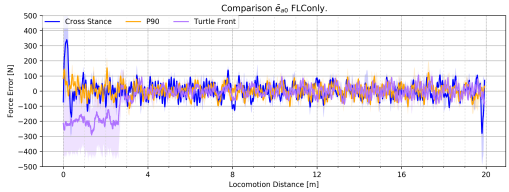

(b) Comparison with *FLConly* setting

Figure 21: Force tracking errors in Flat-Terrain. Comparison of effects of GAP-modes and between three footprint configurations on FL-RR axis.

in Moderate-Slope. Table 13 lists all deviation values.

As expected, in Cross-Stance without active adaption, the force error shows high deviations from the reference values which is due to tilting over the strong contact axis, c.f. Section 5.4.1. The errors in Quasi-Tripod are smaller, as the configuration is close to a tripod which is intrinsically stable in rough terrain.

Activating the force leveling control improves the force tracking significantly: In Cross-Stance, the RMS error value $\hat{e}_{a0}$ drops by 92%, the improvement is less significant in Quasi-Tripod (drop by 79%), which is due to the smaller error value in the case without active adaption which is used as baseline. The absolute errors, however, are in a comparable range (34.3 N in Cross-Stance and 36.7 N in Quasi-Tripod), showing the capability of the FLC component adapt the forces independently of the footprint.

Additionally activating the RPA component does not noticeably affect the force values. The force errors are in the same range, a comparison of the force-error plots in Figures 22(b) and 22(c) shows no significant difference between the two active adaption modes.

Concerning the RMS error values $\hat{e}_r$ and $\hat{e}_p$ of the errors in the body's roll and pitch angle, the force leveling alone has not much effect on the body angles of the rover. The improvement of 10% for $\hat{e}_r$ in Cross-Stance has to be considered due to the natural terrain and possible changes in the exact trajectory of the rover. Note that the absolute improvement is as small as 0.15°. The RPA component, however, improves the attitude control of the rover's body by as much as 97% without a significant effect on the FLC component. From the absolute values, it can be observed that the roll adaption in Quasi-Tripod seems to be slightly less accurate while the pitch correction reduces the errors for both footprints to 0.1° and 0.12°.

In Steep-Slope, higher slippage of the robot is present due to the slope the robot is driving on. The different slippage events over the individual runs do not allow to build means over all runs as done for analysis of runs in settings Flat-Terrain and Moderate-Slope. Hence, an evaluation interpreting the data of the separate runs is necessary for Steep-Slope. Figure 23 shows the RMS error values $\hat{e}_{a0}$, $\hat{e}_r$, $\hat{e}_p$ for all single runs in Steep-Slope, Table 14 lists the values and additionally the values for single legs $\hat{e}_{fi}$ and force axis 1, $\hat{e}_{a1}$.

All $\hat{e}_{a0}$ values, except for Run 6, are in the same range regardless of the footprint or active or inactive roll-pitch adaption. Furthermore, the values are in the same range of $\hat{e}_{a0}$ in Cross-Stance with *FLConly* in Flat-Terrain. The slip event in Run 6 (see also Section 6.3), caused loading/unloading of the wheels, hence higher force tracking errors occurred which are visible in the RMS value of this run. Figures 20 and 26 show the forces f_0 and f_3 during that run, the unloading down to ground contact loss ($f_0 < 100\,N$) is visible starting from about 7.5 m into the slope.

As can be expected, without roll-pitch adaption, the body angles are basically following the slope the robot is driving on, hence the comparatively huge errors in pitch (rover is driving up/down slope) and moderate roll angles in *FLConly* mode. The relatively high scattering of the RMS pitch error with max 21° in Run 11 and min 15.1° in Run 5 can be explained by the rough natural terrain which caused the rover to change its ori-

Table 13: RMS error values of forces, roll and pitch in Moderate-Slope. Percentual change when compared to *noAdap*. Gravitational force of rover is $F_g \approx 1628\,\text{N}$.

Footprint	GAP mode	$\hat{e}_{f0}$	$\hat{e}_{f1}$	$\hat{e}_{f2}$	$\hat{e}_{f3}$	$\hat{e}_{a0}$	$\hat{e}_{a1}$	$\hat{e}_r$	$\hat{e}_p$
	*noAdap*	229.18 N	236.76 N	223.00 N	233.83 N	455.91 N	455.91 N	1.39°	3.97°
	FLConly	40.31 N -82 %	35.91 N -85 %	34.71 N -84 %	40.61 N -83 %	34.30 N -92 %	34.30 N -92 %	1.24° -10 %	4.03° +1 %
	FLC+RPA	39.07 N -83 %	26.48 N -89 %	25.22 N -89 %	39.69 N -83 %	37.98 N -92 %	37.98 N -92 %	0.11° -92 %	0.10° -97 %
	*noAdap*	59.58 N	47.20 N	133.92 N	134.81 N	178.46 N	178.46 N	1.56°	3.98°
	FLConly	35.20 N -41 %	19.29 N -59 %	29.71 N -78 %	43.81 N -68 %	36.69 N -79 %	36.69 N -79 %	1.53° -2 %	3.95° -1 %
	FLC+RPA	38.08 N -36 %	16.01 N -66 %	25.71 N -81 %	44.43 N -67 %	33.19 N -81 %	33.19 N -81 %	0.20° -87 %	0.12° -97 %

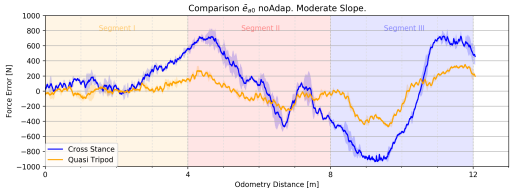

(a) Contact axis FL-RR: Comparison between Cross-Stance and Quasi-Tripod without active ground adaption

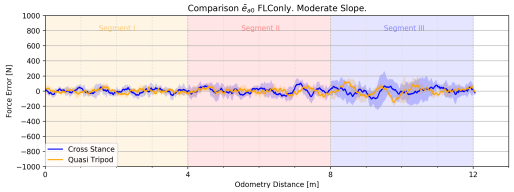

(b) Contact axis FL-RR: Comparison between Cross-Stance and Quasi-Tripod with only FLC active

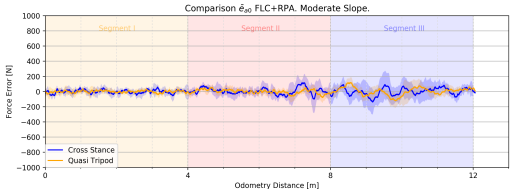

(c) Contact axis FL-RR: Comparison between Cross-Stance and Quasi-Tripod with FLC and RPA active

Figure 22: Force tracking errors in Moderate-Slope. Comparison of effects of GAP-modes and between two footprint configurations on FL-RR axis.

entation due to slip. The separate runs had different slip conditions and hence the trajectory on the slope might vary slightly from run to run. Furthermore, the runs are time/odometry based: More slip in one run leads to more time in steeper slope, which in turn increases the RMS value of the body angle. Activating the RPA module (Runs 6-9 and 12, 13) reduces both RMS errors, $\hat{e}_r$ and $\hat{e}_p$, to below 1°. Again the error values in Run 6 are slightly higher than in the other runs due to the slip event causing the robot to shake for a period of time in mid-slope as described in Figures 20 and 26.

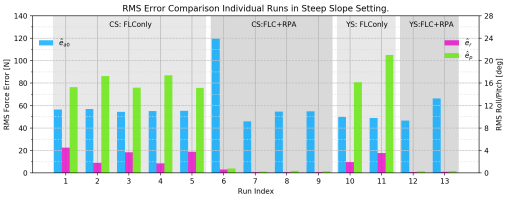

Figure 23: RMS error results of individual runs in Steep-Slope

6.4.3 Conclusion: Force-Levelling and Body Angle Control Analysis

A simplified force leveling control was implemented for SherpaTT. In the experiments discussed above, an evaluation of different footprints in natural terrain was conducted to asses the generality of the simplifications for different footprints.

From the data presented, the force leveling control works comparable in different terrains and with different footprints. A clear improvement of the ground adaption in terms of force distribution is achieved with the force leveling control module. The errors between actual contact forces and expected contact forces are reduced by up to 92%. Absolute RMS errors for the contact forces are reduced well below 100 N for all runs in all footprints. In several settings, the errors were reduced to around 35 N, on the force-axes (common error for two wheels), compared to an overall gravitational force of $F_g \approx 1628\,\text{N}$. Error values that significantly differ from the range of values are explained by single events as for example active wheel unloading with jumps in reference

Table 14: RMS error values of forces, roll and pitch in of individual runs in Steep-Slope. Values from highlighted rows are plotted in Figure 23. Gravitational force of rover is $F_g \approx 1628\,\mathrm{N}$.

	FLConly					*FLC+RPA*				*FLConly*		*FLC+RPA*	
idx	1	2	3	4	5	6	7	8	9	10	11	12	13
$\hat{e}_{f0}$	36.9 N	37.4 N	37.6 N	30.7 N	37.1 N	91.3 N	57.9 N	66.1 N	51.2 N	20.2 N	24.3 N	57.1 N	44.2 N
$\hat{e}_{f1}$	36.8 N	42.2 N	35.6 N	49.1 N	36.3 N	82.7 N	34.9 N	65.7 N	42.8 N	27.5 N	32.0 N	35.3 N	30.3 N
$\hat{e}_{f2}$	30.5 N	41.7 N	29.8 N	47.4 N	31.0 N	72.4 N	36.2 N	61.6 N	42.1 N	42.3 N	41.0 N	45.5 N	50.8 N
$\hat{e}_{f3}$	33.2 N	38.5 N	32.7 N	34.4 N	31.2 N	87.9 N	57.9 N	63.5 N	50.7 N	39.5 N	34.0 N	67.0 N	57.8 N
$\hat{e}_{a0}$	56.6 N	57.0 N	54.5 N	55.2 N	55.3 N	119.6 N	45.8 N	54.6 N	55.0 N	50.1 N	48.9 N	46.5 N	66.4 N
$\hat{e}_{a1}$	56.6 N	57.0 N	54.5 N	55.2 N	55.3 N	119.6 N	45.8 N	54.6 N	55.0 N	50.1 N	48.9 N	46.5 N	66.4 N
$\hat{e}_r$	4.5°	1.8°	3.7°	1.7°	3.8°	0.6°	0.1°	0.1°	0.2°	1.9°	3.6°	0.2°	0.2°
$\hat{e}_p$	15.3°	17.3°	15.2°	17.4°	15.1°	0.8°	0.3°	0.4°	0.3°	16.1°	21.0°	0.3°	0.3°

force values, causing temporary high error values.

Concerning the body angle control, RMS error values of both, roll and pitch angle were reduced to below 0.5° in all tested slopes and footprints with active RPA module. In moderate slopes the RMS errors are reduced to 0.2° or below.

With the experiments it was shown that a combined, multi-objective control is possible: The robot's wheel-ground contact forces can be controlled with simultaneous body roll-pitch angle control. Especially do FLC and RPA not influence each other, the force tracking quality does not change significantly between settings with or without active body roll-pitch control.

6.5 Terrain Slope Estimation

This section shows the results from validating the *Ground Plane Estimator* module presented in Section 5.1.

6.5.1 Presumption

The plane estimator fits a plane through all wheels with ground contact; using the time series of fitted planes, an estimation of the terrain profile the rover is driving on is possible. As only wheels with ground contact are used for the plane estimation, independence of the current footprint is expected. Hence, even when combining the runs from different GAP modes to one mean value, the respective standard deviation is expected to be low.

6.5.2 Results

Figure 24 shows the result of the slope estimation in Moderate-Slope. In the Subplots 24(a) and 24(b) the slope profile estimates of all forward and backward runs of a single footprint are combined to get a mean with standard deviation. Consequently, deviations for each footprint are calculated across the three types of runs (i) without active ground adaption (*noAdap*), (ii) only force leveling control active (*FLConly*), and (iii) force leveling together with roll-pitch adaption (*FLC+RPA*).

The highest deviations occur when the slope angle changes from increasing to decreasing and vice versa, hence when the rover enters or leaves the slope. Most likely this is due to slight inaccuracies in the synchronization of the individual runs which is based on odometry. Another reason for deviations in the plane estimates is to be found in the setting in a natural environment: Slight variations of the tracks driven in the individual runs can introduce variations in the actual slope profile the rover is driving on in the current experiment run.

Table 15 shows all maximum and mean deviation values of the runs in Moderate-Slope. Even though the settings of ground adaption modes are varying, the observable standard deviations are small, overall the mean deviation in the slope angle estimates is around one quarter of a degree. The maximum deviation in the slope profile height observed in all runs in Moderate-Slope is at 3 cm (Quasi-Tripod fwd) or 4.8% of the total estimated mean slope height (0.63 m).

From the plot of the slope angle estimates it can be seen that the terrain in Segment I has an incline around -1° that increases before the rover enters Segment II. The locomotion distance is based on the front wheel pair, hence the slope angle is at the manually measured -8° only when the rover is fully in Segment II. This is the case for approximately 6-8 m locomotion distance when driving forward and for 4-6 m locomotion distance when driving backwards, based on a wheel base $w \approx 2\,\mathrm{m}$.

The results for the slope estimation in Steep-Slope are shown in Figure 25 in a similar manner as for Moderate-Slope. Since Steep-Slope was not conducted without active force leveling, the run means are composed from the ground adaption settings with

- only force leveling control active (*FLConly*), and
- force leveling together with roll-pitch adaption (*FLC+RPA*).

By building a mean over the runs with partially high slippage, high standard deviations are to be expected as the rover might not be at the same spot in the slope at each locomotion distance sample. In fact a wider

Table 15: Slope estimation experiment in Moderate-Slope. Maximum deviations over all runs of one footprint and RMS values of deviations.

Footprint	Slope pitch fwd max(σ)	Slope pitch fwd RMS(σ)	Slope pitch bwd max(σ)	Slope pitch bwd RMS(σ)	Slope profile fwd max(σ)	Slope profile fwd RMS(σ)	Slope profile bwd max(σ)	Slope profile bwd RMS(σ)
	0.46°	0.24°	0.57°	0.26°	0.02 m	0.01 m	0.02 m	0.01 m
	0.45°	0.22°	0.38°	0.19°	0.03 m	0.02 m	0.02 m	0.01 m

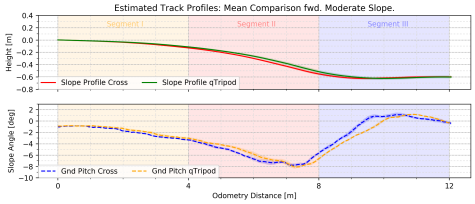

(a) Means and standard deviation of all runs with forward velocity. Driving starts in Front of Segment I.

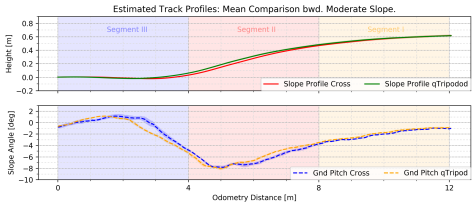

(b) Means and standard deviation of all runs with backward velocity. Driving starts in Segment III.

Figure 24: Test track profile from estimated plane in Moderate-Slope.

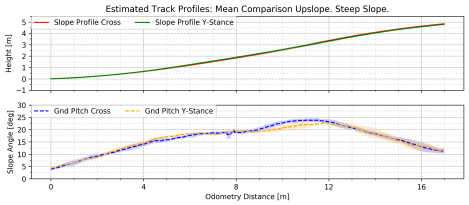

(a) Slope estimation uphill runs in Steep-Slope

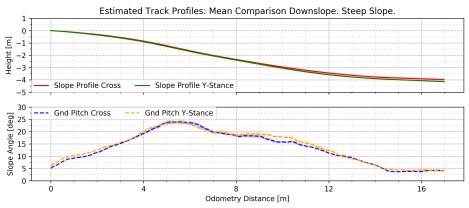

(b) Slope estimation downhill runs in Steep-Slope

Figure 25: Slope estimation with slip in Steep-Slope.

band of deviations can be seen around the slope pitch estimates, Table 16 lists the maximum deviations with up to 2.24°. However, the terrain profile estimates show relative small deviations with a maximum of 10 cm (Y-Shape upslope) which is corresponding to 2.1% of the total estimated mean slope height (4.79 m).

Comparing the estimated terrain profiles of upslope and downslope runs shows that the upslope runs estimate a higher terrain delta than the downslope runs. Manually measured was a height delta of 4.73 m, the estimate for upslope in Cross-Stance is 4.84 m, and in Y-Shape 4.79 m; while downslope estimates are -3.98 m and -4.14 m, respectively. The reason for this is slippage in the slope: Upslope slippage leads to a longer amount of time/odometry distance in steeper parts of the slope, while this is the opposite while driving down the slope. However, in similar terrain, the estimation yields similar results, hence a systematic error due to slip can be identified in the terrain estimates.

In Figure 25(a) a jump in the mean value for the ground pitch estimation in Cross-Stance can be seen at approximately 7.5 m locomotion distance. The jump is caused by a temporary loss of ground contact of the front left wheel due to slip in Run 6. The wheel without ground contact is excluded from the ground plane calculation, hence a jump in the plane estimate occurs. The data from the single run is plotted in Figure 26.

6.5.3 Conclusion: Slope Estimation Analysis

From the data subsumed in Tables 15 and 16, it can be confirmed that the terrain estimation is invariant of the footprint. Furthermore, the small deviations for the means over different GAP-modes show that it is also independent of the chosen adaption mode.

However, since the module relies on proprioceptive data only (forward kinematics of legs and IMU measurements), the influence of the footprint, more precisely the wheel base, is always present in the measurements: The footprints used in the experiments have a different baseline in forward/backward-direction of the rover. While the baseline is w_{cs}=2.04 m for Cross-Stance, the difference between front and rear wheel pair is w_{qtp}=2.29 m for Quasi-Tripod configuration and w_{ys}=2.30 m for Y-Shape.

The effect of this difference can be found when comparing the slope estimates. Consequently, different footprints can result in different ground plane estimates for a given path on natural terrain. The deviation values are comparable between the different footprints, indicating

Table 16: RMS values slope estimation experiment in Steep-Slope.

Footprint	Slope pitch up max(σ)	Slope pitch up RMS(σ)	Slope pitch dwn max(σ)	Slope pitch dwn RMS(σ)	Slope profile up max(σ)	Slope profile up RMS(dev)	Slope profile dwn max(σ)	Slope profile dwn RMS(dev)
	1.81°	0.94°	0.85°	0.41°	0.10 m	0.06 m	0.09 m	0.06 m
	2.24°	1.03°	1.33°	0.64°	0.10 m	0.05 m	0.09 m	0.05 m

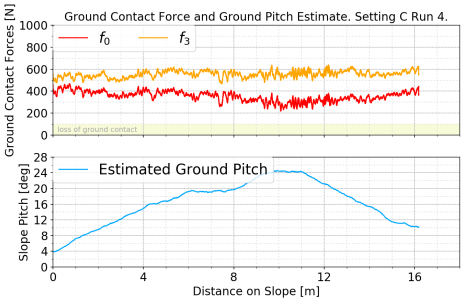

(a) Run 4 in Steep-Slope. Regular slip in slope, all wheels with permanent ground contact: Constant ground plane angle estimate.

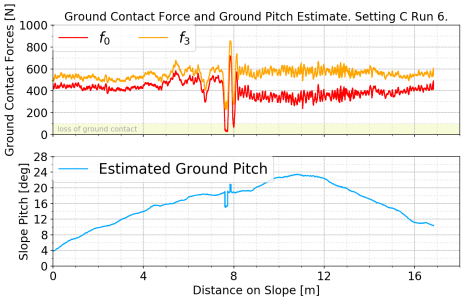

(b) Run 6 in Steep-Slope. Heavy Slip (100%) in the middle of the slope leads to loading and unloading of the wheels. Loss of ground contact for front left wheel around 7.5 m into the slope leads to exclusion of this wheel in ground plane estimate and hence to a jump in the estimated plane pitch angle.

Figure 26: Comparison of regular run and run with heavy slip: Forces FL and RR and Estimated ground pitch angle.

a similar performance independent of the footprint.

As shown in Steep-Slope with higher slip ratios than in Moderate-Slope, the slippage of the system has an impact on the ground plane estimate, which is currently based on the odometry of the system. Slip when driving up a slope leads to a higher ground plane estimate than actually travelled, while driving down the slope with skid leads to a lower ground plane estimate.

6.6 Slope Climbing

The slope climbing experiments in Steep-Slope are used to identify an influence of ground adaption mode and/or footprint on the climbing abilities of SherpaTT in natural terrain.

6.6.1 Presumption

For the slope climbing ability it is expected, that shifting the CoG to the front wheels (the "upslope-wheels") has a positive influence on the slippage of the system. Hence, for the tested footprint Y-Shape a better result is expected.

The main investigation in this test is based on the slip/skid data which is calculated from the difference of odometry and DGPS-data. Following definition is used for slippage analysis:

$$s = 1 - \frac{d_{gps}}{d_{odo}}, \tag{13}$$

where d_{gps} is the travelled distance on slope as recoded by the gps-system and d_{odo} is the locomotion distance as output from odometry. When $s > 0$, the odometry distance is greater than the gps distance, hence the rover was subject to slip, which is expected to happen during the upslope runs. When $s < 0$, the odometry distance is smaller than the gps distance, hence the rover was skidding, which might happen mostly during downslope drives. By normalizing with the odometry distance, the final s value is always normalized by 17 m, while the GPS distance is different depending on slip and skid events during each run.

6.6.2 Results

Figure 27 shows an overview of the results for the two footprints Cross-Stance and Y-Shape. Plotted are the means of d_{odo} over the means of d_{gps} for all runs of one

footprint regardless of the ground adaption mode but separated into uphill and downhill runs. Ideally without slip or skid, $d_{odo} = d_{gps}$, thus the values would be on the 45° line indicated in both plots. However, the plots show that the uphill runs are subject to slip (red line), while the downhill runs are subject to skid. Uphill the slippage starts around d_{gps} ≈6-8 m, which is around the beginning of the steepest part of the slope (see Table 5). The uphill plots for both footprints become roughly parallel to the 45° line at about $d_{gps} \approx 12$ m, meaning that the slip is close to zero, only the accumulated slip is still present. A slope distance of 12 m is approximately when the front wheel pair leaves the steepest part of the slope in uphill runs.

In the downhill runs (rover driving backwards), skid starts after around $d_{gps} \approx 2$ m which means the front wheels enter segment 14-15 while the rear wheels leave segment 13-14 (wheel base of roughly 2 m). At around d_{gps} ≈12 m, the plot is more or less parallel to the 45° line, indicating close to zero skidding in that part of the slope, which is the 4-5 m segment from Table 5 for the front wheels, thus when the rover is past the steepest part of the slope.

Table 17 lists the final slip/skid values according to Equation (13). In the case of combining all up- and downhill runs of one footprint no significant difference between the footprints can be found. Overall both footprints seem to be working similar on the tested slope, where the Cross-Stance shows a slightly better performance. Both footprints perform better in downhill than in uphill runs.

The results when splitted according to the GAP-mode are presented in the right part of the table. Activating the roll-pitch adaption degrades the results for both footprints in uphill runs, while it improves the results of the downhill runs.

The development of the slip/skid values over driven distance is plotted in Figure 28. Since the plotted slip value is dependent on $\frac{d_{gps}}{d_{odo}}$ the value s decreases for phases without slip during the traverse. Note that, in the beginning, small values (<1 m) for d_{gps} and d_{odo}, in combination with sensor noise cause high fluctuation in the values.

When comparing the same GAP-settings in different footprints, a similar development of the slip/skid values over the traverse can be found. Most prominent is the case for *FLC+RPA* when driving downslope. Both plots have nearly the same development and end up with a total skid ratio of -6.5% and -7%, respectively. The least similar plots are for the case *FLC+RPA* in upslope runs: In Y-Shape, the rover has less slip in the beginning of the slope but has a massive slippage event around 9 m of odometry distance. However, in the end the slippage is similar for both footprint configurations. Note that for both cases, uphill and downhill, each plot for Y-Shape is based on a single run, while the plots for Cross-Stance are the mean of two runs. These results indicate that the GAP-mode seems to have a higher influence on the slope climbing ability than the footprint.

Consequently, a clear distinction of a favorable footprint for slope climbing is not possible from the data gained in these experiments. Using the combined up/-down power requirements from Table 10, it seems that a Cross-Stance is slightly favorable for downslope drives and a Y-Shape is slightly favorable for upslope driving.

6.6.3 Conclusion: Slope Climbing Analysis

The conducted experiments in Steep-Slope setting show that the robot is able to cope with natural terrain with up to 28° inclination. All presented runs were successful runs in terms of climbing the slope and reaching the top of the hill with reduced velocity.

However, as stated in Section 6.1.3, runs with a velocity of 0.1 m/s were successful only before the duri-crust on the slope was broken. With lose soil on the slope and velocity setting $\dot{x} = 0.1$ m/s, the rover ended with 100% slip in the steepest part, the runs had to be aborted.

Two different footprints are analysed for the slope climbing. Neither in terms of slip nor in terms of energy consumption there is a significant difference between both footprints observable. Comparing the applied GAP modes, a slightly increased power requirement for active roll-pitch adaption with decreased upslope climbing performance is observable when compared to only force leveling active. Hence, *FLConly* mode should be preferred when a defined body orientation is not required.

In Turtle-Front footprint, structural loads seemed to endanger the robot's integrity. This assessment was done based on the optical impression of the rover in the slope, runs in this footprint were skipped for safety reasons.

7 Conclusion and Future Work

This paper presents the development and an in-field evaluation of the hybrid wheeled-leg rover system SherpaTT. SherpaTT is developed for usage in a heterogeneous multi-robot exploration system with modular components. The main focus of this paper is the electromechanical design of the rover and its locomotion performance. A four week field deployment was conducted in the desert of Utah, USA to validate the system in natural terrain. The results of this outdoor field campaign extend the former indoor laboratory experimental results published in (Cordes and Babu, 2016) and (Cordes et al., 2017).

The rover is equipped with four identical suspension units ("legs") that are used for active ground adaption. Each leg has five active DoF, three of which are mainly used for ground adaption and body roll-pitch control, while two are used to steer and drive the wheel at the end of the leg.

To achieve a coherent behavior in rough terrain, a Motion Control System (MCS) for SherpaTT is introduced. The MCS takes in motion, body posture and footprint

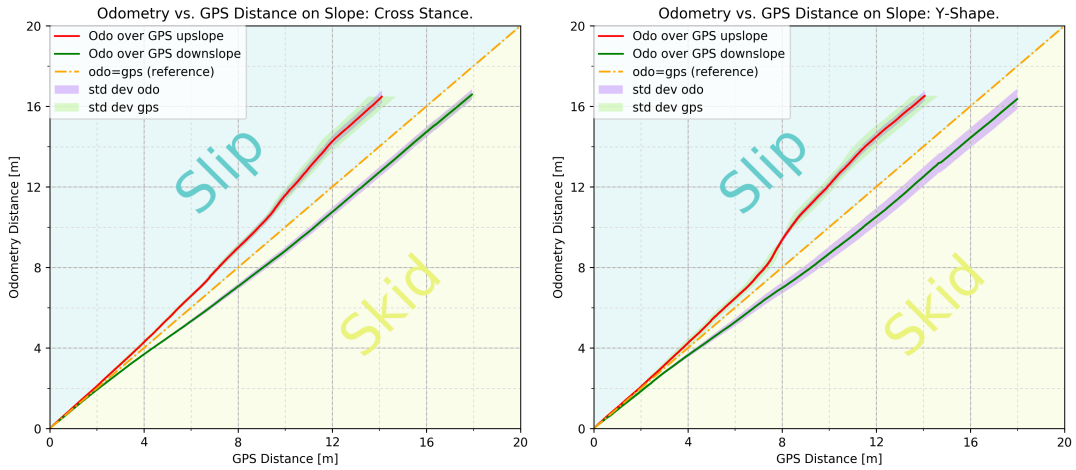

(a) Overall slippage in Cross-Stance up (red) and down (green).

(b) Overall slippage in Y-Shape up (red) and down (green).

Figure 27: Odometry distance vs. GPS distance on slope. Means over all adaption modes.

Table 17: Slip (positive) and skid (negative) values for runs in Steep-Slope.

Footprint		Combined Upslope	Combined Downslope	Separated according to GAP-mode Up *FLConly*	Up *FLC+RPA*	Dwn *FLConly*	Dwn *FLC+RPA*
	CS	+14.3%	-8.2%	+10.2%	+18.5%	-9.2%	-6.5%
	YS	+14.8%	-10.1%	+10.1%*)	+19.5%*)	-13.1%*)	-7.0%*)

*) single run values

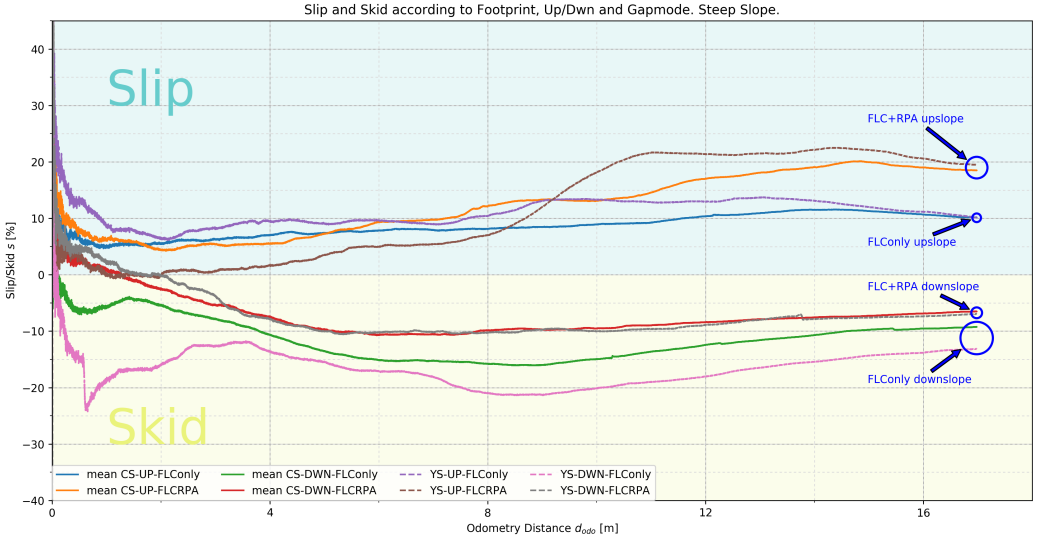

Figure 28: Slip/Skid values separated by footprint, movement direction and GAP-mode.

commands as well as force and body roll-pitch measurements. From these inputs, a coordination of the legs is realized with the goal of permanent wheel-ground contact with optimal force balancing. Optionally the body's roll-pitch angle can be controlled in natural terrain. The force balancing presented in this paper is optimal in terms of the to-be-expected forces at each wheel resulting from the current footprint and the position of the center of mass within the support polygon spanned by the wheels with ground contact.

In the field tests, the rover was driven through three different terrain categories, ranging from mostly flat terrain over moderate slopes to a steep slope with up to 28° inclination covered with loose soil and duri crust. In each terrain set, different footprints and combinations of active GAP modes were tested. The data gathered from these runs is analysed with emphases on (i) energy consumption for locomotion/active ground adaption, (ii) reference force tracking and body roll-pitch control, (iii) ground plane estimation, and (iv) slope climbing abilities in steep slopes.

The experiments showed that the suspension system with its 12 active DoF is not the main power consumer during locomotion. The four wheels and four steering actuators that are also required for passive suspension systems are responsible for the majority of power consumption. Main increase in absolute power requirement from flat terrain to steep slopes is resulting from the drive system, while the suspension system's power requirement is more related to "roughness" of terrain. The test tracks in the presented experiments are rather smooth; in undulating terrain, the power draw of the suspension is expected to increase. This will be quantified in upcoming experimental setups.

In terms of Force Leveling Control (FLC), the presented experiments show that the FLC component is capable of coping with different footprints. The component is able to keep all wheels in ground contact and reduce the force tracking RMS error down to as low as 16 N for individual wheels (gravitational force of the rover: $F_g \approx 1628\,\mathrm{N}$). Additionally activating the roll-pitch adaption does not impede the results of the FLC component, while being able to reduce the roll-pitch tracking RMS errors to below 0.5° in all settings (one run with heavy slipage and robot body oscillations showed RMS errors of $\hat{e}_r = 0.6°$ and $\hat{e}_p = 0.8°$, though).

The ground plane estimation from proprioceptive data showed to have very small deviations across footprints and GAP-modes. Slippage and skidding down slopes, however, affects the results of the plane estimation. The data indicates that the effects are reproducible, in further developments of SherpaTT the proprioceptive ground plane estimates could be used to refine exteroceptive data originating from lidar or camera data and vice versa. Using the plane estimate together with a WCP estimation on the circumference of the wheel, improvements in LEP positioning for active ground adaption are aspired for future work.

From the slope climbing experiments it can be confirmed, that the rover can climb natural terrain slopes with up to 28° inclination. From the data of the experiments it seems that the choice of the GAP-modes has a higher influence than the choice of the footprint on the slippage conditions in the slope. If not required, the RPA-mode should be preferably inactive in slope climbing.

Further analysis of the data shows that changing the pitch angle in the slope gives more workspace and additionally has an influence on the reference forces generated by FLC. This analysis is not presented in detail in this paper, more investigation is needed to realize a reference force balancer by manipulating the reference pitch in an adequate way, this is left for the future work on the system.

Currently also in development is an active leg movement for steering support. When a new steering reference occurs, a trajectory for the LEP shall be generated, that ensures a smooth position and velocity trajectory for the WheelSteering joint without high deltas between current angle and new reference angle.

Additionally the realization of virtual 3D springs for each leg is currently being investigated. Using the force vector measured at each wheel, a virtual compliance can be realized. The effects of this virtual spring on the locomotion shall be investigated in future works.

Finally, evaluation of a combination of reactive control and planning algorithms is aspired. A three dimensional model of the environment can be generated using SherpaTT's lidar scanner. A trajectory for each LEP and the body's center can then be planned in the terrain map. Reactive control then only needs to accommodate for model inaccuracies, while the knowledge of the terrain profile ahead might improve the response-time in ground adaption.

Acknowledgments

The authors would like to thank the *TransTerrA* and *FT-Utah* team members and supporting staff at the DFKI Bremen Robotics Innovation Center. Special acknowledgement is due for the efforts of Leif Christensen, Steffen Planthaber, Thomas M. Roehr, Roland U. Sonsalla, and Tobias Stark of the field team in Utah. Without the joint effort of all field team members, the experiments would not have been possible to conduct. The projects TransTerrA and FT-Utah are funded by the German Space Agency (DLR, Grant number: 50RA1301 and 50RA1621) with federal funds of the Federal Ministry of Economics and Technology (BMWi) in accordance with the parliamentary resolution of the German Parliament.

References

Advanced Navigation (2017). Spacial dual datasheet. `http://www.advancednavigation.com.au/sites/advancednavigation.com.au/files/`

`Spatial%20Dual%20Datasheet.pdf`, last call 2017-09-19.

Apfelbeck, M., Ku, S., Rebele, B., Michaud, S., Boesch, C., Krpoun, R., and Schfer, B. (2011). Exomars phase b2 breadboard locomotion sub-system testcampaign. In *Proceedings of Advanced Space Technologies for Robotics and Automation, (ASTRA'11)*.

Azkarate, M., Zwick, M., Carrio, J. H., Nelen, R., Wiese, T., Joudrier, P. P. A., and Visentin, G. (2015). First experimental investigations on wheel-walking for improving triple-bogie rover locomotion performances. In *Proceedings of Advanced Space Technologies for Robotics and Automation, (ASTRA'15)*.

Balme, M., Curtis-Rouse, M., Banham, S., Barnes, D., Barnes, R., Bauer, A., Bedford, C., Bridges, J., Butcher, F., Caballo, P., Caldwell, A., Coates, A., Grindrod, C., Gunn, M., Gupa, S., Hansen, R., Harris, J., Holt, J., Huber, B., Huntly, C., Hutchinson, I., Jackson, L., Kay, S., Kyberd, S., Lerman, H., McHugh, M., McMahon, W., Muller, J.-P., Paar, G., Preston, L., Schwenzer, S., Stabbins, R., Tao, Y., Traxler, C., Turner, S., Tyler, L., Venn, S., Walker, H., Wright, J., and Yeomans, B. (2017). UK Space Agency 'Mars Utah Rover Field Investigation 2016' (MURFI 2016): Overview of Mission, Aims and Progress. In *Proceedings of the Lunar Planetary Science XLVIII*.

Bartlett, P., Wettergreen, D., and Whittaker, W. L. (2008). Design of the scarab rover for mobility and drilling in the lunar cold traps. In *International Symposium on Artificial Intelligence, Robotics and Automation in Space (i-SAIRAS'08)*.

Bartsch, S., Cordes, F., Haase, S., Planthaber, S., Roehr, T. M., and Kirchner, F. (2010). Performance evaluation of an heterogeneous multi-robot system for lunar crater exploration. In *Proceedings of the 10th International Symposium on Artificial Intelligence, Robotics and Automation in Space (iSAIRAS'10)*, Sapporo, Japan.

Bartsch, S., Manz, M., Kampmann, P., Dettmann, A., Hanff, H., Langosz, M., v. Szadkowski, K., Hilljegerdes, J., Simnofske, M., Kloss, P., Meder, M., and Kirchner, F. (2016). Development and control of the multi-legged robot mantis. In *Proceedings of ISR 2016: 47st International Symposium on Robotics*, pages 1–8.

Bickler, D. B. (1989). Articulated suspension system. US-Patent US4840394 (A) – 1989-06-20 `https://ntrs.nasa.gov/search.jsp?R=19900007837`. Last access: 2018-02-06.

Caudill, C., Galofre, A. G., Pontefract, A., and Osinski, G. (2016). 2015 CANMARS MSR Analog Mission: In situ geochemical insights from x-ray fluorescence spectrometry. In *Proceedings of the 47th Lunar and Planetary Science Conference*.

Clarke, J. D. and Stoker, C. R. (2011). Concretions in Exhumed and Inverted Channels near Hanksville Utah: Implications for Mars. *International Journal of Astrobiology*, 10(3):161–175.

Cordes, F. and Babu, A. (2016). SherpaTT: A versatile hybrid wheeled-leg rover. In *Proceedings of the 13th International Symposium on Artificial Intelligence, Robotics and Automation in Space (iSAIRAS 2016)*.

Cordes, F., Babu, A., and Kirchner, F. (2017). Static force distribution and orientation control for a rover with an actively articulated suspension system. In *Proceedings of the 2017 IEEE/RSJ International Conference on Intelligent Robots and Systems (IROS 2017)*, Vancouver, Canada.

Cordes, F., Dettmann, A., and Kirchner, F. (2011). Locomotion modes for a hybrid wheeled-leg planetary rover. In *Proceedings of the IEEE International Conference on Robotics and Biomemetics (IEEE-Robio 2011)*, Phuket, Thailand.

Cordes, F., Oekermann, C., Babu, A., Kuehn, D., Stark, T., and Kirchner, F. (2014). An active suspension system for a planetary rover. In *Proceedings of the International Symposium on Artificial Intelligence, Robotics and Automation in Space (i-SAIRAS 2014)*, Montreal, Canada.

Dettmann, A., Roemmermann, M., and Cordes, F. (2011). Evolutionary development of an optimized manipulator arm morphology for manipulation and rover locomotion. In *Proceedings of the IEEE International Conference on Robotics and Biomemetics (IEEE-Robio 2011)*.

Dupuis, E., Picard, M., Haltigin, T., Lamarche, T., Rocheleau, S., and Gingras, D. (2016). Results from the csa's 2015 mars analogue mission in the desert of utah. In *Proceedings of the 13th International Symposium on Artificial Intelligence, Robotics and Automation in Space (i-SAIRAS'16)*, Bejing, China.

Gingras, D., Allard, P., Lamarche, T., Rocheleau, S. G., Gemme, S., and Picard, M. (2017). Overview of the 2016 canadian mars sample return analogue deployoment and the technology behind. In *Proceedings fo the 14th Symposium on Advanced Space Technologies in Robotics and Automation (ASTRA'17)*.

Haarmann, R., Jaumann, R., Claasen, F., Apfelbeck, M., Klinkner, S., Richter, L., Schwendner, J., Wolf, M., and Hofmann, P. (2012). Mobile payload element (mpe): Concept study for a sample fetching rover for the ESA lunar lander mission. *Planetary and Space Science*, 74(1):283 – 295. Scientific Preparations For Lunar Exploration.

Harrington, B. D. and Voorhees, C. (2004). The challenges of designing the rocker-bogie suspension for the mars exploration rover. In *In 37th Aerospace Mechanisms Symposium*.

Haynes, G. C., Stager, D., Stentz, A., Vande Weghe, J. M., Zajac, B., Herman, H., Kelly, A., Meyhofer, E., Anderson, D., Bennington, D., Brindza, J., Butterworth, D., Dellin, C., George, M., Gonzalez-Mora, J., Jones, M., Kini, P., Laverne, M., Letwin, N., Perko, E., Pinkston, C., Rice, D., Scheifflee, J., Strabala, K., Waldbaum, M., and Warner, R. (2017). Developing a robust disaster response robot: Chimp and the robotics challenge. *Journal of Field Robotics*, 34(2):281–304.

Heverly, M., Matthews, J., Frost, M., and McQuin, C. (2010). Development of the tri-athlete lunar vehicle prototype. In *Proceedings of the 40th Aerospace Mechanisms Symposium*, NASA Kennedy Space Center.

Huntsberger, T., Stroupe, A., Aghazarian, H., Garrett, M., Younse, P., and Powell, M. (2007). Tressa: Teamed robots for exploration and science on steep areas. *Journal of Field Robotics*, 24(11-12):1015–1031.

Iagnemma, K., Rzepniewski, A., Dubowsky, S., and Schenker, P. (2003). Control of robotic vehicles with actively articulated suspensions in rough terrain. *Autonomous Robots*, 14(1):5–16.

Kroemer, O., Beermann, D., Cordes, F., Lange, C., Littau, B., Rosta, R., Scharringhausen, M., van Zoest, T., and Grimm, C. (2011). Adaptive flexible wheels for planetary exploration. In *Proceedings ot the 62nd International Astronautical Congress (IAC2011)*, Cape Town.

Krotkov, E., Hackett, D., Jackel, L., Perschbacher, M., Pippine, J., Strauss, J., Pratt, G., and Orlowski, C. (2017). The darpa robotics challenge finals: Results and perspectives. *Journal of Field Robotics*, 34(2):229–240.

Lamon, P. and Siegwart, R. (2003). 3d-odometry for rough terrain - towards real 3d navigation. In *2003 IEEE International Conference on Robotics and Automation (Cat. No.03CH37422)*, volume 1, pages 440–445.

Lindemann, R. and Voorhees, C. (2005). Mars exploration rover mobility assembly design, test and performance. In *IEEE International Conference on Systems, Man and Cybernetics, 2005*, volume 1, pages 450–455 Vol. 1.

Manz, M., Dettmann, A., Hilljegerdes, J., and Kirchner, F. (2012). Development of a lightweight manipulator arm using heterogeneous materials and manufacturing technologies. In *Proceedings of the International Symposium on Artificial Intelligence, Robotics and Automation in Space (i-SAIRAS 2012); September 4-6, Turin, Italy.* o.A.

Manz, M., Sonsalla, R. U., Hilljegerdes, J., Oekermann, C., Schwendner, J., Bartsch, S., and Ptacek, S. (2014). Design of a rover for mobile manipulation in uneven terrain in the context of the spacebot cup. In *Proceedings of the International Symposium on Artificial Intelligence, Robotics and Automation in Space (i-SAIRAS'14).*

Michaud, S., Gibbesch, A., Thueer, T., Krebs, A., Lee, C., Despont, B., Schfer, B., and Slade, R. (2008). Development of the exomars chassis and locomotion subsystem. In *Proceedings of i-SAIRAS 2008 - 9th International Symposium on Artificial Intelligence, Robotics and Automation in Space.*

Michaud, S., Schneider, A., Bertrand, R., Lamon, P., Siegwart, R., van Winnendael, M., and Schiele, A. (2002). SOLERO : Solar Powered Exploration Rover. In *None.*

Mishkin, A., Morrison, J., Nguyen, T., Stone, H., Cooper, B., and Wilcox, B. (1998). Experiences with operations and autonomy of the mars pathfinder microrover. In *Aerospace Conference, 1998 IEEE*, volume 2, pages 337 –351 vol.2.

Mumm, E., Farritor, S., Pirjanian, P., Leger, C., and Schenker, P. (2004). Planetary cliff descent using cooperative robots. *Autonomous Robots*, 16(3):259–272.

Nesnas, I. A., Matthews, J. B., Abad-Manterola, P., Burdick, J. W., Edlund, J. A., Morrison, J. C., Peters, R. D., Tanner, M. M., Miyake, R. N., Solish, B. S., and Anderson, R. C. (2012). Axel and duaxel rovers for the sustainable exploration of extreme terrains. *Journal of Field Robotics.*

Reid, W., Prez-Grau, F. J., Gktoan, A. H., and Sukkarieh, S. (2016). Actively articulated suspension for a wheel-on-leg rover operating on a martian analog surface. In *2016 IEEE International Conference on Robotics and Automation (ICRA)*, pages 5596–5602.

Roehr, T. M., Cordes, F., and Kirchner, F. (2014). Reconfigurable integrated multirobot exploration system (RIMRES): Heterogeneous modular reconfigurable robots for space exploration. *Journal of Field Robotics*, Special Issue on Space Robotics, Part 2:3–34.

Schenker, P. S., Huntsberger, T. L., Pirjanian, P., Baumgartner, E., Aghazarian, H., Trebi-ollennu, A., Leger, P. C., Cheng, Y., Backes, P. G., Tunstel, E. W., Propulsion, J., and Dubowsky, L. S. (2001). Robotic automation for space: Planetary surface exploration, terrain-adaptive mobility, and multirobot cooperative tasks. In Hall, D. P. C. E. L., editor, *Intelligent Robots and Computer Vision XX: Algorithms, Techniques, and Active Vision*, volume 4572, pages 12–28, Boston, MA, USA.

Smith, P. (2004). The phoenix mission to mars. In *Aerospace Conference, 2004. Proceedings. 2004 IEEE*, volume 1, page 342 Vol.1.

Sonsalla, R., Cordes, F., Christensen, L., Planthaber, S., Albiez, J., Scholz, I., and Kirchner, F. (2014). Towards a Heterogeneous Modular Robotic Team in a Logistic Chain for Extraterrestrial Exploration. In *Proceedings of the International Symposium on Artificial Intelligence, Robotics and Automation in Space (i-SAIRAS 2014).* International Symposium on Artificial Intelligence, Robotics and Automation in Space.

Sonsalla, R. U., Cordes, F., Christensen, L., Roehr, T. M., Planthaber, S., Stark, T., and Kirchner, E. (2017). Field trials to demonstrate a cooperative multi-robot mission in mars analogue environment. In *Proceedings fo the 14th Symposium on Advanced Space Technologies in Robotics and Automation (ASTRA'17)*.

Thueer, T., Lamon, P., Krebs, A., and Siegwart, R. (2006). Crab - exploration rover with advanced obstacle negotiation capabilities. In *Proceedings of the 9th ESA Workshop on Advanced Space Technologies for Robotics and Automation (ASTRA'08)*.

Townsend, J., Biesiadecki, J., and Collins, C. (2010). Athlete mobility performance with active terrain compliance. In *Aerospace Conference, 2010 IEEE*, pages 1–7.

Volpe, R. (2005). Rover technology development and mission infusion beyond mer. In *Aerospace Conference, 2005 IEEE*, pages 971–981.

Welch, R., Limonadi, D., Samuels, J., Warner, N., and Morantz, C. (2013). Verification and validation of mars science laboratory surface system. In *System of Systems Engineering (SoSE), 2013 8th International Conference on*, pages 64–69.

Wenzel, W., Cordes, F., and Kirchner, F. (2015). A robust eletro-mechanical interface for cooperating heterogeneous multi-robot teams. In *Proceedings of the 2015 IEEE International Conference on Intelligent Robots and Systems (IROS-15)*, pages 1732–1737, Hamburg.

Wettergreen, D., Jonak, D., Kohanbash, D., Moreland, S. J., Spiker, S., Teza, J., and Whittaker, W. L. (2009). Design and experimentation of a rover concept for lunar crater resource survey. In *47th AIAA Aerospace Sciences Meeting Including The New Horizons Forum and Aerospace Exposition*.

Wilcox, B., Litwin, T., Biesiadecki, J., Matthews, J., Heverly, M., Morrison, J., Townsend, J., Ahmad, N., Sirota, A., and Cooper, B. (2007). Athlete: A cargo handling and manipulation robot for the moon. *Journal of Field Robotics*, 24(5):421.

Wilcox, B. H. (2012). Athlete: A limbed vehicle for solar system exploration. In *2012 IEEE Aerospace Conference*, pages 1–9.

[2]: **Reconfigurable Integrated Multirobot Exploration System (RIMRES): Heterogeneous Modular Reconfigurable Robots for Space Exploration**
Thomas M. Roehr, Florian Cordes, and Frank Kirchner
in: Journal of Field Robotics 31(1) (2014)

RIMRES: Heterogeneous Modular Reconfigurable Robots for Space Exploration

Thomas M. Roehr
DFKI Robotics Innovation Center Bremen
28359 Bremen, Germany
thomas.roehr@dfki.de

Florian Cordes
DFKI Robotics Innovation Center Bremen
28359 Bremen, Germany
florian.cordes@dfki.de

Frank Kirchner
DFKI Robotics Innovation Center Bremen and University of Bremen
28359 Bremen, Germany
frank.kirchner@dfki.de

Abstract

This paper presents the multi-robot team RIMRES[1] that comprises a wheeled rover, a legged scout and several immobile payload-items. The heterogeneous systems are employed to demonstrate the feasibility of reconfigurable and modular systems for lunar polar crater exploration missions. All systems have been designed with a common electro-mechanical interface, allowing to tightly interconnect all these systems to a single system and also to form new electro-mechanical units. With the different strengths of the respective subsystems a robust and flexible overall multi-robot system is built up to tackle the, to some extend, contradictory requirements for an exploration mission in a crater environment. In RIMRES the capability for reconfiguration is explicitly taken into account in the design phase of the system, leading to a high degree of flexibility for restructuring the overall multi-robot system. To enable the systems' capabilities the same distributed control software architecture is applied to rover, scout and payload-items, allowing for semi-autonomous cooperative actions as well as full manual control by a mission operator. For validation purposes we present results of a critical part of the aspired mission, the autonomous docking procedure between the legged scout robot and the wheeled rover. This allows to illustrate the feasibility of a complex, cooperative, and autonomous reconfiguration maneuver with the developed reconfigurable team of robots.

1 Introduction

In space exploration scenarios of different agencies, Moon is seen as a stepping stone in human space exploration (ISECG – International Space Exploration Coordination Group, 2011). For an extended stay of humans on the lunar surface in-situ resource utilization is crucial for a successful mission and for preparation of human exploration of more remote destinations such as for example Mars. Robotic precursor missions are part of the roadmaps for human space exploration. Apart from in-situ production of building materials for shelter, water ice is an important resource that is needed for generating fuel or oxygen for human habitats on Moon.

[1] Reconfigurable Integrated Multi-Robot Exploration System

Building up deposits of water ice on the lunar surface is possible by different mechanisms, such as water ice contained in meteorites or comets that make impact on the lunar surface, hydrogen from the solar winds that reacts with lunar oxides or outgassing of water from the inner parts of the Moon (Arnold, 1979). The deposits of water ice are diminished by dissociation of photons coming from the sun, which leads to the assumption, that water ice is most likely to be found in permanently shaded regions – the so-called cold traps – of the lunar surface as can be found in the polar crater regions of the Moon (Zuber et al., 2012).

The LCROSS mission (Colaprete et al., 2010) showed indications for presence of water ice and other volatiles in the Cabeus crater at the lunar south pole. However, the proofs for water ice are up to now only indirect measurements via spectral analysis. Thus, in-situ confirmation and a better understanding of the distribution of the resources are still open questions that need to be addressed.

As indicated, not only water ice as a volatile might be present in the cold traps on Moon, but other volatiles are likely to be found there as well (Mosher and Lucey, 2006). The main scientific goals for a mission for exploring the lunar cold traps for volatiles include

- determination of the volatile composition (isotopic, elementary, mineralogically),
- mapping of the local distribution and the identification of the volatile's sources,
- mineralogical diversity at the landing site, including age, distribution, origin and composition, and
- the lunar environment including dynamic processes, such as weathering and meteoroid impacts.

Technologically more challenging than orbiting missions and with higher risk are landing missions that make use of surface deployable probes such as landing units and/or mobile systems. However, this approach can provide deeper insight into the above mentioned scientific goals (Mosher and Lucey, 2006).

(a) RIMRES systems as CAD models. The six-legged scout CREX is beneath the wheeled rover Sherpa. Attached to Sherpa's manipulator are two payload-items that form a surface-deployable payload.

(b) Photograph of final integration status of RIMRES mobile systems. Wheeled Rover Sherpa with manipulator arm and docked six-legged scout robot CREX.

Figure 1: Systems in the heterogeneous modular multi-robot system RIMRES

In this paper a heterogeneous modular multi-robot approach is presented that is intended to bring a robotic system down into the permanently shaded regions of a lunar polar crater in search for volatiles bound to the lunar regolith. In the presented approach, a wheeled rover (Sherpa[2]) and a legged scout robot (CREX[3]) are used together with surface-deployable modular payloads. The idea is to combine the energy efficient locomotion principle of wheels with the high mobility of a legged system. Both systems can be combined via an electro-mechanical interface (EMI); in the connected state the robots act as a monolithic system, whereas in detached mode, both systems act independently of each other. In Figure 1 the systems are depicted. In general, the EMI serves several use-cases: (1) docking of Sherpa and CREX, (2) manipulating modular

[2]Sherpa: Expandable Rover for Planetary Applications
[3]Crater Explorer

payload-items, (3) stacking of payload-items to form payloads, and (4) attaching payload-items to the mobile systems is made possible by using the EMI (Wenzel et al., 2011).

This paper is structured as follows: In the following section, a short overview on some field of related work for RIMRES is provided. A more elaborate discussion on reconfiguration in terms of system design and levels of reconfiguration is provided in section 3, while section 4 presents details about the hardware components constituting the overall system. Section 5 presents the software framework that is developed for representing the hardware reconfiguration possibilities and modularity in software and mission control. Experiments with the systems and a comparison to a former multi-robot approach are discussed in section 6. Section 7 explicitly describes the lessons learned before concluding the paper in section 8.

2 Related Work

To the authors, no system directly comparable in terms of reconfiguration capabilities, technological complexity of the single subsystems involved in modular reconfiguration and seamless integration of self-contained systems into a new system to the approach presented here is known. However, there are several systems, that are related to the RIMRES system in one way or the other. This section gives a brief overview of some relevant systems and research activities. Because RIMRES tackles a broad range of topics, the following descriptions do not aim at being complete, but are meant to give an overview on some of the relevant systems.

2.1 Modular and Reconfigurable Systems

Mostly, modular reconfigurable systems in literature are systems that provide a kind of atomic modularity, meaning, that the systems are built up from identical modules or modules at least in the same scale with slightly different functions. The approach followed in RIMRES is opposed to that, since the systems that interconnect range from cubic modular payload-items (150 mm × 150 mm × 150 mm, mass < 5 kg) over the legged scout system (around 27 kg) to the wheeled rover with a (variable) footprint of up to 2.5 m × 2.5 m and a weight of around 160 kg. Thus, sizes and weights of subsystems in RIMRES range over two and three orders of magnitude, respectively. A similarity between the common modular (self-)reconfigurable systems in literature and the approach presented here is the need for a common EMI that is shared between all systems.

In literature, a broad range of designs realizing a connector mechanism for connection of single modules in a multi module system (MMS) exist. Approaches using permanent or electro-magnets like the Telecubes (Suh et al., 2002) are elegant because no moving parts are necessary. However, these approaches might need high powers when loads of several kilograms have to be securely fastened in environments with mechanical shocks and high probability of dirt accumulations on the systems.

A pin/hole mechanism combined with a shape memory alloy is an alternative to build latch mechanisms only requiring actuation for detaching the single systems from each other. Conro (Castano et al., 2002) or PolyBot (Yim et al., 2002) are examples of this class of latching mechanism.

The systems M-TRAN III (Kurokawa et al., 2007) and Atron (Ostergaard et al., 2006) make use of active hooks and appropriate bails for connecting mechanically to other modules of the system. Even though the two systems make use of a similar principle for mechanical connection, data connections are different between both systems: M-TRAN makes use of electrodes to transfer data electrically, while Atron modules communicate with each other via infrared signals.

The minimal requirement for the physical connection is that the mechanism can withstand forces that might occur during operation. Typically, these forces depend on the weight of the attached modules. In (Sproewitz et al., 2008) a connection mechanism is presented that can withstand tensile and shear forces of approximately

180 N and shear torques of 7 Nm. A heavy-duty connector for self-reconfigurable robots that withstands forces of more than 700 N is presented in (Nilsson, 2002).

2.2 Examples for Rover Systems with Reconfiguration Capabilities

The ATHLETE (All-Terrain, Hex-Limbed, Extra-Terrestrial Explorer) uses six wheels on actuated legs to walk and to drive (Wilcox et al., 2007). This concept combines the advantages of both locomotion possibilities: energy efficiency and high mobility. Each leg possesses six Degree of Freedom (DoF) (seven DoF in case of the Tri-ATHLETE version (Wheeler et al., 2010)).

A quick-disconnect tool adapter is employed, so each leg can be used as general purpose manipulator as a second use-case. Different tools can be applied. This incorporates drilling devices, grippers and by using two legs in combination scoops for shifting greater amounts of soil can be attached. Thus, the legs of the ATHLETE family of robots are reconfigurable devices, that can be used for both, locomotion (driving motions and undulating behaviors) and manipulation tasks.

The design with the 6 limbs arranged in a hexagon allows to operate in inverted position and even more important helps to prevent tipping over. Each face of the hex frame possesses a stereo camera with appropriate lighting to navigate and avoid hazardous objects. The cameras are also used for visual odometry and visual docking in case of a desired cooperative maneuver. The current version is powered by a gasoline-motor generator and lead-acid batteries, while a future flight model is intended to be powered by solar panels and H2O2 fuel cells.

Scarab (Wettergreen et al., 2009) is a four wheeled rover that combines a rather classical bogie suspension with an active DoF to enhance the ability to climb and drive along slopes. Furthermore, the control of the body height as well as the roll angle of the robot is possible. The aspired mission for the system is to take drilling cores within perpetual darkness of lunar polar craters. Therefore, an upright drill is employed in the center of the robot. The suspension system is used to lower the body of the rover in preparation for the drilling process. Since the drill is in upright position the structure has a dual use: Apart from the drill itself it supports navigation sensors and thus works as a navigation mast (Bartlett et al., 2008).

Tri-Star IV (Aoki et al., 2011) is a three-wheeled rover, able to reconfigure and adapt to changing terrain types by rotating its wheeled arms and using flexible wheels. It represents the latest advancement in the development of a series of three-wheeled rovers. The capability to recover from an upside down position is an essential feature of this rover along with an optimized storage posture. Furthermore, it is embedded into a multi-robot architecture consisting of so-called parent and child type rovers, which shall be deployed for lunar crater exploration using tether-based connections to allow drilling and collecting samples.

2.3 Walking and Climbing Robots

In general, walking systems provide a high mobility, since they have the ability to position the ground contact points (i.e. the feet) nearly arbitrarily within the work space of the respective leg. This enables them to step over obstacles or to cling to foot holds in steep slopes. Furthermore, the lifting of a leg off the ground avoids a so called bulldozing effect wheeled systems have to cope with in loose soils.

The climbing robot Dante II demonstrated in extensive field experiments its capability of climbing into a volcanic crater (Bares and Wettergreen, 1999). The movements in the crater were partially remotely operated by human supervisors and partly autonomous, relying on on-board vision systems (laser-range finder and video cameras). The robot is a framewalker with eight legs. Additionally, a winch/tether mechanism is used to support the robot in steep slopes.

The LEMUR family of robots are six-legged (LEMUR I and LEMUR IIa) and four-legged (LEMUR IIb)

robots that are designed for use in orbital tasks as well as for exploring planetary surfaces (Kennedy et al., 2001; Bretl, 2006). The robots provide tool-exchange interfaces for reconfiguring the legs and equipping them with different tools for a task at hand. By making use of a stereo vision system, appropriate foot holds for freely climbing nearly vertical surfaces is made possible.

The Scorpion robot (Spenneberg and Kirchner, 2007) is an eight-legged system for traversal of various terrain types and can still operate when suffering leg loss (Spenneberg et al., 2004). The robot makes use of a decentralized locomotion control approach and is able climb in steep slopes and can use the front pair of legs as manipulation devices. Not specifically designed for a multi-robot team, it was still possible to act as a scouting robot in a scenario similar to the one presented in this approach (Cordes et al., 2010). Based on the experiences with Scorpion different types of legged walking robots have been developed, e.g. the four-legged Aramies (Spenneberg et al., 2005) and the six-legged SpaceClimber (Bartsch et al., 2012). SpaceClimber is a walking and climbing robot that successfully demonstrated the locomotive abilities of multi-legged robots in steep terrains. In contrast to previous robot designs, SpaceClimber's kinematics have been optimized using evolutionary computation (Rommerman et al., 2009) – an approach which has been reused to optimize the rover's manipulator in RIMRES. The walking robot CREX used as scout in RIMRES is based on the robot SpaceClimber and thus benefits from this series of developments towards walking robots specialized for steep terrains.

2.4 Standards and (Software-)Technologies

A crucial part for reconfiguration and modularization and its reflection in higher levels of software is the underlying framework. Within RIMRES the framework Foundation for Autonomous, Modular Systems (FAMOS) was developed, which build upon and extends common standards in networking and control. If the following some of the parts that constitute FAMOS are presented.

Service Oriented Architectures (SOA) are a common approach to support a modular software design and are inherently more robust, due to component's single responsibility. A similar approach is also propagated by the Foundation of Intelligent Physical Agents (FIPA) (Foundation of Intelligent Physical Agents, 2002) and Consultative Committee for Space Data Systems (CCSDS) (CCSDS/AIAA Inc., 2012). While FIPA developed a standard for a complete abstract architecture, the CCSDS published a "Reference Architecture for Space Data Systems" (CCSDS/AIAA Inc., 2008). Multiple implementations of the FIPA standard exist with JACK (Winikoff, 2005), FIPA-OS (Poslad et al., 2000), Mobile-C (Chen et al., 2006) and JADE (Bellifemine et al., 1999) to name only a few. These frameworks implement the (experimental) FIPA standards to wide parts, but are mostly using JAVA; Mobile-C as a rare exception. These implementations originate from the software-agent domain, and due to the choice of programming language are not directly applicable to RIMRES which relies on C/C++ software to large parts. Another JAVA based framework can be found with Cougaar (Snyder et al., 2004). Cougaar implements a blackboard-based communication for a multi-agent system and allows for highly scalable systems. However, it does not rely on additional standards such as FIPA for building up its infrastructure.

Developing software for the robotics domain comes with a number of common and repetitive tasks, and has triggered the development of different frameworks such as Microsoft Robotics Studio Developer (Microsoft, 2011), MIRO (Utz et al., 2002), Orocos (Bruyninckx et al., 2003), Rock (DFKI Bremen Robotics Innovation Center, 2011), ROS (Willow Garage, Inc., 2011), and Yarp (Metta et al., 2006). These frameworks usually wrap functionality in a single kind of component though using different terminology such as task, node, or service. All of these frameworks deal with communication and dedicated peer-to-peer connection management and publish-subscribe mechanisms exist. MIRO, Orocos and frameworks which build upon those (such as Rock) include an application of CORBA (Common Object Request Brokering Architecture), and Yarp allows an easy integration of it. CORBA has been around since 1991 and reached a level of maturity and broad acceptance.

Since CORBA requires a central name-service, it does not directly fit into a fully distributed setup. A

tool that can act as replacement for the central name-service in a distributed context - and has been used in RIMRES - is Avahi (Poettering et al., 2012). As so-called zeroconf solution (IETF Zeroconf Working Group, 2011) and operating on the two complementary technologies mDNS (Multicast Dynamic Name Service) (Cheshire, 2011) and DNS-SD (DNS-Service Discovery) (Cheshire and Krochmal, 2011) Avahi allows name-based resolution for service records, which can be detailed using multiple, customizable text records. In addition to a simple name-service it also allows to detect when a service is started or stopped.

Only establishing communication is not sufficient, and thus FIPA allows for reasoning on communication using a message specification in combination with so-called performatives. Communication between two agents is looked at as a speech-act, and interaction protocols, e.g. for a contract net implementation, allows validation of the message flow. Lyell et. al (Lyell et al., 2009) already apply these standards in the domain of space robotics.

3 Designing for Reconfiguration

Assuming the usage of mobile robots for further exploration of volatiles in the lunar polar cold traps, some basic requirements for the system design can be established. The systems have to be robust and reliable in order to survive the harsh conditions on the lunar surface. The mobile units have to provide and sustain a general framework for the planned scientific experiments. This includes the power system, environmental protection, the capability of placing the right instruments in the right place and safely transporting measurement equipment to designated places. For a maximized impact, the amount of local surface coverage is also a determining factor. The systems should be able to cover distances in the order of several tens of kilometers. The locomotion should be efficient, since power in the permanently shaded regions is a critical resource. In general, the system has to be able to react to unforeseen circumstances in an appropriate way.

Some of these requirements are partly contradicting, e.g. an energy efficient surface coverage in the order of tens of kilometers might not coincide with a system that is capable of climbing steep slopes that often are to be found in areas of scientific interest, i.e. target areas for exploration and in-depth measurements. However, by combining the benefits of heterogeneous systems into one overall robotic team, the respective strengths of each system can be exploited to maximize outcome of a mission and a larger safety margin is kept – upcoming problems can also be handled by collaboration, e.g. wheeled locomotion is more efficient in general in terms of energy consumption than legged locomotion, while a legged system is more appropriate for challenging terrain type. Combining both locomotion types appears to be logical and thus in RIMRES one exploration system consisting of a main rover (a wheeled system) and a legged scout robot are designed for the task of exploring the inner of the lunar polar cold traps.

To meet these challenges, we propose the usage of heterogeneous reconfigurable systems, an approach we already successfully presented within the project LUNARES and extended substantially with the RIMRES system (Cordes and Kirchner, 2010). The proposed systems are modular and allow for physical reconfiguration, i.e. are able to react with the physical adaptation to different challenges that might occur during mission time. The modular design also allows for extension in successive missions, so that exploration missions and hardware can be gradually implemented to build a lunar exploration infrastructure and prepare for human presence on the Moon.

Since reconfiguration is a main characteristic of the system design, the following section gives a theoretical discussion on that topic in the context of strategic adaption.

3.1 Strategic Flexibility

One of the main elements in the project RIMRES is the integration of reconfiguration capabilities into a system of heterogeneous robots to allow for "strategic flexibility" (Evans, 1991). This is a major distinction

Table 1: Terms of strategic flexibility as defined in (Evans, 1991)

adaptability:	"a singular and permanent adjustment to a newly transformed environment"
flexibility:	"the ability of successive, but temporary approximations to this state of affairs"
robustness:	"a system's ability to absorb, deflect, or endure the impacts of unanticipated changes"
resilience:	"the tendency to rebound or recoil, [...] and the capability to withstand shocks without permanent damage or rupture"

to similar projects since reconfiguration becomes an integral part of the system design.

Reconfiguration comprises three essential states: (1) an actual (stable) configuration, (2) a (stable) target configuration as result of the reconfiguration process, and (3) the (unstable) transition phase between the two configuration states. This process description does not give any idea on how significant the changes of a single reconfiguration might be, yet, a transition has to involve changes, and in that context reconfiguration can be viewed as a "controlled type of evolution" (Dunin-Keplicz and Verbrugge, 2010). The desired outcome of the reconfiguration – the target configuration – is known, while the transition might be initially unknown, but needs to be performed in a controlled manner to produce the desired outcome. Thus, knowing start and target configuration asks for an application of a planner to outline the transition phase and minimize the side effects of such configuration. While a planner is required for an autonomous exploitation of this kind of flexibility, RIMRES uses predefined semi-autonomous action sequences or lets a human operator perform a transition.

Reconfiguration can be found in a variety of domains – robotics being just one – and organization theory has studied the issue of reconfiguration as part of improving on strategic flexibility. The goal of improving strategic flexibility lies in providing a better response to external changes, e.g. here of a market, suppliers, etc., but in general to improve characteristics of an organization in terms of adaptability, flexibility, robustness, or resilience. For these terms we use the semantic description as listed in Table 1 and collected by (Evans, 1991) which serves as our primary source for the discussion on strategic flexibility:

Primarily and following (Evans, 1991), an improvement of these characteristics produces a higher DoF for an organization and allows for a better operational range. The additional DoF increase the solution space and an organization has better chances to find an appropriate solution to upcoming and potentially unforeseen problems. Yet, for more advanced reconfiguration and comparison of reconfiguration strategies, response time or speed of tackling and solving a problem will become a decisive factor for either success or failure (Dignum, 2009). The complexity of the discussion increases when looking at additional dimensions of strategic flexibility in the temporal domain and considering reactiveness, pro-activeness and a differentiation between offensive and defensive actions. For now, we will leave out a detailed discussion on these additional dimensions and focus an applying the basic capability of reconfiguration.

Transferring these findings to a physical system, RIMRES targets the increase of the DoF of the overall system by embedding reconfiguration capabilities at hardware and software levels – initially aiming at higher adaptability and resilience.

3.2 Dimensions of Change

Adaptation of the systems in RIMRES involves change and affects both, hardware and software. On a low level, reconfiguration of hardware can involve the exchange of mechanical parts or a rearrangement of physical links. Similarly for software: a change of the setup of running components and relinking communication channels and data processing chains is a low-level reconfiguration. On a higher level, reconfiguration can take advantage of the parametrization of components using hardware switches or configuration properties of

software modules and allows for more sophisticated reconfiguration approaches. This can be compared to an online system optimization – again supporting the view of a "controlled type of evolution". Generally, we are looking at adaptation in the dimensions listed in Table 2.

Table 2: Dimensions of change

	physical / hardware	**virtual / software**
structural	change of morphology, tool exchange	change of distribution of modules across physical devices, reorganizing and relinking data flow, changing dependencies for running components
functional	tool exchange, modes of operation: wheel also being used as foot or sensing device, manipulator also being used supporting leg	modalities, application of various solution strategies, parametrization of components, e.g. adaption of thresholds, configuration parameters in a signal processing chain
mixed	change of morphology changes the set of active capabilities, and for exploitation requires adaption of the high-level software stack	

In most of the cases a change in structure is followed by a change of functionality. This can on the one hand result in an extension of available functionalities, but on the other hand particular functionalities can also be disabled since they cannot be performed with the new system structure.

3.3 Reconfiguration Examples

Reconfiguration of (robotic) systems can be considered in almost all phases of system design and at all levels of the system architecture. Considering the basic reconfiguration capability i.e. reconfiguration by exchange of (structural) parts of the system, one has to account for (1) mechanical interfaces allowing reconfiguration and (2) a mechanism to perform reconfiguration. Industrial robots provide a practical example by exchanging tools as preparation for different tasks. This kind of reconfiguration is tightly connected to the modularity of systems and the one targeted in this project.

A core element for mechanical reconfiguration in this and other projects is the design of an EMI (see section 4 for details). This interface allows to connect to previously independent systems. However, reconfiguration in general also contains less extreme examples. Accounting for different locomotion modes and a morphology change of a system is an example with a lesser impact on the overall system structure. The change of morphology can be of special benefit for improving locomotion capabilities for specific terrain types or tasks, e.g. the Scarab rover (Bartlett et al., 2008) while driving, uses the suspension system for leveling the robot's body in changing slopes. In the so called inch-worming locomotion mode, the suspension system is actively used to increase the locomotive abilities of the system in steep slopes. Furthermore, the suspension can be used to lower the body of Scarab to the ground in order to prepare for drilling the lunar surface.

The system designer accounts for predefined reconfiguration options using a modular architecture, and reconfiguration can almost always be achieved by (re)using parts of the system in other ways than originally intended. The Hayabusa mission is one prominent example where reconfiguration and re-use of structural parts of the system were successfully applied to lead the overall mission to success. In this case anomalies were detected in one of the thruster engines, but by reconfiguring the two engines the return cruise of the space craft to earth was made possible (JAXA, 2009).

Thus, embedding reconfiguration options into a system is not a novel idea and already present in various

applications, e.g. to perform error recovery or situation adaptation. However, existing applications operate either at very low-level or use systems with lower complexity, e.g. activities of swarm-based research take a very general approach to reconfiguration, at the price of practicality and decreased system performance, while this project tries to maintain the specialized capabilities of robots like Sherpa and CREX and provide the capability for structural reorganization of these systems a the same time.

4 RIMRES – A System of Systems

The aspired mission in RIMRES tries to simulate typical elements of a situation in an exploration mission and/or infrastructure build up. The mission is operated from an earth-bound (mission) control center, which communicates with a system control station at the lunar surface. This system control station is the focal point for communication of all robotic systems that are part of the mission: in RIMRES this encompasses two mobile subsystems as well as immobile payload-items and assembled payloads.

The two mobile subsystems are a wheeled rover and a legged scout. Both systems can act completely independently from each other, but at the same time a close electro-mechanical connection between both systems can be established combining both separated systems into one combined system. Further reconfiguration abilities are added by the introduction of modular payload-items that (1) can extend the capabilities of the mobile systems or (2) can be used to create payload stacks[4] during the mission. These payloads can either be part of a science mission or represent basic infrastructure elements, e.g. for communication. For the RIMRES scenario, four types of so-called payload-items are aspired: (1) a battery module for extending the range of the mobile units and for powering the assembled science packages, (2) a camera module, simulating a data-generating science payload, (3) the mole subsurface sampling system that already flew on the Beagle-2 mission was planned to be implemented in the RIMRES framework, and (4) a communication/navigation item (REIPOS[5]) (Bindel and Bruns, 2010). The wheeled rover serves as transporter and provides a manipulation arm. This manipulator allows to combine payload-items and deploy individual or combined payload-items in the lunar environment. Alternatively, payload-items can be attached to the legged scout.

The overall system in RIMRES serves as a technology demonstration and is used under earth conditions. For demonstration and validation, an artificial lunar crater (surface area $105\,\mathrm{m}^2$) with realistic slopes and lighting conditions has been set up in the DFKI laboratories. Thermal management, radiation and other environmental issues are not explicitly taken into account at this stage of development.

While a mission with the RIMRES system can be arbitrarily complex, the following outline of actions illustrates a feasible mission. The rover starts transport of the scout and six payload-items – three battery modules and two science modules – to the rim of a lunar polar crater. As mentioned, the rover's manipulator can be used to assemble scientific payloads from payload-items, and on the way to the crater rim it deploys two payloads consisting of one science and one battery module each. Furthermore, during transport with the rover, the scout is fully functional, thus its scientific instruments can also be used during this phase to probe the terrain. With one battery module and the scout attached the rover reaches the crater rim, where it detaches the scout and deploys an additional battery module on the back of the scout. Subsequently, the scout climbs into the permanently shaded regions of the crater to conduct in-situ measurements in search for water ice or other volatiles. During the travel to the crater rim the scout has been supplied with energy from Sherpa via the EMI, so that it requires its own internal energy only for the descend into the shaded crater and for the return. While the scout is exploring the crater, the rover ferries between the lander to pick up additional payload-items available at the lander to extend or maintain the infrastructure and experiments. It will also use the lander's infrastructure to replenish its own energy supplies. Eventually, the rover will reunite with the scout at a designated meeting point at the crater rim to continue the exploration from a

[4] In the context of RIMRES payload-items are single cubic modules that can be stacked to form scientific or infrastructural elements which are called payload stacks or payloads.

[4] While the battery module and the camera module are integrated to the status of fully functional payload-items, the REIPOS-system is in the state of a laboratory example, and the setup of the mole module has only been investigated theoretically

[5] Relative Interferometric Position Sensor, development by the project partner ZARM

different starting point.

In RIMRES, reconfiguration aspects are part of various layers. Firstly, the overall system and team of robots can be reconfigured by either stacking of payload-items (onto each other or onto the mobile systems) or by docking the legged scout and the wheeled rover. Secondly, on subsystem level the individual systems are capable of different operating modes which we also describe as reconfiguration property: (1) the wheeled rover can be reconfigured in the sense that the active suspension system can be used in various ways to propel the robot, (2) in addition its manipulator can be used for handling the payload-items as well as for locomotion support, system inspection and system supervision, and (3) the legged scout is reconfigurable in the sense that the legs used for locomotion are equipped with gripper elements and using a gripper mode are able to pick up geological samples at a site of interest.

The following paragraphs describe the single systems of RIMRES in more detail. The EMI as central part of the system is described in section 4.1, while the rover as main mobile unit is presented in section 4.3. A description of the scout is provided in section 4.4, the payload-items are described in section 4.2.

4.1 Electro-Mechanical Interface for Modular Reconfiguration

The electro-mechanical interface (EMI) developed in RIMRES is the central device for interconnecting subsystems with each other. Thus, it is of special importance for realizing the reconfiguration capability in RIMRES. The design of the EMI was driven by the requirements of establishing a reliable and robust physical connection between two systems (Wenzel et al., 2011), i.e. allowing Sherpa to carry CREX, building subsystems of combinations of payload-items, and at the same time providing data and energy transfer between systems via this interface. Additionally, to fulfill these requirements in a lunar environment, dust-resistance of the interface was a primary objective and experiments as illustrated in Figure 3 proved the working of the interface even under these extreme conditions.

The current design of the EMI – achieved after multiple iterations – provides a secure mechanical connection and routes data signals as well as energy in a combination of subsystems. The interface consists of a male (passive) and a female (active) part as shown in Figure 2. Apart from the mechanical parts that are displayed in the figure, a dedicated electronics board is part of the EMI. A microcontroller controls the latch mechanism and the illumination LEDs of each bottom interface. When two system get connected these microcontrollers establish local communication (LOC) in order to gather topology information and route high-level commands. Furthermore, the module electronic provides power management within a system connected via an an EMI. Details on the general concept, mechanical design, and power management can be found in (Dettmann et al., 2011; Wenzel et al., 2011; Wang et al., 2011).

4.2 Modular Payload-Items

Specifically designed to allow construction of additional payloads, or to extend the functionality of some of the main systems, payload-items are cubic modules with an active EMI in the bottom face and a passive EMI in the top face (Wenzel et al., 2011). By stacking the payload-items, different scientific payloads and infrastructure elements can be assembled. All payload-items come with a processing unit (Gumstix) to run the high-level software framework and a micro-controller to support low-level intelligence, e.g. to communicate with an EMI. As part of the low-level intelligence an internal communication protocol has been designed allowing to infer the current topology of a stack of payload-items from the EMI connections, and control basic operations such as opening and closing the mechanic latch to attach an active EMI to a passive one. These capabilities are exposed to higher levels of control, to allow for more complex reconfiguration activities.

The following sections briefly describe the specialized module types that have been developed in RIMRES.

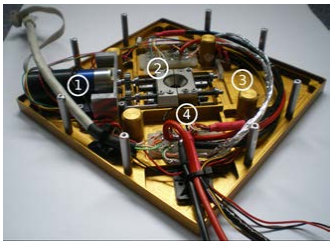

(a) Inside of the bottom interface

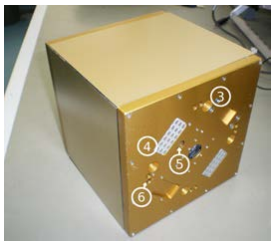

(b) Bottom interface from the outside

(c) Top interface with unique visual servoing markers

Figure 2: Description of the RIMRES electro-mechanical interface in real implementation of a payload-item (cube with side-length of 15 cm): (1) actuator for latch mechanism, (2) bottom latch mechanism and top central connection pin, (3) bottom receptor cylinder and top guidance pin as counterpart, (4) contact blocks for electrical connections via 18 pins, (5) camera opening (camera is not illustrated in (a)), and (6) LED openings

(a) Latch mechanism after closing and opening with basalt of grain size 0.02 mm-0.2 mm

(b) Latch mechanism after closing and opening with basalt of grain size 0.7 mm-1.3 mm

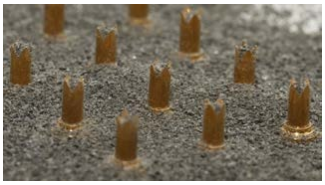

(c) Close-up of crown shaped electrical pins when covered with basalt dust

Figure 3: Situation after covering movable parts of the EMI with amounts of dust exceeding by far the expected amount in normal operation

4.2.1 Battery Module

Within the earth demonstration scenario of RIMRES, battery modules are used as replacement for energy-harvesting payload-items. In later stages, additional solar modules for actually harvesting energy are conceivable. A battery module always constitutes the basis of a payload stack, since functional modules and energy modules are separated within the modular framework of this project. The battery module comprises power switching intelligence and therefore it is possible to connect multiple systems and multiple battery modules at the same time. Each payload-item can be a power sink while the battery modules can be a power source as well. In order to protect the systems from uncontrolled charging and connecting two power sources with different power levels at the same time, a power management system (Wang et al., 2011) – as previously mentioned – has been set up.

4.2.2 Science Modules

In order to simulate science payload-items, a camera payload-item serves as primary example for a science module. The camera payload-item is a placeholder for more sophisticated scientific equipment, but it demonstrates the core feature: attached to a battery payload-item it can form an active payload. It can receive control commands from the mission control, e.g. to set the orientation of the camera that is mounted on a rotational table and provides image data. Thus, this example payload allows to verify the process for data acquisition and distribution, and communication of high volume data from the payload-items to the system control station via WLAN communication. Using the general communication framework which is used by

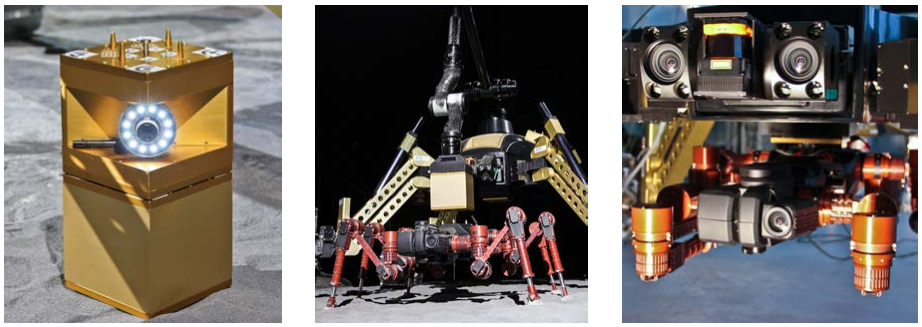

(a) Active payload composed of battery payload-item and camera payload-item. This stack simulates a data generating scientific payload in the RIMRES context.

(b) CREX is being equipped with a battery payload-item for extending its range of operation. The payload-item is handled with Sherpa's manipulator.

(c) CREX is docked to Sherpa via Sherpa's Bottom-EMI

Figure 4: Electro-Mechanical Interface (EMI) and Payload-Items in RIMRES: Used to form scientific payloads, to extend the mobile systems capabilities, and to interconnect the mobile systems.

Table 3: Key dimensions of Sherpa

Description	Value
Max. ground clearance	711 mm
Min. ground clearance (wheels above body)	-189 mm
Square-shaped footprint in cross stance	2100 mm (high stance) to 2500 mm (body low)
Mass (w/o scout or payload-items, incl. manipulator)	approx. 160 kg
Mass of manipulator	25 kg
Length of fully stretched arm	1955 mm
Max. static load on stretched arm (stretched wrist)	183 N
Max. static load on stretched arm (hanging wrist)	537 N

all subsystems, this payload is seamlessly integrated into the system control and communicates within the software framework using the same means as CREX and Sherpa.

4.3 Four-Wheeled Rover Sherpa

The wheeled rover Sherpa is the key team member in our multi-robot system. Only Sherpa is capable of assembling payloads (on demand) using the manipulator arm attached to the central body. It is also capable of transporting the legged scout to the crater rim and transporting payload-items, thus increasing the reach of less efficient or even immobile systems.

Sherpa makes use of an active suspension system that allows to select from a set of locomotion modes depending on the current terrain situation. These modes range from various postures to enhance the relation of center of gravity and center of the support polygon to substantially different drive modes, for example planar omnidirectional movements or inchworming modes, (Cordes et al., 2011). Figure 5 displays the final state of the integration of Sherpa. The key properties of Sherpa are summarized in Table 3.

Sherpa shows great flexibility to adapt to various terrain conditions. The active suspension allows to adapt the footprint of the rover according to the challenges the current terrain imposes on the rover. This can also be interpreted as a posture reconfiguration. Furthermore, the active suspension can be used to propel

(a) Sherpa using its active suspension to step onto an obstacle. The arm was used to support the robot while lifting each of the front legs.

(b) Sherpa using its manipulator as fifth limb. The manipulator is strong enough to bear the weight of the robot, when two legs are lifted off the ground.

Figure 5: Photographs of Sherpa, hybrid wheeled-leg mobile rover in RIMRES

the robot: instead of just using the wheel actuators, the suspension actuators can be incorporated into locomotion, as for example in an inchworming fashion or for (short traverses of) undulating behaviors.

Another main property of Sherpa is the manipulator arm attached to the rover's main body. Its primary use is to handle payload-items that are attached to the four EMIs located around the central tower. By manipulation of payload-items, various scientific and infrastructural payloads can be assembled. Furthermore, the arm can be used as a fifth limb, thus reconfiguring an arm into a leg, cf. Figure 5(b). The manipulator's palm camera is normally used for grasping the payload-items in a visual servoing process, but it can be used to allow a human operator to supervise the rover system. Additionally, payload-items attached to the arm can further extend the functionality of the manipulator, e.g. for scooping or sophisticated gripping (these types of payload-items are not part of the development in the RIMRES project). Details of the manipulator design are provided in (Manz et al., 2012).

In the final stage of expansion, the wheels[6] are planned to be adaptable subsystems of the rover. In the current stage of development, however, the wheels are flexible metallic wheels with passive adaptation to the ground (Kroemer et al., 2011). Figure 5 displays the wheels mounted on Sherpa. Similarly to the manipulator, the rover's functionality can be extended using payload-items. For example, additional sensors can be attached via one of the fixed EMIs of Sherpa that are attached to the main body. Currently, we assume an additional battery pack to extend the operational time of the system, or scientific payloads attached to the docking interface beneath Sherpa.

4.4 Six-Legged Scout CREX

The six-legged scout CREX is the second mobile system in RIMRES. It is based on the SpaceClimber robot (Bartsch et al., 2012) and adapted to the requirements of the multi-robot system RIMRES, e.g. to carry payloads or dock to Sherpa an EMI has been placed at the back of CREX. Further improvements compared with SpaceClimber have been made concerning the mechanic design of the single joints and the lower legs as well as a new sensor head with two degrees of freedom for camera and laser range finder.

Apart from the reconfiguration of the overall system by (un)docking CREX and Sherpa, CREX also provides several reconfiguration capabilities by itself. Firstly, gripping elements are employed in the front legs in order to be able to pick up geological samples. Thus, the legs used to propel the robot can be reconfigured to be used as manipulation/sampling devices.

[6]The wheels are a development of the project partner DLR-RY

(a) CREX robot in artificial crater environment. CREX is equipped with an electro-mechanical interface for attaching to Sherpa and for carrying payload-items.

(b) CREX beneath Sherpa after release from Sherpa's electro-mechanical interface (yellow square in the center of Sherpa's belly)

Figure 6: Photographs of CREX: Scouting robot in RIMRES

Via the EMI on its back, CREX can be connected to the wheeled rover, Figure 1(b). However, the EMI can also be used in the same manner as on Sherpa: arbitrary payload-items can be stacked onto CREX for extending its capabilities. This ranges from additional batteries to specialized sensors for a task at hand. In later stages, a second EMI on the belly of the scout system is conceivable, allowing to dock specific and bigger sampling devices. By using the high degree of mobility of the system, these devices can be positioned precisely over a spot of interest. Figure 6 shows the integrated scout robot CREX in DFKI's Space Exploration Hall.

Table 4: Key dimensions of CREX

Description	Value
Min. / max. body height	150 mm / 400 mm
Min. / max. longitudinal body shift	-150 mm / 150 mm
Min. / max. lateral body shift	-50 mm / 50 mm
Dimensions in standard posture [L×W×H]	850 mm × 1000 mm × 220 mm
Stretched leg length (front and rear)	640 mm
Stretched leg length (middle)	650 mm
Body Dimension (incl. head, central joint in neutral pos.) [L×W×H]	895 mm × 208 mm × 165 mm
Mass (with battery)	27 kg

4.5 Combinations of Subsystems

Table 5: Possible combinations of subsystems in RIMRES. In principle it is possible to connect the manipulator of one rover to a payload-bay of another rover, resulting in the check mark for the rover-rover connection.

	Rover	Scout	Manipulator	Payload-Item
Rover	✓	✓	✓	✓
Scout	✓	×	✓	✓
Manipulator	✓	✓	×	✓
Payload-Item	✓	✓	✓	✓

Table 5 displays the currently possible physical combinations of subsystems in RIMRES. Note that the

combination rover-manipulator is static in the current setup[7] and here illustrates a theoretic modularization. Otherwise, the table shows the range of reconfiguration the system is currently capable of. The connection rover-rover refers to the possibility of connecting a rover's manipulator to the payload-bay of another rover, which – due to the lack of a second rover – is not part of RIMRES. The example of transporting CREX with the manipulator is illustrated in Figure 7(a). Specific capabilities of the systems can be improved, but also disabled in specific configurations, e.g. a combination of Sherpa and CREX is more limited with respect to terrain difficulty it can traverse – the maximum ground clearance is lower. However, the main benefit of this cooperation is energy efficient transport on rather planar surfaces and over long distances. Though possible, we do not expect this monolithic configuration to be applied in very rough or steep terrain.

(a) Photograph of Sherpa using its manipulator to lift CREX. A possible use-case is the deployment of CREX off a landing unit. Furthermore, a reconfiguration-scenario where CREX is used as a six-fingered hand is also conceivable.

(b) CREX docked to Sherpa. CREX has four orientation possibilities to dock to Sherpa (in 90° steps). In this image CREX is oriented with its head towards the primary movement direction of Sherpa.

Figure 7: Feasible combinations of Sherpa and CREX

5 Software Foundation for a Reconfigurable System

The project RIMRES serves as a terrestrial demonstrator and assumes a traditional setup of a ground / mission control station. As already mentioned a system control station at the lunar surface represents the focal point for the communication of the robotic team, and represents the main link to the earth bound mission control. The use of this control station introduces a centralized control approach in the first place, since all robots need to communicate with the system control station. However, to achieve robustness a distributed setup has been selected for the robotic team using peer-to-peer communication. This communication setup minimizes the effects of a single-point of failure and accounts for flexible robot-to-robot interaction schemata when a central communication hub is not available.

As a project targeting a space application the project RIMRES embeds ESA's Functional Reference Model (Ferrarini and Carpanzano, 1999; Visentin, 2007) as illustrated in Figure 8 as general architecture model. This architecture comprises three layers: subsystem control (Level A), task control (Level B) and mission control (Level C) [8]. For our scenario we assume a predefined mission sequence, which can be split into several main tasks. Each task again can be split into sequences of trivial to complex actions, e.g. a trivial probe action allows to verify the communication between two distributed system and validates the full communication stack, while a complex and even cooperative docking action commands a main system to start and control a docking maneuver.

The mission control is responsible for scheduling actions, while the actual management is done via system

[7]However, the manipulator is detachable (by loosening the bolt flange) and was used for development purposes as singular unit without the rover.

[8]The mission control infrastructure for Level C and B has been developed by the project partner EADS Astrium

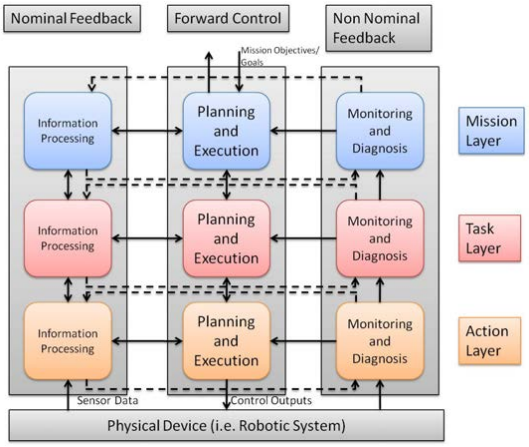

Figure 8: FRM model with three control layers, following (Visentin, 2007)

control, which applies a forward control to the subsystem level. Subsystems in the context of RIMRES are represented by the robots Sherpa and CREX, as well as payload-items or payloads.

The team of robots will be operated from a mission control center and three different operation modes are considered: (1) manual operation: the team of robots executes given actions or action sequences that are forwarded by the mission control center to achieve a certain objective, (2) semi-autonomous operation: the mission control relies on (complex) task sequences to achieve a mission objective, or to reconfigure systems to compensate for errors, and (3) autonomous operation: mission control or system control fails to operate or cannot communicate with the robotic team - the architecture allows for self-organization of the robotic team, either to continue with the still known objectives or to reestablish communication with the mission control. All autonomous operations can be interrupted by intervention from an operator, representing the so-called human-initiated switch between autonomy modes. Meanwhile, the architecture also accounts for a system-initiated switch, i.e. allowing subsystems to request for an interaction by their operator.

In the following we describe the approach taken in RIMRES to design the subsystem control level (Level A) from three different perspectives: the intra-robot, inter-robot perspective and mission control perspective.

5.1 Intra-robot Architecture

The intra-robot perspective has its focus on the individual robot and management of robot resources. The software stack applied on a single robot in RIMRES is mainly based on Rock (DFKI Bremen Robotics Innovation Center, 2011) which itself uses the Orocos Realtime-Toolkit (RTT) (Bruyninckx et al., 2003; Soetens, 2012) for its components. Rock uses a model-based approach to create an infrastructure of software components, and designing a system with Rock has proven to be useful not only for the RIMRES project, but for multiple others in our institute which try to solve complex tasks.

5.1.1 Components and Compositions

The first step towards designing the subsystem control level and enabling the reconfiguration capability in the software architecture is the development of appropriate, specialized drivers for the hardware. These driver libraries are then used or wrapped in Orocos components. Each such component (or software module)

has dedicated input and output ports, allows for remote procedure call and can perform a specific task. Components are specified using an (oroGen) model description, e.g. Figure 9 illustrates the specification of the system monitor component. The system monitor component depends on a number of libraries and inherits functionality from a component called system_state, which is a key value store that is accessed to apply a given rule-base on. The main driver that is wrapped by this component implements the rule_engine. The component will output monitoring events as soon as a rule fires, and the event can be used and interpreted by other components, allowing to isolate the pure monitoring functionality to this specific component.

```
name "system_monitor"
version "0.1"

using_library 'rule_engine'
using_library 'base-lib'
using_library 'utilmm'

using_task_library 'system_state'
import_types_from "SystemMonitorTypes.hpp"

task_context "Task" do
   subclasses 'system_state::Core'
   needs_configuration

   property("rulebase", "/std/string").
       doc("File which contains the rule descriptions")

   output_port("monitoring_events", "system_monitor/MonitoringEvent").
       doc("Output port for the monitoring events")
end
```

Figure 9: The oroGen specification of the system monitor component

Components can be viewed as the lowest level of modularity in the software stack and are specialized to fulfilling one task. Aggregating multiple such components allows to solve more complex tasks, but since this aggregation can get very complex a plan manager (Joyeux et al., 2010) is applied to provide supervision. This supervision can be easily applied to manage component networks since the interfaces of the underlying Orocos tasks are specified by the models. Figure 13 outlines the basic set of components available in RIMRES.

So-called compositions specify component networks in detail, i.e. they define required components and the data flow between these components. Figure 10 illustrates the specification of a composition to connect producers and consumers of monitoring events. Compositions can be nested, so that a single composition can be designed either in a very general way to allow reuse in other compositions or rather to fulfill the very special requirements of one application. The definition of a composition can be enhanced by additional (Ruby) code attached to the model to handle component events or newly defined events. This way compositions can wrap complex capabilities of the underlying system.

```
composition 'Monitoring' do
    add SystemCore::Task, :as => 'system_core'
    add Monster::InterfaceModule, :as => 'monster'
    add SystemMonitor::Task, :as => 'monitor'

    connect monster.telemetry_out => monitor.monster_telemetry_in
    connect monitor.monitoring_events => system_core.monitoring_events
end
```

Figure 10: Component model of the monitoring composition

A single component can be part of multiple compositions as long as the same component configuration can be used, and the supervision evaluates if there is a need for a specific component to run and stops it otherwise. Hence, the supervision also represents a resource-saving means. However, having a single component that

is part of multiple compositions can lead to conflicts which may arise at runtime; a parallel usage might be impossible due to different required configurations. The supervision is responsible for detecting such conflicts and thus prevents the startup of invalid network configurations.

The active management of the component network eventually allows to control granularly (1) which instances are up and running, and (2) the data flow, i.e. while in one configuration a camera might forward its images only to a visual servoing component in another setup it forwards them to the mission control. The development and architecture levels involved to create a robot action are illustrated in Figure 11.

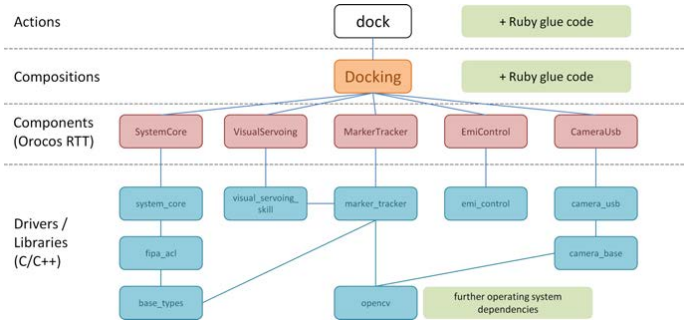

Figure 11: Development levels on Sherpa to allow for the dock action - which starts and controls the reconfiguration procedure to dock CREX.

5.1.2 Reconfiguration at Various System Levels

In RIMRES aspects of reconfiguration can be found at various levels of the hardware and software design. Clearly, the EMI represents the essential piece of hardware towards designing a heterogeneous reconfigurable multi-robot system. The EMI allows reconfiguration and combination of robots such as Sherpa and CREX, and allows to extend the robots' functionality using existing payload-items. In addition, subsystems can appear at runtime of a mission by creating payloads from existing payload-items. Depending of the number of existing payload-items it will be undesirable to account for all possible permutations of such system. Nevertheless, the standardized mechanical interface allows to easily extend a system with new add-ons, which can be even designed after the mission has already been started and the robots have been deployed.

An EMI allows to query for attached neighboring devices and provides an interface to transparently communicate with all payload-items attached to it. To handle EMI information programmatically and embed it into high-level processing, each EMI can be uniquely identified in the overall robot team; a low-level device id is used for this purpose and mapped to individual systems as part of a static configuration. This allows to infer the current physical configuration state by gathering the stati from all available EMIs attached to a robot.

For inference of the physical configuration state an organization model has been implemented using a Ruby based domain specific language (DSL). At the current stage the organization model represents the physical connection status of the team of robots, and is based on the agent-group-role model (Ferber and Gutknecht, 1997). Currently, all systems which serve as a basis for a larger system are represented as a group which comes with a persistent actor, e.g. the group *sherpa* requires a single robot Sherpa as persistent actor, and similarly for CREX and payloads. Figure 12 outlines the current description of the organization model for RIMRES and includes an instance description, i.e. defining dedicated actors and groups. By querying the EMIs for available neighbors with a regular frequency a monitoring of the configuration state can be achieved. Thereby, a system can validate a successful reconfiguration and can also recognize dynamically attached payload-items or docked systems (in case of Sherpa and CREX). While a dynamic detection might

not be necessary in a space application context, it still allows to validate a reached configuration state in an event based fashion.

```
require 'famos'
include Famos::Organization

domain 'rimres' do
    actor_model :payloaditem

    group_model :payload do
        requires Role => :payloaditem, :min => 2 do
            requires ActorModel => :payloaditem
    end

    group_model :sherpa do
        persistent_actor

        # Is associated with the bottom interface
        requires Role => :client, :min => 0 do
            requires ActorModel => :crex
        end

        requires Role => :extension, :min => 0 do
            requires ActorModel => :payloaditem
        end
    end

    group_model :crex do
        persistent_actor

        requires Role => :extension, :min => 0 do
            requires ActorModel => :payloaditem
        end
    end

    # Initial configuration/setup of the rimres scenario
    group_instance :sherpa => "sherpa_0"
    group_instance :crex => "crex_0"

    group_instance :payload => "payload"

    actor_instance :payloaditem => "payloaditem_0"
    actor_instance :payloaditem => "payloaditem_1"
    actor_instance :payloaditem => "payloaditem_2"
end
```

Figure 12: Organization domain model combined with the organization instance description

While generic tools such as the supervision contribute to reconfiguration capabilities, further individual component design does as well. The telemetry provider serves as another example and represents the adoption of recommendations given by the CCSDS (CCSDS/AIAA Inc., 2008). The telemetry provider acts as a generic packaging component to support multiplexing of the sensor data streams towards the mission control station. Acquiring sensor data and forwarding to the mission control center might be costly in terms of processing power and energy and a continuous delivery of all camera images will not be feasible regarding communication bandwidth. Thus, mission control has to carefully select active devices such as cameras. The actual transferred data can be of any format, i.e. images are provided in an internal (standardized) binary format, which adds meta information to a jpeg encoded image. On an operator's request, devices will be activated and the output data stream of the sensor is dynamically attached to the telemetry provider component. This component will convert the images to the target format as expected by the system control station and add them to a generic telemetry container package. This container package is then forwarded to the system control station and can be transparently routed through the network without a need for inspecting the payload data. At its final destination the package is unwrapped and split into the sensor specific packets.

While this is a rather common procedure, this dynamic multiplexing of sensor data allows to manage the existing sensor data in a dynamic fashion, leading to an efficient use of a robot's limited resources.

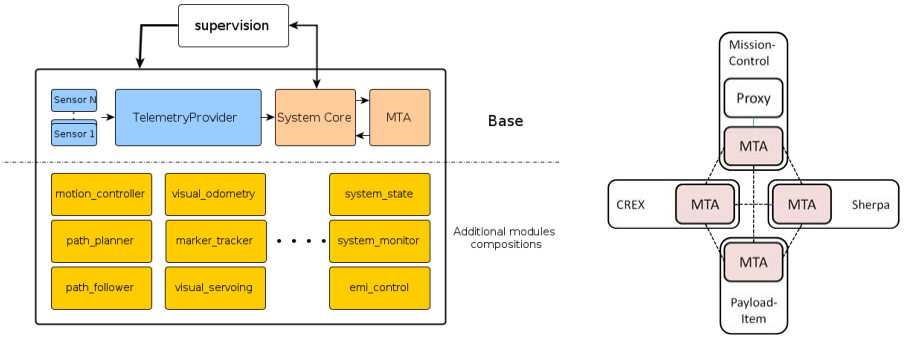

(a) Intra-robot perspective showing the structure of base elements such as the system core which performs communication protocol validation and mediates between the system control center and supervision

(b) Inter-robot perspective illustrating the peer-to-peer network comprising subsystems and mission control

Figure 13: Schematics of the architecture from an intra- and inter-robot perspective.

5.2 Inter-robot Architecture

For the inter-robot challenges we build upon achievements of the multi-agent community. FIPA[9] has defined a number of standards that have been applied mainly in the domain of software agents. The team or robots uses elements of the abstract architecture described by FIPA (Foundation of Intelligent Physical Agents, 2002) to build up the inter-robot infrastructure.

The communication infrastructure is built with message transport services (labeled MTA in Fig. 13) to create a distributed communication network. Each robotic system, i.e. Sherpa, CREX and payload-item, runs a local message transport service. All these local message transport services create a peer-to-peer communication network.

This communication network is created dynamically, since each message transport service announces its existence on the network using the zeroconf solution Avahi (Poettering et al., 2012). This mechanism enables the message transport services to dynamically find each other in a network – this mechanism can be also used for other components (or services) to announce their presence, thus providing a dynamic view on appearing or disappearing components. Thereby, payloads which are stacked during a mission are automatically included in the peer-to-peer communication and will visible to other modules after powering up. Service discovery comes with an additional benefit: appearing and disappearing systems due to communication losses, power down or similar can be detected in the network, i.e. adding an additional means to monitoring.

All participating robots in RIMRES communicate via FIPA messages (which take any type of messages as payload), i.e. communication between MTAs uses bit-efficient FIPA messages. Furthermore, we use so-called interaction protocols to validate conversations within the MTA based communication network. FIPA messages are described by performatives, such as *request* or *inform*, which allow validation of the flow of conversation. For all communication between robots and for communication between system-control and subsystems a simple request based protocol as illustrated in Figure 14 is applied – this interaction protocol is a single request, single response protocol.

[9] Foundation of Intelligent Physical Agents

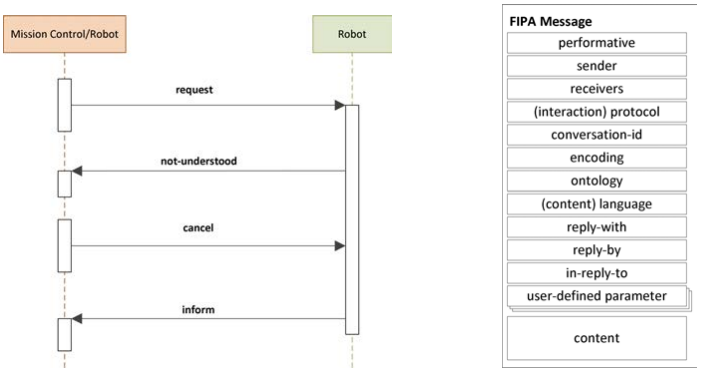

(a) Interaction protocol in use for robot-to-robot and mission-control-to-robot communication

(b) Elements of a FIPA message

Figure 14: Communication in the RIMRES project is using FIPA messages and interaction protocols as a basis for autonomous cooperative robot activities

Without an EMI based connection, systems in RIMRES communicate via WLAN. In order to extend the coverage of the communication, message relaying can be applied. The presented communication stack works on top of existing meshing protocols such as BATMAN (Open-mesh, 2012), and can thus easily benefit from message relaying, only at the cost of additional bandwidth consumption.

5.3 Embedding Mission Control

The team of robot in RIMRES does not operate in a completely autonomous fashion. The dominating operation mode is semi-autonomous. Mission control outlines the major mission timeline and serves as a planning interface (cf. Figure 5.3 – it is possible to pause or stop a running mission and upload a new mission timeline to the system control station. Thus, while no automated planner has been embedded, the mission control uses the operator as main planner for the initial mission and also for handling errors.

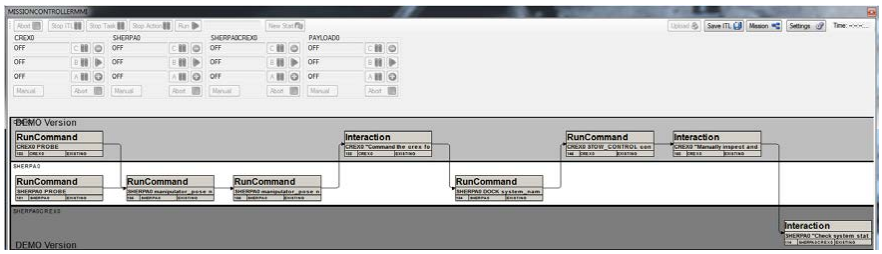

Figure 15: Interface for the mission timeline management. The illustrated timeline applies to Sherpa and CREX and the combined systems.

The mission control center has already been used in the project LUNARES (Cordes et al., 2010) and was adapted to cope with the requirements for reconfiguration in RIMRES. Mission control communicates via a Moon-based system control with the team of robots. In order to establish the communication between the system control and the team of robots a proxy has been put into place. The proxy connects the socket

based communication with the FIPA-message based communication. Similarly to LUNARES, a human-readable content-language has been defined to communicate commands, stati and alike, e.g. to request a robot to perform an action to probe the communication: ACTION probe EXEC. The text-based content-language facilitates both debugging and implementation, and allows to easily enable communication between previously incompatible systems. While this selection does not represent a high-performance solution, it has proven to be practical.

Apart from specific functionality such as querying the set of available actions from reach robot, the definition of this content-language allows a high-level abstraction to commanding all available robots. In RIMRES all systems, i.e. Sherpa, CREX and payload-items, support this content-language, showing the capability of scaling the system, and facilitating to embed dynamically created payloads.

5.4 Modularization and Heterogeneity

The generally adopted development approach in RIMRES (and the one of Rock) outputs highly modularized software, which allows to reuse components to a large extend within the overall system. Modularization starts by designing low-level drivers that will be embedded into the Orocos modules, and continues regarding robot capabilities. While there is common functionality for all systems, e.g. such as the communication infrastructure, each system has specific skills, which needs to be accounted for in the software design.

To keep the mentioned balance between generalization and specialization – and in order to keep the code base maintainable – at the level of supervision all robots use a hierarchical structuring which bundles generic functionalities and extensions to enable specific capabilities. This approach minimizes the effect of quantity and heterogeneity of the systems in RIMRES and allows to run the same basic software stack on Sherpa, CREX, and all payload-items.

Clearly, an identical configuration cannot be applied to all these systems. Configuration and fine-tuning of parameters has to be performed especially to account for lower system resources on the payload-items or for CREX. However, a common high-level software framework can be deployed on the robotic team in RIMRES, which offers a standardized interface for robot-to-robot and human-to-robot communication.

6 Experiments

The multi-robot system presented in this paper has a range of capabilities comprising locomotion, navigation, manipulation, distributed communication and visual servoing. The latter one is a central capability in the context of reconfiguration of Sherpa and CREX, and can also be used for attaching Sherpa's manipulator arm to a payload-item. In the following description the reconfiguration process to assemble payloads using Sherpa's manipulator is called stacking, while reconfiguring Sherpa and CREX to form a combined, mechanically connected robotic system as illustrated in Figure 7(b) is called docking. We selected stacking and docking as the two essential reconfiguration maneuvers involving all subsystems designed in RIMRES to verify the current system setup.

Due to the complexity of the experimental setup a number of soft and not yet quantified parameters exist, such as effects of longer term[10] operation of the robots. These experiments however investigate on the following aspects: (1) feasibility and practicality, but also weaknesses of the hardware and software architecture to control a reconfigurable, multi-robot system, (2) behavior of the multi-robot system under typical communication load, and (3) achievable precision and accuracy of the – compared with the former approach improved – hardware platform CREX to allow for an improved visual docking procedure.

[10] This denotes a continuous operation of the robots for a factor $n > 1$ battery cycles (CREX: approx. 1.5 h, Sherpa: approx. 3 h)

The stacking procedure allows an evaluation of the reconfiguration capabilities using the manipulator and payload-items. The docking procedure allows this evaluation for Sherpa and CREX, but also adds a good test coverage of the software architecture of the multi-robot system, since it involves elements such as: (1) communication and synchronization between two robotic systems, and (2) communication between an operator and a robot. Both experiments cover: (1) dynamic activation and deactivation of (software) components and devices (on a distributed subsystem), and (2) controlling the EMI. In the following paragraphs we present the experimental setup and results for the stacking and docking procedures.

6.1 Stacking procedure

The stacking procedure is applied to assemble payloads from payload-items. The stacking procedure is a semi-autonomous experiment where a human operator activates each individual step in the experiment. The main purpose of this experiment is a qualitative analysis, i.e. an evaluation of reliability, speed or energy consumption is not part of the experiment. Figure 16 illustrates the sequence of actions (also refer to the video material available (DFKI Bremen Robotics Innovation Center, 2013)).

6.1.1 Experimental Setup

The stacking experiment involves the robot Sherpa and two payload-items: one battery payload-item and one scientific (camera) payload-item. Both payload-items are already attached to the Sherpa system. The positions of the manipulator have been previously taught so that Sherpa can extract payload-items from the storage bays without a requirement for visual servoing. A force torque sensor is part of the manipulator's wrist and embedded into the procedure; it allows safe deployment of the payload in the absence of visual information.

6.1.2 Experiment Procedure

Sherpa uses the manipulator to pick the scientific payload-item and detaches the payload-item from Sherpa's main body, cf. Figures 16(a)-16(c). Subsequently the payload-item is stacked on top of the battery payload-item (cf. Figures 16(d) and 16(e)). Note, that the scientific payload-item is activated before attaching to the battery module to validate the capabilities of the power management system. After locking the bottom interface of the scientific payload-item and unlocking the bottom interface of the battery payload-item, the assembled payload is extracted from the storage bay. To prepare deployment of the payload the force torque sensor needs to recalibrate for the new weight attached to the manipulator's EMI. Recalibration is performed in a previously taught position of the manipulator as illustrated in Figure 16(f). After switching from the payload's external power supply (the rover's battery) to its internal one (the battery payload-item), the assembled and now power-independent payload is finally detached from the manipulator.

6.1.3 Experiment Results

The stacking experiment successfully verified the capability to assemble a payload at mission time. Subsystem features that contributed to the success are: (1) functionality and precision of the manipulator, in combination with (2) effective guidance of the EMI, (3) locking and unlocking capabilities of the EMI, and (4) power switching of the EMI. The active LED ring of the scientific payload-item indicates that the power switching has been successfully performed and the software stack has been started properly. The full procedure required approximately ten minutes in real time.

(a) Initial setup with two payload-items attached to Sherpa

(b) Attaching the manipulator to the scientific payload-item

(c) Detaching the scientific payload-item from Sherpa's main body

(d) Preparing to stack

(e) Detaching the fully assembled, active payload

(f) Recalibration of the force-torque sensor

(g) Approaching ground position

(h) Finally deployed payload

Figure 16: Stacking sequence for assembly and deployment of a payload consisting of one scientific payload-item and a battery payload-item

6.1.4 Experiment Discussion

The stacking experiment illustrates that Sherpa is capable of assembling and deploying a subsystem. The deployment can be performed even without visual means if necessary, which makes further automation even easier. However, the stacking procedure is currently limited to the deployment of payloads. Embedding visual data is part of future developments and required to allow pick up payload-items from the environment or to select suitable places for deployment of a payload. Currently, the procedure shows the benefits of power management, since stacking and thus any upcoming maintenance procedures for payloads can be performed in a hot-swap manner. Due to safety reasons and the direct interaction of the operator, the procedure has been executed with low manipulator joint speeds. This could be easily changed given a higher degree of automation and using higher joint speeds for the operation of the manipulator.

6.2 Docking procedure

The docking procedure transforms the separate robots Sherpa and CREX into one monolithic system. Before docking between Sherpa and CREX is possible, a reference pose of CREX has to be taught. This reference position is the position, that shall be reached during the visual servoing process. Within the teaching process the Jacobian for the relative target pose is computed. Preceding experiments to find optimal conditions for the marker detection identified that for optimal results a minimum distance of 15 cm to the camera needs to be kept. Under varying lighting conditions (from completely dark over only using ambient light to ambient light with additional lighting from the EMI LEDs) most robust results are achieved using the available LED lighting in the EMI. Further, preliminary docking and teaching procedures eventually resulted in an optimal teaching position with the markers being approx. 21 cm below the actual camera. Teaching has been performed at a body height of 194 mm of CREX and by shifting CREX' pose around the reference position with offsets of 1 mm and 1°. The positions of the visual markers are extracted and the corresponding

Jacobian is computed. The core algorithms for marker extraction and visual servoing have been developed by the project partner Astrium and have already been used successfully in the project LUNARES (Roehr et al., 2010).

6.2.1 Experimental Setup

The conducted experiment evaluates the performance of main parts of the docking procedure. The steps involved in the docking procedure and part of this performance evaluation are the following:

1. Initiating the docking procedure by an operator
2. Startup of software components by the supervision which are needed to perform the docking
   - Auto-calibration of the electro-mechanical-interface as preparation for the mechanical docking
   - Switching on LEDs of Sherpa's bottom EMI
   - Starting camera in Sherpa's bottom EMI
   - Starting marker extraction component and visual servoing component
   - Creating data connections between components
3. Executing control loop till target position (termination condition) is reached
   - Marker detection and extraction
   - Calculation of current offset and generation of new posture command
   - Direct robot to robot commanding and feedback

We assume that the main approach of the docking procedure (CREX walking beneath Sherpa) has already been performed and the final step to align CREX with the EMI at Sherpa's bottom has to be conducted. To evaluate the accuracy of this approach, we perform the experiments with an initial and isolated offset regarding translation along the x, y and z axis and rotation around the z axis (yaw). For this setup we further assume a planar surface where the docking is performed and thus this experiment does not need to evaluate a compensation for roll and pitch offsets. While this assumption might not hold perfectly for a real mission, it anticipates an advanced docking procedure, where Sherpa and CREX would be independently responsible to setup or maintain a level posture using their inertial measurement sensors. Alternatively, the visual servoing can be used to compensate for the additional degree of freedom – this approach depends on an improvement of the visual marker setup and will demand fine-tuning of the visual servoing controller, otherwise easily leading to prolonged time required for convergence. A perfect docking procedure is not required, but one the EMI can compensate for.

The initial offset regarding translation and rotation is 50 mm and 5° respectively.

All pose measurements represent CREX' telemetry data based on the inverse kinematic of the locomotion controller, i.e. no external tracking system has been used.

6.2.2 Experiment Procedure

The docking procedure in RIMRES relies on a set of six markers which are located at the EMI on the back of CREX. The convergence (stopping) criteria for the visual servoing is set to a translation error of 1.2 mm and a rotation error of 0.5°. In addition, the pixel error for all visible marker needs to be below a threshold of 30 px. The target pose is defined to be reached when these criteria are met for four subsequent controller cycles.

[10] Ideally, the set of markers is distributed in three dimensions.

Once the control loop is started, Sherpa computes posture commands for CREX in order to correct the pose. Sherpa does not change its pose throughout the experiment and docking procedure, while CREX is adapting its posture in order to reach the previously taught position – this position is relative to the EMI at Sherpa's bottom. The control loop works across system boundaries (cf. Figure 17) so that synchronization is needed. Using the FIPA based message infrastructure each communication between Sherpa and CREX involves a short interaction consisting of a request to set the posture and a response about success or failure once the action has been executed. When Sherpa receives the latest response on a posture setting request, it waits for an up-to-date marker extraction result. Marker results are timestamped using the corresponding marker image. The pose of CREX is corrected in small increments and controlled by Sherpa, which serves as the controller of the overall docking procedure. The visual servoing controller allows for a maximum translation step of 1 mm and a rotation of 1° to be performed by CREX – this corresponds to the maximum resolution for setting the posture of CREX.

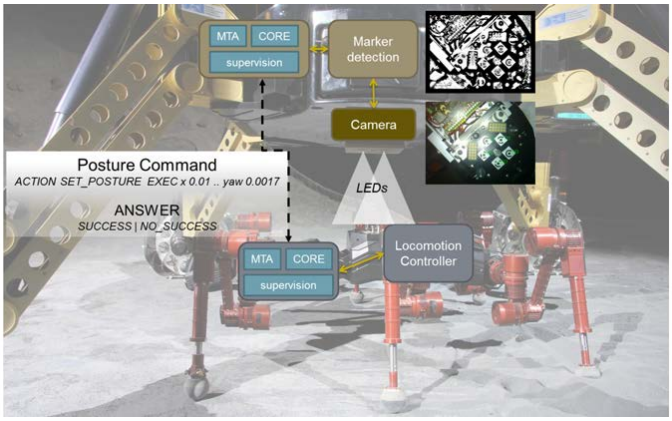

Figure 17: Process of visual servoing: The camera in Sherpa's bottom EMI identifies the visual markers placed on CREX' EMI. From the extracted positions of the markers in the video image, appropriate posture shifts of CREX are commanded, until the reference pose is reached. Subsequently a blind docking is executed to mate the two EMIs. (MTA: Message Transport Agent)

The experiment has been performed with ambient lighting conditions. However, the main light source to allow marker detection are the LEDs which are part of the EMI at Sherpa's bottom and as already mentioned marker detection is working best with this additional illumination. Overall a set of 100 (+20, due to wear, see below) runs was performed, spread over multiple days and involving restarts (power-off) of both of the systems. Five different test-setups were used for the experimental series. The setups have to be distinguished based on the pose offsets that were given for the reference position:

1. Offset in x-direction (forward/backward of CREX) only
2. Offset in y-direction (sideways movements of CREX) only
3. Offset in z-direction (up/down movements of CREX) only
4. Offset in yaw (rotation around z-axis only)
5. Offset simultaneously and randomly applied to all four DoF

For each daily test-setup ten runs were conducted beforehand in order to calculate a mean pose as reference pose. For the actual evaluation, offsets are used to shift CREX' pose away from this target pose. In case of the single-DoF-runs, ten runs with the minimum and maximum offsets from Table 6 are conducted,

respectively. For the simultaneous shift in all DoF, random offsets are generated. The random offsets are limited in order to keep CREX' EMI within the field of view of Sherpa's bottom EMI's camera. The range of the applied offsets is given in Table 6. In the runs with offsets given only in one DoF, still all four used DoF of CREX are commendable by the visual servoing process running on Sherpa.

Table 6: Range of random numbers for the posture offset for each experimental run.

DoF	min	max	unit
x	-50	+50	mm
y	-50	+50	mm
z	-50	+50	mm
yaw	-5	+5	deg

6.2.3 Experimental Results

This section presents the results of the experiments conducted to perform visual servoing as part of an overall docking maneuver. After more than 6 h of continuous operation of the systems in the course of the experiments presented here, a wear in CREX' position accuracy was observable. The wear expressed itself in an increase of convergence time, eventually leading to timeouts. The corresponding experiment for the set -x was therefore aborted after two subsequent timeouts and the results excluded from this presentation. The experiment was repeated the next day. However, including these failed runs, i.e. two additional runs with timeouts for -x, still an overall termination rate of approx. 94% (6 out of 102 runs failed to terminate) is reached, and the effect can be still observed looking at the duration statistics of the preceding experiment (+x offset) (cf. Table 7). Limiting the evaluation to the runs with a random initial offset a termination rate of 95% (1 out of 20 runs failed to terminate) is reached.

The following presentation illustrates selected experiment samples as well as the accuracy and precision of the approach in Tables 7-10. Finally this approach is compared to a previous application of the same visual servoing control algorithm in combination with different hardware systems.

6.2.4 Pose Accuracy and Precision with Offsets in Single DoF-Runs

The following section presents the results for the visual servoing procedure for experiments which started with an offset on a single DoF. In the graphs in the following subsections the error is stepwise corrected. Each of the steps corresponds to one correction step and thus one cycle as shown in Figure 17. Thus, if present, delays during the control and the startup times of the process can be identified in the plots. Note that startup and execution times are increased due to a maximum logging level during the course of these experiments. Note further, that all following graphs represent single runs, since an averaging over multiple runs into one plot is not reasonable due to varying convergence times.

The statistic describes the final pixel error per marker – with an overall set of 6 visible markers. Duration describes the time from sending the operator command to start the visual servoing until the time of final convergence to the taught position. Precision describes which position with what kind of deviation has eventually been reached. Compared to that, accuracy describes the error of the reached position compared to the reference position, which is the taught position being expected to be reached. Even though some of the given values in the following table contain redundant information, the presentation is chosen to allow an easier understanding of both statistics. Note that while all measurements are taken in mm the statistical values have been rounded to the tenth of a mm.

The first approximately 30-40 s with not changing errors in each plot is the startup time between starting the logging and the start of the actual visual servoing loop. Within this time the start-up procedures described

Table 7: Precision and accuracy results of runs with offset in x-direction

initial offset		+x		**initial offset**		-x	
number of timeouts (out of 10 runs)		2		number of timeouts (out of 10 runs)		0	
		mean	**stdev**			**mean**	**stdev**
final pixel error per marker		2.24	1.32	final pixel error per marker		3.67	1.26
duration in s		322.43	373.82	duration in s		168.6	35.49
precision: reached pose	**ref pose**			precision: reached pose	**ref pose**		
x (mm)	-5	-6.1	0.9	x (mm)	0	-0.6	1.4
y (mm)	-4	-6.9	0.7	y (mm)	5	3.7	0.6
z (mm)	194	194.6	0.6	z (mm)	195	196.2	0.4
yaw (deg)	1	0.7	0.5	yaw (deg)	0	0.0	0.0
accuracy: pose error				accuracy: pose error			
x (mm)		-1.1	0.9	x (mm)		-0.6	1.4
y (mm)		-2.9	0.7	y (mm)		-1.3	0.6
z (mm)		0.6	0.6	z (mm)		1.2	0.4
yaw (deg)		-0.3	0.5	yaw (deg)		0.0	0.0

in section 6.2.1 are executed. In the following we highlight the experiments starting with an x offset, since they have been performed after multiple hours of operation time of CREX. The visual servoing procedure timed out for two times during the set of ten experiments for the positive offset – also shown by the high mean and standard deviation of the duration time in Table 7 compared to other experiments. The directly afterwards performed experiment for the negative offset suffered from increasingly higher convergence times and – as already mentioned in the introduction – has been aborted with the assumption of increased system wear.

The results show, that the duration of experiments with a positive x offset is significantly higher, though this is due to significant outliers. Only terminated runs are part of the precision and accuracy computation, the results show that the visual servoing procedure is still able to reach good precision, e.g. see experiment sample in Figure 18. We assume the outliers to be an effect of system wear after multiple hours of operation, since the continuation of the experiments with a fresh system (after cold start the next day) did not show such kind of timeout, as also observed in earlier runs.

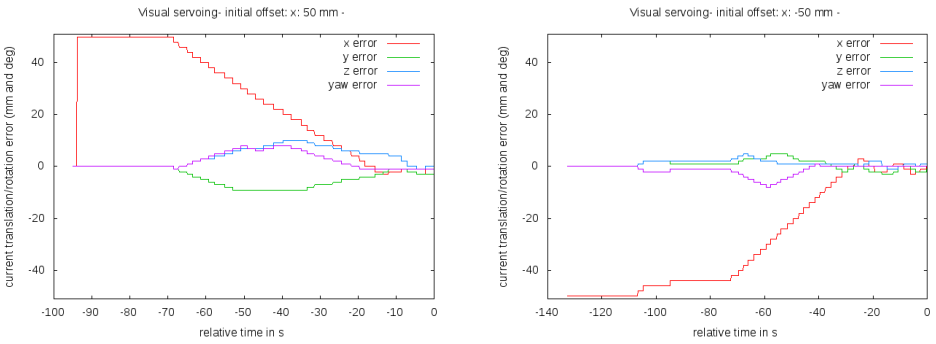

(a) Positive x-offset

(b) Negative x-offset

Figure 18: Example trends for runs with offset in x-direction

Table 11 shows the final results concerning pose accuracy and pose precision for moving in all four DoF with random pose offsets. This can be considered as the standard case during system operation.

Table 8: Precision and accuracy results of runs with offset in y-direction

initial offset		+y		**initial offset**		-y	
number of timeouts (out of 10 runs)		0		number of timeouts (out of 10 runs)		0	
		mean	**stdev**			**mean**	**stdev**
final pixel error per marker		2.96	1.39	final pixel error per marker		2.15	1.58
duration in s		127.63	125.43	duration in s		149.4	82.53
precision: reached pose				precision: reached pose			
	ref pose				**ref pose**		
x (mm)	-5	-6.6	0.8	x (mm)	-5	-6.4	0.7
y (mm)	-4	-2.8	0.7	y (mm)	-4	-4.7	1.6
z (mm)	194	194.9	0.3	z (mm)	194	194.7	0.8
yaw (deg)	1	0.9	0.3	yaw (deg)	1	0.5	0.5
accuracy: pose error				accuracy: pose error			
x (mm)		-1.6	0.8	x (mm)		-1.4	0.7
y (mm)		1.2	0.7	y (mm)		-0.7	1.6
z (mm)		0.9	0.3	z (mm)		0.7	0.8
yaw (deg)		-0.1	0.3	yaw (deg)		-0.5	0.5

Table 9: Precision and accuracy results of runs with offset in z-direction

initial offset		+z		**initial offset**		-z	
number of timeouts (out of 10 runs)		0		number of timeouts (out of 10 runs)		1	
		mean	**stdev**			**mean**	**stdev**
final pixel error per marker		2.44	0.9	final pixel error per marker		2.43	1.31
duration in s		128.67	46.76	duration in s		192.1	231.13
precision: reached pose				precision: reached pose			
	ref pose				**ref pose**		
x (mm)	-5	-5.9	1.0	x (mm)	-5	-6.3	0.6
y (mm)	-4	-1.9	0.3	y (mm)	-4	-2.3	0.5
z (mm)	194	194.4	0.5	z (mm)	194	195.0	0.0
yaw (deg)	1	1.0	0.0	yaw (deg)	1	0.9	0.3
accuracy: pose error				accuracy: pose error			
x (mm)		-0.9	1.0	x (mm)		-1.3	0.6
y (mm)		2.1	0.3	y (mm)		1.7	0.5
z (mm)		0.4	0.5	z (mm)		1.0	0.0
yaw (deg)		0.0	0.0	yaw (deg)		-0.1	0.3

In Figure 19 two experiment samples of the temporal course of CREX' pose are presented. With the beginning of the actual visual servoing control loop, it is observable, that the position errors in x and y are basically continuously decreasing. In both displayed examples, the yaw error is increasing in the first place, but finally gets corrected. Noticeable is the fact, that the z-DoF seems to be only correctable when x- and y-error are already close to being corrected, e.g. in Figure 19(a) the z-error decreases only after x- and y-error are significantly reduced, while in Figure 19(b) the error even increases until x-error and y-error are significantly reduced. However, for concluding a direct relation in the described way, a broader data base than collected in this experimental series is needed.

The experiment starting with random offsets on all four DoF confirms previously received results from the experiments of the single DoF. The typical (mean) convergence time is just lower than 3 min while the final accuracy achieved shows a very low rotation error, but a translation error of multiple millimeters. The to be expected translation offset of about 4 mm can be compensated by the mechanical tolerances in the EMI design using the guidance pins. The guidance pins allow either compensation of an offset of 6 mm or a rotation of 7° (for details see (Wenzel et al., 2011)). The error in z is not of great significance and can also be easily compensated for by the final docking process using a force torque measurement by CREX[11]. A

[11]The flange of each of CREX' legs is a 6 DoF force-torque sensor

Table 10: Precision and accuracy results of runs with offset in yaw-direction

initial offset		+yaw	
number of timeouts (out of 10 runs)		0	
		mean	**stdev**
final pixel error per marker		2.99	1.49
duration in s		51.9	22.34
precision: reached pose			
	ref pose		
x (mm)	0	-0.9	0.8
y (mm)	5	2.9	0.7
z (mm)	195	195.8	0.4
yaw (deg)	0	0.0	0.0
accuracy: pose error			
x (mm)		-0.9	0.8
y (mm)		-2.1	0.7
z (mm)		0.8	0.4
yaw (deg)		0.0	0.0

initial offset		-yaw	
number of timeouts (out of 10 runs)		0	
		mean	**stdev**
final pixel error per marker		2.47	1.01
duration in s		54.6	20.91
precision: reached pose			
	ref pose		
x (mm)	0	-0.7	1.1
y (mm)	5	2.5	0.8
z (mm)	195	195.7	0.6
yaw (deg)	0	0.0	0.0
accuracy: pose error			
x (mm)		-0.7	1.1
y (mm)		-2.5	0.8
z (mm)		0.7	0.6
yaw (deg)		0.0	0.0

slight bias regarding a higher pose error along y compared with x can be seen and leads to the assumption of a systematic error introduced by the hardware. Further experiments on the hardware accuracy and precision will be performed with CREX to investigate on this matter.

Overall this evaluation shows, that the accuracy and precision of the visual servoing is high enough for the outlined docking procedure of CREX and Sherpa.

Table 11: Final results of docking experiment.

initial offset		random	
number of timeouts (out of 20 runs)		1	
		mean	**stdev**
final pixel error per marker		1.78	1.11
duration in s		161.72	80.69
precision: reached pose			
	ref pose		
x (mm)	0	0.0	0.9
y (mm)	5	2.0	1.1
z (mm)	195	195.6	0.6
yaw (deg)	0	0.0	0.2
accuracy: pose error			
x (mm)		0.0	0.9
y (mm)		-3.0	1.1
z (mm)		0.6	0.6
yaw (deg)		0.0	0.2

6.2.5 Comparison with Former Approach

In a former approach, it was already possible to demonstrate the feasibility of visual servoing as a means for docking preparation. In the project LUNARES, a mechanical connection between a wheeled rover and an eight-legged scout robot was successfully established after autonomous positioning via visual servoing. Figure 20 illustrates a typical scene from the docking process.

In the approach, the scout had four rear-facing visual markers, that were identified by the camera system of the rover. The algorithm calculated movement commands for the scout robot in order to bring the scout into a previously defined reference pose. For the docking, three DoF were commanded: forward/backward (x direction) and sideways movements (y direction) and the heading (yaw angle) of the robot.

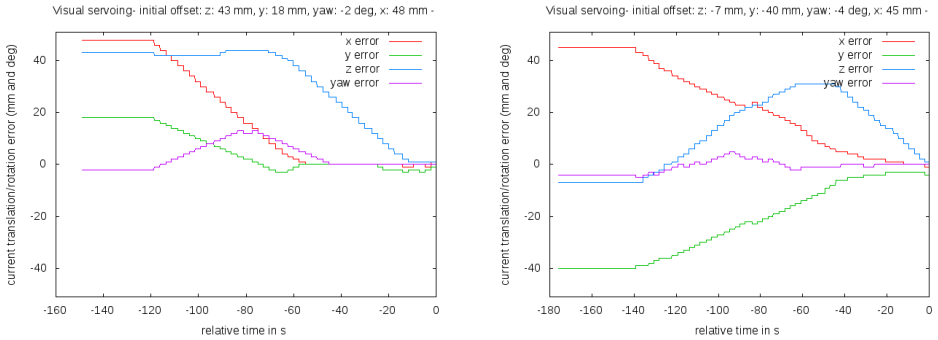

(a) Trend for pose corrections (x, y, z, yaw) for initial offset from taught pose of (48 mm, 18 mm, 43 mm, -2°)

(b) Trend for pose corrections (x, y, z, yaw) for initial offset from taught pose of (45 mm, -40 mm, -7 mm, -4°)

Figure 19: Examples for the trend of pose corrections in experiments with a (bounded) random offset for dimension x, y, z and yaw

As already presented in (Cordes et al., 2010), the standard deviations achieved in the docking procedure were within the mechanical tolerances of the docking mechanism and the play in the commanded robot's joints. Table 12 displays the results achieved in the former approach.

The approach in LUNARES did not require a high precision approach, since the connection was only mechanical and no electrical contact needed to be established. In RIMRES however the EMI and its design (including contact pins for the electrical-connection) requires a much more precise approach, which is mainly feasible only due to the improved design of CREX.

Nevertheless, it has to be noted again, that the measurement in LUNARES were taken by a tracking system and using the walking mode of the robot, while the experiment performed for RIMRES relies on internal measurements of CREX, and need to be extended with an additional evaluation of the pose precision of CREX posture control. Still, the results are significant, since the final docking procedure relies on the combination of internal measurement and the marker detection.

Table 12: Results of docking in the LUNARES project

initial offset	random	
	mean	**stdev**
duration (s)	184	35.5
pose accuracy/final pose error		
x (mm)		9
y (mm)		4
z (mm)		12
yaw (deg)		0.7

6.3 Experiment Discussion

The experiment has been setup to investigate on (1) feasibility and practicality, but also weaknesses of the software architecture to control a reconfigurable, multi-robot system, (2) behavior of the multi-robot system

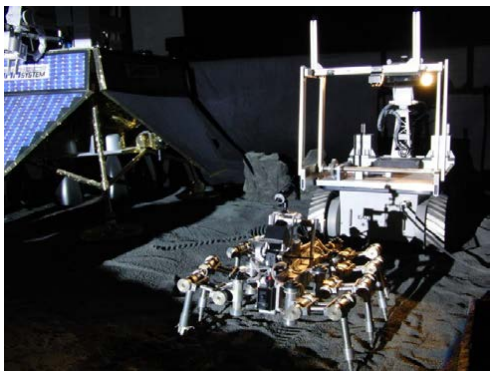

Figure 20: Visual servoing as preparation for docking in LUNARES. The rover identifies the rear-facing visual markers and generates movement commands for the scout. Once the goal position is reached, the docking lever is lowered and by shifting the body backwards and down, the scout places its bail in the docking adapter's hook. The connection is purely mechanical.

under typical communication load, and (3) achievable precision and accuracy of the – compared with the former approach improved – hardware platform CREX to allow for an improved visual docking procedure. The presented experiment allows a direct extraction of the results regarding precision and accuracy of the approach. The experiment also validated the infrastructure regarding tight cooperation of two mobile systems Sherpa and CREX using a master-slave approach in a closed-loop. This approach requires only a set of visible markers for teaching and visual servoing of the slave system, and has to support setting the posture from the master system. Hence, due to the simple and standard command interface for robot to robot communication this approach could be easily applied using a different slave system.

A major weakness of the current architecture can be seen in the complexity compared to rather specialized solutions. Multiple layers of abstraction and the distribution of the multi-robot systems make debugging harder. A variety of tuning parameter exists and details of the underlying software stack such as Orocos can become significant, e.g. during the set of experiments and related to the second aspect under investigation, we observed that components on a slow system did not stop properly as expected and commanded by the supervision. This was due to a fixed timeout setting within Orocos RTT which was only relevant in this context, e.g. the Gumstix which was responsible in this context to manage the EMI camera.

In addition, embedding standards such as FIPA seem to add to this complexity without any initial benefit. However, we can confirm the practicality of this approach especially regarding system cooperation, conversation monitoring and a dynamic setup of robot communication. With respect to the long-term goal of autonomous cooperative systems we expect the application of standards such as FIPA to be of even higher significance. Meanwhile, we have already shown the feasibility of the overall approach by applying it to a multi-robot reconfiguration.

The complexity of the current approach is a draw back, but it is needed to allow for a consistent, generalized approach which scales to a multi-robot system such as presented here. We believe that our approach is effective and facilitates transfer to other robotic systems outside of the scope of this project and thus serves a long-term development plan.

7 Lessons learned

The project RIMRES allowed to expand our knowledge not only regarding the technology, but also regarding the overall development approach. In the following, we highlight the lessons learned for each of the systems developed as part of a reconfigurable multi-robot system.

7.1 EMI Design

The validation of selected requirements for the EMI was successfully performed in isolated test setups, e.g. such as the mechanical stability. Still, applying the EMI in the real systems showed that the guidance pins of the EMI were initially too short to provide actual guidance, i.e. having the same height than the central pin. For visual servoing a marker pattern was imprinted using a laser to the central pin's head. The final result was a small and too light black imprint on a highly reflective material. The central pin was the only marker outside of the payload-items' top face plane, and for good visual servoing performance, markers should be distributed in three dimensions.Thus marker detection required special tuning of the parameters to include the top marker into the visual servoing process. Meanwhile, limiting the DoF for docking to 90° orientation-steps was sufficient for all tested applications. Mechanical and electric connections with EMIs in RIMRES are sufficiently stable and reliable, but cannot replace a dedicated monolithic design. The connection between Sherpa and CREX, however, showed to be sensitive to play between the connecting interfaces, i.e. while the interface is capable of creating a persistent mechanical and electrical connection, any available play can lead to an undesired shaking effect during traveling when CREX is attached to Sherpa.

Establishing serial LOC between all EMIs was a useful backup in situations when a wireless connection did not work fully reliably or had not been established yet[12]. In addition to power management, LOC allows to increase the system's resilience in particular use cases, e.g. communication and controlling EMIs.

Since the EMIs build a topology of the overall system, inferring structure and verifying the identity of a system can be easily performed, e.g. when connecting the manipulator to a payload-item; due to LOC the high-level software stack does not need to be active on the payload-item in order to identify it.

The EMI is seemingly a simple device, and the complexity of the EMI can be easily underestimated compared to systems like Sherpa or CREX. In RIMRES the central importance of the interface for a reconfigurable system and the set of detailed requirements for the EMI design led to an out-stretched development involving multiple iterations.

7.2 Payload-items

All payload-items come with the same set of infrastructure components in order to provide processing power and robust interfacing capabilities. This serves the purpose of redundancy, but in future designs the ratio between infrastructure and actual available payload volume has to be improved. Furthermore, scientific instruments such as REIPOS or the aspired integration of the mole module demand a special design, so that the constraint of a $15\,\mathrm{cm}^2$ interface can be a too limiting factor for some real missions. For developing multiple system of the same type it has been beneficial to maintain a database to keep track of components, changes and issues.

7.3 Rover Design

Sherpa is the most complex system developed in RIMRES considering the integration density of EMIs, the manipulator and the active suspension system.

[12]Payload-items require a few minutes until they are fully functional and embedded into the communication infrastructure.

Regarding the development of the manipulator an exploration of multiple sensors and setups had to be performed to achieve a sufficiently good precision of the joint control and allow for blind stacking procedures. Though the required precision had eventually been reached, the current setup still requires an initial calibration procedure after startup of the system to guarantee precise operation. Meanwhile, the manipulator proved its practicality regarding manipulation and inspection – since the EMI contains a camera the manipulator can be used for visual inspection. It also showed its suitability for locomotion support, i.e. as fifth leg. The manipulator also confirms the benefits of evolutionary optimization; most likely designers would not have considered a bent first link of the manipulator otherwise.

The active suspension system of Sherpa has been designed with six DoF per leg. In most cases we limited the actual application to four DoF, so that the initial design can be considered overly complex. The actual benefit of the additional and currently locked DoF can be questioned and needs further evaluation, also with respect to redundant functionality since flexible wheels are used. Thus, further experiments have to be performed to evaluate this matter.

Sherpa is the key player in the multi-robot system and therefore remains a bottleneck and single point of failure for a mission. In the current setup it is the only mobile system which can manipulate payload-items. Hence, Sherpa has to be highly reliable. Alternatively, the deployment of additional robots with the capability for manipulation or at least detaching and attaching payload-items should be considered.

7.4 CREX

Main features of CREX are inherited from SpaceClimber and thus the lessons learned are focused on new additions to the system, e.g. up to now a depleting battery posed a significant risk for a mission since CREX and SpaceClimber require energy to hold a position other than lying on the ground. In the RIMRES, however, Sherpa's manipulator can be used to attach to CREX and recharge using the facilities of the power management, thus minimizing this operational risk. CREX can be manually operated and to start the docking process we assumed an operator guiding CREX underneath of Sherpa. Nevertheless, the existing and to be expected additional delay between control commands and visual feedback makes the remote operation unsafe and a higher degree of automation is desirable. Future procedures should therefore rely on visual information and on-board processing on either CREX or Sherpa.

7.5 Software Architecture

Developing the software architecture for this multi-robot system has been a challenge especially due to the quantity and heterogeneity of the systems involved. Establishing dedicated development procedures, multiple layers of abstraction and a model-driven design have been essential contributors to a finally successful application. Having a large quantity of subsystems means that even small (systematic) errors – regarding hardware or software – can lead to a severe setback. Main efforts went into enabling the system's basic functionality and making them reliably working including reconfiguration. Any system development in that context – if even if not aiming at a high TRL (Technology Readiness Level) – has to go thoroughly through the steps of (hardware) component selection, verification and integration testing. In addition, detailed debugging and message tracing capabilities across systems need to be available. To limit the impact of heterogeneity it should be actively controlled and reduced in the system design phase by fostering reuse of hardware components, e.g. using a limited set of camera types.

Additional layers of abstraction can add constraints on accessing low-level components or might reduce functionality exposed to higher-layers. Still, access to low-level components should be generally maintained for remote operation. Furthermore, our architecture for a heterogeneous multi-robot had to cope with limited computing resources. The payload-items required special performance optimization, e.g. allowing image processing by activation of the Digital Signal Processor (DSP) and minimizing the overhead of infrastructure components. This shows that performance optimization is well needed to achieve a broadly applicable

software stack.

7.6 Mission Control

The configuration of mission control in RIMRES is static and requires previous configuration of all known individual systems and possible combinations. In addition, the multi-layered control design requires information replication. While the multi-layered approach allows better generalization, it also introduces a source of error if workflows for configuration generation are not fully automated. Furthermore, the current level of autonomy of the multi-robot system is limited and restricted to (semi-)autonomous operation such as docking and stacking. For full exploitation of a reconfigurable multi-robot system we think that a higher degree of autonomy is a requirement. Similarly, the handling of errors and deviations from original plan sequences should be an integral part of manual and autonomous mission control and thus a the center of further improvements.

8 Conclusion and Future Work

This paper presents the state of the project RIMRES. Within this project, a novel approach of tightly cooperating heterogeneous robotic systems is pursued. Reconfiguration of the subsystems themselves and the overall system by combining the individual subsystems is considered in the design phase and enables a wide range of actions to be taken in cases of failure.

A central role in the design of the reconfigurable system takes the electro-mechanical interface (EMI) that is common in all subsystems. The EMI is a standardized interface allowing for a modular hardware design of the team of robots. The wheeled rover Sherpa not only shows high adaptability to terrains that should be covered in planetary exploration, it also plays a central role in the reconfiguration of the robotic team: in order to reconfigure other robots it uses its manipulator and stacks payload-items, which provide additional functionalities for the mobile subsystems or can be combined with other items to form independent (immobile) surface-deployable subsystems.

Throughout this paper we have shown, that reconfigurability and modularity are present on different levels of the overall system. While reconfiguration capabilities already exist in systems without even designing for it, RIMRES intentionally makes it part of the design and shows a great range of flexibility towards new applications. Regarding an increase of adaptability by physical reconfiguration RIMRES opens new directions for (field) research by providing a platform for studying complex physical reconfigurations. Most importantly though, this project shows that despite the modularity of the developed systems they are capable of performing complex maneuvers such as stacking and docking. Both maneuvers have been presented as part of an experimental evaluation. While stacking has been used for a qualitative evaluation of the hardware and verification of low-level software functionality, the high-level software stack was evaluated by the docking maneuver. We were able to show the adaptability of the multi-robot systems using basic functionalities. We assume that increasing the autonomy of the multi-robot system using an improved organization model will lead to a more sophisticated exploitation of the hardware capabilities.

Clearly, the modularization and flexibility of the reconfigurable multi-robot system in RIMRES comes at a cost. Using EMIs introduces a management overhead and the complexity of this new piece of hardware introduces a point of failure, especially having to maintain two interface types: male and female. This demands an equally strong focus on the design, verification and integration testing of this device compared to the more complex systems. Generalizing from this observation, the modularized design facilitates the exploitation of existing redundancies in the multi-robot system. However, the design comes with increased complexity and probability of error. Therefore, the capability for reconfiguration cannot replace existing safety measures, but has to be seen as an add-on.

Evaluation of the general EMI concept and resulting reconfiguration capabilities provided good evidence regarding feasibility and practicality of the approach towards supporting reconfigurable systems. The detailed design elements have to be further improved and a thorough evaluation of the efficiency gain has to be performed. A future improvement is the reduction to a homogeneous EMI design, and we expect a benefit regarding design and maintenance efforts when using a single gender interface. Generally, improving the individual systems is a next step to make the overall multi-robot system more capable and reliable, e.g. the wheels of the rover are planned to be extended to actively adapt their stiffness in order to react to changes in the environment and in a further step be able to act as a sensor for characterization of soil properties. A final integration of a relative positioning system, which already started in RIMRES, will be another research direction to continue on.

Future applications similar to RIMRES can benefit from flexibility in the system design for proactive actions as well as for reactive actions. Improving the overall outcome of a multi-robot mission remains the main intention and will be achieved by a reduction of the operational risk as well as increasing the efficiency of the overall team of robots. Further development will target system modeling for the intelligent and automated use of the additional degrees of operational freedom and investigate deeper on how to exploit the systems' capabilities in order to balance efficiency and operational risk for multi-robot activities.

Acknowledgments

The authors would like to thank the RIMRES team members, partners and supporting staff at the DFKI Bremen Robotics Innovation Center. The project RIMRES was funded by the German Space Agency (DLR, Grant number: 50RA0904) with federal funds of the Federal Ministry of Economics and Technology (BMWi) in accordance with the parliamentary resolution of the German Parliament. RIMRES was a cooperation between the DFKI Bremen – Robotics Innovation Center and ZARM – Center of Applied Space Technology and Microgravity. Further partners were DLR-RY, EADS Astrium, and OHB System.

References

Aoki, T., Murayama, Y., and Hirose, S. (2011). Mechanical design of three-wheeled lunar rover ẗri-star iv:. In *Proc. IEEE International Conference on Robotics and Automation (ICRA) 2011,*, pages 2198 –2203.

Arnold, J. R. (1979). Ice in the lunar polar regions. *Journal of Geophysical Research (JGR)*, 84(B10):5659–5668.

Bares, J. and Wettergreen, D. (1999). Dante ii: Technical description, results and lessons learned. *International Journal of Robotics Research*, 18(7):621–649.

Bartlett, P., Wettergreen, D., and Whittaker, W. R. L. (2008). Design of the scarab rover for mobility and drilling in the lunar cold traps. In *International Symposium on Artificial Intelligence, Robotics and Automation in Space*.

Bartsch, S., Birnschein, T., Roemmermann, M., Hilljegerdes, J., Kuehn, D., and Kirchner, F. (2012). Development of the six-legged walking and climbing robot spaceclimber. *Journal of Field Robotics*, 29(3):506–532.

Bellifemine, F., Poggi, A., and Rimassa, G. (1999). Jade - a fipa-compliant agent framework. pages 97–108.

Bindel, D. and Bruns, R. (2010). Reipos - relative interferometric position sensor. In *Proceedings of the 61st International Astronautical Congress, IAC 2010*, number IAC-10-A3.2C.5.

Bretl, T. (2006). Motion planning of multi-limbed robots subject to equilibrium constraints: The free-climbing robot problem. *The International Journal of Robotics Research*, 25(4):317–342.

Bruyninckx, H., Soetens, P., and Koninckx, B. (2003). The real-time motion control core of the Orocos project. In *IEEE International Conference on Robotics and Automation*, pages 2766–2771.

Castano, A., Behar, A., and Will, P. (2002). The conro modules for reconfigurable robots. *IEEE/ASME Trans. Mechatronics*, 7(4):403–409.

CCSDS/AIAA Inc. (2008). Reference architecture for space data systems.

CCSDS/AIAA Inc. (2012). The consultative committee for space data systems - the official web site. CSSDS Homepage. last access 2012-12-06.

Chen, B., Cheng, H. H., and Palen, J. (2006). Mobile-C: a mobile agent platform for mobile C-C++ agents. *Softw. Pract. Exper.*, 36(15):1711–1733.

Cheshire, S. (2011). Multicast dns. Homepage Multicast DNS. last access 2011-10-04.

Cheshire, S. and Krochmal, M. (2011). Ietf internet draft - dns-based service discovery. IETF Tools Internet-Draft Archive. last access 2011-10-04.

Colaprete, A., Schultz, P., Heldmann, J., Wooden, D., Shirley, M., Ennico, K., Hermalyn, B., Marshall, W., Ricco, A., Elphic, R. C., Goldstein, D., Summy, D., Bart, G. D., Asphaug, E., Korycansky, D., Landis, D., and Sollitt, L. (2010). Detection of Water in the LCROSS Ejecta Plume. *Science*, 330(6003):463–468.

Cordes, F., Ahrns, I., Bartsch, S., Birnschein, T., Dettmann, A., Estable, S., Haase, S., Hilljegerdes, J., Koebel, D., Planthaber, S., Roehr, T., Scheper, M., and Kirchner, F. (2010). Lunares: lunar crater exploration with heterogeneous multi robot systems. *Intelligent Service Robotics*, pages 61–89. 10.1007/s11370-010-0081-4.

Cordes, F., Dettmann, A., and Kirchner, F. (2011). Locomotion mode control for a hybrid wheeled-leg planetary rover. In *Proceedings of the IEEE International Conference on Robotics and Biomemetics (IEEE-Robio 2011)*, Phuket, Thailand.

Cordes, F. and Kirchner, F. (2010). Heterogeneous robotic teams for exploration of steep crater environments. In *Planetary Rovers Workshop (ICRA2010)*, Anchorage, Alaska, USA. IEEE Conference on Robotics and Automation 2010 (ICRA10).

Dettmann, A., Wang, Z., Wenzel, W., Cordes, F., and Kirchner, F. (2011). Heterogeneous modules with a homogeneous electromechanical interface in multi-module systems for space exploration. In *Proc. of the IEEE International Conference on Robotics and Automation (ICRA-2011)*.

DFKI Bremen Robotics Innovation Center (2011). The robot construction kit. `http://www.rock-robotics.org`. last access 2011-10-04.

DFKI Bremen Robotics Innovation Center (2013). Sherpa: Stacking camera payload. `http://youtu.be/ikUM8nUBMjI`. last access 2013-03-09.

Dignum, V. (2009). *Handbook of Research on Multi-Agent Systems: Semantics and Dynamics of Organizational Models*. IGI Global.

Dunin-Keplicz, B. M. and Verbrugge, R. (2010). *Teamwork in Multi-Agent Systems: A Formal Approach*. Wiley Publishing, 1st edition.

Evans, J. S. (1991). Strategic flexibility for high technology manoeuvers: A conceptual framework. *Journal of Management Studies*, 28:69–89.

Ferber, J. and Gutknecht, O. (1997). Aalaadin: A meta-model for the analysis and design of organizations in multi-agent systems.

Ferrarini, L. and Carpanzano, E. (1999). Reference models for the supervision and control of advancedindustrial manipulators. In *American Control Conference*, volume 4, pages 2440–2444.

Foundation of Intelligent Physical Agents (2002). Fipa abstract architecture specification. FIPA Homepage. last access 2011-10-04.

IETF Zeroconf Working Group (2011). Zero Configuration Networking (Zeroconf). Zeroconf Homepage. last access 2011-10-04.

ISECG – International Space Exploration Coordination Group (2011). The global exploration roadmap. online.

JAXA (2009). Hayabusa: Resumption of return cruise by combining two ion engines. `http://www.isas.jaxa.jp/e/topics/2009/1119.shtml`. last access 2012-11-26.

Joyeux, S., Kirchner, F., and Lacroix, S. (2010). Managing plans: Integrating deliberation and reactive execution schemes. *Robotics and Autonomous Systems*, 58(9):1057–1066.

Kennedy, B., Agazarian, H., Cheng, Y., Garrett, M., Hickey, G., Huntsberger, T., Magnone, L., Mahoney, C., Meyer, A., and Knight, J. (2001). Lemur: Legged excursion mechanical utility rover. *Autonomous Robots*, 11:201–205. 10.1023/A:1012474603861.

Kroemer, O., Beermann, D., Cordes, F., Lange, C., Littau, B., Rosta, R., Scharringhausen, M., and van Zoest, T. (2011). Adaptive flexible wheels for planetary exploration. In *Proceedings ot the 62nd International Astronautical Congress*.

Kurokawa, H., Tomita, K., Kamimura, A., Kokaji, S., Hasuo, T., and Murata, S. (2007). Self-reconfigurable modular robot m-tran: distributed control and communication. In *RoboComm '07: Proceedings of the 1st international conference on Robot communication and coordination*, pages 1–7, Piscataway, NJ, USA. IEEE Press.

Lyell, M., Webb, A., Nanda, J., and Chen, W. (2009). Human-autonomous system interaction framework to support astronaut-multi-agent system interactions. *Aerospace Sciences Meeting*. AIAA Paper Number AIAA-2009-428.

Manz, M., Hilljegerdes, J., Dettmann, A., and Kirchner, F. (2012). Development of an lightweight manipulator-arm with selective laser sintering parts combined with fibre-reinforced plastic structures. In *Proceedings of the 11th International Symposium on Artificial Intelligence, Robotics and Automation in Space (iSAIRAS'12)*.

Metta, G., Fitzpatrick, P., and Natale, L. (2006). Yarp: Yet another robot platform. *International Journal of Advanced Robotics Systems, special issue on Software Development and Integration in Robotics*, 3(1).

Microsoft (2011). Microsoft robotics studio developer. Microsoft Robotics Studio Developer Homepage. last access 2011-10-03.

Mosher, T. J. and Lucey, P. (2006). Polar night: A lunar volatiles expedition. *Acta Astronautica*, 56:585–592.

Nilsson, M. (2002). Heavy-duty connectors for self-reconfiguring robots. In *IEEE International Conference on Robotics and Automation, 2002. Proceedings. ICRA '02*, volume 4.

Open-mesh (2012). B.a.t.m.a.n. (better approach to mobile ad-hoc networking). `http://www.open-mesh.org/projects/open-mesh/wiki`. last access 2012-12-04.

Ostergaard, E., Kassow, K., Beck, R., and Lund, H. (2006). Design of the atron lattice-based self-reconfigurable robot. *Autonomous Robots*, 21(2):165–183.

Poettering, L., Lloyd, T., and Estienne, S. (2012). Avahi. Avahi Homepage. last access 2012-10-04.

Poslad, S., Buckle, P., and Hadingham, R. (2000). The fipa-os agent platform: Open source for open standards. page 14.

Roehr, T. M., Cordes, F., Kirchner, F., and Ahrns, I. (2010). Cooperative docking procedures for a lunar mission. pages 1–8.

Rommerman, M., Kuhn, D., and Kirchner, F. (2009). Robot design for space missions using evolutionary computation. In *Evolutionary Computation, 2009. CEC '09. IEEE Congress on*, pages 2098 –2105.

Snyder, R. D., Douglas, D., and Mackenzie, C. (2004). Robustness infrastructure for multi-agent systems. In *Applications, Survivability Infrastructure and Architecture of the Cougaar Agent Software – Proceedings of the 1st Open Cougaar Conference*.

Soetens, P. (2012). RTT: Real-Time Toolkit. Orocos Homepage. last access 2012-10-04.

Spenneberg, D. and Kirchner, F. (2007). The Bio-Inspired SCORPION Robot: Design, Control \& Lessons Learned. *Climbing and Walking Robots, Towards New Applications*, (October):197–218.

Spenneberg, D., Mccullough, K., and Kirchner, F. (2004). Stability of walking in a multilegged robot suffering leg loss. In *in Proceeding of ICRA 04*, page 2004.

Spenneberg, D., Strack, A., Hilljegerdes, J., Zschenker, H., Albrecht, M., Backhaus, T., and Kirchner, F. (2005). Aramies: A four-legged climbing and walking robot. In *Proceedings of 8th International Symposium iSAIRAS*.

Sproewitz, A., Asadpour, M., Bourquin, Y., and Ijspeert, A. (2008). An active connection mechanism for modular self-reconfigurable robotic systems based on physical latching. In *Robotics and Automation, 2008. ICRA 2008. IEEE International Conference on*, pages 3508 –3513.

Suh, J., Homans, S., and Yim, M. (2002). Telecubes: Mechanical design of a module for self-reconfigurable robotics. In *Proceedings- IEEE International Conference on Robotics and Automation*, volume 4, pages 4095–4101. Citeseer.

Utz, H., Sablatnog, S., Enderle, S., and Kraetzschmar, G. (2002). Miro - middleware for mobile robot applications. *Robotics and Automation, IEEE Transactions on*, 18(4):493–497.

Visentin, G. (2007). Autonomy in ESA Planetary Robotics Missions. PPARC KITE Club/Sensors KTN. Workshop on Autonomous Sensors. last access 2013-03-08.

Wang, Z., Cordes, F., Dettmann, A., and Szczuka, R. (2011). Evaluation of a power management system for heterogenous modules in a self-reconfigurable multi-module system. In *Proceedings of the International Conference on Intelligent Robots and Systems (IROS'11)*, San Francisco, CA, USA.

Wenzel, W., Cordes, F., Dettmann, A., and Wang, Z. (2011). Evaluation of a dust-resistant docking mechanism for surface exploration robots. In *Proceedings of the 15th International Conference on Advanced Robotics (ICAR'11)*, Tallinn, Estonia.

Wettergreen, D., Jonak, D., Kohanbash, D., Moreland, S., Spiker, S., and Teza, J. (2009). Field experiments in mobility and navigation with a lunar rover prototype. In *Proceedings of the 7th International Conference on Field and Service Robotics*, Cambridge, Massachusetts.

Wheeler, D., Chavez-Clemente, D., and SunSpiral, V. (2010). Footspring: A compliance model for the athlete family of robots. In *Proceedings of the 10th International Symposium on Artificial Intelligence, Robotics and Automation in Space (iSAIRAS'10)*, pages 644–651.

Wilcox, B., Litwin, T., Biesiadecki, J., Matthews, J., Heverly, M., Morrison, J., Townsend, J., Ahmad, N., Sirota, A., and Cooper, B. (2007). Athlete: A cargo handling and manipulation robot for the moon. *Journal of Field Robotics*, 24(5):421.

Willow Garage, Inc. (2011). Robot operating system. ROS Wiki. last access 2011-10-03.

Winikoff, M. (2005). Jack(tm) intelligent agents: An industrial strength platform. 15:175–193.

Yim, M., Zhang, Y., Roufas, K., Duff, D., and Eldershaw, C. (2002). Connecting and disconnecting for chain self-reconfiguration with polybot. *IEEE/ASME Trans. Mechatron*, 7:2002.

Zuber, M. T., Head, J. W., Smith, D. E., Neumann, G. A., Mazarico, E., Torrence, M. H., Aharonson, O., Tye, A. R., Fassett, C. I., Rosenburg, M. A., and Melosh, H. J. (2012). Constraints on the volatile distribution within shackleton crater at the lunar south pole. *Nature*, 486:378–381.

[3]: **Lunares: Lunar Crater Exploration with Heterogeneous Multi Robot Systems**
F. Cordes et. al
in: Journal of Intelligent Service Robotics, 2010

LUNARES : Lunar Crater Exploration with Heterogeneous Multi Robot Systems

Florian Cordes[1] Ingo Ahrns[2] Sebastian Bartsch[1] Timo Birnschein[1]
Alexander Dettmann[1] Stéphane Estable[2] Stefan Haase[1] Jens Hilljegerdes[1]
David Koebel[3] Steffen Planthaber[1] Thomas M. Roehr[1] Marc Scheper[3]
Frank Kirchner[1]

[1]DFKI Robotics Innovation Center [2]EADS Astrium GmbH [3]OHB System AG

July 14, 2010

Abstract

The LUNARES project emulates the retrieval of a scientific sample from a in a robotic mission. The reference of this demonstration scenario is the Shakelton crater at the lunar south pole, where samples of scientific interest are expected in permanently shadowed regions.

For accomplishment of such kind of mission an approach of a heterogeneous robotic team consisting of a wheeled rover, a legged scout as well as a robotic arm mounted on the landing unit was chosen. All robots act as a team to reach the mission goal. To prove the feasibility of the chosen approach, an artificial lunar crater environment has been established to test and demonstrate the capabilities of the robotic systems. Figure 1 depicts the systems in the artificial crater environment. For LUNARES , preexisting robots were used and integrated into a common system control.

A ground control station has been developed considering conditions of a real mission, requiring information of autonomous task execution and remote controlled operations to be displayed for human operators.

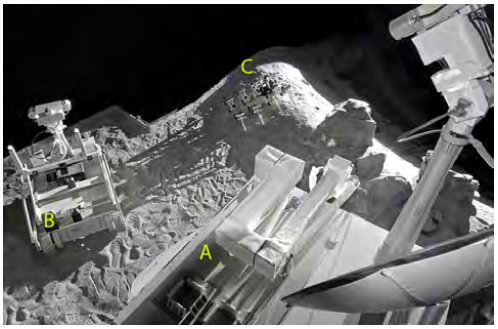

Figure 1. LUNARES systems: Landing unit (A), wheeled rover (B) and legged scout (C) in the artificial crater environment

1 Introduction

Water to be found on Moon would be a crucial requirement for extended human presence on Moon. By splitting up water into hydrogen and oxygen, fuel for spacecrafts as well as oxygen for human habitats might be obtained. Currently, evidence is growing for water ice on the lunar surface. In addition multiple theories try to explain a possible existence of water on the Moon:

J.R. Arnold [1], for example, names four main mechanisms building up deposits of water on the lunar surface: (1) water was brought down to the lunar surface as part of the meteoritic bombardment the Moon is exposed to, (2) hydrogen of the solar wind reacts with lunar oxides and leaves water molecules. (3) Cometary impacts and (4) outgassing of water from the lunar interior are also considered as sources. The latter one is considered to be the least probable source. At the same time, Arnold identifies effects that counteract building up significant deposits of water ice on the Moon. These include for example dissociation of H_2O molecules through photons. This leads to the assumption that deposits of water ice reside, if at all, at permanently shadowed areas of the lunar surface, as already described by Watson, Murray, and Brown in 1961 [23].

Additionally, several satellite missions indicate that regolith-bound water ice can be found in such

permanently shadowed craters at both lunar poles: In 1996 the Clementine bistatic radar experiment suggested the presence of water ice at the lunar south pole [17]. Differences in the polarization of radar echoes from permanently shadowed and sunlit areas led to this conclusion. In 1998, measurements from Lunar Prospector implied the presence of hydrogen, possibly in from of water ice at both lunar poles [8].

In November 2009, the LCROSS mission [16] detected water ice in the Cabeus crater at the lunar south pole. In this mission a part of the satellite hit the ground of the permanently shadowed crater, resulting in an ejection of a material plume to be analyzed by the instruments of LCROSS. Additionally by the end of 2009, NASA announced the detection of several hundred tons of water ice at both lunar poles within the MINI-RF experiment that flew with India's Chandrayaan-1 mission [15].

Current satellite missions can detect water only indirectly. For direct detection of water, an in situ sample has to be taken and analyzed. It is clear that such missions will be executed by robotic systems since these missions for exploration of lunar environments operate with lower risk and higher efficiency compared to missions with direct human involvement [3]. Such robotic mission could include taking core samples and might give insight in the history of volatiles brought to Moon by asteroids and meteorites.

Various approaches are proposed to explore lunar craters. These approaches employ different means such as "classical" single rover systems, cooperative robotic systems, tethered systems and new hybrid approaches. Some of the approaches are presented in the following paragraphs.

Barlett et al. [2] intend to use a four wheeled rover with a drilling tower to explore the bottom of dark lunar polar craters. The Scarab rover is designed to be deployed directly in the interior of the crater. The rover will solely operate in dark regions, thus an Radioisotopic Thermoelectric Generator (RTG) for power generation will be used in the flight system. In various experiments Scarab proved to be able to safely overcome terrains with slopes of up to 20° on different soils [24]. The instrumentation is feasible to take 1 m drill cores and to demonstrate the extraction of water from the taken soil sample.

In October 2008 the robot CESAR was the only robot to fulfill all mission objectives of the *Lunar Robotic Challenge (LRC)* hosted by the European Space Agency (ESA). The robot uses a hybrid legged-wheel approach for locomotion in steep crater environments [19]. The objective of the LRC was to send a robotic device into a crater at the Teide Volcano on Tenerife to find and pick up 100 g of colored sand. The sample had to be delivered back to a designated site outside the crater. The challenge simulated missions where the scientific equipment has to reside outside of the crater itself; requiring robots to collect the samples. The robots in the challenge were remotely operated from a simulated ground control station.

With the TRESSA system, Huntsberger et al. [12] employ a team of three rovers to explore hard-to-access terrain. The system comprises a *Cliff-Bot* that is tethered down a slope by two so called *Tether Bots*. The tether bots act as anchors with winches for the tethering system. The cliff bot is equipped with an instrumented arm for scientific experiments to be conducted directly in the slope. The system proved to be able to successfully operate in steep canyon walls with slopes of up to 85°.

In comparison, the LUNARES project aims at a reconfigurable cooperative system of heterogeneous robots to accomplish the task of analyzing material from a permanently shaded region at the lunar south pole [5].

The system consists of three main elements: (1) a landing unit that has to transport all subsystems safely to the lunar surface and provide manipulation support using its robotic arm (2) a wheeled rover to allow locomotion in moderate terrain and to provide an energy efficient vehicle for long distance and (3) a legged scout robot that can advance into the dark areas of a lunar crater and return a sample from the crater bottom. The aim of the project was to provide a proof of concept based on existing technology, i.e. reusing existing robotic systems.

The subsystems involved are described in detail in Section 2. Section 3 gives an overview over the lunar crater testbed, that has been build up as simulation environment to demonstrate and test the feasibility of the approach within the project LUNARES . The demonstration mission conducted in the testbed is presented in Section 4. An overview on the readyness level compared to a real mission is described in Section 5 and finally the conclusion of the project as well as an outlook on following activities is given in Section 6.

2 Systems of the LUNARES Scenario

The following section describes the systems being part of the LUNARES mission. The section is subdivided into a description of the lander mock-up's superstructural parts, namely sensor tower and manipulator arm. Section 2.2 describes the wheeled rover system, which is used for longer distances in moderate terrains. Section 2.3 presents the details of the legged

scout system (aka Scorpion). Finally, system and mission control elements of the LUNARES system are discussed in Section 2.4 and Section 2.5, highlighting the required functionality of a ground segment for a real exploration mission.

2.1 Landing Unit and Superstructural Parts

The landing unit is represented by a non functional mock-up and serves as mounting platform for the robotic arm and the sensor tower, these components are described in the following paragraphs. However, the design of the lander is inspired by a real landing unit, though in a 1:1.6 scale.

2.1.1 Lander Manipulator

The lander manipulator is a 6 DOF robotic manipulator (Figure 2(a)). The main tasks for the robotic manipulator in the LUNARES reference mission involves the following components:

- reconfiguration of rover by grasping a payload element from the lander and installing it at a special payload bay on the back of the rover.
- recollecting a payload by grasping the payload element from the back of the rover and placement of the element on the lander
- grasping the sample container from the back of the scout which contains the collected lunar sample, and transport of the sample container to the lander

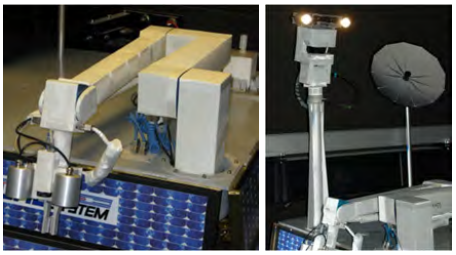

(a) The 6 DOF lander manipulator in its space saving configuration on top of the lander mock-up

(b) The sensor system including a stereo camera, a 3D laser scanner and two spotlights

Figure 2. The lander's superstructural components

2.1.2 Lander Sensor System

The sensor system of the lander (Figure 2(b)) includes a pan-tilt unit which contains a stereo camera system, a laser scanner and spotlight for illumination. By swiveling the laser line over the scene, the reconstruction of static scenes of the environment is performed. The sensor system fulfills several tasks:

1. The stereo camera system provides camera images for the ground control station enabling a visual monitoring of the robotic systems, when the robots are in the vicinity of the lander[1].
2. The pan-tilt unit allows the ground operator to control the viewing direction in order to focus on parts of the scene that are of greater importance for the current task execution.
3. The 2D laser scanner works together with the tilt-unit as an imaging 3D-LIDAR (Light Detection And Ranging), thus providing dense 3D images of the vicinity of the lander, Figure 3. By using the values of remission, the 3D laser scanner can also be used as a convenient 3D feature tracker. For this purpose, retro-reflective markers are attached to the rover which enable an accurate tracking of the rover pose in the neighborhood of the lander (See also Figure 23 in Section 4.4).
4. The spotlight can be used to illuminate the close vicinity of the lander for improved imagery.

2.2 Rover

One of the preconditions of the LUNARES project was to reuse existing robotic systems. Therefore the LUNARES rover is based on an industrial mobile platform which was not designed as a lunar rover. The existing platform was utilized to demonstrate the basic idea of combining two different mobility systems, i.e. a wheeled rover for the coverage of larger distances in moderate terrain and the legged scout for the exploration of shorter distances in more difficult terrain (with more obstacles and terrain inclination). Nevertheless, the existing mobile platform had to be adapted to fit the demonstration requirements: (1) carry an additional payload (i.e. a lifting mechanism for the scout and the scout itself) of approximately 20 kg mass (14 kg for the scout and 6 kg for the lifting mechanism), (2) operate in very dusty terrain and (3) negotiate inclinations of about 15°.

[1] Up to now, the operator at ground control only receives monoscopic cameras. However, for future enhancement of the system a visual control through a stereoscopic display is possible

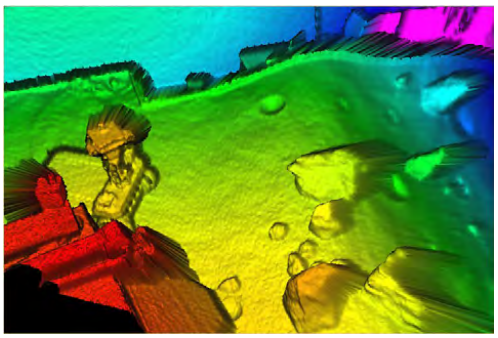

Figure 3. Scan data provided by the 3D laser scanner showing parts of the lander (red, lower left corner), the rover in front of the lander, and parts of the crater rim (right half of the picture).

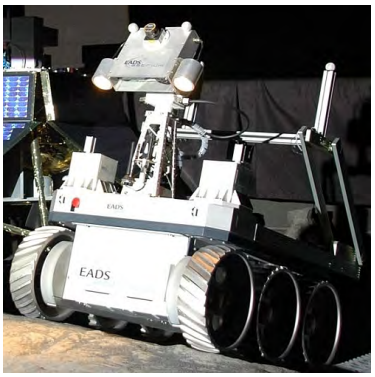

Figure 4. Image of the LUNARES rover reaching the crater rim and looking into the crater where the scout is working.

This resulted mainly in modifications to the traction systems, which are actually still not applicable for a real lunar mission. Figure 4 shows the modified LUNARES rover.

For intelligent and cooperative behaviour, the rover was equipped with an additional processing unit and additional sensors. The sensor system of the rover comprises a sensor head including a stereoscopic camera system and a laser scanner. The sensor head is mounted on a pan-tilt unit. Additionally, an inclination sensor allows to detect hazards resulting from too large ground inclinations. To support the self-localization of the rover an Inertial Measurement Unit (IMU) including an accelerometer and a gyro based on Micro-Electro-Mechanical-System (MEMS) technology were added.

The pan-tilt unit enables the control of the viewing direction of the camera system as well as the usage of the 2D laserscanner as an imaging 3D LIDAR. The data of the laser scanner are mainly used for reactive obstacle avoidance and sensor data driven emergency stops.

The camera serves two purposes: (1) It allows the monitoring of the operation via the ground control station. (2) It is required for the autonomous docking behaviour between rover and scout. This is discussed in more detail in Section 4.4.

Rover Control

The rover is one of four robotic subsystems in the LUNARES system architecture is embedded into the system control which will be described in Section 2.4.

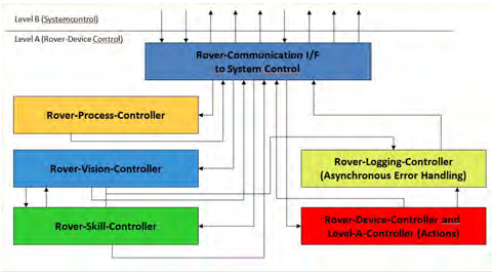

Figure 5. Control system of the rover hosted on the rover on-board computer.

The structure of the rover specific control is depicted in Figure 5. The rover is controlled by five components:

1. The rover device controller (level A controller) controls the H/W of the rover, the movements, reactive emergency behaviors, spline-interpolation, trajectory generation, the pan-tilt unit and the data acquisition of the 3D imaging LIDAR.
2. The rover skill controller is a scheduler that controls the execution of skills such as the autonomous scout-docking behavior depending on the specific tasks.
3. The rover vision controller acquires image data from the stereo camera system and distributes these data via WLAN.

Figure 6. Cubic splines and circle segments are used to generate more complex trajectories for the rover

4. The rover process controller starts and stops all processes of the rover's on-board computer and performs a health check of all components of the rover.

5. The logging controller of the rover records all incoming and outgoing messages and generates an asynchronous error signal to the higher levels of the system control in case of severe error signals from one of the components of the rover control.

6. The rover communication interface provides a central interface program to the higher levels of the system control.

Rover Motion Planning

The level A controller of the rover provides different types to control it's motion, i.e. velocity control (left and right wheels control, jog-rate etc.), control of certain distances at defined velocities, as well as more complex trajectories which can be assembled from simpler trajectory parts. Possible parts can be segments of circles as well as cubic splines which reach a certain point with given heading direction (Figure 6).

The general concept of motion planning of the rover consists of three main steps:

- Depending on the task a trajectory is planned, either automatically as it is the case during the automatic docking to the lander mockup, or controlled by the operator from ground.

- The trajectory is transferred to the controller which commands the motion system and the specific velocities for the left and right wheel system (differential drive).

- During the motion execution the motion is monitored via the odometry system which estimates a rough information of the position and heading direction of the rover.

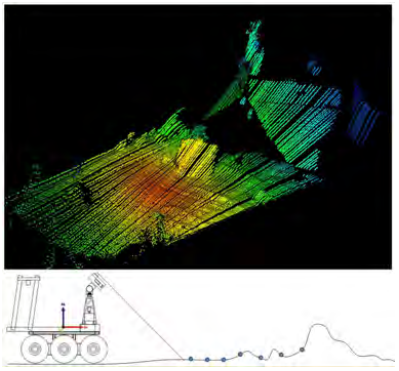

Figure 7. Collecting several laser scans while driving and combining these scans to a 3D reconstruction using the rover's odometry provides enough information in order to assess the terrain.

In the vicinity of the lander, the estimation of the rover position and heading direction is supported by the 3D laser scanner of the lander system which estimates the rover pose from retro-reflective markers. Sensor data is processed and monitored to apply a reactive emergency behavior that stops the rover. Potential reasons for an emergency stop are:

- Loss of WLAN connection checked by continuous pinging the system control at the lander.

- Obstacles in front of the rover detected by the laserscanner.

- Too large inclination indicating the start of a crater rim or any other obstacle which has not been not detected by the laserscanner.

The reactive emergency stop-behavior gathers range information from the 3D laser scanner and assembles a rough estimation of the terrain in front of the rover using the self-localization resulting from the rover odometry. The 3D data allows to extract information whether there is an obstacle, a hill or the beginning of a hole (e.g. a crater). This principle is shown in Figure 7.

The ground control station (Section 2.5) provides different methods for monitoring and control the rover. A mission involving the rover contains automatic tasks and interactive tasks which are monitored or even solved by the operators. The LUNARES system does not include autonomous path planning and obstacle avoidance with trajectory replanning. In-

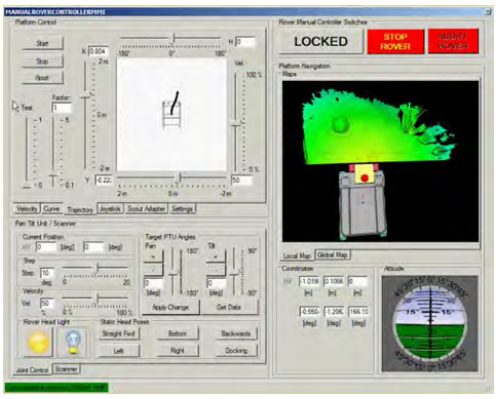

Figure 8. MMI at the ground control station dedicated to rover. The MMI provides monitoring (e.g. artificial horizon, lower right) and trajectory planning (white area, top left). The window in the top right area shows the acquired 3D-data from a scan while not driving. The planned trajectory can be applied to the simulated rover in the 3D scan image.

stead, for safety issues, every movement of the rover is preceded by the acquisition of a 3D range image.

This image supplies the ground operators with a good impression of the near terrain and is used to plan a small trajectory which does not exceed 1.5 m (Figure 8). This movement can be simulated on ground and finally send to the flight system which executes the planned trajectory. Unforeseen hazards can still be avoided by the emergency system of the rover.

2.3 Scout

The Scorpion robot [13, 14] serves as legged scout in the LUNARES mission. Scorpion is an eight-legged biomimetic walking robot. Each of its legs has three active DOF and one passive DOF in the lower leg. The locomotion control employs the biological inspired pattern generator and reflexes for efficient locomotion. The following paragraphs describe the modifications that have been executed in order to adapt the existing robot Scorpion for the LUNARES scenario. Figure 9 shows the Scorpion as fully equipped LUNARES -scout.

Scout's Basic Locomotion Principle

The scout's locomotion is controlled by a microprocessor running a micro-kernel for behavior-based control of robots [20]. The higher behavioral levels are executed on an embedded PC separately. This principle of separation is biological inspired: Human or animal locomotion and reflexes are produced in the spinal cord, whereas higher level understanding is located in the brain. In case of the Scorpion the microprocessor replaces the spinal cord and the higher level behaviors are executed on the PC system.

Beside real-time capabilities and reflexes, the micro-kernel also offers an inverse kinematics layer which is used to describe the scout's rhythmic movement patterns in Cartesian coordinates.

This inverse kinematics layer is important for the climbing task of the robot, because it prevents the feet from slipping due to a reduction of tension between the legs while walking.

The micro-kernel allows to write multiple inputs to single hardware drivers using different merging functions, e.g. the normal posture of the robot is written to the joints, the walking itself is defined as offsets to this position. The micro-kernel merges both values by adding and relays the value to the inverse kinematic resulting into the final control values for the joints.

Due to this approach an automatic merging of walking patterns is possible. Thus, forward- and sideward-walking can be combined to a diagonal walking pattern. The posture (e.g. body height, lean forward, tilt angle, etc.) can be set independently from walking patterns.

The representation of the movements allows to modify the walking speed by changing the frequency of the curve and to modify the step height by changing the amplitude.

Reflexes for Secure Locomotion

In order to enable a secure locomotion in crater slope of up to 35°, several reflexes had to be implemented or adapted. Already existing reflexes were the *hole reflex* and *stumbling correction*, additionally a *ridge reflex* and a *balance reflex* were introduced specially for the locomotion in steep environments with obstacles.

The *hole reflex* is triggered when, due to the state of the walking behavior, ground contact of a foot is expected but not measured by the linear potentiometer in the spring-damped lower leg (passive DOF). As a result the reflex stretches the leg until ground contact is measured. The "opposite" reflex is the *ridge reflex*: This reflex is triggered, when in touchdown phase of the leg ground contact is sensed before it is expected. In this case the reflex inhibits further stretching of the leg in order to keep the body of the robot in level.

The *stumbling correction reflex* is triggered when a leg is stuck in swing phase. To detect this, the

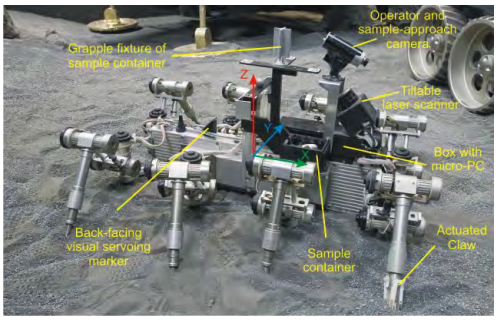

Figure 9. Scorpion robot: Scout system for LUNARES . One of the eight legs is equipped with a gripper for sample pick up. The sample container with a grapple fixture for the lander's arm is mounted on the scout's back. Main sensors are an operator camera, also used for automatic sample approach and a tiltable laser scanner.

currents of the thorax joint are measured and compared with a threshold. If the current raises above the threshold, the basal and distal joints are moved reflex-like in order to lift the foot over the obstacle, i.e. the foot swings with a much higher amplitude over the obstacle like when using the regular gait pattern. A second indication to trigger this reflex is the difference of actual position and desired position of the foot.

The *balance reflex* shifts the body accordingly to the slope of the terrain in order to keep the load as equally distributed on all legs as possible.

Reusing a Leg as Manipulator
The complex system of an walking robot can increase its advantages with the adaption of an functional element on the footprint. With this element, e.g. grabber or sensor, the legs of the system can perform as a manipulator or sensor arm. Furthermore, a robots gripping device can support locomotion, when used to increase the footprint of the robot.

For the LUNARES scenario, the Scorpion is equipped with a gripper. The main function of this device is to collect probes on the ground and to place them in a container on the robot. More information on the gripping device is provided in [5].

Autonomy Framework for the Scout
The Scorpion's task requirements within the scenario exceeded the existing online processing capability of the Scorpion. To handle this issue, a software framework was introduced. This framework provided the communication infrastructure to remotely control the Scorpion and eventually allowed the introduction of high level action commands such as "collect sample" - a command which is executed after the position of this sample was determined (described in Section 4.5).

This framework also allowed the distribution of software on different processing units such as workstations or embedded PCs, and also allowed for conducting simulation experiments with "hardware in the loop", e.g. using the real sensors of the robot for a obstacle detection task, while controlling the robots in simulation.

Additional Sensors
In order to fulfill the task of detecting a sample autonomously as described in Section 4.5, the scout has been equipped with a laser scanner. Since the laser scanner was added to the existing robot in the project, a compact additional module has been designed, consisting of controller electronics, a power converter, a digital servo motor and the laser scanner itself.

The controller is executed on a microcomputer with a Linux operating system and uses wireless communication to connect to the mission control station. This enables the controller to be embedded into the control station and communicate within the autonomy framework (see Section 2.3).

The pan-tilt laser scanner unit is controlled by a high level software module, which collects the information of the laser scanner and constructs a height map. This map is then used for localization of samples (see Section 4.5). Similarly, the camera output is processed by another high level software module, which controls the approach of the scout (see Section 4.5).

2.4 System Control

The control of the systems is based on the Functional Reference Model (FRM) defined by the European Space Agency (ESA) [22, 9]. FRM divides autonomous robot control into three layers:

- Mission Layer (Level C)
- Task Layer (Level B)
- Action Layer (Level A)

In case of LUNARES , the Action Layer defines basic actions like movements or gripping. The Task Layer is responsible for sequences of actions and defines tasks like "go to the next position while avoiding obstacles" or "deliver sample". The Mission Layer is responsible for the overall mission execution. It de-

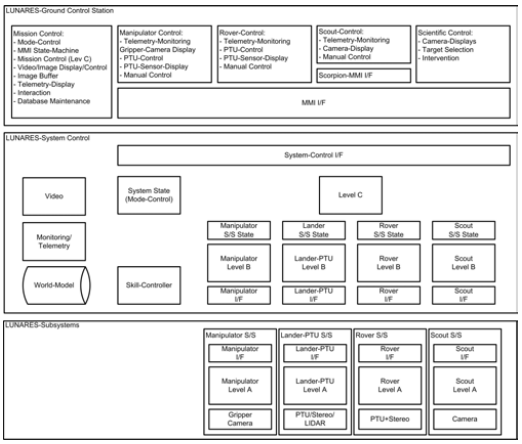

Figure 10. Overview of the LUNARES control architecture: Bottom: Subsystem control with all level A controllers of rover, scout, lander, and manipulator. Middle: System control with level B and C, and other support functions like monitoring, telemetry, vision server, world model, and skill controller. Top: LUNARES ground control distributed over several workstations.

fines which task is executed when and how to handle dependencies of tasks between all robots. Due to this approach the Level B and C Controllers can make use of the existing Level A Controllers.

Also the three main columns of information flow (forward control, nominal feedback, non-nominal feedback) typical for the FRM [22] have been implemented for the LUNARES control system. The first column is the feed forward control which sends commands from the top (mission level) via level B to the bottom (action level close to the robotic hardware).

The second column of the FRM is the nominal feedback channel which is implemented as a synchronous communication channel where nominal responses to the commands of the feed forward command channel are send and evaluated. Normally, this channel serves to acknowledge simple commands, or to generate errors. In case of an error generated by a lower level, the next higher level has to react on that error, or in case of no possible error recovery, the error has to be reported to the next higher level.

In addition, the FRM foresees a third column which is called the non-nominal feedback channel. On that channel, asynchronous error messages can be generated, which are reported from a lower level to the next higher level. Again, the next higher level can try to recover from the problem if possible. This channel is the most complicated due to its asynchronous character.

For the LUNARES system control, this has been solved by a simple error handling mechanism so far and should be enhanced in the future. Besides the three control levels, the LUNARES system control also contains a global state machine which controls different operating modes and error states of the system. The overall mode controller comprises vector states which contain component states for every subsystem. This allows an error handling for single subsystems whereas other subsystems operate in nominal automatic or manual operating mode.

Furthermore, the system control contains a world model database, a skill controller which provides a library of higher skills (such as cognitive skills for grasping or docking) and a monitoring controller which gathers telemetry information from the system itself and all connected subsystems, i. e. the different robots. The telemetry data is permanently analyzed and is used to throw asynchronous error messages. A vision server collects all video and image related data and provides a central service for all other skills and functions that need these type of data. Figure 10 depicts the main components of the system architecture.

The Level B Controller (i.e. task controller), applies a PHP script interpreter. So every task is coded as a small PHP snippet of code. Via network communication these scripts call actions of the level A controller and skills of the skill controller. On this control level, most of the data representations are

symbolic, like "move to payload-bay". By accessing the world model database from the task script, the Level B controller resolves the symbolic data and obtains the corresponding numeric data. This type of data is then send to the Level A, which normally understands numeric data and parameters only.

2.5 Ground Control Station

The benefit of robotic missions is the ability to achieve various mission objectives within the same mission based on a mission specific set of programmable robots and payloads. The LUNARES mission foresees for instance to retrieve samples from a crater relying on a heterogeneous robotic team including the remote system control and a ground control station. The Ground Control Station (GCS) has to support the LUNARES mission activities at different levels: (1) generate the mission database and the associated mission tasks, (2) edit and verify the mission timeline, (3) execute the mission timeline in a supervised autonomy mode, (4) direct control of all the subsystems. These features are not specific to the LUNARES mission but can be found for a wide variety of robotic missions. The LUNARES GCS integrates these requirements and has been used within the experiments to prepare the missions and to execute automatically the mission timelines including manual recovery actions.

2.6 Operational Concept

Using state-of-the-art robotic systems for mobility and manipulation, only a low level of autonomy can be expected, especially in an unstructured environment like the moon. The knowledge about the mission and their subsystems has then to be shared among the elements of the whole system including the operators:

1. Complex operations which cannot be performed autonomously by the robots are coded in the Level B Tasks of the system control
2. Complex operations which can be performed autonomously by the robot are coded in the Level A actions of the system control as well as simple operations
3. The generation of the mission structure leading to the timeline (Level C Timeline) which necessitates reasoning capabilities is performed by the operator
4. Mission execution which requests as well analysis capabilities is supervised by the operator. The operational concept is based on the supervised autonomy which shall involve the operator in all critical phases of the mission.

In order to improve the safety and the reliability of the mission, the operator shall be able to manage the system from full automatic (automatic execution of the timeline) to full manual (direct commanding of all the subsystems including the sensors). In case of errors and contingencies, or for complex operations beyond routine activities, the operator shall be able to stop the mission, to operate manually the faulty subsystem, and to resume the mission.

The GCS shall also be user friendly in order to reduce the training effort and to increase the operational safety. The primary operation of the Man Maschine-Interface (MMI) consists of selecting an operational mode or context (i.e. Standby, Automatic, Manual) with the mode controller in which the modes and their transitions are represented as a finite state machine. The accessibility of the commanding tools (i.e. manual controller or vision server) or part of them is set according to the operational modes.

As the LUNARES mission involves several robots that could operate in parallel the mission responsibilities are shared among several operators: (1) mission director for supervising and monitoring the mission state and delegating activities to the Mission Operators, (2) mission operators for commanding directly the robots in specific mission phases. The ground control station has then the capability to involve several operators in a coordinated way for monitoring and commanding a mission.

2.7 Functions

The operational functionality consists of standard system status telemetry (TM) monitoring and the remote manual commanding of the subsystems (TC). To interact with the environment the operator can command the subsystems from the GUIs.

Each robotic and sensor subsystem has a dedicated GUI to configure and command that subsystem. The remote operator can obtain situational awareness of the worksite environment by viewing images from the head cameras of the rover, the scout and the lander. The mission preparation steps and the mission configuration, planning and execution are performed via dedicated GUI interfaces.

2.8 Architecture

The control station architecture applies the Thin Client Three Tier (TCTT) architecture model (Figure 11). In this architecture the three levels *User Interface*, *Domain Application* and *Data Access* are strictly separated (Three Tier). According to the selected TCTT architecture model, the implementation of each function is split into a kernel application and a GUI unit.

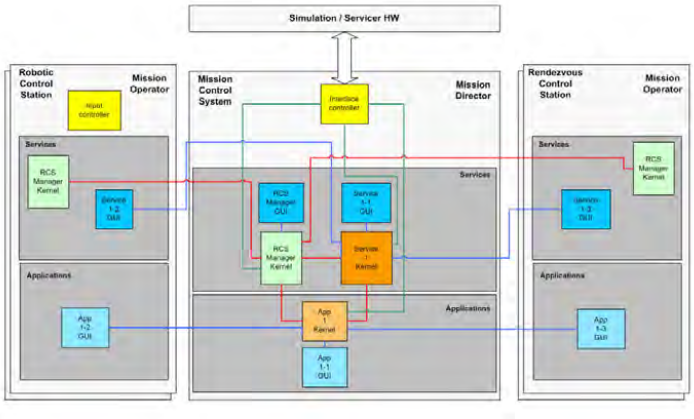

Figure 11. Basic Architecture of the robotic Ground Control Station

The kernel application runs the main processing related to the function while the GUI unit enables the GUI-based commanding of the kernel application. The GUI units are not linked to each other but only with their dedicated kernel application. In addition the kernel and GUI applications are shared between the core applications which manage the basic functionalities and the robot applications which directly depend on the robot. While the core applications are robot independent or fully configurable, the robot applications are either partially configurable or need a re-design according to the robot needs.

The communication between the kernel applications as well as between the kernel and the GUI applications rely on the design patterns (i.e. observer and mediator patterns). In order to reach the multi-operator capability the GUI of the subsystems to be commanded by additional operators are started on a parallel control station and linked to their kernel application, while the kernel application remains on the central control station of the mission director.

2.9 Configurability

The control station provides a variety of configuration files for the definition of the environment, mode control and mode transition, telemetry, and commanding. Robot commands are specified as macros in an Excel sheet. The assembly of binary telemetry streams coming from the system control is defined via another Excel sheet. The sheet holds information about subsystem, name, position, type, length, and monitoring values (warning and error minimum and maximum limits). The mission database (access file) contains the path definitions of the manipulator and the rover, intermediate points used in the Level B tasks, as well as the position of objects (i.e. payloads) on the subsystems (i.e. lander, rover).

Figure 12. MMI environment with the Mission Controller (left) and the camera controller of the Head and the Manipulator (right). Error and warning messages are displayed in upper part of MMI, status messages are displayed at the bottom, the upper right provides commanding tools to be opened in the central workspace.

2.10 MMI environment

The main MMI consists of fixed areas split around the screen (Figure 12). (1) error and warning messages, (2) status message, (3) commanding tools, (4) monitoring, (5) workspace in the center where the commanding tools can be opened and used. The commanding tools are selectable according to the current

Figure 13. Ground Control Station in a multi-operator configuration. Above the monitors the related subsystems are pasted into the photograph.

mode of the control station, so the operator can only select context specific operations. This allows to ease the utilization of the MMI and to increase the operational safety. So, different workspaces can be configured for the different mission phases like planning, monitoring, or commanding of a subsystem.

In multi-operator mode the ground control station is started on two computers allowing a parallel monitoring and commanding of the LUNARES application scenario (see Figure 13). The MMI environment is the same for both control stations. The *Director MMI* has full functionality over the robotic system and can distribute rights to the operators of the subsystems. The *Operator MMI* is configured according to the role assigned by the director, so the operator has only access to the commanding tools of the subsystem he is in charge of.

3 Test Environment and Test Equipment

The scenery for experiments conducted in LUNARES is an artificial lunar crater environment called *Space Testbed* (STB). The STB simulates the conditions at lunar polar regions. The surface of the STB consists of hard rocks with gray basalt chips as regolith substitute including stones and small craters. The STB provides slopes between 30° and 45° (Figure 14).

In addition, a lighting system is installed which is able to create very bright areas (14500 lux at 10 m/12^o per spotlight) at the crater rim as well as complete darkness in the interior of the crater in order to simulate the lighting conditions at the lunar polar regions.

A visitor platform is installed allowing to spectate the experiments and demonstrations. The control center is located below the crater. Thus, the operators have to depend on sensor data from the systems for control and supervision, resulting in a situation similar to real mission scenarios.

The STB is equipped with supervision tools to acquire experiment data for evaluation of the systems under test. To collect, archive, and synchronize the experiment data and to control the cameras a software is implemented called STB-Control. The test equipment is controlled automatically in order to support the operators. The equipment comprises

- a Motion Tracking System (MTS),
- two Pan-Tilt-Zoom (PTZ) cameras,
- a fixed observation camera,
- and a gantry crane equipped with an observation camera and a tracking camera.

The following paragraphs provide a rough overview of the automatic surveillance system, [7] offers more detailed information.

3.1 Automatic Supervision Using Pan-Tilt-Zoom Cameras and a Motion Tracking System

Besides position determination of the scout in the slope, the MTS is used to automatically focus the PTZ cameras on the robot under test. Therefor, the position of a reflective marker fit to the robot is tracked by the MTS and its position is used to align the cameras. The continuous video material from different points of view including a constant bird's eye view (Section 3.2), combined with the recorded trajectory helps to improve locomotion in the slope by discovering malfunctions and improving walking behaviors.

The camera alignment is realized by a camera calibration using the known position of the reflective markers and their position in the camera image. Thus, the extrinsic parameters describing the position and orientation of the camera in the coordinate system of the MTS (WCS) can be calculated and can be used to transfer the positions of the markers into the camera coordinate system (CCS). The following sections describe the algorithm used to detect the markers within the camera image, the CMA-ES optimization [11] of the extrinsic parameters and the final camera alignment on the markers in the CCS which have been realized by a spherical coordinate transformation.

The camera alignment is realized by a camera calibration using the known position of the reflective markers and their position in the camera image. Thus, the extrinsic parameters describing the position and orientation of the camera in the coordinate

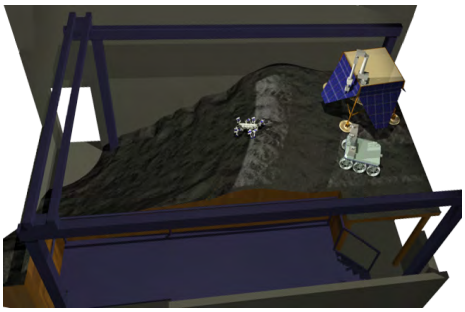

(a) CAD-model of STB, including landing unit, rover and legged scout.

(b) Panoramic view from within the crater. The picture is stitched from several single shots.

Figure 14. Space Testbed (STB): CAD-model and view from interior. The main slope is 30° to 35°, the environment additionally provides a slope of 45° (special area in lower left corner of CAD-picture)

system of the MTS (WCS) can be calculated and can be used to transfer the positions of the markers into the camera coordinate system (CCS).

The following sections describe the algorithm used to detect the markers within the camera image, the CMA-ES-optimization [11] of the extrinsic parameters and the final camera alignment on the markers in the CCS which have been realized by a spherical coordinate transformation.

Detection Algorithm
The camera calibration requires a reliable detection of the markers used by the MTS. Therefore, the cameras are equipped with infrared emitters and the infrared cut filters of the cameras are switched off. The detection algorithm uses a run-length encoding algorithm to build horizontal intervals of pixels, whose brightness reaches a certain threshold, and an union-find algorithm to connect the intervals to regions [10]. The detection algorithm allows the collection of passpoints which consist of a marker position in the WCS and its corresponding pixel in the camera image. These passpoints are used during the optimization to rate the different camera positions.

Optimization of the extrinsic parameters
The CMA-ES optimization uses a camera calibration function containing the intrinsic parameters of the camera, which have been extracted from the data sheet, and the six extrinsic parameters describing the position and orientation of the camera in the WCS.

Each camera pose is rated by transferring the 3D point of the collected passpoints into the camera image and compares the calculated image coordinates with the desired ones. Thus a set of extrinsic parameters is rated by the average deviation over all passpoints in pixel-related units. If rough start parameters are supplied, a deviation of 6.79 to 7.84 pixel is achieved (Figure 15(a) and Figure 15(b)). This fitness value can be further improved by optimizing the algorithm which is responsible for the passpoint collection.

Camera Alignment
To focus each camera on a 3D point within its coordinate system, modified spherical coordinates are used. Mapping function (2) restricts the tilt angle ϑ to $[-90, 90]$ and the pan angle φ to $[-179, 180]$ using the right-handed coordinate system shown in Figure 16. Together with the calculated camera pose this mapping function allows a fast, calculation cost-effective and accurate alignment on each marker-equipped robotic system within the STB.

$$\begin{aligned} \vartheta &= -\arctan\frac{z}{\sqrt{x^2+y^2}} && -90° \leq \vartheta \leq 90° \\ \varphi &= \begin{cases} \arccos\frac{x}{\sqrt{x^2+y^2}} & y \geq 0 \\ -\arccos\frac{x}{\sqrt{x^2+y^2}} & y < 0 \end{cases} && -180° < \varphi \leq 180° \end{aligned} \quad (1)$$

$$\text{with } x^2 + y^2 \neq 0$$

3.2 Automatic Robot Tracing using a Gantry Crane

The gantry crane's purpose is to autonomously trace the scout during movements in the slope in order to

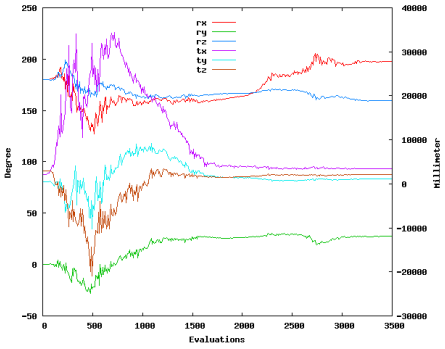

(a) Optimization of the extrinsic parameters

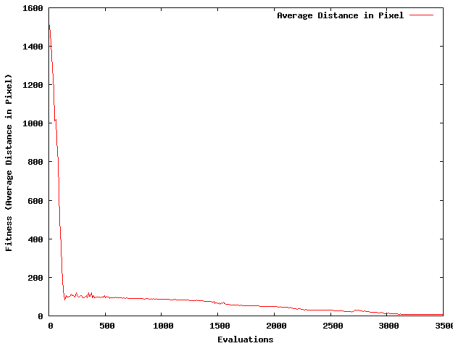

(b) Fitness optimization from a distance of 1509.54 to 6.79 pixel (4446 evaluations in 0.08 seconds)

Figure 15. Optimization of the extrinsic parameters using CMA-ES and camera coordinate systems

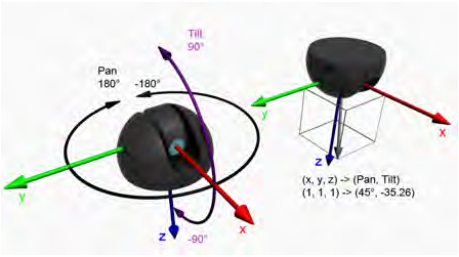

Figure 16. Coordinate system of the PTZ cameras in standing and hanging orientation, direction of rotation, and an example mapping on point (1,1,1)

maintain a constant top view. In LUNARES , the crane is used only for documentation, but in later projects it can be used to provide a simple simulation of lower gravity for the robot by using a counterweight and deflection rollers. Therefor, it is crucial for the gantry crane to reside over the robot all the time, even when the robot is moving. A tracking camera is utilized to capture the infrared light reflected from a retro-reflective marker on the robot and emitted from an IR source, mounted next to the camera.

The detection algorithm (Section 3.1) is used to determine the marker position in the tracking camera image. The center position of the marker has to be kept on a constant reference position in the image in order to automatically trace the robot. Since the gantry crane needs absolute desired positions as control input, a transformation from image to world coordinates is necessary.

If the actual position of the robot is used directly for the new desired position of the gantry crane, an error would remain, which is proportional to the speed of the robot. This is due to the time the gantry crane needs to reach the desired position, while the traced robot is still moving. For this reason, the velocity of the robot has to be taken into account. The velocity is calculated using the actual position and the last known position as well as the time between measurements which is defined by the control frequency of the gantry crane. A constant speed between two measurements is assumed.

However, the gantry crane is not designed for realtime interactions. The control frequency is limited to 4 Hz and a delay between command and action of around 0.5 s can be observed. In order to cope with uncertainties and to realize a smooth tracing, a particle filter similar to [21] is used.

The algorithm uses a linear perceptual model. This improves the dynamic behavior compared to a Gaussian weighting. Afterwards, a resampling step filters out poor predictions and draws new ones. The motion model uses the actual velocity added with Gaussian noise and position to move each particle. The new desired position results from the average of all particle positions.

4 Sample Retrieval from a Permanently Shadowed Lunar Crater

In this section, a reference mission for the LUNARES scenario is presented, then the steps of the LUNARES

demonstration mission are described. Additionally, three key elements of the mission are described in detail: Section 4.3 displays the exchange of rover's payloads and the handling of the sample container through the lander's manipulator arm. Section 4.4 demonstrates the autonomous docking of rover to lander and scout to rover. Finally, Section 4.5 shows how the sample pick up in the crater bottom is accomplished.

4.1 Reference Mission

The choice of a lunar mission, which is used as reference for the system of LUNARES and its successors, is established with the help of the following selection criteria (ordered by importance):

1. Maximum scientific payload possible
2. Realisation of the mission in a realistic time frame
3. Visionary character, specifically the inventiveness level
4. Public Outreach Value

Some robotic missions which are in the long term planning (e.g. the ones that are necessary for the build up of a lunar infrastructure for a permanent lunar base), are seen as non-realistic in the near future and from the standpoint of science they are seen as unattractive. Because of this, missions which are orientated around "hot" scientific topics are given the priority. The mission objectives of this narrowed choice of missions are:

1. Deployment of a Geophysical Environment Package (GEP) with seismometers and thermal fluxsensor.
2. In-Situ analysis of soil samples or sample return to a central measurement station (e.g. GeoChronology, interstellar particles in the lunar regolith)
3. Sample-return mission for samples from the landing zone (Measurement station on the Lander or with a sample-return module)
4. Radio telescope, more specifically an antenna array for radio science
5. Measurements in the earth magnetic field tail
6. Astro-habitat with biological experiments in a radiation environment

From this list, mission 2 was chosen. In addition, the possibility for a sample-return mission was investigated. As destination for the mission, the rim of the Shackleton Crater has been chosen (Figure 17).

The mission profile foresees that a wheeled rover drives to the rim and deploys a walking robot. After this the walking robot descents into the crater and takes a sample in the shadowed area, which it takes back to the wheeled rover. After this, the walking robot is merged with the wheeled rover again and the combination drives back to the lander. After arrival, the lander's robotic arm takes the soil sample and places it in the central analysis unit or in the sample-return vehicle.

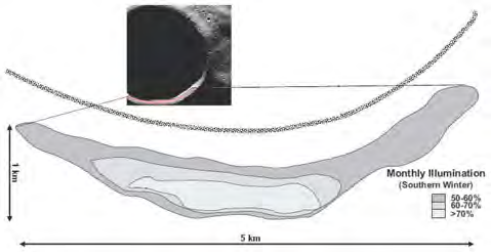

Figure 17. Illumination Characteristics at the Shackleton Crater Rim, picture taken from [4].

4.2 LUNARES Demonstration Mission

Figure 18 illustrates the demonstration scenario in eight subsequent steps. The following paragraphs give a more detailed description of each step, and thus provide a detailed summary of the complete LUNARES demonstration scenario.

Starting Position
The landing procedure on the surface of the moon is not part of the LUNARES demonstration. Also, due to space limitations, the rover egress is not addressed. Instead, the demonstration scenario starts after the rover has been deployed on the lunar surface. For the demonstration the rover is in view distance to the landing unit simulating the arrival of the rover from another mission part in order to be reconfigured for the next part. Figure 18(a) shows the start configuration.

Rover Docks to Landing Unit
The rover has to be equipped with payloads from the lander. For that purpose the docking procedure between lander and rover has to be initiated. Initially, the lander extracts the rover's relative position and generates a trajectory for the rover. Then, the lander leads the rover into the workspace of the lander's manipulator to allow for payload exchange, see Section 4.4 for more details.

Payload Exchange on the Rover
After reaching the workspace of the lander's manipulator, the rover is equipped with a payload (P/L)

(Figure 18(b)). The P/L is picked from the lander and placed into a designated payload bay of the rover (Section 4.3). The payloads used in the demonstration scenario are mock-ups representing scientific instruments in a real mission. By equipping the rover with different payloads, it is possible to configure the system for the current mission at hand.

Movement of Rover and Scout to the Crater Rim
When the rover is equipped with a new P/L, rover and docked scout drive towards the crater rim. In principle, the rover is able to negotiate moderately rough terrain and can travel longer distances in an energy efficient way compared with the legged scout. However, due to space constraints in the LUNARES mission the distance to be covered by the rover is limited to several meters. Figure 18(c) illustrates rover and scout collectively driving towards the crater's rim.

Undocking of Scout and Rover
Once the unit consisting of rover and scout arrived at the crater rim, the scout undocks from the rover (Figure 18(d)). The docking adapter allows the scout's deployment onto the surface. The process of detaching the scout from the rover is described in Section 4.4.

Scout Descends into Crater
After the undocking, the scout has to overcome the crater rim (Figure 18(e)) and enter the dark interior of the crater. To arrive at the crater bottom the scout has to safely climb down the crater slope which is covered with small rocks and small impact craters. In the LUNARES mission the movements of the scout in the crater slope are remotely controlled by an operator, using the camera which is mounted on top of the scout.

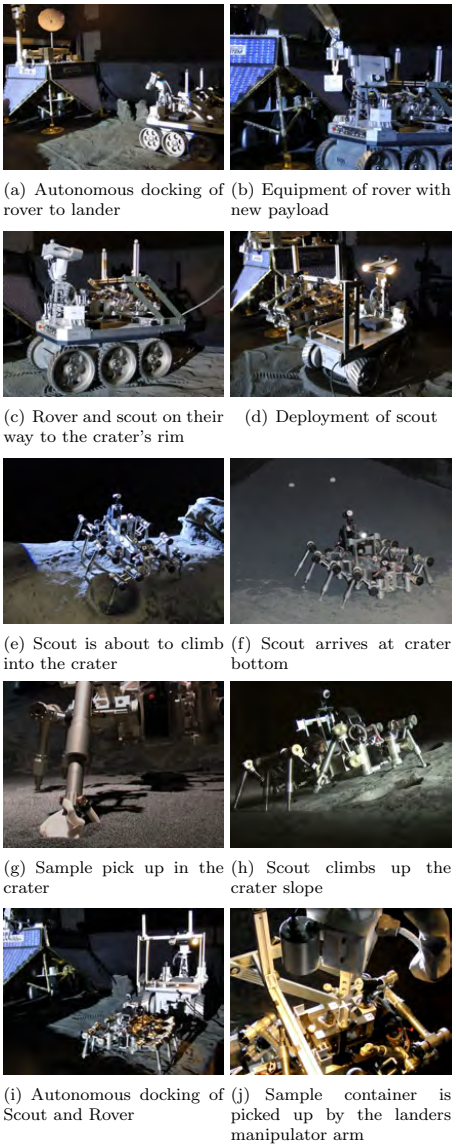

(a) Autonomous docking of rover to lander
(b) Equipment of rover with new payload
(c) Rover and scout on their way to the crater's rim
(d) Deployment of scout
(e) Scout is about to climb into the crater
(f) Scout arrives at crater bottom
(g) Sample pick up in the crater
(h) Scout climbs up the crater slope
(i) Autonomous docking of Scout and Rover
(j) Sample container is picked up by the landers manipulator arm

Figure 18. Scenes from the LUNARES sample return demonstration mission

Sample Collection at Crater Bottom
After arriving at the crater bottom (Figure 18(f)) a scientific operator chooses a geological sample using the video image provided by the scout. The scout positions itself in front of the selected sample, using a visual servoing approach (Section 4.5). When the coarse positioning is done, the scout executes a fine detection of the samples's coordinates by making use of its laser scanner (Section 4.5). When the coordinates of the sample are determined, a leg is used as manipulator to place the sample into a sample container on the scout's back (Figure 18(g)).

Scout Climbs Back up the Crater
When the sample has successfully been collected and stored in the sample container, the scout starts to climb the crater slope and back towards the rover. The scout climbs freely in the crater slope (Figure 18(h)), i.e. no tethering system is applied. However, it remains remotely controlled.

Cooperative Docking of Rover and Scout
After arrival at the rover, the scout turns its back to the rover (Figure 18(i)) to prepare for the autonomous docking procedure as described in Section 4.4. For this procedure, the rover detects the four markers on the scout and commands the scout into a predefined docking pose. When the scout is in the correct pose, the hook of the docking adapter is lowered so that the scout is able to hang itself into the hook.

Return of Rover and Scout to Landing Unit
Similar to the initial procedure, rover and scout collectively drive back to the landing unit using the docking procedure between rover and lander. The docking process ends, when the rover and thus the scout's sample container are within the workspace of the lander's manipulator arm.

Transfer of Sample Container to Landing Unit
The last step of the LUNARES demonstration mission consists of unloading the sample container from the docked scout (Figure 18(j)) and to transferring the sample onto the landing unit. The process is performed autonomously, a visual servoing approach allows to determine the exact position of the sample container with respect to the manipulator (see Section 4.3).

4.3 Automatic Payload Exchange

One of the main goals of the LUNARES system and the corresponding reference mission was to demonstrate the cooperation between a team of heterogeneous robotic subsystems all working together in order to achieve a common goal – collecting a sample from the inner of a lunar crater and returning the sample to the lander for further analysis.

For this purpose, the robotic subsystems had to be reconfigured by the system. One example is the exchange of payload dummies. The most important step concerning the exchange of payloads is the return of the sample container to the lander.

Manipulation is based on a visual servoing approach [18], avoiding the need for a thoroughly performed calibration of the camera systems. However, instead of calibration, a teaching phase is necessary which replaces the calibration.

The LUNARES visual servoing approach detects visual markers in monocular camera images. The markers are black filled circles on white background with a binary ring code around the circle. An adaptive binarisation technique followed by blob analysis generates a set of marker hypotheses which can be identified very robustly by their ring codes. Every image contains a set of n markers $\{(m_x^1, m_y^1)^T, \cdots, (m_x^n, m_y^n)^T\}$. For any static scene, the locations of these markers only depend on the configuration of the manipulator as long as the camera is mounted to the end effector. Thus, the marker locations can be regarded as the result of the perceptual kinematic map π (PKM):

$$\pi : \mathbb{R}^6 \to \mathbb{R}^{2n}, \quad c \mapsto (m_x^1, m_y^1, \cdots, m_x^n, m_y^n)^T. \quad (2)$$

where

c :	$(x, y, z, \alpha, \beta, \gamma)$
x_r,y_r,z_r:	robot coordinates (WKS)
α,β,γ:	rotation around x_r,y_r,z_r-axis
m_x^n, m_y^n:	x/y-image coordinates of the n-th feature

The grasping can be solved as a fixed movement starting from a well-known reference position $c_0 \in \mathbb{R}^6$. Therefore, the task of grasping reduces to the recovery of the reference position. By linearizing the PKM around that reference configuration c_0, the following direction $\Delta(c)$ in the configuration space is obtained. Moving the end-effector in that direction minimizes the differences between the current marker locations and marker locations of the reference image.

$$\Delta(c) = \left(D\pi(c_0)^T D\pi(c_0)\right)^{-1} D\pi(c_0)^T \cdot (\pi(c_0) - \pi(c)). \quad (3)$$

The Jacobian $D\pi(c_0)$ can be determined by applying test movements along all six directions. Figure 19 depicts the result of the visual servoing approach for a payload with four markers attached.

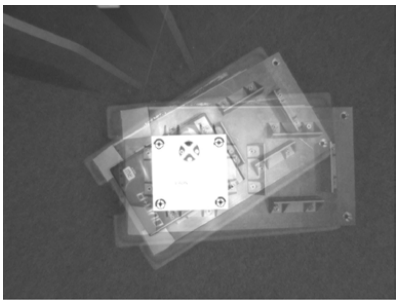

Figure 19. Overlay of the reference image used for the teaching process of the Jacobian and the image of the camera view after successful control of the manipulator. The visual servoing was able to perfectly align the marker locations whereas the differences of the background clearly show the different situations.

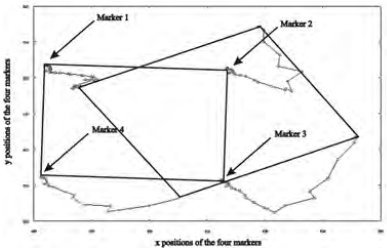

Figure 20. Positions of the markers in the image plane tracked during the visual servoing process.

Figure 20 shows the movements of the visual markers during the visual servoing process. The process runs on standard PC hardware (Intel Core 2 Duo) at 10 Hz and requires approximately 10 s for convergence. The accuracy is high enough to perform a "blind grasping" through a predefined trajectory afterwards.

4.4 Autonomous Docking Procedures

In the LUNARES reference mission, the global mission goal is achieved by splitting the task into several sub tasks which are solved by specialized robotic subsystems. For instance, the required high degree of mobility is achieved by splitting up the requirement into two different mobility systems the rover for larger distances in moderate terrain and the scout for shorter distances in more difficult terrain.

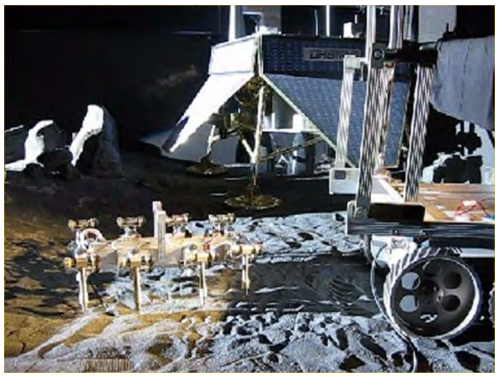

Figure 21. Typical situation for the docking between the scout and the rover.

This splitting however, requires new capabilities of the robotic subsystems. In this section two autonomous and also cooperative behaviors of the robotic subsystems shall be discussed. The first behavior is the docking between the scout and the rover which is required after the scout has returned from its crater exploration. Second is the autonomous docking of the rover to the lander in order to reach a working position from which the lander manipulator can reach the sample canister.

Docking of Scout to Rover

The scout and the rover have not been specifically designed for a docking procedure. However, the LUNARES mission required the scout to dock to the rover. Different possibilities for docking procedures have been evaluated, e.g. such as the scout walking onto the rover.

Here we present the final choice for the docking procedure, which requires the scout to approach the rover by stepping backward. This eliminates the possibility to use the scout's visual sensors for the docking procedure. Instead, the vision system of the rover acquires images of the docking scout and generates correction manoeuvres of the scout to reach a certain goal position. From there a mechanical hook is able to lift the scout to the back of the rover.

The autonomous docking procedure has to perform within given constraints. These constraints depend on the mechanical docking mechanism, i.e. the docking adapter. The adapters capability to deal with position errors and to compensate for such errors define with what precision the scout has to get to the target position. In order to increase robustness of

the given docking scenario we identified three critical elements: (1) the predefined actions of the docking procedure, (2) design of the docking adapter and its ability to compensate for alignment errors, (3) fallback safety range for scout's pose correction.

While predefining the actions, the docking procedure has to account for errors in the x-alignment as well as in the z-alignment within some limitation[2], i.e. the final procedure requires security distances for the mechanical docking, so that the risk of a collision of docking adapter and the scout's docking handle is minimized. Eventually and for a worst case scenario, the scout has to maintain a fallback range for manual pose correction leading to the semi-autonomous docking approach.

The overall docking procedure comprises multiple steps. For the start of the docking procedure the rover's camera requires capture the scout and the visual markers attached to the scout. Then, the rover takes control of the scout movements by applying a visual servoing approach. The control target is to reach a certain target position with the scout such that the position of the visual markers is identical to the marker positions of a reference image which has been taken during a teaching phase of the visual servoing approach. The visual servoing approach is exactly the same as described in Section 4.3.

A training phase is required to generate the Jacobian matrix of the PKM to linearise the mapping function around the target configuration. For that purpose several test movements along six different degrees of freedom in positive and negative directions have been performed to setup the Jacobian of the PKM. As a controller we utilized a proportional controller.

Once the position has been successfully reached, a number of predefined actions will be executed[3]:

1. scout shifts its body forward (approx. 2 cm away from the rover), to increase the clearance between its handle and a lowered hook,

2. moving down the docking adapter including a clearance distance (approx. 3 cm),

3. scout shifts its body backward (approx. 5.5 cm) to guarantee that the scout's handle has contact to the lowered docking adapter's hook,

4. docking adapter lifts the scout (12°) just so that the scout's legs do not touch the ground anymore,

[2]The coordinate system is depicted in Figure 9

[3]Since the scout has play in joints the distances of the pose changes are only approximate.

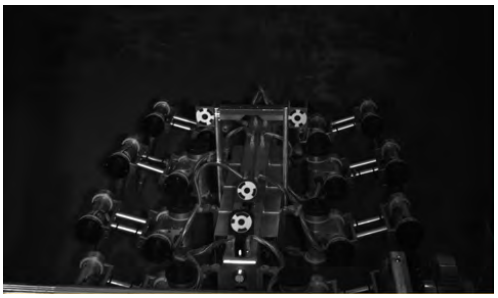

Figure 22. The scout as seen from the rover camera. The coded ring markers are clearly visible in the image and extracted from the rover's image processing system.

5. scout folds its legs into docking position so it can be loaded onto the rover,

6. docking adapter lifts the scout into its final docking position.

The docking procedure will be performed with disabled reflexes, to allow for the predefined posture setting.

Docking of Rover to Lander

The second autonomous docking manoeuvre concerns the placement of the rover in front of the lander in order to achieve a sufficiently precise starting point for the manipulation and sensor based grasping of the payloads or the sample canister. For that purpose a certain accuracy of the rover position in front of the lander has to be reached.

The docking between rover and lander is solved by utilization of the lander's sensor system. Here, the lander acquires a range image from the 3D laser scanner providing two types of information: (1) 3D information for every pixel, and (2) the intensity of the reflected laser pulse. Especially the latter enables the detection of special retro-reflective targets in the scene. Four of these visual markers have been placed at the rover and can easily be detected by the rover to lander docking skill. Using the 3D positions of the detected markers, a graph matching method [6] has been implemented to assure an identification of the single markers, Figure 23. Finally, a pose estimation of the rover with respect to the lander system is obtained.

Using this pose information, a spline trajectory is planned to reach the desired target position from the current pose of the rover. However, due to drift errors

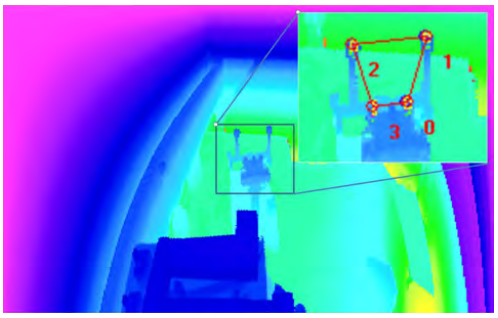

Figure 23. Laser scan image with detected marker configuration for graph matching

in the rover's odometry, that trajectory is only iteratively executed. In one step, the rover only drives along half the pre-planned trajectory. After that distance, a new measurement with the 3D laserscanner is applied and a new trajectory is planned.

This process is repeated until the distance between target position and current position is below a certain threshold. If the position has been reached, the orientation is corrected in a similar manner. After 3-4 iterations, the rover reaches the target with a precision of about 2 cm which is sufficient for further reconfiguration steps and the unloading of the sample canister.

4.5 Sample Pick Up by a Legged Scout System

Before collecting samples, the robot has to position itself in front of an sample of interest. This sample is selected by a human operator using a graphical user interface. Afterwards, the robot starts an automatic approach to the sample until the scout is close enough to grab the sample.

The approach is vision based and utilizes a single camera with an analog transmitter and receiver. Due to limited processing power on the scout robot itself, the computer vision algorithms are executed on an external processing system, a flight system would have to embed such system into the deployed robots itself. Wireless transmission is used for the camera images. Transmission can be easily affected by other wireless systems, and result in image distortions. To cope with these distortions a particle filter was used to track the sample's position in the camera image.

The sample detection process can be separated into three steps:

1. Detect the object
2. Update the particle filter with the position in the image (if detected)
3. Control the scout's movements

Step one is accomplished currently by a threshold on image brightness, it is assumed that samples of interest have different color compared to "regular" stones in the scenario. After selecting the sample of interest, the characteristics are saved and used to find the same object in subsequent images. After the threshold was applied to the camera image, fitting objects are searched beginning at the expected position of the object. The starting point is extracted from the particle filter, which includes a movement model of the object in the camera images.

Only if an object fitting to the characteristics of the selected sample is found, the particle filter and its movement model are updated (step two).

The final step is the control of the scout. Depending on the object's distance to the target area (the area where the gripper can reach the sample), values for the forward speed and turn values are set appropriately.

Figure 24 shows a labeled camera image of the approach, extracted objects are highlighted in the image (green colored areas from brightness threshold), the points are the single particles of the particle filter, the cross marks the expected position of the sample extracted from the particle filter and the box marks the target area where the robot stops moving when the sample resides in that box for some time. The only light comes from some infrared diodes attached to the camera on scout's back (bright spot is visible in the image).

When the robot reaches its final position, it notifies the Ground Control Station, which then can initiate the actual collecting procedure. After finishing the approach, the location of the target sample has to be determined with high precision to allow for sample pick up. It can be assumed that the manipulation will take place in a planar environment. Hence, that target sample can be easily determined after generating a height map of the environment, given a certain region of interest (ROI). One of the influencing factors for the ROI is the accuracy of the approach. Experiments showed that manipulation works best for sample distances of 22 cm in a straight line of the scout's right thorax joint ('shoulder' joint). This knowledge allowed the definition and extraction of the ROI. Currently a target area of 121 cm^2 (11 cm×11 cm) applies.

The scout uses the mounted laserscanner driven by a servo motor to extract an distance image of the environment, which is subsequently transformed into a height map. The essential procedure to extract a sample's position consists of the following steps:

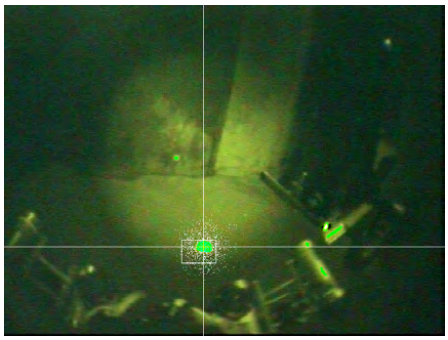

Figure 24. Labeled camera image of the approach action (post processed in brightness and contrast). Around the green highlighted object to approach to, the particles of the filter are displayed as white dots. The approach ends, when the object is completely in the goal region (white rectangle)

1. Extraction of a laser scan of the direct environment within a horizontal range of ±30°
2. Transformation of the scan data from the world coordinate system into the robot coordinate system
3. Generation of the height map in the robot coordinate system
4. Extraction of the region of interest, defining the allowed manipulation area of the scout
5. Extraction of the local minimum within the ROI
6. Extraction of the region around the local minimum to extract the likely target center

The height map is actually transformed into a grey scale image to allow further processing steps such as median filtering (Figure 25). During the sample pickup process the operator can get hold of the images and validate the extracted final target position. If no object can be extracted, the operator will receive an error message. Additionally, if the operator identifies a false positive, he can initiate a second scan.

5 Potentials for a Real Lunar Mission

The realisation of a robotic Moon mission necessitates the timely development and qualification of a series of technologies, which do not possess the required high development status. More precisely, for the start of

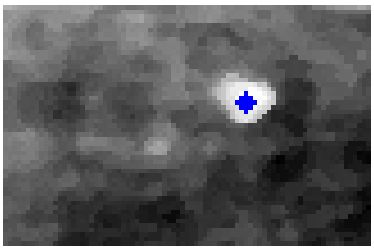

Figure 25. Resulting grey scale image. The centre of the detected sample is marked by an diamond-shaped marker.

Phase C (actual mission planning), a TRL (technology readiness level) of 5 - 6 is required, representing a technology demonstrator or prototype which has already been tested in a representative environment. The identification of technologies which do not have a sufficient TRL level is necessary to minimize the technical and programmatic risks associated with a system development.

In the LUNARES study critical technologies and requirements for the realisation of a multiple-configuration robotic concept were investigated and a stepwise plan for the development was elaborated.

For the LUNARES project, three mission classes have been investigated:

1. Single Moon exploratory missions, e.g. for spectral analysis of surface samples from a Moon crater or even sample return of these samples.
2. The construction of a scientific Moon infrastructure
3. Cargo transportation for support of human missions

For handling of surface samples by the walking robot and the lander, an appropriate gas tight moveable sample container has to be developed. By this it can be ensured that no volatile gases are lost during transport from crater bottom to landing unit.

For the lander, the rover, and the walking robot a higher-level system control of the board computer via an appropriate ground station for automation and robotics has to be developed.

For appropriate programs for technology verification, the DLR program On-Orbit-Verifikation (OOV[4]) is very suited. For this program the German Small Satellites Platform TET[5] can be used. On

[4] http://www.dlr.de/rd/en/desktopdefault.aspx/tabid-2265/3376_read-9781/
[5] http://www.dlr.de/rd/en/desktopdefault.aspx/tabid-2274/3396_read-5085/

the ESA side, there is the Technology Research Programme (TRP), which is specifically for early technology development, or the General Support Technology Programme (GSTP), which is for the development of more developed technologies for market ready products. The following demonstration methods for components, subsystems or the complete LUNARES follow-on system are applicable:

- Software-based simulations
- Earth-based component tests
- Piggy-back Technology Flight Opportunities for component in-orbit tests
- Test campaigns for system prototypes on the Earth

For the qualification and testing philosophy, the classical qualification with structure- and thermal models, engineering model, qualifications model (QM) as well as a flight model (FM) is recommended.

6 Conclusion and Outlook

The project LUNARES provides a terrestrial demonstrator to evaluate the feasibility of a heterogeneous robotic team for lunar crater exploration. Existing robots not specifically designed for the chosen mission scenario have been employed.

The systems came from different project partners. Despite the differences concerning hardware as well as control approaches of the systems, an overall system containing the different subsystems was successfully implemented in the presented project. In numerous demonstrations the combination of the various subsystems were constituted successfully.

For the purpose of experiments and demonstrations, an artificial lunar crater environment comprising realistic slopes and illumination has been established in the project. The testbed is equipped with various surveillance sensors such as video cameras and a motion tracking system. Automated experiment documentation has been implemented in the testbed.

A docking procedure for a walking machine and a wheeled rover was developed. It is based on visual information from the rover's camera system, which is used to control the legged scout. Furthermore, a docking procedure allowing the precise placement of a rover in front of a landing unit was developed using the lander's sensor system. For exchanging payloads and sample containers between rover, scout, and landing unit, visual servoing methods were implemented.

During the project, important experiences with locomotion of walking machines in crater environments were made and the locomotion principle was significantly improved. With appropriate control mechanisms even the Scorpion robot, not explicitly designed for this terrain, was able to climb in the artificial crater with slopes of up to 35°. The locomotion was safe and reliable, even with leg failure, the robot could negotiate the slope with the remaining seven legs.

Overall, LUNARES successfully demonstrated the feasibility of the chosen approach. In the project RIMRES we want to further pursue the idea of heterogeneous robotic systems. Here mobile systems will be newly developed in a co-design process. This allows for a closer coupling between rover and scout. A standardized mechatronic interface and a connection providing interfaces for exchange of data and energy will be developed. An additional focus will be the modularity of the system, several payload modules, each equipped with the mechatronic interface, will be developed.

References

[1] James R. Arnold. Ice in the lunar polar regions. *Journal of Geophysical Research (JGR)*, 84(B10):5659–5668, September 1979.

[2] P. Bartlett, D. Wettergreen, and W. L. Whittaker. Design of the scarab rover for mobility and drilling in the lunar cold traps. In *International Symposium on Artificial Intelligence, Robotics and Automation in Space*, February 2008.

[3] Andrew J. Coates. Limited by cost: The case against humans in the scientific exploration of space. *Earth, Moon, and Planets*, 87(3):213–219, 1999.

[4] Doug Cooke. Exploration lunar architecture. In *Proceedings of the NASA Advisory Council Workshop on Science Associated with the Lunar Exploration Architecture*, Feb. 27–March 2, 2007 2007.

[5] Florian Cordes, Steffen Planthaber, Ingo Ahrns, Timo Birnschein, Sebastian Bartsch, and Frank Kirchner. Cooperating reconfigurable robots for autonomous planetary sample return missions. In *ASME/IFToMM International Conference on Reconfigurable Mechanisms and Robots (ReMAR-2009)*, London, United Kingdom, June 22-24 2009.

[6] Thomas H. Cormen, Clifford Stein, Ronald L. Rivest, and Charles E. Leiserson. *Introduction to Algorithms*. McGraw-Hill Higher Education, 2001.

[7] Alexander Dettmann, Stefan Haase, and Frank Kirchner. Automatic robot supervision within a lunar crater environment. In *Joint 41st International Symposium on Robotics and 6th German Conference on Robotics (ISR Robotik-2010), June 7-9, Munich, Germany*, Munich, Germany, 2010.

[8] W. C. Feldman, S. Maurice, A. B. Binder, B. L. Barraclough, R. C. Elphic, and D. J. Lawrence. Fluxes of fast and epithermal neutrons from lunar prospector: Evidence for water ice at the lunar poles. *Science*, 281:1496–1500, September 1998.

[9] L. Ferrarini and E. Carpanzano. Reference models for the supervision and control of advancedindustrial manipulators. In *American Control Conference*, volume 4, pages 2440–2444, 1999.

[10] C. Fiorio and J. Gustedt. Two linear time union-find strategies for image processing. *Theoretical Computer Science*, 154(2):165–181, 1996.

[11] N. Hansen and A. Ostermeier. Completely derandomized self-adaptation in evolution strategies. *Evolutionary Computation*, 9(2):159–195, 2001.

[12] T Huntsberger, A Stroupe, H. Aghazarian, M. Garrett, P. Younse, and M. Powell. Tressa: Teamed robots for exploration and science on steep areas: Field reports. *J. Field Robot.*, 24(11-12):1015–1031, 2007.

[13] Bernhard Klaassen, Ralf Linnemann, Dirk Spenneberg, and Frank Kirchner. Biomimetric walking robot scorpion: Control and modeling. In *Robotic and Autonomous Systems Journal*, 2002.

[14] Ralf Linnemann, Bernhard Klaassen, and Frank Kirchner. Walking robot scorpion - experiences with a full parametric model. In E.J.H. Kerckhoffs, editor, *15th European Simulation Multiconference: Modelling and Simulation*, pages S.1012–1018, Prague, Czech Republic, June 6-9 2001. International Society for Computer Simulation -SCS-.

[15] NASA.gov – Mini-RF. Exploring the lunar poles, March 2010.

[16] NASA.gov – Mission Update. Lcross impact data indicates water on moon. NASA Homepage, 11/2009.

[17] S. Nozette, C.L. Lichtenberg, P. Spudis, R. Bonner, W. Ort, E. Malaret, M. Robinson, and E. M. Shoemaker. The clementine bistatic radar experiment. *Science*, 274:1495–1498, November 1996.

[18] A. C. Sanderson and L. E. Weiss. Adaptive visual servo control of robots. *Robot Vision*, pages 107–116, 1983.

[19] J. Schwendner, F. Grimminger, S. Bartsch, T. Kaupisch, M. Yuksel, A. Bresser, J. Bessekon Akpo, A. Dieterle, S. Schmidt, M. Seydel, and F. Kirchner. Cesar: A lunar crater exploration and sample return robot. In *Intelligent Robots and Systems. IROS 2009*, St. Louis, Oktober 2009.

[20] D. Spenneberg, M. Albrecht, and T. Backhaus. M.O.N.S.T.E.R.: A new behavior–based microkernel for mobile robots. In *ECMR 2005*, 2005.

[21] S. Thrun, D. Fox, W. Burgard, and F. Dellaert. Robust monte carlo localization for mobile robots. *Artificial Intelligence*, 128(1-2):99–141, 2001.

[22] Gianfranco Visentin. Autonomy in ESA Planetary Robotics Missions.

[23] Kenneth Watson, Bruce Murray, and Harrison Brown. On the possible presence of ice on the moon. *Journal of Geographical Research (JGR)*, 66(5):1588–1600, 1961.

[24] David Wettergreen, Dominic Jonak, David Kohanbash, Scott Jared Moreland, Spencer Spiker, James Teza, and William (Red) L. Whittaker. Design and experimentation of a rover concept for lunar crater resource survey. In *47th AIAA Aerospace Sciences Meeting Including The New Horizons Forum and Aerospace Exposition*, January 2009.

[4]: **Static Force Distribution and Orientation Control for a Rover with an Actively Articulated Suspension System**
F. Cordes, A. Babu, F. Kirchner
in: IROS 2017 ©IEEE 2017

Static Force Distribution and Orientation Control for a Rover with an Actively Articulated Suspension System

Florian Cordes[a], Ajish Babu[a], and Frank Kirchner[a,b]

***Abstract*— This paper presents the control strategies used to adapt the actively articulated suspension system of the rover SherpaTT to irregular terrain. Experimental validation of the approach with the physical system is conducted and presented. The coordinated control of the legs constituting the suspension system is encapsulated in a Ground Adaption Process (GAP) that operates independently from high level motion commands. The GAP makes use of force and orientation measurements to control the suspension system with 20 active degrees of freedom. The active suspension is used to achieve multi-objective terrain adaption encompassing (i) active force distribution at the wheel-ground contact points, (ii) keeping all wheels in permanent ground contact, and (iii) body orientation w.r.t. gravity.**

I. INTRODUCTION

Currently, planetary exploration is conducted exclusively by robotic means. Stationary landers with manipulators, scoops and remote sensing devices provide the possibility to collect information around a fixed landing site, one such example being the Phoenix lander on Mars [9].

A substantially larger area can be explored using mobile robots. For stable and robust locomotion an adaption to the irregular surface (dunes, slopes, boulders, soft soil, hard soil, etc.) is mandatory. Passive suspension systems allow an adaption to the ground with comparatively low complexity and little or no computational effort. Suspension systems as the triple bogie ExoMars suspension [6] or the well-known rocker-bogie suspension (as used for example in all four successfully deployed Mars rovers, [4, 5, 7]) are examples for passive suspensions providing a good terrain capability. In case of the rocker-bogie suspension, a differential reduces the angles experienced at the rover's body due to sloping terrain and climbing boulders. The size of obstacles that can be overcome is in the range of the wheel's diameter. To climb an obstacle with a wheel, the suspension system needs the other wheels to provide enough traction in order to push the wheel up the obstacle. Once stuck in soft soil or with a wheel in a crevice it might be hard for a system with passive suspension to free itself from that situation, as can be seen for example with the Spirit rover[1]. Furthermore, high peak rim thrusts that are far from the nominal thrust in regular operation have to be provided to drive a wheel vertically out of such a hole with up to half of the vehicle's weight on that wheel [12].

Fig. 1. SherpaTT in an artificial crater environment. Inset shows compact stow pose.

Current research is also directed towards active suspension systems for mobile robots. Active suspension has the potential to deliberately influence the robot's center of gravity, distribute forces between wheels, lift wheels off of the ground, or actively control the body's pose, e.g. roll and pitch w.r.t. a plane perpendicular to gravity. Hence, being more complex in general, an actively articulated suspension can yield substantially improved rough terrain mobility.

JPL's Sample Return Rover (SRR) is able to articulate its two shoulder joints in order to actively conform to sloping terrain [3]. By changing the suspension geometry, the position of the center of mass w.r.t. to the support polygon can be changed. In the experiments described in [3], the rover (1) drove a short traverse with a fixed suspension, and (2) stopped for adjustment of the suspension according to a planned sequence and then repeated (1)-(2) for the test track. A comparison of the stability margin with a fixed suspension showed a vast improvement with the articulated suspension.

The ATHLETE family of rovers [12] makes use of a fully actuated suspension without passive elements in the legs, apart from the flexible wheels. Each leg of a robot has six (seven in case of Tri-ATHLETE) active Degrees of Freedom (DoFs) to achieve active terrain adaption. Variances in absolute and relative position encoders are used to estimate the joint torques and an Inertial Measurement Unit (IMU) in the central body is used to measure the orientation of the central platform.

There are many more systems with active suspension to be found in the literature. An all-encompassing literature survey would be beyond the scope of this paper; [2] provides more literature concerning active and passive suspension systems.

*This work is part of the project TransTerrA and funded by the German Space Agency (DLR, Grant number: 50RA1301) with funds of the Federal Ministry of Economics and Technology (BMWi).

[a]DFKI Robotics Innovation Center Bremen, Bremen, Germany `firstname.lastname@dfki.de`

[b]University of Bremen, Faculty 03: Mathematics/Computer Science, Bremen, Germany

[1]`http://mars.nasa.gov/mer/mission/status.html#spirit`

This paper focuses on the rover SherpaTT, which is part of a multi-robot exploration system, built for and tested in an earth bound demonstration scenario [10]. Fig. 1 shows the rover in an artificial crater environment. The rationale for developing the active suspension system in SherpaTT is twofold: (i) the suspension design allows high terrain mobility for the rover, with active influence on the center of gravity's position in three dimensions, control of contact forces at wheel-ground contact points (load distribution), and orienting the main body irrespective of the terrain and (ii) the design allows the body to be moved with the wheels not changing their position on the ground. Hence, the system is able to deploy and pick up other compatible modules with its bottom electro-mechanical interface [10]. With the force sensors directly in the legs and an orientation measurement in the body, the complex system can be controlled with a minimal set of inputs. All leg movements for ground adaption can be done without the need to stop for reconfiguration of the legs. All controls demonstrated in this paper are based on these low-level sensors and a reactive control approach. Path planning for the system or suspension configuration planning is not needed for ground adaption and consequently not part of this work.

Controllers for actively articulated robots can be found in the literature. Wheeler in [11] develops a compliance model for wheel deflection to be used with walking gaits. In [8] Reid uses an RGB-D sensor to generate a terrain map and perform ground adaption using this information. In contrast to this high-level approach, in this paper, we discuss the solution with force measurement in each wheel and hence vastly simplified control, without relying on complex modeling and sensor processing.

II. MOTION CONTROL SYSTEM

This section gives an overview of SherpaTT's *Motion Control System (MCS)*. The DoF of the suspension system are described along with the general mechanical structure. Furthermore, the design of the ground adaption controller and insights of data processing such as the estimation of an ideal force distribution on the four ground contact points is provided.

A. Suspension System Kinematics

The suspension system consists of four leg-like structures with a wheel at the end of each leg. Each of the legs has five DoF in total, Fig. 2. Due to the design of the legs, a four dimensional workspace for each leg is achieved (3D position, 1D orientation). The robot is able to change its footprint from nearly six square meters (square with $2.4\,m \times 2.4\,m$ edge length) down to around one square meter in its *stow pose*, see also inset in Fig. 1.

The *Pan* joint rotates the leg around its pivot point on the central body. This allows changing the foot print from long stance to wide stance or a square stance, the latter being the standard configuration, also referred to as cross-stance [1]. The two joints, *InnerLeg* and *OuterLeg*, are designed as parallelograms to keep the wheel parallel to the rover's body.

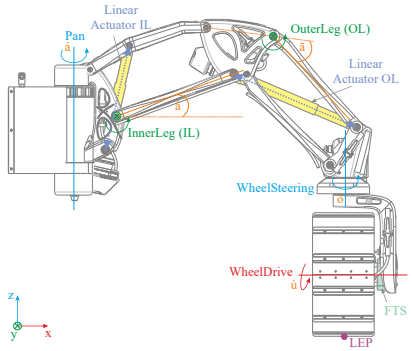

Fig. 2. Degrees of freedom of a suspension unit of SherpaTT, LEP, and location of the FTS.

Each parallelogram is equipped with a linear actuator. Using non-backdrivable linear spindle drives for actuation allows an energy-efficient self-locking, hence, the rover keeps its body height even when powered off. The *WheelSteering*-DoF is used for orienting the wheel while the *WheelDrive* actuator rotates the wheel to propel the robot and avoid wheel dragging during posture changes.

B. Overview of the Control Structure

An overview of the MCS is provided in Fig. 3. The control system has three main input classes, that can be used by human operators via a graphical user interface or from higher level processes (navigation, path follower and alike). The inputs encompass (i) a three dimensional motion command $\dot{\xi} = (\dot{x}, \dot{y}, \dot{\Theta})^T$ with velocities for forward, lateral and rotational movements of the robot, (ii) a footprint command consisting of four three dimensional vectors $\mathbf{g}_i$ ($i = \{0 \dots 3\}$), defining the relative position of each Leg End Point (LEP) to the body, and (iii) a footprint-independent six-dimensional body posture $\mathbf{b} = (x_b\ y_b\ z_b\ \Omega\ \Phi\ \Psi)^T$.

The inputs are fed forward to a drive mode module, generating wheel orientation φ_i and wheel velocity ω_i commands from the motion command and a LEP command generator, that merges the body posture command with the footprint command to a single LEP command $\hat{\mathbf{p}}_i$ for each leg i.

The LEP command is then sent to an interpolation module in order to generate smooth trajectories between actual LEP ($\mathbf{p}_i$) and (newly) commanded LEP. The active *GAP* (see next subsection) writes z-offsets that are added to the interpolated LEP commands to be finally written (as $\bar{\mathbf{p}}_i$) via an inverse kinematics module to the hardware.

C. Active Ground Adaption: Overview

The GAP is composed of different submodules. Each contributes to the ground adaption of the suspension system by reacting to measured sensor values, as indicated within the orange box in Fig. 3. The GAP's submodules calculate individual offsets for each of the four legs that are added to the actual LEPs before the inverse kinematics layer generates the joint command $\bar{\mathbf{q}}_i$. The two key components of GAP are

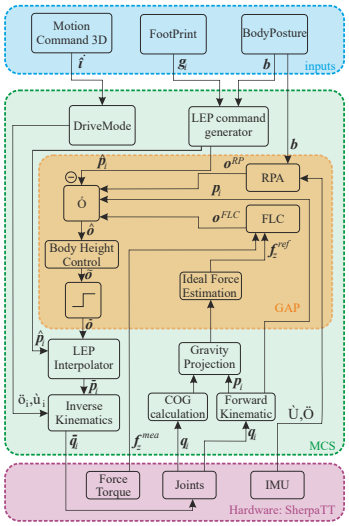

Fig. 3. Simplified structure of MCS with user/high-level inputs and details of the structure of the GAP (orange box)

the *Roll Pitch Adaption (RPA)* and *Force Leveling Control (FLC)* which ensure desired body orientation, and adequate wheel-ground contact, respectively.

The single offsets of RPA ($\mathbf{o}_i^{RP}$) and FLC ($\mathbf{o}_i^{FLC}$) are added in an accumulator module and then passed to the *Body Height Control* module that (i) removes common offsets from the legs (in case all accumulated offsets have the same sign), and (ii) limits the offsets such that the resulting LEP command is kept within the work space of a leg. By limiting the absolute offset outputs $\tilde{\mathbf{o}}$ in a saturation component, the final offsets $\bar{\mathbf{o}}$ for each leg are generated.

D. Force Leveling Control

The FLC component is implemented to maintain the expected force for each wheel in the current footprint, projected along the vector of gravity. The values measured from the force-torque sensors and the location of the Center of Gravity (CoG) within the support polygon are inputs to FLC. Note that the calculated "ideal" forces are those that are expected in the current foot print configuration of the robot, simply put, the closer the wheel to the body, the higher its load share. Ideal force distribution for locomotion improvement needs to change the location of the CoG within the support polygon. Driving up a slope, this might be achieved by shifting the robot's body upslope. Such a posture adaption is not the task of the FLC component.

The ideal forces are estimated under the assumption of static equilibrium with only the gravitational forces and their reaction forces from the ground acting on the robot. The static equilibrium assumption produces three constraint equations and four unknowns. This underdetermined system is solved using a Moore-Penrose pseudoinverse. By correcting each LEP's z-position with an offset o_i^{FLC} in order to match the measured forces with the expected forces, an optimal ground contact can be ensured for each LEP in the current posture of the robot.

For this goal, the LEPs and the CoG of the robot are projected onto a gravity perpendicular 2D plane using the IMU's attitude measurements. Let the position of the LEPs in the 2D plane be $\begin{pmatrix} x_i & y_i \end{pmatrix}^T$, with $i = \{0, 1, 2, 3\}$ representing each leg and the position of the CoG be $\begin{pmatrix} x_c & y_c \end{pmatrix}^T$. Let $\mathbf{t} = \begin{pmatrix} 0 & 0 & mg \end{pmatrix}^T$, be the vector consisting of zero-moments around x and y axis and gravitational force. Let the expected vertical reaction forces vector be $\mathbf{f}_z^{ref} = \begin{pmatrix} f_{z,0}^{ref} & f_{z,1}^{ref} & f_{z,2}^{ref} & f_{z,3}^{ref} \end{pmatrix}^T$ where $f_{z,i}^{ref}$ is the scalar value for each leg. The constraint equation for the static equilibrium case is given by

$$\mathbf{t} = \mathbf{A} \cdot \mathbf{f}_z^{ref} \tag{1}$$

where

$$\mathbf{A} = \begin{pmatrix} x_0 - x_c & x_1 - x_c & x_2 - x_c & x_3 - x_c \\ y_0 - y_c & y_1 - y_c & y_2 - y_c & y_3 - y_c \\ 1 & 1 & 1 & 1 \end{pmatrix} \tag{2}$$

Solving for $\mathbf{f}_z^{ref}$ yields

$$\mathbf{f}_z^{ref} = \mathbf{A}^+ \cdot \mathbf{t} \tag{3}$$

where $\mathbf{A}^+$ is the Moore-Penrose pseudoinverse for matrices with independent columns given by

$$\mathbf{A}^+ = \mathbf{A}^T \cdot (\mathbf{A} \cdot \mathbf{A}^T)^{-1} \tag{4}$$

$\mathbf{f}_z^{ref}$ is taken as reference input for FLC during each time step. The CoG is computed using the approximated inertial properties of the robot links. Inaccuracies in computation of CoG increase inaccuracy in the computation of ideal forces.

E. Roll-Pitch Adaption

The RPA component takes roll and pitch from the IMU data, and compares it against the desired roll Ω and pitch Φ for the body. The orientation error is computed in angle-axis form and used to compute the offsets o_i^{RP} necessary for roll-pitch correction. Let the orientation error be represented in angle-axis as $\{\mathbf{e}, \theta_e\}$, where $\mathbf{e}$ is the normalized rotation axis and θ_e is the rotation error in the Body Coordinate System. Since only roll and pitch errors are considered, $\mathbf{e}$ is always in the xy-plane. The desired offset for correcting the roll/pitch is dependent on the LEP's distance d_i to the rotation axis, while the sign is determined by the sign of θ_e and the LEP location $\mathbf{p_i} = \begin{pmatrix} p_{x,i} & p_{y,i} & 0 \end{pmatrix}^T$ in the xy-plane w.r.t. $\mathbf{e}$ ("left or right side").

$$o_i^{RP} = \pm d_i \tan\theta_e \tag{5}$$

$$d_i = \|\mathbf{e} \times \mathbf{p}\| \quad \text{because } \|\mathbf{e}\| = 1 \tag{6}$$

$$o_i^{RP} = \text{sgn}(\mathbf{p} \cdot \mathbf{n}) \, \|\mathbf{e} \times \mathbf{p}\| \, \tan\theta_e \tag{7}$$

where $\mathbf{n_i}$ the normal of the plane spanned by the rotation axis $\mathbf{e}$ and the basis vector along the robot's z-axis $\hat{k} = \begin{pmatrix} 0 & 0 & 1 \end{pmatrix}^T$.

F. Controller Implementation

The general approach for the active ground adaption is to keep the calculation efforts as low as possible for implementation on low performance hardware in future developments. Therefore an approach without sophisticated control-architecture, planning or exteroceptive sensors (e.g. laser scanner or camera) is chosen deliberately.

The FLC and RPA controllers are activated only if all the wheels are in contact with the ground, otherwise the legs which are not in contact are lowered until there is a minimal contact. The outputs from the FLC and RPA are position offsets for each leg in the vertical direction. The combined unsaturated offsets for each leg $\hat{o}_i$ are given by

$$\hat{o}_i = p_{z,i} - \hat{p}_{z,i} + K_f \cdot \left(f_{z,i}^{mea} - f_{z,i}^{ref} \right) + K_o \cdot o_i^{RP} \quad (8)$$

where K_f is the force-leveling gain, K_o is the orientation gain defining the overall influence of the modules on the GAP output. The values $\hat{\mathbf{o}} = (\hat{o}_0\ \hat{o}_1\ \hat{o}_2\ \hat{o}_3)^T$ are then shifted by the body height control module and a saturation module as described in Section II-C to generate the final output value $\bar{\mathbf{o}}$.

The FLC module offset output is calculated as a scaled difference of measured force and reference force. The scaling is mainly done to transform the calculated scalar from force domain to distance domain. The effect is that of a simple proportional controller in velocity domain. In the experiments described below, the gains are hand-tuned, resulting in $K_f = 0.1 \frac{mm}{N}$ and $K_o = 1.0$.

The ability of the controller to overcome terrain height variations depends on the terrain slopes and on the robot speed. It is limited by the possible maximum speed of the leg movement, which in turn depends on the current leg configuration. The strategy is to linearly adapt the speed of the robot if the combined force and orientation errors crosses a predefined threshold. Experimental results in the regard are not included here.

III. EXPERIMENTS

All experiments presented are conducted in a laboratory environment with obstacles built up from modular components, Fig. 4. The experiments are conducted with a fixed commanded forward speed of $\dot{x} = 50 \frac{mm}{s}$. SherpaTT is in a symmetrical square-shaped footprint in all experiments with a commanded roll and pitch of zero degree for the body. The edge length of the foot print's square is about 2.1 m, i.e. when the front-left (FL) wheel is about to leave the obstacle which is 2.4 m in length, the rear-left (RL) wheel just entered the obstacle. The right side wheels roll over the even laboratory floor. The overall mass of the rover is about 150 kg in the experiments. With the symmetrical footprint, a symmetrical force distribution of $f_{z,i}^{ref} \approx 375\,N$ is to be expected. However, the manipulator's pose shifts the COG, imposing a slightly higher force on the front wheels. All experiments are conducted with rigid wheels. As shown in the image of the setup, the rover was in an early integration state for the experiments presented in this paper.

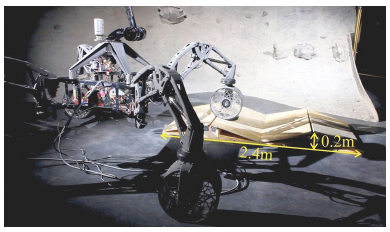

Fig. 4. Experimental setup (screenshot from experiment video). Overlay indicates dimensions of obstacle.

For reference, experiment markers are manually set in the data plots indicating the position of the wheels on the obstacle. The markers are shown in each of the following plots. A marker has the value zero, when the corresponding wheel is on the laboratory floor, the value one when the wheel is on an upward slope and the value two when the wheel is on a down slope of the obstacle. Preliminary tests showed only marginal deviations between single runs, hence the data shown here, even though from single runs, can be considered as relevant for the evaluation of the approach.

A. No Adaption: Rigid Suspension

A run without adaption is conducted as the baseline. The plots for the rover's roll and pitch angle and the z-forces at the four wheels are shown in Fig. 5(a) and Fig. 5(b), respectively. As expected, the forces strongly deviate from an ideal distribution throughout the run. While being on the obstacle, at least one wheel is without ground contact with $f_{z,i}^{ref} \approx 0\,N$.

As can be seen from the roll/pitch data, the rover tilts over its front-left/rear-right (FL/RR) axis at about 45 s during the run, effectively shifting the pitch angle to the roll angle. The touchdown of the front right wheel can be seen in a minimal force spike around the same time in the forces plot. The tip-over is the result of the slightly front-shifted COG due to the manipulator pose.

After starting the system and before entering the obstacle (≈5 s-25 s in the plot) the force distribution yields a *strong contact pair* (FL/RR) and a *weak contact pair* (front-right/rear-left; FR/RL). This can be explained by slightly different stiffness in the separate legs and minor inaccuracy in joint position calibration. During the run over the obstacle the strong contacts change from FL/RR to FR/RL when the rear wheel drives onto the obstacle. Slight deviations in leg stiffness and the preference for the FL/RR axis as strong contacts also explain, why at around 95 s there is a short period of ground contact of all four wheels (RL wheel is in "valley" between the two obstacle's peaks) while this is not the case around 45 s when the FL wheel is in that valley.

B. Using Roll/Pitch Adaption only

Fig. 6 shows the data when driving over the obstacle with active RPA and inactive FLC. At around 35 s the FL wheel is on the first top of the obstacle when the rover tips over (peak of 1.5deg in roll and pitch in the plot). While the wheel drives

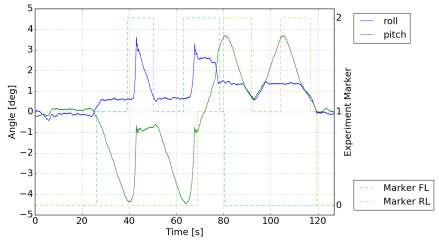

(a) Roll and pitch of body without any adaption

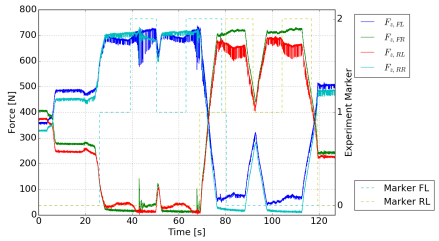

(b) Forces F_z on wheel contact points without any adaption

Fig. 5. Results from run without adaption, e.g. stiff suspension system

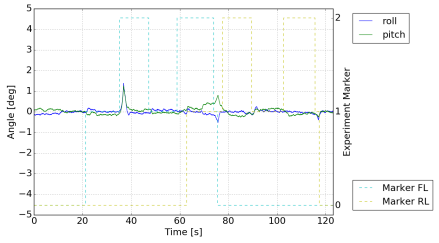

(a) Roll and pitch of body with RPA

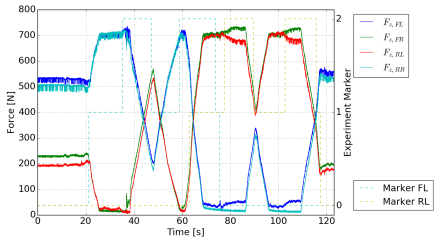

(b) Forces F_z on wheel contact points with RPA

Fig. 6. Results from run with RPA only. As expected the forces are similar to rigid suspension, while roll and pitch errors are clearly reduced.

down the slope, the forces at FL and RR decrease resulting in a short switch over of the strong contact axis.

Since the RPA module itself does not guarantee ground contact, contact loss is still observable. Even more: When entering the obstacle with the FL wheel, both, FL and FR wheels are moved up synchronously in order to reach the desired pitch, hence the FR wheel is moved up by the RPA module, when it actually should move down to keep ground contact. Apart from the roll/pitch deviations due to tipping over (at around 35 s onto FR wheel and at around 75 s onto FL wheel), the RPA module keeps both angles well within $\pm 0.5^\circ$ with a commanded angle of zero degree, whereas deviations of -4.5° to $+3.5^\circ$ are present in the reference experiment without active adaption.

C. Using Force Leveling only

The experiments with FLC active and RPA inactive showed that the FLC has the tendency to impose a drift on the pitch angle of the robot. This is due to inaccuracies in the modelled weights of each of the links of the robot and the resulting inaccuracy in the position of the robot's COG. Due to this drift, these experiments are not presented in detail in this paper. The FLC alone in its implementation state while conducting the experiments discussed here is not feasible for usage in the active ground adaption.

D. Using Roll/Pitch Adaption and Active Force Leveling

In this experiment, the rover is commanded to keep the body's roll and pitch at zero degrees and simultaneously maintaining each wheel's desired z-force. Keeping the force at each wheel at the commanded value also ensures that the wheels do not loose ground contact. Due to the continuous ground contact of all wheels, no tip-over of the system occurs. Thus the roll and pitch angles are limited within $\pm 0.5^\circ$ during the whole run, as shown in Fig. 7(a).

The forces at each wheel are displayed in Fig. 7(b). A clear improvement in distribution of the robot's weight onto all four wheels can be seen. After activating the FLC component (around 5 s in the plot), the forces are kept permanently between 250 N and 450 N (peaks around 15 s, 55 s, 60 s, and 110 s where wheels are entering or leaving the obstacle) and between 320 N and 400 N most of the time.

IV. CONCLUSION & OUTLOOK

The design of the presented Ground Adaption Process within SherpaTT's Motion Control System with modules for orientation adaption and force leveling provides an effective, yet simple-to-implement controller.

The experiments conducted and presented in this paper show a clear improvement from using no active adaption over only body orientation control to the combination of two adaption modules for achieving a multi-objective ground adaption. Fig. 8 shows the RMS errors from the three experiment settings. Roll/pitch control improvement is observable with the RPA active, reducing the RMS from 1.19° and 2.07° to values below 0.25°. The mean force error is lower (from 265 N to 253 N) but shows no significant improvement in this setting. Enabling FLC and RPA shows a greatly reduced force error (average error is 39 N) and reduces the roll error slightly in comparison with RPA only. The pitch error seems not to be influenced by activating the FLC.

While writing this paper, the system SherpaTT successfully finished a four week field deployment in the desert

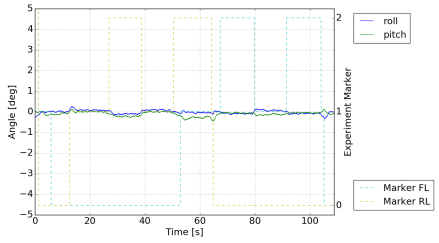

(a) Roll and pitch of body with RPA and FLC

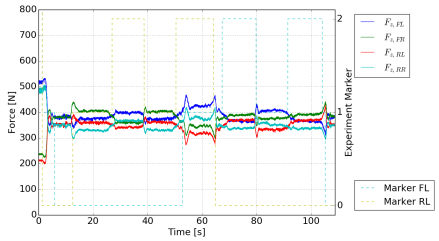

(b) Forces F_z on wheel contact points with RPA and FLC

Fig. 7. Results from run with RPA and FLC active. Both, forces at LEPs and roll/pitch error benefit from active FLC.

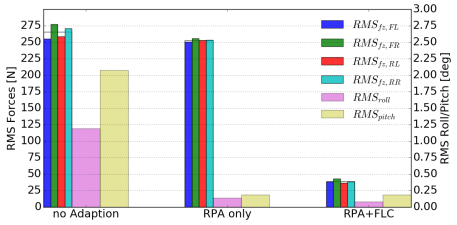

Fig. 8. RMS error of the three experiment settings. Average of force error of the four LEPs is displayed as underlying rectangle.

of Utah, USA[2] using the control approaches presented in this paper. The system was able to climb slopes of up to 28° covered with loose soil and duricrust. The data of these trials is currently being analyzed and will be published accordingly. Fig. 9 shows the system during a slope run on natural terrain.

Fig. 9. SherpaTT during field trials in Utah, USA in Oct/Nov 2016. Slope in this image is about 28°/53% and covered with duricrust. SherpaTT uses FLC and RPA modules to climb the slope.

References

[1] F. Cordes, A. Dettmann, and F. Kirchner. "Locomotion Modes for a Hybrid Wheeled-Leg Planetary Rover". In: *Proceedings of the IEEE International Conference on Robotics and Biomemetics (IEEE-Robio 2011)*. Phuket, Thailand, Sept. 2011.

[2] F. Cordes et al. "An Active Suspension System for a Planetary Rover". In: *Proceedings of the International Symposium on Artificial Intelligence, Robotics and Automation in Space (i-SAIRAS 2014)*. Montreal, Canada: o.A., June 2014.

[3] Karl Iagnemma and Steven Dubowsky. *Mobile Robots in Rough Terrain – Estimation, Motion Planning, and Control with Application to Planetary Rovers*. Vol. 12. Springer Tracts in Advanced Robotics 1. Springer-Verlag Berlin Heidelberg, 2004.

[4] NASA JPL. *Wheels and Legs*. http://mars.nasa.gov/msl/mission/rover/wheelslegs/. 2017-01-24.

[5] R.A. Lindemann and C.J. Voorhees. "Mars Exploration Rover mobility assembly design, test and performance". In: *Systems, Man and Cybernetics, 2005 IEEE International Conference on*. Vol. 1. Oct. 2005, 450–455 Vol. 1.

[6] S. Michaud et al. "ExoMars Locomotion Subsystem Analytical Tool Development and Correlation". In: *11th Symposium on Advanced Space Technologies in Robotics and Automation, ASTRA-11*. 2011.

[7] A.H. Mishkin et al. "Experiences with operations and autonomy of the Mars Pathfinder Microrover". In: *Aerospace Conference, 1998 IEEE*. Vol. 2. Mar. 1998, 337–351 vol.2.

[8] William Reid et al. "Actively articulated suspension for a wheel-on-leg rover operating on a Martian analog surface". In: *Robotics and Automation (ICRA), 2016 IEEE International Conference on*. IEEE. 2016, pp. 5596–5602.

[9] P.H. Smith. "The Phoenix mission to Mars". In: *Aerospace Conference, 2004. Proceedings. 2004 IEEE*. Vol. 1. Mar. 2004, 342 Vol.1.

[10] R. Sonsalla et al. "Towards a Heterogeneous Modular Robotic Team in a Logistic Chain for Extraterrestrial Exploration". In: *Proceedings of the International Symposium on Artificial Intelligence, Robotics and Automation in Space (i-SAIRAS 2014); June 17-19, Montreal, Canada*. o.A., June 2014.

[11] D. Wheeler, D. Chavez-Clemente, and V. SunSpiral. "FootSpring: A Compliance Model for the ATHLETE Family of Robots". In: *Proceedings of the 10th International Symposium on Artificial Intelligence, Robotics and Automation in Space (iSAIRAS'10)*. 2010, pp. 644–651.

[12] B. H. Wilcox. "ATHLETE: A limbed vehicle for solar system exploration". In: *2012 IEEE Aerospace Conference*. 2012, pp. 1–9.

[2] Video available at: `https://youtu.be/pvKIzldni68`

SherpaTT: A Versatile Hybrid Wheeled-Leg Rover

Florian Cordes[1] and Ajish Babu[1]

[1] DFKI Robotics Innovation Center Bremen, Germany
e-mail: *firstname.lastname@dfki.de*

Abstract

This paper subsumes the first experiences with the hardware of the robotic system SherpaTT. The mobile platform consists of four legs, each equipped with a wheel at its end. All legs are connected via a central body. The chosen control design and approach are validated with experiments using the robotic hardware. Autonomous active ground adaption is able to significantly improve the system's stability in terms of ground contact force tracking and body roll/pitch stability. For adaption, the robot makes use of a one dimensional force measurement per wheel and the roll and pitch angles as measured by an inertial measurement unit in the central body. The results of the experiments are an excellent base for further development of the motion capabilities of the rover.

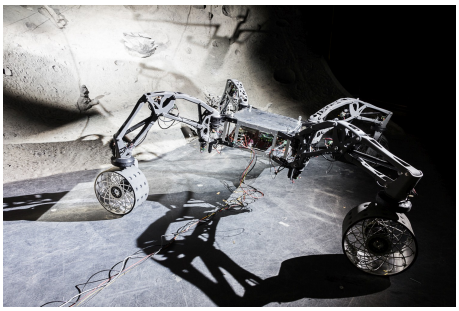

Figure 1. First integration stage of SherpaTT: four fully functional legs and a central body for locomotion mode development. Manipulator, high level sensors and protective hull are not mounted, yet.

1 Introduction

Mobile robots provide the possibility to collect data from remote locations and explore places that are too far away or too dangerous to be reached by humans. Since this implies that no humans are around once the robot is deployed, the robot needs to be self-sufficient, robust and possibly as autonomous as possible. Planetary exploration (currently primarily on Mars) is one example were mobile robots are deployed for exploration and gathering of scientific data.

From nature, walking and climbing seems to be the best solution for stable locomotion in a wide variety of terrains. Even though there are promising advancements in legged robotic locomotion [1, 9], the complexity and a persisting lack of robustness currently prevents these systems from being deployed in space missions.

As opposed to walking systems, wheeled robots offer a low complexity and high robustness. When equipped with appropriate suspension mechanisms these systems can provide a high mobility in natural terrain. So far, the mobile systems deployed on Moon (e.g. LRV [14], the Lunokhod rovers or Chang'e-3) and Mars (Pathfinder, MER [5], Curiosity [15]) are wheeled systems with passive suspension systems. The passive suspension known as rocker-bogie reduces the angular displacement the body of the robot is experiencing while traversing sloping terrain and allows to overcome obstacles such as rocks in the range of the wheel's diameter. A variation of the rocker-bogie is the triple bogie suspension with three independent rocker-arms that each interconnect two wheels of a six-wheeled rover [7, 8]. Another type of passive suspension system can be found in the rover CRAB [17], where three wheels on each side of the robot are connected via two links, creating a parallel bogie configuration. The mechanisms on each side of the rover are connected via a differential to level pitch angles of the body.

Hybrid systems with legs-on-wheels like presented in [3, 12] or wheels-on-legs as presented in [10, 13] provide a possibility to close the gap between walking and driving locomotion. A leg-on-wheel system imitates the movements of a walking system with a limited range of possible foot placements but vastly reduced kinematical complexity and often increased movement speed. On the other hand, wheel-on-leg (or wheeled-leg) systems are first and foremost driving systems. For adaption to sloping/rough terrain they need sensors, actuation and control algorithms. Depending on the design of the legs / the active suspension system, these systems provide the possibility to exhibit walking locomotion as well. Furthermore, active control of the central body's pose with respect to the

footprint in up to six degrees of freedom (DoF) is possible while simultaneously adapting to the terrain they are driving on.

This paper presents the first experiences with the hardware of the hybrid wheeled-leg system SherpaTT, which is depicted in Figure 1. The rover consists of four identical legs with a wheel at the end. For the experiments in this paper the first integration stage with fully functional legs mounted on the central body is used. In the final integration stage an additional manipulator will be mounted on top of the system. SherpaTT is part of a multi-robot team for an aspired lunar sample-return mission [11]. Following this introduction chapter, the second chapter gives an overview of the kinematics of the suspension system that is formed by the four legs, the third chapter highlights the motion control system implemented in SherpaTT.

2 SherpaTT: System Overview

In this section the general design of SherpaTT is presented. Currently, SherpaTT is in its first integration stage with all four leg units attached to a central body and the basic electronics implemented in the system for hardware testing (focus on the suspension system). The last paragraph of this section highlights some of the upcoming extensions of the system, that will be conducted to make SherpaTT a full member of the planned multi-robot system in the project TransTerrA [11]. SherpaTT is the successor of Sherpa, differences of both systems are highlighted in [4].

2.1 Leg Design and Definitions

As can be seen from Figure 1, SherpaTT features four leg-like units that constitute its active suspension system. A total of 20 active DoF distributed in four identical suspension units ("legs") are present.

For calculations of the kinematics, the Leg End Point (LEP) is defined as the point on a rigid wheel below the steering axis of that wheel as indicated in Figure 2. The LEP is used under the assumption of a rigid wheel on a rigid and flat surface. The LEP might be different from the Wheel Contact Point (WCP) which could be calculated using force/torque measurements [2] and the known stiffness of a flexible wheel. However, for the experiments and descriptions in this paper, we focus on the LEP as a first approximation.

The three DoF of each leg closest to the body (named *Pan*, *InnerLeg*, *OuterLeg*) are responsible for the movements of the LEP with respect to the body. The outermost DoF do not influence the LEP's position with respect to the body. These actuators rotate the wheel around its vertical axis (*WheelSteering*) and drive the wheel to create rolling motions of the robot (*WheelDrive*).

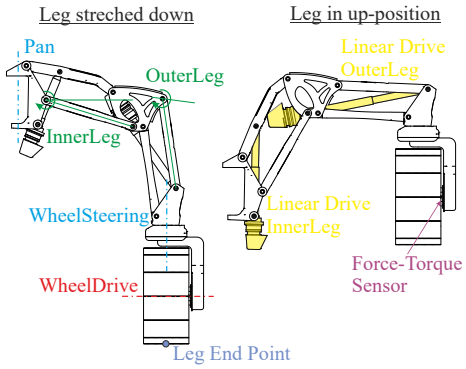

Figure 2. Degrees of Freedom of a Suspension Unit. Left: Configuration for high ground clearance, right: configuration with body on ground.

2.2 Leg Workspace

Figure 3 shows a cross-section of the toroid-shaped workspace built by the actual (still conservatively set) joint limits. Three preferred poses are indicated. These are LEP positions in the workspace, which provide maximum z-movement (up/down) for ground adaption (PrefPoseA), a compromise between radius movements and z-movementrange (PrefPoseB) and maximum body height (PrefPoseC). Note that the horizontal and vertical elements of the mock-up leg shown in the image keep horizontal/vertical due to the parallelogram structure used in the actual leg design.

The workspace is made up by moving the LEP towards or away from the body (changing the radius in the cylindrical leg coordinate frame, see also Section 3.1), moving the LEP up/down (z-component) and rotating around the pan joint.

A preferred pose is independent of the Pan joint position. Hence, different foot prints such as square, rectangular or any arbitrary four-sided polygon is possible. A preferred pose is used as standard commanded pose which is altered by offsets written from adaptive processes as described in Section 3.

2.3 Extensions of Current Integration State

Currently, SherpaTT is in an integration state, where the active suspension is put into operation while all other features of the system are still under development. A major mechanical upgrade is the mounting of the manipulator which was already used on the predecessor Sherpa [6]. The manipulator is used for payload-handling and optionally for locomotion support.

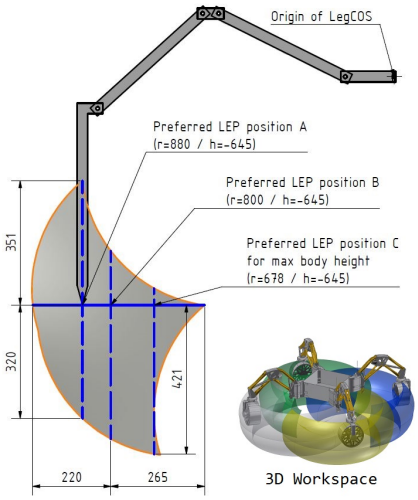

Figure 3. Workspace dimensions (cross section) and preferred poses in cylindrical leg frame. Inset depicts the overlapping workspaces of all four legs. Dimensions are in millimeters.

For a seamless integration into the multi-robot system [11], SherpaTT will be equipped with four payload interfaces (EMI: electro-mechanical interface [16]) around the manipulator tower and at the bottom of the body. The interfaces are used to transport payloads or to expand the rover's capabilities by attaching additional sensors and devices.

Finally a protective hull will be mounted on SherpaTT for protection against dust and other contaminants.

3 Motion Control

In this section, we present the motion control system (MCS) for SherpaTT. The MCS is the connecting layer between low-level control on one hand – i.e. firmware running on the hardware boards such as joint controllers, relay-boards and alike – and high level control (navigation, planning, and other autonomous behaviors) on the other. For the purpose of development of the MCS, a graphical user interface is used to command the robot's movement (forward, lateral and turn), its body attitude with respect to gravity (roll, pitch) and body height, and the footprint of the robot (where the LEPs of the suspension unit are with respect to the body). These are also

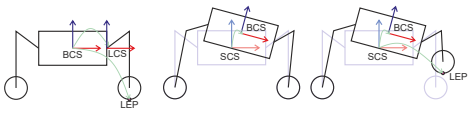

Figure 4. Coordinate Frames for Locomotion

the possible inputs for high-level processes to command the rover. Generation of joint commands from the mentioned high-level commands is completely encapsulated in the MCS.

3.1 Locomotion Coordinate Frames

Figure 4 illustrates the most important coordinate frames used in SherpaTT. The following main coordinate frames are used for locomotion control:

- The *Body Coordinate System* (BCS) is attached to the center of the main body of SherpaTT. Its z-axis is pointing upwards, the x-y plane is at the same height as the Leg Coordinate System's x-y plane (see below). This frame is used for all internal computations.
- The *Leg Coordinate System* (LCS) has its origin in the Pan joint of a leg. It is aligned with the Pan-CS when the Pan angle $\alpha = 0°$.
- The *Shadow Coordinate System* (SCS) is used to describe the motion commands independent of the body posture. The center image and the right hand image of Figure 4 illustrate the SCS. It is a virtual CS that remains at the "nominal pose" of SherpaTT. Body posture changes, externally commanded Leg End Point (LEP)-positions and movement commands are described in this frame.

3.2 Basic Structure of the Motion Control System

SherpaTT's *Motion Control System* (MCS) is setup to encapsulate the control of the robot's complex kinematics such that the high level process only needs to provide control inputs via a simple command interface. Figure 5 shows how the MCS is used to control the robot. In this simplified diagram the main command inputs are shown at the top:

- The *Motion Command* is used for basic robot movement. The command is three dimensional and allows commanding forward (x) and lateral (y) as well as turn movements (about z).
- *BodyPosture* commands are used to control the six DoF of the robot's main body.
- A *FootPrint* command is used to describe the three DoF of each LEP.

This results in a total of 21 possible command inputs. Three of which are velocity commands, the rest are

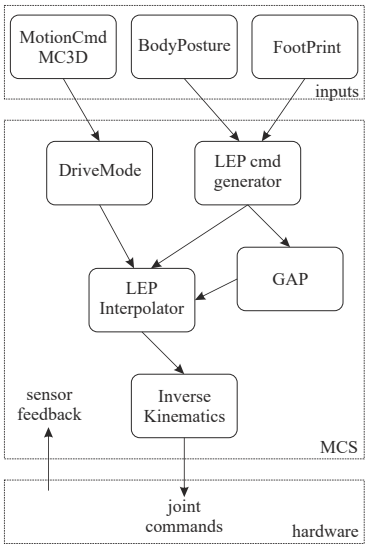

Figure 5. Simplified structure of SherpaTT's Motion Control System. Only central components are displayed.

position commands. Note that height commands (z-component) for single LEPs can be set freely, however these commands have an influence on the BodyPosture. Hence, even if possible in the actual MCS implementation, direct z-commands for the LEPs should be avoided by the human operator or the high-level processes.

Internally, the BodyPosture command and the FootPrint command are merged into one LEP position (in BCS) per leg of the suspension system. The MotionCommand is used to control the WheelSteering and WheelDrive joints according to the DriveMode. The commanded values are merged together with LEP offsets originating from the *Ground Adaption Process* (GAP, see Section 3.3) into the LEP Interpolator. Here the trajectories of the LEP positions are generated to reach a new desired LEP from the actual LEP position.

In each cycle of the MCS (which is executed at 100 Hz), the actual LEP command is finally converted into joint commands by the Inverse Kinematics task and sent to the joints of the suspension system. The sensor feedback contains telemetry from each joint as well as IMU data for the actual body orientation and data from the force-torque sensors at each wheel.

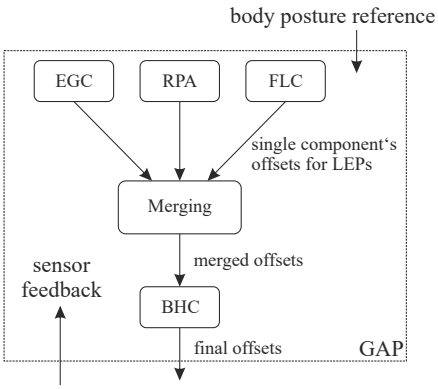

Figure 6. The components of the Ground Adaption Process (GAP): Ensure Ground Contact (EGC), Roll/Pitch Adaption (RPA), Force Leveling Control (FLC), and Body Height Correction (BHC).

3.3 Active Ground Adaption

The Ground Adaption Process (GAP) is the part of the MCS that manipulates the LEPs of each leg to conform to the terrain. This is achieved by following reference values for forces at the LEP and roll and pitch angle of the central body as measured by the Inertial Measuring Unit (IMU). The reference values are tracked using PI-controllers for each of the setpoint goals. Figure 6 displays the general scheme in which the values for active ground adaption are generated.

Currently, three subcomponents constitute the ground adaption. The three offset generating subcomponents of GAP are described in more detail in the following paragraphs. Each of the components independently calculates an LEP offset (in z-direction) for each of the wheels. The offsets are then merged into one offset for each wheel. Before writing the merged offsets out to the MCS, the *Body Height Control (BHC)* module checks whether all offsets have the same sign, when this is the case, the offsets are cut such that the smallest offset is set to zero. Hence, a body height drift can be prevented.

Ensure Ground Contact (EGC) This module is responsible for keeping all wheels in continuous ground contact. Once the measured force on a wheel drops below a threshold, the corresponding wheel offset is adapted such that the wheel moves down with $\dot{z}_{LEP,i} = -10\,mm/s$.

Roll/Pitch Adaption (RPA) In the RPA subcomponent, two separate PI controllers are active for each wheel's offset, resulting in eight PI-controllers in total. One controller generates offsets to match the commanded roll, the second controller to match the commanded pitch angle of the body. In the implementation used for the experiments presented in this paper, both controllers assume a distance of the wheel to the rotation axis of 1 m. An extension to arbitrary foot prints is possible by incorporating the x and y component of the LEP in body coordinates as scaling factor. Both offsets of the RPA module are added and written as combined RPA offset.

Force Leveling Control (FLC) The force leveling module needs the expected forces at the wheels as input for the PI controller. Currently, the forces are calculated as expected forces for the footprint the robot is driving. In other words, when driving in a symmetrical square foot print configuration, each wheel is expected to share the same fraction of the robot's mass. Wheels that are closer to the body would share a higher load. Since the system with four ground contact points is underdetermined, an approximation using a Moore-Penrose pseudoinverse is used to generate the reference forces for the wheels. For this static equilibrium is assumed. In later development stages, other ground adaption modules will actively change the position of the center of gravity within the support polygon to generate an appropriate force distribution between the wheels for locomotion in rough and sloping terrain.

4 Experiments

For validating the systems's ground adaption capabilities, experiments on a wooden obstacle track are conducted. The initial experiments using the first integration study of SherpaTT and the results thereof are presented in this section.

4.1 Setup

Figure 7 shows the experimental setup. An obstacle with two up-down slopes of 20 cm height is used. During the experiment the rover is commanded in such a way, that it drives "one-sided" over the obstacle with its left wheels, while the wheels front-right (FR) and rear-right (RR) roll over flat laboratory floor. In the chosen foot print of the robot each wheel contact point is in the corner of a square with an edge length of ~2 m. Hence, during most of the run only one wheel is on the obstacle; when the front wheel is about to drive off the obstacle, the rear wheel has just been driven onto the first slope.

All experiments use a constant forward velocity of $\dot{x} = 50\,mm/s$ and a symmetrical, square-shaped footprint. Each wheel is approximately at a distance of 1 m from

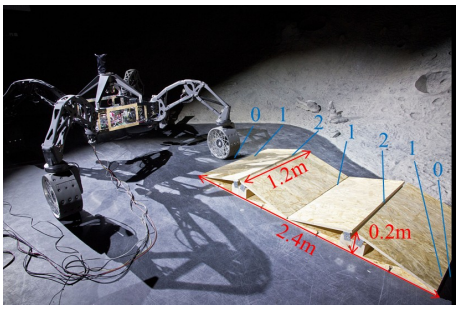

Figure 7. Obstacle track with dimensions as used for the presented experiments. Blue digits identify the experiment markers for the wheel position in the log data stream. Note that during the experiments the manipulator flange was already mounted on SherpaTT.

the rover's roll and pitch axis, respectively. For reference, the experiment is conducted without ground adaption, i.e. with a stiff suspension system, and then compared with the data using active ground adaption. During the run, experiment markers are set manually for the position of the front-left (FL) and rear-left (RL) wheel on the obstacle: A marker value of "0" indicates a wheel on laboratory floor, changing the value to "1" marks the beginning of an upslope, while setting the marker to "2" indicates the beginning of a down-slope. The experiment markers are shown in Figure 7 as blue digits at the point where they are set.

In the data plots of Figure 8 and Figure 9, the experiment markers are shown for the front left and rear left wheel as light blue and yellow line, respectively. Please note that due to the manual setting, the markers are not precisely set. However, orientation in the data is more easy with these markers. Furthermore, in between the run without adaption and the run with active adaption, the manipulator flange was mounted on the rover. This is reflected in the slightly higher overall weight of the rover ($F_{g1} \approx 1200\,N$ in the run without adaption vs. $F_{g2} \approx 1400\,N$ in the run with active ground adaption).

All presented plots are single-run data. Comparison of different runs showed a high repeatability, with in only marginal differences between the single runs.

4.2 Results

Figure 8(a) shows the roll and pitch data from a run without active adaption of the suspension system. The roll angle is more or less constant at around 1°, once a wheel is on the obstacle (blue line). A peak of about 3° in roll is visible when wheel FL is still on the last slope and wheel

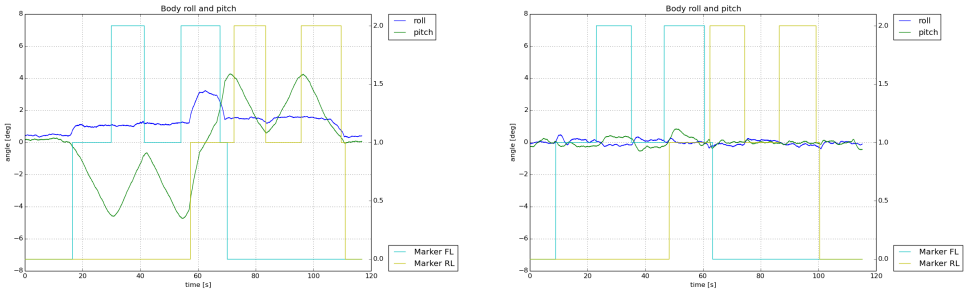

(a) Without adaption, the obstacle-course is well visible in the pitch of the robot.

(b) Active adaption limits the values within ±1deg max

Figure 8. Roll/Pitch deviation without and with active GAP.

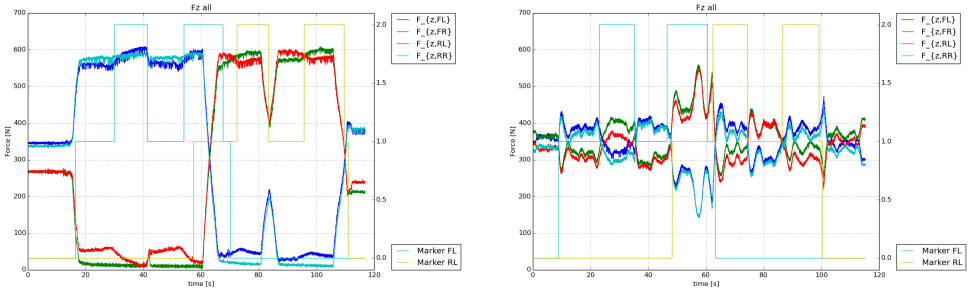

(a) Without adaption, wheels loose ground contact (F_z ≈0 N). Two diagonally opposite wheels (FL/RR and FR/RL) share the main load of the robot's weight.

(b) Active adaption limits the values mostly to ±100 N of the desired value (≈300 N). A higher deviation is visible in the middle of the experiment, where the rear wheel enters the obstacle while the front wheel leaves the obstacle

Figure 9. Wheel-ground contact forces without and with active GAP.

RL drives up the first slope (around $t = 60\ s$).

In the pitch data of the rover, the obstacle is quite well recognizable, with a negative pitch following the two peaks of the obstacle when the FL wheel is on the obstacle and a positive pitch, when the rear wheel is on the obstacle. From the corresponding force plot in Figure 9(a) it can be seen that the wheels FR and RR loose ground contact (z-force drops close to zero).

The force plot also shows that with the stiff suspension there are always two *strong contacts* and two *weak contacts*. Both types are diagonally opposed to each other, i.e. FL/RR and FR/RL are contact pairs. The robot is driving with a symmetrical foot print. With a weight of $F_{g1} \approx 1200\,N$, each wheel contact should ideally remain at around $300\,N$. Actually, due to the stiff suspension and the resulting lift off the ground of single wheels, the forces deviate about $\pm 300\,N$ from the desired reference force.

Figure 8(b) and Figure 9(b) show the results of driving over the same obstacle with active GAP. With active control of roll and pitch angles both are kept within ±0.5°, apart from one deviation of about 1° around 50 s (ref. Figure 8(b)). In the second half of the experiment (RL wheel on obstacle) the angles are kept within ±0.2°.

From the plot of the wheel contact forces, it can be seen that all wheels keep ground contact during the complete experiment run. Control oscillations lead to more frequent switching between strong and weak contact pairs. The oscillations are a result of a limited velocity of the wheel's z-component, which is due to the single joint velocity limits in each leg. Apart from greater force deviations during the change over of FL and RL wheel on the obstacle, the force levels are kept approximately $\pm 50\,N$

around the setpoint of $\frac{1}{4}F_{g2} = 350\,N$.

5 Conclusion and Outlook

This paper gives a first impression of the newly integrated hybrid driving and walking rover SherpaTT.

The structure and kinematics of the suspension system are highlighted, and the implemented control system is presented. Core part of the motion control system is the active ground adaption process (GAP). This process is implemented in such a way that offsets to the commanded wheel position are written to adapt to sloping terrain. Measurement inputs are currently one-dimensional force measurements at the wheels and orientation measurements (roll/pitch) in the central body.

The initial experiments presented in this paper show that a clear reduction in loads of a single wheel by active force balancing is possible. The deviation of forces was reduced to $\pm 50\,N$ as opposed to deviations of $\pm 300\,N$ in case of no adaption to the obstacle. The implemented roll and pitch controller is able to keep the body's pose close to the desired values ($\pm 0.5^\circ$ vs. $\pm 4.5^\circ$ without active adaption) on the obstacle used for the experiments, significantly reducing the ground's effect onto the body's orientation. In the presented experiments, rough control gain setting was done, it is to be expected that tuning of control parameters will improve the oscillating behavior and reference value tracking. A high repeatability was observed, differences between single runs with same settings are only marginal.

Even though the experiments in this paper indicate a good behavior of the robot concerning the active adaption to sloping terrain, only a limited subset of system configurations was investigated so far. Further developments are currently directed into arbitrary foot prints (non-symmetric stance and LEPs in other distances than 1 m from rotation axis), three dimensional force tracking and LEP offset generation, and less regular as well as bigger obstacles.

Acknowledgment

The project TransTerrA is funded by the German Space Agency (DLR, Grant number: 50RA1301) with federal funds of the Federal Ministry of Economics and Technology (BMWi) in accordance with the parliamentary resolution of the German Parliament.

References

[1] S. Bartsch. "Development, Control, and Empirical Evaluation of the Six-Legged Robot SpaceClimber Designed for Extraterrestrial Crater Exploration". In: *KI - Künstliche Intelligenz* 28.2 (2014), pp. 127–131. URL: http://dx.doi.org/10.1007/s13218-014-0299-y.

[2] A. Bicchi, J. K. Salisbury, and D. L. Brock. *Contact Sensing from Force Measurements*. A.I. Memo No. 1262. Massechusetts Institute of Technology, Artificial Intelligence Laboratory, 1990, pp. 249–262. URL: ftp://publications.ai.mit.edu/ai-publications/pdf/AIM-1262.pdf.

[3] Y. C. Chou et al. "Bio-inspired step crossing algorithm for a hexapod robot". In: *Intelligent Robots and Systems (IROS), 2011 IEEE/RSJ International Conference on*. 2011, pp. 1493–1498.

[4] F. Cordes et al. "An Active Suspension System for a Planetary Rover". In: *Proceedings of the International Symposium on Artificial Intelligence, Robotics and Automation in Space (i-SAIRAS 2014); June 17-19, Montreal, Canada*. o.A., June 2014.

[5] R.A. Lindemann and C.J. Voorhees. "Mars Exploration Rover mobility assembly design, test and performance". In: *Systems, Man and Cybernetics, 2005 IEEE International Conference on*. Vol. 1. 2005, 450–455 Vol. 1.

[6] M. Manz et al. "Development of a Lightweight Manipulator Arm using Heterogeneous Materials and Manufacturing Technologies". In: *Proceedings of the International Symposium on Artificial Intelligence, Robotics and Automation in Space (i-SAIRAS 2012); September 4-6, Turin, Italy*. o.A., Sept. 2012.

[7] Paul Meacham, Nuno Silva, and Richard Lancaster. "The Development of the Locomotion Performance Model (LPM) for the ExoMars Rover Vehicle". In: *Proceedings of ASTRA 2013*. 2013. URL: http://robotics.estec.esa.int/ASTRA/Astra2013/Papers/meacham_2811294.pdf.

[8] S. Michaud et al. "Development of the ExoMars Chassis and Locomotion Subsystem". In: *Proceedings of i-SAIRAS 2008 - 9th International Symposium on Artificial Intelligence, Robotics and Automation in Space*. 2008. URL: http://elib.dlr.de/55365/1/i-sairas2008_ExoMars.pdf.

[9] M. Raibert et al. *BigDog, the Rough-Terrain Quadruped Robot*. online. 2008. URL: http://www.bostondynamics.com/img/BigDog_IFAC_Apr-8-2008.pdf.

[10] W. Reid, A. H. Göktogan, and S. Sukkarieh. "Moving MAMMOTH: Stable Motion for a Reconfigurable Wheel-On-Leg Rover". In: *Proceedings of Australasian Conference on Robotics and Automation*. 2014.

[11] R. Sonsalla et al. "Towards a Heterogeneous Modular Robotic Team in a Logistic Chain for Extraterrestrial Exploration". In: *Proceedings of the International Symposium on Artificial Intelligence, Robotics and Automation in Space (i-SAIRAS 2014); June 17-19, Montreal, Canada*. o.A., June 2014.

[12] R. U. Sonsalla et al. "Design of a High Mobile Micro Rover within a Dual Rover Configuration for Autonomous Operations". In: *Proceedings of the International Symposium on Artificial Intelligence, Robotics and Automation in Space (iSAIRAS-2014)*. Montreal, 2014.

[13] J. Townsend, J. Biesiadecki, and C. Collins. "ATHLETE mobility performance with active terrain compliance". In: *Aerospace Conference, 2010 IEEE*. 2010, pp. 1–7.

[14] NASA Webpage. *The Apollo Lunar Roving Vehicle*. `http://nssdc.gsfc.nasa.gov/planetary/lunar/apollo_lrv.html`. last visit: 2016-02-09.

[15] R. Welch et al. "Verification and validation of Mars Science Laboratory surface system". In: *System of Systems Engineering (SoSE), 2013 8th International Conference on*. 2013, pp. 64–69. URL: `http://ieeexplore.ieee.org/xpl/articleDetails.jsp?arnumber=6575244&queryText=Verification%20and%20Validation%20of%20the%20MSL%20Curiosity%20Rover&newsearch=true`.

[16] W. Wenzel, F. Cordes, and F. Kirchner. "A Robust Electro-Mechanical Interface for Cooperating Heterogeneous Multi-Robot Teams". In: *Proceedings of the 2015 IEEE International Conference on Intelligent Robots and Systems (IROS-15)*. Hamburg, 2015, pp. 1732–1737.

[17] B. Xu et al. "Composite control based on optimal torque control and adaptive Kriging control for the CRAB rover". In: *Robotics and Automation (ICRA), 2011 IEEE International Conference on*. 2011, pp. 1752–1757.

An Active Suspension System for a Planetary Rover

Florian Cordes*, Christian Oekermann*, Ajish Babu*, Daniel Kuehn*, Tobias Stark*, and Frank Kirchner*‡

*DFKI Robotics Innovation Center Bremen
Bremen, Germany
‡University Bremen FB3
Bremen, Germany
e-mail: *firstname.lastname@dfki.de*

Abstract

This paper reviews the design of the hybrid wheeled-leg rover Sherpa[1]. Focus is set on the mechanical design of the suspension system that is constituted by four independently controllable legs with a wheel mounted at each leg. Achievements and drawbacks of the current design are outlined and lead together with the new application range to a revised design of the suspension. The new design and its modular actuation components are presented in this paper.

1 Introduction

Autonomous robots for exploration of extraterrestrial surfaces require reliable and robust locomotion systems. Passive suspension systems such as the well-known rocker bogie system which is applied for example in all successfully deployed Mars rovers so far [9, 8, 10] provide high motion capabilities with low control complexity. The passive suspension allows to negotiate obstacles in the size of the order of a wheel diameter of the rover. With passive suspension no extra efforts in controlling the configuration of the suspension system or its reaction to the ground are necessary, since the mechanical structure adapts to the external loads.

A major drawback in passive suspension systems becomes obvious in situations where the vehicle is stuck, for example in soft soils. Relieving the vehicle might become difficult or impossible without external intervention.

Compared with passive suspension, active suspension systems come with a higher cost concerning the control of the adaption to the ground. However, these systems provide a high maneuverability and reconfiguration capabilities that are not possible with purely passive suspension. Depending on the layout, the suspension can be used in substantially different ways to propel the robot. Apart from mere adaption to the ground, the suspension system's actuators can be used to actively take part in the robot's movements [3] and, for example, to increase the traction on the ground [1]. On a higher complexity level of the suspension, wheels that are mounted on leg-like structures even enable the robot to exhibit undulating locomotion capabilities, resulting in a reconfiguration space of the locomotion system from driving to walking [6]. As described with the skating motions of the RollerWalker system [3] the locomotion modes are not necessarily discrete driving vs. walking. Rather, a potential for mixed modes or gradual mode changes is created using active suspension systems.

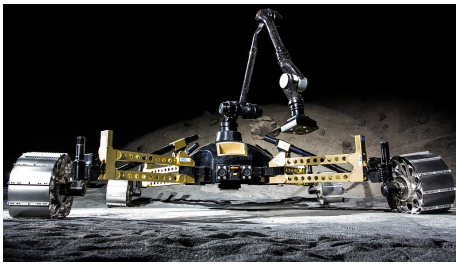

Figure 1. Sherpa in low stance mode. The body is very close to the ground and a wide footprint is adopted.

Not only rough terrain robots benefit from reconfigurable suspension: In indoor environments a change of the footprint allows high stability when needed, for example, in heavy load manipulation (i.e. health care robots) while compact configurations facilitate driving through narrow passages such as, for example, doors or crowded hallways [4].

Active suspension systems are defined by employing actuators for changing the kinematics of the sus-

[1] Sherpa: Expandable Rover for Planetary Applications

pension. The Sample Return Rover (SRR) [7] and Scarab [1] are both four wheeled systems that make use of one bogie on each side of the robot. The bogies are connected via a differential. Furthermore, one active degree of freedom (DoF) per bogie is used to reconfigure the suspension system. In case of the SRR, the main purpose of actively controlling the suspension system is to increase the rover's tipover stability by actively shifting the center of mass (CoM). Scarab, as well as the SRR make use of a shoulder joint to actively change the footprint of the system. Apart from increasing the stability in slopes the suspension system allows alternative motion modes and is used to lower the body for increased stability for subsurface drilling. For the SRR not only the suspension system is considered for locomotion purposes but the manipulator can be used to stabilize the robot in slopes (i.e. by shifting the CoM).

The ATHLETE family of rovers makes use of a highly actuated suspension system. It can be considered to be constituted by legs that are equipped with wheels at the ground contact points [6]. This configuration allows high adaption capabilities to irregular ground. Even discontinuous paths can be realized, since active lifting of the wheels off the ground is possible. This further increases the possibilities of motions and obstacles that can be negotiated. Using tool adapters mounted at the driving axes of the wheels, a leg of the system can be used as manipulator as well.

An important role in the flexibility of terrain negotiation plays the possibility of decoupling path following from the attitude of or attitude changes in the suspension system. High level control such as autonomous navigation should provide a path planning through the terrain ahead and a path following process. An appropriate suspension system controller can then provide a decoupled control of path following and terrain adaption by posture changes [5]. In order to enable path following in rough terrain, the posture of the suspension system is actively changed decoupled from high level commands.

In the remainder of this paper, the rover Sherpa (Fig. 1) will be highlighted in Section 2. Apart from benefits of the system, drawbacks are outlined as well, leading to a mechanical re-design of the suspension system as described in Section 3. In Section 4 a conclusion and an outlook on the next development steps are provided.

2 Sherpa Review

The hybrid wheeled rover Sherpa was initially developed within the project RIMRES [11]. It features

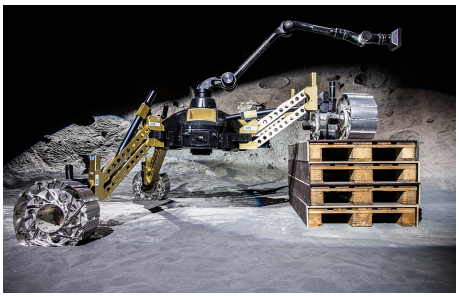

Figure 2. Benefits of negative ground clearance: Sherpa stepping onto a high obstacle. The manipulator was used to support the rover while lifting the wheel onto the obstacle.

an active suspension system for increased maneuverability and a multi-purpose manipulator arm that can be used for both, manipulation and locomotion purposes. The suspension system is constituted by four independent legs each equipped with a wheel, Figure 2.

The design of the suspension system uses active and passive suspension on different scales. Flexible metal wheels are employed to cope with ground irregularities on a small scale (several centimeters) and to provide high traction in soft soils. Springs in the lifting actuators of the rover form a kind of serial elastic actuator that copes with bigger irregularities below one wheel diameter. Big obstacles and body leveling in sloped terrain are dealt with by actively actuating the suspension system.

Sherpa has a maximum ground clearance of 711 mm. The ground clearance can be altered with the active suspension. This allows Sherpa even to put the central body to the ground and lift the wheels 189 mm off the ground, resulting in a negative ground clearance. In square footprint configuration, the edges of the square have a length of 2100 mm in high stance and 2500 mm in low stance (as shown in Fig. 1). Overall the system has a mass of approximately 160 kg.

A design point that proved to be beneficial is using self locking gears in the actuator design of the suspension. Due to this construction, Sherpa is able to maintain its body height without expending electrical energy. High additional payloads are realizable. A maximum of 90 kg impact load was successfully tested on Sherpa. A drawback is, however, an estimation of the load of a leg based on currents in the individual

joints is not possible.

The wide range of motions of each single leg allows a wide range of postures (footprint/body height and attitude combinations) the robot can achieve. A change of stance width can be used for narrow passages, the center of mass of the robot can be shifted with respect to the support polygon etc. The manipulator can be used for locomotion i.e. serving as a fifth leg. This further increases the flexibility of the rover.

The chosen control approach for regular driving [2] is able to cope with the loss of one wheel. More precisely, no reconfiguration of the controller is necessary. If a wheel has a failure, the leg can be lifted off the ground, the remaining three legs are rearranged for a stable stance and the controller can work identically with three wheels as it did with four wheels.

The passive flexibility as described above allows to control the robot with a comparatively low number of sensors for the locomotion software-layer. Joint positions/speeds and a gravity sensor in the body are enough for basic terrain adaption. However, a sophisticated load balancing between the wheels/legs would need, for example, force-torque sensors for each leg since this information is not available by comparing the single joint's loads (due to the self locking gears).

A non-optimal point in the current design turned out to be the arrangement of the individual joints in a leg. Currently the first two joints (DoF0 and DoF1, c.f. Fig. 3) are responsible for the main positioning of the wheel contact point in x, y, and z coordinates. Consequently, the wheel cannot be freely positioned in the whole workspace of the leg. Furthermore, the second set of joints (DoF2 and DoF3, c.f. Fig. 3) does not have a considerable effect on the actual position of the wheel. Those DoF are intended to tilt and flip the wheel for proper steering in slopes and to provide a foothold with the wheel being lifted off the ground. During experiments with the system it became obvious that the flexible wheels sufficiently adapt to slopes so that the two DoF were used sparsely.

While the offset of the wheel from the steering axis allows the wheel to support the steering motion, at the same time the re-orientation of the wheel during steering imposes a movement of the wheel-ground contact point (WCP) relative to the rover. Thus, wheel steering is always coupled to a x,y-movement of the WCP within the rover's body coordinate frame. This imposes control issues when adapting the footprint during locomotion.

Thorough analysis of the mechanical structure and the distribution of loads originating from the wheel contact points revealed potential for weight reduction in the mechanical structure of the legs. Since most of the mechanical loads are carried by the linear actuator (lift DoF) and the upper beam of the parallelogram, it is possible to reduce stiffness and thus the mass of the lower beam.

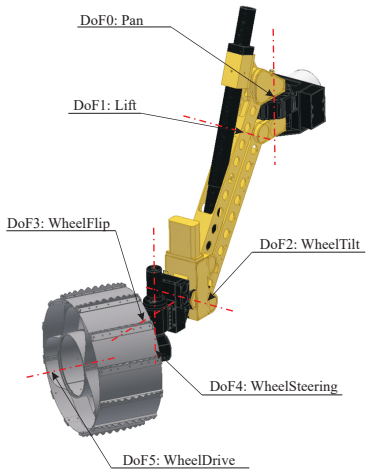

Figure 3. One leg of Sherpa's suspension system with numbering and naming of the degrees of freedom.

Since four of the in total six actuators of each leg are clustered close to the wheel, a rather unflexible geometry of the leg is achieved. This results in the above mentioned coupling of DoF and in a non compact stow position of the robot. The minimum volume envelope of Sherpa is with front and back legs stretched forward and backward, respectively at $2.25\,m \times 0.8\,m \times 1.35\,m = 2.43\,m^3$. Figure 4 illustrates the minimum volume configuration for Sherpa.

Sherpa was designed as a member in a heterogeneous robotic team in which a six-legged robot can be attached to the bottom interface of its central structure [11]. In the original scenario, the flexibility of the legged robot was exploited and allowed an autonomous docking manoeuver. For the docking process, Sherpa did not need to control its body attitude independently in several DoF; adapting the body height and limiting the roll and pitch angle were sufficient for successful docking maneuvers.

In the new application range also passive payloads shall be picked up with the electromechanical interface. In the new scenario, Sherpa is used to deploy

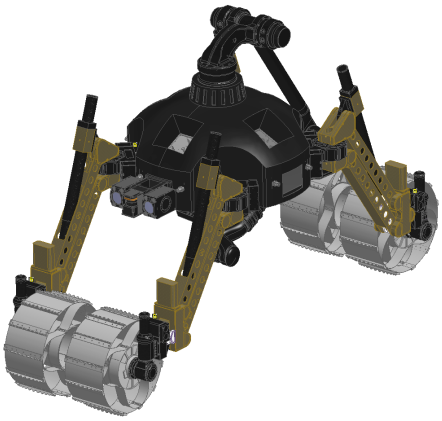

Figure 4. Sherpa in its minimal volume configuration. Due to the clustering of four out of six actuators at the end of each leg, more compact configurations are not possible.

base camps in a lunar logistics chain [12]. These base camps constitute node for (geological) sample storage and are planned to be used as communication relays and for energy harvesting in a multi robot scenario.

The placement of base camps and the pickup of those passive structures requires a higher maneuverability of the central body than currently possible. For precise docking of the two corresponding interfaces, the rover's body-attitude should be controllable in all 6 DoF independently, which is not possible with the current design of the suspension.

3 Sherpa-Redesign

Based on the drawbacks as indicated in the previous chapter, a redesign of Sherpa's suspension system is currently executed. The main focus is to further increase the flexibility of the suspension system and trying to reduce the weight at the same time. In order to reduce the development effort, a modular actuator concept shall be used.

3.1 Suspension design

The new leg design is shown in Fig. 5. As previously described, the wheel flip function (DoF3 in Fig. 3) was rarely used and therefore subducted in the new design. The WheelTilt actuator of the old design is exchanged for a second lifting actuator ('outer actuator'), resulting in a knee in each of Sherpa's legs. The new knee couples a set of two parallel structures that are coupled as main actuators for controlling the height and the width of Sherpa's footprint, Figure 5.

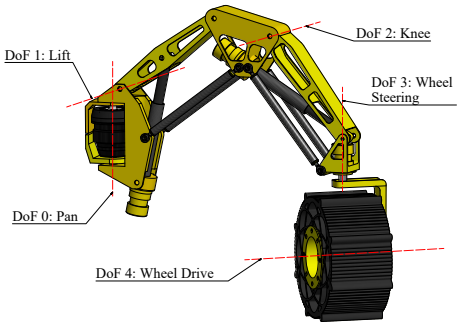

Figure 5. New leg design for Sherpa based on two serial aligned parallel kinematics

The linear actuators are installed in such a way that they experience tensional forces while the wheel has contact with the ground. This leads to a stiffer system compared to the original Sherpa design where the actuator has to provide a push-force and mechanical slackness leads to high position variance.

The new rover design in the regular driving pose is shown in Figure 6. With the proposed suspension design, the wheel contact point (WCP) can be moved $\approx 800\,mm$ in vertical direction. Due to the introduced knee, the wheel can be lifted independently from movements in x-y plane which is not possible with the original Sherpa suspension. Depending on the body height, a shift of up to $\pm 250\,mm$ is possible. When moving all legs synchronously, this results in an according body lean in the horizontal plane. Figure 7 depicts the movement range of the wheel contact point (WCP).

To measure the wheel loads (force and torque), a six DoF sensor will be installed between the drive motor and fork-type wheel attachment. The sensor input will be used for improved load balancing and terrain adaption. The additional sensor input is expected to facilitate the rover's terrain adaption capabilities and stability due to explicit load balancing.

The original version of Sherpa's suspension did not allow compact storage volumes. A compact stow volume is desired to be realizable with the new design. This demonstrates a possible launching configuration

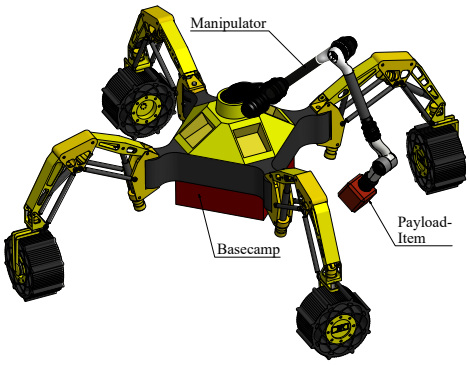

Figure 6. New rover suspension design. The suspension is shown in the normal pose: A cross shaped suspension alignment and at medium body height.

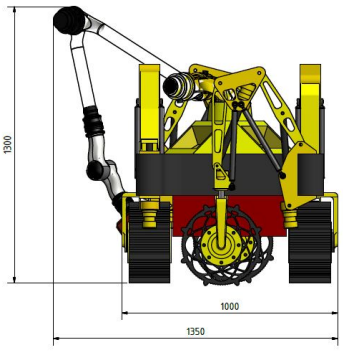

Figure 8. New stow pose of Sherpa. Note that the manipulator is unchanged in this design and might be adapted in a later development stage. Indicated dimensions are in mm.

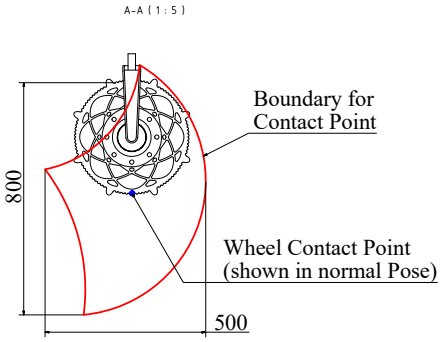

Figure 7. Movement range for the wheel contact point using DoF1 and DoF2. DoF0 has a movement range of $\pm 135°$ that creates a toroid of the denoted cross section. Normal pose denotes the expected nominal driving position (WCP in center of movementrange) in cross shaped stance. Dimensions are in mm.

and in terms of practical use facilitates transporting the rover for experimentation. The new suspension design with the newly introduced knee allows a way more compact bounding box than the original Sherpa suspension, Figure 8 shows Sherpa in the new stow configuration. Its new minimal volume envelope is approximately $1.0\,m \times 1.35\,m \times 1.3\,m = 1.76m^3$

3.2 Modular Actuator Design

A set of modularized actuators of different power classes has been developed at the author's institute, these modules are used for the Sherpa redesign, reducing the number of different actuators in the system for improved maintenance and control. Basic components of the actuator modules are electronically commutated internal rotor DC motors of different classes and accompanying ellipto-centric gears of varying gear reductions in single or two stage configurations. For a better maintainability of the electronics, each actuator module has its own electronic stack with a base-board which provides all necessary connector plugs without any active components. Main sensors for position, speed and torque control are two magnetic encoders implemented on the drive side and the gear side, respectively as well as a bi-directional current measurement in each motor phase. For communication between the actuator modules and the central control electronics a high speed daisy chained serial communication is used with a communication

speed up to $320Mbit/s$. Additionally temperature monitoring is implemented to avoid overheating of the motors.

From the experiences with the initial Sherpa design and using simulation tools, the required mechanical power for each DoF is estimated. The result is that both linear actuators and the steering actuator do require a comparable power and therefore can be based on the same motor module. The pan actuator has to provide a very high torque and therefore will be designed around a two stage cycloid gear. The same motor size as the leg pan actuator can be used for the wheel drive, but due to lower torque requirements a single stage gear is appropriate.

In the design phase it could be shown that the modular concept offers a great reduction in development time and costs. However, a drawback in modular devices with discrete performance classes are weight and efficiency. In case of Sherpa's suspension redesign, costs and time where favored over explicitly for this system developed actuator modules.

For the linear actuators in the legs, a relatively high rotational speed is required, therefore RoboDrive ILM50×8 motors (nominal speed: $5500rpm$) are used. For wheel steering, an ILM50×14 offers higher torque at lower speeds (nominal speed: $3500rpm$). Advantageous on the modular actuator concept is that the same casing can be used for both type of motors. For the wheel drive and the leg pan actuators, higher power is required, therefore ILM70×10 is used.

All of the actuators use HarmonicDrive gears to match the motors' speed and torque to the given requirement. For the linear actuators self-locking is desired, therefore ball-screw type screwjacks can not be used. Instead, ACME-type spindles get driven by an HarmonicDrive Series 17 gear, the same type which is used for the steering actuators. To provide the required torque, a two staged gear (double HarmonicDrive combination) is used for the leg pan actuator.

4 Conclusion and Outlook

4.1 Conclusion

This paper gives an overview of the current state of the exploration rover Sherpa. Current drawbacks are outlined and a new design improving the suspension system is proposed. The mechanical fabrication of the new components is currently in progress.

The original design of the suspension system featured some degrees of freedom (DoF) that were used sparsely, since the employed flexible wheels proved to exhibit a sufficient adaption to the ground that was planned to be done by two of the six DoF per leg. In the new design these DoF are thus subducted. For improving the independence of the wheel contact point's x, y, and z-coordinate, an additional knee joint is introduced. Furthermore, the offset of the wheels to their steering axis is removed to decouple steering direction from the positioning of the wheels ground contact point in the rover's coordinate frame.

The joints in the new suspension system are designed as modular units that can be adapted in terms of motor power and gear reduction. This reduces design efforts and facilitates maintenance of the system.

4.2 Outlook

The original rover motion control system (MCS) was ported into the Rock framework and is currently re-structured to exploit the tools and workflow provided by this framework. To exhaust the systems' capabilities, a distributed control software architecture is applied to the rover, allowing autonomous or semi-autonomous modes as well as full manual control by a mission operator. The underlying rock component model bases on the Orocos real time toolkit. Rock provides all tools required to set up and run robotic systems with a wide range of well tested modules for sensors, actuators and high-level operations like path planning or map generation.

Within rock, an encapsulated motion control will be implemented. The MCS is structured in different layers, e.g. a *motion generation* layer, the *motion control* layer or the *MCS core* layer. In the *motion generation* layer, high level inputs are used to generate the locomotion of the robot and the motions associated with reconfiguring the suspension system. These are feed forward modules, mainly transforming the inputs to desired outputs in the form of wheel orientation, wheel speed, and foot print.

The *motion control* layer takes the outputs of the *motion generation* layer and modifies the values based on the chosen control modes (e.g. terrain adaption). The terrain adaption controller changes the wheel contact point so as to actively adapt to changes in the terrain. This is achieved by estimating the loads expected from each of the legs in the current configuration and varying the height of the WCP in order to achieve this load. This ensures proper ground contact for all the wheels even when terrain changes. Roll/pitch adaption controls the body roll and pitch such that the body is leveled with respect to the gravity vector or, if desired, is parallel to the inclined ground. Still the operator can modify any given value with an offset, if required.

In the *MCS core* layer, the inverse kinematics are

calculated in order to generate the appropriate joint commands from the cartesian commands generated in the layers before. Safety modules implement a self collision avoidance or a center of mass (CoM) stability checker to prevent damages to the hardware. A trajectory interpolator generates smooth joint reference trajectories taking into account speed and acceleration limits. The output of these module is sent as reference to the robot's joints. In the current state, the joints internally make use of cascaded position-speed-current control, which can actively limit the maximum position, speed, and currents, ensuring a safe operation.

The future Sherpa will benefit from its increased range of motion combined with additional sensors to allow reactive actions to given situations. Improving the overall outcome of a certain mission remains one of the main intention and will be achieved by reducing the operational risks due to more autonomous functionality like navigation and planning introduced by the rock framework.

Acknowledgment

The work presented in this paper is part of the finished project RIMRES[2] (initial version of Sherpa) and the ongoing project TransTerrA[3].

References

[1] Bartlett, P. ; Wettergreen, D. ; Whittaker, W. L.: Design of the Scarab Rover for Mobility and Drilling in the Lunar Cold Traps. In: *International Symposium on Artificial Intelligence, Robotics and Automation in Space*, 2008

[2] Cordes, F. ; Dettmann, A. ; Kirchner, F.: Locomotion Modes for a Hybrid Wheeled-Leg Planetary Rover. In: *Proceedings of the IEEE International Conference on Robotics and Biomemetics (IEEE-Robio 2011)*. Phuket, Thailand, September 2011

[3] Endo, G. ; Hirose, S.: Study on Roller-Walker - Adaptation of characteristics of the propulsion by a leg trajectory -. In: *Intelligent Robots and Systems, 2008. IROS 2008. IEEE/RSJ International Conference on*, 2008, S. 1532–1537

[4] Giordano, P. R. ; Fuchs, M. ; Albu-Schaffer, A. ; Hirzinger, G.: On the kinematic modeling and control of a mobile platform equipped with steering wheels and movable legs. In: *Robotics and Automation, 2009. ICRA '09. IEEE International Conference on*, 2009. – ISSN 1050–4729, S. 4080–4087

[5] Grand, Ch. ; BenAmar, F. ; Plumet, F. ; Bidaud, Ph.: Decoupled control of posture and trajectory of the hybrid wheel-legged robot hylos. In: *Robotics and Automation, 2004. Proceedings. ICRA '04. 2004 IEEE International Conference on* Bd. 5, 2004. – ISSN 1050–4729, S. 5111–5116

[6] Heverly, M. ; Matthews, J. ; Frost, M. ; McQuin, Ch.: Development of the Tri-ATHLETE Lunar Vehicle Prototype. In: *Proceedings of the 40th Aerospace Mechanisms Symposium*. NASA Kennedy Space Center, May, 12-14 2010

[7] Iagnemma, K. ; Rzepniewski, A. ; Dubowsky, S. ; Schenker, P.: Control of Robotic Vehicles with Actively Articulated Suspensions in Rough Terrain. In: *Autonomous Robots* 14 (2003), Nr. 1, S. 5–16. – ISSN 0929–5593

[8] Lindemann, R.A. ; Voorhees, C.J.: Mars Exploration Rover mobility assembly design, test and performance. In: *Systems, Man and Cybernetics, 2005 IEEE International Conference on* Bd. 1, 2005, S. 450–455 Vol. 1

[9] Mishkin, A.H. ; Morrison, J.C. ; Nguyen, T.T. ; Stone, H.W. ; Cooper, B.K. ; Wilcox, B.H.: Experiences with operations and autonomy of the Mars Pathfinder Microrover. In: *Aerospace Conference, 1998 IEEE* Bd. 2, 1998. – ISSN 1095–323X, S. 337–351 vol.2

[10] NASA JPL. *Homepage of Curiosity Mission*. Web. April 2014

[11] Roehr, T. M. ; Cordes, F. ; Kirchner, F.: Reconfigurable Integrated Multirobot Exploration System (RIMRES): Heterogeneous Modular Reconfigurable Robots for Space Exploration. In: *Journal of Field Robotics* 31 (2014), Nr. 1, S. 3–34. – ISSN 1556–4967

[12] Sonsalla, R. U. ; Cordes, F. ; Christensen, L. ; Planthaber, S. ; Albiez, J. ; Scholz, I. ; Kirchner, F.: Towards a Heterogeneous Modular Robotic Team in a Logistics Chain for Extended Extraterrestial Exploration. In: *Proceedings of the 12th International Symposium on Artificial Intelligence, Robotics and Automation in Space - i-Sairas 2014*. Montreal, Canada, June 2014

[2]The project RIMRES was funded by the GermanSpace Agency (DLR, Grant number: 50RA0904) with federal funds of the Federal Ministry of Economics and Technology (BMWi) in accordance with the parliamentary resolution of the German Parliament.

[3]The project TransTerrA is funded by the GermanSpace Agency (DLR, Grant number: 50RA1301) with federal funds of the Federal Ministry of Economics and Technology (BMWi) in accordance with the parliamentary resolution of the German Parliament.

[7]: **Locomotion Modes for a Hybrid Wheeled-Leg Planetary Rover**
F. Cordes, A. Dettmann, F. Kirchner
in: RoBio 2011

Locomotion Modes for a Hybrid Wheeled-Leg Planetary Rover

Florian Cordes*, Alexander Dettmann*, and Frank Kirchner*,◇

***Abstract*— This paper introduces locomotion modes for the planetary rover Sherpa[1]. The rover's locomotion system consists of four wheeled-legs, each providing a total of six degrees of freedom. The design of the active suspension system allows a wide range of posture and drive modes for the rover. Self-locking gears in the suspension system allow to maintain the body height without the need of actively driving the actuators. Thus, energy-efficient wheeled locomotion and at the same time high flexibility in ground adaption and obstacle negotiation are possible, as well as high payload capabilities. Furthermore, the rover will be equipped with a manipulator arm explicitly designed to be used for locomotion support. Thus, all degrees of freedom of the system can be used to enhance the locomotive capabilities. This paper gives an overview of the mechanical design of the rover, kinematic considerations for movement constraints on the wheel contact points are presented. Based on these constraints, the wheel motions due to the commanded velocities of the platform can be calculated, taking into account the flexible posture of the rover. A first set of possible locomotion modes for the rover is presented in this paper as well.**

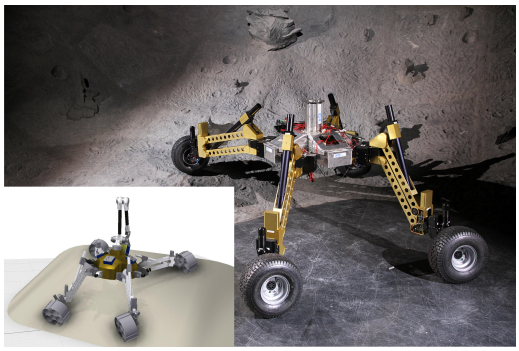

Fig. 1. Current state of the integration study of Sherpa in DFKI's artificial crater environment. The active DoF are used in a way that the central platform is horizontally aligned. The inset depicts the CAD model of the rover.

I. INTRODUCTION

Today, extraterrestrial exploration is conducted nearly exclusively by robotic means. This includes satellites for remote sensing (e.g. *LCROSS* [1]) as well as surface deployable probes (e.g. *Phoenix Lander* [2]) and mobile exploration robots (e.g. *Spirit* and *Opportunity* [3]). In order to investigate a planetary terrain closely, mobility has to be provided to allow for collecting scientific samples from various locations. Canyons and impact craters are of special scientific interest, but these terrains are also challenging for locomotion systems. Thus, these areas can only be accessed with sophisticated mobile devices.

Mobile systems that have been deployed up to now on Mars and Moon make use of passive suspension systems. The rocker-bogie system, used for example in *Pathfinder*, the *Mars Exploration Rovers*, and also implemented for the *Mars Science Laboratory* [4], is a sophisticated suspension system for a wide range of terrains. However, experiences with the Mars Exploration Rovers show, that a robot with a purely passive suspension system has limitations for instance in stuck situations, as appeared when *Spirit* drowned in a spot of soft soil [5]. Furthermore, the size of the obstacles that can be overcome is limited to the range of a wheel diameter.

An active suspension system overcomes these limitations and can maintain the advantages of wheeled locomotion such as energy efficiency. With the *ATHLETE* family of rovers, NASA/JPL introduced a rover with wheels mounted on a six degrees of freedom (DoF) (*ATHLETE*) and a seven DoF (*Tri-ATHLETE*) leg [6], respectively. This rover is able to use its wheels for locomotion in moderate terrain, whereas the DoF of the legs can be used for egression off the landing unit and overcoming big obstacles. The robot is meant to serve as crew assistant and cargo transporter on the Moon. Furthermore the robot can be used to transport habitat modules, thus serving as a mobile platform for heavy loads. The final version of ATHLETE aims at limb sizes of 4 m length.

Scarab [7] is a four wheeled rover that combines a classical bogie suspension with an active DoF to enhance the ability to climb and drive along slopes. Furthermore, the control of the body height as well as the roll angle of the robot is possible. The system is designed to work in places of perpetual darkness at the lunar poles in order to search for deposits of water ice.

Outstanding surface mobility can be provided by legged locomotion, since the foot contact points do not need a constant trajectory on the ground plane but can be placed arbitrarily within the workspace of the leg, enabling walking machines to climb even vertical surfaces [8]. However, purely legged locomotion suffers the disadvantage of complexity and worse energy efficiency compared to wheeled locomotion. This makes legged robots more suitable for relatively short traverses in extreme terrains [9] [10].

The combination of wheeled and legged locomotion provides the possibility to combine the advantages of both approaches. In the RIMRES-project [11] we pursue this approach on different levels: (1) We combine two separate

*DFKI Robotics Innovation Center Bremen, 28359 Bremen, Germany.
◇University of Bremen, FB3, Robotics Lab, 28359 Bremen, Germany.
Contacting Author: Florian.Cordes@dfki.de
[1]Sherpa: Expandable Rover for Planetary Applications

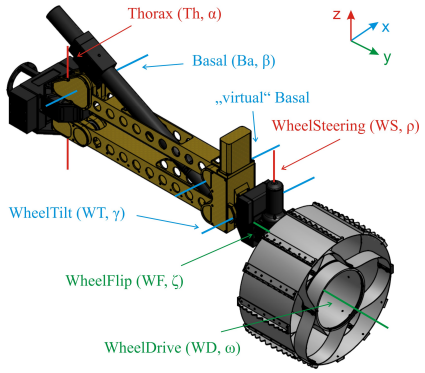

Fig. 2. The four DoF of a swing unit and two DoF for actuating the wheel. The virtual Basal DoF results from the parallel kinematic. All angles are shown in their respective zero position.

systems, namely a wheeled rover (Sherpa, Fig. 1) and a legged scout (CREX[2]) into one multi-robot system. (2) The rover that is responsible to carry the scout to the crater rim is designed with an active suspension system to be highly manoeuvrable itself and to transport the scout safely to the crater rim.

Sherpa is designed to transport moderate loads. Its main tasks are transporting the scout robot to scientific interesting places and setting out science packages. Since Sherpa is embedded into a heterogeneous multi-robot system another design issue is the compatibility with the hardware developed for the multi-robot system RIMRES. A distinct new feature of the robot is its ability to use the robotic arm for multiple purposes: (1) Manipulating payload-items, fig.3, (2) using the embedded camera for system supervision (hazard cam) and (3) active locomotion support.

This paper is structured as follows: In Section II, the mechanical design of Sherpa is briefly described. Section III presents kinematic considerations based on the wheel contact point's motion restrictions. Section IV presents a subset of manually designed postures and drive modes for Sherpa to give a first insight into the locomotion capabilities of the system. The last section concludes the paper and gives an outlook on the next steps of the work with Sherpa.

II. DESIGN OVERVIEW

Sherpa is a four wheeled rover that is capable to connect tightly to a legged scout robot via an electromechanical interface beneath the body [12]. The same interface is used to transport payload items in the four payload bays that are oriented around the central manipulator tower. The manipulator itself makes use of the interface for manipulating the payload items. The whole design of Sherpa is driven by the need to safely carry the legged scout and to manipulate the payload-items. Table I provides some of the key values of Sherpa.

[2]Crater Explorer

TABLE I
KEY DIMENSIONS OF SHERPA

Description	Value
Max. ground clearance	711 mm
Min. ground clearance (Wheels above body)	-189 mm
Propellant torque per wheel	59 Nm
Max. speed of wheel drive	$165° \frac{1}{s}$
Expected mass	≈ 200 kg
Additional Payload	≈ 60 kg
Length of fully stretched arm	1772 mm

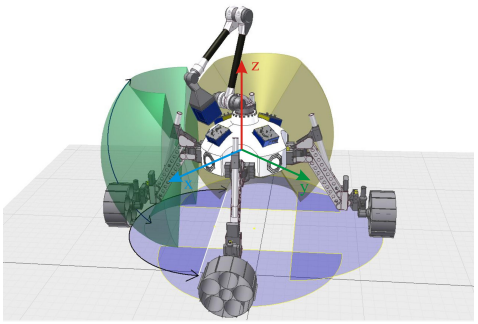

Fig. 3. Movement range of the two main DoF of Sherpa's active suspension system, depicted for two legs. The two DoF result in a spherical shape of the workspace of the swing unit. The thorax movement range for all four and the combination of basal an thorax for two of the swing units is shown. The manipulator is shown with one payload item attached, in each of the four payload bays around the manipulator base is another payload item mounted.

Currently, the hardware integration is ongoing, Fig. 1 depicts the state of the integration. The first drive modes have been implemented for the real system, however, intensive testing and verification is still work in progress.

A. Active Suspension System

The suspension system makes use of actively controllable swing units in order to change the posture of the robot or to lift a wheel off the ground and replace it in a suited place. Short passages of ambulating locomotion are possible. Fig. 2 shows one swing unit with all joints in zero position and the naming of the joints. The Basal joint has a "virtual counter joint" resulting from the usage of a parallel structure. The possible range motion of the two main degrees of freedom of Sherpa's swing units is depicted in Fig. 3. The Thorax joint has a range of $\pm 90°$, whereas the Basal joint has a moving range of $\pm 60°$, resulting in a maximum vertical stroke of 900 mm. The combination of the auxiliary DoF WheelTilt and WheelFlip can be used to orient the wheel towards a slope.

The DoF are driven by highly reduced gears for supporting the rover without the need for actively maintaining the body height. All four DoF of a swing unit use brushless DC motors with a planetary gear. For further reduction and a self-locking feature, worm gears (Thorax, WheelFlip) and spindle drives (Basal, WheelTilt) are used. The actuators only have to be driven when a change in the locomotion system is

desired. Thus, the energy efficiency of wheeled locomotion is maintained.

In order to adapt to the ground on a smaller scale, passive suspension is provided through springs and adaptive flexible wheels. Sherpa's wheels make use of adaptronics in order to sense the properties of the interaction of wheel and surface and to actively adapt the stiffness of the wheels to the actual situation[3]. This will reduce the danger of digging to deep into the ground and get stuck in loose surface material. In case the rover is stuck nonetheless, the active suspension system can be employed to lift the leg out of a sand pit or a comparable situation.

For each DoF of a swing unit, an absolute position sensor is used to be able to measure the deflections of the springs in the passive part of the suspension system. In the mounting point of the swing units to the body, a customized force-torque load cell will be employed to measure the loads that are acting on a swing unit. These measurements can be used for load balancing between the legs and to detect stuck situations, contact with obstacles, and alike.

B. Manipulator Arm

The manipulator arm is designed to be used for various applications: (1) Manipulation of payload items, (2) Supervision of the rover and its closer surroundings, (3) Locomotion support by shifting center of gravity (COG) and using the manipulator arm as an additional leg.

For manipulation and assembly tasks, the arm is equipped with an electromechanical interface which is also used for connecting payload items as well as rover and scout. This interface provides mechanical, electrical, and data connection between two units of the RIMRES system [12].

As proposed for a tracked robot in [13] or a planetary rover in [14], a robot's manipulator arm can also be used for locomotion support. This can improve the locomotive abilities of the system, thus increasing the robustness of the system in unknown environments.

From the beginning of the design phase, the manipulator arm of Sherpa is meant to be a multi-functional tool as stated above. In order to support the rover's weight, considerable torques have to be generated by the manipulator joints. In an evolutionary approach using a physical simulation environment in combination with CMA-ES[4], the optimal joint lengths and required torques for the given use-cases were determined.

Fig. 3 shows the resulting design of the manipulator as mounted on the rover. Currently, the mechanical construction of the first and second joint as well as of the connecting link is finished based on the simulation results. The second joint will be driven by two parallel brushless DC motors in order to generate the required torques for supporting the rover's weight. The link lengths are chosen in a way, that the arm is able to reach the surface over an attached payload item in a radius of 900 mm around the center of the body when the rover has maximum ground clearance ($\beta = 60°$).

Since the manipulation interface is not designed to withstand the loads that occur during the support of the rover, the wrist of the manipulator arm is moved aside and a dedicated footplate is used for ground contact.

[3]The wheels are currently under development by the project partner DLR-RY: Institute of Space Systems, Bremen, Germany. The rubber wheels in Fig. 1 are a substitute for first experiments with the active suspension system.

[4]Covariance Matrix Adaption Evolutionary Strategy

III. KINEMATIC CONSIDERATIONS

In this section, the movement constraints at the contact points of the wheels are used to deduce the wheel orientations and velocities for given commanded velocities. Furthermore, it is shown how the orientation of the wheels (including the robot's posture in Thorax and Basal joints) affects the general mobility of the robot.

A. Assumptions

For the calculations conducted in this section, the wheels are assumed to experience no slippage or skidding. The calculations in the following are derived from [15] and extended to Sherpa's flexible morphology.

The three-dimensional vector ξ^W describes the pose of the robot with respect to the fixed world coordinate frame.

$$\xi^W = \begin{pmatrix} x^W \\ y^W \\ \theta^W \end{pmatrix} \quad \text{and} \quad \dot{\xi}^W = \frac{d}{dt}\xi^W = \begin{pmatrix} \dot{x}^W \\ \dot{y}^W \\ \dot{\theta}^W \end{pmatrix} \tag{1}$$

With the orthogonal rotation matrix $R(\theta)$, the coordinates can be transformed into the body frame. Note that the superscript ^{B} is omitted for the body coordinates in the following. For planar movements, the body frame's z-axis can be assumed to be collinear with the world frame's z-axis without loss of generality. Thus, $\dot{\theta}$ is the rotational velocity of the robot around its z-axis. The origin of the body frame is located in the geometric center of the robot, fig. 4. $\dot{\xi}^B$ is used as input vector of the currently active drive mode (section IV) for commanding the robot's velocities.

$$\xi^B = R(\theta) \cdot \xi^W \tag{2}$$

$$\mathrm{R}(\theta) = \begin{pmatrix} \cos(\theta) & \sin(\theta) & 0 \\ -\sin(\theta) & \cos(\theta) & 0 \\ 0 & 0 & 1 \end{pmatrix} \tag{3}$$

B. Description of Wheel Motions

In the following, the dimensions and angles needed for setting up the movement constraints on the rover's wheels are illustrated. The values are depicted in fig. 4. As also depicted in fig. 2, α_i, β_i and ϕ_i describe the angular positions of the Thorax, Basal and WheelSteering joint, respectively. The point $\mathcal{PWS}$ is the position of the WheelSteering axis. The length of the connecting line from the robots center $\mathcal{O}$ to $\mathcal{PWS}$ is denoted l_i. The length l_i is dependent on both, α and β. However, note that the calculations presented here are projected into the x-y-plane of the robot, so the z-component of $\mathcal{PWS}$ can be neglected in this case.

$$l_i = \sqrt{(x_{\mathcal{PWS},i})^2 + (y_{\mathcal{PWS},i})^2} \tag{4}$$

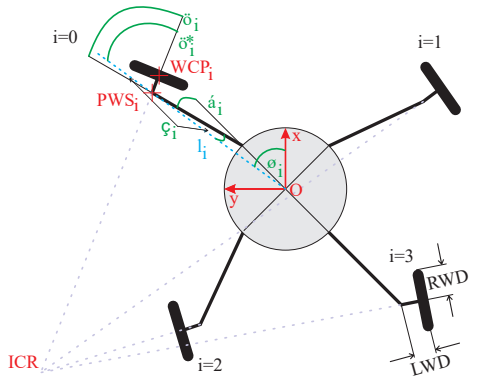

Fig. 4. Schematic view of Sherpa in arbitrary pose for kinematic calculations. α_i: angle of the thorax joint; φ_i: angle of the wheel steering DOF to swing unit; ψ_i: angle of connection line from origin to wheel contact point; l_i length of that line.

The angles ψ_i are the angles between l_i and the x-axis of the robot.

$$\psi_i = \arctan 2(y_{\mathcal{PWS},i}, x_{\mathcal{PWS},i}) \qquad i = \{0, \ldots, 3\} \quad (5)$$

To be able to proceed with the calculations as proposed by Campion et. al [15], we introduce the *virtual steering angle* φ_i^*, measured between the wheel axis of wheel i and l_i, fig. 4. The connection between the virtual steering angle and the actual steering angle φ is given by eqn. (6).

$$\varphi_i = \varphi_i^* - \eta_i \quad (6)$$

The angle η can be calculated using simple geometric dependencies:

$$\eta_0 = \alpha_0 - \Psi_0 + \frac{\pi}{4} \quad (7)$$

$$\eta_1 = \alpha_1 - \Psi_1 - \frac{\pi}{4} \quad (8)$$

$$\eta_2 = \alpha_2 - \Psi_2 + \frac{3 \cdot \pi}{4} \quad (9)$$

$$\eta_3 = \alpha_3 - \Psi_3 - \frac{3 \cdot \pi}{4} \quad (10)$$

With these terms defined and the no slip-condition, the following two constraints for velocities along the wheel plane and orthogonal to the wheel plane can be established for the four wheels ($i = 0, \ldots, 3$), where ω_i denotes the turning speed of wheel i.

Constraints along wheel plane:

$$\begin{pmatrix} \sin(\psi_i + \varphi_i^*) \\ \cos(\psi_i + \varphi_i^*) \\ l_i \cos(\varphi_i^*) + \text{LWD} \end{pmatrix}^T \dot{\xi} - \text{RWD}\,\omega_i - \text{LWD}\,\dot{\varphi}_i = 0 \quad (11)$$

Constraints orthogonal to wheel plane:

$$\begin{pmatrix} \cos(\psi_i + \varphi_i^*) \\ \sin(\psi_i + \varphi_i^*) \\ -l_i \sin(\varphi_i^*) \end{pmatrix}^T \dot{\xi} = 0 \quad (12)$$

In difference to [15], the velocity of the off-centered wheel adds to the motion along the wheel plane, since Sherpa's wheel is orthogonal to the lever (LWD; denoted d in [15]) and not parallel, as in the castor wheels described by Campion et al.

For simplification, the velocity $\dot{\alpha}$ of the thorax joint has been omitted here. It is assumed that in each calculation step, the posture of the robot can be regarded as fixed. However, the posture is still included in the calculations, since l_i is dependent of α_i and β_i.

C. Robot Control with Flexible Suspension System

For a given velocity vector $\dot{\xi}$ the angle φ_i^* can be calculated from constraint (12), the required wheel velocity ω can then be calculated from constraint (11). Effectively this means, that the wheels will be oriented according to the instantaneous center of rotation (ICR) for a given $\dot{\xi}$, see also section IV-C.1.

$$\varphi_i^* = \arctan \frac{-1 \cdot (\cos\Psi_i \cdot \dot{x} + \sin\Psi_i \cdot \dot{y})}{\cos\Psi_i \cdot \dot{y} - \sin\Psi_i \cdot \dot{x} + \dot{\Theta} l_i} \quad (13)$$

$$\omega_i = \frac{\sin(\Psi_i + \varphi_i^*)\dot{x} + \cos(\Psi_i + \varphi_i^*)\dot{y}}{\text{RWD}} - \frac{(\cos(\varphi_i^*) l_i + \text{LWD})\,\dot{\Theta} - \text{LWD}\dot{\varphi}_i}{\text{RWD}} \quad (14)$$

D. Restrictions to Robot Mobility

The constraints (11) and (12) can be written under the following matrix form to summarize the constraints for all four wheels:

$$J_1 \dot{\xi} + J_2 \omega + J_3 \dot{\varphi} = 0 \quad (15)$$

$$C_1 \dot{\xi} = 0 \quad (16)$$

In which the matrices J_1 and C_1 are defined as follows. J_2 and J_3 are diagonal matrices containing the wheel diameters RWD and the offset length LWD on their diagonal, respectively.

$$J_1 = \begin{pmatrix} \sin(\psi_0 + \varphi_0^*) & \cos(\psi_0 + \varphi_0^*) & l_0 \cos(\varphi_0^*) + \text{LWD} \\ \sin(\psi_1 + \varphi_1^*) & \cos(\psi_1 + \varphi_1^*) & l_1 \cos(\varphi_1^*) + \text{LWD} \\ \sin(\psi_2 + \varphi_2^*) & \cos(\psi_2 + \varphi_2^*) & l_2 \cos(\varphi_2^*) + \text{LWD} \\ \sin(\psi_3 + \varphi_3^*) & \cos(\psi_3 + \varphi_3^*) & l_3 \cos(\varphi_3^*) + \text{LWD} \end{pmatrix} \quad (17)$$

$$C_1 = \begin{pmatrix} \cos(\psi_0 + \varphi_0^*) & \sin(\psi_0 + \varphi_0^*) & -l_0 \sin(\varphi_0^*) \\ \cos(\psi_1 + \varphi_1^*) & \sin(\psi_1 + \varphi_1^*) & -l_1 \sin(\varphi_1^*) \\ \cos(\psi_2 + \varphi_2^*) & \sin(\psi_2 + \varphi_2^*) & -l_2 \sin(\varphi_2^*) \\ \cos(\psi_3 + \varphi_3^*) & \sin(\psi_3 + \varphi_3^*) & -l_3 \sin(\varphi_3^*) \end{pmatrix} \quad (18)$$

The rank of the matrix C_1 is an indicator for the mobility of the robot system [15]. If $rank\,[C_1] = 3$, no motion of the robot is possible, since $\dot{\xi} = 0$ is needed to fulfill constraint (16), thus the rank has to be less than 3; due to the dimensions of C_1, the rank is always less than or equal to 3.

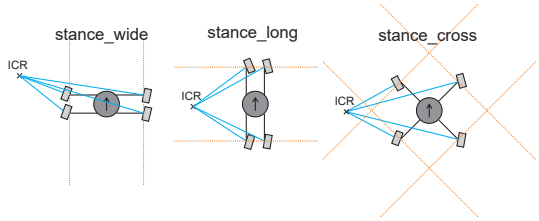

Fig. 5. Three basic stance modes and the dependency of ICR-singularities of the stance mode. When the ICR is moved across a line, at least one wheel has to flip to the opposite end point in a realignment phase.

When the wheels are not coordinated in a way, that the normals of the wheels cross in one singular point (the instantaneous center of rotation, ICR), clearly no directed movement is possible. This is also reflected in the fact that for such configurations $rank\,[C_1] = 3$ (we assumed no slipping motion of the wheel's contact point).

When for instance a point turn is commanded, $\varphi_i^* = 0$ and thus $rank\,[C_1] = 2$. Note that the commanded value of φ_i^* is independent of α and β, which means that the movement is possible for each posture of the corresponding swing unit. However, the real commanded value φ_i obviously is dependent on the posture of the swing unit.

IV. POSTURE AND DRIVE MODES: LOCOMOTION USING ALL DOF

This section first gives definitions of the terms *behavior*, *posture mode*, and *drive mode* as used in this work and then presents some of the possible posture and drive modes for Sherpa.

A. Definitions

Behavior A behavior is a process that is implemented in the robot's operating system. A behavior controls the robots actuators and/or collects sensor data.

Posture Mode A posture mode is a behavior that controls the robot's extremities in order to achieve a goal such as keeping the robot's center of gravity within the stability margin of the support polygon. The posture is not fix, it can be adapted to changes in the environment.

Drive Mode A drive mode is a behavior that is commanding the robot's actuators in a way that the robot moves in the fixed world coordinate frame.

Locomotion Mode A locomotion mode is a combination of drive and posture modes that is used for propelling the robot.

B. Posture Modes for Sherpa

By presenting a basic set of posture modes, this section provides an insight into the flexibility of Sherpa's suspension system. As given in the above definition, posture modes are used for adapting the robot's pose to the environment, for example to facilitate locomotion in slopes. Different posture modes can be combined by different merging functions. The robot's operating system MONSTER [16] allows writing multiple joint position/velocity commands to one single hardware driver using an appropriate merge function.

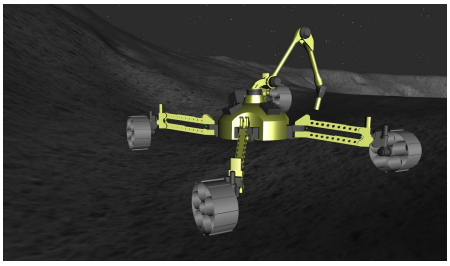

Fig. 6. Roll and pitch adaption for locomotion in slopes. The picture shows a screenshot taken from the physical simulation where the main body's roll and pitch angle are kept below 1°. The manipulator arm is oriented towards the slope.

1) Posture Stance: Fig. 5 illustrates three possibilities of the basic posture mode *stance*. This posture mode varies the support polygon of the robot. Narrow passages can be passed in a long stance, while the wide stance can be used to overcome medium sized craters or boulders without needing to traverse them with any wheel. For varying the stance, this posture mode controls the thorax angle of the legs. The regular stance mode for Sherpa has been chosen as a cross shaped footprint. A relatively high stability is ensured with this posture, while high flexibility concerning changes of the posture is achieved.

2) Posture Roll/Pitch: The posture mode *roll/pitch* keeps the roll and pitch angle of the robot within specified boundaries. This posture mode is important for negotiating moderate slopes and during traversing rugged terrain. If the body angles are kept approximately constant, mechanical stress induced into the manipulator arm mounting can be reduced. Fig. 6 shows a snapshot from the physical simulation environment, where Sherpa controls its roll and pitch angle by adapting the height of the wheels. The input for this posture mode is given by an inertial measurement unit. For the real system, the measurements of a force-torque load cell in the shoulder (currently under development) can be included additionally.

In principle, this posture mode can be superimposed with other posture modes. When the wheels are lifted (due to the morphology, a pure z-motion is not possible), stress might be induced in the structure. However, by combining the movements in the first two joints, the circular motion around the x-axis (Basal joint) can be transformed into a circular motion around the y-axis. In projection to the ground plane, this is a straight movement along the x-axis of the robot. This movement can easily be compensated by adapting the turning speed of the respective wheel.

3) Posture Tripod: Driving in a tripod configuration is necessary, if a wheel drive or wheel steering actuator fails. Then, the robot does not have to drag a malfunctioning wheel behind, which would affect energy efficiency and stability. If needed, the leg can still be used in some kind of stepping motion, where steering and/or wheel drive actuator are not needed. In order to increase the stability of the tripod

stance, this posture mode can be combined with the posture *manipulator balance*.

4) Posture Manipulator Balance: This posture mode makes active use of Sherpa's manipulator arm to support locomotion so as to increase the stability of locomotion. For this posture mode, the relation between COG and spanned support polygon is constantly checked. If the COG moves to close towards the border of the support polygon, an appropriate action of the arm is taken in order to move the COG back towards the center of the support polygon. The arm is not kept in a fixed pose, since its pose is constantly adapted to compensate for the movements of the rover in the terrain.

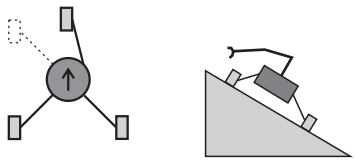

(a) Tripod posture: If a wheel unit fails, the robot can lift the corresponding leg.

(b) Using the manipulator for balancing the center of mass

Fig. 7. The posture modes *Tripod* and *Manipulator Balance*

C. Drive Modes for Sherpa

In this section, a subset of possible drive modes is presented. The drive modes are combined with the posture modes (and optional reflexes) into locomotion modes. Some drive modes are incompatible with certain posture modes. Only one drive mode is possible to be active at a time, while various posture modes can be activated simultaneously with the drive mode.

1) Omnidirectional Control: The instantaneous center of rotation (ICR) is a common tool to describe the translational and rotational movement of a rigid body as a purely rotational movement. It is also widely used in order to control wheeled vehicles, the control approach is not limited to flat terrains [17]. The ICR follows the rover movement and in each time instant, the ICR is the current center of rotation of the rover's body. By steering the wheels in order to cross their normals of their respective wheel plane in the ICR, a smooth trajectory following of the robot is made possible. Generally, for Sherpa all kinds of postures are compatible to the *ICR control*.

In case of Sherpa, there is no fixed geometry concerning the suspension system, i.e. the footprint of the robot is time-varying. Thus, the calculations for the wheel orientations always have to be adapted to the current posture mode of the robot, cf. section III.

A second issue arises with the mechanical design of the wheel modules. Since it is not possible to turn the wheel freely in 360°, several lines of singularities exist. If the ICR is moved across such a line, the wheel theoretically has to move in zero time from one limit to the opposing one (resulting in a 180° turn in 0 s). Fig. 5 illustrates the change between the singularity lines for three different stance modes.

For an ICR that temporarily reaches the singularity line, a correction movement with the thorax joint can avoid the singularity. When the ICR is set completely on a different side, the robot has to stop and re-orient the wheels in order to move on with the new ICR.

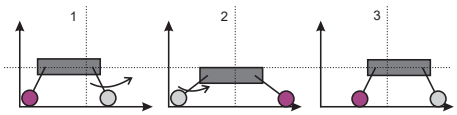

(a) By keeping one pair of wheels fixed with respect to the ground (colored wheel) the grip of the system is increased. The basal joints account actively for propelling the system.

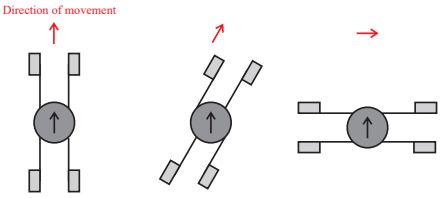

(b) "Omnidirectionality" of inch worming behavior: Due to the flexibility, inching can be executed in arbitrary directions. The arrow depicts the x-axis of the robot's body frame

Fig. 8. Drive mode *inch worming* and direction variations

2) Inch Worming: The drive mode *inch worming* utilizes the fact that in this mode at least two wheels have fixed ground contact at all times to reduce the slippage of the vehicle [7]. Fig. 8(a) depicts the three steps of this drive mode: (1) The rear wheels are fixed and the body is lowered by rolling over the front wheel pair. (2) At the lowest point, the front pair of wheels is kept fixed, while the rear wheels roll forward and the body hight is increased. (3) The procedure repeats itself.

Due to the flexibility of Sherpa's locomotion system, an arbitrary direction for this mode is possible. The Thorax joints are aligned in a way that ensures the desired direction of motion, fig. 8(b). First tests with the real system on a supporting frame proved that the inch worming mode can be used in an arbitrary 2D direction.

3) Stepping with Manipulator Arm Support: In general the active suspension system also allows stepping or walking motions. These can be useful when obstacles have to be overcome or single wheels have to be freed from stuck situations. To support stability, the manipulator arm can be used to stabilize the robot at the spot where the swing unit is lifted. The stepping behavior should only be used for short traverses and to free the robot since it is expected to be less energy-efficient than rolling motions.

The scheme for this locomotion behavior is as follows: (1) Place the manipulator's footplate close to the wheel that is next to be lifted, (2) lift the wheel and place it according to

the desired direction of movement, (3) when the wheel is on the surface again, move the manipulator to the next wheel that is to be lifted and start the procedure again.

Since the manipulator arm is designed to support the rover when two wheels are lifted, it should be possible to mount even obstacles that are higher than the 900 mm maximum vertical stroke of the rovers legs. However, this has still to be verified with the real system when the integrated manipulator arm is available.

V. CONCLUSION AND OUTLOOK

In this paper, posture and drive modes for the planetary rover Sherpa are introduced. By combining a drive mode with one or more posture modes, a locomotion mode for the rover is realized. The presented modes are an initial set that has been manually designed and partially implemented in a physical simulation environment and on the real system.

The design of the robot facilitates a multitude of postures and drive modes that can be implemented for locomotion in various terrains. Furthermore, the manipulator arm on the robot is explicitly designed for locomotion support. The possibilities for using the arm for locomotion include shifting of the COG to enhance the stability during the traverse of slopes. Furthermore, actively incorporating the arm into locomotion patterns is possible, so it can be used, for example, to support the rover when a leg is in a stuck situation.

The wheel configuration space for smooth movements without slipping and skidding under the constraint of a variable locomotion system is presented. In the next steps the model will be extended for application in rough environments.

The presented locomotion modes will be extended and evaluated experimentally in various terrains with the real system. Up to now the implementation has been validated on flat laboratory floor. The comparison of the results from the locomotion experiments in relevant terrain then feeds into a locomotion mode controller, which will be responsible for choosing the appropriate locomotion mode for the current terrain based on a metric that incorporates stability, maneuverability and energy considerations.

VI. ACKNOWLEDGMENTS

The project RIMRES is funded by the German Space Agency (DLR, Grant number: 50RA0904) with federal funds of the Federal Ministry of Economics and Technology (BMWi) in accordance with the parliamentary resolution of the German Parliament. RIMRES is a cooperation between the DFKI Bremen – Robotics Innovation Center and ZARM – Center of Applied Space Technology and Microgravity. Further partners are DLR-RY, EADS Astrium, and OHB System.

REFERENCES

[1] P. H. Schultz, B. Hermalyn, A. Colaprete, K. Ennico, M. Shirley, and W. S. Marshall, "The LCROSS Cratering Experiment," *Science*, vol. 330, no. 6003, pp. 468–472, 2010. [Online]. Available: http://www.sciencemag.org/cgi/content/abstract/330/6003/468

[2] B. Goldstein and R. Shotwell, "Phoenix: The first mars scout mission," in *Aerospace Conference, 2009 IEEE*, New York, USA, mar. 2009, pp. 1 –20.

[3] NASA Jet Propulsion Laboratory, "Mars exploration rover mission," Homepage of MER-Mission, last access 2011-07-20. [Online]. Available: http://marsrovers.jpl.nasa.gov/overview/

[4] NASA, "Webpage of Mars Science Laboratory," http://marsprogram.jpl.nasa.gov/msl/, last access 2011-07-20.

[5] NASA-JPL, "Free Spirit: Homepage on stuck situation of MER-A Spirit," http://www.jpl.nasa.gov/freespirit/, last access 2011-07-20.

[6] D. Wheeler, D. Chavez-Clemente, and V. SunSpiral, "Footspring: A compliance model for the athlete family of robots," in *Proceedings of the 10th International Symposium on Artificial Intelligence, Robotics and Automation in Space (iSAIRAS'10)*, 2010, pp. 644–651.

[7] D. Wettergreen, D. Jonak, D. Kohanbash, S. Moreland, S. Spiker, and J. Teza, "Field experiments in mobility and navigation with a lunar rover prototype," in *Proceedings of the 7th International Conference on Field and Service Robotics*, Cambridge, Massachusetts, July 14-16 2009. [Online]. Available: http://www.rec.ri.cmu.edu/fsr09/

[8] T. Bretl, "Motion Planning of Multi-Limbed Robots Subject to Equilibrium Constraints: The Free-Climbing Robot Problem," *The International Journal of Robotics Research*, vol. 25, no. 4, pp. 317–342, 2006. [Online]. Available: http://ijr.sagepub.com/content/25/4/317.abstract

[9] S. Bartsch, T. Birnschein, F. Cordes, D. Kuehn, P. Kampmann, J. Hilljegerdes, S. Planthaber, M. Roemmermann, and F. Kirchner, "SpaceClimber: Development of a six-legged climbing robot for space exploration," in *Proceedings of the 41st International Symposium on Robotics and 6th German Conference on Robotics, (ISR Robotik-2010)*, 2010.

[10] D. Spenneberg and F. Kirchner, *Climbing and Walking Robots Towards New Applications*. I-Tech Education and Publishing, October 2007, ch. The Bio-Inspired SCORPION Robot: Design,Control & Lessons Learned. [Online]. Available: http://sciyo.com/articles/show/title/the_bio-inspired_scorpion_robot__design_control___lessons_learned

[11] F. Cordes, D. Bindel, C. Lange, and F. Kirchner, "Towards a modular reconfigurable heterogenous multi-robot exploration system," in *Proceedings of the 10th International Symposium on Artificial Intelligence, Robotics and Automation in Space (iSAIRAS'10)*, August 2010, pp. 38–45.

[12] Z. Wang, F. Cordes, A. Dettmann, and R. Szczuka, "Evaluation of a power management system for heterogenous modules in a self-reconfigurable multi-module system," in *Proceedings of the International Conference on Intelligent Robots and Systems (IROS'11)*, San Francisco, CA, USA, September 2011.

[13] P. Ben-Tzvi, "Hybrid mobile robot system: Interchanging locomotion and manipulation," Ph.D. dissertation, University of Toronto – Department of Mechanical & Industrial Engineering, July, 30th 2008. [Online]. Available: https://tspace.library.utoronto.ca/handle/1807/11181

[14] P. S. Schenker, T. L. Huntsberger, P. Pirjanian, E. T. Baumgartner, and E. Tunstel, "Planetary rover developments supporting mars exploration, sample return and future human-robotic colonization," *Autonomous Robots*, vol. 14, no. 2-3, pp. 103–126, November, 1st 2004. [Online]. Available: http://www.springerlink.com/content/g55m107335658367/

[15] G. Campion, G. Bastin, and B. Dandrea-Novel, "Structural properties and classification of kinematic and dynamic models of wheeled mobile robots," *Robotics and Automation, IEEE Transactions on*, vol. 12, no. 1, pp. 47 –62, feb. 1996. [Online]. Available: http://ieeexplore.ieee.org/xpls/abs_all.jsp?arnumber=481750

[16] D. Spenneberg, M. Albrecht, and T. Backhaus, "M.o.n.s.t.e.r.: A new behavior-based microkernel for mobile robots," *Proceedings of the 2nd European Conference on Mobile Robots*, 2005.

[17] H. Xu, W. Huang, F. Peng, K. Xue, S. Yu, X. Gao, Q. Ouyang, Q. Chang, and Z. Lu, "Maneuver control of mobile robot based on equivalent instantaneous center of rotation in rough terrain," in *Proceedings of the 2007 IEEE International Conference on Mechatronics and Automation*, Harbin, China, aug. 2007, pp. 405 –410. [Online]. Available: http://ieeexplore.ieee.org/xpls/abs_all.jsp?arnumber=4303577&tag=1

[8]: **Heterogeneous Robotic Teams for Exploration of Steep Crater Environments**
F. Cordes, F. Kirchner
in: Planetary Rovers Workshop (ICRA 2010) ©IEEE 2010

Heterogeneous Robotic Teams for Exploration of Steep Crater Environments

Florian Cordes and Frank Kirchner
DFKI – German Research Center for Artificial Intelligence
Robotics Innovation Center Bremen
28359 Bremen, Germany
Florian.Cordes@dfki.de

***Abstract*— This paper describes three projects that are concerned with the exploration of the interior of steep craters, with special focus on exploring lunar craters with heterogeneous robotic teams. Within the project LUNARES (Lunar Exploration System), a terrestrial demonstrator for a lunar sample return mission has been created. The task of fetching a soil sample from within a permanently shadowed lunar crater had to be accomplished by a heterogeneous team of robots consisting of a wheeled rover and a legged scout. By means of different locomotion principles, the unique skills of these systems have been combined in order to increase the overall performance in the team. The follow-up project RIMRES (Reconfigurable Integrated Multi-Robot Exploration System) develops a rover and a six legged scout in a co-design process. The key idea remains: Robots with different locomotion capabilities cooperate as a team, in order to explore permanently shaded craters at the lunar poles. The third project, SpaceClimber, focusses on developing a six-legged free-climbing robot for crater environments. The SpaceClimber robot is likely to be used as antetype for the scout system in RIMRES. For more detailed information on the projects, references are provided.**

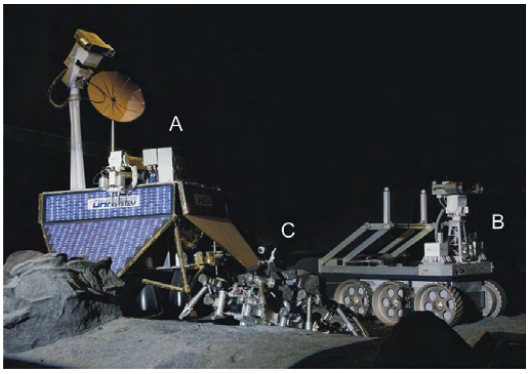

Fig. 1. LUNARES-Systems in artificial lunar crater test environment. A Lander mock-up with sensor tower and manipulator arm is installed (A). For mobility a wheeled rover (B) with parallel crank lever docking adapter and a legged scout (C) are used.

I. Introduction

Space exploration is currently dominated by exercising robots for fulfilling the scientific goals, since robots provide a better cost-efficiency for exploration along with lower risks for humans [1]. Robotic probes have already been send to extraterrestrial missions, Mars and Moon being the most prominent. Recently, Moon came into focus of scientific interest since the detection of possibly vast amounts of water ice at both lunar poles [2].

There are various approaches for lunar robotic technology of the next generation, including single robot systems like ATHLETE [3] and Scarab [4]. Multi robot systems are also under consideration, e.g. TRESSA [5] and the Robotic Contruction Crew (RCC) [6].

This paper presents the approach of a heterogeneous robotic team used for crater exploration at the lunar poles. The recently finished project LUNARES served the main purpose of demonstrating the general feasibility of the heterogeneous robotic team. This project is presented in the following section. Section III introduces the recently started project RIMRES and its current state of work. In this project a modular, heterogeneous multi-robot system is developed to provide high mobility on planetary surfaces. Section IV gives an overview of the SpaceClimber-project, developing a six-legged robot that is currently being developed for exploration of steep crater environments. In Section V this paper is concluded and an outlook on the next activities is given.

II. LUNARES

The recently finished project LUNARES [7] had the aim to combine existing robots in order to build up a heterogeneous robotic team for a terrestrial demonstration mission. The goal of the demonstrations was to show the general feasibility of the chosen approach. Space qualification of the single systems was of no concern in this project. The following chapters only give an overview on the systems and the chosen demonstration mission. For more details and experimental results, the reader is asked to follow the given references.

A. Systems

The LUNARES-team (Fig. 1) consists of two mobile units: (1) a wheeled rover for energy efficient locomotion in moderate terrains, and (2) a legged scout robot – the Scorpion robot [8] – is employed to fulfill the task of climbing into an otherwise inaccessible area, more specifically the interior of a steep crater. Furthermore, the team provides a manipulator

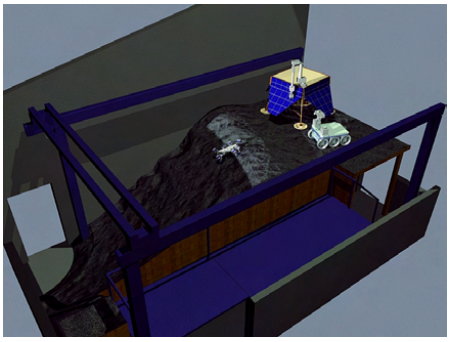

(a) CAD model of the artificial crater environment. The environment provides slopes of 30° to 45° in the interior of the crater and a small plateau for rover movements. Floodlights (not displayed) with narrow angle simulate lighting conditions at the lunar poles.

(b) Panoramic view from the crater bottom of the Space-TestBed (STB)

Fig. 2. The Space-TestBed, CAD-Model and photograph of the interior of the crater

and a sensor tower on a landing platform, which itself is a wooden mock-up in the case of the LUNARES-project.

Existing robots were used, but modified to meet the requirements of the project. As wheeled rover system an industrial transportation platform has been used and modified by adding a sensor tower (providing a stereo video camera, a laser scanner and illumination), exchange of the pneumatic tires with metallic wheels and addition of a docking adapter for picking up the scout.

For usage of the Scorpion robot as LUNARES-scout, the microkernel MONSTER [9] has been employed for locomotion control of the scout. Beside real-time capabilities and reflexes, the micro-kernel also offers an inverse kinematics layer which is used to describe the scout's rhythmic movement patterns in Cartesian coordinates. MONSTER allows for merging different behaviors, so that changing postures (i.e. lean forward, change roll-angle etc.) do not affect the walking pattern.

Additionally, one leg of the scout has been equipped with a sampling device for picking up a geological sample. To be able to identify the relative position of the sample with respect to the robot, a laserscanner and a mikro-PC system have been added to the Scorpion robot.

The feasibility of this approach with a wheeled and a legged robot acting as a team for lunar crater exploration has been tested and successfully demonstrated in an artificial lunar crater environment. The crater design is derived from pictures of Apollo missions and data from real craters at the lunar south pole. The artificial crater provides slopes between 30° and 45° within the crater and a slope of 15° at the outer rim. The crater has been set up in a laboratory of $45\,m^2$. Fig. 2(a) shows a CAD model of the artificial lunar crater environment with a grandstand for observing the experiments. In Fig. 2(b) a panoramic view into the main slope of the crater is given. To document experiments conducted in the environment, several surveillance tools have been installed: (1) a motion tracking system, (2) pan-tilt-zoom cameras and (3) a gantry crane that follows autonomously the system under test in order to give a constant top view video image and to provide the possibility for gravity compensation with counterweights. In [10] more detailed information is presented on automatic experimental data acquisition in the test environment.

B. Demonstration Scenario

In the demonstration scenario, a lunar sample return mission has been simulated using the heterogeneous systems of the LUNARES team in the artificial crater environment. The mission steps are presented in detail in the following paragraphs.

1) Autonomous Docking of Rover and Lander: At the start of the demonstration mission, the rover is situated in the vicinity of the lander, Fig. 3(a). In order to be able to equip the rover with a new payload (P/L), the rover has to be positioned in the workspace of the lander's manipulator. This is achieved by an autonomous docking, which makes use of the lander's laser scanner. The payloads used in the demonstration scenario are mock-ups representing scientific instruments of a real mission. By equipping the rover with different payloads, it is possible to configure the system for the current mission at hand. The docking approach and experimental results are described in detail in [11].

2) Payload Exchange on the Rover: After reaching the workspace of the lander's manipulator, the rover is equipped with a payload – Fig. 3(b). The P/L is picked from the lander and placed into a designated payload bay of the rover.

3) Movement of Rover and Scout to the Crater Rim: After finishing the task of reconfiguration, the manipulator arm is retracted, Fig. 3(c). Rover and docked scout then drive towards the crater rim. This demonstrates the ability of the wheeled system to move in an energy-efficient way in moderate terrain. Generally the rover should negotiate longer distances. However, due to space constraints in the Space-TestBed, the distance covered by the rover is limited to a

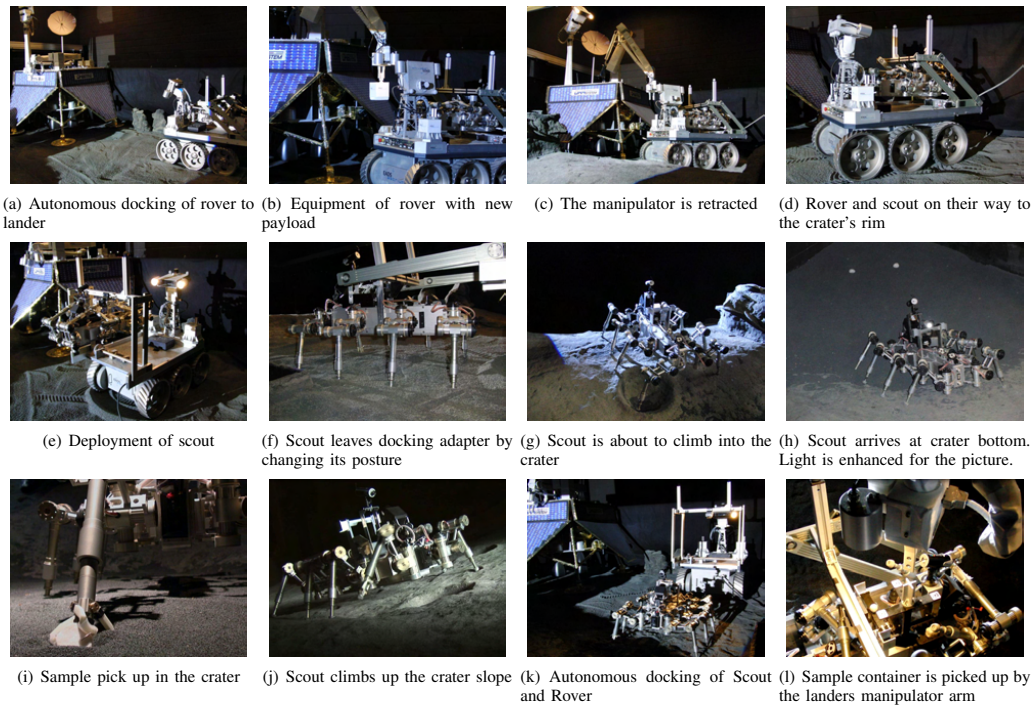

(a) Autonomous docking of rover to lander
(b) Equipment of rover with new payload
(c) The manipulator is retracted
(d) Rover and scout on their way to the crater's rim
(e) Deployment of scout
(f) Scout leaves docking adapter by changing its posture
(g) Scout is about to climb into the crater
(h) Scout arrives at crater bottom. Light is enhanced for the picture.
(i) Sample pick up in the crater
(j) Scout climbs up the crater slope
(k) Autonomous docking of Scout and Rover
(l) Sample container is picked up by the landers manipulator arm

Fig. 3. Scenes from the LUNARES sample return demonstration mission. The mission provides autonomous behaviors as well as remotely controlled sequences. Especially positioning of the robots for docking, sampling and manipulation is achieved by autonomous approaches in order to enhance the performance of the systems.

few meters. Fig. 3(d) illustrates rover and scout collectively driving towards the crater's rim.

4) Undocking of Scout and Rover: Once the team consisting of rover and scout arrives at the crater rim, the scout undocks from the rover. Therefor the docking adapter mounted on the back of the rover is used. The parallel crank lever facilitates the scout's deployment onto the surface as depicted in Fig. 3(e). By adjusting the posture of the scout, it leaves the hook of the docking adapter, Fig. 3(f).

5) Scout Descends into Crater: After the detaching from the rover, the scout heads for the crater rim and enters the dark interior of the crater, Fig. 3(g). On the way to the bottom of the crater, small impact craters and rocks buried into the regolith have to be overcome or circumnavigated in the slope. In the LUNARES mission the movements of the scout in the crater slope are remotely controlled by an operator, using the camera which is mounted on top of the scout, deeply buried rocks are simulated with rocks fixed to the surface – Fig. 2(b).

6) Sample Collection at Crater Bottom: Figure 3(h) depicts the arrival of the scout at the crater bottom. The normally dark environment is lighted up for better visibility on the picture. A scientific operator chooses a geological sample using the video image provided by the scout. In an autonomous approach behavior, the scout positions itself in front of the selected sample. When this coarse positioning is done, a fine detection of the samples's coordinates is executed. By using its laser scanner the scout generates a 2.5D-height map of its direct vicinity. The coordinates of the sample are extracted from the 2.5D-height map, to position the scout's leg on the sample of interest. After grabbing the sample with the integrated manipulator, the sample is placed in the sample container on the back of the scout, Fig. 3(i). More information on the sample approach and sample pick up is provided in [12].

7) Scout Climbs Back up the Crater: When the sample has successfully been collected and stored in the sample container, the scout starts to climb the crater slope and back towards the rover. The scout climbs freely in the crater slope as depicted in Fig. 3(j). No tethering system is applied. However, due to calculation power the locomotion in the slope remains remotely controlled.

8) Cooperative Docking of Rover and Scout: After arrival at the rover, the scout turns its back to the rover as depicted in Fig. 3(k) to prepare for the autonomous docking procedure. For this procedure, the rover detects specific optical markers on the scout and commands the scout into a predefined docking pose. The docking procedure of rover and scout as well as experimental results are described in detail in [11].

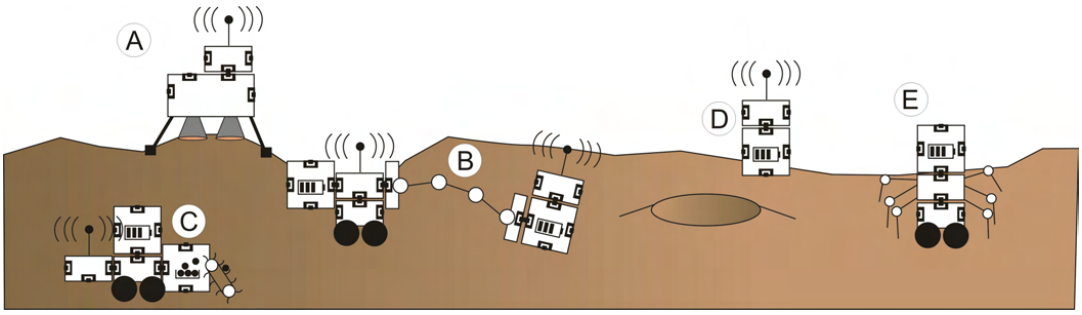

Fig. 4. Illustration of the envisioned RIMRES system. A: Landing unit with radio module and free module slots; B: Rover with radio module and additional battery module deploys radio beacon; C: Rover with additional battery and radio module makes use of a sampling module; D: Operating radio module stack; E: Connected rover and scout on their way to a crater for exploration.

9) Return of Rover and Scout to Landing Unit: Similar to the initial procedure, rover and scout collectively drive back to the landing unit using the autonomous docking procedure between rover and lander. The docking process ends, when the rover and thus the scout's sample container are within the workspace of the lander's manipulator arm.

10) Transfer of Sample Container to Landing Unit: The last step of the LUNARES demonstration mission consists of unloading the sample container from the docked scout, as depicted in Fig. 3(l). The sample is then transferred onto the landing unit. This process is performed autonomously, a visual servoing approach allows to determine the exact position of the sample container with respect to the manipulator.

C. Conclusions

The project LUNARES dealt with the topic of using a heterogeneous team of robots to cope with the task of fetching a soil sample from within a permanently shadowed crater at the lunar south pole. The system that has been build up consists of previously existing robots, that were modified to achieve the given task. LUNARES showed, that even with existing robots, the chosen approach in principle is feasible [12]. Only minor modifications were needed to achieve the task with not specifically designed robots. The experiences made in the LUNARES project can directly be exploited for projects such as SpaceClimber and RIMRES, being described in the subsequent chapters.

III. RIMRES

RIMRES [13] picks up the ideas of LUNARES and additionally addresses the modularity of the systems. The purely mechanical connection of rover and scout in LUNARES is extended by introducing a mechatronic interface, providing a mechanical connection as well as data and energy connections. Utilizing the interface, two robots can closely connect and act as one single robotic system, as well as two independent systems when needed. Figure 4 illustrates an envisioned scenario for the RIMRES system.

A. Systems

As opposed to LUNARES, in RIMRES the new mobile units are meant specifically for the purpose of forming a tightly coupled team. Thus this requirement is considered in the design phase already. Parts of the systems can be switched off during connection to save energy, i.e. the legs of the scout and parts of its sensors not needed when coupled with the rover can be shut down.

Because of the tight coupling of rover and scout via the mechatronic interface (data, electrical and mechanical energy connection), there are multiple ways to enhance the redundancy. In case of rover sensor faults, the scout could take over control of the rovers actuators and navigate the rover/scout team using its own sensors. Alternatively, the rover could directly control the scout's legs while both robots are coupled, allowing the rover to make use of the sampling device in the scout's legs. Figure 5 on the next page shows an artist drawing of the RIMRES system: A rover with connected scout is visible in the foreground. The rover is about to set out a module stack, while the connected scout analyzes a small rock with its front legs. A second scout climbs a slope in the background.

The following paragraphs give an overview of the planned design of the systems. A wheeled rover, a legged scout and additional payload modules representing scientific and functional modules will be implemented.

1) Rover: For RIMRES, a rover is designed from scratch. This rover will feature four wheels each one suspended by an actuated parallel kinematic. These "legs" of the rover can be actuated with four degrees of freedom (DOF), allowing an adaption to slopes and providing the ability to actively lift a leg from a stuck situation. Additionally, big obstacles can be overcome. By using spindle drives, the actuators of the rover do not require energy for keeping the rover's body height.

The wheels of the rover will be equipped with sophisticated adaptronics. Thus the wheels can adapt their stiffness to changing ground properties as well as to changing mass of the rover. For example the rover's mass is changed by docking and undocking of the scout, whose mass will be

around 20 kg.

On top of the rover there will be four payload-bays implemented, each providing a mechatronic interface for placement of the immobile payload-modules. To be able to handle the modules, a robotic arm is implemented in the center of the robot. The scout system will be situated beneath the rover, coupled with the rover via the mechatronic interface. The placement of the scout will be designed in a way, that the scout is still able to use its front pair of legs as manipulators/sampling device.

2) Scout: The scout design will follow the design of the SpaceClimber, a six legged robot currently under development, see also Section IV. To allow for coupling with the rover, a mechatronic interface will be implemented on the back of the scout.

The main task of the scout is to access areas that are not reachable by the wheeled system. This includes steep craters as well as elevated planes. In general the scout can use its front legs as sensing devices, for example by implementing the external optical head of a combined Raman-LIBS (Laser Induced Breakdown Spectroscopy) spectrometer. The laser source and electronics for analysis could be placed in the scouts body. However, in RIMRES this analysis tool will be represented by a sampling device similar to that one implemented on the Scorpion robot [7].

3) Additional Modules: Along with two mobile units, the RIMRES system provides immobile payload modules that can be attached to the rover as well as to the scout. The modules can be stacked using the mechatronic interface and deployed by the rover. This way, more complex scientific packages consisting of different modules may be set up in order to be deployed on the lunar surface.

A battery module is planned to represent an energy harvesting module (solar-module) for the immobile payload stacks and to enable longer operations in shaded regions for the mobile units. A radio module will be implemented, featuring data relay as well as navigation functionalities. The REIPOS (Relative Interferometric Position Sensor) will be able to detect the direction and distance of other REIPOS-Modules, thus building a rudimentary navigation infrastructure. Camera modules will represent scientific payloads to be placed on the lunar surface, for example seismic experiments. The PLUTO Mole [14] that flew with Beagle-2 in the Mars Express mission, will be incorporated in a module frame in order to demonstrate the modular approach of scientific payload design.

B. System Control

As described above, the RIMRES-System consists of different mobile and immobile subsystems, constituting a reconfigurable, modular overall system. To be able to control the system, a representation of the current system configuration has to be mapped in the software. A new module in a module network has to be made known and propagate its functionalities to the existing system of modules. A ”new” module can enter or leave a system of modules by

- reaching or leaving the range of the radio signal

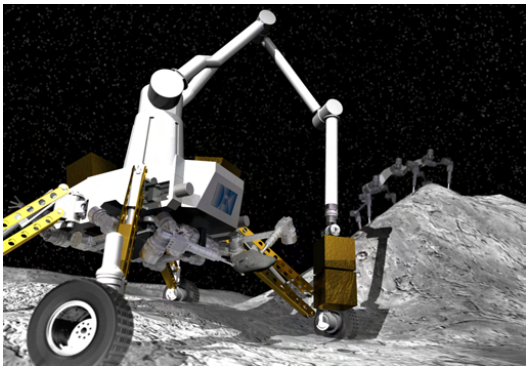

Fig. 5. RIMRES-scenario in an artist drawing. The rover in the foreground is about to set out a stack of two modules. The connected scout beneath the rover analyzes a small rock sample. In the background, a second scout climbs a slope to steep for the wheeled system.

- mechanically (dis)connecting to (from) another module

The software framework will support communication between two modules providing the possibility of using individual modules as relay station, remote software updates, control of modules by other modules, search for modules with specific functionalities and other control options. The communication of modules can be divided into remote communication (of modules that are not connected via the mechatronic interface) and direct communication via the mechatronic interface.

The control system incorporates human interaction and support as well as autonomous behaviors of the systems. The concept provides a continuum of autonomy levels, ranging form full autonomy to direct (tele operated) control. There are three main events, that induce the change of autonomy level:

- Human initiated autonomy switch (the operator demands for control)
- Planned autonomy change (the mission time line provides a change of the autonomy level)
- Robot initiated autonomy change (the robot recognizes, that it cannot fulfill its task under the given circumstances)

Especially the robot initiated autonomy switch requires research on the self-assessment of the robot. The concept and first results of the pursued sliding autonomy approach are described in more detail in [15].

IV. SpaceClimber

The goal of the SpaceClimber project is the development of a biologically inspired, energy-efficient, free-climbing robot for steep slopes. SpaceClimber should prove that walking robotic systems present an option for future missions on difficult terrain, in particular missions in craters or rock fissures. The robotic system that is developed should be able to conquer irregular slopes of up to 80% and should be in

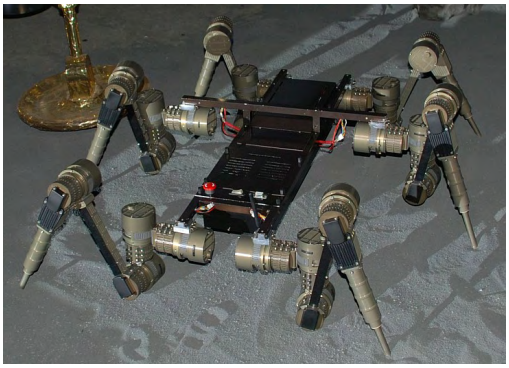

Fig. 6. The integration study of SpaceClimber in the Space TestBed. The legs are fully integrated and operational. The body itself is up to now a "carrier-platform" for the legs and central electronics. It is to be replaced with a new body including one DOF for lifting the front third of the torso.

a position to navigate with local autonomy using built-in sensors [16].

SpaceClimber is a six-legged walking robot with four active DOF per leg plus an additional passive DOF in the lower leg, Fig. 6. The morphology of the robot has been determined with evolutionary strategies. In simulation a fitness function for minimizing energy consumption was set up to evaluate the locomotion on flat ground and walking on slope of 30° up and down, respectively. For the evolution, certain constraints were defined: (1) The system should have six legs, (2) each leg consists of four joints in a given orientation with respect to the body and (3) the six legs are mounted in three pairs of two symmetrical legs. The parameters that were influenced by the evolutionary process were (1) the length of the last link and the lower leg (the first three joints are connected to form a shoulder joint), (2) the horizontal position of a leg-pair, (3) the vertical position of a leg-pair, and (4) the width of a pair of legs. Simultaneously with the morphology, walking patterns were learned to optimize the locomotion in both, flat ground as well as slopes. More details on the evolutionary design of the robot are given in [17].

The actuators for the joints of the robot provide a BLDC motor with a harmonic drive gear. The actuator modules furthermore provide electronics containing power electronics, electronics for sensor data acquisition as well as an FPGA for implementation of control algorithms, logging capabilities and communication with other actuators and the central processing unit. The power consumption of the joints is 30 W, 18 W and 13 W while exerting 23 Nm, 16 Nm and 12 Nm at 3 rpm respectively [18].

V. Conclusion and Outlook

In this paper we reviewed the LUNARES project and the achievements of this first approach of a heterogeneous team of robots for space application. In LUNARES an artificial lunar crater environment has been set up to test the feasibility of the chosen approach. A wheeled rover is used to overcome moderate terrain and slopes in an energy efficient way. A legged scout, equipped with sampling/sensing devices, is used to advance into the permanently shaded regions of a lunar crater. In these regions a sample is taken or in situ measurements with integrated sensor equipment are undergone.

The RIMRES project picks up the idea of heterogeneous robots acting as a team for crater exploration. In RIMRES, a new rover and a scout are developed, these systems are able to connect to each other and further immobile payload-modules via a mechatronic interface. The autonomy of the systems will be addressed in a sliding autonomy framework, providing autonomy continuously ranging from remote control to full autonomy. The SpaceClimber robot in a modified version will serve as scout system in the RIMRES scenario.

The next steps in the project RIMRES are to finish the concept phase and finalize the design of rover, mechatronic interface and system control. The modifications of SpaceClimber to suit the needs of the RIMRES scout will be of interest in the near future.

Acknowledgements

The authors would like to thank all members of the project teams of LUNARES, RIMRES and SpaceClimber.

The project LUNARES is funded by the German Space Agency (DLR, Grant number: 50RA0706) and the Investment Association Bremen (BIG, Grant number: INNO1036A) and is a cooperation between DFKI RIC Bremen, EADS Astrium GmbH, and OHB-System AG.

The project RIMRES is funded by the German Space Agency (DLR, Grant number: 50RA0904). RIMRES is a cooperation between the DFKI RIC Bremen and ZARM – Center of Applied Space Technology and Microgravity.

The project SpaceClimber is funded by the European Space Agency ESA (Contract no.: 18116/04/NL/PA) and the German Space Agency (DLR, Grant number: 50RA0705)

References

[1] Andrew J. Coates. Limited by cost: The case against humans in the scientific exploration of space. *Earth, Moon, and Planets*, 87(3):213–219, 1999.

[2] NASA.gov – Mini-RF. Exploring the lunar poles. `http://www.nasa.gov/mission_pages/Mini-RF/multimedia/feature_ice_like_deposits.html`, March 2010.

[3] Brian H. Wilcox, Todd Litwin, Jeff Biesiadecki, Jaret Matthews, Matt Heverly, Jack Morrison, Julie Townsend, Norman Ahmad, Allen Sirota, and Brian Cooper. ATHLETE: A cargo handling and manipulation robot for the moon. *Journal of Field Robotics*, 24(5):421, 2007.

[4] David Wettergreen, Dominic Jonak, David Kohanbash, Scott Jared Moreland, Spencer Spiker, James Teza, and William (Red) L. Whittaker. Design and experimentation of a rover concept for lunar crater resource survey. In *47th AIAA Aerospace Sciences Meeting Including The New Horizons Forum and Aerospace Exposition*, January 2009.

[5] Terry Huntsberger, Ashley Stroupe, Hrand Aghazarian, Mike Garrett, Paulo Younse, and Mark Powell. Tressa: Teamed robots for exploration and science on steep areas: Field reports. *J. Field Robot.*, 24(11-12):1015–1031, 2007.

[6] Terry Huntsberger, Ashley Stroupe, and Brett Kennedy. System of systems for space construction. *2005 IEEE International Conference on Systems, Man and Cybernetics*, 4:3173 – 3178 Vol. 4, Oct. 2005.

[7] Florian Cordes, Steffen Planthaber, Ingo Ahrns, Sebastian Bartsch, Timo Birnschein, and Frank Kirchner. Cooperating reconfigurable robots for autonomous planetary sample return missions. In *ASME/IFToMM International Conference on Reconfigurable Mechanisms and Robots (ReMAR-2009)*, London, United Kingdom, June 2009.

[8] Dirk Spenneberg and Frank Kirchner. Scorpion: A biomimetic walking robot. In VDI, editor, *Robotik 2002*, volume 1679, pages 677–682. VDI, 2002.

[9] Dirk Spenneberg, Martin Albrecht, and Till Backhaus. M.O.N.S.T.E.R.: A new behavior-based microkernel for mobile robots. In *ECMR 2005*, 2005.

[10] Alexander Dettmann, Stefan Haase, and Frank Kirchner. Automatic robot supervision within a lunar crater environment. In *Proceedings of the ISR/Robotik2010, accepted*, Munich, Germany, 2010.

[11] Thomas M. Roehr, Florian Cordes, Ingo Ahrns, and Frank Kirchner. Cooperative docking procedures for a lunar mission. In *Proceedings of the ISR/Robotik2010, accepted*, Munich, Germany, 2010.

[12] Sebastian Bartsch, Florian Cordes, Stefan Haase, Steffen Planthaber, Thomas M. Roehr, and Frank Kirchner. Performance evaluation of an heterogeneous multi-robot system for lunar crater exploration. In *Proceedings of the 10th International Symposium on Artificial Intelligence, Robotics and Automation in Space (iSAIRAS'10), accepted*, Sapporo, Japan, 2010.

[13] Florian Cordes, Daniel Bindel, Caroline Lange, and Frank Kirchner. Towards a modular reconfigurable heterogenous multi-robot exploration system. In *Proceedings of the 10th International Symposium on Artificial Intelligence, Robotics and Automation in Space (iSAIRAS'10), accepted*, August 2010.

[14] Carol R. Stoker, Lutz Richter, William H. Smith, Larry G. Lemke, Philip Hammer, Brad Dalton, Brian J. Glass, and Aaron Zent. The Mars Underground Mole (MUM): A Subsurface Penetration Device with In Situ Infrared Reflectance and Raman Spectroscopic Sensing Capability. In S. Mackwell & E. Stansbery, editor, *Proceedings of the Sixth International Conference on Mars*, volume 34 of *Lunar and Planetary Inst. Technical Report*, March 2003.

[15] Thomas M. Roehr, Yuping Shi, and Frank Kirchner. Using a self-confidence measure for a system-initiated switch between autonomy-levels. In *Proceedings of the 10th International Symposium on Artificial Intelligence, Robotics and Automation in Space (iSAIRAS'10), accepted*, August 2010.

[16] Sebastian Bartsch, Timo Birnschein, Florian Cordes, Daniel Kuehn, Peter Kampmann, Jens Hilljegerdes, Steffen Planthaber, Malte Roemmermann, and Frank Kirchner. SpaceClimber: Development of a six-legged climbing robot for space exploration. In *Proceedings of the 41st International Symposium on Robotics and 6th German Conference on Robotics, (ISR Robotik-2010), accepted*, 2010.

[17] Malte Roemmermann, Daniel Kuehn, and Frank Kirchner. Robot design for space missions using evolutionary computation. In *IEEE Congress on Evolutionary Computation. IEEE Congress on Evolutionary Computation (IEEE CEC-2009), May 18-21, Trondheim, Norway*. -, 2009.

[18] Jens Hilljegerdes, Peter Kampmann, Stefan Bosse, and Frank Kirchner. Development of an intelligent joint actuator prototype for climbing and walking robots. In *Mobile Robotics - Solutions and Challenges. 12th International Conference on Climbing and Walking Robots and the Support technologies for Mobile Machines (CLAWAR-09), September 9-11, Istanbul, Turkey*, pages 942–949. o.A., 2009.

FIELD TESTING OF A COOPERATIVE MULTI-ROBOT SAMPLE RETURN MISSION IN MARS ANALOGUE ENVIRONMENT

Roland U. Sonsalla, Florian Cordes, Leif Christensen, Thomas M. Roehr, Tobias Stark, Steffen Planthaber, Michael Maurus, Martin Mallwitz, and Elsa A. Kirchner

DFKI Robotics Innovation Center, Robert-Hooke-Str. 1, 28359 Bremen, Germany, Email: Roland.Sonsalla@dfki.de, firstname.lastname@dfki.de

ABSTRACT

This paper presents the evaluation of a heterogeneous robotic team for planetary exploration purposes. An extensive test campaign with a duration of four weeks was conducted in October/November 2016 in the desert of Utah, USA. The employed robotic systems were tested on natural and unstructured Mars analogue terrain and remotely operated from a control station in Bremen, Germany. The paper details the performed system tests as well as the conducted cooperative mission sequences in the scope of a sample return mission. Furthermore, the planning and preparation of the field trial campaign as well as the infrastructure set-up in Utah and Bremen and the test execution are presented with regard to lessons learned in the field and at the control center in Bremen.

Key words: Mars Rover, Field Trial, Robot Team, Modularity.

1. INTRODUCTION

Mars is the most attractive planet within our solar system for human exploration, providing an atmosphere, moderate temperatures and is in general similar to Earth. Currently, geological and biological robotic exploration is of main interest for gathering knowledge on the history of Mars and possible former or present life on Mars.

In the future, more sophisticated and complex mission scenarios are envisaged for Mars exploration as it is one of the main targets announced by NASA and ESA [1, 2]. Ranging from robotic exploration over sample return to human exploration missions, including the potential set-up of support infrastructure, a need arises for highly capable robotic systems to meet the requirements. One approach to tackle these challenges is to introduce a multi-robotic team in contrast to the common single system set-up, e.g. for sample acquisition and return [3] and/or to increase the overall safety, speed and exploration range of robotic systems [4]. In order to test such systems against their suitability for Mars exploration, field tests provide a good way to deploy the systems in natural analogue environments along with the whole mission command and control architecture [5].

Figure 1. The employed systems in the field trials: Hybrid wheeled-leg rover SherpaTT (left, with modular sampling tool attached to the manipulator arm), Coyote III (center background and inset, with modular manipulator arm SIMA) and BaseCamp (right, with attached sample container)

Geological sampling and sample-return might be conducted by a multi-robot team where single units are specialized on taking samples from various locations or fetching stored sample containers to transfer them to a return stage for sending the samples back to Earth. Such a scenario was tested in a four week field trial, as described in this paper. For the experiments, the TransTerrA system [6] was deployed in the desert of Utah during October and November 2016. Fig. 1 displays the systems in the test environment. The multi-robot system is composed of (i) the main exploration and sampling rover SherpaTT, (ii) the shuttle/scout system Coyote III, equipped with (iii) the modular manipulator arm SIMA, (iv) various modular payload-items (PLIs) for sample collection, storage and transfer, (v) a BaseCamp with five docking bays for the PLIs, additionally, a (vi) "Ground Control Station" in Bremen, Germany was used to control the execution of the mission sequence via a satellite link.

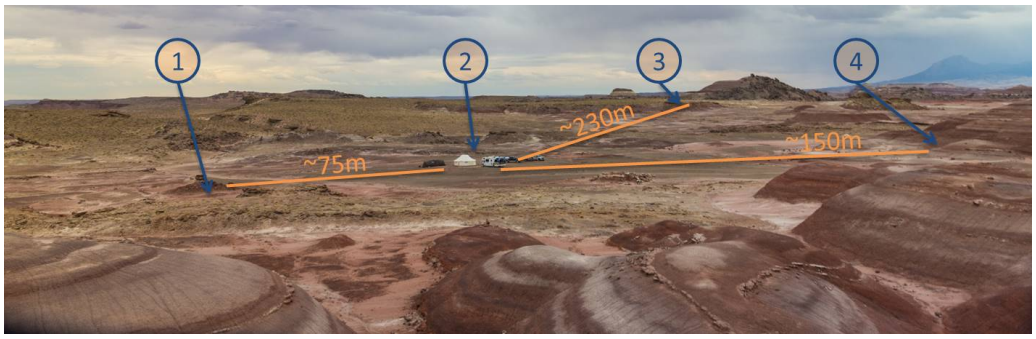

Figure 2. Overview on the testing area with indications of main test spots and distances. (1) The testing area for the mission sequence, see also Figure 9, (2) The camp with materials tent, working tent for repair and local mission control (3) Spot for cliff exploration (4) Slope climbing with SherpaTT and Coyote III

2. TEST SITE AND INFRASTRUCTURE

The test site for the field trials is located near Hanksville in Utah, USA, at 38° 24' 46.141" N and 110° 47' 1.118" W. The landscape represents a Mars analogue environment as described in [7, 8] and is marked by vast plains, rocky hill formations and mesas as shown in Fig. 3. The landscape was formed due to erosion, leaving inverted river beds with steep slopes and fluvial channels formed by clay-rich soils and sandstone. Similar formations were found on Mars and are of high interest for further exploration. The test site presents a wide variety of soils and slopes, ranging from flat terrain to steep slopes with inclinations of over 50° and even cliffs with overhangs. Firm clay-based soils as well as gravel and very loose sandy soils are present in the plain. Different slopes with unstructured rocky terrain, layered sandstone as bed-rock and duricrust are within the vicinity of the test site (cf. Fig. 5). Due to its analogue features other test campaigns have been conducted at the test site by the Canadian Space Agency (CSA) in 2015 and 2016 [8, 9] and the UK Space Agency (UKSA) in 2016 [10, 11].

As no infrastructure was available at the test site, a base station was set-up in the desert. The core elements of the base station were a materials tent, a working tent and a caravan, as shown in Fig. 2. The materials tent with approximately 20 m^2 was mainly used as storage space for equipment boxes and robot transport cases. The working tent with approximately 30 m^2 was used for local mission control and system maintenance. The tent was equipped with a local control station, as well as a small electro-mechanical workshop for in-field repair of the systems. Moreover, all robotic systems were placed in the tent and the tent was heated by two fan heaters during night. This precaution was taken, to avoid water condensation due to a temperature drop and to keep sensitive electronic parts as well as the robot batteries above 0° C during the night. The base station was completed by a caravan, which was mainly used as sleeping place for the night crew. Furthermore, it served as food and water storage and was used as gathering and working place with reduced wind and dust pollution.

Figure 3. Overview of the main testing area with SherpaTT in the foreground and inverted river beds in the background

The power supply was realized with three independent systems. These were two fuel driven power generators as well as a solar array. A coupling of these systems to a stand-alone power station was not realized. The working tent was connected to a solar array bench, consisting of five 100 W solar arrays which were connected to a 12 V secondary battery for energy storage and a voltage converter providing 230 V. The power generated by the solar arrays was e.g. used to recharge the batteries of laptops, walkie-talkies, cameras and portable floodlights. Furthermore, the working tent was equipped with LED based illumination tubes, which ran on solar power. In addition a 100 W solar array in combination with a secondary battery was used to provide the power for a transportable communication relay link in the field. The two power generators were mainly used stationary at the base station. They provided the power for the local control station as well as additionally needed laboratory power supply.

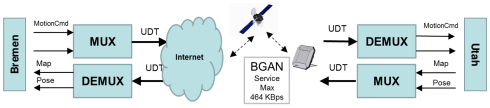

Figure 4. Schematic representation of the established satellite communication link between the test site in Utah, USA and Mission Control in Bremen, Germany

For robot communication in the field a local WiFi-based communication mesh was established enabling the robotic team to operate independently of a central access point. All robotic systems, the local control station and the remote control station were linked through this mesh. Each of the participating nodes served also as communication relay, resulting in an extended communication coverage in the field. To communicate with the mission control in Bremen an Inmarsat/BGAN satellite modem was used, providing up to 464 kbps of bandwidth. The satellite modem was connected via Ethernet to the local control station which managed the exchange of telemetry data and commands between the control station in Bremen and the robots in the field. A schematic diagram of the communication link architecture is shown in Fig. 4.

3. ROBOTIC SYSTEMS

This section provides an overview on the mobile and immobile robotic systems involved in the field trials. Both mobile systems are shown in Fig. 5. The mission control is described in Section 5.

3.1. Exploration Rover SherpaTT

SherpaTT is a rover of about 150 kg mass with a hybrid wheeled-leg actively articulated suspension system [12]. With its suspension, the system is able to actively adapt to irregular, natural terrain and slopes. Each of the four legs that constitute the suspension has a total of five active Degree of Freedom (DoF). Apart from its four legs forming the suspension, the rover features a 6 DoF manipulation arm. As part of the modular multi-robot system, the rover is equipped with six electro-mechanical interfaces (EMIs) [13], four passive interfaces are mounted around the central manipulation tower, an active interface is used as end-effector of the manipulator for grasping the passive counterpart on any other modular payload or mobile system. A second active interface is mounted beneath the rover's main body structure, mainly for transporting and deploying a BaseCamp (see Section 3.4).

A rotating lidar sensor is used for generating point clouds of the environment which are transformed into Multi-Level Surface (MLS) and traversability maps. The lidar is mounted on the manipulator tower such that it rotates with the first joint of the arm. This configuration allows

Figure 5. SherpaTT during a single system test concerning slope driving capabilities (top) and Coyote III in preparational tests for cliff exploration scenarios (bottom)

the sensor to be mounted on top of the rover where it can provide the best environment data while at the same time a rotation of the sensor/manipulator allows full view around the rover without occlusion by the arm structure.

3.2. Shuttle and Scout System Coyote III with SIMA manipulation arm

Designed as a micro rover with a mass of approximately 15 kg Coyote III is considerably smaller than its teammate SherpaTT. By use of four directly driven hybrid legged-wheels on a passive chassis the rover gains a high mobility performance in unstructured terrain and steep slopes as can be seen in Fig. 5. Equipped with its own power source, computer and on-board sensor suite, including a laser range finder and a camera, Coyote III is able to perform autonomous exploration tasks. The communication subsystem allows to cooperate with other systems, such as SherpaTT.

Coyote III is equipped with two passive EMIs and its own payload management system, allowing to dock additional payload elements such as PLI to the rover. Due to the lightweight and robust structural design of Coyote III, it is possible to apply several kilograms of additional payload to the rover. In this way, Coyote III can not only act as a scouting system for SherpaTT but as a support system by transporting PLIs and providing shuttle services. In

order to handle the PLI, e.g. for deployment, Coyote III can be equipped with the SIMA module. SIMA is a full 5 DoF manipulator arm which is equipped with two active EMIs. The arm can be docked as additional payload to one of Coyote III's payload bays. Fig. 10 shows Coyote III with attached manipulator arm during rendezvous with SherpaTT. Both systems, Coyote III and the manipulation arm SIMA are described in more detail in [14].

3.3. Modular Payload-Items

Modular payload-items in the sense of the system presented here are cubic modules with an edge length of 15 cm. Each PLI has a passive EMI on the top and an active EMI on the bottom face of the cube [13]. A PLI can generally contain any payload needed for a specific mission purpose, PLIs with a height of more or less than 15 cm are possible, for ground truth, a D-GPS (differential GPS) system was integrated in a PLI and used in the field trials in Utah.

For the mission sequence during the field trials, battery and sampling modules were implemented. A battery module can be used to power any system (mobile and immobile) via the connecting EMIs of each subsystem, a battery module is typically integrated in a standard (15×15×15cm) cube. The sampling module features a retractable shovel, simulating a sealing of a sample within the sample container and is also integrated into a standard cube. For taking a soil sample, the module is attached to SherpaTT's manipulation arm (as depicted in Fig. 1), pulled over loose soil and than closed by retracting the shovel.

3.4. BaseCamp

A BaseCamp is a special type of immobile payload. It has roughly the size of five standard PLIs arranged in a cross-like manner with one PLI in the center and the remaining four PLIs attached to each side of the central cube, a deployed BaseCamp can be seen Fig. 1.

A BaseCamp is transported by SherpaTT via the EMI located in the central body's ground plate. By lowering the rover's body and releasing the mechanical connection by opening the EMI's latch, the BaseCamp can be deployed on the ground. It can however, be handled by SherpaTT's manipulator as well, as it uses the same EMI. Main tasks for the BaseCamp are (i) to act as a communication relay for the mobile units, and (ii) to provide a sample/battery cache. In later development stages, the BaseCamp might be equipped with solar panels in order to be able to recharge battery modules.

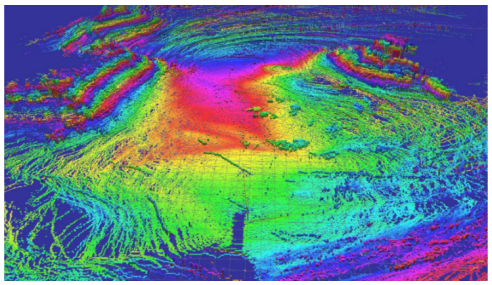

(a) Multi Level Surface (MSL) Map. Color indicates height, color cycle repeats each 1 m in height

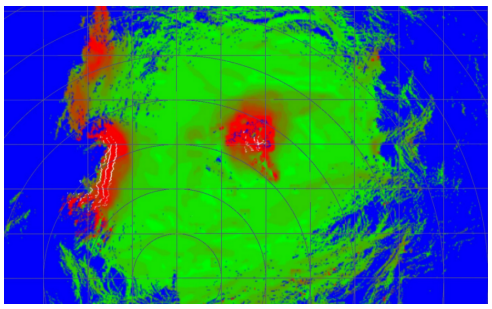

(b) Traversability Map. Red is not traversable, green areas are possible to be navigated through.

Figure 6. SLAM-based maps as created by the rovers at the Utah test site

4. SOFTWARE DESIGN

Establishing a common platform for autonomy for a distributed, heterogeneous and reconfigurable team of robots has been the major driver of the software design. The key requirements were autonomous navigation in unknown environment including a distributed mapping approach, manipulation capabilities, and establishing a general decentralized infrastructure to allow for reconfigurability.

As a baseline for all robotic systems the Robot Construction Kit (Rock) [15] has been used in order to support a modular development approach. The high modularity of the software components allows high reusability for the heterogeneous team of robots, so that for example the mapping infrastructure can be designed generically. In this context, the field test served also as evaluation of a Debian-based binary package distribution which was used for a common set of packages on all robotic systems.

The starting point of autonomous operations has been the consistent creation of a shared environment representation. The robots used throughout the field testing comprise different set of sensors which might result in distinct environment representations when operated stan-

dalone. However, to enable rendezvous maneuvers for reconfiguration a consistent shared environment representation on each of the robots has to be created. This has been achieved by operating the team of robots as a sensor network, and sharing pointcloud data among all navigating robots; the communication mesh was used in combination with a distributed communication architecture to multicast sensor data (cf. [16] for further details).

To plan a path to an exploration or rendezvous target, the environment map is converted by each robot into a robot specific traversability map, Fig. 6. This traversability map is synchronized with new environment information in regular intervals and updates trigger a replanning of the path. Hence, obstacles can be avoided without a highly reactive layer, but based on the assumption of a low dynamic environment. Both navigating robots use the same mapping software infrastructure, though require an individual parameter tuning to deal with sensor characteristics.

5. MISSION CONTROL

For the control of the mission and for interfacing with the robotic systems in Utah via satellite link a ground control station (GCS) was developed. It makes use of a 3D virtual control environment, i.e., a Cave Automatic Virtual Environment (CAVE) running the custom simulation software "Machina Arte Robotum Simulans" (MARS) [17]. Hence, the robots were displayed by means of close to realistic physical simulations of the real robots in a map generated from their sensors' input. In comparison to video live feed, a generated map displayed in virtual environment is especially advantageous for steering robots under visually challenging conditions like sandstorms.

In addition to showing the robots' pose in the virtual environment, a graphical user interface was needed to display additional data and especially to send commands to the robots. The operator was able to set waypoints, request a camera image, a pose update or a map update, stop the robot or set the update rate for automatically sending telemetry data. A direct control mode was implemented to control SherpaTT's manipulator arm. The map as well as widget-based icons for control are optimized in appearance to minimize load on the operator. For this design optimization, online as well as offline EEG analysis was performed, [18]. Fig. 7 gives an overview of the mission control facility.

The telemetry for Bremen was collected in Utah by a single control station. After the robot telemetry was collected using the native, CORBA-based communication of the Rock framework [15], the samples were multiplexed into a single data package. The resulting telemetry container package was compressed and sent to Bremen via satellite using the UDT protocol [19]. UDT was able to handle conditions with ping times of up to 22 seconds without suffering package loss. The control station in Utah ran an HTTP-based API server to control

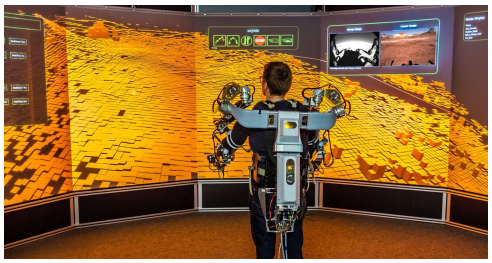

Figure 7. Mission control in Bremen using an exoskeleton. The operator is in the center of a multi-projection area ("CAVE"), in the image a 3D environment representation generated from SherpaTT in Utah (yellow tiles) and nav-cam images of SherpaTT and Coyote III are shown (top right)

the telemetry contents and data intervals to be included in packages sent to Bremen.

To control the robots, the CAPIO exoskeleton [20] or a wand was used as an input device. The wand was tracked by an inertial-ultrasonic hybrid tracking device. It was mainly used to set waypoints for the robots and to change the virtual camera by rotating, zooming and translating. The exoskeleton could be used for this as well but was further used to intuitively control SherpaTT's arm in manipulation tasks while providing force feedback. Therefor the exoskeleton is equipped with seven active DoF at each arm and a multi-input hand-interface. It provides two tele-operation modes. In case of exploration the exoskeleton uses the virtual environment in order to control the virtual cursor and therefore choose a robot, send way points, update and navigate the map and request photos from a rover, as shown in Fig. 7. In case of manipulation mode the operator controls SherpaTT's manipulator with the right exoskeleton arm and can request a force feedback. The usage of the exoskeleton enables the operator to interact with the robot in a natural, intuitive and haptic way. This could be shown over a distance of 8.300 km with performance restricted by the lack of bandwidth due to the chosen communication. The field test showed the applicability of an exoskeleton over a large distance and supports its usage during extraterrestrial exploration and manipulation.

6. SYSTEM TESTS AND MISSION SEQUENCE

The field trial campaign was based on a three layered system evaluation: (i) single system tests concerning locomotion capabilities and performance parameters, (ii) single system tests concerning autonomy and cooperative tasks and (iii) full system test in a simulated mission scenario with the primary focus on the execution of a semi-autonomous sample return mission sequence, including all robotic systems as previously described.

Table 1. Slope inclination profile for slope tests

Distance [m]	0-1	1-2	2-3	3-4	4-5	5-6
Inclination	9.5°	10°	10°	11°	15°	16°
Distance [m]	6-7	7-8	8-9	9-10	10-11	11-12
Inclination	28°	22°	25°	28°	28°	20°
Distance [m]	12-13	13-14	14-15	15-16	16-17	17-18
Inclination	20°	15°	10°	10°	0°	0°

The following paragraphs present an overview of the conducted tests. A detailed description of the experiments and outcomes is, however, beyond the scope of this paper. Further publications are currently prepared, elaborating in detail on the experiments and their results.

6.1. SherpaTT and Coyote III Single System Tests

Prior to the mission scenario several single system tests regarding locomotion and autonomous behavior were conducted with SherpaTT and Coyote III. Both systems performed odometry tests after their deployment. The tests were performed on flat and relatively firm terrain. The tests were used to assess (i) the wheel based odometry of the systems as well as (ii) the influence of the implemented trajectory followers and the active ground adaption of SherpaTT on the quality of the odometry performance.

During slope tests both systems showed their climbing capability. Both systems performed a test series on a slope with a varying inclination profile as given in Tab. 1 and shown in Fig. 5 (top). The slope was covered by loose soil and thin duricrust. SherpaTT mastered the slope with up to 28° inclination in upward and downward direction. Further successful test drives have been performed with Coyote III on slopes with duricrust at inclinations of up to 42° and up to 32° inclined slopes with bed-rock.

Furthermore, different general mobility tests were performed with SherpaTT, especially to evaluate the active suspension system. These tests included the active force leveling (load sharing of wheels) with different foot prints (suspension system configurations) in flat terrain and moderate slopes as well as the evaluation of active roll/pitch adaption. With Coyote III a general mobility assessment was performed with regard to static and dynamic stability, driving over steps and tranches as well as on very unstructured terrain. Additionally, different cliff driving tests have been performed to assess the behavior of Coyote III in precipitous slopes as shown in Fig. 5 (bottom).

In preparation for the cooperative mission sequence, both systems were first put to single autonomous operations tests and later on tested in a cooperative manner. These tests were used to test and tune the self localization and mapping (SLAM) capabilities of the systems (see Fig. 6), as well as to perform and evaluate autonomous operations, such as path planning, obstacle avoidance and autonomous waypoint based navigation.

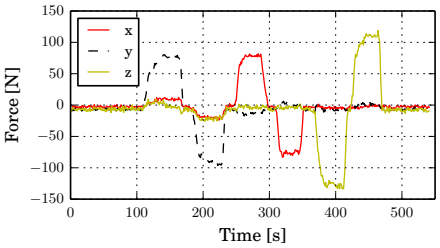

Figure 8. Measured forces at SherpaTT's end effector

6.2. Manipulator Control with an Exoskeleton

The CAPIO exoskeleton was used as input device for SherpaTT's manipulator. In this mode the Cartesian position of the exoskeleton's end effector was up scaled and transferred from Bremen to Utah on SherpaTT's manipulator.

Vice versa the exoskeleton was used as output device to the human operator. In order to gain initial experiences under the given circumstances, the first force feedback test was done with prerecorded data from the test side. Following this pretest the experiment was repeated successfully with the entire communication chain and live data. A human pushed and twisted SherpaTT's manipulator in orthogonal directions generating forces and torques. An example of the measured and transferred data is depicted in Fig. 8.

The measured data where then downscaled by a factor of 10 and applied as force-torque-vector to the end effector. The distribution of the joint torques at the exoskeleton is calculated by the RBDL-library [21]. Thereby the exoskeleton triggered a forced movement of the operator. Further work will focus on the employment of the force feedback on the soil sample process.

6.3. Mission Sequence

In the demonstrated mission sequence, SherpaTT acted as exploration and sample acquisition rover. Coyote III took the role of a scout and shuttle rover, supposed to collect sample containers and to transport them back to a fictional sample return stage. An overview of the area of operations is given in Fig. 9, highlighting the key waypoints of both systems and their approximate traversal.

The mission's command and control was based in the GCS located in Bremen. All steps of the mission were controlled from the GCS in Bremen by operators with no direct knowledge of the area of operations [22]. The operator used the exoskeleton to request a three dimensional map of the environment and to order photos from the camera of both rovers. The mission control in Bremen commanded the systems to target waypoints, where

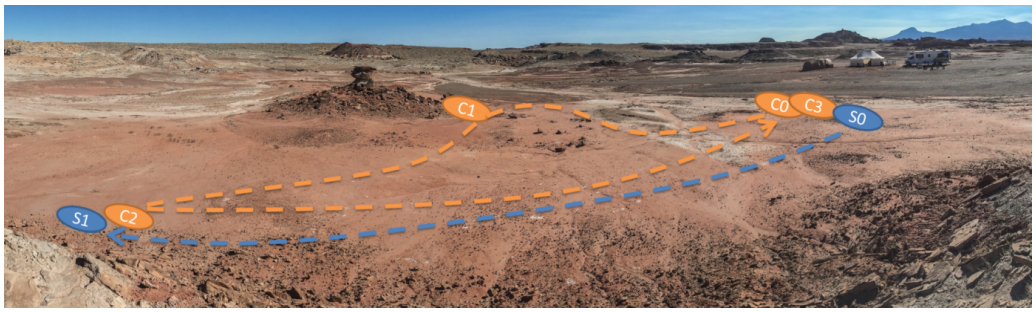

Figure 9. Mission sequence with waypoints for SherpaTT (blue) and Coyote III (orange). Both systems had a rendezvous at S1/C2. Panoramic image stitched from single pictures.

Figure 10. Rendezvous of SherpaTT and Coyote III during the mission sequence. Coyote III's manipulation arm SIMA is in a pose to give room for transfer of the sample container.

each of the waypoints was associated with an assumed (but not performed during the test sequence) activity such as soil sampling or robot rendezvous. Rovers were navigating autonomously to all waypoints by relying on the distributed mapping approach described in Section 4 and planning a path through known, traversable terrain. Successive updates of the environment map and image data improved the operator's situational awareness for the remote area.

While SherpaTT started directly off to its sampling point S1, Coyote III was heading towards C1 for scouting. Due to this maneuver SherpaTT could not be seen by the operator on Coyote III's camera any longer and was operating outside the mapping area of SherpaTT. Simultaneously to the scouting operation of Coyote III SherpaTT's manipulator was remotely controlled by an operator in Bremen, using the exoskeleton to simulate soil sampling actions. Thereafter, Coyote III and SherpaTT met up for a rendezvous at S1/C2 for payload hand-over simulation. After the rendezvous of both rovers Coyote III drove autonomously back to its starting point by a manually given goal way point.

The actual soil sampling process as well as the payload exchange were not included in the mission sequence controlled from Bremen but have been performed by SherpaTT and Coyote III in previous cooperative tests. Soil sampling, using a modified PLI, could successfully be demonstrated by SherpaTT, as well as a payload hand over from SherpaTT to Coyote III during a rendezvous as shown in Fig. 10. The PLI was than transported to its goal destination by Coyote III and deployed using the SIMA module.

7. LESSONS LEARNED, CONCLUSION AND OUTLOOK

During the field test campaign described in this paper, single system and cooperative multi-robot system tests were conducted. The single system tests were focused on the locomotion capabilities of both deployed mobile systems, while the multi-robot scenario explored the capabilities concerning cooperative mapping, rendezvous and handover of sample containers between the two systems.

In the locomotion experiments, the exploration rover SherpaTT was able to climb slopes of up to 28° covered in soft soil/duricrust, while the shuttle and scouting rover Coyote III was tested in slopes of up to 52°, successfully managing slopes of 42°. Additionally, vertical cliff walls and overhangs were negotiated with Coyote III where a human simulated a tether management system. Experiences from these tests are going to be exploited for future developments with a robotic tether management system, mounted on SherpaTT or with an new type of PLI with an anchoring and cable winch mechanism. Both systems showed a very high mobility performance in natural and unstructured terrain, mastering various obstacles.

In preparation for a sample return mission sequence, both rover were taken through thorough tests, regarding their sensor calibration and autonomous behavior. Both systems were independently able to perform autonomous go to goal way point navigation while mapping their environment, using a graph-based SLAM approach. In order to allow cooperative tasks and perform rendezvous

maneuvers, a distributed mapping approach was successfully tested with both systems, enabling to merge the independently generated maps into a consistent global map.

All key aspects of a sample return mission sequence have been demonstrated by the heterogeneous robot-team during the field trials. The soil sampling task has been conducted by SherpaTT, using a specifically equipped PLI. The soil sampling device could successfully be docked and deployed by SherpaTT's manipulator. Autonomous docking by using visual odometry and handling of the PLI could be demonstrated in natural terrain with representative lightning conditions. Both rovers were applied in a closed mission sequence which was controlled from a ground station in Bremen, Germany. The control station was equipped with a multi-projection area and a dual-arm upper body exoskeleton to perform the mission execution. It proved to provide a good mission overview and situational awareness, allowing to perform complex multi-robot mission sequences. For a smooth mission operation, a clear role allocation among the operational staff proved to be very helpful. A stable communication link between mission control and the robots in the field is, however, an important prerequisite.

Overall important insights and results could be gathered during the field trails regarding the robustness and mobility of the systems as well as their autonomous and cooperative behavior for exploration in naturally unstructured terrain. The results of the field trial campaign will be further investigated and serve as additional input for the TransTerrA project. The gathered results, know-how and impressions will further drive the improvement of all involved systems and may lead to follow up analogue test campaigns in the future.

ACKNOWLEDGMENTS

The authors would like to thank the FT-Utah team and all supporting staff at DFKI Robotics Innovation Center Bremen, especially the TransTerrA team, and at the Robotics Group of the University of Bremen. The work presented is part of the projects Field Trials Utah and TransTerrA which are funded by the German Space Agency (DLR Agentur) with federal funds of the Federal Ministry of Economics and Technology in accordance with the parliamentary resolution of the German Parliament under grant no. 50 RA 1621/50 RA 1622 (FT-Utah) and 50 RA 1301 (TransTerrA).

REFERENCES

[1] Strategic Planning and Outreach Office of the ESA Directorate of Human Spaceflight and Operations, ESTEC, the Netherlands. *Exploring Together - ESA Space Exploration Strategy*, 2015.

[2] International Space Exploration Coordination Group (ISECG). *The Gloabal Exploration Roadmap*, August 2013.

[3] E. Allouis, T. Jorden, and P. Falkner. Sample fatching rover - concept and operation of a lightweight long-range rover for MSR. In *Proc. of the Global Space Exploration Conference (GLEX2012)*, Washington, DC., 2012.

[4] E. Allouis et al. FP7 FASTER project - demonstration of multi-platform operation for safer planetary traverses. In *Proc. of the Symp. on Advanced Space Technologies in Robotics and Automation (ASTRA2015)*, 2015.

[5] S. Gunes-Lasnet et al. SAFER: The promising results of the mars mission simulation in atacama, chile. In *Proc. of the Int. Symp. on Artificial Intelligence, Robotics and Automation in Space (iSAIRAS2014)*, 2014.

[6] R.U. Sonsalla et al. Towards a heterogeneous modular robotic team in a logistic chain for extraterrestrial exploration. In *Proc. of the Int. Symp. on Artificial Intelligence, Robotics and Automation in Space (iSAIRAS2014)*, 2014.

[7] J. D.A. Clarke and C. R. Stoker. Concretions in exhumed and inverted channels near hanksville utah: implications for Mars. *Int. Journal of Astrobiology*, 10(3):161–175, 2011.

[8] Erick Dupuis et al. Results from the CSA's 2015 Mars analogue mission in the desert of Utah. In *Proc. of the Int. Symp. on Artificial Intelligence, Robotics and Automation in Space (iSAIRAS2016)*, 2016.

[9] C.M. Caudill et al. 2015 CANMARS MSR analog mission: In situ geochemical insights from x-ray fluorescence spectrometry. In *Proc. of the Lunar and Planetary Science Conf.*, 2016.

[10] M.R. Balme et al. UK Space Agency 'Mars Utah Rover Field Investigation 2016' (MURFI 2016): Overview of mission, aims and progress. In *Proc. of the Lunar Planetary Science XLVIII*, 2017.

[11] L.J. Preston et al. Mars Utah Rover Field Investigation 2016 (MURFI 2016): Targeting, localization, and in-situ science operations. In *Proc. of the Lunar Planetary Science XLVIII*, 2017.

[12] F. Cordes and A. Babu. SherpaTT: A versatile hybrid weeled-leg rover. In *Proc. of the Int. Symp. on Artificial Intelligence, Robotics and Automation in Space (iSAIRAS2016)*, 2016.

[13] W. Wenzel, F. Cordes, and F. Kirchner. A robust electromechanical interface for cooperating heterogeneous multi-robot teams. In *Proc. of the IEEE/RSJ Int. Conf. on Intelligent Robots and Systems*, 2015.

[14] R.U. Sonsalla, J. Bessekon Akpo, and F. Kirchner. Coyote III: Development of a modular and highly mobile micro rover. In *Proc. of the Symp. on Advanced Space Technologies in Robotics and Automation (ASTRA2015)*, 2015.

[15] S. Joyeux, J. Schwendner, and T. M. Roehr. Modular software for an autonomous space rover. In *Proc. of the Int. Symp. on Artificial Intelligence, Robotics and Automation in Space (iSAIRAS2014)*, 2014.

[16] T. M. Roehr and S. Herfert. *A FIPA-Based Communication Infrastructure for a Reconfigurable Multi-robot System*, pages 665–676. Springer International Publishing, Cham, 2016.

[17] DFKI - RIC. Mars - a cross-platform simulation and visualization tool. `http://rock-simulation.github.io/mars`, 2015.

[18] E. A. Kirchner et al. An intelligent man-machine interface - multi-robot control adapted for task engagement based on single-trial detectability of p300. *Frontiers in Human Neuroscience*, 10:291, 2016.

[19] Y. Gu and R. L. Grossman. UDT: UDP-based data transfer for high-speed wide area networks. *Computer Networks*, 51(7):1777–1799, 2007.

[20] Martin Mallwitz et al. The CAPIO active upper body exoskeleton and its application for teleoperation. In *Proc. of the Symp. on Advanced Space Technologies in Robotics and Automation (ASTRA-2015)*, 2015.

[21] Martin Felis. Rigid body dynamics library. `https://rbdl.bitbucket.io/index.html`, 2013.

[22] S. Planthaber et al. Controlling a semi-autonomous robot team from a virtual environment. In *Companion of the 2017 ACM/IEEE Int. Conf. on Human-Robot Interaction*, 2017.

[10]: **Performance Evaluation of an Heterogeneous Multi-Robot System for Lunar Crater Exploration**
S. Bartsch, F. Cordes, S. Haase, S. Planthaber, T. M. Roehr, F. Kirchner
in: i-SAIRAS 2010

Performance Evaluation of an Heterogeneous Multi-Robot System for Lunar Crater Exploration

Sebastian Bartsch, Florian Cordes
Stefan Haase, Steffen Planthaber, Thomas M. Roehr

DFKI – Robotics Innovation Center Bremen; 28359 Bremen, Germany
e-mails: firstname.lastname@dfki.de

Abstract

This paper presents the results of the project LUNARES, in which a heterogeneous multi-robot system and a realistic lunar environment replica have been realized in order to evaluate a lunar crater sample return mission. The evaluation shows the general validity and usability of the described approach. The presented experiments include: precision of autonomous docking between heterogeneous robotic systems, parameter selection and energy considerations for climbing a lunar crater with a legged robot, and precision and repeatability of autonomous sample localization and pick up. Critical elements within the mission procedures are identified and improvements to individual components are suggested.
Keywords: Reconfigurable Robots, Heterogeneous Robot Team, Space Robotics, Lunar Crater Exploration, Sample Return

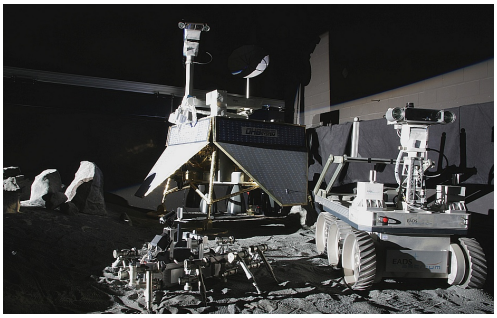

Figure 1. LUNARES systems in artificial crater environment. Left foreground: Legged scout, back in the middle: the landing unit with robotic arm and sensor tower, right foreground: wheeled rover.

1 Introduction

Space missions so far have been performed with single robots equipped for various mission goals. However, all mobile robotic systems deployed on celestial bodies have in common that they use wheeled locomotion, though in different variations, e.g. recent deployments commonly make use of a rocker-bogie suspension system.

Descending into a (lunar) crater is a challenging task for wheeled robots, and legged locomotion can serve as an alternative solution. A comparison between legged and wheeled motion [7, 9] shows that planar environments are best suitable for wheeled locomotion especially regarding energy efficiency. However, legged systems [10] are able to cope with very rough terrain and slopes, or even climb vertical surfaces [5].

Combining both locomotion principles seems therefore desirable. Huntsberger et al. [4] propose a heterogeneous robotic team for infrastructure/inter-robot servicing and repair. They use a six-legged robot for repairing a rover's wheel. Abad-Manetrola et al. [1] present an approach of using a "classical" rover for longer distances and a scout system for exploration of steep crater environments. The scout system in this approach is a two wheeled system connected via a tether to the main rover.

The project LUNARES evaluates the capabilities of a heterogeneous, reconfigurable robotic team relying on cooperation to fulfil a lunar sample return mission [3]. The project allows a general evaluation of a lunar crater exploration mission, broken down into multiple aspects: cooperation of heterogeneous robotic systems, reconfiguration of robotic systems, control of a mixed human-robot team, and (semi-)autonomous operations in space missions. Furthermore, it shows the usability of a bio-inspired legged robot in space missions [2]. In this paper we will address the following technical issues: (1) autonomously approaching a target sample, (2) collecting the target sample, (3) climbing with a legged robot, and (4) docking of heterogeneous systems.

The anticipated space mission in the project LUNARES is built upon three different robotic systems, Figure 1: a lander, a wheeled rover, and a legged scout.

The current setup assumes that the lander has surfaced the moon, and rover and scout have already disembarked the lander unit. Though the lander has been realized as a scaled down mockup, it provides a robotic arm and a sensor tower. Rover and scout are separate systems, but they can cooperate to form a combined system; the rover can serve as a transport platform for the scout.

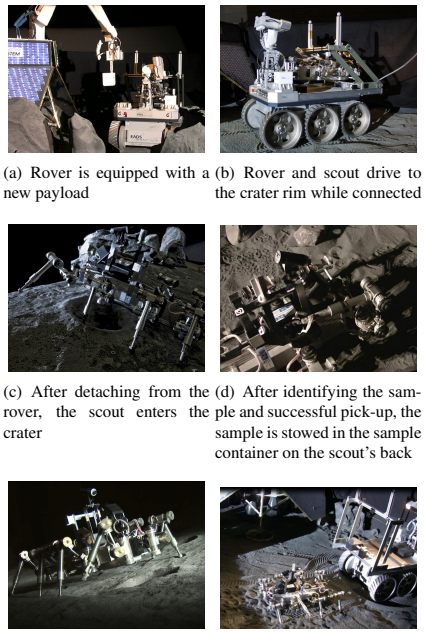

(a) Rover is equipped with a new payload

(b) Rover and scout drive to the crater rim while connected

(c) After detaching from the rover, the scout enters the crater

(d) After identifying the sample and successful pick-up, the sample is stowed in the sample container on the scout's back

(e) Scout climbs back up to the rover

(f) Scout docks to the rover, the rover commands the scout

Figure 2. Selected mission steps from the LUNARES demonstration mission.

The mission consists of the following steps (see also Figure 2: After being equipped with a payload (in order to demonstrate the reconfigurability of the system), the rover transports the scout to a crater rim, and unloads the scout. Subsequently, the scout climbs into the crater and requests an operator to select a sample. The scout autonomously approaches the sample and collects it, before carrying it back to the rover. After leaving the crater, the scout docks to the rover for being transported back to the lander. The collected sample is retrieved by the manipulator and stored on the lander where it has to be prepared for its final submission to earth or further analysis. The submission/analysis is not part of the demonstration of the LUNARES project.

2 Autonomous Sample Approach

After reaching the crater bottom, a sample to be picked up is selected by a human operator. The sample is selected by using the camera signal provided by the scout. Using the video image, the scout adapts its position, until the selected sample is in a goal region of the video image. For stability of the approach, the sample is tracked using a particle filter. Due to occlusion the sample can be tracked until it has an approximate distance of 22 cm straight in front of the front right leg of the robot.

2.1 Experimental Setup

The approach has been tested in a dark planar section of the crater bottom. The ground is covered with lunar regolith substitute. The area has not been illuminated directly, except for the robot's infrared lights, which are part of the attached camera, and weak ambient light (which is caused by having a sunlight simulation for the crater rim within a wall-constrainted environment).

The approach has been tested for different sample-positions within the robot's coordinate system. The x-axis of the right-handed coordinate system correlates to the forward direction of the robot and the z-axis points upwards.

Because only the approach should be evaluated but not the sample detecting strategy, a retro-reflective ball-shaped marker with a diameter of 21 mm is used as the sample. An single experiment procedure consists of the following steps: (1) operator selects the marker, (2) autonomous approach starts, and (3) autonomous approach ends or is interrupted by the operator. The difference of the reached positions relative to the optimal one - measured within the coordinate system of the robot - are listed in Table 1. The set of experiments covers direct and curved approaches.

For each starting position the sample was approached ten times. The number of manual corrections (reselecting the sample), which were solely necessary due to noisy analog camera transmission[1], has been regarded by the evaluation.

2.2 Experimental Results

The set of experiments and its results are listed in Table 1. The set is designed to reflect the approach under different angles of attack, i.e. approx. 12° and 28° deviation from a straight line. Corrections represents the average number of manual interventions. For our experiments we rely on markers in order to guarantee reproducibility and to avoid influences from the sample detection algorithm. The algorithm does not adapt contrast dynamically but requires an operator to do so.

[1] Currently, the processing unit for the camera images remains outside of the actual robot. Thus, analog transmission within the 2.4 GHz band was required to allow image processing.

Table 1. Results of the approach experiments using a reflective marker and a stone as target

start position x/y cm	Ø duration min:sec	goal position variance x/y cm	goal position corrections Ø
68 / -31.70	1:05	9.45 / 0.92	0.29
68 / -12.00	1:02	3.61 / 1.57	0.1
48 / -22.40	1:46	5.39 / 1.88	0.3
48 / -8.50	0:52	1.06 / 1.75	0.1
38 / -17.70	0:46	0.73 / 0.18	0.0
38 / -6.70	0:41	0.72 / 1.42	0.0
Ø	1:02	3.49 / 1.29	0.132

2.3 Discussion

The task of approaching the sample has been performed with success and sufficient accuracy. However, the approach showed to be sensitive towards a large distance to the target.

The approach suffered from noisy camera images due to interferences within the wireless network. However, this will not be a problem for robots that have onboard processing capabilites.

The movement of the robot in basalt did not have a major impact on the overall performance. We will show that any inaccuracies of this approach can be compensated by the subsequent steps of sample detection and pick up.

3 Sample Detection and Laser Scanner Evaluation

To start the pickup process of a specific sample, the location of the sample has to be determined accurately. The target sample can be easily determined after generating a height map of the environment and will be further simplified by considering only a region of interest (ROI). This ROI and its size depend on the accuracy of the approach which precedes the sample collect procedure (previous section).

Due to occlusion in the camera image during the autonomous approach, the sample has to be around 22 cm in front of the scouts right "shoulder" (thorax) joint. On this basis the ROI is defined.

Currently a target area of 121 cm^2(11 cm×11 cm) applies. The ROI is centered at 22 cm ahead of the thorax joint, which has a static position within the scout's coordinate system.

The scout uses a 3D laser-scanner system to extract a distance image of the environment, which is subsequently transformed into a height map. The essential procedure to extract a sample's position consists of the following steps:

1. Extraction of a laser scan of the direct environment within a horizontal range of ±30°
2. Transformation of the scan data from the scanner coordinate system into the robot coordinate system
3. Generation of the height map in the robot coordinate system
4. Extraction of the region of interest, defining the allowed manipulation area of the scout
5. Extraction of the local extremum within the ROI
6. Extraction of the region around extremum to reconstruct the target center

The height map is transformed into a gray scale image to allow further processing steps such as median filtering.

Table 2. Experimental parameter sets

object type	object size mm	ground material	color grayscale
reflective marker	9	printed paper	161
reflective marker	9	printed paper	127
reflective marker	9	printed paper	69
reflective marker	9	printed paper	0
reflective marker	9	regolith	24-100
reflective marker	19	regolith	24-100
white stone	40	regolith	24-100
white stone	40	regolith	24-100

3.1 Experimental Setup

Repeated tests with the laser scanner have been performed, using the following variables: (1) various sizes of target: spherical with a diameter of 9 mm up to 40 mm, (2) varying types of targets: reflective markers vs. real stone sample, (3) varying grounds: four types of grayscale printed A4 sheets, and regolith covered, and (4) activation of the final software compensation step.

We used a test setup with a table mounted laser scanner, and scanning a sample lying on a fix position. Experiments have been performed in combinations shown in Table 8, where greyscale refer to a printed color sheet.

The regolith used is mainly of darker color, but also contains lighter material resulting in the listed color range from gray scale values of 24 to 100. For each combination 100 scans have been performed. A short warm-up phase of the laser scanner is employed, with five subsequent scans for warm-up. Though this number seems to be small, it proved to be sufficient to create consistent scan results in our scenario.

3.2 Experimental Results

The experiments have shown, that the object detection using the laserscanner is influenced by the color of surface and target object, while the structure of the surface is less important. The grayscale range of 69 to 161 provides a standard deviation of 2 mm up to 5 mm. In contrast a completely black surface causes deviations of 6 mm up to 17 mm depending on the size of the object.

Additionally the deviation increases with the size of the object. Further, the experiment showed a standard de-

viation of about 4 mm for a 19 mm sized sample (20 % of its diameter) versus 14 mm for a 40 mm sized sample (35% of its diameter). However, this deviation is also caused by the fact, that the applied algorithm searches for a pixel with minimum color value within the ROI and thus can be easily affected by measurement noise even after applying a median filter. However, to deal with the measurement noise region growing proofed to be an effective measurement, increasing the accuracy of the sample detection to to standard deviation of 2 mm.

3.3 Discussion

The lunar crater environment creates specific requirements for the approach. The algorithm for autonomous sample detection using laser-scan data has to consider surface and sample color. However, our algorithm would need further evaluation and adaption for inclined or heavily irregular surfaces, since both conditions affect the analysis of the ROI. Nevertheless, we achieved high accuracy after consideration of the environment characteristics and applying region growing to improve the sample center determination. Eventually, this accuracy is sufficient to forward the extracted coordinates to the manipulator leg, which has to deal with play in the joint which is a factor of ten higher than actually needed due to the restricted accuracy of the positioning of the leg (play in the joints).

4 Sample Pickup

To realize the sample collection with the scout a grabbing device has been integrated into the right front leg. The grabber consists of three claws attached to the bottom of the lower leg. One motor is mounted in the shaft of the shank driving the claws through a bevel gear.

After approaching and localizing the sample as described in Section 2 and 3, the grabber has to be moved just above the object in order to collect it. The scout's legs operate with three degrees of freedom. However, due to the kinematics the angle of attack directly depends on the distance to the sample, i.e. the larger the distance to the sample the higher the angle of attack for the grabber (measured from the (vertical) z-axis). The design of the claws has to compensate the kinematic constraint, in order to achieve a high success rate of sample pickups in a wide range of positions. Hence, three different types of claws as illustrated in Figure 3 have been designed and evaluated.

4.1 Experimental Setup

The grabbing process is tested on the bottom of the simulated crater. One out of two different rock samples with a diameter of approx. 45 mm and 30 mm (see Figure 4(a)) is placed at a distance of 170 mm and at

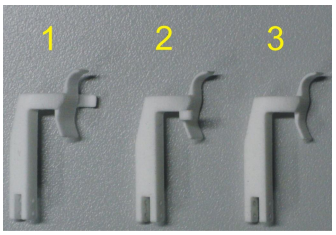

Figure 3. Claw types for scout robot, the claws are with and without a third "finger" at the side.

220 mm from the thorax joint of the right front leg (see Figure 4(b)).

The scout is commanded to collect the sample at the predefined, known position. For each combination of rock samples, claw types and distances ten trials to pick up the sample were performed.

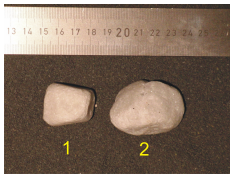

(a) The used rock samples

(b) Experimental setup in the crater bottom

Figure 4. Rock sample and experimental setup

4.2 Experimental Results

The evaluation of the results as presented in Figure 5 shows that the task was performed successfully in 70% over all combinations of experimental paramters with claw type two and three, whereas type one was only successful in 63.5% of the trials. Note that a trial has been counted only as successful if the sample was deposited in the storage unit on the back of the robot. A trial is not successful when (1) grabbing aside of the target, (2) pushing the object away and creating the necessity for a new scan, and (3) loss of the sample while transferring it to the storage unit.

In a more differentiated analysis regarding the rock sample, it can be observed that both the size and shape of the object have a big influence on the success of the collecting process. The smaller sample (1) was collected successfully in 88,33% of all trials but the larger sample (2) only in 46,67%. Claw type two showed most successful trials with sample (1). For sample (2) claw type three was most suitable.

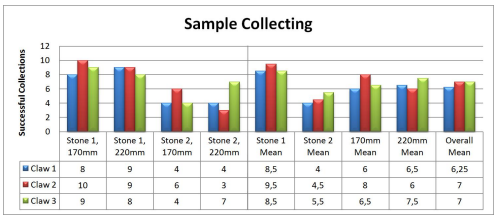

	Stone 1, 170mm	Stone 1, 220mm	Stone 2, 170mm	Stone 2, 220mm	Stone 1 Mean	Stone 2 Mean	170mm Mean	220mm Mean	Overall Mean
Claw 1	8	9	4	4	8,5	4	6	6,5	6,25
Claw 2	10	9	6	3	9,5	4,5	8	6	7
Claw 3	9	8	4	7	8,5	5,5	6,5	7,5	7

Figure 5. Results of the experimental series

Regarding the different distances in median the sample collection showed a slightly better performance with the smaller distance of 170 mm (68,33%) than with 220 mm (66,67%). This is a slight confirmation of our initial statement, since the angle of attack increases with the distance to the sample.

4.3 Discussion

Due to the fact that the sample gradually leaves the field of view of the camera at a distance smaller than 220 mm this range should not be under-run for the autonomous positioning to the sample described in Section 2. Hence, the third claw type was selected as best suited for the LUNARES mission. With an average success rate of 75% it showed the best performance at this distance. Though the grabbing process can be executed serveral times within the mission, and thus this success rate has a minor impact on the overall mission success.

5 Climbing with Legged Scout Robot

In this experimental series the climbing capabilities of the Scout are evaluated. For locomotion in steep slopes, the original CPG-based locomotion approach [6] has been extended by a state machine containing the four states *stance*, *lift*, *shift* and *touchdown*. The locomotion control allows to set a wide rage of parameters for locomotion of the eight legged robot. In general, the locomotion is cyclic, with the parameter *pulse*, measured in milliseconds. While the allowed time for the three states within the swing phase can be set, the remaining cycle time is used for the stance phase according to Equation 1.

$$t_{stance} = t_{pulse} - (t_{lift} + t_{shift} + t_{touchdown}) \quad (1)$$

Further parameters include the step width in lateral and transversal direction, and the turning in degrees per cycle. Additionally, body height and body shift can be adjusted. The robot control is also equipped with several reflexes, such as *stumbling correction*, *hole-reflex* for stretching the leg until touching ground to step through small craters, and a *balance-reflex* to shift the center of mass to optimize stability during climbing.

5.1 Experimental Setup

The experimental setup consists of a series of runs in which the scout climbs up the artificial crater slope (distance on optimal path ca. 5 m), guided by an operator. Various locomotion parameters are applied, but are fix for each set of runs. Ten runs with one fix set of locomotion parameters are conducted. The only parameter changing is the heading of the robot, since we need to guide the robot safely to the crater rim.

A power meter installed on the robot is used to evaluate the consumed energy during a single run. Before each run, supply voltage and overall consumed current are recorded. During a run the current and power consumption is recorded for each third of the total distance. After reaching the top of the crater, elapsed time, supply voltage and overall consumed current are recorded. For comparison, similar experiments are conducted on 5 m of flat laboratory floor.

Table 3 lists the walking parameters that were combined in the experimental series. The combination of the parameters results in 12 different parameter sets. Each of the sets is used for at least ten successful runs of the robot in the slope. Since the lean value depends on the slope, a lean value of zero has been used for Scout movements on the laboratory floor. This results in a minimum of 180 runs, since few runs, e.g. due to failed hardware, had to be repeated.

In the following, a pulse value of 3000 (three thousand milliseconds for a full cycle) is noted P3000, the parameter Body Height is abbreviated B150 for a height of 150 mm (distance between center of body and ground). The shift of the body into the slope is denoted as L0, L50 and L100 for zero, 5 cm and 10 cm maximum offset, respectively.

Table 3. Locomotion parameters during climbing experiments

Parameter	Values		
Pulse	3000	4500	
Body Height	150	180	
Max Lean	0	50	100

All experiments were conducted using a phase shift of 0.7. The phase shift denotes the shift between the movement of the single legs of the robot. A phase shift of 1 results in an equally distributed walking pattern, whereas a phase shift of 0 results in a quad-pod-gait, thus four legs are synchronous in stance phase and four legs in swing phase.

5.2 Experimental Results

The experiments showed, that the scout is not able to negotiate the slope at all, when the lean value is restricted

Table 4. Categories of Body Height and maximum Lean value combinations for the conducted experiments

Category	Body Height	Lean Value	Environment
#1	B150	L100	artificial crater
#2	B180	L100	artificial crater
#3	B150	L50	artificial crater
#A	B150	L0	laboratory floor
#B	B180	L0	laboratory floor

Table 5. Average results from runs with P3000 in crater (1-3) and on flat laboratory floor (A,B)

Cat. #	Chrg. mAh	Dev. mAh	Time mm:ss	Dev. mm:ss	Energy Wh	Power W
1	181	26	02:20	00:11	5.62	144
2	262	42	03:28	00:26	8.29	139
3	305	42	03:52	00:29	9.63	151
A	111	6	01:14	00:01	3.49	169
B	132	4	01:16	00:01	4.03	191

to zero (no posture change caused by the inclination). The robot's center of mass (COM) is situated at the lower end of the support polygon, resulting in an increased load on the hind legs, whereas the front legs are hardly supporting traction at all.

With L50 and L100, the robot is able to cope with a slope of approximately 35°. However, using the parameter combination L50, B180 results in heavy slippage and a high risk of tilting over, due to the non-optimal position of the COM. Thus, these experiment series were aborted. Table 4 gives an overview of the combined parameter sets and a category name that is used in the subsequent tables.

Table 5 gives the results of the experiments with P3000, while Table 6 gives the results of the same experiments with P4500. Within one experimental series with the same pulse, the time needed for negotiating the slope represents an indirect measurement of the stability of the locomotion, since heavier slippage results in prolonged climbing to reach the crater rim. This also corresponds with the difficulties, the operator experiences when commanding the robot in the slope. Clearly, the ascend times of the two different series (P3000, P4500) can not be compared to evaluate the stability of the locomotion, since a reduced pulse results in a slower locomotion speed. The average power consumption (W) of the robot is calculated from the measured energy consumption (Wh) and the measured time (s) needed for climbing the slope.

From the data given in the tables it is clearly visible, that the robot's locomotion gets less stable with reduced maximum allowed lean value and increased body height respectively. This can be inferred from the average time needed for ascend as well as in the increased deviation of the run times. This holds for both experimental series (P3000 and P4500). In both series, the stability of

Table 6. Average results from runs with P4500 in crater (1-3) and on flat laboratory floor (A,B)

Cat. #	Chrg. mAh	Dev. mAh	Time mm:ss	Dev. mm:ss	Energy Wh	Power W
1	216	22	03:19	00:10	6.53	118
2	250	29	04:04	00:23	7.80	115
3	342	30	04:59	00:28	10.49	126
A	159	3	02:06	00:02	4.99	143
B	168	20	02:11	00:01	5.28	145

locomotion drops significantly from category #1 (B150, L100) to category #2 and #3, whereas the difference between category #2 and #3 concerning the deviation is not that significant. While the deviation of the ascending time is nearly the same in categories #2 and #3, the overall time needed for ascend is longer when the maximal lean value is restricted (cat. #3) then with increased body height but same max. lean (cat. #2).

Directly dependent on the ascend time is the energy consumption of the robot. This is a general observation, but especially true for legged systems, since in contrast to a wheeled system the robot's actuators have to produce torques constantly, even when the system stands still on even ground. Thus, as expected, the energy consumption increases with the duration of a run.

The comparison of the two series shows another expected result: A slower movement of the robot (P4500) leads to a reduced power consumption. Unexpectedly, the power consumption of category #2 in the slope is less than category #1 for both series. This result cannot be verified in the reference series on even laboratory floor. Here, the expected result of higher power consumption with an higher COM can be observed. Interestingly, the average power consumption in the slope is less than in the reference experiments. The explanation for this observation can be found in the morphology of the scout robot. In thorax and distal joint a high gear ratio is used (higher torques), whereas in the basal joint, a lower gear ratio is used (higher speed). On flat ground, the basal joints have a higher load than in the slope, where a part of the load is transferred to the thorax joints.

For reference, Figure 6 depicts some trajectories of the robot in the slope during the P4500-series. The fastest, slowest and an intermediate run are shown for each parameter category.

5.3 Discussion

As can be seen from the experimental results, a correct parameter choice is crucial for the locomotion of the legged scout in the terrain. Compared to the space of possible parameter sets, the used parameter set for the presented experimental series is relatively small. However, the chosen parameter set shows the whole range of results of different parameters: The results range from not being

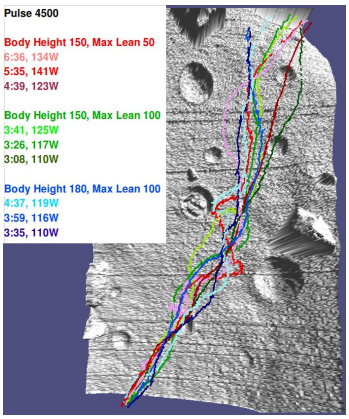

Figure 6. Trajectories of slowest, fastest and intermediate run with P4500 for three parameter sets (B150,L50/ B150,L100/ B180,L100).

able to complete the task at all to success with varying performance concerning energy, power and time needed to ascend in the artificial crater slope.

The mechanical design of the robot also plays an important role in the efficiency for locomotion. The experimental results show, that it is possible to adapt the robot for locomotion in steep slopes by using a specific set of gears in the joints. By optimizing the locomotion for the slope, the efficiency on even terrain might be affected. The reduced gravity on the Moon also has to be taken into account for an actual deployable system.

In general, a trade off between power (W) and energy (Wh) consumption has to be made. For the aspired application of locomotion in a dark crater, the energy consumption plays a greater role, since the robot can not use solar panels for power generation and has to rely on it's batteries completely. Thus, a faster gait should be chosen, since this reduces the energy consumption but yields a higher power consumption.

As a second impact, the reliability of the locomotion has to be taken into account. Clearly, a slower locomotion increases the safety of the locomotion. Dependent on the specific task (how long is the path in darkness, how long is the expected mission duration...) a suitable set of locomotion parameters has to be chosen.

6 Docking

For the LUNARES mission autonomous docking procedures were required for the following situations: (1) The landing unit deploys or extracts a payload from the rover, (2) the scout is transported on the rover. Both docking procedures are discussed and evaluated in detail in [8]. Hence, and only for completeness, we will present a short summary here.

6.1 Experimental Setup

We evaluated the provided accuracy of the two docking approaches over multiple test sequences using a motion tracking system, which allows tracking with millimeter-precision. The docking of rover to lander, and docking of scout to rover have been evaluated based on ten runs.

Docking Rover to Lander The rover has been placed in various starting positions, though with limited variance due to the constraint of operating in the lunar simulation environment. For the docking process the lander uses a laser scanner to localize the rover based on retro-reflective markers which are attached to the rover. A path is computed from the current rover's position to the target position which the rover follows. When half of the trajectory is completed, a new measurement is done and a new trajectory is generated. This guiding process is repeated until the rover reaches its target position with sufficient accuracy, i.e. it has to be within 0.14 m of the target position and have an orientation error of less than 2.5°.

Docking Scout to Rover The scout starts the docking process in various positions and orientations with respect to the rover. The path of the scout is recorded with a motion tracking system. The deviation to the ideal pose of the scout after finishing the docking process is measured.

6.2 Experimental Results

Docking Rover to Lander This docking process showed high accuracies in reaching the final rover target position. The standard deviations are listed in Table 7.

Table 7. Ø-deviations to the target position

x-error	y-error	yaw-error
0.0138 m	0.0098 m	0.36°

Docking Scout to Rover Over the evaluated trials the scout was able to reach the predefined target destination with high accuracy. The given deviations from the target position are listed in Table 8 separately for each degree of freedom. The time for convergence had an average of 184 s with a standard deviation of 35.5 s.

Table 8. Ø-deviations to the target position

x-error	y-error	yaw-error
0.009 m	0.004 m	0.7°

6.3 Discussion

The evaluation performed on the docking procedures in this project has shown, how cooperation of two previously independently operating robots - one being a behaviour-based legged robot - can be achieved by applying visual servoing. The applied control and docking strategy has been robust enough to cope with inaccuracies introduced by the scout. This accuracy allowed to use predefined subsequent mechanical linking procedures.

7 Conclusions and Outlook

In LUNARES we built up an earth demonstrator of a complex robotic mission. The demonstrator is used for evaluation of the heterogeneous robotic approach for retrieval of a sample from within a permanently shadowed crater at the lunar south pole. Preexisting robots have been used for that goal, the robots were not explicitly designed for the chosen mission scenario.

An autonomous approach of the walking scout towards a selected geological sample has been evaluated in this paper. The performance of this rough positioning in front of a promising sample showed to be accurate enough for the following fine detection of the sample's coordinates using a laser scanner. The robustness of the approach was increased using a particle filter for estimation of the sample in the video image.

The fine detection of the sample is done using a laser scanner. A greyscale height map is generated from the laser scan. Using a region growing algorithm the center of the sample is extracted with higher precision than actually needed due to play in the robots joints.

A docking procedure for a walking machine and a wheeled rover was developed. It is based on visual information from the rover's camera system, which is used to control the legged scout. Furthermore, a docking procedure allowing the precise placement of a rover in front of a landing unit was developed using the lander's sensor system. For exchanging payloads and sample containers between rover, scout, and landing unit, visual servoing methods were implemented.

Important experiences with locomotion of walking machines in crater environments were made and the locomotion principle was significantly improved. With appropriate control mechanisms even the Scorpion robot, not explicitly designed for this terrain, was able to climb in the artificial crater with slopes of up to 35°. The locomotion was safe and reliable, even with leg failure, the robot could negotiate the slope with the remaining seven legs.

The evaluated parts of the mission that are presented in this paper were successfully demonstrated in a complex overall mission. This demonstration showed the ability of the project partners to deal with a complex multi-robot mission and proved the overall system to be capable fetching a soil sample from within a dark crater.

In the project RIMRES[2] (Reconfigurable Integrated Multi-Robot Exploration System [3]) the idea of heterogeneous robotic systems is further pursued. The mobile systems will be newly developed in a co-design process. A standardized mechatronic interface and a connection providing interfaces for exchange of data and energy will be developed, allowing for a closer coupling between rover and scout.

References

[1] Abad-Manterola, Pablo ; Burdick, Joel W. ; Nesnas, Issa A. D. ; Chinchali, Sandeep ; Fuller, Christine ; Zhou, Xuecheng: Heterogeneous Robotic Teams for Exploration of Steep Crater Environments. In: *Proceedings of the 2010 IEEE International Conference on Robotics and Automation (ICRA'10)*. Anchorage, Alaska, USA, 2010

[2] Cordes, F. ; Planthaber, S. ; Ahrns, I. ; Birnschein, T. ; Bartsch, S. ; Kirchner, F.: Cooperating Reconfigurable Robots for Autonomous Planetary Sample Return Missions. In: *ASME/IFToMM International Conference on Reconfigurable Mechanisms and Robots (ReMAR-2009)*. London, United Kingdom, June 22-24 2009

[3] Cordes, Florian ; Kirchner, Frank: Heterogeneous Robotic Teams for Exploration of Steep Crater Environments. In: *Planetary Rovers Workshop (ICRA2010)*. Anchorage, Alaska, USA, 2010

[4] Huntsberger, Terry ; Rodriguez, Guillermo ; Schenker, Paul S.: Robotics Challenges for Robotic and Human Mars Exploration. In: *Proceedings of ROBOTICS 2000*, 2000, S. 84–90

[5] Kennedy, B. ; Aghazarian, H. ; Cheng, Y. ; Garrett, M. ; Hutsberger, T. ; Magnone, L. ; Okon, A. ; Robinson, M.: Limbed Excursion Mechanical Utility Rover: LEMUR II. In: *53rd International Astronautical Congress*, 2002

[6] Linnemann, Ralf ; Klaassen, Bernhard ; Kirchner, Frank: Walking Robot Scorpion - Experiences with a Full Parametric Model. In: Kerckhoffs, E.J.H. (Hrsg.): *15th European Simulation Multiconference: Modelling and Simulation*. Prague, Czech Republic, June 6-9 2001, S. S.1012–1018

[7] Patel, Nildeep ; Scott, Gregory P. ; Ellery, Alex: Application of Bekker Theory for Planetary Exploration through Wheeled, Tracked and Legged Vehicle Locomotion. In: *Proc. of Space 2004 Conference*, 2004, S. 1–9

[8] Roehr, Thomas M. ; Cordes, Florian ; Ahrns, Ingo ; Kirchner, Frank: Cooperative Docking Procedures for a Lunar Mission. In: *Proceedings of the ISR/Robotik2010*, 2010

[9] Schenker, Paul S. ; Huntsberger, Terry L. ; Pirjanian, Paolo ; Baumgartner, Eric T. ; Tunstel, Eddie: Planetary Rover Developments Supporting Mars Exploration, Sample Return and Future Human-Robotic Colonization. In: *Autonomous Robots* 14 (2003), Nr. 2-3, S. 103–126

[10] Silva, Manuel F. ; Machado, J.A. T.: A Historical Perspective of Legged Robots. In: *Journal of Vibration and Control* 13 (2007), S. 1447–1486

[2]RIMRES is funded by the German Space Agency DLR, Grant No. 50RA0904

Towards a Heterogeneous Modular Robotic Team in a Logistics Chain for Extended Extraterrestrial Exploration

Roland U. Sonsalla[1], Florian Cordes[1], Leif Christensen[1], Steffen Planthaber[1], Jan Albiez[1], Ingo Scholz[1] and Frank Kirchner[1,2]

[1] DFKI Robotics Innovation Center Bremen, Germany
e-mail: *firstname.lastname@dfki.de*

[2] University of Bremen, Robotics Lab, Germany

Abstract

Future extraterrestrial exploration missions ask for robotic systems able to handle tasks with increasing complexity. A reference mission within Amundsen crater near the lunar south pole for volatiles and rogolith analysis is outlined in this paper. The focus is on implementing a logistics chain introducing various heterogeneous mobile and immobile robotic systems. Within this context the robot cooperation as well as communication architecture is outlined. The reference mission serves as base line for later field trials. Furthermore, an overview is given on the robots to be used within the terrestrial test campaign.

1 Introduction

Future exploration of the solar system is calling for robotic missions with increasing complexity. Scientific concepts for the exploration of the Moon and Mars ask for advanced instrumentation and experiments such as sample acquisition and return, while pushing into more hostile environments such as permanently shaded areas at the lunar poles. These missions get increasingly difficult to handle with common single rover architectures but call for the combination of multiple, specialized exploration vehicles. A first attempt in this direction is e.g. the proposed ESA/NASA Mars Sample Return (MSR) mission, including one rover for taking samples and a second rover for fetching these samples and returning them to the sample return stage [6].

The primary mission objective of the presented project seeks to extend the exploration capabilities and handle complex mission tasks in a (semi-)autonomous manner by introducing a semi-autonomous and heterogeneous team of cooperating mobile robots, able to establish a logistics chain based on stationary modules (so-called base camps) as well as portable modular payload items. The general idea of implementing a logistics chain including various robotic systems is depicted in Figure 1. An exploration rover is paired with one or more small supporting rovers (so-called shuttles) building up a logistics chain between the rover and the lander via the aforementioned base camps.

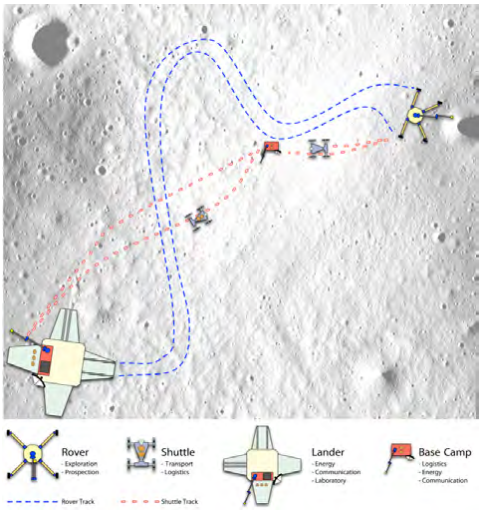

Figure 1. Schematic drawing of the implementation of a logistics chain using a heterogeneous team of mobile and stationary robots

In this paper a reference lunar exploration mission is outlined. First the mission concept is presented, providing the overall mission design concept as well as the mission subject and landing site. Furthermore, the mission architecture is addressed, providing an idea how the different robotic systems are working together. This mission set-up provides the basis for terrestrial implementations, tests, and demonstrations of logistics chain applications. The different robotic systems which are used for implementing a logistics chain, referencing to the previously outlined mission design, are conceptualized and introduced

as well. Finally a conclusion and outlook for further work is given.

2 Mission Design Concept

The mission design concept is motivated by the need of robotic systems able to handle exploration tasks with increasing complexity. This includes e.g. (multi-) sample return missions as well as tasks in the field of resource utilization and even the preparation of (long term) manned missions. The overall mission concept is oriented around the implementation of a logistics chain, including various robotic systems. As shown in Figure 1, this includes: (1) a team of mobile surface robots, (2) stationary elements and (3) portable modular payload items. The proposed mission concept addresses basically the surface exploration of the above mentioned elements.

The exploration rover is the primary mobile element within the mission concept. It serves as main exploration device, able to conduct the major mission tasks and serves as transporter for the deployment of base camps.

The exploration rover is paired up with one or more shuttle rover(s). The shuttle is a compact, highly mobile system and the core element for establishing a supply chain between stationary infrastructure elements - such as lander and/or sample return stage, base camps and the exploration rover. The base camps are stationary elements providing infrastructure to support the logistics chain. They can serve as junction point as shown in Figure 1 to exchange, e.g., payload items between the different systems. Further functionality for energy harvesting, communication or scientific instrumentation may also be provided by base camps depending on the needs of the mission.

In order to implement a supply chain the shuttles need to cooperate tightly with the exploration rover. Further surface elements that may be included in the logistics chain are potentially the lander and a sample return stage. Independently of the chosen landing system, a dedicated *home base*, i.e. main supply and communication link to the ground station, is part of the mission concept. The home base serves as depot for base camps and portable payload items and may be equipped with additional scientific and/or mission relevant functionality as well.

The mission concept proposes to realize the logistics chain by including the different mobile and stationary surface elements and establish the links using a modular approach. While each of the surface elements has to satisfy specific needs to execute the mission tasks, a high interconnectivity between the different elements is envisaged. An overview of the physical connectivity between the various elements is shown schematically in Figure 2. Especially the portable and modular payload items play a key role for establishing the logistics chain. They serve as multipurpose payload containers which can be attached to several elements. This approach allows to add specific functionality to the various systems and to handle different tasks in a distributed manner. A closer look on the different robotic systems is provided in Section 6.

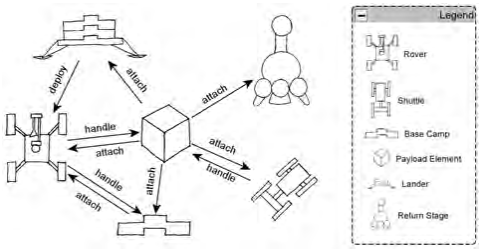

Figure 2. Schematic drawing of the modular interconnectivity of the different surface elements

3 Mission Subject and Landing Site

For the reference mission scenario the robotic systems are designated to operate inside Amundsen crater, located close to the lunar south pole. This landing site was chosen based on a trade-off between different scientific goals for lunar exploration, as identified by [4, 7]. The trade-off process was conducted to identify an adequate scientific context and an appropriate landing site for the reference mission. This was done mainly with respect to which scientific mission concept would benefit the most of the previously described mission design concept. As most of the described science goals in [4, 7] require field work, like sample collection and return to Earth, four high potential sites are identified which would benefit from a logistics chain set-up. These are in particular: 1. Amundsen Crater, 2. Tycho Crater, 3. Montes Harbinger and 4. Schrödinger Basin. The four sites are shown in Figure 3, with potential landing and exploration sites highlighted as identified by [4].

The primary scientific objective within Amundsen crater is to study volatiles and their flux in the lunar pole regions. Due to its location and crater diameter of approximately 150 km, only some parts of the crater are permanently shadowed regions (PSR) (cf. Figure 3(a)). This allows to land and deploy the robots directly on the flat crater floor in a sunlit region such that no descent on a steep crater wall is required as it would be the case e.g. at Shackleton crater. Another benefit is the possibility to send the robots for short exploration excursions into the thermally and power-wise more challenging PSR environment.

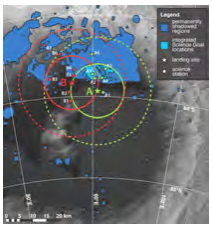

(a) Amundsen Crater

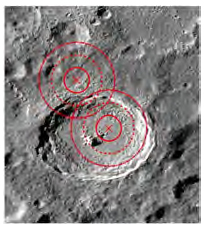

(b) Tycho Crater

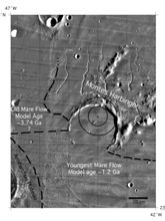

(c) Montes Harbinger

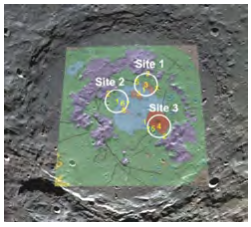

(d) Schrödinger Basin

Figure 3. The four most favorable lunar landing sites following the mission design concept [4]

The main needs which arise from the scientific mission setup with respect to the mission and system design are:

Operation in shadowed/dark areas Exploration and analysis tasks need to be conducted in PSR which provide continuous low temperatures. These areas are of main interest to study the accumulation of volatile materials as well as regolith processes.

Sample analysis The current state of volatile materials and regolith at very cold spots may need to be analyzed by in-situ measurements. Taking the samples out of its environment can change the composition drastically due to temperature change.

Sample return to Earth In order to study regolith composition and processes in cold areas in-situ analysis is needed. However, the science goals ask for the return of regolith samples allowing a deeper investigation within terrestrial laboratories. As proposed in [2] returning frozen samples should be considered as well, calling for sealable sample containers.

The mission needs introduce quite challenging and complex exploration tasks which would benefit from a logistics chain e.g. in terms of sample transport, energy and communication support and assembling special base stations for keeping-alive support.

Especially the deployment of different base camps can support the mission in terms of, e.g., energy supply, position tracking, and communications. Furthermore, they can serve as stationary laboratories for in-situ analysis of samples taken by the exploration rover. Paired with suitable modular payload items it would be possible to introduce instrument and/or tool change for the different rover platforms in order to handle a wide range of different tasks.

The investigation on establishing and maintaining a robotic logistics chain provides the possibility of increasing the maturity level and demonstrating the state of robotic technologies in terms of (1) robotic cooperation, (2) multi-robot mission planning and execution, (3) robotic long-term autonomy, and (4) robotic infrastructure setup and maintenance. These robotic technologies are currently considered to be main issues in preparation for (long-term) human presence on any celestial body.

The aspired mission definition provides a wide range of exploration and assembly tasks with the possibility to prepare In-Situ Resource Utilization (ISRU) and/or long-term manned missions. Especially the potential of harvesting volatile materials, e.g., for future long term manned missions makes the Amundsen crater a quite interesting place.

This concept highly depends on the logistics chain considering that the base camps will be needed as communication relay stations (cf. Section 5) and potentially for power supply and sample analysis. Especially for solar powered rover systems the base camps can be used for energy harvesting. This would allow to extend the PSR excursions of the exploration rover due to the possibility to supply recharged energy packages via the logistics chain. Most likely, however, this concept would not hold for the surface exploration as described in Section 4. For extensive PSR traversal an appropriate power supply system is needed on the exploration rover which can, e.g., be based on wireless power transmission techniques or radio thermal generators. In any case a reliable cooperation between the robotic systems is required in order to support exploration and sample analysis in PSR.

4 Surface Exploration

The main scientific and technical focus is on establishing a logistics chain utilizing a team of robots to sample regolith and evaluate the presence of volatile material in difficult to reach areas inside the Amundsen crater. The chosen landing and exploration site is shown in Figure 4. The image is a multi-level surface map with a satellite mosaic overlay [5], the markers for the science goals refer to [4]. The paths were chosen to avoid craters on transients using the tools available in [5].

The rover starts at the landing site L and passes the

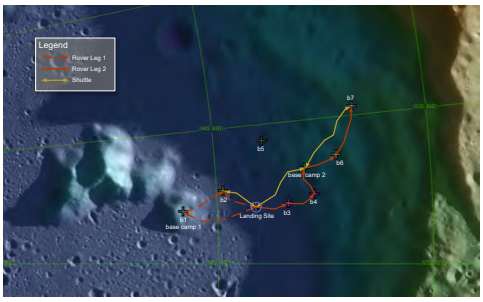

Figure 4. Overview of the surface exploration scenario in Amundsen crater

science sites *b1* to *b7*. The following enumeration gives more detail on the approach sequence and tasks carried out at the specific science sites:

1. Following the touchdown of the lander at landing site *B*, 83.82° S, 87.53° E (cf. Figure 3(a)) with crater floor slopes < 5°, both, the shuttle as well as the exploration rover, begin the commissioning phase.

2. After commissioning, the rover, already equipped with a base camp assembly for communication and power supply, travels towards the central peak foothills and then starts approaching point *b1* on the slopes of the central peaks.

3. At point *b1* the exploration rover deploys (utilizing it's manipulation capabilities) the base camp communication/power assembly. The elevation above the crater floor will increase visibility both to Earth and Sun for communication purposes and energy harvesting. The base camp may also be utilized for navigation purposes by serving as a beacon.

4. A second task at point *b1* for the exploration rover is to take regolith samples, which are of specific interest due to the potentially layered structure of the central peak slopes. The gathered samples do not need to be analyzed in-situ but can be stowed away in a modular sampling container (payload item) for sample return.

5. Subsequently, the exploration rover descents the central peak slopes, heading for point *b2* to take further regolith samples.

6. *b2* is also the first rendezvous point for the exploration rover and the shuttle, at which the exploration rover can reequip itself with fresh battery payload elements brought there by the shuttle, as well as exchanging the filled sampling payload elements with new ones. Additional sample containers are probably required to take samples at *b2* which is proposed for sensor calibration by [4].

   Following the first rendezvous, both robots head for the lander, the exploration rover in order to fetch the second base camp assembly (sample drop-off / power supply type) and the shuttle to deposit the regolith samples.

7. Thereafter, the exploration rover is approaching and entering the PSR heading towards point *b3* and *b4*, taking geological samples in places of utmost scientific interest due to the expected thermally trapped volatiles.

8. Having sampled at point *b3* and *b4*, the exploration rover leaves the PSR again in a left side arc toward *b6*, deploying the second base camp. At this point also a rendezvous with the supplying shuttle takes place again.

9. While the shuttle is returning exchanged sampling and battery payload elements to the lander, the exploration rover is entering the PSR again in order to sample at *b6* and *b7* subsequently while being resupplied by the shuttle.

10. In an extended phase that could follow the mission procedure stated above, the exploration rover can continue to climb the Amundsen crater rim sampling the interesting heavily terraced and layered slopes looking for ancient regolith.

Following the depicted exploration scenario, the exploration rover needs to travel a total distance of approximately 47.75 km with a maximum distance from the landing site of 20 km, and 3915 m of cumulative elevation gain. In Figure 5(a) a distance profile for the exploration rover path within Amundsen Crater is plotted. The landing site, scientific exploration points of interest as well as base camp deployment locations are marked within the diagram. Accordingly, the travel profiles for the different shuttle legs are given in Figure 5(b). For each shuttle path the distances to the target and back are plotted since this is considered a typical shuttle support mission. Specifically these cover the shuttle traversal from the landing site to *b2* and back, again from the landing site to base camp 2 and back and from base camp 2 to *b7* and back.

The travel profiles follow the exploration scenario as shown in Figure 4 and outlined in the previous descriptions. For compiling the traversal profiles and distance measurements the data available in [5] were used. For all measurements the direct path between the depicted points of interests are taken into account. Hence, no additional traversal for performing exploration tasks and/or obstacle

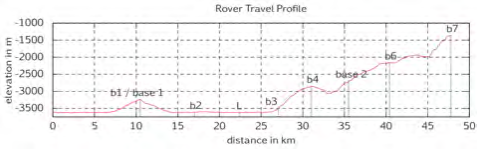

(a) Distance profile for the exploration rover path

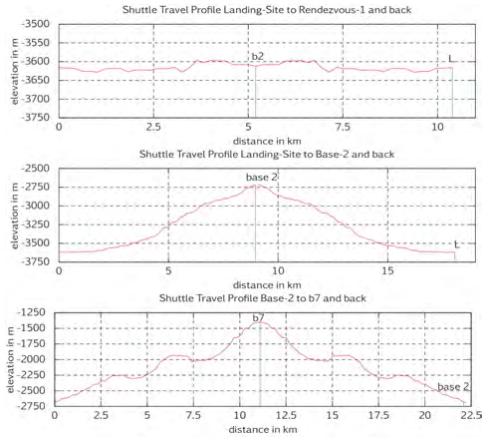

(b) Distance profile for the shuttle rover paths

Figure 5. Travel distance profiles for the exploration and shuttle rover

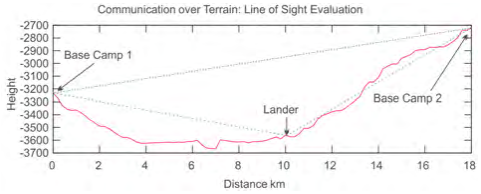

Figure 6. Free line of sight evaluation for communication within Amundsen crater

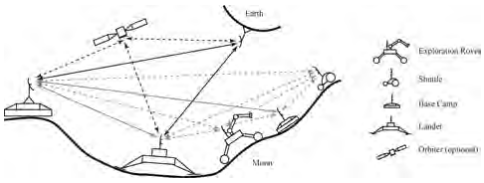

Figure 7. Proposed communication architecture with optional orbiter displayed. Dashed lines depict temporary and/or optional communications and solid lines mark fixed communication links.

avoidance is considered in the given distance measurements. These need to be included during a detailed mission design process.

5 Communication Architecture

To allow the implementation of a logistics chain with various cooperating surface elements a proper communication architecture needs to be taken into account for operations. A short range communication ability between the exploration rover and shuttle(s) is necessary to allow the handling of cooperative tasks. For longer ranges base camps can serve as communication relays, e.g. for transmitting the relative positions of the systems for rendezvous. This implies that the exploration rover as well as the shuttle need a direct communication link to each other or at least to one base camp when trying to communicate with each other. Therefore, each base camp should be able to link to neighboring base camps to establish a supporting communication network for the surface elements.

The communication range on the Moon strongly depends on antenna heights and terrain. A direct line of sight (LoS) is necessary in order to establish communication. Figure 6 illustrates the communication possibilities over the terrain between the base camps and the landing unit representing a cross section of Amundsen crater based on the data available in [5]. As shown the LoS between the lander and base camp 2 is blocked by terrain. A communication between lander and base camp 2 is possible using base camp 1 as relay.

Using this information, Figure 7 illustrates the proposed communication architecture. As outlined previously, base camp 1 should be placed on the central peak of Amundsen crater. This has two main reasons besides the scientific mission needs: (1) As shown in Figure 6 no direct LoS can be established between the lander and base camp 2. Therefore, a relay is needed to set up a communication network, covering the points of interest *b3* to *b7*. (2) Due to the landing site at 83.82° S, 87.53° E the lunar libration with max. angles of ±7.7° longitude and ±6.7° latitude has a major impact on the LoS to Earth (cf. [3]). Placing a base camp on the central peak reduces the angle to the crater rim to ~ 2.5° while the horizon seen from the crater floor is at ~ 5°. Taking the libration into account the total time with direct communication ability to Earth increases by placing the antenna on the central peak. Optionally, communication times with mission control can be increased by introducing a lunar orbiting satellite or

placing a relay on the outer crater rim of Amundsen. During the traverse of the exploration rover to the deployment destination of base camp 1 the lander is considered to serve as communication link to Earth, providing a communication back-up for the later on mission.

For cooperative tasks between the exploration rover and the shuttle(s) short range communication is required. For longer ranges base camps serve as communication relays, e.g. for communicating the relative positions of the systems for rendezvous. This implies that the exploration rover as well as the shuttle need a communication connection to each other or at least to one base camp to build up a communication link. Many aditional types of deployable units are conceivable when regarding the modular setup of the overall system. These units are for example surface deployable scientific experiments. While this modality is not depicted in Figure 7, such elements need to be connected to the local communication network set up by the base camps and lander.

6 Robotic Systems Overview

There are several systems involved in the approach of forming a logistics chain on a celestial body. The systems include, as mentioned above, mobile units, namely an exploration rover and one or more supporting shuttle systems. Immobile units are present in form of base camps and payload items, extended by the possibility of including the landing unit. The main tasks are distributed as follows.

The exploration rover is responsible for carrying and deploying base camps and payload items to establish the basic infrastructure of the logistics chain. By means of the payload items, the rover can be equipped with additional tools to fulfill different science tasks.

The shuttle rover has to be able to quickly (w.r.t. the exploration rover) cover rough terrain. Its task is carrying payload items between stationary nodes to the exploration rover and back, thus keeping the logistics chain active.

Payload items are containers for scientific instruments, infrastructure elements or tools. They can be connected with other payload items, base camps or mobile robots via a uniform electro-mechanical interface (EMI). Connecting different payload items into a stack allows to build up functional units from modular items.

Base camps shall provide stationary points in the logistics chain. They can be used for energy harvesting, communication relay, payload storage etc. Base camps are equipped with EMIs to be able to integrate modular payload items for extension of functionality or battery recharging.

Following the previously described reference mission, it is intended to perform demonstration scenarios in terrestrial testing facilities. The robotic systems that

Figure 8. Designated systems for terrestrial proof of concept demonstration of the described scenarios

are employed in the context of these demonstration scenarios are based on already available systems as shown in Figure 8. The wheeled-leg exploration rover Sherpa (background), the hybrid legged-wheel shuttle Asguard (foreground) and some payload items (stack of cubes). The systems are displayed in their initial state, adaptions are currently conducted. A brief description of the core robotic systems and their adaptation to the special needs for establishing the envisioned logistics chain is given in the following sections.

6.1 Exploration Rover

The hybrid wheeled-leg system Sherpa is designated as exploration rover. This system has already demonstrated its ability to work in a heterogeneous robotic system and is capable of transporting modular payload items, a partner robot, and is equipped with a manipulator for payload handling [8]. Currently, the main adaption work for Sherpa is focusing on the suspension system and a new locomotion control scheme that is being implemented.

A concept study of the Sherpa adaptation as presented in [1] is shown in Figure 9. The rover is shown with a base camp attached under its belly and a payload item attached to the manipulator arm. The main body of the rover holds four modular payload item bays for reconfiguration purposes or storage of payload containers.

The main dimensions of Sherpa are $2.4 \times 2.4 \times 1.2\,\mathrm{m}$, with a mass of $\sim$ 160 kg. The adaptation of Sherpa as shown in Figure 9 is considered to stay within this mass and size frame.

6.2 Shuttle

The task of a quick and highly mobile shuttle is assigned to one of the robots of the Asguard family. These robots make use of hybrid legged-wheels for propulsion.

Figure 9. Conceptual drawing of the proposed adaptation of Sherpa as exploration rover with attached base camp and payload item

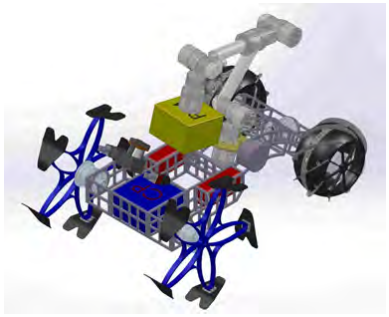

Figure 10. Conceptual drawing of a shuttle rover equipped with a manipulator for payload item handling

The special design of the wheels allows fast movement in very rough terrain. The system exhibits a generally low control complexity and a robust design. In its latest version, Asguard presented high autonomous capabilities while moving in rough terrain [9].

From the family of Asguard rovers an adaptation of the Coyote II rover (cf. [10]) is considered for the terrestrial proof of concept trials. A major adaptation of the rover is to enable the transport and handling of modular payload items. An initial idea of a possible shuttle concept is given in Figure 10. The rover concept is equipped with a payload item bay and a manipulation device to handle the payload items. While Coyote II has a mass of 9.2 kg at 850 × 580 × 410 mm outer dimensions, it is considered that the adopted rover will have a higher mass due to its additional mechanisms.

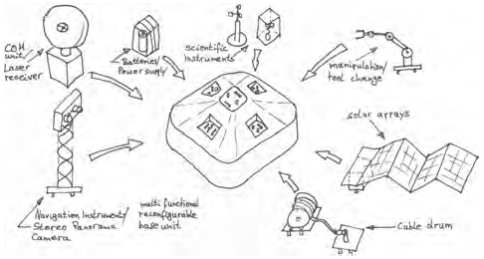

Figure 11. Schematic drawing of the modularity concept for a general base camp

6.3 Payload Items

The payload items are based on previous developments as described in [8] and shown in Figure 8. Each payload item is equipped with an EMI on the top and bottom. The EMI with its accompanying electronics is responsible for connecting payload items electronically and mechanically with other payload items or robots that provide an EMI.

The EMI and the payload items play a key role in establishing the logistics chain. They provide the modularity and reconfiguration capabilities of the different robotic systems due to a standardized EMI and payload container shape. The interface as well as the payload items allow to establish tool and system change for the remaining robotic systems and can be equipped with different tools, instruments, systems or goods. It is foreseen to use the payload item e.g. for energy supply, sample catching and positioning purposes during the planned terrestrial tests. A basic payload item has a cubical shape with 154 mm edge length and is designed for an overall mass of 5 kg. The EMI itself is designed for operation under mechanical loads of up to 300 N in order to support base camp deployment.

6.4 Base Camps

Base camps are considered to either serve as specialized base stations designed for a specific task or as mutlifunctional modular base stations providing the main functionality in terms of communication (cf. Section 5) and a set of EMI, for reconfiguration purposes. The general idea of modularity for a base camp is outlined in Figure 11. The base camp, equipped with several EMIs, serves as multi- functional note within the logistics chain. It can be equipped with different payload items according to the mission need and progress. This allows to provide a defined assembly point for payload items in order to build up a supply chain for the mobile robots or to build up a scientific and/or mission relevant system.

The base camps are carried and deployed by the ex-

ploration rover (cf. Figure 9). It is proposed to connect them to the bottom of the exploration rover's main body using an EMI. Therefore, the dimensions of a base camp are dependent on the rover body dimensions and are initially considered at 600 × 600 × 150 mm with a mass of ≤ 30 kg.

7 Conclusion and Outlook

In the previous sections a mission design concept is presented, introducing a heterogeneous modular robotic team for extended extraterrestrial exploration tasks. In order to handle tasks with increasing complexity in future exploration missions the approach of implementing a highly modular logistics chain is presented. For this, a team of mobile robots is accompanied by stationary surface elements as well as portable and modular payload items.

The analysis of present scientific questions for future lunar exploration missions yields a high potential for multi-robot missions. The proposed approach of implementing a logistics chain promises to gain benefits in terms of long term exploration, sample transport for sample analysis and return, energy and communication support and last but not least providing the ability to handle complex cooperative tasks like setting up infrastructure elements. Based on the scientific context a reference mission within Amundsen crater is presented, motivating the proposed mission design concept. The mission outline focuses on the implementation of a logistics chain, allowing to analyze volatiles and regolith processes at various points of interest within Amundsen crater. A set-up including one exploration rover and one ore more shuttle rovers is presented. These mobile robots are accompanied by stationary base camps which build up a local communication network to support the logistics chain. Furthermore, base camps are considered to be used for energy harvesting in order to provide life support within the thermally and power-wise difficult environment of Amundsen crater.

Based on the lunar reference mission a set of demonstration scenarios will be derived for terrestrial proof of concept trials. The intended robotic systems for the implementation of a logistics chain are presented along with their proposed functional adaptations. Furthermore, it is intended to analyze the benefits of all systems proposed for space exploration purposes within Earth-bound applications. This includes, e.g., search and rescue, management of maritime resources and rehabilitation. It is believed that the installation of a logistics chain and the cooperation of a heterogeneous robotic team can add major benefits to these domains as well.

Acknowledgment

The project TransTerrA is funded by the German Space Agency (DLR, Grant number: 50RA1301) with federal funds of the Federal Ministry of Economics and Technology (BMWi) in accordance with the parliamentary resolution of the German Parliament.

References

[1] F. Cordes et al. "An Active Suspension System for a Planetary Rover". In: *Proc. of the 12th Int. Symp. on Artificial Intelligence, Robotics and Automation in Space - i-Sairas 2014*. Montreal, Canada, 2014.

[2] ESA. *Moon Exploration - Lunar Polar Sample Return*. ESA - Human Space Flight and Operations (HSO). ESA Thematic information day BELSPO, 2012.

[3] G.H. Heiken, D.T. Vaniman, and B.M. French, eds. *Lunar Sourcebook: A User's Guide to the Moon*. Cambridge University Press, 1991.

[4] D.A. Kring and D.D. Durda, eds. *A Global Lunar Landing Site Study to Provide the Scientific Context for Exploration of the Moon*. LPI Contribution No. 1694. LPI-JSC Center for Lunar Science and Exploration, 2012.

[5] LROC-Team. *LROC Quickmap Tool*. online. 2013. URL: `http://target.lroc.asu.edu/q3/`.

[6] E. Nilsen, C. Whetsel, and R. Mattingly. "Mars Sample Return Campaign Status". In: *Proc. of the 2012 IEEE Aerospace Conference*. Big Sky, MT, 2012.

[7] G.A. Paulikas et al., eds. *The Scientific Context for Exploration of the Moon: Final Report*. Washington, D.C.: National Academies Press, 2007.

[8] T.M. Roehr, F. Cordes, and F. Kirchner. "Reconfigurable Integrated Multirobot Exploration System (RIMRES): Heterogeneous Modular Reconfigurable Robots for Space Exploration". In: *Journal of Field Robotics* 31.1 (2014), pp. 3–34.

[9] J. Schwendner, S. Joyeux, and F. Kirchner. "Using Embodied Data for Localization and Mapping". In: *Journal of Field Robotics* 31.2 (2014), pp. 263–295.

[10] R.U. Sonsalla et al. "Design of a High Mobile Micro Rover within a Dual Rover Configuration for Autonomous Operations". In: *Proc. of the 12th Int. Symp. on Artificial Intelligence, Robotics and Automation in Space - i-Sairas 2014*. Montreal, Canada, 2014.

[12]: **Heterogeneous Modules with a Homogeneous Electromechanical Interface in Multi-Module Systems for Space Exploration**
A. Dettmann, Z. Wang, W. Wenzel, F. Cordes, F. Kirchner
in: ICRA 2011

Heterogeneous Modules with a Homogeneous Electromechanical Interface in Multi-Module Systems for Space Exploration

Alexander Dettmann, Zhuowei Wang, Wiebke Wenzel, Florian Cordes, and Frank Kirchner

DFKI Robotics Innovation Center
28359 Bremen, Germany

***Abstract*— The work presented in this paper is part of the RIMRES[1] project. We describe the design and development of an electromechanical interface for combining heterogeneous modules. The interface has a male and a female face and allows docking in 90-degree steps. The developed concept guarantees a secure connecting and disconnecting in rough environments with fine dust as existing on celestial bodies such as Mars and Moon. A short introduction into the project RIMRES is given with focus on the modularity of the system. After providing the design considerations for the interface, experimental results with the hardware are presented. The experiments show that the interface is capable of operating mechanically with heavy loads of up to 40 kg. The proposed latch mechanism tolerates layers of dust of up to 2 mm. Thus, an electrical as well as mechanical connection in dusty environments is realized.**

I. Introduction

Multi-module systems can change their shape and functionality by adding or removing modules. In this way, modular systems can be dynamically adapted to unforeseen tasks. The majority of current developments is in the field of homogeneous reconfigurable multi-robot systems. These systems make use of a high number of modules of one distinct type. These modules, typically with one or two degrees of freedom, can be found in systems like M-TRAN [1], ATRON [2], SuperBot [3], and CKBot [4].

There are other concepts where a main system's functionality can be enhanced or extended by adding various payload modules. The main system is fully functional by itself and already covers key functionalities such as locomotion. Each limb of the ATHLETE [5] with six degrees of freedom, for example, is equipped with a quick-disconnect tool adapter, so that it can be used as general purpose manipulator which can perform different tasks with various tools.

The XROB [6] study by the European Space Agency (ESA) analyzes the needs for exploration missions and defines robotic concepts that can fulfill these needs in a cost-efficient way. The authors conclude that modular robotic systems are essential for exploration tasks to limit load, cost, and development time. In their preliminary modular system concept, they declare standardized interfaces as crucial for manipulating as well as for mechanically and functionally connecting modules to the main system.

The goal of the project RIMRES is to develop key technologies for modular reconfigurable robot systems for extraterrestrial exploration missions and to demonstrate them under earth conditions. The robotic system consists of mobile units to explore extraterrestrial surfaces as well as immobile payload items which either can be stacked to form a scientific package or connected to the mobile units to enhance their functionality or to extend their life cycles [7], [8].

Planetary exploration involves additional difficulties which the RIMRES system has to resolve. The communication delay especially to Mars complicates tele-control, so an intelligent autonomous behavior is needed to automatically explore the surface and deploy scientific payloads [9]. In particular fine dust is a serious threat [10], especially when using a modular system which needs to dock and undock its modular elements to use its full potential. This has also been identified for the PolyBot-system [11], however, this requirement has not been taken into special account in the design of the interface for the modules. In the future, the SINGO connector [12] for the SuperBot system shall be improved to endure dirt. In literature, heavy-duty capability is more common, like the DRAGON connector [13] which can hold over 70 kg load or the active connection mechanism based on physical latching by Sproewitz et al. [14]. The design of the electromechanical interface (EMI) for the RIMRES system pays special attention to the robustness and dust-resistance of the mechanical latching mechanism and the electric connections.

The paper is structured as follows: The basic concept of the overall system is given in section II. The requirements for the interface in the context of the RIMRES system as well as its design are given in section III. The experiments for verifying the interface and their results are provided in section IV. The last section concludes the paper and gives an outlook on future work.

II. Modular Concept of RIMRES

The multi-module system RIMRES consists of mobile units and immobile payload items (see Fig. 1). The rover Sherpa[2] provides four wheeled legs for energy-efficient locomotion in lunar landscapes. It is the main system which is able to carry all other modules and to deploy payload items with a manipulator arm on its back. The walking robot CREX[3] serves as scout and can climb steep inclines to reach areas which the rover cannot access.

[1]Reconfigurable Integrated Multi-Robot Exploration System

[2]Sherpa: Expandable Rover for Planetary Applications
[3]Crater Explorer

[12]: **Heterogeneous Modules with a Homogeneous Electromechanical Interface in Multi-Module Systems for Space Exploration**
A. Dettmann, Z. Wang, W. Wenzel, F. Cordes, F. Kirchner
in: ICRA 2011 ©IEEE 2011

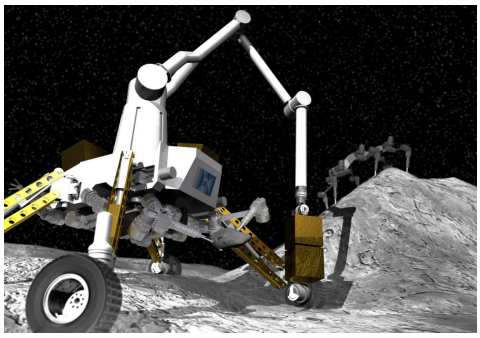

Fig. 1. Artist drawing of the RIMRES system. One legged scout is climbing a steep slope while a second is mounted beneath the rover. The wheeled rover is deploying a stack of two payload items on the surface.

The payload items can be arranged to autonomous module stacks as well as to enhance the performance of the mobile units by providing extra energy, communication, or sensors [7]. For an independent configuration of the modular system, an EMI is developed to exchange data and energy among all kinds of modules and to securely connect them. Each payload item is equipped with one EMI on the top side and one on the bottom side. Sherpa makes use of four docking bays with integrated EMIs on the back for transporting payload items, one EMI on the bottom to connect to the scout and one EMI as end effector of the manipulator arm. CREX has one EMI on its back to connect to the rover and to carry payload items.

A. Communication

Communication plays a significant role in modular robotic systems. Varying communication approaches are applied in many developed multi-robot systems, e.g., SuperBot [3] with local communication (infrared), M-TRAN II [1] with global communication (Controller Area Network), and CKBot [4] with local and global communication. By reason of the heterogeneity of the RIMRES modules, diverse channels are employed to cover different communication levels as outlined in Fig. 2. The proposed components were chosen for an earth demonstrator, but can easily be exchanged for a flight system.

1) *Local Communication* is used to exchange simple, yet important information between neighboring modules, e.g., identification and fitness status of modules. The acquired information makes cooperation and topology recovery of a formed subsystem possible. The widely used infrared approach is not suitable for application in dusty environments, since the communication channel can easily be obstructed by loosely bound dust. In order to implement a reliable data connection, EIA RS-422 using balanced signaling is employed as physical transmission layer for local inter-module communication. The information acquired over this channel facilitates many other applications in the system, e.g., docking and power sharing among the modules.

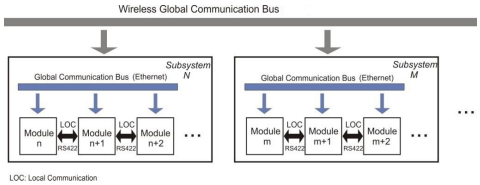

Fig. 2. Three communication levels in the RIMRES system: Modules can communicate with their direct neighbors via local communication (RS-422) (used for docking procedure and topology recovery), Ethernet is used for wired communication in a physically connected system. Wireless communication is employed between remote subsystems.

2) Cooperation and sharing of computational resources between individual modules inside of a subsystem is based on *Global Communication* via Ethernet. The hardware used within the modules is 100BaseT compatible which provides high speed transmission and robust performance.
3) The RIMRES system can be divided into several spatially separated subsystems. Thus, a *Wireless Global Communication* is needed as well. It is realized via the REIPOS[4]-system [15], a subsystem developed within RIMRES for communication and navigation purposes.

B. Power Management

Since all modules in one physical connected subsystem share a common power bus, a homogeneous power management system was developed. On the one hand, it supplies passive payload items with energy from the power bus to activate their functionality. On the other hand, the power management guarantees safe power supply of active modules to the power bus. The 48 V of the power bus will be converted down by the power management to the needed voltages of the module consumers. Since several power sources can be autonomously assembled in one subsystem, the power management is able to securely connect and disconnect the modules via a hot swapping functionality allowing just one power supply on the power bus.

C. Module Components

Fig. 3 gives an overview of the components that are common in each RIMRES module. A microprocessor provides high-level functionalities and uses global communication to cooperate with other modules. In addition, its computational power is used to process sensor data. The microprocessor can be shut down when its capability is not needed. It directly communicates with a microcontroller unit which handles the latch mechanism of the EMI, controls the power management, and communicates via local communication with potential module neighbors. The module-dependent special hardware is controlled by the microprocessor and supplied by the power management.

[4]Relative Interferometric Position Sensor

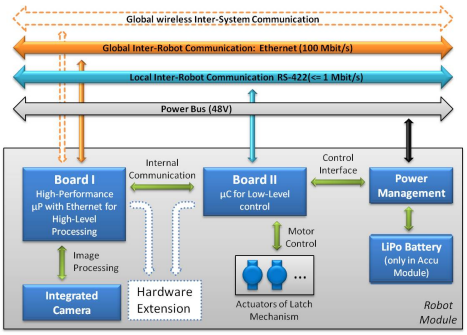

Fig. 3. Basic components in each module. The three bus systems energy, local communication via RS-422, and global communication via ethernet are provided by the electrical part of the EMI.

III. Electromechanical Interface

This section describes in detail the design of the EMI which securely connects and disconnects all RIMRES modules in dusty environments. The EMI is a key element for modularity in the RIMRES system. Since RIMRES is an earth demonstrator for extraterrestrial exploration missions, the challenges of Martian and lunar surfaces have to be taken into account. Even though space qualification is not necessary in this project phase, the components should be exchangeable to facilitate a potential qualification in follow-up phases.

A. Requirements on the Electromechanical Interface

The following requirements were considered to assure a secure mechanical and electrical connection.

Robust Connection The latch mechanism has to be able to hold complete module stacks as well as CREX with a mass of approx. 25 kg.

Energy Efficiency Because energy is a valuable resource in space applications, the latch should not consume energy in closed or opened state.

Mechanical Guidance The docking procedure is supposed to run autonomously, the interface itself should eliminate small positioning errors caused by sensor and actuator inaccuracies.

Play The play should be kept to a minimum when modules are attached to each other, in order to ensure a reliable electrical connection.

90°-Steps Docking To reduce the handling complexity and maximize the multi-module robot flexibility, the modules should support docking in 90°-steps of orientation.

Size The interface is limited to the quadratic size of a payload item's ground plate (150 mm x 150 mm). The height of the EMI itself has to be kept to a minimum to allow maximum space for module components.

Dust-Resistance The latch mechanism should be able to work in dusty environments and also prevent dust from entering into the module.

Energy Bus The EMI has to withstand currents which can be considered around 5 A, if in the worst case the actuators of the rover are supplied by energy payload items.

Data Transmission Local and global communication signals are transmitted over the EMI.

Sensors To achieve a successful autonomous docking, the module surfaces have to be aligned. Therefore, the sensor data have to be accurate and work from long distances of about 2 m to short distances where the remaining offset can be eliminated by a given trajectory to complete the docking procedure.

Actuators The latch mechanism needs a reliable drive which is able to open and close the latch.

Contact Probes The contact probes actually have to realize the electrical connection for energy and data transfer. Since dust is one of the major concerns, the heads of the contact probes should cope with that.

B. Mechanical Structure and Latch Mechanism

We decided to develop an EMI which consists of an active female part located on the bottom side of each module and a passive male part located on the top side of each module. This male/female combination has several advantages: (1) The top side of each module, where it is more likely that dust particles can accumulate, is completely closed. (2) The end effector of the manipulator arm that is always powered from the rover's main batteries has an active part of the EMI included, thus it is always possible to connect to unpowered modules. (3) A simple, yet robust design is possible.

Due to the main concern of robustness even in tough environments, an active opening and closing of the latch was chosen. After experiments with different concepts, a design employing a small motor with a spindle drive to open and close two braces was chosen (Fig. 4). The counterpart is a pole on top of the passive part of the EMI which is held by the closed braces. Due to the conical shape, the two modules are firmly pressed against each other when the latch is closed. A housing surrounds the latch mechanism protecting the module interior from potentially entered dust.

As depicted in Fig. 5, the latch mechanism is located in the center of the module face. A linear potentiometer is attached to the latch mechanism to signalize the opened or closed state. The closing of the latch is initiated when the pole of the passive part of the EMI reaches its end position which is detected by an inductive distance sensor. Four cylinders with conical mouths are located around the electronic parts. Their purpose is to receive four dome-shaped centering pins from the passive part of the EMI to avoid rotations between modules while they are connected and locked. Their conical

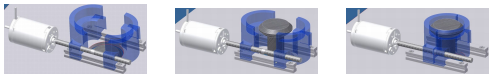

(a) Opened Latch Mechanism (b) Bolt of passive part of EMI inserted (c) Closed Latch Mechanism

Fig. 4. Latch mechanism

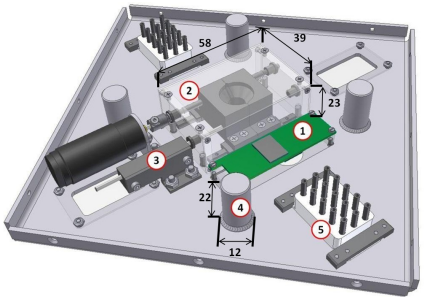

Fig. 5. Active part of electromechanical interface integrated in module bottom with dimensions in mm 1) Camera 2) Mechanical latch mechanism with spindle drive and dust protection housing 3) Linear potentiometer 4) Cylinder with conical mouth 5) Block of contact plates

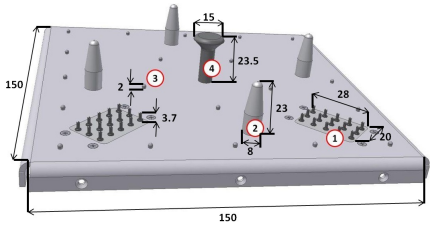

Fig. 6. Passive part of electromechanical interface on module top with dimensions in mm 1) Block of contact probes 2) Dome-shaped centering pins 3) Distance pins 4) Bolt for latch mechanism

shape increases the tolerance during docking procedure by providing mechanical guidance. The active part of the EMI also includes a camera with additional light-emitting diodes which are used for visual servoing during docking procedure. Two blocks of contact plates for energy and data transfer between modules which withstand physical force are aligned kitty-cornered, while two blocks of contact probes on the passive EMI are located on one half of the module (see Fig. 6). In that way, connecting in 90°-steps is possible with a minimum number of connectors. Smaller mechanical distance pins all over the module surface lead to a gap when two modules are docked. So, minor dust accumulations do not influence the docking procedure.

C. Spring-Loaded Contact Probes

The electrical connection is established by blocks of spring-loaded contact probes integrated in the passive part of the EMI and blocks of contact plates integrated in the active part (Fig. 7(a)). The chosen components are resistant to the required currents during power transmission and support high-frequency data streaming. The spring in the contact probes allows a variable length which creates a vertical docking tolerance of 2.2 mm. In addition, the spring force secures a constant electrical contact while the system is exposed to vibrations. Each probe is equipped with a 4-point crown head. The pointy endings are able to penetrate a layer

(a) 4-point crown head and contact plate

Pin	Description
1	RS-422 CH1 H
2	Ethernet TX+
3	RS-422 CH2 H
4	RS-422 CH1 L
5	Ethernet TX-
6	RS-422 CH2 L
7	Current (RC)
8	Ethernet RX+
9	Enable (RC)
10	Position (RC)
11	Ethernet RX-
12	Phase (RC)
13	VCC (+ 48 V)
14	NC
15	GND

(b) Pinout of the contact blocks (view from connection side)

Fig. 7. Contacts and Pinout

of dust. The round contact plates have a larger diameter than the probes. So, a horizontal docking tolerance of 3 mm is obtained.

Each contact block consists of 15 contact probes or plates. Two pins are used by the power bus. The global communication over Ethernet and the local communication via RS-422 need four pins each. Additional four pins will be used to implement a fault-tolerant interface control which enables the lower module to open the latch mechanism of the upper module. In this way, defect modules can be removed from the system. Fig.7(b) illustrates the pinout.

D. Sensor System

In the LUNARES project [16], we demonstrated successfully that visual servoing is a feasible approach for equipping systems with payloads in environments similar to the lunar surface. Thus, a docking mechanism based on visual servoing will be implemented for the RIMRES system as well. Since the cubic modules might obstruct a wrist cam on the manipulator arm, a small camera board is implemented in the active part of the EMI (Fig. 5).

A linear potentiometer is used to verify the absolute position of the braces of the latching mechanism. An inductive distance sensor attached on the latch housing signals the success of a docking approach.

IV. Experimental Results

This section presents experiments proving basic functionalities of the EMI. Since dust resistance is an important aim, we use two different kinds of regolith substitute for our dust experiments. On the one hand, we test the interface with basalt chips of 0.7 mm to 1.3 mm graining representing rough dust. On the other hand, crystalline Durubas micro basalt of of 0.02 mm to 0.2 mm graining is used to simulate very fine dust. Both regolith substitutes have a weak magnetic character.

A. Load Test for the Latch Mechanism

To test the heavy-duty capability of the proposed design, we fixed the active part of the EMI with reduced complexity on a rigid support frame. Weights were attached to the central

bolt of the passive part, which was then fixed in the latch mechanism of the active part. With the load hanging free under the latch mechanism, the actuator was driven in order to open up the latch. The aim was to test whether the latch mechanism gets jammed under loads or not. Currently we were able to test with loads of up to 40 kg in steps of 5 kg. Each weight was tested 10 times.

The latch mechanism is able to open properly to masses of up to 40 kg in all cases. In average, it takes around 2 s to open or close the latch. 3.1 W are needed and both power and time are independent from the applied load. Because no power is used in opened and closed state, the proposed design is suitable for multi-module systems. Since the scout robot with its mass of approx. 25 kg will be the highest load for the interface, the tested 40 kg are more than sufficient for the RIMRES scenario. However, in a new test setup we want to test even higher loads.

B. Docking with Dust

This experiment shows how the proposed design copes with varying layers of the above-mentioned dust types. In our setup, we established a plain layer of dust on the top of a module (Fig. 8(a)), afterwards connected both EMI parts and and finally closed the latch mechanism. Each layer of dust was tested ten times before increasing the thickness of the layer in 1 mm steps.

In general, dust layers of up to 2 mm cause no problems while docking. Most of the dust slides down from the conical distance pins of the lower module. Potential rest accumulations are pressed aside by the lower surface of the top module. In this way, the distance pins always build a constant contact surface for the upper module. At a layer of 3 mm and above, dust particles are trapped between the mechanical distance pins and the lower surface of the active part, thus causing a gap which prevents the latch mechanism from closing. We discovered that the rough basalt chips are loosely bound together and slight vibrations cause the dust to fall from the sides which continuously decreases the layer of dust. So, shaking makes a connection between two modules possible again. In contrast to the rough dust, the fine dust compressed by the pressure of the top module starts to stick to the surface. Shaking the module does not help to reduce the layer of dust (Fig. 8(b)). Thus, a docking above a layer of 3 mm is impossible with fine dust.

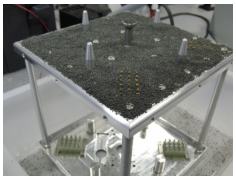

(a) Plain layer of rough dust

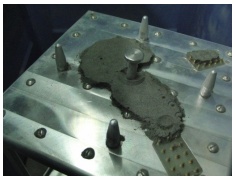

(b) Rest of compressed fine dust after experimental trial

Fig. 8. Dust experiments: Contamination of the interface

In addition, we tested the docking with four small spots of fine dust accumulations across the surface. In this case, debris cones up to 12 mm height are not causing any problems. Higher accumulations cannot be pressed aside to reach the needed docking distance due to the adhesive characteristic of the compressed fine dust.

During these experiments, dust could enter the module interior because the proposed bristles, which prevent dust from entering the module, were missing. Anyway, the entered dust did not harm the latch mechanism. The distance pins fulfilled their task of guaranteeing a safe docking to dust layers of up to 2 mm.

The experiments were conducted under worse conditions than could be expected for a real scenario. A homogeneous layer of dust was applied to the module face, Fig. 8(a). In reality smaller deposits of dust are likely. However, in the experiments we showed, that the interface can cope with extreme contaminations.

C. Reliability of the Electrical Connection

In this experiment we distributed a layer of approx. 1 mm of the above-mentioned rough and fine dust over the passive part of the EMI and manually connected it with the active part to test how the spring-loaded contact pins with their 4-point crown heads cope with dust. After the connection was established, the microcontroller of each module was supposed to start the local communication with its neighbor. Since the established contacts do not always stand statically in practice, we provoked external dynamic disturbances which could cause negative influence to the contacts, e.g., manipulator moves immobile payload items or Sherpa crosses rough terrain. Table I summarizes the results of the 50 trials per dust type.

Without dust, the microcontrollers start to communicate with each other as soon as the connection is established. It works reliably and shaking the module stack does not influence the connection. Rough dust can cause connection problems when bigger dust particles accumulate in the middle of a a 4-point crown head. This happened in 12% of our test cases, thus preventing one or both microcontrollers to start the communication. If the communication starts, shaking does not disturb the established data transfer. In just 78% of our test cases during the fine dust experiment, all necessary pins connected from the beginning with their counterparts, thus enabling the communication to start. A failure occurs when either the 4-point crown heads are filled with dust or a layer of dust sticks to the flat surfaces of the contact plates due to magnetic force. But in most

TABLE I
SUCCESS OF DATA TRANSFER

without dust	communication started	100%
	after disturbances	100%
rough dust	communication started	88%
	after disturbances	88%
fine dust	communication started	78%
	after disturbances	92%

of the failure cases, shaking the module causes the dust particles separating the contacts to fall off, thus resolving the connection problem.

Summing up, the heads basically work but not reliably enough. Consequently, more head types have to be evaluated, e.g, a spike or a sharp angle, which could potentially prevent dust accumulations. The usage of spring-loaded contacts turns out to be a good choice. Besides the redundancy in horizontal and vertical direction, the established connection is reliable regarding possible external disturbances.

D. Power Transmission

We connected two modules and distributed power over two pins of the EMI to test the power transmission. An electrical load represented potential consumers in an active multi-module system. In this experiment, we tested with and without dust a nominal current of 5 A and over-current of 8 A at a constant voltage of 25 V. Temperature and resistance of the contact were measured periodically during the test.

As shown in the temperature-time diagram in Fig. 9, the temperature of the contact rises drastically at the beginning of the connection. After the first minute, the temperature tends to be stable. The comparison between the two currents shows that higher current increases the contact temperature. Due to reduced heat conduction, the temperature is even higher when the probes are covered with dust. Nevertheless, the temperature is not critical in our application since the contact temperature is always lower than 80°. The resistance of the connections remains almost constant.

V. Conclusion and Outlook

This paper shows the development of an EMI for a heterogeneous multi-module system. Mechanical as well as electric connections of a first laboratory sample of the EMI have been tested. The data gained from the presented experiments suggest that the chosen approach has the potential to be used in a complex multi-robot scenario during operations in rough surface environments. The latch mechanism can hold a load of up to 40 kg and tolerates dust accumulations between module faces of up to 2 mm. The work presented here is preliminary and will be substantiated in additional experiments in the upcoming phase of the project. Additionally, the EMI will be integrated into payload items and mobile systems.

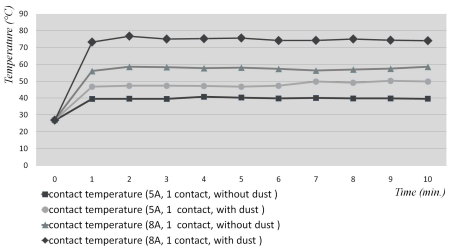

Fig. 9. Temperature of the contact probes

Acknowledgements

The project RIMRES is funded by the German Space Agency (DLR, Grant number: 50RA0904) with federal funds of the Federal Ministry of Economics and Technology (BMWi) in accordance with the parliamentary resolution of the German Parliament. RIMRES is a cooperation between the DFKI Bremen – Robotics Innovation Center and ZARM – Center of Applied Space Technology and Microgravity.

References

[1] H. Kurokawa, K. Tomita, A. Kamimura, S. Kokaji, T. Hasuo, and S. Murata, "Self-reconfigurable modular robot m-tran: distributed control and communication," in *RoboComm '07: Proceedings of the 1st international conference on Robot communication and coordination*. Piscataway, NJ, USA: IEEE Press, 2007, pp. 1–7.

[2] E. Ostergaard, K. Kassow, R. Beck, and H. Lund, "Design of the atron lattice-based self-reconfigurable robot," *Autonomous Robots*, vol. 21, no. 2, pp. 165–183, 2006.

[3] B. Salemi, M. Moll, and W.-M. Shen, "Superbot: A deployable, multi-functional, and modular self-reconfigurable robotic system," in *Proc. 2006 IEEE/RSJ Intl. Conf. on Intelligent Robots and Systems*, Beijing, China, oct 2006, inproceedings, pp. 3636–3641.

[4] M. G. Park, "Configuration recognition, communication fault tolerance and self-reassembly for the ckbot," Ph.D. dissertation, University of Pennsylvania, 12 2009.

[5] B. Wilcox, T. Litwin, J. Biesiadecki, J. Matthews, M. Heverly, J. Morrison, J. Townsend, N. Ahmad, A. Sirota, and B. Cooper, "Athlete: A cargo handling and manipulation robot for the moon," *Journal of Field Robotics*, vol. 24, no. 5, p. 421, 2007.

[6] P. Schoonejans, F. Didot, and A. Gily, "The xrob study: Exploration robotics requirements and concepts," in *Poceedings of the 11th ILEWG Conference on Exploration and Utilisation of the Moon (GLUC)*, 2010.

[7] F. Cordes, D. Bindel, C. Lange, and F. Kirchner, "Towards a modular reconfigurable heterogenous multi-robot exploration system," in *Proceedings of the 10th International Symposium on Artificial Intelligence, Robotics and Automation in Space (iSAIRAS'10)*, August 2010.

[8] F. Cordes and F. Kirchner, "Heterogeneous robotic teams for exploration of steep crater environments," in *Planetary Rovers Workshop of 2010 IEEE International Conference on Robotics and Automation (ICRA2010)*, Anchorage, Alaska, USA, 2010. [Online]. Available: http://ewh.ieee.org/conf/icra/2010/workshops/PlanetaryRovers/

[9] T. M. Roehr and Y. Shi, "Using a self-confidence measure for a system-initiated switch between autonomy modes," in *Proceedings of the 10th International Symposium on Artificial Intelligence, Robotics and Automation in Space (iSAIRAS'10)*, August 2010.

[10] M. P. Golombek, "Planetary science: The surface of mars: Not just dust and rocks," *Science*, vol. 300, no. 5628, pp. 2043–2044, 2003. [Online]. Available: http://www.sciencemag.org

[11] M. Yim, K. Roufas, D. Duff, Y. Zhang, C. Eldershaw, and S. Homans, "Modular reconfigurable robots in space applications," *Autonomous Robots*, vol. 14, pp. 225–237, 2003, 10.1023/A:1022287820808. [Online]. Available: http://dx.doi.org/10.1023/A:1022287820808

[12] W. Shen, R. Kovac, and M. Rubenstein, "Singo: A single-end-operative and genderless connector for self-reconfiguration, self-assembly and self-healing," in *Robotics and Automation, 2009. ICRA'09. IEEE International Conference on*. IEEE, 2009, pp. 4253–4258.

[13] M. Nilsson, "Heavy-duty connectors for self-reconfiguring robots," in *IEEE International Conference on Robotics and Automation, 2002. Proceedings. ICRA'02*, vol. 4, 2002.

[14] A. Sproewitz, M. Asadpour, Y. Bourquin, and A. Ijspeert, "An active connection mechanism for modular self-reconfigurable robotic systems based on physical latching," in *2008 IEEE International Conference on Robotics and Automation, Conference Proceedings*, 2008. [Online]. Available: http://birg2.epfl.ch/publications/fulltext/aSproewitz08.pdf

[15] D. Bindel and R. Bruns, "Reipos - relative interferometric position sensor," in *Proceedings of the 61st International Astronautical Congress, IAC 2010*, no. IAC-10-A3.2C.5, September 2010.

[16] F. Cordes, I. Ahrns, S. Bartsch, T. Birnschein, A. Dettmann, S. Estable, S. Haase, J. Hilljegerdes, D. Koebel, S. Planthaber, T. Roehr, M. Scheper, and F. Kirchner, "Lunares: lunar crater exploration with heterogeneous multi robot systems," *Intelligent Service Robotics*, pp. 1–29, 2010.

[13]: **A Robust Electro-Mechanical Interface for Cooperating Heterogeneous Multi-Robot Teams**
W. Wenzel, F. Cordes, F. Kirchner
in: IROS 2015 ©IEEE 2015

A Robust Electro-Mechanical Interface for Cooperating Heterogeneous Multi-Robot Teams

Wiebke Wenzel[1], Florian Cordes[1], and Frank Kirchner[1,2]

***Abstract*— This paper presents the mechanical development and testing of a docking device for a highly heterogeneous self-reconfigurable multi-module/multi-robot system. The overall system is meant to emulate a robotic lunar exploration mission. The docking device, more precisely the electro-mechanical interface (EMI), is an advancement of the reliable electro-mechanical connection of the project RIMRES. Since possible combinations and roles of modules in the multi-robot system are defined before a mission, a gender-principle approach with one active and one passive face to be mated was chosen. The experiments in this paper are conducted to compare the improved mechanical design with the previous design. With the new design, docking is successfully tested under loads up to 800 N. The experiments presented include attaching and detaching in different EMI orientations with various loads, exceeding those expected for the application scenario. In further experiments operations under heavy dust/small particle contamination are presented.**

I. Introduction

Tightly interacting heterogeneous robotic teams need common interfaces to be able to exchange data and energy. A uniform electro mechanical interface for all subsystems of a heterogeneous multi-robot system is thus a necessity. Modular robotics is a field where such interfaces are employed to connect modules with each other. Most commonly, the term *modular robot* refers to a robot that is comprised of interconnected units called *modules*. An overview on current developments of these systems is given in [1].

The SMART system for example is a heterogeneous modular robot system which attempts to give a quick solution to a diversity of tasks such as manipulation and different types of locomotion [2]. Further modular robots with docking systems, which are rotationally locked after docking are ModRED [3], M3Express [4] and JL-2 [5].

Self-assembly modular robot systems as Sambot [6] can form a new robotic structure through self-assembly and self reconfiguration. The main task of the employed docking mechanisms is to connect fast and within a certain range of misalignment.

In [7] three kinds of reconfiguration classes are defined for a modular robotic system: (i) lattice style, (ii) chain style and (iii) mobile reconfiguration. Being able to work in all classes of reconfiguration is claimed to be a step towards a universal modular robot.

*This work was supported by the German Space Agency (DLR) and conducted under grant agreement 50RA1301 (BMWi)
[1]DFKI GmbH Robotics Innovation Center, Bremen, Germany `firstname.lastname@dfki.de`
[2]University of Bremen, Bremen, Germany

The electro-mechanical interface (EMI) presented in this paper is a development for a heterogeneous multi-robot system (MRS) in project TransTerrA. It is meant to interconnect various elements of the MRS with each other [8] as shown in Fig. 1.

For tightly coupling different robots into one single system in TransTerrA, an appropriate interface is required. This interface should at least ensure:

1) Mechanical connection
2) Power transmission
3) Data exchange

In addition the design should permit a rapid and low cost fabrication. The main challenge for the docking mechanism presented here is to be suitable for systems that differ over several orders of magnitude in weight and dimensions.

In the predecessor project RIMRES [9], a heterogeneous multi-robot team was developed, using an EMI. This paper presents the improvements in the mechanical design of the interface and its application to a new scenario: a set-up of a multi-robot logistics chain for planetary exploration and sample return missions [8]. The logistics chain is implemented between the different robotic systems (see Figure 1) (i) payload-item, (ii) base camp, (iii) exploration rover and (iv) shuttle rover, whereby most of the systems are based on already existing robots and are adopted with regard to their specific tasks. The objectives of the overall project TransTerrA are(i) to extend exploration capabilities, (ii) to handle semi-autonomous tasks, (iii) to improve the Technology Readiness Level (TRL) of certain subsystems and (iv) to

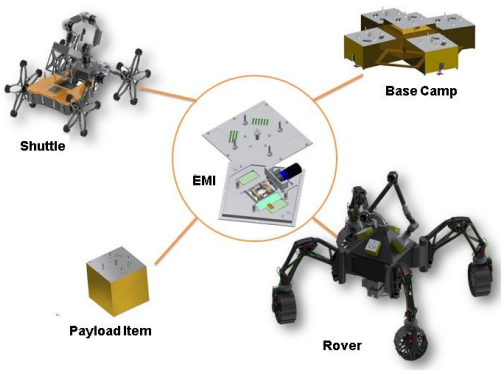

Fig. 1: Interconnection of the robotic systems in TransTerrA

develop an interaction through innovative human-machine-interfaces.

In preparation for manned spaceflight missions, robots can be used for exploring the surface of unknown celestial bodies to identify potential endangerments, to extend the knowledge about the target area as well as to enable the logistics and infrastructure for astronauts. By cooperation between a rover and a shuttle, in the TransTerrA-scenario these surfaces shall be explored. The Amundsen-crater was chosen for a reference landing-area, which has typical slopes below 5° to be negotiated by the robotic systems on the crater floor [8].

In the scenario a shuttle (*Coyote III*) supplies an exploration rover (*Sherpa*) through a logistics chain, which shall ensure the channels of supply through several stations. *Base camps* are helping to bridge long distances and build up the logistics chain. These base camps function as intermediate stations for shuttle and rover and serve as functional modules either as relay station for communication, intermediate store for samples and required modules or as energy deposit. Because of their compatible docking interface (the EMI presented here), the rover as well as the shuttle can modify and exchange the base camps through payload-items. To guarantee a safe transport and a high mobility even over rough terrain, the rover is equipped with hybrid wheel-legs [10], while the shuttle makes use of legged-wheels [11].

On earth the human operators can intervene in the mission through innovative human-machine-interfaces [12]. Thereby an exoskeleton attached on the upper part of the body is responsible for the system control and for visualization modern technologies such as VR-Glasses and a multi-screen projection area are used.

II. Electro-Mechanical Interface Overview

The EMI of TransTerrA is responsible for (dis-)connection between the different robot systems. The EMI presented in this paper is an advancement of the RIMRES-EMI [13] and was altered with respect to the required needs of the new scenario and shortcomings identified during the work with the previous design.

During the development of the EMI, focus is on robustness against dust, accurate guiding during the mating of two interfaces, ability to carry high loads in non-energy-state and limited space within a cubic payload-item. A connection of two sub-systems is always done by mating two different EMI-faces, namely an active part that is typically mounted on the bottom of a robot or payload-item, and a passive face that is typically mounted on top of a sub-system or payload-item. The active part consists of the actuated latch mechanism, a camera for the autonomous docking approach, LEDs for illumination, electrical receptor plates (Fig. 2) and cover flaps (Fig. 3). The passive part consists of a central docking bolt, four rotation protection and guidance pins, spring-loaded electrical connectors and four visual markers for detection through the active interface (Fig. 4). Since the upper face of payload-items is prone to dust accumulations, the passive part of the EMI provides distance pins to allow

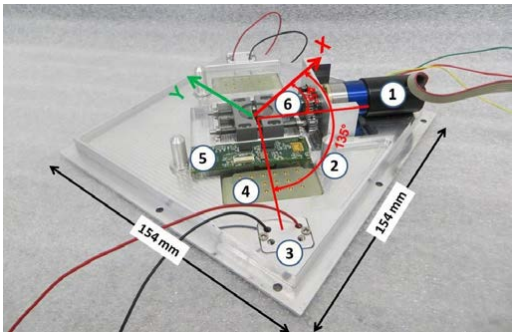

Fig. 2: Active part of the EMI, consisting of (1) actuator (2) counter-acting cylinder (3) LED (4) signal block (5) camera (6) braces with threaded spindles and gears. Coordinates and directions of tilt and roll within the load experiments are indicated

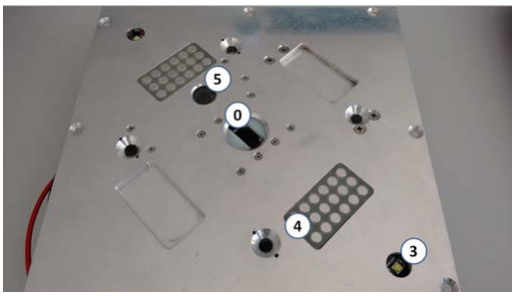

Fig. 3: Back of the active part of the EMI. (0) shows the cover flap in half opening position

for a 2 mm dust layer on the complete face. Both, the passive and active side of the EMI, have an universal design, which can be mounted on each used robotic system in TransTerrA.

For maintaining the electrical connection between interfaces during movements in possibly rough environments, two solutions are employed: (i) when closing, the latch mechanism pulls the central pin of the mating passive interface up to tightly fixate the mechanical connection; (ii) in case of dust accumulations or in the event of remaining mechanical play between the two interfaces, spring loaded electrical pins level out those movements and ensure a constant electrical connection.

A. Latch Mechanism / Active EMI

The latch mechanism's design in the active interface had two main design goals: (i) effective dust resistance and (ii) no consumption of energy in either closed or opened state. Thus the latch mechanism, which is located in the center of the module face, consists of two conical shaped braces, driven by a spindle drive. The two threaded spindles are driven by one actuator. Once the central bolt of the passive face is inserted

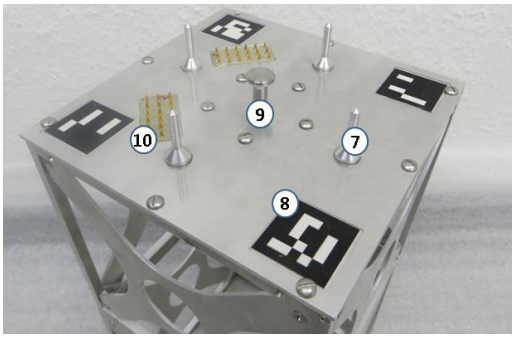

Fig. 4: Passive part of the EMI, consisting of (7) guiding pins (8) marker (9) bolt for latch mechanism (10) contact block and distance pins

between the braces, the spindle drive closes the latch. In the last few millimeters, the central bolt is pushed up through the conical shape of the bolt and braces so that the passive face is tightly pressed against the active face.

To protect the latch mechanism against small particles and dust, the opening is protected with cover flaps as shown in Fig. 3. The cover flaps operate by a spring mechanism, which ensure correct positioning of cover flaps in interconnected or undocked state of EMI.

Each time the latch mechanism is to be opened or closed, the spindle mechanism needs to be actively driven. A micro-controller is used to control position and current consumption of the latch mechanism. A blocked latch mechanism can be detected by merging the position information of the latch with the current the mechanism actually consumes.

As the conducted experiments proved, the design of the latch mechanism ensures a failure-free docking operation with heavy loads under high tilt and roll orientations of the interface with respect to the gravity vector. Moreover, the conical shaped braces and bolts constitute a mechanical guidance and prevent vertical play during the closure of the latch because they are pressed firmly against each other.

Four counter-acting cylinders are mounted around the latch mechanism with openings to the bottom face. These cylinders are meant to house the guidance pins of the passive face in connected state. Due to their conical inlet, a high displacement error is allowed in the initial state of the docking process, while a tight rotation protection is guaranteed in fully docked state, since the main part of the guidance housing is of cylindrical shape.

B. Passive EMI

The passive face of the EMI features a central pin to be grabbed by the latch mechanism and four rotation protection or guidance pins. The central pin has a conical shape at its lower side so that it fits to the concave conical shape formed by the closed latch of the active interface. The guidance pins make use of a short conical tip, whereas the main length is of cylindrical shape to be taken by the counter-acting cylinders of the active face.

To ensure a stable electrical connection, spring loaded contact probes are used in the passive (upper) face of the EMI. The crown-headed contact pins are used to contact the appropriate contact plates of the mating active interface. Due to the variable length of the spring loaded pins, a vertical docking tolerance of 2.2 mm is possible. The shape of the pin headers allows a penetration of dust layers and guarantees a secure electrical connection even in dusty environments.

The contact probes are used with up to 10 A continuous current within the system. The same electrical connection is used for high-frequency data streaming such as Ethernet. Each passive interface provides two blocks with 18 contact pins each. The blocks are redundant, the same holds for the active face. The arrangement of the blocks in each face allows four possible orientations for a connection with 90° rotation between each allowable configuration.

C. Docking procedure

The docking procedure between two interfaces can be divided into four steps:

1) Detection of the relative pose
2) Docking operation
3) Locking with the latch mechanism
4) Power bus activation and start of communication

The disconnection is conducted in reverse order.

In the first step the camera in the active EMI is used to find the markers on the passive EMI. Using a visual servoing approach, both interfaces are brought into a predefined relative pose to each other using the rover's (either exploration rover or shuttle rover) manipulator.

In the second step, a "blind docking" takes place. Here, a known change of poses brings the two interfaces together. Remaining uncertainties can be accounted for by the mechanical design of the two interfaces. The design of both parts of the EMI allows mechanical uncertainty in horizontal positioning of $\pm 5\,mm$ between the top of a guiding pin on the passive side to the conical shape of the counterpart cylinder on the active interface (Fig. 5). An initial misalignment of 40° is allowed by the mechanical design. However, in case of such extreme misalignments, a force control needs to properly align the interfaces during the remaining process. Typically, the visual servoing approach does not result in misalignments of this magnitude [9]. In the further process of docking the allowed angle may be 7° when the docking pins reach the cylindrical counterpart of the active EMI (see Fig. 5(b)). A rotational tolerance of 7° is allowed as depicted in Fig. 6.

Once the interfaces are brought together properly with contact detection pin on blocks, the mechanical latch is closed. A proper connection of the interfaces is indicated by one electrical probe pin that at the same time is used to identify the relative orientation of the two faces. Specific experiments will follow with the manipulator.

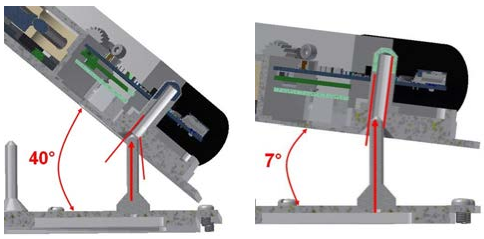

(a) Docking with angle is possible up to 40° in the conical area of counter-acting cylinder (b) Docking with angle is possible up to 7° while guiding in counter-acting cylinder

Fig. 5: Allowed docking tolerances due to horizontal angle between passive and active side of the EMI

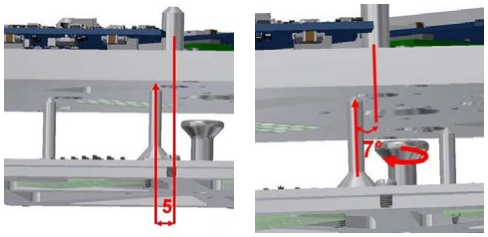

(a) Docking with horizontal displacement is possible up to 5 mm (b) Docking with rotation around vertical axis is possible up to 7°

Fig. 6: Allowed docking tolerances due to centering pins and counter-acting cylinders

D. Technical improvements in the new EMI design

With the development of the second generation of the EMI the following technical improvements were made:

1) Shorter central connection pin to allow for a longer guidance period, which means guiding pins lead the whole passive EMI along the counter acting cylinders on active EMI for correct alignment, before docking the central connection pin.
2) Thinner guiding pins for mass reduction and tight rotation protection
3) Smaller braces for reduced mounting space requirements
4) New high-power LEDs with improved positions in terms of reflections in the camera image
5) Improved visual positioning markers for a better detection in the camera image
6) Additional sealing of the docking hole with cover flaps to avoid dust penetration in case of no attached passive interface

The guiding pins of the EMI have a small conical tip, which allows play during the docking procedure. The cylindrical part allows an almost playless guiding of $5\,mm$ in the counter-acting cylinders before the central pin is inserted into the active EMI face. Fig. 7 depicts the main changes in the pin design of the interface.

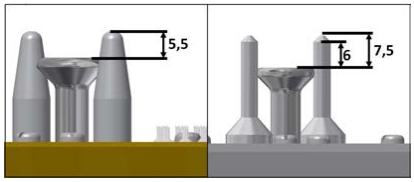

Fig. 7: Difference in heights between the EMI pins of RIMRES-EMI (left) and EMI of TransTerrA (right)

III. Experiments

To evaluate the mechanical robustness of the electro-mechanical interface, two series of experiments are conducted: (i) opening and closing of the latch under load and (ii) opening and closing of the latch under heavy contamination with dust/dirt.

In the mission scenario a base camp shall be deployed by the exploration rover. Due to its degrees of freedom in the suspension system, the rover is able to deploy a base camp vertically to the gravity vector in nominal circumstances. However, situations during the mission might occur, where the base camp needs to be dropped in slopes where, i.e. due to stability issues of the rover, a complete roll/pitch adaption is not possible. Hence, the EMI was tested for closing and opening under load in rolled and pitched state. Fig. 2 indicates the nominal x- and y-direction of the interface and the tested orientations. For the load experiment, misalignments in direction of the actuator and in the direction of the spindles were tested to separate these two load cases from each other (which would not be the case by rotating around x- and y-axis, respectively).

A. Heavy Load Test

For the heavy load test, a tray is fixed to a central pin of the passive interface. The tray carries weight discs to generate different loads for opening and closing of the active interface. The active interface is mounted in a rack and operated by the electronic that is used later in the payload-items and robotic subsystems for operating the EMI. The tray with the central pin is placed below the interface so that it is lifted by closing the latch mechanism and thus the full weight is lifted and carried by the latch. During the opening under load, the tray can fall down freely. Fig. 8 shows the experiment setup with a horizontally displaced EMI with slope of 10° and a small weight on the tray, which together results 50 N.

The fixed lever of the tray with the central pin is 78 mm, after that lever, the weights are always oriented with the gravity vector. In the experiment series, the weight on the tray is stepwise increased by 50 N from 0 N (without load) up to 400 N in each orientation. Each load condition is applied at least 20 times for opening and closing. For zero roll and pitch angle higher loads up to 800 N while undocking are tested. Additionally, a maximum static load of 1300 N has shown the robustness of latch mechanism. More load may possible, only the tray limited the test of higher weight.

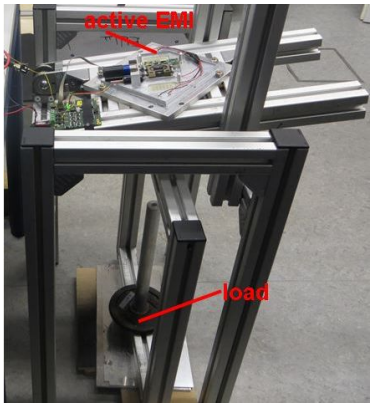

Fig. 8: Load test setup: EMI in slope of 10° with load of 50 N.

In all tested load cycles (approximately 2000 cycles), the EMI was able to completely open and close the latch properly. In average two seconds are needed for an opening or closing cycle with the chosen gear reduction. The power consumption is at 1 W in the least critical load case and reaches up to around 15 W in the worst case while opening with load of 400 N. With the nominal loads of around 50 N (max. for payload-item) and 250 N (carrying the shuttle system) in horizontal plane for closing/opening the latch, the average power consumption is at 1.6 W/1.2 W and 2.3 W/2.1 W, respectively.

With tested loads of up to 800 N, a safety factor of operation of 3.2 was achieved. Furthermore, it was proved that opening and closing under displacements from the horizontal plane is possible even in presence of high loads. The average test results for each actuator are plotted in Fig. 9 (latch closing) and Fig. 10 (latch opening), respectively.

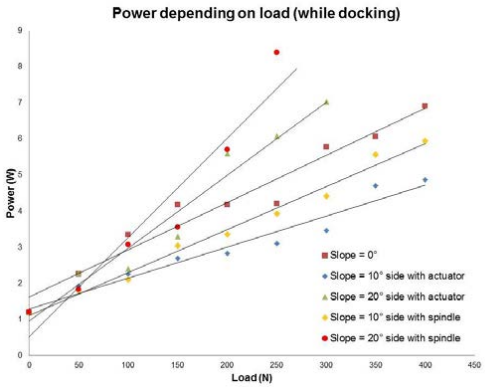

Fig. 9: Required power depending on load while closing the latch

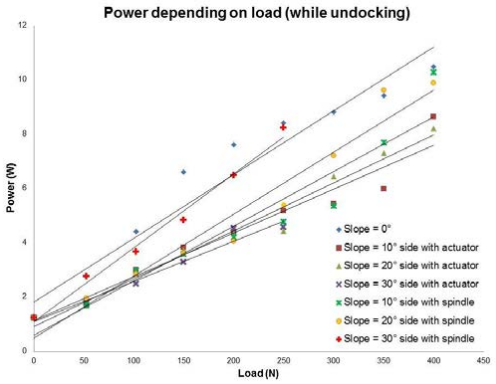

Fig. 10: Required power depending on load while opening the latch

Overall, the average of the consumed power while docking under load (closing the latch) is lower than in undocking (opening the latch). This difference is due to the fact of the position of the central pin in both scenarios: While docking the central pin of the passive face will be moved only in the last few millimeters of brace-movement, while the rest of the movement is basically without load. This results in a low average load over the whole closing process.

In case of opening the latch mechanism, the central pin and the attached load are pressing the braces apart for a longer time period than the closing presses the load, thus the higher average power consumption. Pushing the braces apart leads to higher friction due to the spindle gears, the load is not supporting the opening process.

Due to the set current limitation closing under load with slopes of 30° were not possible. However, the system allows for higher currents, thus the current limit could be adapted for operation in such situations.

B. Operation of the Latch Mechanism with Dirt Contamination

In the aspired scenario, payload-items will house surface deployable loads. This implies that the active face of the EMI is in direct contact with dusty and dirty environments. Furthermore, dust accumulations on the passive EMI might introduce contamination in the active part of the EMI. A bristle covering the inlet hole minimizes the amount of dust able to enter the EMI in most operation scenarios.

Although contamination might enter the active part of the EMI, the amount that might enter through the reception hole for the central pin is expected to be small. Nonetheless, the experiments presented in this section are assuming heavy contamination with basalt of three different granularities. Following granularity types where tested:

- Type A, grain size 0.02 mm up to 0.2 mm
- Type B, grain size 0.7 mm up to 1.3 mm
- Type C, grain size up to 5 mm

(a) EMI with contamination of basalt Type C (b) EMI with contamination of basalt Type B (c) EMI with contamination of basalt Type A

Fig. 11: EMI with different types of dust

TABLE I: Experiment results for contamination test.

Grain size	Average Power	Max. Power	Av. Time
Clean	1.1 W	1.3 W	2.2 s
Type C	1.4 W	4.6 W	2.4 s
Type B	2.3 7W	7.8 W	2.2 s
Type A*	4.2 W	17.4 W	2.3 s

*: Series with Type A contamination were aborted after 739 cycles due to damaged bearings of the mechanism.

In the experiment the latch mechanism was covered with the basalt of the different types from the top. Since in operation the dust can only enter from the bottom, this already represents a higher contamination than that to be expected during operation of the system. With the contaminated latch mechanism, 1000 cycles of closing and re-opening were attempted.

Introducing heavy contaminations increases the load for the actuator. The finer the granularity, the higher the load that is introduced to the actuator. This is due to the small grains sticking to the spindle mechanism and thus increasing the friction in the whole mechanism.

Experiments started with contamination of Type C, proceeded with Type B and ended with Type A. For Type C and B the planned 1000 cycles were conducted completely. In the series with Type A after 739 full cycles, the bearings of the linear brace guidance were destroyed.

Considering the amount of cycles with Type C and Type B contamination, and adding those to the cycles with contamination of Type A, a very robust design of the latch mechanism can be claimed. Especially since the applied contaminations were way beyond the to be expected contamination in the real system operation. The mechanical latch design is thus considered to be fully appropriate for the current project's needs.

IV. Conclusion

This paper highlights the improvements introduced in an upgraded electro-mechanical interface (EMI) used in heterogeneous multi-robot systems. The EMI is constituted by an active and a passive face that can be connected in four relative orientations with respect to each other. The EMI provides a secure mechanical and electrical (power and data) connection. This present paper focusses on the mechanical design and the mechanical reliability of the interface.

The presented experiments were conducted with loads exceeding those of nominal operation by a factor of 3.2 (tested 800 N load, while nominal extreme load case is 250 N, regular operation is below 50 N). Furthermore, undesirable docking and undocking orientations with misalignments from the horizontal plane of up to 30° were successfully tested. During nominal operation, those misalignments can be levelled out by the manipulator or by correcting the rover's attitude using its active suspension system.

A severely contaminated latch mechanism is still able to operate. After 2000 opening and closing cycles with basalt of high and medium granularity the mechanism failed after further 739 operations in fine dust. However, the contaminations applied are way beyond those to be expected in nominal operations. The mechanical design prevents excessive contamination of the moveable parts of the EMI.

Overall, the mechanical part of the interface proved to be more than feasible. For future experiments, operation in vacuum and with varying ambient temperatures are considered.

References

[1] P. Moubarak and P. Ben-Tzvi, "Modular and reconfigurable mobile robotics," *Robotics and Autonomous Systems*, vol. 60, no. 12, pp. 1648 – 1663, 2012.

[2] J. Baca, M. Ferre, and R. Aracil, "A heterogeneous modular robotic design for fast response to a diversity of tasks," *Robotics and Autonomous Systems*, vol. 60, no. 4, pp. 522 – 531, 2012.

[3] J. Baca, S. Hossain, P. Dasgupta, C. A. Nelson, and A. Dutta, "Modred: Hardware design and reconfiguration planning for a high dexterity modular self-reconfigurable robot for extra-terrestrial exploration," *Robotics and Autonomous Systems*, vol. 62, no. 7, pp. 1002 – 1015, 2014, reconfigurable Modular Robotics.

[4] K. Wolfe, M. Moses, M. Kutzer, and G. Chirikjian, "M3express: A low-cost independently-mobile reconfigurable modular robot," in *Robotics and Automation (ICRA), 2012 IEEE Int. Conf. on*, May 2012, pp. 2704–2710.

[5] W. Wang, W. Yu, and H. Zhang, "Jl-2: A mobile multi-robot system with docking and manipulating capabilities," *Int. Journal of Advanced Robotic Systems*, vol. 7, no. 1, pp. 009–018, 2010.

[6] H. Wei, Y. Cai, H. Li, D. Li, and T. Wang, "Sambot: A self-assembly modular robot for swarm robot," in *Robotics and Automation (ICRA), 2010 IEEE Int. Conf. on*, May 2010, pp. 66–71.

[7] J. Davey, N. Kwok, and M. Yim, "Emulating self-reconfigurable robots - design of the smores system," in *Intelligent Robots and Systems (IROS), 2012 IEEE/RSJ Int. Conf. on*, Oct 2012, pp. 4464–4469.

[8] R. U. Sonsalla, F. Cordes, L. Christensen, S. Planthaber, J. Albiez, I. Scholz, and F. Kirchner, "Towards a heterogeneous modular robotic team in a logistic chain for extraterrestrial exploration," in *Proc. of the Int. Symp. on Artificial Intelligence, Robotics and Automation in Space (i-SAIRAS 2014), Montreal, Canada*. o.A., 6 2014.

[9] T. M. Roehr, F. Cordes, and F. Kirchner, "Reconfigurable integrated multirobot exploration system (rimres): Heterogeneous modular reconfigurable robots for space exploration," *Journal of Field Robotics*, vol. Special Issue on Space Robotics, Part 2, pp. 3–34, 2014.

[10] F. Cordes, C. Oekermann, A. Babu, D. Kuehn, T. Stark, and F. Kirchner, "An active suspension system for a planetary rover," in *Proc. of the Int. Symp. on Artificial Intelligence, Robotics and Automation in Space (i-SAIRAS 2014), Montreal, Canada*. o.A., 6 2014.

[11] R. U. Sonsalla, J. B. Akpo, and F. Kirchner, "Coyote III: Development of a modular and highly mobile micro rover," in *Proc. of the 13th Symp. on Advanced Space Technologies in Robotics and Automation (ASTRA-2015)*, 2015.

[12] M. Mallwitz, N. Will, J. Teiwes, and E. A. Kirchner, "The capio active upper body exoskeleton and its application for teleoperation," *Proc. of the 13th Symp. on Advanced Space Technologies in Robotics and Automation (ASTRA-2015)*, 2015.

[13] W. Wenzel, F. Cordes, A. Dettmann, and Z. Wang, "Evaluation of a dust-resistant docking mechanism for surface exploration robots," in *Proc. of the 15th Int. Conf. On Advanced Robotics 2011 (ICAR-11),Talinn, Estonia*. o.A., 6 2011, pp. 495–500.